

# **Experimental and mathematical modelling of the culture and cryopreservation of a bioartificial liver device utilizing a 3D cell scaffold construction**

A thesis submitted for the degree of Doctor of Philosophy (PhD)

**Peter James Kilbride**

University College London, 2016

MRC Industrial Case Studentship, no. 9203 (UCL/Asymptote Ltd.) and UCL Graduate School Interdisciplinary Scholarship (Mathematics/Medicine).

Some of the work in this thesis was part-funded by Innovate UK (101103)

**Declaration:** I, Peter Kilbride confirm that the work presented in this thesis is my own. Where information has been derived from other sources, I confirm that this has been indicated in the thesis

# 1. Abstract

Acute Liver Failure has poor prognosis; current treatment - liver transplant - cannot keep up with demand. Due to its regenerative capabilities, a damaged liver could heal if its functions were temporarily carried out by a separate device.

A bioartificial liver device (BAL) could provide functional support while the organ heals, eliminating transplant and lifelong immunosuppression requirements. This device consists of a 2 litre biomass of alginate encapsulated HepG2 liver cells.

The aim of this PhD is to cryopreserve this biomass in a single cassette and recover viable cell number within 72 h of thaw by researching the physical and biological implications of scaling-up cryopreservation from 2ml to 2 litres.

Heat transfer, ice formation patterns, ice nucleation, and thawing profiles were examined and used to optimise cryopreservation protocols.

Ice structure was substantially different after scale-up, with network solidification present in 2ml but progressive solidification in 2 litre volumes – this reduced post-thaw viable cell number 24 h post-thaw, but faster recovery eliminated differences by 48 h. There was a strong spatial element after scale-up - biologic freezing later demonstrated reduced post-thaw function. This was solved by inclusion of supernatant medium acting as a solute and heat sink.

The warming rate of the 2.3 litre mass was reduced to  $<1^{\circ}\text{C}/\text{min}$  – the critical step during thawing was the final melting step – this should be rapid.

The effect of cold on hepatocyte proliferation was studied and a new method, termed here cryoanaptiksi, developed that uses chilling to induce rapid cell proliferation. Oxygenation and fluidisation of the bioreactor was modelled to determine more effective cell culture methods.

Using optimised protocols, successful cryopreservation of the BAL has been demonstrated – a 4 times greater volume than any cryopreserved mammalian biomass recorded in the literature. This work gives strong foundation towards successful clinical delivery of a BAL.



## Acknowledgements

I would like to thank all those who made this PhD possible, I will always be grateful for their bountiful contributions.

Little could have been achieved without the help and support of my fiancée, Eleni. On long and testing avenues she was always a stable rock of calm for me. Very likely I wouldn't have gotten through the project without her. Ευχαριστώ!

Elizabeth and Malcolm Kilbride, my parents, must be commended for super decision to go to bed early sometime in mid-May 1990. Life would have been difficult without that and of course I thank them for energizing an early interest in science and life opportunities. Extensive assistance and stimulating discussions with John Morris was of immeasurable benefit to this project and my experience and I am greatly indebted to him.

Never will I forget the welcoming nature of the UCL Maths Department where I spent a year of my PhD, in particular I would like to thank the KLB post-graduates for one of the best years of my PhD, and Nick Ovenden & Frank Smith who guided me through that year.

I dedicate this thesis to Eleni.

---



# CONTENTS

---

|           |   |           |
|-----------|---|-----------|
| <b>1.</b> | <b>ABSTRACT</b>   | <b>3</b>  |
| 1.1.      | Frequent Abbreviations  | 21        |
| <b>2.</b> | <b>INTRODUCTION</b>   | <b>22</b> |
| 2.1.      | Overview of the Liver and its Failure                               | 22        |
| 2.1.1.    | The Liver   | 22        |
| 2.1.2.    | Physiological Changes in Damaged Livers                             | 22        |
| 2.1.3.    | Causes of Liver Damage and Failure                                  | 23        |
| 2.2.      | Bio-Artificial Livers   | 23        |
| 2.2.1.    | Current Treatments  | 23        |
| 2.2.2.    | The Liver Group Bio-Artificial Liver                                | 23        |
| 2.2.1.    | Advantages and Disadvantages of the Liver Group Bioartificial Liver | 25        |
| 2.2.2.    | Alternative Developmental Treatments and Liver Support Devices      | 28        |
| 2.2.3.    | Timescales with the Bio-Artificial Liver and Acute Liver Failure    | 30        |
| 2.3.      | Cryopreservation  | 31        |
| 2.3.1.    | Cryopreservation Injuries and Solutions                             | 31        |
| 2.3.2.    | Cryoprotective Additives  | 35        |
| 2.3.3.    | Nucleation  | 36        |
| 2.3.4.    | Cryoconcentration   | 37        |
| 2.4.      | Modelling and Culture of the Bioartificial Liver Device             | 37        |
| 2.4.1.    | Fluidisation  | 37        |
| 2.4.2.    | Oxygenation   | 38        |
| 2.4.3.    | Scale-up  | 38        |
| 2.4.4.    | Previous Work and Other Aspects to Consider                         | 39        |
| 2.5.      | Detailed Aims, Motivations, and Strategy of the Thesis              | 40        |
| 2.5.1.    | Hypotheses  | 42        |
| 2.5.2.    | Chapter by Chapter Aims   | 42        |
| 2.5.3.    | List of Novel Contributions   | 43        |
| 2.5.4.    | Published Work from the Thesis                                      | 43        |
| <b>3.</b> | <b>METHODS</b>  | <b>45</b> |
| 3.1.      | Cell Culture Methods  | 45        |

|             |  |           |
|-------------|--|-----------|
| 3.1.1.      | Growing Cells in Monolayer   | 45        |
| 3.1.2.      | Preparing Culture Medium   | 46        |
| 3.1.3.      | Passaging Cells  | 47        |
| 3.1.4.      | Encapsulation of Cells in Alginate   | 48        |
| 3.1.5.      | Culturing ELS in Static Culture  | 50        |
| 3.1.6.      | Culturing ELS in an RCCS Environment   | 50        |
| <b>3.2.</b> | <b>Freezing and Warming Methods</b>  | <b>51</b> |
| 3.2.1.      | Concentration Terminology  | 51        |
| 3.2.2.      | Preparing Freezing Solution Materials  | 51        |
| 3.2.3.      | Freezing of Encapsulated Liver Spheroids (ELS)   | 52        |
| 3.2.4.      | Use of the Planer Kryo Freezer   | 53        |
| 3.2.5.      | Use of the Adapted Asymptote EF600 Freezer for use in a Scale Down Process                   | 53        |
| 3.2.6.      | Thawing of Encapsulated Liver Spheroids in Cryovials   | 54        |
| 3.2.7.      | Temperature Measurements   | 55        |
| <b>3.3.</b> | <b>Cell Functional Assays</b>  | <b>57</b> |
| 3.3.1.      | Viability using Trypan Blue  | 57        |
| 3.3.2.      | Viability of Encapsulated Liver Spheroids (ELS) using Fluorescent Dye Staining               | 58        |
| 3.3.3.      | Cell Counts using the Nucleocounter Device   | 60        |
| 3.3.4.      | MTT Viability Assay  | 61        |
| 3.3.5.      | Secreted Protein Synthesis Measurement: Albumin ELISAs (Enzyme Linked Immune Sorbent Assays) | 61        |
| 3.3.6.      | Alpha-Fetoprotein ELISAs   | 63        |
| 3.3.7.      | Alpha-1-Antitrypsin ELISAs   | 64        |
| 3.3.8.      | Fibrinogen ELISAs  | 64        |
| 3.3.9.      | Glucose Consumption and Lactate Production   | 64        |
| 3.3.10.     | Statistics   | 66        |
| <b>4.</b>   | <b>CRYOPROTECTIVE ADDITIVES AND THERMAL PROFILE OPTIMISATION</b>                             | <b>67</b> |
| <b>4.1.</b> | <b>Introduction</b>  | <b>67</b> |
| <b>4.2.</b> | <b>The Uses and Impacts of CPAs</b>  | <b>67</b> |
| 4.2.1.      | Forms of Cryo-injury   | 67        |
| 4.2.2.      | Cryoprotectants in Nature  | 68        |
| 4.2.3.      | Effects and Uses of CPAs   | 69        |
| 4.2.4.      | Application of, and Specific CPAs  | 73        |
| 4.2.5.      | Summary  | 76        |
| <b>4.3.</b> | <b>Materials and Methods</b>   | <b>76</b> |

|  |            |
|--|------------|
| <b>4.4. Results</b>  | <b>76</b>  |
| 4.4.1. Toxicity of DMSO  | 77         |
| 4.4.2. Adding Anti-Oxidants and Glucose to the Cryopreservation Medium | 78         |
| 4.4.3. Effect of pre-cryoconcentration conditions on cell growth       | 79         |
| 4.4.4. Pre incubation with CPAs  | 80         |
| 4.4.5. The complete cryopreservation profile                           | 82         |
| 4.4.6. Carrier Medium  | 83         |
| <b>4.5. The cooling profile</b>  | <b>84</b>  |
| 4.5.1. Cooling rate  | 84         |
| 4.5.2. Between what temperatures is the cooling rate most important?   | 85         |
| 4.5.3. Holding temperature at -80°C                                    | 87         |
| <b>4.6. The warming profile</b>  | <b>88</b>  |
| 4.6.1. Consistent Warming Rate   | 88         |
| <b>4.7. Discussion</b>   | <b>89</b>  |
| 4.7.1. Overview  | 89         |
| 4.7.2. Use of CPA and Carrier Medium                                   | 90         |
| 4.7.3. Cooling and Warming Rates                                       | 90         |
| <b>5. TRANSPORT AND STORAGE OF ELS</b>                                 | <b>93</b>  |
| <b>5.1. Introduction</b>   | <b>93</b>  |
| 5.1.1. Chapter Overview  | 93         |
| 5.1.2. General Introduction  | 93         |
| <b>5.2. Study Design</b>   | <b>95</b>  |
| 5.2.1. Thawing Protocols   | 95         |
| <b>5.3. Results</b>  | <b>97</b>  |
| 5.3.1. Thawing Profiles  | 97         |
| 5.3.2. Glucose Consumption   | 99         |
| 5.3.3. Protein synthesis by AFP ELISAs                                 | 100        |
| <b>5.4. Discussion</b>   | <b>101</b> |
| <b>6. SCALE UP – LARGE SCALE BIOLOGICAL FREEZING</b>                   | <b>104</b> |
| <b>6.1. Introduction</b>   | <b>104</b> |
| 6.1.1. Overview  | 104        |
| 6.1.2. Advantages of Freezing Large Scale Biological Samples           | 105        |

|             |  |            |
|-------------|--|------------|
| 6.1.3.      | Vitrification of Large Biological Samples  | 105        |
| 6.1.4.      | Slow Cooling of Large Scale Biological Samples   | 106        |
| 6.1.5.      | Inside the Large Volume  | 107        |
| <b>6.2.</b> | <b>Methods</b>   | <b>109</b> |
| 6.2.1.      | Cryopreserving the 13cm Prototype Chamber with a Planer Controlled Rate Freezer.   | 109        |
| 6.2.1.      | Cryopreserving the 30cm Prototype Chamber with an Asymptote Large Volume Viafreeze<br>Controlled Rate Freezer.                                   | 110        |
| <b>6.3.</b> | <b>Modelling for the BAL</b>   | <b>110</b> |
| <b>6.4.</b> | <b>Simulating the Large Scale Chamber</b>  | <b>112</b> |
| 6.4.1.      | Modelling  | 113        |
| 6.4.2.      | Calculations for a Large Scale Chamber   | 117        |
| 6.4.3.      | Empirical testing of a large scale chamber   | 117        |
| <b>6.5.</b> | <b>Physical Parameters of the Asymptote Large Volume Liquid Nitrogen Free Large Volume<br/>Freezer</b>   | <b>119</b> |
| 6.5.1.      | Cooling and Equilibrium with 10% Glycerol  | 119        |
| 6.5.2.      | Thawing the Chamber with 10% Glycerol Solution   | 121        |
| <b>6.6.</b> | <b>Summary and Conclusions</b>   | <b>121</b> |
| <b>7.</b>   | <b>A NOVEL METHOD TO SIMULATE LARGE SCALE FREEZING</b>   | <b>124</b> |
| <b>7.1.</b> | <b>Introduction</b>  | <b>124</b> |
| 7.1.1.      | Chapter Overview   | 124        |
| 7.1.2.      | Recap of the Need for Large Volume Cryopreservation  | 125        |
| 7.1.3.      | Smaller Volume Cryopreservation  | 125        |
| 7.1.4.      | Bulk Samples   | 126        |
| <b>7.2.</b> | <b>Materials and Methods</b>   | <b>127</b> |
| 7.2.1.      | Establishment of cooling profiles in a representative large scale volume containing an ELS<br>thermal mimic.                                     | 127        |
| 7.2.2.      | Modification of the Controlled Rate Freezer to Achieve NS or PS in small volumes during<br>cryopreservation                                      | 128        |
| 7.2.3.      | Cryopreservation Protocol  | 129        |
| 7.2.4.      | Cryo Scanning Electron Microscopy (CryoSEM) of samples cooled by PS or NS  | 130        |
| <b>7.3.</b> | <b>Results</b>   | <b>131</b> |
| 7.3.1.      | Measurement of the Thermal Histories of the Different Cooling Processes in both the Large<br>Volume Prototype Chamber and the Scale-Down Modules | 131        |

|             |  |            |
|-------------|--|------------|
| 7.3.2.      | Characterization of the Ice Morphologies in the Different Freezing Processes in the Scale-Down Modules | 132        |
| 7.3.3.      | Viability and Viable Cell Number   | 134        |
| 7.3.4.      | Metabolic Activity   | 134        |
| 7.3.5.      | Protein Synthesis  | 135        |
| <b>7.4.</b> | <b>Discussion</b>  | <b>136</b> |
| <b>7.5.</b> | <b>Conclusion</b>  | <b>139</b> |
| <b>8.</b>   | <b>CRYOCONCENTRATION</b>   | <b>141</b> |
| <b>8.1.</b> | <b>Overview</b>  | <b>141</b> |
| 8.1.1.      | Chapter Specific Nomenclature and Abbreviations  | 142        |
| 8.1.2.      | Metallurgy and Inverse Segregation   | 143        |
| <b>8.2.</b> | <b>Factors Impacting on Magnitude of Cryoconcentration</b>   | <b>144</b> |
| 8.2.1.      | Effect of Ice Front Speed  | 144        |
| 8.2.2.      | Effect of pre-freeze Concentration   | 145        |
| 8.2.3.      | Interactions between Solutes   | 145        |
| 8.2.4.      | Effect of Solute Size on Diffusion Rate  | 146        |
| 8.2.5.      | Effect of Temperature  | 146        |
| 8.2.6.      | Biological Solutes   | 147        |
| 8.2.7.      | Dissolved Gas  | 148        |
| 8.2.8.      | Location of Solutes in Ice Matrix  | 148        |
| 8.2.9.      | Effect on Glass Transition Temperature   | 149        |
| 8.2.10.     | Ice Front Structure  | 149        |
| 8.2.11.     | Ice Crystal Spacing  | 149        |
| 8.2.12.     | Rapid Solidification   | 151        |
| 8.2.13.     | Methods to Increase and Reduce Cryoconcentration   | 151        |
| <b>8.3.</b> | <b>Mathematical Modelling</b>  | <b>152</b> |
| 8.3.1.      | Determining Diffusivity  | 152        |
| 8.3.2.      | Diffusivity of Common Cryoprotectants  | 154        |
| 8.3.3.      | Solute Concentration in Solid and Liquid Phases  | 155        |
| 8.3.4.      | Partition Coefficient  | 160        |
| 8.3.5.      | Rapid Solidification   | 161        |
| <b>8.4.</b> | <b>Summary of Mathematics</b>  | <b>163</b> |
| <b>8.5.</b> | <b>Experimental Measurements</b>   | <b>164</b> |
| 8.5.1.      | Materials and Methods  | 164        |

|             |  |            |
|-------------|--|------------|
| 8.5.2.      | Results  | 169        |
| <b>8.6.</b> | <b>Adding Gravity to the Model</b>   | <b>179</b> |
| <b>8.7.</b> | <b>Conclusions</b>   | <b>181</b> |
| <b>8.8.</b> | <b>Appendices</b>  | <b>182</b> |
| 8.8.1.      | Appendix 1 –To Equation ( 19 )   | 182        |
| 8.8.2.      | Appendix 2 – To Equation ( 20 )  | 183        |
| 8.8.3.      | Appendix 3 – Diffusion Coefficients  | 184        |
| <b>9.</b>   | <b>SPATIAL CONSIDERATIONS DURING CRYOPRESERVATION OF LARGE VOLUME SAMPLES.</b>                     | <b>187</b> |
| <b>9.1.</b> | <b>Introduction</b>  | <b>187</b> |
| 9.1.1.      | Overview of Chapter  | 187        |
| 9.1.2.      | General Introduction and Large Volume Re-cap   | 188        |
| <b>9.2.</b> | <b>Materials and Methods</b>   | <b>189</b> |
| 9.2.1.      | Modification of the Controlled Rate Freezer to Achieve PS in Small Volumes during Cryopreservation | 189        |
| 9.2.2.      | Modification and Application of 2 Litre Cryopreservation Chamber by Adding Warming Device          | 190        |
| 9.2.3.      | Cryopreservation Protocol for 6ml PS Samples   | 191        |
| 9.2.4.      | Cryopreservation Protocol for 2 litre PS Samples without Warming Device.                           | 192        |
| 9.2.5.      | Thawing and Dissection of 6ml Volume PS Samples  | 192        |
| 9.2.1.      | Thawing of 2 Litre PS Sample without Warming Device  | 193        |
| <b>9.3.</b> | <b>Results</b>   | <b>195</b> |
| 9.3.1.      | Progressive Solidification (PS) in 6ml Samples   | 195        |
| 9.3.2.      | Progressive Solidification in a Pouch in a 2 Litre Volume  | 196        |
| 9.3.3.      | Thawing of a 2 Litre Volume  | 198        |
| 9.3.4.      | Warming Rates Impact on Viability and Viable Cell Number   | 199        |
| <b>9.4.</b> | <b>Discussion</b>  | <b>200</b> |
| 9.4.1.      | 6ml Samples Experiencing Progressive Solidification (PS)   | 201        |
| 9.4.2.      | Comparison of 6ml Samples to 2 Litre Volumes   | 201        |
| 9.4.3.      | Spatial Effects of Warming a Large Volume  | 202        |
| 9.4.4.      | Progressive Solidification   | 202        |
| <b>9.5.</b> | <b>Conclusion</b>  | <b>204</b> |

|   |            |
|---|------------|
| <b>10. SCALED UP – CRYOPRESERVATION AND RE-CULTURE OF A 2.3 LITRE BIOMASS FOR USE IN A BIOARTIFICIAL LIVER DEVICE</b> | <b>205</b> |
| <b>10.1. Introduction</b>   | <b>205</b> |
| 10.1.1. General Chapter Overview  | 205        |
| 10.1.2. General Introduction and Re-Cap   | 205        |
| <b>10.2. Methods</b>  | <b>207</b> |
| 10.2.1. Large Volume Cell Culture   | 207        |
| 10.2.2. Optimised Large Volume Cryopreservation Protocol  | 208        |
| 10.2.3. Scale Down Process Protocol   | 209        |
| 10.2.4. Large Volume Thawing and Re-culture Protocol  | 209        |
| 10.2.5. Thawing and Re-Culture Protocol of Scale Down Process and Cryovial Samples.                                   | 209        |
| 10.2.6. Temperature Profiles  | 209        |
| <b>10.3. Results</b>  | <b>210</b> |
| 10.3.1. Warming Rates Significance  | 210        |
| 10.3.2. Excess Medium Significance  | 211        |
| 10.3.3. Large Volume Warming Profile  | 212        |
| 10.3.4. Viability and Viable Cell Number  | 212        |
| 10.3.5. Glucose Consumption   | 214        |
| 10.3.6. Lactate Production  | 215        |
| 10.3.7. Alpha-fetoprotein Production  | 215        |
| <b>10.4. Discussion</b>   | <b>216</b> |
| 10.4.1. Warming Rates Significance  | 216        |
| 10.4.2. Excess Medium Significance  | 218        |
| 10.4.3. Recovery Timeframe  | 218        |
| <b>10.5. Conclusions and Future Work</b>  | <b>219</b> |
| <b>11. ENGAGING COLD TO INCREASE CELL PROLIFERATION IN ALGINATE ENCAPSULATED LIVER SPHEROIDS</b>                      | <b>221</b> |
| <b>11.1. Introduction</b>   | <b>221</b> |
| 11.1.1. Chapter Overview  | 221        |
| 11.1.2. Overview of Literature  | 222        |
| <b>11.2. Materials and Methods</b>  | <b>223</b> |
| 11.2.1. Cooling/Warming Methods   | 223        |
| 11.2.2. Cryopreservation Protocol – DMSO with Viaspan   | 224        |

|              |   |            |
|--------------|---|------------|
| 11.2.3.      | Cell Culture  | 224        |
| <b>11.3.</b> | <b>Results</b>  | <b>224</b> |
| 11.3.1.      | Comparing ELS Cryopreserved on Encapsulation with those Cultured in a FBB Directly. | 224        |
| 11.3.2.      | Spheroid breakout from Alginate   | 225        |
| 11.3.3.      | Cold Treatment in Culture Medium  | 226        |
| 11.3.4.      | Time and Temperature Dependence of Low Temperature                                  | 227        |
| 11.3.5.      | Cooling Rate Dependency of Low Temperature Treatment                                | 228        |
| 11.3.6.      | Effect of Cell Density  | 230        |
| 11.3.7.      | Effect of Cryopreservation over Simple Chilling.                                    | 232        |
| 11.3.8.      | Effect of Cryopreservation Reagents.  | 232        |
| 11.3.9.      | Time-course of Cryoanaptiksi Cell Proliferation.                                    | 233        |
| 11.3.10.     | Impact on Cell Function and Extended Culture  | 234        |
| <b>11.4.</b> | <b>Discussion</b>   | <b>235</b> |
| <b>12.</b>   | <b>FLUIDISATION</b>   | <b>240</b> |
| <b>12.1.</b> | <b>Introduction</b>   | <b>240</b> |
| <b>12.2.</b> | <b>Types of Fluidisation</b>  | <b>241</b> |
| 12.2.1.      | Gas-Solid   | 241        |
| 12.2.2.      | Liquid-Solid  | 241        |
| 12.2.3.      | Gas-Liquid-Solid  | 242        |
| 12.2.4.      | Circulating Fluidised Bed Reactors  | 242        |
| 12.2.5.      | Inverse Fluidisation  | 242        |
| 12.2.6.      | Semi-Fluidised Beds   | 243        |
| <b>12.3.</b> | <b>Applications of Fluidisation</b>   | <b>243</b> |
| 12.3.1.      | Mixing  | 243        |
| 12.3.2.      | Particle Separation   | 243        |
| 12.3.3.      | Particle coating  | 244        |
| 12.3.4.      | Biomass Combustion  | 244        |
| 12.3.5.      | Application to the Bioartificial Liver  | 244        |
| <b>12.4.</b> | <b>Mechanical Considerations during Fluidisation (solid-liquid)</b>                 | <b>245</b> |
| 12.4.1.      | Linearising Flow  | 245        |
| 12.4.2.      | Effect of Particle Size and Shape   | 246        |
| 12.4.3.      | Collisions between Particles  | 246        |
| <b>12.5.</b> | <b>Modelling System Parameters</b>  | <b>247</b> |
| 12.5.1.      | Nomenclature  | 248        |

|              |  |            |
|--------------|--|------------|
| 12.5.2.      | Reynolds Number  | 249        |
| 12.5.3.      | Archimedes Number  | 250        |
| 12.5.4.      | Drag Coefficient   | 251        |
| 12.5.5.      | Minimum Fluidisation Velocity and Pressure Drop                                      | 253        |
| 12.5.6.      | Mathematically Modelling Pressure Drops and Minimum Fluidisation Velocity            | 253        |
| 12.5.7.      | Maximum Fluidisation Velocity  | 254        |
| 12.5.8.      | Bed Expansion and Voidage  | 256        |
| 12.5.9.      | Particle distribution  | 257        |
| 12.5.10.     | Usefulness of Theory to Practice   | 258        |
| <b>12.6.</b> | <b>Materials and Methods</b>   | <b>259</b> |
| 12.6.1.      | The Bioartificial Liver Vessel   | 259        |
| 12.6.2.      | Mini-columns   | 260        |
| 12.6.3.      | Viscosity  | 261        |
| <b>12.7.</b> | <b>Results</b>   | <b>262</b> |
| 12.7.1.      | Construction and Operation of the System.  | 262        |
| 12.7.2.      | Effect of Volume of ELS  | 262        |
| 12.7.3.      | Flow Rates required for Fluidisation   | 263        |
| <b>12.8.</b> | <b>Discussion, Conclusions, and Future Work</b>                                      | <b>264</b> |
| <b>13.</b>   | <b>OXYGENATION OF THE BIOARTIFICIAL LIVER DEVICE (BAL) AS A DIAGNOSTIC TOOL. 266</b> |            |
| <b>13.1.</b> | <b>Introduction</b>  | <b>266</b> |
| 13.1.1.      | Chapter Outline  | 266        |
| 13.1.2.      | Oxygenation  | 266        |
| 13.1.3.      | Overview   | 267        |
| 13.1.4.      | Design of the BAL Culture Chamber  | 268        |
| 13.1.5.      | Converting % Measurements to Molar Consumption                                       | 268        |
| <b>13.2.</b> | <b>Materials and Methods</b>   | <b>269</b> |
| 13.2.1.      | Measuring Oxygen Pressure in Silicone Tubing   | 269        |
| 13.2.1.      | Measuring Oxygen Levels in the BAL Chamber without ELS                               | 270        |
| <b>13.3.</b> | <b>Mathematical Approximations</b>   | <b>270</b> |
| 13.3.1.      | Determining Oxygen Diffusion through the Silicone Tubing                             | 270        |
| 13.3.2.      | Determining the Partial Pressures between the Silicone and the Culture Medium        | 272        |

|  |            |
|--|------------|
| <b>13.4. Modelling oxygenation of ELS during low external oxygen flow rates during FBB culture – Steps</b> | <b>273</b> |
| <b>13.5. Higher Oxygen Flow Rates</b>  | <b>274</b> |
| <b>13.6. General System</b>  | <b>274</b> |
| 13.6.1. Oxygen Pressures at Specific Flow Rates  | 274        |
| <b>13.7. Estimating Oxygen Consumption during the FBB Culture</b>  | <b>277</b> |
| 13.7.1. Problems with the Model  | 280        |
| <b>13.8. Oxygenation as a Diagnostic Tool</b>  | <b>281</b> |
| 13.8.1. Experimental Design  | 281        |
| 13.8.1. Oxygen Consumption after Cryopreservation  | 284        |
| <b>13.9. Discussion and Conclusions</b>  | <b>285</b> |
| <b>14. CONCLUDING REMARKS, THOUGHTS, AND POTENTIAL FUTURE DIRECTIONS</b>                                   | <b>287</b> |
| <b>15. REFERENCES</b>  | <b>291</b> |

|   |     |
|---|-----|
| Figure 1 - Schematic of the BAL device.....   | 24  |
| Figure 2 - Standard deviation between n=8 k-type Pico-technology thermocouples at different temperatures.....                         | 56  |
| Figure 3 - An example of the typical images used to determine viability.....  | 59  |
| Figure 4 - Looking at the effects of Raffinose, Raffinose and DMSO combined, and DMSO, on the success of cryopreservation of ELS..... | 77  |
| Figure 5 - Cell viability after being held in cryopreservation solution containing 12% DMSO in viaspan .....                          | 78  |
| Figure 6 - Effect of anti-oxidants and glucose when added to the freezing solution.. .....  | 79  |
| Figure 7 – Effects on viable cell number of pre incubating under different conditions for 24h. ....                                   | 80  |
| Figure 8 – Impact of pre-incubation .....   | 81  |
| Figure 9 - The effects of removing any additional supernatant .....   | 82  |
| Figure 10 - Testing new carrier solutions. ....   | 83  |
| Figure 11 - Cell viability 24hrs post-thaw with cells of different cooling rates and cell densities .....                             | 84  |
| Figure 12 - The effect on viable cell number of different cooling rates with different initial cell densities .....                   | 85  |
| Figure 13 - The effects on viability of plunging ELS into liquid nitrogen.....  | 86  |
| Figure 14 - Viable cell number 24 h after thaw of samples plunged into LN <sub>2</sub> at different temperatures. ....                | 87  |
| Figure 15 - Effects of a 72h dehydration stop on viable cell number .....   | 88  |
| Figure 16 - Cell membrane and metabolic viability: the impact of different warming rates. ....  | 89  |
| Figure 17 - Thawing cryovials temperature profiles .....  | 97  |
| Figure 18 – Impact of hold on warming (days).....   | 98  |
| Figure 19 – Impact of hold on cooling (hours) .....   | 99  |
| Figure 20 – Impact of hold on warming on glucose consumption.....   | 99  |
| Figure 21 – Impact of hold on warming on protein production .....   | 100 |
| Figure 22 - The set-up of the Asymptote Large Volume Viasfreeze. ....   | 110 |
| Figure 23 - Comparing the theoretically predicted and actual temperatures inside a cooling centrifuge tube.....                       | 117 |
| Figure 24 - Temperature profiles inside 2L volume being cryopreserved in a chamber .....  | 118 |
| Figure 25 - Thermal profiles in the LVCRF system during cooling and at the equilibrium level. ....                                    | 120 |
| Figure 26 – Thawing profiles the 30m chamber. ....  | 121 |
| Figure 27 - Schematic and image of the large volume cylindrical chamber.. .....   | 127 |
| Figure 28 - The two different heat transfer modules designed for the EF600-103 CRF.....   | 129 |
| Figure 29 - Measured temperature profiles inside the BAL chamber during cooling of a thermal mimic. ....                              | 131 |
| Figure 30 - Temperature profiles in the heat transfer modules measured on the EF600-103 controlled rate freezer.....                  | 132 |
| Figure 31 - Cryo-Scanning Electron Microscopy (Cryo-SEM) presenting differences in ice structure ...                                  | 133 |

|  |     |
|--|-----|
| Figure 32 – Viability between PS and NS .....  | 134 |
| Figure 33 – MTT between PS and NS .....  | 135 |
| Figure 34 – Impact of PS and NS on protein production. ....  | 136 |
| Figure 35 - Solute concentration profile in the liquid phase, for a long sample. ....  | 158 |
| Figure 36 - Solute concentration profile in the solid phase, for a long sample.....  | 159 |
| Figure 37 - Cryoconcentration vial experimental setup. ....  | 166 |
| Figure 38 - The EF600 freezer adapted for the scale down process.....  | 167 |
| Figure 39 - The levels of DMSO measured in the ice after cryopreservation,.....  | 170 |
| Figure 40 - Measured DMSO concentrations in the taller 5ml vials, .....  | 171 |
| Figure 41 - DMSO concentration in the solid phase after being cooled in a -20°C freezer horizontally..<br>.....  | 172 |
| Figure 42 - Data comparing samples cooled to -100°C at 5°C/min in the aluminium module of the<br>EF600 controlled rate freezer to investigate the effect of supercooling. .... | 174 |
| Figure 43 - Cryoconcentration observed in a sample where ice develops downwards in a sample.....   | 175 |
| Figure 44 - Typical cooling profiles obtained with thermocouples attached to the pico-logger system.<br>.....  | 176 |
| Figure 45 - Standard curve relating the refractive index of NaCl solution to a % weight.....   | 177 |
| Figure 46 - Cryoconcentration measured in NaCl samples cooled at different ice growth in the acetal<br>module, and at the aluminium module.....                                | 177 |
| Figure 47 - Cryoconcentration measured in taller 5ml vials, both for samples frozen vertically .....   | 178 |
| Figure 48 - Figure of relative measured mass density of DMSO at varying concentrations and with a<br>linear line of best fit added. ....                                       | 180 |
| Figure 49 – Schematic of the BAL thawing device.....   | 191 |
| Figure 50 – Schematic of the Scale Down Process .....  | 193 |
| Figure 51 – Spatial impact on viability in large volume cryopreservation .....   | 194 |
| Figure 52 - Functional outcome on ELS experiencing PS on cooling in 6ml vials,.....  | 196 |
| Figure 53 – Viability and viable cell number of samples cryopreserved in porous pouches  | 197 |
| Figure 54 - MTT viability of samples cryopreserved in porous pouches in a 2 litre mass of alginate<br>beads .....  | 198 |
| Figure 55 – Temperatures measured in the warming fluid (ethanol) the thawing tubes of the chamber<br>with warming device. ....   | 199 |
| Figure 56 – Spatial impact on thawing.....   | 200 |
| Figure 57 – Relationship between total thawing time of a BAL, and the cell viability on thaw. ....   | 200 |
| Figure 58 – Impact of warming rates in cryovials.....  | 211 |
| Figure 59 – Impact of excessive supernatant on cryopreservation .....  | 211 |
| Figure 60 - Warming profiles experienced during warming of the large volume cryopreservation<br>cylindrical chamber.....   | 212 |
| Figure 61 – Viability after large volume cryopreservation .....  | 213 |
| Figure 62 - Glucose consumption and lactate production following large volume cryopreservation..   | 214 |

|   |     |
|---|-----|
| Figure 63 – AFP production of large volume cryopreserved samples.....   | 216 |
| Figure 64 – Comparison between ELS encapsulated and cultured directly in an FBB environment, with ELS cryopreserved and thawed before RCCS culture. ....                          | 225 |
| Figure 65 – Images of cell breakout at high cell densities, .....   | 226 |
| Figure 66 - Comparison in viable cell number between samples experiencing cryoanaptiksi induced by either simple chilling or cryopreservation and untreated control samples. .... | 227 |
| Figure 67 - Viable cell number of samples experiencing various chilling times and chilling temperatures to induce cryoanaptiksi.....  | 228 |
| Figure 68 - Viable cell number after 12 days of culture following cryoanaptiksi induced through various cooling conditions. ....  | 229 |
| Figure 69 - Top shows effect of 0°C chill at a high cell density, after 12 days prior culture. ....   | 230 |
| Figure 70 – Comparison of viable cell number between ELS sets experiencing different levels of cryodamage,.....   | 231 |
| Figure 71 - Comparison between viable cell number 12 days after cryoanaptiksi induced by either simple chilling, or cryopreservation .....  | 232 |
| Figure 72 - Viable cell number of samples experiencing different reagents when undergoing cryoanaptiksi. ....   | 233 |
| Figure 73 - Comparing temporal cell growth between samples undergoing cryoanaptiksi and an untreated control. ....  | 234 |
| Figure 74 – Functional assays of ELS having undergone cryoanaptiksi.....  | 235 |
| Figure 75 - Example of a solid-liquid fixed bed of particles, an expanded (fluidised) bed and an over fluidised bed .....   | 240 |
| Figure 76 - A false colour representation of possible fluid flow through the bioartificial liver device at any particular moment. ....  | 245 |
| Figure 77 - The mini-column set up with 6 circuits in series.....   | 260 |
| Figure 78 - The mini-column set-up.....   | 261 |
| Figure 79 - One minicolumn during use of a fluidisation experiment. ....  | 262 |
| Figure 80 - Flow rate versus pump rotation rate for different volumes of ELS. ....  | 263 |
| Figure 81 – Level of bed expansion compared to linear flow rate of different volumes of ELS in identical minicolumns.....   | 264 |
| Figure 82 - A Schematic of the BAL device during oxygenation tests.. ....   | 269 |
| Figure 83 - Standard curves of oxygen pressure related to flow rate at different exit conditions.....   | 275 |
| Figure 84 – Average pressure measured in the inlet pressure transducer at different oxygen flow rates. ....   | 276 |
| Figure 85 - The additional pressure supplied by the silicone tubing related to the measured increase in oxygen levels .....   | 277 |
| Figure 86 - Measured oxygen consumption rates of the BAL during 5 different experiments.....  | 279 |
| Figure 87 - Considering the oxygen consumption rates of an FBB experiment where poor cell growth was seen .....   | 281 |

**Figure 88 - Considering the oxygen consumption rates of an FBB experiment where an overheating event occurred .....282**

**Figure 89 - Considering the oxygen consumption rates of an FBB experiment where the external oxygen tubing started to leak . .....283**

**Figure 90 - Oxygen consumption measured during the pre-cryopreservation culture phase of the large volume compared with values post-thaw. ....284**

## **1.1. Frequent Abbreviations**

ALF – Acute liver failure

BAL – Bioartificial liver device

CPA – Cryoprotective additive

CV – Cryopreservation in cryovials

DMSO – Dimethyl sulfoxide

DOCD – Delayed onset cell death

DS – Directional solidification

ELS – Encapsulated Liver Cell Spheroids

FB – Fluidised bed

FBB – Fluidised bed bioreactor

FDA - Fluorescein diacetate

FFP – Fresh frozen plasma

IIF – Intra-cellular ice formation

LG – Liver group (team with which I was doing my PhD)

LN<sub>2</sub> – Liquid nitrogen

LV – Large volume

NS – Network solidification

PI - Propidium iodide

PS – Progressive solidification

SDP – Scale down process

## 2. Introduction

### 2.1. Overview of the Liver and its Failure

#### 2.1.1. The Liver

The liver is the human body's largest internal organ - it weighs ~ 1.5kg and is located in the upper right of the abdominal cavity [213, 225], coming after the spleen and intestine in the human corporal system [397, 398]. The liver has a wide range of functions, over 500 have been identified: it is involved in protein, fat, and carbohydrate metabolism; nutrient storage as well as many forms of blood detoxification. The most common cell type in the liver is the hepatocyte, which accounts for ~ 60% of the organ's mass [213, 357]. These cells fulfil many of the liver's functions and are arranged into lobules *in situ*. Each lobule contains as many as 200,000 hepatocytes, which are formed in thin layers to allow for maximum contact area with the blood being treated [213, 225, 357, 397, 398].

Although hepatocytes are the most common cell type in the liver, there are many others, such as kupffer cells - a type of phagocyte - and stellate cells that provide a structured environment for the hepatocytes to function. Most of the primary metabolic functions of the liver are carried out by hepatocytes [213, 225, 357, 397, 398].

#### 2.1.2. Physiological Changes in Damaged Livers

The liver has a remarkable ability to heal itself after injury. Even with two thirds of its mass removed, the remaining cells can proliferate readily, returning the liver back to its healthy size within only a few days or weeks [101, 251, 300].

Sustained damage over a longer term however, can impair the organ's ability to fully recover, therefore hindering the liver's function and efficiency. As a liver recovers from damage, collagenous scar tissue forms in the extra-cellular space. If the liver repairs itself on many occasions, this scar tissue can become so dense that it cuts off blood supply to hepatocytes. This condition is known as fibrosis, which can further develop into a more severe form – cirrhosis. These stop hepatocytes from interacting with the blood and so reduce the operation of the liver [225, 357, 359].

Acute Liver Failure (ALF) is a rare condition, with fewer than 1 case per 100,000 per year in the developed world in which severe loss of liver function presents itself in a patient who normally has not shown any signs of liver problems up to that point [30, 31, 239, 313]. If this severe failure becomes encephalopathic - that is if it leads to confusion, loss of consciousness, and coma - within one to four weeks of jaundice onset, the condition will usually be described as ALF [30, 31, 239, 444].

### **2.1.3. Causes of Liver Damage and Failure**

The causes of liver failure are varied though can often be attributed to viral infection or drug overdose. ALF in the UK is most commonly caused by Acetaminophen (paracetamol) overdose, accounting for 57% of cases between 1999-2008, and around half of cases in the United States [30, 31, 239, 313]. Other causes include mushroom poisoning, hepatitis B, Acute Fatty Liver of Pregnancy Syndrome that can affect women in later stages of pregnancy, and ingestion of many noxious chemicals results in the onset of ALF. In around 15% of cases the cause remains unknown [31, 239, 397].

## **2.2. Bio-Artificial Livers**

### **2.2.1. Current Treatments**

Currently the only treatment for ALF short of spontaneous recovery is liver transplantation [313, 334, 397]. However, this is problematic; there are shortages of organ donors, resulting in many deaths on the waiting list [313]. In addition, there are the general risks associated with major surgery and specific issues of organ rejection. The survival outcome for patients with ALF receiving liver transplantation is lower than that for patients receiving an elective liver transplant [31, 126, 239].

Moreover, if a liver is transplanted successfully, the recipient of that organ will have to be on immunosuppressants for the rest of his or her life, to prevent the body's immunological response to foreign tissue. This makes the patient more susceptible to disease and illness in the future, reducing quality of life, although new techniques which allow for the removal of immunosuppression are being developed [54, 117, 144, 225, 252].

### **2.2.2. The Liver Group Bio-Artificial Liver**

Considering the mass of a healthy liver, the total number of cells is approximately between  $10^{11}$  and  $2 \times 10^{11}$  [373, 374, 445]. However as a human liver can support life and recover with when a substantial portion of its mass is removed [251, 300], and the fact that a patient with ALF will retain some liver function, it is envisaged that a BAL would only need to contain between 30-50% of normal liver mass to operate satisfactorily ( $7 \times 10^{10}$ - $10^{11}$  hepatocytes) [213, 389]. These cells are grown in the Liver Group at the Royal Free Hospital Campus, UCL. This cell line (HepG2) is grown from cells originally taken from a *hepatoblastoma* in a 15-year-old boy in 1979 [216, 375].

The cells are grown in a 3-dimensional environment by encapsulation in alginate spheres, each spherical being approximately 0.5 mm in diameter. This culture system mimics the conditions inside the liver for the cells, making them proliferate and function more effectively than levels seen in monolayer culture [63, 137, 206].

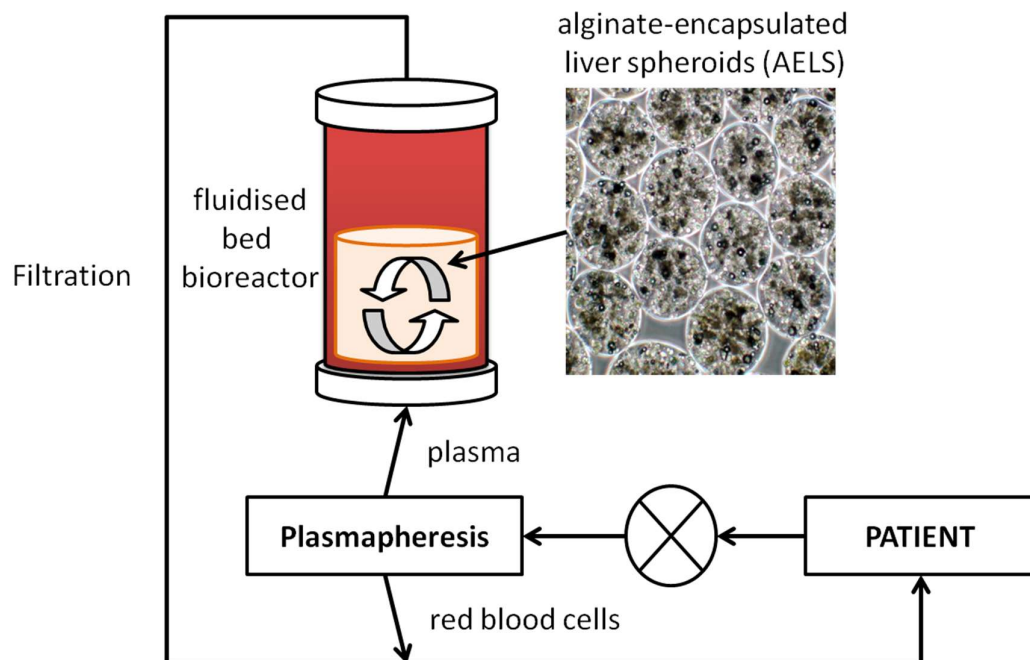


*Figure 1 - Schematic of the BAL device. The device will be attached extra-corporally to a patient, with the patient's blood plasma fraction separated, and passed through the BAL chamber containing ELS. After several passages, this treated plasma will be filtered for endotoxins and returned to the patient, mimicking the condition of blood that has passed through a functioning liver. Image taken from LG stock images.*

These spheres are then held in a chamber within the BAL, cultured in a fluidised bed bioreactor (FBB) [101, 137, 240]. After sufficient biomass has been cultured, patient plasma will be passed through the chamber and will come into contact with the ELS (ELS – Encapsulated Liver Spheroids) [363]. This plasma makes contact with the hepatocytes that subsequently carry out liver functions. Sophisticated filter methods must be in place to stop any material, such as DNA from the BAL cells, returning to the patient intravenously.

## **Improvement on Current Treatment**

As a consequence of the poor prognosis for ALF sufferers, it is desirable to find a new form of treatment. Survival rates are very low when no transplant is available [30, 50].

A potential solution to this problem is the use of a bioartificial liver (BAL), such as is being developed by the Liver Group (LG), in the UCL Institute for Liver and Digestive Health [101, 363]. This is a device that sits outside the patient and incorporates living liver tissue and which mimics functions of a human liver. As no completely artificial device that emulates the functions of the liver currently exists, and there has been little success in developing one, a BAL device that incorporates living liver tissue may be the most promising avenue [9, 50, 389].

A BAL would contain hepatocyte cells; with blood being diverted from the patient's impaired liver through the device, with the hepatocytes within the BAL acting as a replacement for those within the liver. This would prolong the life of those with ALF, and allowing them more time to wait for a suitable donor organ to become available [363, 389].

It would also give the patient's liver the time and opportunity to recover on its own. As discussed in section 2.1.2, the liver can heal itself rapidly. The BAL should allow the patient's recovery while it carries out the liver's functions. This will lead to a full recovery for the patient without the need for a transplant [9, 168, 213, 307]. Recovery without transplant is much preferable to transplantation due to post-transplant treatments, and would represent a marked improvement on current treatments.

### **2.2.1. Advantages and Disadvantages of the Liver Group Bioartificial Liver**

#### **Advantages**

The BAL being tested here has substantial improvements over other liver assist devices (LADs). A major advantage is the fact that the HepG2 cell line is human-derived [216]. This ensured that human proteins are produced, as opposed to other devices where animal cell lines have been attempted producing some non-human proteins [9, 389]. While many of the proteins produced are the same in human and non-human liver cells, the differences that do exist will reduce non-human based devices efficiencies.

Non-human cell lines also carry a greater risk of cross-species disease [437]. This can lead to the introduction of non-human viruses into the cell line; resulting in a risk of that virus crossing the

species barrier and infecting a patient. Of particular risk is porcine endogenous retro-viruses, (amusingly abbreviated to PERVs)[333]. Pig cells and tissues are often used for pre-clinical trials [9] as their physiology is similar to humans, resulting in an increased contamination risk. Several other BAL attempts in the past have used porcine derived cells as their primary mode of function [9, 168, 292, 333]. If there is the possibility of any contaminated cells in a BAL, it cannot be used clinically.

The extra-corporeal nature and cell encapsulation used in the BAL studies here also gives it an edge. As there is no direct contact between the patient's plasma and the cell line, the risk of foreign DNA entering a patient is reduced. The device sitting outside the body also substantially reduces this risk, and allows for easier attachment and removal.

The HepG2 cell line's rapid proliferation in culture allows for the production of a large biomass in a relatively short period of time [63, 101]. Alternative sources of biomass, such as primary cells, can take many times longer to achieve sufficient biomass size resulting in uneconomical culture costs.

A major advantage of the BAL studied here is the delivery method. A single cassette will be used for the culture, cryopreservation, and treatment of a patient. This reduces the risk of contamination during biomass transfer. It also enables many BALs to be produced and stored on demand and thawed for direct use. Cryopreservation in another format such as cryobags would require additional trained technicians for the thawing and decanting process in an expensive GMP facility. This is the reason this thesis focuses on the cryopreservation in the 2 litre cassette.

A recent animal trial using the BAL showed the ability of the ELS to improve clinically relevant parameters, such as a reduction in bilirubin levels and intracranial pressure [363].

### **Disadvantages**

With the many advantages of using the HepG2 cell line comes some disadvantages which must be addressed before the BAL studied here can become a realistic clinical treatment. A cause of concern is the functionality of the HepG2 cells [308]. A healthy human liver produces between 5-15g of albumin per day, for example [23, 32, 136]. Encapsulated HepG2 cells in a microgravity culture produce 20µg albumin per million cells per day [63]. Approximately  $50 \times 10^{10}$  HepG2 cells would then be required to fully replace a liver function, an order of magnitude higher than the total cell count within the BAL [101].

This is not as bad as it appears – the BAL would only be needed to replace around 25-30% liver function as a fully functional human liver has substantial over capacity [32, 136]. The 20µg figure

is also for cells grown in fetal calf serum medium [63]. In the BAL this has been replaced with human plasma and function per cell may be higher. The rate of production of proteins carried out in a healthy human liver is unknown for ELS cultured in 10% human plasma – they cannot be detected above background levels. This fact alone suggests that they are well below levels required for clinical relevance.

To overcome this challenge several options are available. Synthetic albumin and other proteins could be given as additional treatment during BAL delivery, as is done in other systems [22]. Alternatively gene modification could be carried out on the cell line to restore functional capacity that has been lost [96, 305]. A third option would be trying an additional cell line, although this would result in the benefits that HepG2 cell lines bring removed. Finally a system using several cell types at once could be attempted, as this will more accurately mimic a human liver [83, 218, 253].

One major disadvantage of the BAL is the inability of HepG2 cells to carry out the urea cycle [43, 267]. The human body produces ammonium from the metabolism of amino acids. Ammonium build up in the body is fatal as ammonium is highly toxic [42, 391]. One of the functions of the human liver is to convert ammonium into less toxic urea (urea cycle) before it is expelled from the body [229, 391]. HepG2 cells have lost this ability in culture.

While attempts to edit HepG2 cells to re-acquire the ability to detoxify ammonium have been carried out [267], the effect is very short lived before the cells regress and the ability is lost. This must be solved before the BAL can be a clinical treatment, options include adding synthetic devices which separately remove ammonia.

Other challenges to overcome with the BAL include the use of 10% human blood plasma in the culture medium [101]. The bioreactor used for the culture phase has a volume of 116 litres and several medium changes happen during this phase. The volume of human blood required for widespread use of a BAL device is therefore considerable and considering that blood is in high demand with increasing use in ageing populations not counteracted by an increase in supply [146] this may become prohibitive if the use of the BAL as a treatment for ALF becomes widespread. This cost is amplified if a patient requires multiple treatments. Use of a suitable replacement for human blood plasma in the process may therefore be required.

The efficacy of the BAL must also be established before clinical trials can proceed. There is no significant data to suggest that use of the liver group BAL reduces mortality rate after two animal trials, although this may be a consequence of above mentioned limitations in the system. No control group that was not connected to a BAL or cell-free BAL was attempted so baseline

survival is unknown [363]. Improving survival time is the fundamental aim of the BAL device, although many other devices have also struggled with this parameter [168, 224, 304].

The UCL BAL, as is the case with almost all liver assist devices, only contains one cell type (hepatocytes), and so functions or symbiotic relationships between the array of cell types and structures in a liver are not fulfilled. In addition, the fluidised bed nature of the BAL results in the whole biomass experiencing homogeneous conditions. In reality, a human liver experiences heterogeneous metabolic zoning and has areas of higher and lower oxygen availability [139, 203]. This metabolic zoning affects a range of liver functions and is likely critical for optimal cell operation, and oxygen or nutrient gradients in the human liver act as a regulator of this zonation [8, 73, 139, 199, 443]. This zonation is fundamental for proper function of the human liver and its absence in the UCL BAL may hinder its performance.

The focus of this PhD is on the cryopreservation and optimization of culture conditions of the BAL device, not its clinical use.

### **2.2.2. Alternative Developmental Treatments and Liver Support Devices**

The human liver is one of the very few organs for which no, even temporary, medical device can replace. As the liver is vital for numerous physiological applications, many groups are attempting to fill this gap in the medical toolbox, not just for treatment of ALF, but liver failure more generally.

These liver support devices (LADs) can very broadly be categorized into three groups: bioartificial livers where liver function is replaced using cells or tissue; artificial livers where detoxification and liver replacement occurs through mechanical means; and LADs that combine both a biological material with fully artificial components [9, 50, 334]. For clarity, throughout this section and thesis the abbreviation 'BAL' will refer solely to the bioartificial liver studied in this project at UCL and not other similar devices.

One of the most widespread, and controversial, LADs is the MARS (Molecular Albumin Recombinant System). This is an artificial system that uses charcoal and hollow fibre membranes to re-cycle albumin in a patient suffering from liver failure [380]. The albumin molecule is produced in a healthy human liver and enters the bloodstream. In the bloodstream it binds with toxins which are then removed from the body. This makes it one of the most important proteins produced in the liver with a major role in blood detoxification. MARS works extra-corporally by capturing toxins from albumin, thereby allowing it to be re-cycled in a patient whose liver is no longer producing a sufficient quantity of fresh albumin [22, 44, 50, 380].

MARS has been the focus of several clinical studies, however the results are controversial. Patients attached to the device exhibit increased clinical indicators such as a reduction in creatinine and bilirubin levels. While no significant improvement in survival has been seen in the general case [22, 168, 224, 304, 380], it does appear to be of benefit in a small cohort of patients with specific liver problems, ALF being a condition where MARS shows promising results [304].

A similar system to MARS is Prometheus [224]. This also uses membranes to remove toxins from albumin, and some additional haemodialysis is carried out resulting in both water soluble and albumin soluble toxins to be removed. The Prometheus system does improve some clinical measurements such as bilirubin level reduction, however no improvement in patient survival has been observed [168, 224, 304].

Many other artificial devices are in various stages of development. A notable one is also being researched at UCL, the UCL Liver Dialysis Device (LDD) [238]. This device was developed on the hypothesis that the poor performance in the MARS and Prometheus system was due to a failure to reduce immune system response and due to the re-circulating albumin's function not being restored. This device combined albumin and water soluble toxin removal with infusion of human serum albumin and reduced immune response. A recent animal trial has shown potential to reduce mortality rates in ALF [238].

When it comes to bioartificial liver devices, several designs are common – hollow fibre bioreactors where cells interact with blood/plasma through thin meshes or strands [50, 316], or fluidised bed bioreactors, where plasma is passed through a biomass (as is the case with the UCL BAL), amongst others [101, 137]. The choice of cell type is also important – human or animal; primary or cell line?

One of the early bioartificial liver devices is the HepatAssist system (also known as HepaMate). This is a hollow fibre bioreactor. It operates by separating out human blood plasma, which then passes through activated charcoal and an oxygenator before passing through the a bioreactor filled with previously cryopreserved porcine hepatocytes [50, 296]. This device has undergone several large clinical trials, but overall while several clinical parameters are improved, no significant improvement in survival has been reproducible [50, 81]. While this device uses porcine cells, no transmission of PERVs was observed on follow-ups up to 5 years post-treatment [333].

The ELAD (extracorporeal liver assist device), follows a roughly similar design to the HepatAssist device [335]. Human plasma is exposed to a hollow cartridge bioreactor after passing through an oxygenator and activated charcoal. The cell type used here is C3As [50, 335]. These are a clone of the HepG2 cells used in the UCL BAL and so the results from ELAD studies will have

added relevance to this project. There have been several larger clinical studies carried out with this device, but improvement on survival is yet to be shown [95, 335].

Other approaches to the problem are also being attempted. Work being carried out at King's College Hospital involves encapsulating primary hepatocytes into alginate beads which can then (after cryopreservation) be transplanted into a patient. The alginate prevents an immune reaction and localizes the cells. With liver failure, these cells can be transplanted and remain in place for several months assisting the liver. This is being developed in paediatric clinics and the results will have many interesting lessons for the cryopreservation and use of the UCL BAL [83].

Many other variations on liver support devices exists, from growing cells on PTFE fabrics to increase surface area [217], implanting this fabric into the body [378], to using multiple cell types to more accurately mimic liver functions. The reader is pointed towards several good reviews in this area [50, 213, 218, 304, 334, 335].

### **2.2.3. Timescales with the Bio-Artificial Liver and Acute Liver Failure**

Without treatment, death from ALF can occur rapidly following diagnosis. It takes around two weeks of static culture and a further twelve days of bioreactor culture to grow sufficient biomass for the BAL [101]. Currently there is no method to store the biomass for any longer than 2-3 days before cell death becomes too great [361].

Clearly, this limits the effective clinical applications of a BAL and to make the procedure more viable a method of long term storage of the biomass must be found. In fact, for all tissue-tissue engineered constructs Just-In-Time manufacture is not feasible, neither on costs nor logistics, so preservation methods developed here may have wide application outwith the BAL project [110, 111]. An extended preservation time-frame would allow many BALs to be made and then retained in hospitals until needed.

Cryopreserving the biomass could achieve this. This procedure involves cooling the hepatocytes (in the bioreactor culture chamber) down to liquid nitrogen (LN<sub>2</sub>) temperatures (-196°C), to stop all metabolic activity. Once thawed, the cells would return to their normal state and the BAL could be used within a short timeframe.

However, this freezing and thawing process can have many detrimental effects on the viability of the cells, which need to be addressed.

## **2.3. Cryopreservation**

### **2.3.1. Cryopreservation Injuries and Solutions**

#### **The Inverted U Graph**

Mammalian cells can be easily damaged by the freezing process – they normally live at a constant 37°C in the body and have a significant water component. Injury can be split into two main groups – fast and slow freezing injuries [4, 132, 226, 269, 271].

A graph of cell survival post-thaw, shows high cell mortality rates at relatively high cooling rates and again at relatively slow cooling rates. There is usually an area of maximum survival between these two extremes [132, 460]. This results in a graph shape similar to an inverted U. The values of this optimal rate for survival vary widely between cell types; for cell sparse spheroids of HepG2 liver cells, the optimal rate is 2°C/min, for cell dense the rate is somewhere lower; for red blood cells the optimal rate is 200°C/min [269]; there is also a dependence on cryoprotectant additive concentration [269]. Finding an optimal rate is necessary to improve the survival rate of the frozen tissue.

Similar graphs can be drawn for warming rates and cryoprotectant concentration highlighting the need for an optimal and controlled cryopreservation protocol [272, 301].

#### **Slow Cooling Injury**

Cells adjust to remain in osmotic equilibrium with their surroundings. As (solute-excluding) ice forms in extra-cellular areas, the solutes become more concentrated, because more water gets locked away as ice [221, 352]. Internal cell water is lost in order to remain in equilibrium with the extra-cellular space [132, 271, 290, 407]. With a large volume of extra-cellular ice, the increase in solute concentration may become so great as to be toxic to the cells, thereby reducing survival rate [132, 254, 271, 273].

As ice forms in a solution, cells migrate to unfrozen areas. The more ice that forms the smaller this unfrozen area becomes. This results in a high cell density in these liquid areas, and can result in cells being crushed together, damaging the cell membrane and rendering them no longer viable [270, 323].

When cells dehydrate, they shrink. On rehydration, the cell and its membrane expand. This process in itself could cause stress and distortions to the cell, especially if a cell membrane is

brittle at low temperatures, adversely affecting the shape and operation of cells. This potentially leads to cell injury or death [268].

### **Fast Cooling Injury**

If a cell is cooled relatively quickly, it does not have enough time to fully dehydrate. A large volume of intra-cellular water increases the probability of intra-cellular ice formation (IIF). Ice formation within a cell is usually fatal [132, 324, 410]. The precise mechanism by which IIF causes cell death is not definitively known, and the occurrence of IIF in a cell or tissue varies depending on cell type, however, it seems probable that ice crystals inside the cell can damage the cell membrane and internal structures, and so on thawing, the cell lyses [324]. Cells are also sensitive to cooling rates even above 0°C, and rapid cooling can result in cold-shock cell death [89, 288].

### **Thawing**

The warming rate is as important as the cooling rate when it comes to cell survival. In general, cells frozen rapidly are best warmed rapidly, while those cooled slowly have less dependence on warming rate [132, 272] though there is considerable variability and many exceptions. When cooling rapidly, the equilibrium phase diagram is not cooled – osmotic shock can cause death on warming [290], death can also be caused by recrystallization intra-or extra cellularly [51]

For slow cooled cells, the picture is less clear. Most literature with hepatocytes use fast warming [186, 385, 402]. Thawing rates have been largely neglected and poorly examined in the literature with relation to classical, ice present, cryopreservation. With cryopreservation of large volume constructs where rapid rates are difficult to achieve practically this is likely to change.

### **Post-Thaw Death**

The death of cells that becomes apparent between several hours to several days after the freeze-thaw process is complete comes in two principal forms. Necrosis – the death of cells due to external events (usually irreparable damage to the cell), or apoptosis – the programmed self-destruction of the cell [26, 28, 262, 430, 453]. Cell death is not only undesired as it reduces the effectiveness of a BAL; it also releases cell contents into the extracellular environment, which should be removed to prevent transfer risk to the patient [262].

While necrosis is usually a direct consequence of accumulated freezing/thawing injury, apoptosis is usually a result of chemical signals sent to the cells, caspase being a mechanism of apoptosis that can be used to show the process is occurring. Using an additive to reduce these

signalling pathways has been shown to reduce apoptosis [26, 27, 262, 430, 453]. Post-cryopreservation, cells usually continue to lose viability for several hours post-thaw, a phenomenon known as Delayed Onset Cell Death (DOCD) [26, 27], with ELS the nadir of cell membrane viability occurs around 12-24 h after thaw, which coincides with the low of viable cell number.

### **Vitrification**

It is possible to avoid ice induced freezing injury altogether if the cell mass is vitrified as opposed to frozen [109, 110, 340, 450, 451]. Vitrification is the process by which a liquid is cooled down very rapidly, but ice is not nucleated and so the liquid takes on a glassy state. Here the molecular structure of the solution has the same structure and bonding as the liquid state (it has not crystallised), but the motion of the molecules has largely ceased. It can be more accurately described as a super-viscous liquid [109, 112, 340, 400].

Achieving vitrification presents several challenges. The cells and extra-cellular solution must all be cooled quickly, which is difficult to implement for larger cellular masses. The system can also crystallise on thawing, with the same effects as if crystallising on freezing. For this, the solution must be heated rapidly [110, 112, 429, 451]. Further, a large volume of toxic cryoprotective additives (CPAs) must be used to lower the freezing point and inhibit ice formation sufficiently to reduce the risk of spontaneous nucleation [112, 244].

This method has received much attention since it was first proposed in the 1980s, been successfully used on human oocytes and embryos, as well as liver spheroids, and as such is worth further consideration [175, 450].

### **Isochoric and Hyperbaric Cryopreservation**

Other promising avenues for ice-free cryopreservation include hyperbaric or isochoric preservation [352]. These methods engage high pressures to suppress ice formation on cooling. As pressures affect everywhere in a sample instantly and reduce the level of CPA required at any given temperature, so essentially acts as a highly efficient cryoprotectant.

Hyperbaric cryopreservation induces high pressures directly. Isochoric preservation takes place in a constant volume, as standard hexagonal ice is less dense than water, when it forms in a constant (air free) volume, the pressure will increase and ice formation suppressed. Isochoric preservation equilibrates to the lowest required pressure at any given pressure, minimizing pressure damage [338, 352, 393]

Livers have been observed to survive pressures of over 30 MPa, making this a promising avenue for ELS preservation [395]. It was not, however, within the remit of this project.

### **Encapsulation of Liver Cells**

HepG2 cells are encapsulated in alginate spheres in order to boost their function and proliferation [63]. Alginate is a hydrogel, composed primarily of water (99%). The alginate gives a structure for the HepG2 cells to attach to, while also allowing the transport of nutrients, oxygen, and water products between the cells and their environment. Cells contained within encapsulated liver cell spheroids (ELS) have been seen to proliferate faster than those in monolayer cultures. They also show signs of inter-cellular gap junctions and desmosomes between the cells, as well as greater per cell performance than the same cells in monolayer [63, 206]. This suggests that the spheroids replicate conditions inside a human liver, which helps with their functionality and growth.

Initially individual cells are encapsulated in alginate, which then grow into colonies of several hundred cells. Each sphere of alginate will contain many colonies and measure about 0.5mm in diameter [101].

Many different cell types have been encapsulate in alginate for the purpose of cryopreservation. Several cell types such as embryonic kidney cells and neurons, are encapsulated in alginate prior to cryopreservation as the alginate seems to offer some form of cryo-protection – and many types of hepatocytes have been cryopreserved this way [38, 257, 311, 364, 383].

There is also an abundance of literature which considers the effect of alginate encapsulation on the cryopreservation and freeze-drying of plant seeds and embryonic roots and shoots [177, 354, 438]. Part of the mechanism for protection may be due to the ability of alginate to vitrify more readily than a CPA solution reducing ice crystal damage [177, 354].

This protection may be linked to the inhibition of extracellular ice around the alginate beads. Indeed in a previous study in the LG the alginate did seem to act as a barrier to ice growth, which may protect the cells from IIF or from mechanical ice damage. However when ice was present in the inter-spheroid space, previous work in the liver group suggests that the alginate only offers limited protection.

The impact of encapsulation is difficult to test explicitly however in the BAL system. Alginate not only surrounds the cells and cell clusters – it also spaces them apart and immobilizes them. The effects of alginate itself on cryopreservation cannot be readily separated from the effect of cell separation. In a HepG2 cell suspension cells will naturally sink to the base of the vial and may

clump together. On ice formation cells not encapsulated can be 'pushed' by the ice front and therefore stay in a solute dense region ahead of the ice front for longer. It is an involved process to try and separate the impact of alginate directly from the impact of cell separation and immobilization. One potential solution would be to encapsulate cells in some other medium such as agar. However since growth characteristics of HepG2 cells in agar will be different than the growth characteristics in alginate, additional variables will still be present.

As the alginate encapsulation characteristics have already been optimized for cell culture, and due to practice difficulties, the effect of alginate on cell cryopreservation is not explicitly studied in this thesis.

### **2.3.2. Cryoprotective Additives**

#### **The Use of Cryoprotective Additives**

Cryoprotective additives (CPAs) can be broken down into two groups – penetrating and non-penetrating [131, 273, 394]. Their purpose is to protect cells against freezing injury, thereby increasing the cells' survival rates. CPAs can achieve this by lowering the freezing point of a liquid, thereby reducing the solvent concentration at a given temperature, and - by dehydrating cells - reducing the probability of IIF. The choice of CPA is very important; many substances that appear to show the desired characteristics for a CPA can turn out to be unacceptably toxic to the cells [131, 234].

#### **Penetrating CPAs**

Penetrating CPAs are usually small molecules, such as glucose or dimethylsulfoxide (DMSO) [394], that can enter the intra-cellular space. These CPAs are most commonly used to protect against slow-freezing injury. They help do so by reducing the concentration of solutes at low temperatures and so reducing the effects of solute toxicity. This is achieved by two means: firstly by reducing the freezing point of water, less ice is present at a given temperature when compared to water without CPAs, therefore lowering the temperature at which solutes become toxic to the cell. Secondly the CPA also gives the solutes another substance to dissolve into, reducing the amount acting upon the cells [131, 273].

#### **Non-Penetrating CPAs**

Non-penetrating CPAs are those that cannot enter the intra-cellular space. They are usually large molecules with large osmotic coefficients. As a consequence of their osmotic properties, cells

are dehydrated when such a CPA exists in the extra-cellular space. If these dehydrated cells are subsequently fast-frozen, less intra-cellular liquid remains, and so the likelihood of damaging IIF is reduced [131, 132].

In general, CPAs have many other areas of action, such as membrane stability or cold protection, the full mechanism of protection is not definitively understood. Due to their significance, chapter 4 explores CPA in detail.

### **2.3.3. Nucleation**

#### **Thermal Issues with Crystallisation**

As water freezes to form ice, heat is released. This is a result of the lower free energy of crystallised water molecules than those in an unfrozen state. 1ml of water freezing releases 334J of heat energy (the latent heat of melting) [458].

As water cools below 0°C, ice will only form if it is nucleated (in the absence of CPAs, which can change this temperature) [85, 190, 263, 289]. Heterogeneous nucleation is the process by which another material can act as a seed for ice formation, and the amount of undercooling (cooling below the equilibrium melting point) is a function of the surface area and effectiveness of the nucleant [170, 263]. If no nucleator is present, the water will continue to cool below its normal freezing point until an ice crystal forms spontaneously (homogeneous nucleation) [85, 289]. This ice crystal will then spread throughout the inter-cellular volume, releasing heat as it advances [85, 210, 265]. The result is a significant increase the temperature of the cells, and so a disruption of the cell cooling pattern [210]. This disruption can in turn reduce the viability of the cells as an optimal cooling curve is not followed – ELS are particularly sensitive to nucleation temperature [265, 289]. A lack of a nucleating event during cooling will result in vitrification below the glass transition temperature.

#### **Nucleating Agents**

Almost all ice is nucleated by a surface in biological settings, as almost any structure can act as a nucleant.

As a result of the potential damage of nucleation, it is often preferable to deliberately seed nucleation of ice at a specific higher temperature than would happen spontaneously, or use very effective ice nucleants [85, 190]. For ELS systems, reducing the amount of supercooling using effective nucleators is key as post-thaw survival has a strong negative correlation with amount of supercooling [263, 265]. This allows the cooling curve to be more easily controlled, as the

temperature and point of nucleation will be more easily predictable. The cooling device could then be adjusted accordingly.

Previous work in the laboratory had shown that cholesterol was an effective ice nucleator, and improved post-thaw viability of ELS [263]. Cholesterol was found to nucleate ice at  $\sim -9^{\circ}\text{C}$ , although this value is specific to the concentration of DMSO used [263]. Cholesterol will need to be removed fully after thawing, in order to prevent it entering a patient's bloodstream. It would be useful to have another non-organic ice nucleator instead, and so Asymptote Icestart is often used in this thesis [210], which has been shown to be as effective as cholesterol.

#### **2.3.4. Cryoconcentration**

As ice forms through a water-ice system, solutes tend to be re-distributed. This is a consequence of solutes preferring the liquid state of water over the solid phase. This effect has been studied in detail in metallurgy, food engineering, and waste water treatment, but has been relatively neglected in the field of cryopreservation [221, 405, 423].

Cryoconcentration tends to be amplified for slower ice growth rates and in larger volumes [41, 221, 302]. As the BAL has a size of 2 litres, significant cryoconcentration may occur [211]. Optimal cryopreservation protocols are sensitive to CPA and the concentration of other solutes. Cryoconcentration can upset this balance significantly, and so it has been studied in detail in this thesis.

### ***2.4. Modelling and Culture of the Bioartificial Liver Device***

#### **2.4.1. Fluidisation**

The biomass for the BAL is cultured in a fluidised bed bioreactor system [101]. This is a system where innumerable small solid objects (in our case the encapsulated liver spheroids, ELS), sit atop each other in a packed bed format [240]. Culture medium is then passed up through this packed bed, and it becomes fluidised – that is the bed height expands as the upward flow of the medium counteracts the weight of the ELS (or other particles) [240, 247, 455].

Using this method, with a specific value of bed expansion maintained and the 3-D culture ELS provide, it has been previously found that liver cells proliferate more readily and their function is up-regulated relative to a system consisting only of a static bed of a 2-D cell culture [63, 240].

Levels and efficiency of fluidisation is highly dependent of the structure and physical properties of the fluidised particles. By building a model, and comparing fluidisation of ELS in the BAL system before and after cryopreservation, differences in ELS morphology and features can be determined. This has been studied in detail in chapter 12.

### **2.4.2. Oxygenation**

During the culture phase of the biomass, especially as the cell density exceeds around 10 million cells/ml, the culture medium does not contain sufficient oxygen for the hepatocytes to metabolise. Left uncorrected, this could result in significant harm to the biomass.

To overcome this challenge, coils of silicone tubing are added to the BAL chamber, which are pumped through with oxygen [101]. Oxygen diffuses out of the tubing and supplements the oxygen in the medium, allowing standardized cell growth conditions. The aim is to keep oxygen concentration at the levels found in air, 21%.

Being able to determine the rate of oxygen diffusion from the tubing to the medium, and the oxygen content of the medium before and after the biomass would allow the oxygen consumption of the BAL to be determined, and would provide another non-invasive method to assess cell function and health.

Measuring this consumption before and after cryopreservation will provide another invaluable tool to determine the feasibility of the BAL device. This has been studied in detail in chapter 13.

### **2.4.3. Scale-up**

A BAL would have to contain a large number of cells, around  $7 \times 10^{10}$  hepatocytes [101]. A large volume would be needed to accommodate this. Scaling up from a few hundred cells to tens of millions presents issues that must be overcome.

Controlling rates of cooling and heating within a larger space is more difficult – heat energy takes time to travel a finite distance. This leads to difficulties in maintaining a consistent heat profile throughout the BAL, and on creating rapid temperature changes, such as those required for

rapid thawing [210, 211]. Freezing and thawing methods have been explored in detail in this thesis.

Ice nucleation temperature is also more difficult to manage. Ice nucleates spontaneously, with the cooler the liquid the more probable that it will happen over a shorter time. With a larger volume, and so more water molecules, the chance of a spontaneous event increases, as does the time between ice forming in one section of the BAL to ice being present throughout the BAL [210, 211, 289].

Dehydration of cells takes longer with a larger volume. As individual cells in a bead may be surrounded completely by other cells, water has further to travel and therefore takes longer to permeate into the inter-bead space. The resultant reduced rate of water loss in ELS slows the dehydration process, and so the cooling rate must be lowered accordingly, to what may be a sub-optimal level.

#### **2.4.4. Previous Work and Other Aspects to Consider**

##### **Filtration**

Ideally for a BAL, cells derived from the patient in question's own liver would be preferable. There would be little risk of foreign DNA or material entering the patient's system. Unfortunately, this is usually not possible. By the time a patient presents with ALF, it is too late to utilize cells from them. This means that the most practical solution is using a cell line derived from a separate source. In the case of the LG, the carcinoma cell line HepG2 is used, which was originally derived in 1979 [216]. This leads to the possibility of foreign DNA entering a patient, which must be avoided under EU and US regulations if the device is to be used in a clinical setting.

An effective and reliable filtration device is required as a consequence [308]. Many methods have previously been tried, ranging from charcoal through to narrow membranes (which also help with detoxification) [50]. However, no sufficiently effective method has yet been achieved. Future work will have to resolve this in order for a BAL to have clinical applications.

##### **Cell line Contamination**

HepG2 cell lines are susceptible to external contamination. This can often occur through accidental crossing with other cell lines in the same lab [48, 185].

To prevent this, very strict procedures and checks must be in place while handling cell lines. They must be completely isolated and sterile, only worked from in a sterile hood with everything that enters that hood, in the case of the LG, treated with ethanol in aqueous solution, a cleansing agent.

Before a cell line is used in a clinical setting, it must be checked for all possible contaminants. This is especially important for the cell lines used in the LG, as they have been in culture for almost 40 years, and may have been in contact with contaminants before entering the LG, as well as changing genetically over time [48, 185, 216]. This is a long and costly undertaking, and failing contamination checks is clearly best avoided.

The HepG2 cells used in our study have undergone tests by DNA profiling, as well as GMP tests for non-human contents of a broad range of viruses including mycoplasma and are not contaminated in any way.

## ***2.5. Detailed Aims, Motivations, and Strategy of the Thesis***

To be a clinically relevant device, the BAL must be available on demand. Starting to culture one from scratch when a patient presents with ALF is not possible due to the rapid clinical deterioration in this condition.

One solution would be to cryopreserve a clinically ready system that could be thawed and used on demand. This is a primary aim of this thesis. Cryopreservation will damage the biomass and so recovery time will be required – the aim is to have full functional recovery within 72 h as this would be clinically relevant, although the shorter the timeframe the better.

The bulk of this thesis will examine this task. Most previous work in cryobiology involved smaller systems (a few ml at most), and so this will be used as a basis [210]. Early work here examined the impact of cryopreservation of ELS in small volumes, and tried to determine optimal cooling rates, supernatant volume, CPA concentration, and the impact of cell density.

As the BAL will have a final volume of 2 litres, the physical differences between cryopreserving small and large volumes was studied – both from a physical and biological perspective. It was found that there were indeed important differences and so the remainder of the work would be carried out in larger volume conditions.

It was not economical to carry out a large number of repeats on a 2-litre system. To overcome this a scale-down process was developed which allowed the physical and biological characteristics of 2 litre cryopreservation to be carried out in 6ml vials. This allowed for a suitable

range on conditions and repeats of to be carried out in a system relevant to large volume cryopreservation. Work here was then expanded to cover large volume cryopreservation in detail and devise strategies to improve outcome. For clinical delivery of the BAL practical considerations such as transportation were examined.

Also relevant to the scale up process is was the size and make-up of the BAL chamber. The chamber used for the culture phase of the BAL is glass, however this was susceptible to cracking due to the thermal stresses during cooling and warming. For this purpose a new chamber material had to be used. Several parameters had to be optimized to give the system sufficient strength but sufficient heat transfer – the thermal conductivity of different materials, the wall thickness, and diameter of many potential systems had to be tested. It was impractical to manufacture and test a large range of potential devices, and so some mathematical modelling was carried out to optimize chamber design in an economical manner. This model has the additional advantage of allowing an in depth understanding of thermal profiles in the system during cooling – something difficult to achieve using thermocouples alone.

Also significant during the cryopreservation of large volumes is the impact of cryoconcentration – solute concentration increase during cooling. Very little previous work has examined this in biological systems, even though solute increase during cryopreservation is often cited as the primary cause of cell death at low cooling rates. This was studied to determine if it could be reduced in the BAL system and so improve outcome. As it is difficult to sample the BAL during cooling to determine solute concentration (a sampling device would disturb the liquid and so mix more and less concentrated areas), a mathematical models based on literature in other fields such as metallurgy and food preservation were examined. On testing of these models it was found that gravity was a dominant factor during cryoconcentration that had not previously been identified. Due to the way the BAL was cooled base-up cryoconcentration was found not to be a major issue due to gravity. A new relationship was proposed that explicitly included the effect of gravity on cryoconcentration which may have application in fields such as desalination, water purification, metallurgy, and food transportation amongst others.

The work up to this point was then combined in order to cryopreserve a 2.3 litre volume of ELS in a single cassette. This was successful with full functional recovery within 72 h.

During the PhD an interesting observation had been made – namely that cell growth after cryopreservation increased. This has been studied in more detail later in the thesis and a promising new technique using cold to increase cell growth was discovered. Interesting oxygenation patterns were also observed throughout the PhD. This is explored and a novel

method to determine the health of the BAL was proposed which may be used to improve monitoring of the BAL system post-thaw.

### 2.5.1. Hypotheses

1. The 2-litre bioartificial liver device can be successfully cryopreserved, and fully recovered within 72 h of thaw.
2. Parameters of the biomass culture system can be optimised to increase culture effectiveness.

### 2.5.2. Chapter by Chapter Aims

To investigate these hypotheses, there are several distinct aims of this thesis. I shall:

- Examine the ideal cooling and warming rates for the encapsulated liver cell spheroids (ELS) and study and determine optimal CPAs to use in our system, for cell dense ELS – this will allow the practicalities of the large volume freezing to be examined, as a large volume cannot be rapidly cooled or warmed (chapter 4).
- Explore effective transportation methods for ELS after cryopreservation. This is an important practical consideration for effective delivery of the BAL (chapter 5).
- Carry out simple mathematical modelling of the thermodynamic conditions – in a large volume, there will be large thermal gradients. Quantifying them will allow useful study into their effects on ELS. In order to calibrate and validate the mathematical modelling, empirical cryopreservation will be carried out (chapter 6).
- Determine a method by which to mimic large volume freezing – The BAL will have ~2 litres biomass volume. It is impractical to do many large freezing runs on this scale. Using special inserts to create directional heat transfer on the EF600 CRF should mimic the thermodynamics of a large volume, allowing many more experiments to be carried out (chapter 7).
- Model and experimentally calibrate the levels of cryoconcentration in the BAL system and determine methods to minimise any detriment deriving from this cryoconcentration (chapter 8).

- Determine if the spatial location within the BAL impacts on post-thaw outcome. The cryopreservation conditions may not be equal, so determining areas of damage will instruct optimization procedures (chapter 9).
- Combine the knowledge gained in the above chapters to predict and experimentally cryopreserve a whole-volume bioartificial liver device. This would be the largest volume biomass ever cryopreserved, and successfully complete the aim set out at the inception of this PhD (chapter 10).
- Cryoanaptiksi, the cell-chilling phenomenon discovered during this project is examined in chapter 11.
- Examine the fluidisation of the BAL device during culture to expand knowledge of the culture regime (chapter 12).
- Model the oxygenation of the ELS during and after cryopreservation. This should give another parameter to test cell function and post-thaw outcome (chapter 13).

### 2.5.3. List of Novel Contributions

The novel contributions in this thesis include:

- Development of a scale down process allowing physical conditions of large volume freezing to be carried out quicker and more economically.
- A study of the impact these changes in physical conditions has on post-thaw outcome, finding that small volume and large volume cryopreservation are quite different
- The impact of different temperatures relevant to BAL delivery, finding that the BAL requires transportation at either liquid nitrogen temperatures or thawed – dry ice temperatures is not acceptable.
- That gravity is a significant contributor to cryoconcentration.
- A method to successfully cryopreserve a 2.3 litre biomass in a single cassette and recover function within 72 h.
- A method to induce rapid cell proliferation using chilling.
- A method to use oxygenation readings to monitor the health of the bioartificial liver.

### 2.5.4. Published Work from the Thesis

Kilbride et al. A scale down process for the development of large volume cryopreservation. *Cryobiology* 2014 Dec;69(3):367-75. doi: 10.1016/j.cryobiol.2014.09.003 - [210]. This is added to this document as appendix A.

In addition, a paper based on chapter 5 titled “Impact of Storage at -80°C on Encapsulated Liver Spheroids after Liquid Nitrogen Storage” has been accepted for publication in the journal *BioResearch OpenAccess*.

Three other papers, based on chapters 9, 10, and 11 are going through the publication process although, at time of writing, not yet through peer-review.

An additional paper was produced during my time as a PhD student. It is not included in the thesis as it was not directly applicable to the BAL project: Kilbride et al. Modeling the effects of cyclodextrin on intracellular membrane vesicles from Cos-7 cells prepared by sonication and carbonate treatment. *PeerJ*. 2015 Oct 27;3:e1351. doi: 10.7717/peerj.1351 -[212]. This has been added to this document as appendix B.

## 3. Methods

### 3.1. Cell Culture Methods

#### 3.1.1. Growing Cells in Monolayer

##### Materials

- HepG2 cells (human liver cell line) between passages 40 and 60.
- Triple Layer Flasks - filter capped (total growth area 500cm<sup>2</sup>, Nunc, Rochester, NY, USA #132913)
- Culture Medium (see section 3.1.2)
- 50ml Stripette (Corning Costar, Amsterdam, Netherlands; Sigma #4501)
- Pipette Boy – pipette controller (Integra Bioscience, Zizers, Switzerland)
- P200 Gilson Pipette
- 200µl Tips
- Incubator at 37°C and 5% CO<sub>2</sub>, with 95% humidity

##### Method

4 million cells in suspension were added to the Triple Layer flask, and culture medium added to a total volume of 90ml. The flasks were placed in the humidified incubator at 5% CO<sub>2</sub> in air, at a temperature of 37°C. The cells attached to the flask within 2 days. A complete medium change took place every 2-3 days. The cells replicated in the flask, reaching about 90% confluence in 7 days, at which point they were split (see Section 3.1.3).

##### Justification, Benefits, and Limitations of Approach

HepG2 cells are an adhesive cell line and as such are grown on treated culture plates as a standard procedure [266]. In this project, triple layer flasks were used as these gave a higher final cell number than T175 or other flask types due to their large surface area (500cm<sup>3</sup> vs 175cm<sup>3</sup>). Cell numbers required for encapsulation were typically around 2 million cells/ml and on confluence each triple layer flask gives around 100 million cells, approximately 3x that acquired from a T175 flask.

From internal group unpublished observations, the seeding density of 4 million cells per ml is optimal for HepG2 cells – any fewer and cell clusters start to form. Cells in these clusters could grow on top of each other which would reduce viability on passage. Seeding at a higher cell density would result in an earlier passage, which can help in emergencies, but as the final passage concentration is always the same this is inefficient. Cells must be passaged before 100% confluence is reached as cells would start to grow on top of each other reducing viability.

### 3.1.2. Preparing Culture Medium

#### Materials

- $\alpha$ MEM Alpha Medium (Gibco, Paisley, Scotland, UK, #32571-028)
- Fungizone (Amphotericin B 250  $\mu$ l/ml, Gibco, Paisley, Scotland, UK #15290-026)
- Penicillin/Streptomycin (5000 Units/ml Pen. 5000  $\mu$ g/ml Streptomycin, Gibco, Paisley, Scotland, UK #15290-026)
- Insulin (100 iu/ml) (Actrapid, Novo Nordisk, Gatwick, England, UK #041-7642)
- Fetal Calf Serum (PAA, Cambridge, England, UK #A15-101) or human plasma (National Blood Transfusion Service, UK)
- Sodium Selenite (0.1 mg/ml) (Sigma, Dorset, England, UK #S5261)
- Hydrocortisone (1 mg/ml) (Sigma, Dorset, England, UK #H0888)
- BSA/Linoleic Acid (100mg/ml, Sigma, Dorset, England, UK #L9530)
- TRH (2 mg/ml) (Sigma, Dorset, England, UK #P1319)
- 45% Aqueous Glucose (Sigma, Dorset, England, UK #G8769)
- 50ml Centrifuge Tubes
- 0.2  $\mu$ m Hydrophilic Filter (Sartorius, Epsom, England, UK #16534)

#### Method

2.5ml of Fungizone, 5ml of Penicillin/streptomycin, 1.5ml insulin, 95  $\mu$ L of 0.1mg/ml Sodium Selenite aqueous solution, 204  $\mu$ L of 1mg/ml aqueous solution hydrocortisone, 275  $\mu$ L of 100mg/ml BSA/Linoleic Acid, and 102  $\mu$ L of 2mg/ml aqueous TRH were added to a centrifuge tube and filter sterilised into the  $\alpha$ MEM medium bottle.

56ml of heat-inactivated fetal calf serum was added to the bottle.

If the medium was for growth of ELS, 4.4ml of glucose was added (high-glucose medium), for monolayer cells in flasks no extra glucose was added. The medium was kept at 4°C until required (up to a maximum of 2 weeks). In some cases, the calf serum was replaced with an equal volume of human blood plasma. This is referred to as FFP medium in this thesis.

#### Justification, Benefits, and Limitations of Approach

The culture medium used in this project is relatively complicated, which adds to the cost and time of cell culture. However it has been optimized for use with HepG2 cells and ELS and so the extra effort is justified in terms of output (liver group unpublished results), and has been used previously [248, 266]. Fetal calf serum medium (also known as fetal bovine serum) medium is beneficial as it contains no human proteins, and so proteins produced by the HepG2 cells in ELS can be detected [210].

Human blood plasma medium results in higher cell growth and so is preferred (liver group unpublished results). As it contains large concentrations of human proteins, their production by HepG2 cells or spheroids cannot be detected in human plasma medium. To overcome this limitation levels of alpha-fetoprotein are measured instead – this is a protein produced by HepG2 cells but not present in healthy human plasma and is used as an indicator of protein production [101].

### 3.1.3. Passaging Cells

#### Materials

- HepG2s attached to a flask at 90% confluence
- Hank's BSS, CA<sup>+</sup> free (PAA, Cambridge, England, UK #H15-010)
- TrypLE Select (Gibco, Paisley, Scotland, UK #12563)
- 50ml Centrifuge Tubes
- 0.2µm hydrophilic filter (Sartorius, Epsom, England, #16534)
- Centrifuge
- Culture Medium (as section 3.1.2)
- Syringe (20ml)
- Needle (21 Gauge)

#### Method

For each flask - the culture medium was removed. 60ml of HBSS was used to wash the inside of the flask, removing protein, starting to loosen calcium bonds, and removing any un-attached cells. This was repeated twice.

30ml of warmed (37°C) TrypLE Select was then added to the flask. The flask was laid on its side to ensure all the cells were covered in TrypLE Select and placed in an incubator for 5 mins at 37°C and 5% CO<sub>2</sub>.

On removal from the incubator, the flask was tapped vigorously to remove the cells. 60ml culture medium was then added to inactivate the TrypLE Select.

The cell/ TrypLE Select /medium mix was removed from the flask into 50ml centrifuge tubes, and centrifuged for 4mins at 272rcf to pellet the cells. The supernatant was discarded and the cells re-suspended in 10ml of culture medium (per triple flask).

The cells were then syringed 5 times through a 21-gauge needle to de-aggregate them and a cell count was carried out using trypan blue as per section 3.3.1.

#### Justification, Benefits, and Limitations of Approach

The procedure above is typical of standard adherent cell passaging, and has been published previously by the Liver Group [248, 266]. The use of TrypLE Select as a disassociation reagent has been chosen over more common reagents such as trypsin (which had been used previously in the Liver Group [248, 266]) as it uses only one disassociation enzyme as opposed to several making it less harmful to cells. Disassociation reagents work in general by dissolving cellular attachment to culture flasks and so cells can be extracted, these can be harmful to cells as the enzymes can act on other cellular components, the choice of the more expensive TrypLE Select is justified through reduced cellular damage. It is also free from animal origin and GMP (good manufacturing practice) compliant – a necessity for medical devices. Other methods of cell disassociation, such as using a cell scraper, are impractical in triple layer flasks [94].

A feature of HepG2 cells is they are 'clumpy'. That is, they tend to form clusters easily in suspension. When seeding new culture flasks or cells into alginate, it is important to have the cells suspended individually in solution. This makes cell counting more accurate and ensures spheroids in the alginate are approximately the same size. For this reason, on passage cells are passed through a needle 5 times. This treatment cause a large shear force on the cells that can be damaging – it is important not to over stress the cells at this stage and this procedure could be improved in a gentler dis-aggregation method could be developed.

#### 3.1.4. Encapsulation of Cells in Alginate

##### Materials

- Jet Cutter Encapsulation System (GeniaLab, Braunschweig, Germany).
- 90% confluent HepG2 cells on flask.
- 2% Alginate Solution (Manugel GMB, FMC Biopolymer, Girvan, Scotland, UK)
- Glass beads (10µm-50µm diameter, Kisker Biotech, Steinfurt, Germany, # PGB-05)
- Polybuffer (0.204 molar aqueous calcium chloride solution, prepared from Sigma #12022, Dorset, England, UK)
- Pluronic Acid (Sigma, Dorset, England, UK #1300)
- Magnetic Stirrer

##### Methods

Cells were passaged as per section 3.1.3.

2% dissolved alginate in 0.15M NaCl aqueous solution, buffered with hepes, pH 7.4 was added 1:1 to a mix of cells in culture medium, to give a final cell density of  $1.75 \times 10^6$  cells/ml. Glass beads were added to give the beads the correct density for fluidization, at 0.75% w/v.

This cell-alginate-medium mix was added to the jet cutter system. The jet cutter compressed the mix into a steady stream of liquid that passed through a rotating disk, slicing the jet into

sections that formed spherical droplets with a diameter of 500-550  $\mu\text{m}$  before hitting the polybuffer solution that was being slowly stirred. After encapsulating the mix, the spheres were cross-linked for a further 10mins. These spheres were then washed with culture medium, and placed into an appropriate flask with culture medium, then placed into an incubator at 37°C and 5%  $\text{CO}_2$ .

Many encapsulations for ELS experiments in this thesis were carried out by James Bundy, Eloy Erro, assisted by Sunil Modi. The author collected ELS surplus to requirement if available for work on the PhD project.

### **Justification, Benefits, and Limitations of Approach**

There are several methods to encapsulate cells, ranging from simply pipetting droplets of alginate into  $\text{CaCl}_2$  solution (impractical at volume), to electrical systems such as the Inotech device [266], to the large scale JetCutter system used here [101, 210]. The JetCutter system was chosen as it is capable of processing the 2 litre volumes typically required.

This system does have some drawbacks however. The use of a rotating cutting disk results in a loss of around 11% of the alginate/cell mix during the droplet forming stage.

The inclusion of glass beads required for buoyancy regulation can block the nozzles in the system and halt the encapsulation process. To avoid this a filter is included earlier in the system and glass beads are filtered prior to use, however some blockages can still occur.

It takes around 1 h for 2 litres of ELS to be produced. This results in a large variation time of ELS remaining in the  $\text{CaCl}_2$  solution, which may introduce heterogeneity between ELS or be damaging to cells.

The system is manual and very labour intensive, requiring at least 4 people working on it full time to produce 2 litre of ELS – the result is often a large variation in initial cell density in the ELS. While this is acceptable in an experimental set-up, an automated system will be required for mass production.

The JetCutter system allows for a large volume of very accurately sized ELS with good shape and density – the key parameters for the BAL which outweigh its drawbacks.

### 3.1.5. Culturing Encapsulated Liver Spheroids in Static Culture

#### Materials

- T175 Flasks (Nunc, Sigma, Dorset, England, UK #CLS431328)
- Culture Medium (see section 3.1.2)
- 50ml Stripette (Corning Costar, Sigma, Dorset, England, UK #4501)
- Pipette Boy (Integra Bioscience, Zizers, Switzerland)
- Incubator at 37°C and 5% CO<sub>2</sub>, with 95% humidity

#### Methods

Immediately after encapsulation, 6ml ELS were placed into a T175 flask, with culture medium, warmed to 37°C, added at a ratio of 1:32. The flask was then placed into the humidified incubator. Medium was changed every 2-3 days, with the ELS used days 10-14 post-encapsulation [210].

#### Justification, Benefits, and Limitations of Approach

ELS in T175 flasks allows for small volumes to be cultured in a cost and labour effective manner. ELS typically proliferate less in static culture than in a microgravity environment [63], however they can be cultured for longer. They are also easier to monitor as the flasks can be non-invasively imaged directly under the microscope while still in the culture flask.

### 3.1.6. Culturing Encapsulated Liver Spheroids in an Rotary Cell Culture System Environment

#### Materials

- Rotary Cell Culture System (Synthecon, Houston, TX, USA)
- Culture Medium (Section 3.1.2)
- Incubator at 37°C and 5% CO<sub>2</sub>, with 95% humidity

#### Methods

A desired volume of ELS was placed into a 500ml Rotating Cell Culture System (RCCS) chamber. This was usually 15ml to maintain a 1:32 cell culture ratio but could be lowered at higher cell densities. This chamber was then filled with 37°C culture medium. The chamber was placed onto the rotating insert of the RCCS system in the incubator, and a rotation rate of 10 rotations/min set.

To remove samples, the chamber was detached from the rotator and removed from the incubator and placed in a sterile hood. It was replaced into the incubator and the rotating insert.

## **Justification, Benefits, and Limitations of Approach**

The RCCS system allows ELS to be cultured in a microgravity environment without the use of the 2 litre bioreactor [281]. It was particularly useful on thawing as ELS grown in microgravity die in static culture, so these were used to test different cryopreservation conditions – only one FBB chamber was available. Drawbacks include the fact that only 4 were available so experiments took longer to increase repeats. Another drawback is ELS could not be seen inside the RCCS chamber, they have to be removed to be studied under a microscope and could not easily be added back into the RCCS post-imaging.

## **3.2. Freezing and Warming Methods**

### **3.2.1. Concentration Terminology**

At all points in this thesis, % concentrations refer to a v/v percentage, unless otherwise stated.

### **3.2.2. Preparing Freezing Solution Materials**

#### **Materials**

- Viaspan (also known as University of Wisconsin Solution, Bristol-Myers Squibb, New York, NY, USA)
- DMSO (Sigma, Dorset, England, UK #34869)

#### **Method**

A freezing mix was prepared of 24% DMSO in Viaspan. This solution was kept on ice until needed. This was added to ELS at a 1:1 ratio. ELS sediment in this solution so excess supernatant was removed after equilibrating.

Where other cryoprotectants are used, it is specified in the text.

## **Justification, Benefits, and Limitations of Approach**

Viaspan is a solution containing various solutes such as starch and raffinose. It is used for hypothermic preservation of livers prior to transplant through osmotic balance being preserved with metabolically inert substances, with edema and free radical reducing compounds also added [321]. It is used here as a carrier solution for the DMSO to prevent osmotic shock primarily, and is preferred over culture medium due as it is tailored for low temperatures, so may infer protection to the HepG2 cells at low, unfrozen, temperatures. Viapsan is somewhat

expensive, at around £100 per litre. The small volumes used in cryovials of the scale down process help to mitigate this [210].

### **3.2.3. Freezing of Encapsulated Liver Spheroids (ELS)**

#### **Materials**

- Freezing Mix, kept at 0°C (as per section 3.2.2)
- Encapsulated Liver Spheroids (ELS)
- Cryovials (Fisher Scientific, Loughborough, England, UK)
- EF600 Controlled rate freezer (CRF, Asymptote, Cambridge, England, UK)
- Ice Nucleating Agent (INA)

#### **Method**

The required cooling run was entered into the controlled rate freezer before it cooled and stabilised at its starting temperature.

ELS were collected in a centrifuge tube and stored on ice. The freezing mix was kept on ice.

The required INA was added to the cryovials, and an appropriate volume of ELS added to the cryovials, typically 1ml. A 1:1 ratio of freezing mix was added to the spheres with 15 mins allowed for equilibration after which supernatant removed if necessary. The cryovials were moved on ice to the freezer, before the freezing run commenced.

At the end of the program, the cryovials were removed and placed at storage temperature, typically -80°C or -196°C.

Other freezers and vials were also used, where done this is specified in the text.

#### **Justification, Benefits, and Limitations of Approach**

The EF600 controlled rate freezer was used as it gives very accurate control of the cooling profile, is completely sterile, and can be run indefinitely as only electricity (no liquid coolant) is required for use [65, 265, 287]. This allows complicated and long cooling profiles to be carried out. A disadvantage was that this model. The EF600 was therefore used for cryovials and for the scale-down process [210].

An ice nucleant was used in order to reduce the amount of supercooling in the system, which is damaging to ELS [265]. Ice nucleants also homogenise ice nucleation temperature between samples, reducing inter-sample variability [266, 289]. Several ice nucleants were used in this thesis depending on the desired effect, although the most commonly used on was IceStart from

Asymptote, Cambridge, UK. This is a biologically inert powder making it ideal for use in a cell culture system.

### 3.2.4. Use of the Planer Kryo Freezer

#### Materials

- Planer Kryo 10 Freezer (Planer plc, Sunbury-on-Thames, England, UK)
- Liquid nitrogen tank and hose

#### Method

The 35 litre liquid nitrogen reservoir was removed from the hose (that in turn was attached to the freezer) and filled.

The liquid nitrogen reservoir was re-attached to the freezer and the pressure allowed to build up for a few minutes before the freezer was turned on. Once running, the program was then started and the program set to run.

The freezer first went to the desired start temperature and automatically held there. In this time the sample was usually prepared. The sample was placed in the freezer and the program run. The temperature was monitored from a thermometer inside the freezing chamber.

#### Justification, Benefits, and Limitations of Approach

The main advantage of the Planer system is that it had the capacity to cryopreserve the 2 litre bioartificial liver device. For this reason it was used in this project. The disadvantages are the use of liquid nitrogen as a coolant, which is bulky, costly, and non-sterile [34, 65, 152, 287]. The Planer machine could also not be topped-up during a run – this limited the length of cooling profiles and volumes used. Only one cooling run could be carried out per day at the rates typically used in this thesis (0.3°C/min) – it could not be left to run overnight unmonitored.

### 3.2.5. Use of the Adapted Asymptote EF600 Freezer for use in a Scale Down Process

#### Materials

- Adapted Asymptote EF600 Freezer (Asymptote Ltd, Cambridge, England, UK)
- Power Socket
- Laptop with EF600 software installed (Grant Instruments, Cambridge, England, UK)
- Aluminium or acetal modules, as required (Manufactured especially for project)

## Method

This freezer was cooled using electric Stirling engines, and so required no liquid coolant.

The freezer was attached to a laptop with the software installed, and the desired program entered into the freezer software.

The freezer was set to the start temperature, during which time the samples were prepared and samples were then placed into the freezer, and the cooling profile run freezer temperature was displayed on the laptop, and this was recorded.

For uniform cooling, the aluminium holder (with adapted freezer) was placed on top of the cooling plate, into which samples were placed. For cooling on only one side the acetal holder was used. Schematics and details on the use of these holders can be found in Chapter 7 and in [210].

## Justification, Benefits, and Limitations of Approach

This configuration was crucial to the project as it allowed the physical characteristics during large volume cryopreservation to be studied in a more economical manner. This method, and results from it, are the primary focus of Chapter 7, and the reader is directed there for a full discussion.

### 3.2.6. Thawing of Encapsulated Liver Spheroids in Cryovials

#### Materials

- High glucose culture medium (section 3.1.2; chilled to 4°C)
- High glucose culture medium (section 3.1.2; warmed to 37°C)
- Ice Bucket (typically a polystyrene box)
- Strippettes (Corning Costar, Sigma, Dorset, England, UK #4501)
- Pipette Boy (Integra Bioscience, Zizers, Switzerland)
- 50ml Centrifuge Tubes

#### Method

The sample was removed from its storage temperature and warmed (the rate and method dependent on the experiment, and was recorded with the experiments).

Immediately following the melting of the last ice crystal, the contents of the cryovials were poured out into a centrifuge tube stored on ice, and a volume of chilled culture medium equal to the volume of ELS was added.

Thereafter, the volume in the centrifuge tube was doubled at minute intervals for 4 minutes, to dilute out the freezing mix.

The ELS were allowed to settle and the medium removed. Warmed culture medium was added, 32ml per 1ml ELS. The ELS and medium mix was placed into an appropriate volume flask, and incubated in a 37°C humidified incubator.

### **Justification, Benefits, and Limitations of Approach**

The dilution out of cryoprotectant solution (CPA) occurs as soon as the last ice crystal has melted. This is to reduce the toxicity of CPA after warming. The CPA solution was not diluted all out in one step, rather there was a series of 1:1 dilutions at minute intervals to reduce osmotic shock in the cells. ELS are robust in the face of osmotic shock (unpublished observation by author), likely as the alginate dampens solute change before reaching the HepG2 cells, and so the fairly rapid dilution employed here was acceptable.

Dilution happened at low temperatures, as the cells are less metabolically active at low temperatures [57], before warmed medium was added for the culture phase. This method is labour intensive and so only around 5 vials at a time can be carried out per person, and may lead to subtle variations depending on who thawed the samples. The alternative would be using an automated machine which would be prohibitively expensive. To reduce variation the method was made to be as simple as possible, and all cryovial thawing done in this thesis was carried out by the author.

### **3.2.7. Temperature Measurements**

#### **Materials**

- K-type thermocouples (RS Instruments, Corby, England, UK)
- TC-08 -Logger Unit (Pico-technology, St. Neots, England, UK)
- Pico-Logger software (Pico-technology, St. Neots, England, UK)
- Laptop

#### **Method**

The Pico-technology system was used for all temperature measurements unless otherwise stated.

The thermocouples were placed at the desired location inside the sample, and these thermocouples attached to a pico-logger which was in turn connected to a computer with the pico-logger software installed. The thermocouples could be attached to a rig if necessary.

At the end of the experiment, the data was exported to excel and plotted on a graph. The thermocouples had been tested to ensure accurate measurements at low temperatures (Figure 2).

### Justification, Benefits, and Limitations of Approach

Thermocouples are a robust, simple, and well established method of temperature measurements. They use the Seebeck effect and their size allows them to be added to small vials with direct line of sight not required [420]. They do have some drawbacks however. They are less accurate at lower temperatures, as outlined in Figure 2. They are also difficult to manoeuvre into an exact location. Further problems emerge in low temperature science where there is the potential for heat to flow through the thermocouple wire, Seebeck induced temperature changes, and for it to act as an ice nucleant. There is then potential that thermocouples by their presence change the system which they are measuring [420]. For this reason, thermocouple measurements were only used as a rough guide in this thesis, and their results considered in conjunction with other methods such as mathematical modelling and thermal imaging. Many types of thermocouples are available that use different alloys. T-type thermocouples tend to be more accurate at lower temperatures and methods could be improved by using them over k-type.

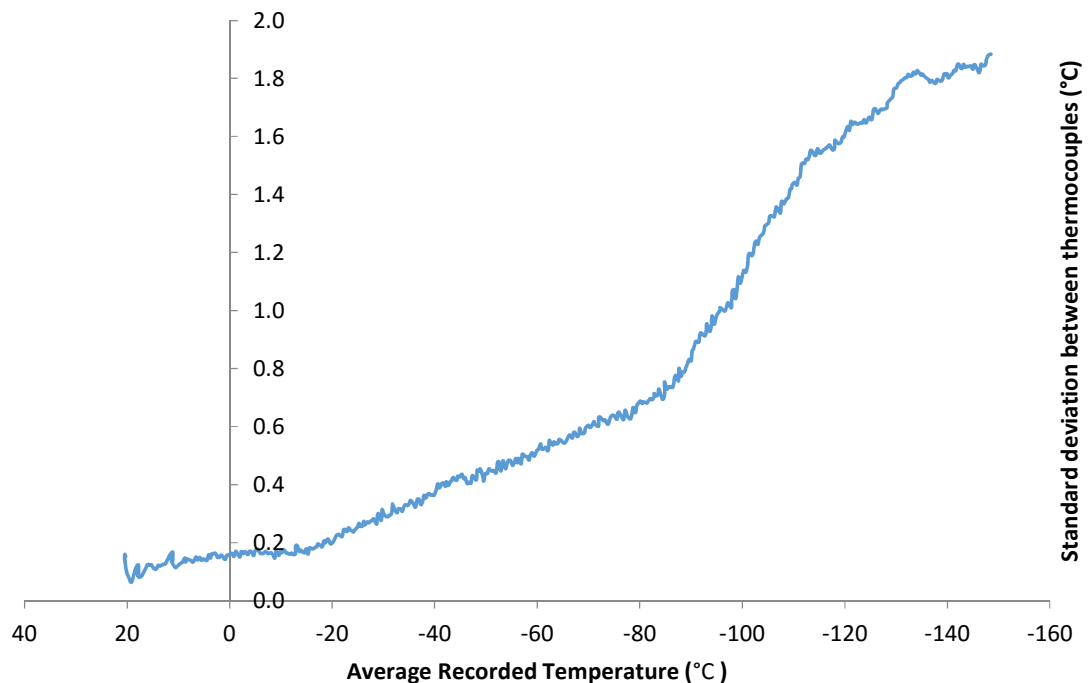


Figure 2 - Standard deviation between  $n=8$  k-type Pico-technology thermocouples at different temperatures. As can be seen, accuracy falls with decreasing temperature, but only by a few degrees and so acceptable for our requirements.

### **3.3. Cell Functional Assays**

#### **3.3.1. Viability using Trypan Blue**

##### **Materials**

- 2% trypan blue in Phosphate Buffered Saline (Sigma, Dorset, England, UK, #T-6146 in #D8662)
- Haemocytometer
- Hank's Buffered Saline Solution (PAA, Paisley, Scotland, UK #H15-010)
- Disaggregated cells in suspension.
- P200 and P20 Gilson Pipettes (Gilson, Luton, England, UK)
- Pipette Tips

##### **Method**

20µl cell mix was added to 160µl HBSS and 20µl trypan blue solution.

This was thoroughly but gently mixed, during which time the trypan blue stained non-viable cells.

9µl of this mix was placed onto each side of a haemocytometer, and placed onto a microscope.

On each side of the haemocytometer, the number of alive and dead cells was counted on a 25-square grid. This was then multiplied by  $10^5$  to give the cell count and viability of the cell mix, to take account of the 0.1mm depth of the sample, its 1/10 dilution, and its  $0.01\text{cm}^2$  area.

##### **Justification, Benefits, and Limitations of Approach**

This method was primarily used during cell passaging. Trypan blue is normally excluded by HepG2 cells, so when visible within the cell membrane (the cell will turn a deep blue) this gives an indication of cell membrane viability. It is a cheap, easy, and well-established method [390], however does have shortcomings. As cell counts are done manually, errors can creep in, and large inter-user variabilities may occur [365]. It also cannot be applied to cell spheroids as each cell must be counted – in a spheroid cells can be behind other cells.

### 3.3.2. Viability of Encapsulated Liver Spheroids (ELS) using Fluorescent Dye Staining

#### Materials

- Propidium Iodide fluorescent dye ( $\lambda_{ex}535/\lambda_{em}617\text{nm}$ ) (PI), 1mg/ml solution (Sigma, Dorset, England, UK #70335)
- Fluorescein diacetate fluorescent dye ( $\lambda_{ex}495/\lambda_{em}520\text{nm}$ ) (FDA) in 1mg/ml in DMSO (Sigma #F7378)
- Microscope slides and cover slips
- Nikon imaging software (NIS Elements Version 4.0)
- 4x zoom inverted, phase contrast, fluorescence microscope
- 100 $\mu\text{m}$  mesh filter (Corning, from Sigma, Dorset, England, UK #CLS431752)
- Phosphate Buffered Saline, PBS (Sigma #D8662)
- Hank's Buffered Saline Solution, HBSS, (PAA, Paisley, Scotland, UK #H15-010)

#### Method

A volume of containing at least 100 ELS were harvested, and washed once with HBSS, and placed on a mesh to remove all of the excess medium/HBSS.

These were removed from the mesh using a small spatula and placed into a 1.5ml centrifuge tube. 1ml of PBS was used to further wash the ELS, before they were suspended in 500 $\mu\text{l}$  PBS.

20 $\mu\text{l}$  of PI and 10 $\mu\text{l}$  of FDA solution was added to the ELS. The centrifuge tube was shaken and left to rest for 90 seconds.

PI stained the nuclei of cells with a non-viable cell membrane, while FDA stained cells with an intact cell membrane and metabolic activity. PI when excited with 535nm light, while FDA at 475nm.

A phase image of the ELS was taken. This was followed by a fluorescent image (exposure time 1s) at 617nm (the emission wavelength) to detect PI, and a fluorescent image (exposure time 150ms) at 520nm to detect FDA emission. 5 images of different fields of view were collected for each dye; the exposure times have been calibrated to give correct viabilities (FDA fluoresces more than PI).

Using a macro, the amount of PI and FDA excitation was found, and these were compared to each other to give viability [101, 210, 266].

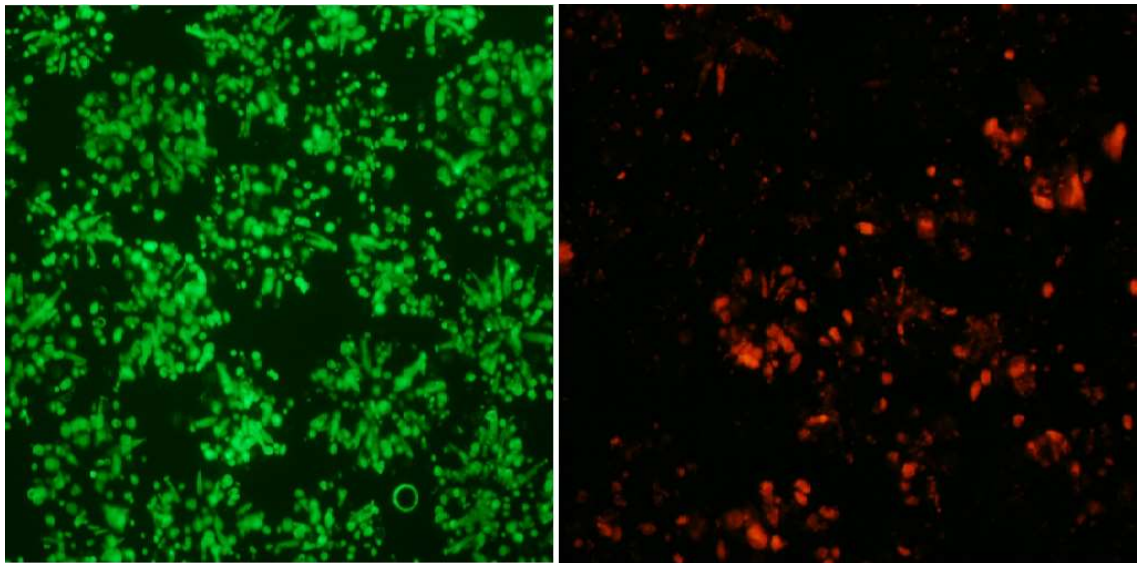


*Figure 3 - An example of the typical images used to determine viability. On the left the FDA fluorescence indicates metabolic activity in the cells, on the right PI fluorescence indicated a non-viable cell membrane. Images taken at 4x zoom at 520nm and 617nm for FDA and PI respectively. The viability readout was determined by comparing fluorescence between the two images using a calibrated macro.*

### **Justification, Benefits, and Limitations of Approach**

The primary benefit of using the FDA/PI membrane staining is that clusters of cells such as ELS can be visualized. This is because the fluorescent readings are strong enough to pass through other cells and be detected. An additional benefit comes from the double nature of the test. PI will highlight permeated cell membranes while FDA highlights both cell membrane integrity and metabolic activity (through hydrolysis by intracellular esterase to fluorescein). This method is well established and used in many cell types [11, 197]. This technique can be used to image ELS in alginate beads with greater contrast.

Limitations of the technique are the speed in which imaging must be carried out after staining. After a few mins FDA will leak out of healthy cells which will interfere with the viability readout. It is also possible that cells identified as dead in this study – through damaged membranes – may recover and so not truly be dead.

This method is used as it gives a simple read out of cell viability, which is indicative of overall health, and the speed in which it can be done makes it suitable for a large range of conditions to be tested during optimization. After optimization, much more time consuming tests on functionality can be carried out.

The word 'viability' in this thesis refers to a PI/FDA viability test, unless otherwise stated. Viability is stated as absolute viability, i.e. percentage of cells in a population viable in this thesis unless otherwise stated.

### 3.3.3. Cell Counts using the Nucleocounter Device

#### Materials

- NC-100 Nucleocounter (Chemometec, Sartorius, Epsom, England, UK)
- Nucleocassettes (Chemometec, Sartorius, Epsom, England, UK)
- 20ml Syringe
- 1.5ml microfuge tubes
- 16mM EDTA (AppliChem, Darmstadt, Germany #A1105)
- Scales
- 100 µm mesh filter (Corning, from Sigma, Dorset, England, UK #CLS431752)
- Nucleocounter reagents A (#910-003) and B (#910-002, Chemometec, Sartorius, Epsom, England, UK)

#### Method

A volume of medium and at least 0.5ml ELS was removed from a flask into a mesh.

A centrifuge tube was weighed, and then a volume of ELS removed from the mesh and placed into the tube. This was weighed, and so the exact weight of ELS was known.

1ml of EDTA was added to the microfuge tube, and this was incubated at room temperature for 5mins to dissolve the alginate, leaving a cell suspension behind. The microfuge tube was then centrifuged at 13000rcf for 5 minutes. The cells form a pellet at the bottom of the tube.

The supernatant was removed and the pellet was re-suspended in 1ml PBS. This was syringed 5 times to de-aggregate the cells, and 500µl of this solution removed and placed into another microfuge tube.

To this was added 500µl of reagent A, the tube was mixed and then 500µl reagent B was added. A nucleocassette was loaded with this solution, the cell nuclei were dyed and the nucleocounter gave a reading for number of cells in that solution. This was then related to an original cell count [210].

#### Justification, Benefits, and Limitations of Approach

The nucleocounter system works by lysing cells, staining the nuclei with propidium iodide (PI), and then imaging a small volume of the cell solution. The number of nuclei in the image is then counted by the nucleocounter automatically and a cell density given. HepG2 cells are mononuclear. This is very advantageous over a trypan blue cell count as human error in the counting is eliminated, and a visual record of the counts can be easily maintained for future reference [365].

### 3.3.4. MTT (Tetrazolium Salt) Viability Assay

#### Materials

- 0.75% w/v MTT solution in aqueous solution (Thermofisher, Waltham Ma, USA, #M6494)
- Acidified isopropanol (4mM hydrochloric acid in isopropanol)
- 16mM EDTA (AppliChem, Darmstadt, Germany #A1105)
- 1.5ml centrifuge tubes
- Humidified incubator
- 96 well plate
- Plate reader

#### Methods

A known weight of ELS were liberated from alginate through a 16mM EDTA solution, and 0.5ml 0.75% w/v MTT solution (tetrazolium salt, Invitrogen, Carlesbad, CA, USA) was added to the ELS in a centrifuge tube tube. After 3 h incubation in an incubator the MTT was inactivated and the crystal product dissolved using acidified isopropanol (4mM HCl in propan-2-ol). After the crystals had dissolved, a known volume was added to a 96-well plate, and total absorbance was measured at 570 nm on an Anthos III microplate reader, and quantified using MANTA software. This was then related to total MTT production per million cells or per ml ELS.

#### Justification, Benefits, and Limitations of Approach

Fully, MTT is 3-(4,5-Dimethylthiazol-2-yl)-2,5-diphenyltetrazolium bromide [406, 421]. It was used as a complimentary measurement to FDA/PI viability in this thesis. It was not used as a primary viability assay as it tended to give larger error bars and gave post-thaw viability as a function of control, not an absolute value. However is a well-established method [406, 421] and gave support to results from other protocols. An absolute value is useful as it indicated health of a population before cryopreservation.

### 3.3.5. Secreted Protein Synthesis Measurement: Albumin ELISAs (Enzyme Linked Immune Sorbent Assays)

#### Materials

- Culture Medium Samples
- Primary Antibody (Dako, Ely, England, UK # A0001, polyclonal rabbit)
- Coating Buffer (0.159% w/v Na<sub>2</sub>CO<sub>3</sub> and 0.293% w/v NaHCO<sub>3</sub> in distilled water, pH adjusted to 9.6)
- 96-well Nunc Immuno-coated plates (ThermoFisher, Waltham, MA, USA #DIS-971-030J)
- Clingfilm

- Plate washer
- Tween solution ( w/v - 0.8% NaCl, 0.02% KCl, 0.152% Na<sub>2</sub>HPO<sub>4</sub>·2H<sub>2</sub>O, 0.02% KH<sub>2</sub>PO<sub>4</sub>. v/v 0.05% tween20, Sigma, Dorset, England, UK #P1379)
- Blocking buffer - 1.25g powdered milk (Marvel) in 25ml tween solution.
- Secondary Antibody (Abcam, Cambridge, England, UK #ab24458-200, mouse anti-human)
- OPD solution (2\*OPD (3.5mg 1.2 phenylenediamine dihydrochloride) tablets Dako cat # s204530) in 12ml distilled water.
- Sulphuric acid (2M in water)
- Anthos ht-III plate reader with Manta software (Dazdaq ltd. Brighton, England, UK).

## Method

Medium samples were taken at set points from cells of ELS in culture, these could be stored at -20°C until required. As the total amount of albumin was measured, cell counts were also carried out (as per section 3.3.3), to give production per cell.

Coating buffer and tween solution are made as per recipe in materials.

The primary antibody was diluted 1 to 1000 in coating buffer. 100µl of this solution was put into each well of the 96-well plate. The plate was then wrapped in cling film and left at 4°C overnight.

The following day, the 96-well plate was washed in the plate washer three times with the Tween solution. The plate was then left to dry, before 100 µl of blocking buffer was added to each well and the plate was placed in room temperature for 1 h.

100 µl of each sample was then added to the wells. The samples were usually done in triplicate. A quality control and standard were also added to wells, before the plate was incubated for 1.5 h at 37°C.

The plate was washed with the plate reader three times with the tween solution and left to dry. The secondary antibody was then diluted 1 to 1000 in coating buffer. 100µl of this solution was then added to each well in use in the plate, before being kept at room temperature for 1 h.

100µl OPD solution was added to each well. This was then kept in the dark for approximately 5mins (until colour developed, dependent on room temperature) before sulphuric acid was added to stop the reaction. It was important to ensure that the time each well was exposed to the OPD solution before the sulphuric acid was added was identical.

The plate was transferred to the plate reader. The standard was used to quantify the albumin in each well, which was related to production rate per cell per unit time [210, 248].

## **Justification, Benefits, and Limitations of Approach**

For the BAL to be a feasible treatment for acute liver failure, they must produce sufficient proteins and it is important that after cryopreservation protein production levels recover – that makes protein ELISAs crucial to the project. They are time consuming, and so are only done on protocols previously optimized using a viability assay – if the cell membrane has no viability the protein functionality will also be low. As albumin is one of the major liver proteins responsible for blood detoxification it has been selected for study (the full range of liver proteins is extremely large and not all can be tested).

Sandwich ELISAs work by measuring the amount of bound antigen between two antibodies. In this case a first antibody is added to the plates. When the sample containing the antigen – in this case albumin acts as antigen – is added, it binds to the first (capture antibody). The sample is then washed off, with the antigen remaining attached to the first antibody. A second antibody is then added which attaches to the antigen. The amount of attached secondary antibody is then measured which on comparison to a standard curve determined protein concentration in each tested sample (the standard curve is prepared using known concentrations of desired protein) [67, 68].

Limitations of the ELISA protocols in general is they are labour intensive, reducing the number of samples that can be tested. They are also very manual and environmentally sensitive and so variations can occur between samples analysed on different days – for this reason a fresh standard curve is carried out with every plate [67, 68]. ELISAs for most human proteins, including albumin, are not sensitive enough to detect albumin produced by ELS over background levels in culture medium using human blood plasma. They can only be done in samples using fetal calf serum medium.

### **3.3.6. Alpha-Fetoprotein ELISAs**

A sandwich ELISA as above except using mouse monoclonal antibodies (Abcam, Cambridge, England, UK # ab10071 and ab10072) as a capture, and as an HRP linked antibody respectively, with Applichem (Darmstadt, Germany, # A6935) used for a standard curve.

## **Justification, Benefits, and Limitations of Approach**

Alpha-fetoprotein is not present in human blood under normal conditions, but is produced by HepG2 cells (it is a cancer marker, and HepG2 cells are from a cancer cell line). This allows protein production levels of ELS growing in human plasma to be approximated [101].

### 3.3.7. Alpha-1-Antitrypsin ELISAs

A sandwich ELISA as above except using rabbit polyclonal antibodies from Dako (cat # A0012) and Abcam (cat # ab7635-s) as a capture, and as an HRP linked antibody respectively, with BBI solutions (Cardiff, Wales, UK) # BBI P165-5 used for a standard curve.

#### Justification, Benefits, and Limitations of Approach

Alpha-1-antitrypsin is involved in regulating inflammation response in the body [360], with experimental benefits and limitations similar to those for albumin.

### 3.3.8. Fibrinogen ELISAs

A sandwich ELISA as above except using goat monoclonal antibodies from Abcam Cat # ab6666 and Cat # ab7539 as a capture, and as an HRP linked (secondary) antibody respectively, with Sigma F3879 used for a standard curve.

#### Justification, Benefits, and Limitations of Approach

Fibrinogen is involved in blood clotting in the body [87], with experimental benefits and limitations similar to those for albumin as above.

### 3.3.9. Glucose Consumption and Lactate Production

#### Materials

- Culture samples
- Analox GM7 (Analox, London, England, UK)
- Glucose reagent (Analox GMRD-002A)
- Glucose standard, 8mmol/L (Analox GMRD-011)
- Lactate reagent (Analox GMRD 092A)
- Lactate oxidase (Analox GMRD 092B)
- Lactate standard, 8mmol/L (Analox GMRD 092C)

#### Method – Glucose

Culture medium samples were taken throughout the culture process and frozen at -20°C. To measure glucose, samples were thawed and left to warm to room temperature with the reagents. As the GM7 is only accurate up to around 24mmol/litre, samples were diluted in filtered water if necessary. The GM7 was primed with reagent, calibrated with the standard, and the 10µl of sample was measured, normally in triplicate or penticate. The GM7 was re-calibrated every 10 measurements. The concentration in the sample was then compared to previous measurements or initial concentration and used to determine glucose consumption of the ELS [101].

### **Lactate Measurements**

The Analox GM7 was also used for lactate measurements on medium samples using an L-Lactate oxidase reaction. The reagent and oxidase were mixed before use (stable chilled for about 2 months), and samples thawed and left to warm to room temperature before experiments began. The same process was followed as glucose to find lactate consumption, with 7µl used instead of 10µl. The measured concentration was then related to total consumption per condition [101].

### **Justification, Benefits, and Limitations of Approach**

ELS consume glucose as part of regular cell metabolism. Measuring consumption rates give a non-specific indicator of general cell function, which can be missed by other indicators. For example, if cells are proliferating rapidly cellular resources will be committed to proliferation and so protein production function will appear lower, if they are producing many proteins cell proliferation functions may be reduced. Glucose consumption can give a wider picture view of all of these functions which can smooth out inhomogeneity in specific functions.

Lactate is produced in cell metabolism, and so these measurements can re-inforce glucose consumption or give an independent overview. Excessive lactate is also harmful to cells so monitoring levels can give an indicator to when medium changes are required.

The GM7 device works by causing an enzyme oxidative reaction, the results of which (glycolic acid or pyruvate) can be measured as a specific indicator of glucose or lactate concentration respectively. The 8mM standard is used to calibrate the readings.

### 3.3.10. Statistics

To determine significance, an appropriate t-test was performed. Significance was determined at  $P < 0.01$  unless otherwise stated. Samples for cell functional analysis and other data contained five independent replicates per experiment unless indicated differently in the text. Each sample taken for analysis contained at least 100 ELS. In binary systems where a t-test was not possible, another system was used and this is stated with the results.

T-tests were applied to all experimental conditions possible over other tests in order to ensure consistency throughout the thesis. This also avoids the 'let's try as many different statistical tests as possible until one shows significance with our data' fallacy.

In general with the ELS used in this thesis, large inter-experimental variations occurred, as is common in biological systems. It is particularly pronounced in the BAL system in the LG as total direct cell culture time before then end of an experiment can be more than a month - incidentally a reason why cryopreservation is carried out near the end of the process, to reduce potential patient wait time - for this reason cell experiments need to be carried out on at least two separate occasions before results are stated even if one experiment has a low p-value. This has been done in this thesis, though in the interests of clarity results are only stated in one place (except for emphasis). Values of n stated in this thesis refer to different experimental samples, although may have been examined at the same time.

## 4. Cryoprotective Additives and Thermal Profile Optimisation

### 4.1. Introduction

Traditionally, cryopreservation has been carried out in small volumes, typically no larger than 4ml and usually much smaller. This is sufficient volume for cryopreservation of spermatozoa, oocytes, embryos, and small tissues.

In the BAL, cryopreserving in small volumes has many advantages, primarily allowing more experiments to be carried out without major increases in cost and logistics and the ability to probe the effects of rapid changes in cooling rates at specific temperatures – something which may prove invaluable information before scale-up. As will be discussed in chapters 5 and 7, larger volumes cannot always be approximated on the smaller scale [210], however in some cases this is not a problem and is preferable on practical grounds when few ELS are available, and so smaller volume experiments have been carried out for studies in this chapter. The BAL being a homogenous mix of ELS allows this to be done.

Previous work in the cryopreservation of HepG2s in the LG were done in small volumes at low cell densities (<2ml, < 5 million cells/ml), with good post-thaw outcome (typically over 80% viability) [263, 264, 266]. Replicating this success in a larger volume and at higher cell densities is the primary aim of this thesis. Previous attempts at cryopreserving in the large volume chamber in the LG resulted in total cell death [266].

This chapter contains an in-depth look at the effects of CPAs during cryopreservation, tried to find new optimised CPAs, and examined work used to determine optimal cooling/warming rates and the effect of CPAs.

### 4.2. The Uses and Impacts of Cryoprotectants

#### 4.2.1. Forms of Cryo-injury

CPAs (Cryoprotective Agents) are chemicals added during cryopreservation to limit the damage caused during the freeze-thaw cycle, making long term storage of cells and cell clusters possible [131, 254, 273, 322, 336].

As discussed in the general introduction, chapter 2, as tissue or cells are cooled for cryopreservation and ice forms in the biological system, they can experience a number of ice related cryo-injury – usually caused by cooling rates which are either too rapid or too slow [268, 271]. The first of these is IIF (Intracellular Ice Formation). As the name suggests, this is defined as ice crystals forming within the cell membrane. Ice easily damages the delicate internal structure of cells and usually results in cell death. IIF often forms when cells are cooled too quickly [135, 269, 271, 408, 414].

As a biological system freezes, ice will form in the inter-cellular space. This ‘locks up’ water with a low solute concentration, leaving the cells experiencing a high osmotic gradient [290]. The cells dehydrate to equilibrate with this solution, reducing their internal water concentration and so the chances of IIF [268, 407]. If a sample is cooled too quickly, the cell cannot dehydrate fast enough so the water volume remains relatively high making IIF more likely, as ice nucleation is (weakly) volume dependant [269, 289, 409].

A second major form of cell death is due to solute toxicity [268, 270, 324]. During cryopreservation, the extra-cellular solution becomes hypertonic. This build-up of solutes can reach a toxic level and result in cell injury or death [254, 270]. This is linked to a too low cooling rate, as the exposure time in the high solute solution above the storage temperature is increased, and the slow cooling rates allow for maximum cell dehydration and ice crystal volume to be maximized [290, 291, 409].

Cryoprotective Agents (CPAs) are used to protect against these effects, and cooling rates are optimised to further reduce harmful conditions [131]. Discussion of warming rates, which are equally as important as cooling rates though often overlooked, will be studied in chapter 10.

#### **4.2.2. Cryoprotectants in Nature**

Many biological systems in the natural world regularly survive sub-zero temperatures. Animals, plants, and bacteria in the polar regions can survive for months or even years in temperatures reaching as low as  $-70^{\circ}\text{C}$  [58, 90, 388, 415]. Identifying and then using the active proteins allowing this survival is of interest [74, 75, 90]. While insects that are freeze tolerant experience extra-cellular and not intra-cellular ice in most cases, some cell types in some insects can even survive intra-cellular freezing [367, 462], an event lethal in the overwhelming majority of mammalian cells.

Animals have two methods of surviving sub-zero body temperatures. They avoid freezing with the use of anti-freeze proteins, or nucleate freezing at a higher temperature using protein ice nucleators [74, 75, 90, 463]. Cryoprotectants - in particular sugars such as glucose and trehalose - also accumulate inside the bodies of insects and other life forms [47, 56, 388, 415], either preventing the freezing of body fluids or protecting freezing injury.

These anti-freeze proteins are not exclusive to land animals. In the Arctic seas the salt content of the sea water can allow its temperature to fall below the normal freezing point of fishes' internal fluids. Here fish species can lower the ice nucleation point of their fluids allowing them to survive where otherwise they would freeze and die [74, 119].

While nature has discovered ways around cold-injury, many of these methods are not applicable to BAL cryopreservation for three reasons – difficulty in determining and synthesizing the active protein; the lower temperatures invoked in cryopreservation (liquid nitrogen temperatures are never experienced in the natural world); and unknown reactions between foreign proteins and the samples which would require extensive research before regulatory approval for use in a human treatment is admissible.

### **4.2.3. Effects and Uses of Cryoprotectants**

#### **Adjustment of Phase Transition Temperature**

One of the simplest ways CPAs can protect against injury is by lowering, or depressing, the freezing point of a cryopreservation solution [160, 162, 243]. As temperature is lowered, cells' metabolism slows down, and as a result they become able to withstand toxic solutions for longer [57]. Lowering the equilibrium phase transition temperature of a freezing mix reduces the amount of water 'locked-up' as ice at any given temperature and so results in a lower solute concentration at that temperature – provided that the agent used to reduce the equilibrium melting point is not toxic itself. Consequently the solute toxicity at any given temperature will be lowered and the cell death due to solute toxicity should be reduced [255].

Adding 12% DMSO to a solution of culture medium reduces its freezing point by around 4.5°C [263, 266]. This is a significant amount for many cell types, and this freezing point suppression is true of most solutes due to the colligative effects of solutes – small molecules being most effective [246].

#### **Solute Dilution**

Adding CPAs to a solution gives the solutes another material in which to dissolve, reducing their total concentration during cryopreservation. This buffering effect lowers the time cells are exposed to toxic concentrations of salts at any given temperature, reducing post thaw necrosis and apoptosis in a sample. Generally this has been proposed as one of the primary methods of CPA protection [132, 255, 273].

### **CPA Toxicity**

Although one of their primary functions is to reduce toxicity, many CPAs are themselves toxic [108, 131, 196, 234]. Their toxicity is a function of their concentration, exposure time, and temperature of sample [196]. This has been shown to be true for many different cell types and species and different CPAs [108, 196, 234, 434]. This CPA toxicity becomes a more significant problem when it comes to cryopreservation by means of vitrification. During vitrification a very high concentration of CPA is required (relative to slow cooling), to prevent any ice formation [10, 107, 109].

Utilizing more than one CPA while cryopreserving may reduce the relative toxicity of these additives. It has also been suggested that using an additional agent to counteract the effects of the CPAs' toxicity can improve post-thaw survival [10].

Sugars on the other hand are generally less damaging to biological material. This is likely a consequence of the organic bases of these chemicals, as well as the exposure many of these cells experience to sugars *in vivo*. The toxicity of CPAs is their limiting factor, and needs to be extensively considered when adding to a system.

At lower temperatures the toxicity effect of CPAs is less dramatic due to the reduction in cell metabolism at low temperatures [57]. Thus DMSO is added to our cells at 4°C, a temperature at which cell metabolism is low.

### **Protein Stabilisation**

The effects of cryoprotectants on proteins have been reviewed in detail by Crowe and Arakawa with their teams [13, 66]. They explored the preferential exclusion mechanism as an explanation for the stabilising effect many CPAs have on proteins.

The mechanism discussed in their review is that when a protectant such as DMSO, trehalose, or polyethylene glycol are present in solution they are preferentially excluded from the surface of proteins. As these co-solvents are hydrophilic, they bind to water in the system in preference to

proteins and so the free energy of the system dictates that they bind to the minimum surface area of the protein possible. For this to happen atoms in the protein remain clustered as to expose the smallest surface area to the cryoprotectant – this is proteins' natural state and so they remain intact [13, 66, 194].

At higher temperatures many CPAs are toxic [131]. This too can be explained in terms of protein stabilisation. As Arakawa notes, DMSO, polyethylene glycol, and ethylene glycol, amongst others, become hydrophobic at higher temperatures. This leads then to bind preferentially with the protein, which will then de-tangle to present the largest possible surface area and in the process denature. Crowe and Arakawa go into details to these effects in their reviews [13].

It has been shown that DMSO can exhibit this exclusion mechanism in certain membrane phospholipids [439], presumably a further method of DMSO cryoprotection.

### **Non-Penetrating CPAs - Cell Dehydration**

Small molecules, such as DMSO, can easily penetrate the cell membrane and enter intracellular space [273, 394, 401]. Larger molecules, such as polymers and hydroxyethyl starch cannot penetrate the cell membrane in normal circumstances. Non-penetrating CPAs are useful for dehydrating cells. They cannot enter a cell and so the osmotic stress over the membrane is greater. This increases the rate of cell dehydration, an effect true of most polymers [273, 387]. Osmosis will dehydrate the cell, reducing its total water fraction at any given temperature and so reducing the incidence of IIF. As IIF is one of the primary causes of cell death the post-thaw function in cryopreserved samples is improved. In mouse sperm cryopreservation, it has been shown that using only non-penetrating raffinose/milk is superior to penetrating CPAs [394].

Along with penetrating CPAs, non-penetrating CPAs can act as a buffer to reduce solute concentration [131].

### **Anti-oxidants**

As cells enter a non-optimal environment they become stressed, which can lead to an increase in oxidation reactions. These reactions result in free-radicals (molecules that react readily with others, also known as reactive oxygen species) which can harm biological systems [125]. Combined with the damage from the freeze-thaw process, free-radicals can produce a significant reduction in post-thaw survival – causing damage to cell membranes and DNA [125, 318, 399].

Free radicals (reactive oxygen species, ROS), such as hydrogen peroxide (H<sub>2</sub>O<sub>2</sub>) are usually removed naturally in a cell by anti-oxidants. If their concentration becomes too high however, they can readily react with molecules in the structure of the cell. Lipid peroxidation can occur at a rapid rate leading to destruction of the cell membrane and other cellular components [125, 318].

Anti-oxidants reduce this occurrence. Agents with anti-oxidant effects can be added, so reducing the amount of free radicals in the cellular environment. Addition of small amounts of antioxidants, such as vitamin E, Vitamin C, L-glutamine, catalase, L-cysteine, and perhaps rosemary have shown to improve functionality of several mammalian species sperm post-thaw [317, 318, 399, 465].

The literature is sparse on non-reproductive cell types, further tests with antioxidants on other cell types is a logical step to enhance their cryopreservation outcome.

### **Membrane Stress/Stability**

The cell membrane encounters extreme stress during cryopreservation – more than it has evolved to cope with. The cell membrane comes under physical pressure from extra-cellular ice, its shape may be distorted when the cell significantly dehydrates [317]. This may result in cells crushed against other cells in an ice-free channel, ROS can attack its structure, ice may form between cells in a cluster - tearing cellular connections attached to the membrane, and so damage can be done to the cell cytoskeleton. Ensuring the survival of the cell membrane is vital to the survival of the cell.

Glycerol may bind to lipids and proteins, such as make up the cell membrane, when used as a CPA during the cryopreservation of human sperm [317]. It is also clear that the membrane acts differently at lower temperatures – glycerol is readily up taken by cells at 37°C, but almost completely excluded at 0°C [401]. Lipid bilayers in mammalian cells become less permeable to water at lower temperatures – an effect that DMSO can help slow [4, 401].

This harm usually comes in several ways. When a cell dehydrates, its volume shrinks. The cell membrane therefore becomes deformed, and if deformed enough this can lead to the membrane folding in on itself and fuse. When the cell re-hydrates there is no longer enough membrane for the internal volume and so the cell lyses.

As the volume of unfrozen liquid in a freezing mix is reduced, cells will increasingly be confined to channels. Cells may find themselves squeezed between walls of ice. Additionally in a high cell dense environment cells can be pressed against each other [53, 270, 303, 427]. Mazur proposed

in his study with human erythrocytes that these cell membranes may become inter-locked, and when this connection is broken the cells' viability is affected. He proposed that at high hematocrit (proportion of a blood solution that is volumetrically composed of erythrocytes, normally determined by centrifuging), the primary cause of cell damage was not solute toxicity as in a low hematocrit, but rather these ice-cell and cell-cell interactions [270]. It has been observed in our work that the density of ELS may have a bearing on the post- thaw survival. Higher density ELS typically cryopreserving less successfully. Hepatoctyes have been shown to have a lower viability at high packing densities, and previous authors have suggested an optimal density of  $1.1 \times 10^7$  cells/ml on cryopreservation of suspensions [78, 176].

A complex cell matrix such as exists in tissues and organs can incur an additional form of viability depletion. As extra-cellular ice expands through the tissues, it can tear through and damage the connective tissues in this matrix [324]. This not only reduces the function of the tissue as a whole, but as many cells will be strongly affixed to their neighbours, the cell membranes can be destroyed when these links are broken or damaged violently.

#### **4.2.4. Application of, and Specific Cryoprotectants**

CPAs are often added to a sample on cooling (usually in a solution freezing mix at a specific CPA concentration) at a lower temperature prior to cryopreservation. Several methods, such as stepwise addition [116] or pre-incubation with CPAs [404] can be used to maximise outcome.

##### **Uses – pre-incubation**

It has been shown in studies that pre-incubation the sample to be cryopreserved with the CPA can improve the beneficial effect of the CPA [47, 148, 261, 404]. This can give CPAs more time to fully equilibrate in the intra-cellular space, improving their effects when the sample is cryopreserved. Pre-incubation of periosteal cells in DMSO for 30 mins at 37°C improves their post thaw function, and is the ideal balance between too little DMSO penetration and too much DMSO toxicity [261]. 24 h pre-incubation with trehalose can improve the post thaw viability of endothelial cells then cryopreserved with trehalose [47].

##### **DMSO**

DMSO (Dimethyl Sulphur Oxide,  $\text{Me}_2\text{SO}$ ), is one of the most widely used cryoprotectants [47, 132]. Generally it is used as the primary and most effective cryoprotectant when cryopreserving

hepatocytes [7, 176, 202, 210, 250]. As discussed above, DMSO protects cells in many different ways, reducing overall damage effectively.

## Sugars

Sugars protect against cryoinjury in many natural environments and are useful too in the lab [202, 415]. Sugars are either monosaccharides, or composed of them – sugars consisting of two monosaccharides are known as disaccharides, sugars consisting of three are trisaccharides etc. [60]

### Monosaccharides

Monosaccharides are the simplest sugars, with chemical formula  $C_6H_{12}O_6$ , the most common members in cryopreservation are glucose, fructose, and galactose. These can often act as penetrating CPAs, due to their small size [60].

### Disaccharides

As the name suggests, disaccharides are made of two monosaccharides, having chemical formula  $C_{12}H_{22}O_{11}$ . The base monosaccharides and bonding determine the chemistry. The disaccharide trehalose has been shown to improve post-thaw function in several hepatocyte functions, and so deserves further attention [194, 202]. Commonly sugars can offer protection by creating an osmotic gradient between the inter and intra cellular space, increasing rates of dehydration [60, 115, 194, 202].

### Trehalose

Trehalose is found in the natural environment, in freeze or drying resistant species such as tardigrades [415]. Trehalose seems to offer protection to dehydrating cells, and has the additional protective property of being an anti-oxidant. A previous study by Katenz et al. have shown the inclusion of trehalose can improve post thaw viability of primary hepatocytes from  $46.9 \pm 11\%$  to  $62.9 \pm 13\%$  [202].

Although the literature is fairly sparse when dealing with trehalose and liver cells, it has been shown to be beneficial in the cryopreservation of other mammalian cells, with trehalose being used primarily but not exclusively as a non-permeating CPA [47, 100, 194, 202].

Trehalose may work best as a permeating cryoprotectant. As it is not normally permeable to the cell membrane, additives such as di-rhamnolipids may be used to allow trehalose into the intracellular space [194].

### Glycerol

One of the earliest used and most useful cryoprotectant is glycerol [336]; it too can act either as a permeable or non-permeable CPA, and is used widely today [291]. It is less effective than DMSO when cryopreserving hepatocytes (unpublished observations), so is not considered within the scope of this study.

### CPA Mixes

Although many cryoprotectants accomplish many tasks, it is likely that using a combination of different cryoprotectants when freezing can lead to an optimised result. Saliem et al. have shown that cryopreservation of primary hepatocytes may be improved by using a freeze-medium containing both DMSO and anhydrous dextrose – a mixture of permeating and non-permeating agents [355]. DMSO mixed Hydroxyethylstarch is preferable to solely DMSO in some cases [387]. Higher recovery of several species' hepatocytes can be achieved by using polyvinylpyrrolidone with DMSO [148]. It is clear that having select additional cryoprotectants during freeze/thaw can be a useful method to increase post-thaw function.

Some research groups have been adding anti-oxidants during hepatocyte cryopreservation to improve their function. Culture medium often contains fetal calf serum (FCS). This helps the cells grow in culture and also results in better cryopreservation outcomes [148, 237], perhaps due to the anti-oxidant properties of FCS. Vitamin E has been used as an anti-oxidant in cryopreservation to improve post-thaw function [399].

In many medical applications it may not be possible to use FCS – it is animal derived so carries with it the risk of zoonoses.

University of Wisconsin (UW) solution, also known and referred to in this thesis as Viaspan, has been shown to be an effective carrier solution for cryoprotectants [236, 237], and is used widely against cold injury. UW solution itself contains 8 chemicals in water including many antioxidants. These are allopurinol, glutathione, adenosine, magnesium sulphate, potassium phosphate, raffinose, potassium lactobionate, and hydroxyethyl starch [314]. These are used to protect against cold injury and maintain osmotic balance. Viaspan is used widely for transport of livers for transplant at hypothermic temperatures [321].

Although DMSO is the CPA of choice when it comes to cryopreservation of hepatocytes, there are many more available [131, 201]. It is prudent to consider other CPAs, either on their own or in conjunction with DMSO.

#### **4.2.5. Summary**

The effects of cryoprotectants are widespread. They can help to dehydrate cells, reduce solute toxicity, stabilise cell membranes and internal proteins, have an anti-oxidant effect and reduce the freezing point of a solution. The full mechanisms are not fully understood and a general theory of cryoprotectant action seems still some way off.

There are also many cryoprotectants to choose from, depending on cell type or desired post-thaw function [201]. From this large quantity of potential CPAs, it is likely that the most optimal combinations are still awaiting discovery. Currently the gold-standard cryoprotectant in the LG is 12% DMSO in UW/Viaspan solution.

### **4.3. *Materials and Methods***

There are no methods unique to this chapter, and as such all methods are as described in Section 3. Unless otherwise stated, all samples in this section were cooled out in 2ml cryovials.

### **4.4. *Results***

Raffinose has been used in cryopreservation of ELS previously at UCL, with some success (internal unpublished data). As sugars such as raffinose are common cryoprotectants and raffinose is the only sugar in Viapsan – the liver cold storage solution and the carrier solution used in this thesis - testing it was an obvious starting point. Testing DMSO on its own in different concentrations, raffinose on its own, and a mixture of the two was carried out using a standard straight cooling from 4°C to -80°C at -0.3°C/min. It should be noted that as viaspan was used in the DMSO-only set, these samples would actually contain 0.68% raffinose – this was taken into account when adding additional raffinose.

## Effects of Raffinose and DMSO - Post-thaw Viable Cell Number

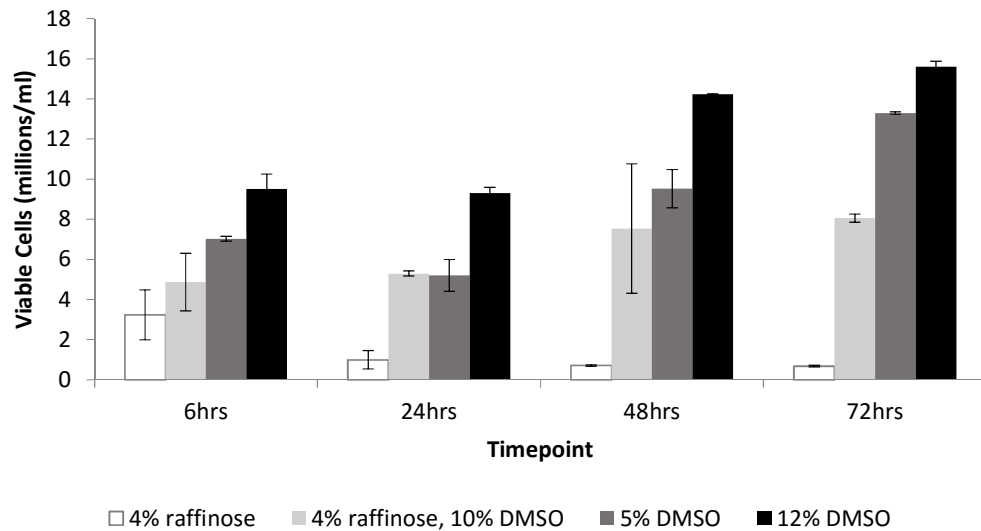


Figure 4 - Looking at the effects of Raffinose, Raffinose and DMSO combined, and DMSO, on the success of cryopreservation of ELS, and comparing it to the 12% DMSO present protocol. Solutions were added to the ELS which were then cooled at 0.3°C/min and stored at liquid nitrogen temperatures. After a rapid thaw, viability tests and cell counts were carried out at set timepoints.  $n=5\pm SD$ , DMSO viable cell number was significantly ( $p<0.01$ ) higher over all other sets at the same time point.

Figure 4 shows that raffinose does not enhance post-thaw survival in this system, in fact adding it with DMSO harms the cells.

The choice of CPA is a complex task, there are many available and one may work very well at only a narrow concentration or cooling rate. More work is needed to understanding the chemistry of the ELS at low cell densities in order to deduce any possible improvement to DMSO, or to help buffer against its toxic effects.

### 4.4.1. Toxicity of DMSO

In the final BAL there will be a substantial time between the cell/freezing mix solution reaching its freezing point, and the whole solution becoming frozen. This is a natural consequence of the large mass of the BAL – ice will grow through the sample taking over 90 minutes from first forming until it has fully solidified.

It was important to ensure that having cells in an unfrozen solution for extended periods was not damaging to their post thaw viability.

ELS were cooled to just above their freezing point (-4.5°C [263]) and held there for different lengths of time, before being re-warmed and their viability monitored.

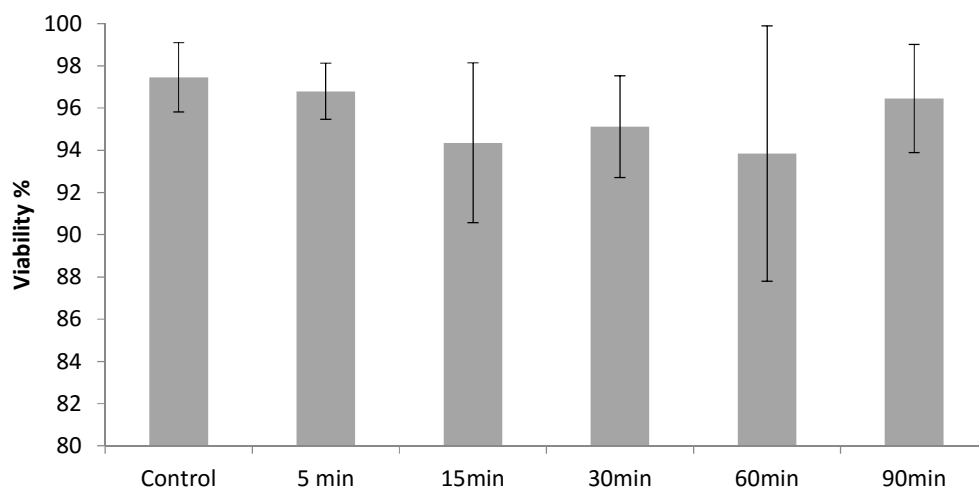


Figure 5 - Cell viability after being held in cryopreservation solution containing 12% DMSO in viaspan (v/v) just above its freezing point of -4.5°C for different lengths of time. Viability was measured through a PI/FDA staining procedure at ELS 24 h post-exposure.  $n=5\pm SD$

Figure 5 shows that at a 12% concentration of DMSO, there was no statistically significant difference between ELS held for up to 90 minutes, at -4.5°C, and the un-chilled control.

Lower cell metabolic activity at lower temperatures may not be the only factor affecting CPA toxicity. Studies have shown that at higher temperatures DMSO binds preferentially to proteins – denaturing them. At lower temperatures the situation is reversed, DMSO being preferentially excluded from the proteins thereby stabilising them [66].

#### 4.4.2. Adding Anti-Oxidants and Glucose to the Cryopreservation Medium

Cryopreserving ELS using some anti-oxidants or glucose may reduce damage and cell stress during cryopreservation. The following reagents had been shown elsewhere in the LG to reduce the fall in viability during 48 h shipping of ELS at room temperature [361], and these were tested to determine if they had a use in cryopreservation.

A control was cooled containing 12% DMSO in Viaspan, while two other samples, one containing 2% glucose (v/v) and another containing 2% glucose plus Hepes (2.5% v/v), valine (0.04% w/v), N-acetylcysteine (0.05% w/v), trolox 0.021% w/v (in ethanol, total concentration during freezing 0.14% v/v), catalase (0.005% w/v) and sodium hydroxide at 0.02M/litre.



Figure 6 - Effect of anti-oxidants and glucose when added to the freezing solution.° While at earlier time points the results look promising, the cells do not proliferate readily and so by day 3 post-thaw both sets are worse than the control group (without any additional CPA)  $n=3 \pm SD$ .

Figure 6 shows that CPA with additional anti-oxidants does not help the freezing process longer term post-thaw in our system. This may be due to the fact that most anti-oxidants are larger molecules, and so will not readily enter the cell membrane, especially at the low metabolic rates exhibited by the cells in the freezing mix. The anti-oxidants do appear to have an advantage over only glycerol, and as such it may be beneficial to include anti-oxidants without added glucose, or pre-incubate with anti-oxidants.

#### 4.4.3. Effect of pre-cryoconcentration conditions on cell growth

To first establish that certain common pre-treatments were not harmful, ELS were cultured in medium under different conditions for 24 h, and the viable cell number compared to ELS in standard culture medium without any additional components. The compounds tested were vitamin E (0.1% v/v), trehalose (2% w/v), and trolox (0.1% w/v). Trolox is a vitamin E substitute, and is much easier to dissolve in culture medium (and even easier to dissolve in ethanol – unpublished observation). Also examined was the effect of holding the ELS at room temperature (21°C) for 24 h. Holding at room temperature may acclimatise the ELS to lower temperatures, thereby reducing the impact of cold injury to the cells.

The effect of the common anti-oxidant Vitamin C was also examined, however as this is acidic (l-ascorbic acid) the 0.3% w/v concentration dissolved the ELS. Figure 7 plots the experimental outcome.

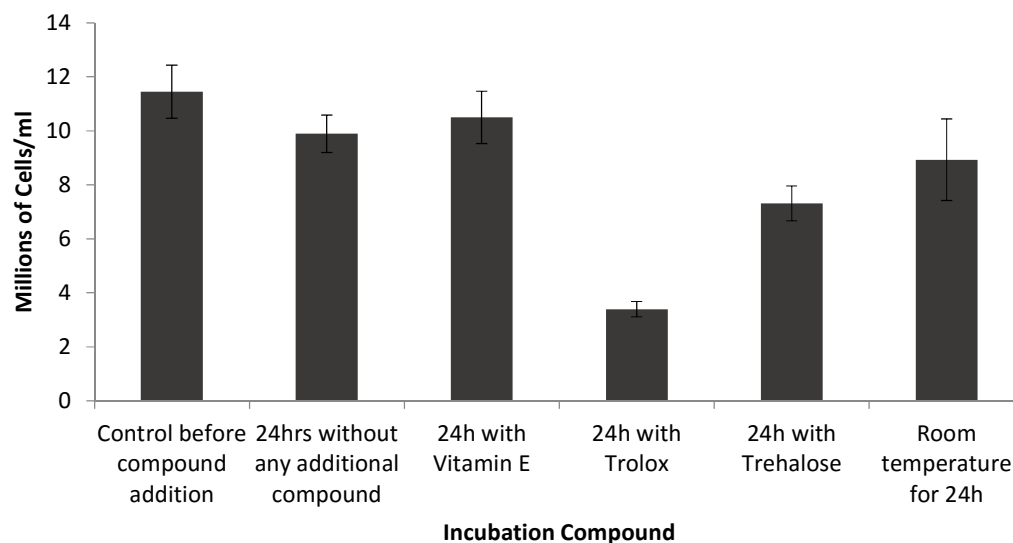


Figure 7 – Effects on viable cell number of pre incubating under different conditions for 24h. Vitamin E (0.1%), Trolox (0.1%), and Trehalose (2%) were added to ELS for 24 h before being washed out and fresh culture medium added. The effect on viable cell number examined immediately after wash-out. Also tested was holding at room temperature and a control with no additional condition, before and after the 24 h,  $n=3 \pm SD$ .

As can be seen from Figure 7, incubating with trolox, trehalose, or at room temperature appears to have a detrimental effect of cell outcome. Unless these are exceptionally good at mitigating cryo-damage they are unlikely to be of use in the freezing process at these concentrations.

#### 4.4.4. Pre incubation with Cryoprotectants

Many chemicals, such as vitamin C, vitamin E, and trehalose are too large to easily penetrate the cell membrane of HepG2s. However, several studies suggest that they are only effective as a cryopreservation medium intra-cellularly. To overcome this problem two methods are common – either add an agent that opens up the cell membrane to a greater degree, or a long incubation step prior to cryopreservation.

The former, while tending to be more effective, is not suitable for the BAL due to high cost of materials and regulatory complications. A pre-incubation step is not problematic and was carried out here, the concentrations were largely reduced from Section 4.4.3, to minimise the damage caused. If these studies were successful, further experiments could be carried out to optimise concentration and incubation time.

ELS were cultured for 11 days in a static culture. After these 11 days, the cells were split into 4 different flasks, into these was added either trehalose (2% w/v), Vitamin C (l-ascorbic acid, 0.03% w/v), or Vitamin E (a-tocopherol, 0.01% v/v) into the culture medium. The cells remained in

static culture in the 37°C incubator for a further 24 h. A control flask without any additional CPAs was maintained.

Cell viability was carried out before the freezing process commenced.

The samples were then cooled and thawed as per sections 3.2.3 and 3.2.6.

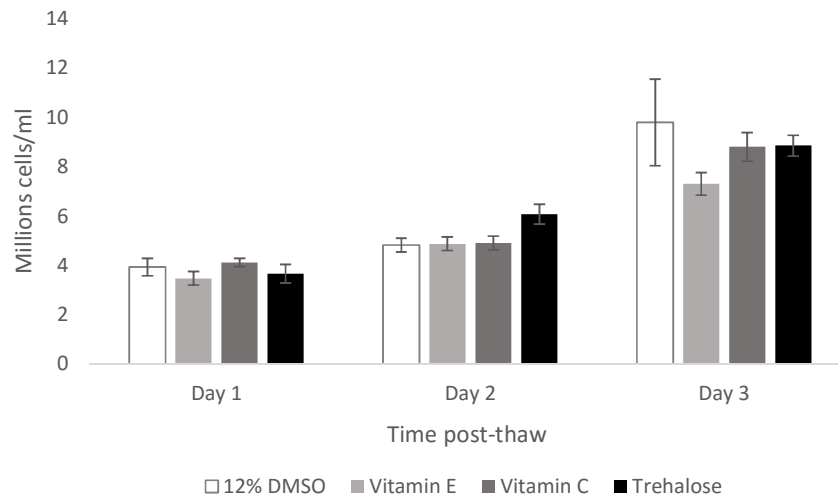


*Figure 8 - The cell membrane viability of ELS before and after cryopreservation having experienced either one or no pre-incubation with an anti-oxidant or trehalose for 24hrs pre-freezing. Potential additional cryoprotectants were added to the samples, which were maintained in culture flasks at room temperature. They were then cryopreserved in 12% DMSO at 0.3°C/min and stored in liquid nitrogen. Viable cell number was assessed at set timepoints after a rapid thaw. No significant difference was noted between any conditions at any time point.  $n=3 \pm SD$ .*

As can be seen from Figure 8, pre-incubation with anti-oxidants does not help post-thaw outcome in our BAL system. This is likely due to lack of transport through the cell membrane or ineffective protection. This highlights the lack of any positive effect from pre-incubating the ELS with either Vitamin C, Vitamin E, or trehalose, over a sample cryopreserved without any additional cryoprotective (other than DMSO) of our HepG2 set-up.

24 h incubations with higher concentrations was also attempted (6% trehalose, 0.1% Vitamin E, 0.3% Vitamin C). The data is not shown here. This test was unsuccessful – after 24 h incubation the cell viability had dropped significantly, indicating that culture with those concentrations is excessively harmful to the cells.

#### 4.4.5. The complete cryopreservation profile

##### Amount of CPA

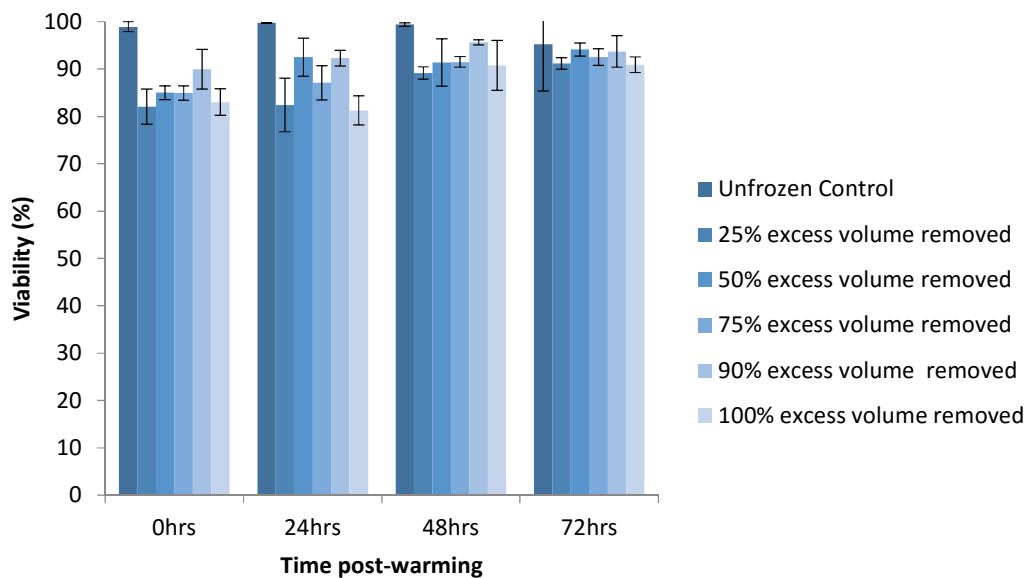


Figure 9 - The effects of removing any additional supernatant after the CPA has been added to the ELS which have then been allowed to sink and settle. Supernatant consisted of the cryopreservation solution of 12% DMSO in viaspan.. After supernatant had been removed, cells were cooled at 0.3°C/min and stored in liquid nitrogen before a rapid thaw. Impact on post-thaw viability determined (using PI and FDA staining as per chapter 3).  $n = 5 \pm SD$ .

The primary engineering challenge in the cryopreservation of the BAL is its sheer volume. Methods to reduce this volume have been explored.

Previously when cryopreserving ELS, CPA has been added to the spheroids and the whole system subsequently frozen. The ratio of ELS to CPA has been approximately 1:1; therefore to cryopreserve 2L of ELS the total volume of the ELS/CPA mix is 4L. Removing excess CPA would be of great benefit as it would reduce the thermal mass of the system. It was tested experimentally whether removing the excess liquid after allowing the CPA to infiltrate the ELS for a few minutes could be carried out without affecting post-thaw viability. Comparisons were made between:

1. Removing none of the excess liquid.
2. Removing a certain percentage of it.
3. And removing all of it.

The results shown in Figure 9 are very encouraging. Removing excess liquid does not harm post-thaw viability and so the total mass to cryopreserve is less. This result can be used to make it

easier to apply optimum cooling and warming rates to the BAL chamber. Later chapters will explore if this effect remains when scaling up to larger volumes, with interesting results.

#### 4.4.6. Carrier Medium

The CPA is diluted in a carrier solution prior to addition to the cells in order to get the correct concentration and to prevent exposing the cells to too high a concentration prior to mixing. Viaspan (University of Wisconsin solution) is used as standard in this thesis, as it has previously shown good results with ELS, and is currently used for low liquid temperature storage of livers for transplantation, due to its protective effect at low temperatures.

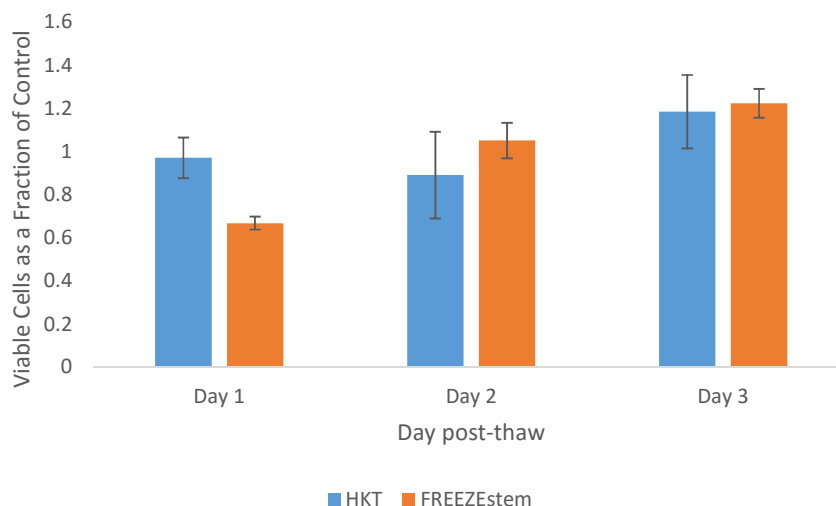


Figure 10 - Testing new carrier solutions. °C/min with 12% DMSO dissolved in either HKT or using only FREEZEstem. Post-thaw viability and cell number was measured at set-timepoints after a rapid thaw, and presented as fraction of samples cryopreserved using the gold-standard treatment of 12% DMSO in Viaspan. HKT is not significantly different from the control at any time point. FREEZEstem is significantly better at 3 days post thaw  $p < 0.05$ .  $n = 3 \pm SD$

Further tests on different carrier solutions were carried out in order to optimise the cryopreservation process. Two alternative solutions were tested, which was compared as a fraction of control using Viaspan. These were Custodial HKT (Histidine-tryptophan-ketoglutarate) and FREEZEstem (Biolaminar). The HKT operates in the same way as Viaspan (for dilution of DMSO). FREEZEstem is added and equilibrated with the ELS with no additional CPA addition – this offers DMSO free cryopreservation.

From Figure 10, it can be seen that HKT does not give a significant difference from the Viaspan control (neither better nor worse) at any time point. While the FREEZEstem is significantly worse at day 1, the cells recover much more rapidly and it is significantly better ( $p < 0.05$ ) by 3 days post thaw. FREEZEstem is prohibitively expensive to use in large volumes, so has not been explored

further in this thesis. Biolamina also stopped selling it suddenly without a given reason, and so further exploration was not carried out.

As no CPA solutions with a better outcome than 12% DMSO could be determined, other aspects of the cryopreservation protocol were examined.

## 4.5. The cooling profile

### 4.5.1. Cooling rate

As discussed in Section 2.3, cells are highly sensitive to cooling rates during cryopreservation. It was important to establish optimal cooling profiles for ELS, taking into account that this optimal rate may vary depending on cell density.

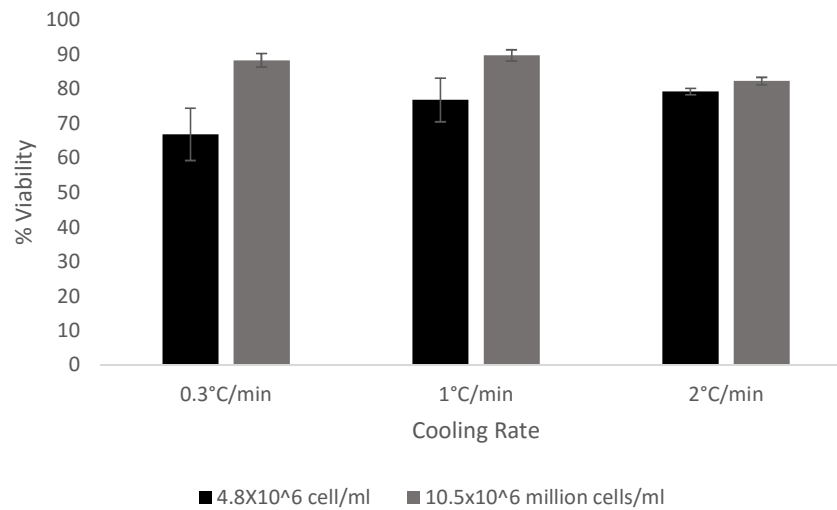


Figure 11 - Cell viability 24hrs post-thaw with cells of different cooling rates and cell densities - either  $4.8 \times 10^6$  million cells/ml (black) or  $10.5 \times 10^6$  million cells/ml (grey). Samples were cooled at different rates and thawed rapidly. Higher cell densities tend to prefer slower cooling rates, while lower cell densities have better post thaw outcome with quicker cooling.  $n=3 \pm SD$

Figure 12 and Figure 11 show the optimal cooling rate varies depending on the density of cells within the ELS. At  $\sim 10^6$  cells/ml, faster cooling rates, between 1-2°C/min are optimal, however when higher cell densities are reached ( $\sim 10^7$  cells/ml) the optimal cooling rate was much lower (as determined from the viable cell number), at around 0.3°C/min. ELS were cryopreserved at increasing time, and so increasing cell densities, from encapsulation and grown in static culture.

While from Figure 11 it appears that ELS with a higher cell density cryopreserve better, this is often not the case when the total surviving cells are taken into account. Often many cells are completely destroyed in the freezing process and so do not register in the viability studies. For

this reason viable cell number is often more useful, as this related viability to a cell count that can be compared to a cell count pre-freeze. In general, it is much more difficult to cryopreserve higher cell densities, especially up to  $\sim 3 \times 10^7$  cells/ml (the optimal BAL concentration) despite changing the cooling rates [266]. It should be noted that cell count and viability errors tended to be around 10-15% using standard LG methods, this means for changes in cooling rates, where warming rates had a small but reproducible impact, significance was difficult to reach without a large number of replicates. As this data agrees with previous cooling rate studies [266], the  $0.3^\circ\text{C}/\text{min}$  cooling rate was deemed acceptable for large volume preservation.

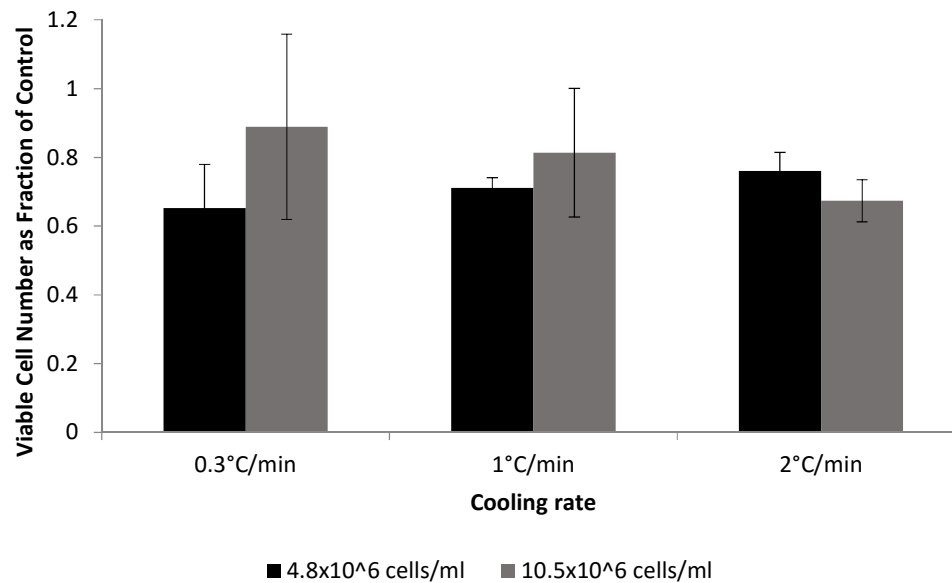


Figure 12 - The effect on viable cell number of different cooling rates with different initial cell densities – either  $4.8 \times 10^6$  million cells/ml (black) or  $10.5 \times 10^6$  million cells/ml (grey). Samples were cooled at different rates and thawed rapidly. Higher cell densities tend to prefer slower cooling rates, while lower cell densities have better post thaw outcome with quicker cooling. Data shown is average of  $n=5$ ,  $\pm$  SD

#### 4.5.2. Between what temperatures is the cooling rate most important?

It is important that a controlled cooling rate is followed in cryopreservation; usually a protocol will be followed, with different cooling rates and profiles giving different results. However it is important to know at what temperature ranges the cooling profile is most significant. By  $\sim -80^\circ\text{C}$ , most metabolic activity in the cells will have ceased, and the ice will be stable enough to allow plunging into liquid nitrogen or its vapour ( $-196^\circ\text{C}/-150^\circ\text{C}$ ), without damaging viability. This liquid nitrogen plunge happens in many protocols and will likely occur with the BAL.

Determining what temperature plunging into liquid nitrogen ceases to be damaging gives clues into the chemistry of the system at low temperatures, as well as being an important practical consideration. If no damage occurs from plunging into LN<sub>2</sub> below a certain temperature, more emphasis can be placed on temperatures above that limit when trying to improve post-thaw function.

Samples were cooled at -0.3°C/minute, and at certain temperatures a set of samples removed and plunged directly into liquid nitrogen. Post-thaw functional assays were then carried out.

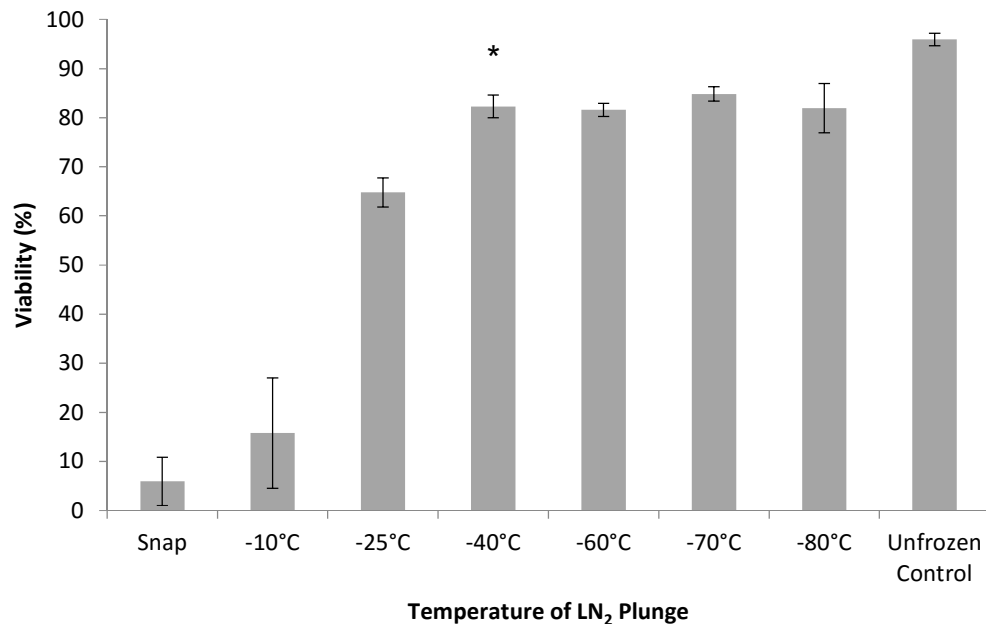


Figure 13 - The effects on viability of plunging ELS into liquid nitrogen, after controlled cooling at 0.3°C/min to certain different temperatures. Samples were added to cryovials and cooled at 0.3°C/min until a set temperature at which point they were plunged into liquid nitrogen. All samples used 12% DMSO in viaspan as cryoprotectant. n=5±SD \*p < 0.01 cf. samples plunged at a temperature higher than -40°C.

Figure 13 and Figure 14 indicate that below -40°C, having a rapid cooling rate imposed by a plunge into LN<sub>2</sub> was not detrimental to post-thaw function. Therefore it is most-important to control cooling above this temperature, with more flexible rates being permissible thereafter.

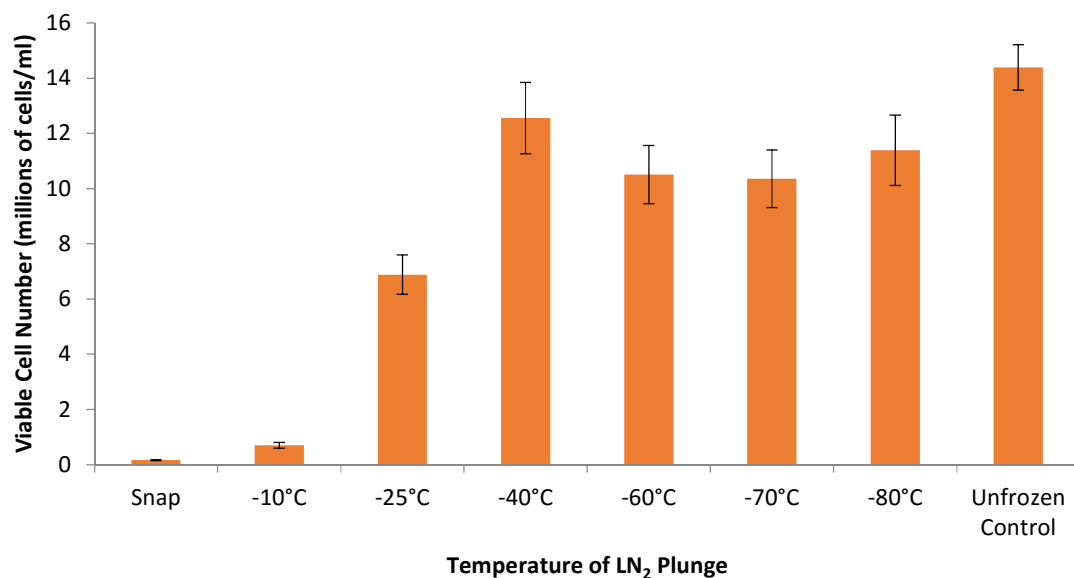


Figure 14 - Viable cell number 24 h after thaw of samples plunged into LN<sub>2</sub> at different temperatures. Samples were added to cryovials and cooled at 0.3°C/min until a set temperature at which point they were plunged into liquid nitrogen and a viability and cell count analysis carried out 24 h after rapid thaw. Below around -40°C, no significant difference is apparent between the sets while samples snap frozen or cooled rapidly from relatively high temperatures present poor recovery.  $n=5\pm SD$ .

#### 4.5.3. Holding temperature at -80°C

Part of the advantage of having a slow cooling rate is that cells have a long time over which to dehydrate, hence reducing IIF formation [273].

It was prudent to consider for how long dehydration can be prolonged. If cells are held at -80°C for a period of time before being plunged into LN<sub>2</sub>, perhaps further crucial dehydration can occur and IIF reduced.

To test this two sets of equal 2ml samples were cooled at -0.3°C/min to -80°C. One of these sets was plunged straight into LN<sub>2</sub> while another was held at -80°C for 72 h before being plunged, in order to further dehydrate. Their post-thaw viability and viable cell number was observed.

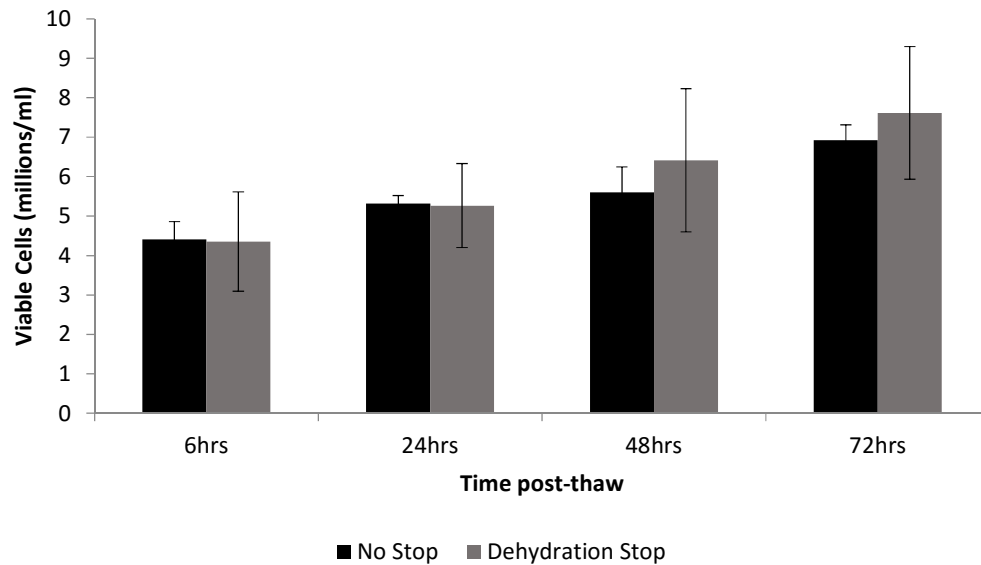


Figure 15 - Effects of a 72h dehydration stop on viable cell number at  $-80^{\circ}\text{C}$  compared to no dehydration stop.  $^{\circ}\text{C}/\text{min}$  to  $-80^{\circ}\text{C}$ . One set was then plunged directly into liquid nitrogen (black) while the other held at  $-80^{\circ}\text{C}$  for 72 h (grey) before being plunged into liquid nitrogen. Viability and cell counts were carried out at set timepoints after a rapid thaw. No significant difference was noted between the pairs of samples at any time point.  $N=5\pm SD$

As can be seen from Figure 15 there was no significant difference between the two pairs, and their growth patterns remained similar. This suggests that the cells were as dehydrated as was optimal by reaching  $-80^{\circ}\text{C}$ , having been cooled slowly at  $-0.3^{\circ}\text{C}$ .

As higher cell densities are reached, the time needed for dehydration will increase, as the cell spheroids will be larger and so liquid has further to travel before exiting the spheroid. This will be examined again in section 5, with a much higher cell density.

## 4.6. The warming profile

### 4.6.1. Consistent Warming Rate

Generally, cryopreserved hepatocytes are warmed rapidly (around  $40^{\circ}\text{C}/\text{min}$ ) in order to retain a high post-thaw viability [186, 385, 402]. However in the large scale BAL which will have a volume of up to 2 litres, this warming rate will be very difficult to achieve. Achieving such a large cylindrical volume warmed consistently at this rate will be even more difficult.

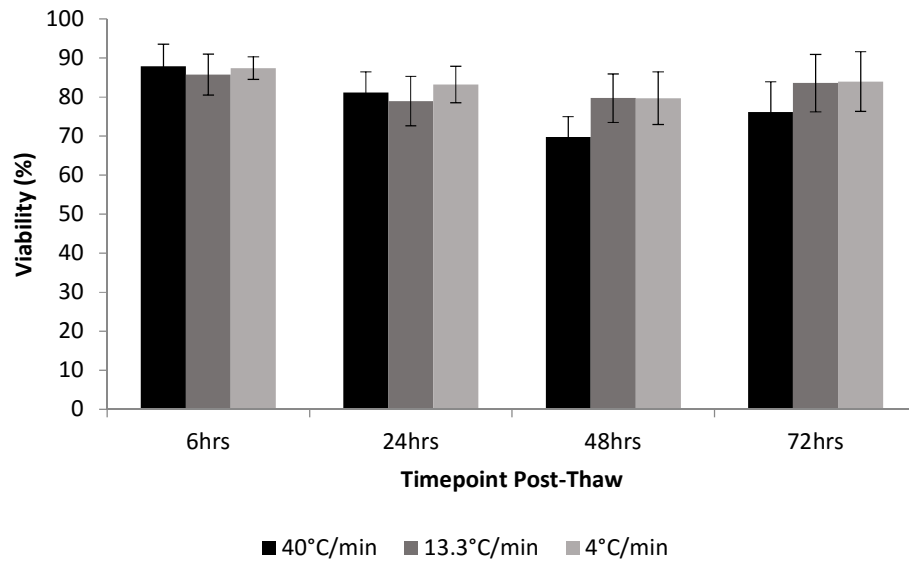


Figure 16 - Cell membrane and metabolic viability: the impact of different warming rates. °C/min, and stored in liquid nitrogen. Various thawing rates were examined. Examining the effects of three different warming rates out to 72 h post-thaw. No significant difference in viability was observed between warming rates of between 40-4°C/min.  $n=5\pm SD$

Samples were warmed at a three different rates, all of which are relatively high for a 2 litre volume, with post thaw viability monitored throughout the following 72 h.

What was distinctive from the above data is the lack of any significant change between samples warmed at different warming rates; in fact slower warming rates seem almost preferable in later time points. One point here was that even though the warming rates were different, the time it took for the ice to melt was roughly the same, as the phase transition takes place over a very narrow temperature range. One might hypothesise the most significant factor in the warming phase related to post thaw viability is the phase transition time.

If confirmed, this would be very useful. It would show that damage in warming was not caused by ice re-crystallisation (it has been suggested many times that damage occurs in warming due to larger crystals forming during warming), but rather when the ice crystals melt and water re-enters the system, though the reason for this is currently unknown.

## 4.7. Discussion

### 4.7.1. Overview

The aim of this chapter was to explore the physical impacts of cryopreservation on a smaller scale, to minimize waste when scaling up to a larger system. This chapter explored the impact of CPAs and cooling/warming rates in a smaller system.

### 4.7.2. Use of Cryoprotectants and Carrier Medium

No individual CPA or mix of CPAs was found in this study that improved the post-thaw outcome over the current standard 12% DMSO in UW solution. This is perhaps unsurprising – huge research has gone into finding new CPAs historically, but the field is still dominated by reagents discovered serendipitously in the mid- 20<sup>th</sup> century when cryobiology was still a developing field [255, 336]. DMSO as a primary cryoprotectant is used in the cryopreservation of other cell types and in particular liver cryopreservation [7, 176, 186]. And encapsulated hepatocytes [265, 403] Many studies with additives such as sugars have been attempted, but none have received widespread use, with the exception of small concentrations of glucose, as present in our culture medium. Some groups have shown that having trehalose as an intracellular cryoprotectant may be beneficial, but as trehalose is too large to penetrate the cell membrane a manipulation must be carried out [100]. No notable success with encapsulated hepatocytes have been reported after these changes.

It should also be noted that fetal calf serum has been used as a cryoprotectant [140]. It was not possible to test its effects here as removing it from the medium caused cell death – so obscuring the impact of cryopreservation, however the serum used in the medium may offer a cryoprotective advantage.

It is likely that in future, if the huge advances in computing power are exploited and new high-throughput screening methods are developed or adapted, many more CPAs are waiting to be discovered. Or someone might just get lucky – glycerol, the first identified CPA was discovered by chance [150].

### 4.7.3. Cooling and Warming Rates

It appears that the denser the ELS, the slower the cooling rate employed while cryopreserving should result in better outcomes. This was not unexpected, and very helpful.

It seems likely that much cell death is caused by IIF [4, 408]. As the spheroids of cells get larger, it takes longer for the water from dehydrating cells in the centre of this cluster to leave the clusters of cells, slowing down the dehydration process – insufficient time for dehydration has long been known as a factor for cell death through IIF. A slower cooling rate is therefore desirable as cells have longer to dehydrate sufficiently.

Work of cryopreservation of encapsulated primary cells by Terry et al. found that a rapid cool to  $-8^{\circ}\text{C}$ , followed by  $1^{\circ}\text{C}/\text{min}$  was optimal [403]. The rapid rate may have been necessary to nucleate ice – something achieved by inclusion of an ice nucleating agent in this system. Terry et al. also found that cooling at a fairly rapid rate ( $10^{\circ}\text{C}/\text{min}$ ) below  $-60^{\circ}\text{C}$  was optimal for primary cells, this is similar to what was seen with the liquid nitrogen plunges at lower temperatures in this chapter.

This chapter found that plunging into liquid nitrogen at lower temperatures (below  $-40^{\circ}\text{C}$ ) was not damaging to cryopreservation outcome, but above was. This is in agreement with other studies that found that cells are sensitive to conditions such as nucleation temperature which occur at relatively high sub-zero temperatures, both in suspensions and spheroids [263, 265]. Another complimentary explanation for this is the greater cell metabolism at these temperatures [57]. Also below  $-40^{\circ}\text{C}$  almost all liquid in the system will be locked up as ice [341], so cellular dehydration will be almost complete at these temperatures, rendering fast cooling injury improbable – indeed the intracellular material may also have entered a glassy state [58, 120].

The impact of cell density has not previously been reported by other groups. However extensive literature is available of the cryopreservation of many types of hepatocytes (HepG2s, C3A cells, primary human, pig etc.). These studies have found that relatively low rates of cooling ( $<2^{\circ}\text{C}/\text{min}$ ) are optimal for hepatocytes in general, agreeing with the present data [7, 176, 186, 202, 266].

A slower cooling rate is also useful for our purpose. To cool a large mass at a consistent rate throughout its structure is difficult at higher cooling rates. The experimental set-up for slow cooling is also simpler to achieve. At faster cooling rates a larger amount of energy must be removed from the sample at any given time, and larger temperature gradients will exist. A Stirling engine has a maximum power removal. To cool faster would require a larger and more expensive system. If liquid nitrogen was being used, a much larger volume would be required in a shorter time, this is an issue that could be overcome more easily but considering the total amount needed to cryopreserve the whole BAL, many technical restraints will be encountered – in addition, it is incredibly difficult to get sterile, GMP liquid nitrogen, limiting its usefulness in a medical setting [65, 287].

Perhaps starting a cryopreservation at a temperature lower than  $4^{\circ}\text{C}$  could help to improve post-thaw function. This would help mitigate the effects of solute toxicity that may become a problem at very slow cooling rates (and so for exposure to DMSO in the liquid state for  $>90\text{mins}$ ).

Another significant observation is that at higher cell densities ( $\sim 10^7$  cells/ml), the highest survival rate is not substantially different than at lower cell densities ( $\sim 5 \times 10^6$ ), as a proportion of original function for cells grown in static culture. Literature for hepatocytes is sparse; higher cell densities seem to be detrimental to fractional survival for some other cell types [270, 332, 402]. A reason for this in our case may be the structure that hepatocytes take on in our system. As individual cells multiply in the alginate, spheres of cells form with each cell being connected to its surrounding ones with an inter-cellular matrix. This is beneficial for the functionality of the cells – it mimics conditions in the liver more accurately – and perhaps culturing in a static flask encourages these spheroids to form closer to the edges of the alginate. Spheroids nearer the edge of the alginate may cryopreserve more easily as they can dehydrate more readily.

Growing ELS in a fluidised bed bioreactor, as will be examined later in this thesis, will not only increase the cell density to even greater heights (up to  $5 \times 10^7$  cells/ml), it also allows for spheroids to form throughout the alginate, as the nutrient exchange is large throughout the ELS. This may be detrimental to cryopreserving outcome and needs to be explored further.

When ice forms, it may slice the connections between cells in spheroids and by doing so damages the cell membrane, ultimately killing the cells. Having ice grow in a slower, more controlled manner through the spheres of cells may put them under less biological stress as the ice has time to grow through the areas of least resistance, being 'gentler' to the cell clusters and the links between them.

# 5. Transport and Storage of Encapsulated Liver Spheroids

## 5.1. Introduction

### 5.1.1. Chapter Overview

Cryopreservation of the BAL device raises the important question of transport of the biomass to the end user- either transport thawed or still cryopreserved are options.

This chapter examined different thermal histories on warming and short holding periods at different sub-zero temperatures on subsequent functional recoveries of ELS to mimic transport at liquid nitrogen (-196°C) or dry ice (approximately -80°C) temperatures. It will be shown that holding at -80°C after -196°C storage (mimicking dry ice transport) led to ELS expressing significant ( $P < 0.001$ ) damage over those thawed directly from liquid nitrogen storage, with viable cell number falling from  $74.0 \pm 8.4$  million viable cells/ml without -80°C storage, to  $1.9 \pm 0.6$  million viable cells/ml 3 days culture after 8 days storage at -80°C. Even 1 day storage at -80°C after -196°C storage resulted in lower cell viability (down 21% 24 h post-thaw), viable cell number (down 29% 24 h post-thaw), glucose consumption (down 59% 48 h post-thaw), and alpha-1-fetoprotein production (down 95% 48 h post-thaw), with storage at -80°C determined to be harmful only the warming cycle.

I concluded that for a bioartificial liver device composed of alginate encapsulated liver spheroids to be used after cryopreservation, it requires transport below dry ice temperatures or must be thawed prior to transport.

### 5.1.2. General Introduction

Successful and reliable transportation and distribution of bioengineered products from point of manufacture to point of use is essential for medical application of bioengineered technology, where it is often not possible to manufacture biomass at the end user site.

Most biological constructs, not just the 2-litre bioartificial liver device [101], require storage at cryogenic temperatures (-196°C), for effective delivery and treatment of Acute Liver Failure (ALF). At these temperatures samples can be stored indefinitely with little or no metabolic activity [77, 132, 323] before thawing on demand. Most complicated bio-engineered products

take many weeks or months to produce and so manufacture on demand is often not logistically or economically feasible.

Methods of transportation have wide consequences for all cryopreserved constructs. Transportation of biological agents - both bioengineered constructs and direct specimens such as spermatozoa, tissue samples, and embryos - is an involved issue but largely can be categorised into two groups. These are either transport at liquid or vapour phase nitrogen temperatures using commercial dry shippers typically between  $-196^{\circ}\text{C}$  and  $-150^{\circ}\text{C}$ , or transport at dry ice temperatures ( $-79^{\circ}\text{C}$ ) [147, 192, 298, 310, 349].

A dry shipper is a liquid nitrogen storage container, pre-charged with cryogen, into which samples can be placed and transported. Being adsorbed there is little risk of liquid nitrogen spillage. Liquid nitrogen is categorised as a dangerous product during shipping, however, and so transport can be relatively expensive. Most dry shippers have a finite transportation window before uncontrolled warming as they cannot easily be 'topped up' during transport. Storage and transport with liquid nitrogen may also come with increased risk of biomass contamination as the cryogen is routinely non-sterile, although this risk may be low for the transport stage [33, 34, 59, 152].

There are many studies where different tissue types have been transported successfully at liquid nitrogen temperatures ( $\text{LN}_2$ ) [1, 147, 192, 310, 349]. Additionally liquid nitrogen temperatures are essential for vitrified samples, where transport at  $-80^{\circ}\text{C}$  (which is above the glass transition temperature of samples cryopreserved in DMSO) would normally result in the samples preserved, for example, with cryoprotectants such as DMSO warming and de-vitrifying extracellularly, inducing significant biological injury.

Transport at dry ice temperatures ( $-79^{\circ}\text{C}$ ) is also used widely and is cheaper to do and easier in many practical senses [310]. The set-up for short transport is generally straightforward, and can be as simple as a polystyrene box filled with dry ice. This allows for the transport of large and irregularly shaped samples easily, and does not require the receiver to have liquid nitrogen handling infrastructure. Also,  $-80^{\circ}\text{C}$  freezers are widely available commercially and found routinely in the majority of potential treatment centres, and so samples transported on dry ice can be placed in a suitable freezer on arrival without temperature disruption for short or longer term storage. This can provide flexibility for the end user if products cannot be used on the day of delivery or operations need to be rescheduled. Transporting on dry ice is also a time dependant procedure, as they cannot be readily 'topped up' during transit either. There are also reports of  $\text{CO}_2$  leakage into samples on dry ice which can cause acidification related protein

denaturation [298], although as the BAL will be hermetically sealed which will prevent this occurring.

Historically for cell therapies, most samples were transported at dry ice temperatures before LN<sub>2</sub> usage became more widespread, and as a consequence procedures and successful studies using storage and transport on dry ice or at dry ice temperatures are often perceived to be sufficient.

In addressing these topics, it has previously been demonstrated by our group that ELS can be stored for at least 1 year at liquid nitrogen temperatures without significant loss of function, whilst they can be stored at -80°C only for periods less than a month; this mirrors results with many other cell types requiring liquid nitrogen temperatures for successful long term storage [59, 264].

As per the premise for the project, the 2 litre biomass of alginate encapsulated HepG2 cells (ELS) in the BAL takes up to 4 weeks to manufacture, however death from ALF can occur within days of diagnosis. Consequently, for the device to be a feasible clinical treatment, long term storage at -196°C will be required. Two options would then be available for patient delivery. The first would be transport to the point of need at cryogenic temperatures. -80°C would be preferable to eliminate the need for staff trained in liquid nitrogen handling at point of use.

The second transport option is to thaw at the location of cryogenic storage, and then transport at in the liquid state to the point of need; mechanisms have already been developed for ambient temperature transport [361], with post-vitrification transport also reported with mouse embryos [396]. However, transporting thawed products can be problematic as re-cryopreserving the device if not used will prove difficult, and thus costly products may be wasted.

This study examined, from a cryobiological viewpoint, which of these two methods is optimal for the ELS comprising the bioartificial liver device.

## **5.2. Study Design**

### **5.2.1. Thawing Protocols**

In this chapter, a consistent cooling rate of 0.3°C minute was applied to every sample down to -80°C, before plunging into liquid nitrogen. The primary conditions under test here were the impact of storage temperatures after the samples reached -196°C.

## **Positive Control**

In this chapter, the positive control was not an unfrozen sample, rather it was samples cryopreserved, stored in, and warmed directly from liquid nitrogen rapidly. These did not include any  $-80^{\circ}\text{C}$  hold step, the condition under review in this set of experiments.

These samples were removed from liquid nitrogen storage after 14 days, and thawed rapidly in 300s in a  $37^{\circ}\text{C}$  water bath, before the cryoprotectant was removed and samples returned to culture. Cooling and materials as per section 3.2.

## **Samples Stored at $-80^{\circ}\text{C}$ after Liquid Nitrogen Storage**

To investigate the effects of storage at  $-80^{\circ}\text{C}$  after liquid nitrogen storage, mimicking warmer transportation temperatures, samples were placed into an insulated box at liquid nitrogen temperatures, this box was then sealed before leaving the  $\text{LN}_2$  and being placed into a  $-80^{\circ}\text{C}$  freezer, with the samples equilibrating to  $-80^{\circ}\text{C}$  after approximately one hour.

Samples were then thawed rapidly in a  $37^{\circ}\text{C}$  water bath (taking 200 seconds) after storage of either 1 day, 4 days, or 8 days at  $-80^{\circ}\text{C}$ . Upon thawing the cryoprotectant was diluted out and the samples returned to culture [210, 264].

All samples in this set were cryopreserved and stored in  $\text{LN}_2$  and at  $-80^{\circ}\text{C}$  for a total of 14 days cryopreservation (ie. the time at  $\text{LN}_2$  + time at  $-80^{\circ}\text{C}$  = 14 days). Cooling and materials as per section 3.2.

## **Samples Stored only at $-80^{\circ}\text{C}$**

To explore the impact of  $-80^{\circ}\text{C}$  storage over the shorter term where the sample was never exposed to liquid nitrogen temperatures even during the cooling step, samples were removed from the EF600 after the cooling profile was reached  $-80^{\circ}\text{C}$  and stored in a  $-80^{\circ}\text{C}$  freezer. Samples were then removed after 1 day, 4 days, and 8 days, thawed in 200s in a  $37^{\circ}\text{C}$  water bath, and returned to culture. Cooling and materials as per section 3.2. This compared the difference in biological outcome between storage at  $-80^{\circ}\text{C}$  before or after  $\text{LN}_2$  storage.

## 5.3. Results

### 5.3.1. Thawing Profiles

The thawing profiles experienced during the early stage of the warming phase is depicted in Figure 17. It was important to ensure that the temperature profiles between -196°C and -80°C were consistent between all samples, to eliminate any artefact effect of warming rates in this range. As can be seen from the figure, both sets had an equal warming profile in this regime.

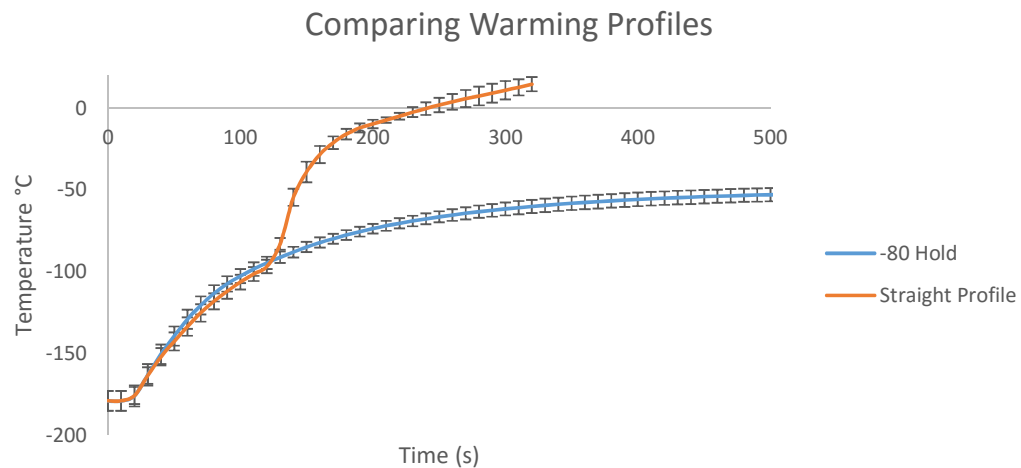


Figure 17 - Thawing cryovials temperature profiles - Temperature profiles between samples thawed directly from LN<sub>2</sub> (grey), and samples that experience a hold at -80°C. The profile to -80°C is equal in both sets. While the -80°C hold samples experience a temperature overshoot of around 10°C when placed into a -80°C freezer, this corrects itself in < 1 h and has no detrimental impact on cell outcome as per Figure 19. Data is average of 5 measurements per condition ± SD.

Comparing samples with different -80°C hold times following cryopreservation storage at -196°C, it can be seen from Figure 18 that samples with storage at any length of time at -80°C have significantly worse viability compared to a sample thawed directly from -196°C at 24 h. This difference is negligible when measured at the 48 h and 72 h post-thaw culture time points in samples held for either 1 or 4 days at -80°C, which can be explained through cell division and recovery of the ELS. Samples held at -80°C for 8 days after liquid nitrogen storage did not recover viability by 72 h post thaw, indicative of major and lasting damage.

Viable cell numbers, which take into account recovered cell densities, show that the controls (thawed directly from -196°C) were significantly better than those held at any time points at -80°C. While those held for 1 and 4 days at -80°C show recovery and proliferation by 48 h post-thaw, those held for 8 days did not show any recovery even by 72 h post thaw.

Figure 18 shows that for samples cryopreserved to and stored at only  $-80^{\circ}\text{C}$ , there was no significant difference between storage times of between 1-8 days. Samples that had been stored at  $-80^{\circ}\text{C}$  for 8 days after liquid nitrogen storage show significantly worse performance over samples stored for 8 days at  $-80^{\circ}\text{C}$  having never been stored in liquid nitrogen for the same 8 day period, at the 48 h post-thaw time point.

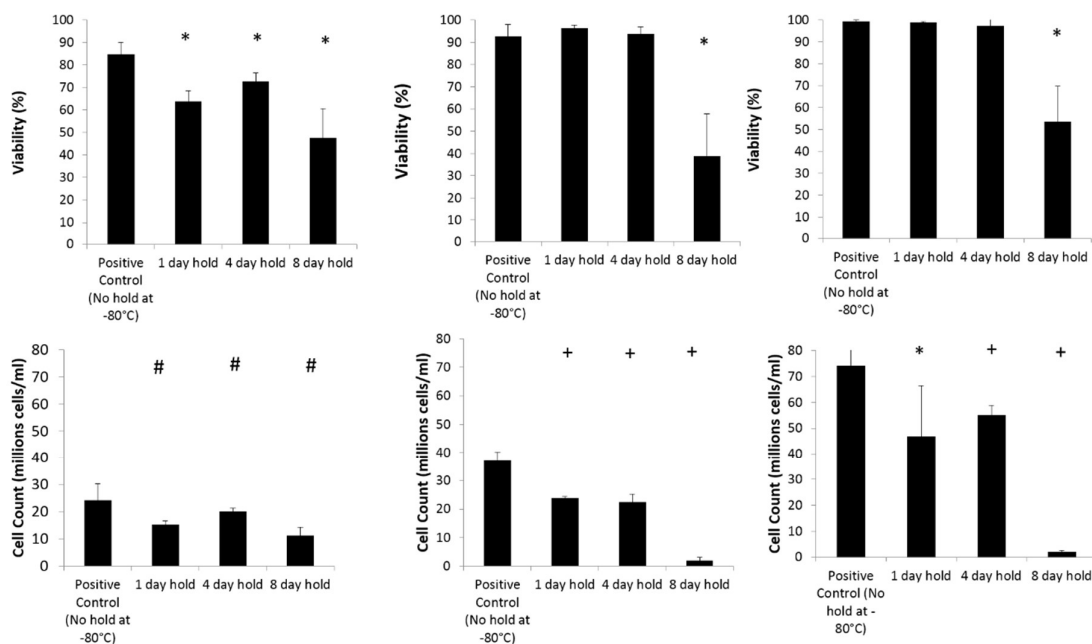


Figure 18 - Viability (top), and viable cell number (bottom) of samples cooled to  $-196^{\circ}\text{C}$ , warmed to  $-80^{\circ}\text{C}$  and held for stated periods of time. The total time from freezing to thaw was 14 days. Viability and cell count measurements were made at 24 h (left), 48 h (centre), and 72 h (right) post-thaw. Significance from a control that was thawed without stopping at  $-80^{\circ}\text{C}$  is denoted by # for  $p < 0.05$ , \* for  $p < 0.01$ , and + for  $p < 0.001$  using an unpaired student's t-test.  $n = 5 \pm \text{SD}$ .

To establish if the interruption to the warming cycle at  $-80^{\circ}\text{C}$  was a factor, a separate set of samples stored at  $-196^{\circ}\text{C}$  were warmed to  $-80^{\circ}\text{C}$  and stopped for a period of either 1 or 4 h. No significant difference was observed between these samples and a set that was thawed directly from  $-196^{\circ}\text{C}$ , as can be seen in Figure 19 at 48 h post-thaw.

It is notable that samples experiencing a one day cryopreservation at  $-80^{\circ}\text{C}$ , having never encountered  $\text{LN}_2$ , have worse outcome than those cryopreserved in  $\text{LN}_2$ . This is interesting and was not expected, based on section 4.5.3. These cells had a much higher cell density than those in the previous section, which is likely the cause of the discrepancy. This is further evidence of higher cell dense ELS having different cryopreservation characteristics compared with lower cell dense ELS. The mechanism behind this is not known fully beyond speculation, and further investigation is required.

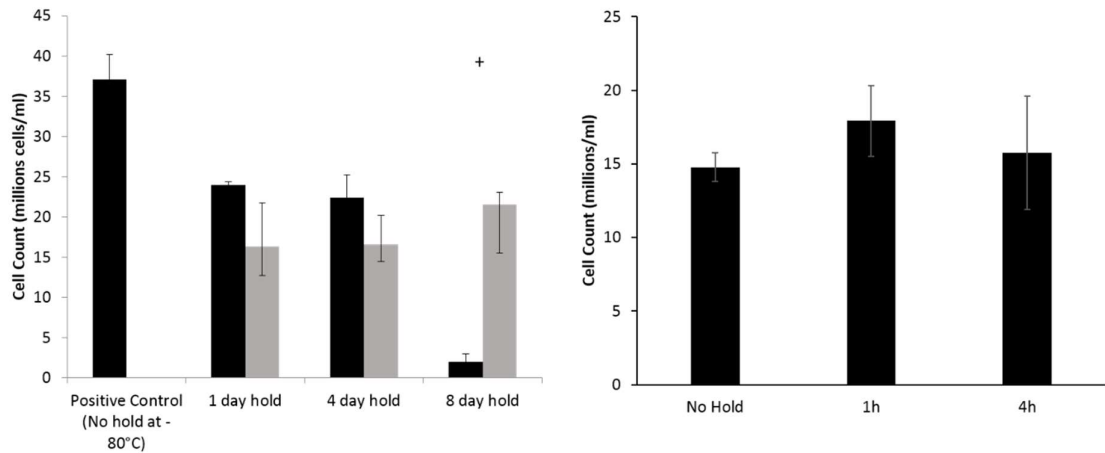


Figure 19 – Left - comparing viable cell numbers of samples stored in liquid nitrogen before storage in  $-80^{\circ}\text{C}$  (black), and those stored only at  $-80^{\circ}\text{C}$  (light grey). Measurements were taken at 24 h (left), 48 h (centre), and 72 h (right) post-thaw. No significant difference was observed between any samples being stored at only  $-80^{\circ}\text{C}$ , whilst samples stored at  $-80^{\circ}\text{C}$  for after  $-196^{\circ}\text{C}$  storage had significantly ( $P < 0.001$ ) worse outcome than those stored for 8 days only at  $-80^{\circ}\text{C}$ . The right figure shows a separate set of samples that were stored for either 1 or 4 h at  $-80^{\circ}\text{C}$  after  $-196^{\circ}\text{C}$ , compared with samples thawed without a stop. No difference was observed between any of these sets using an unpaired student's t-test.  $n = 5 \pm \text{SD}$ .

### 5.3.2. Glucose Consumption

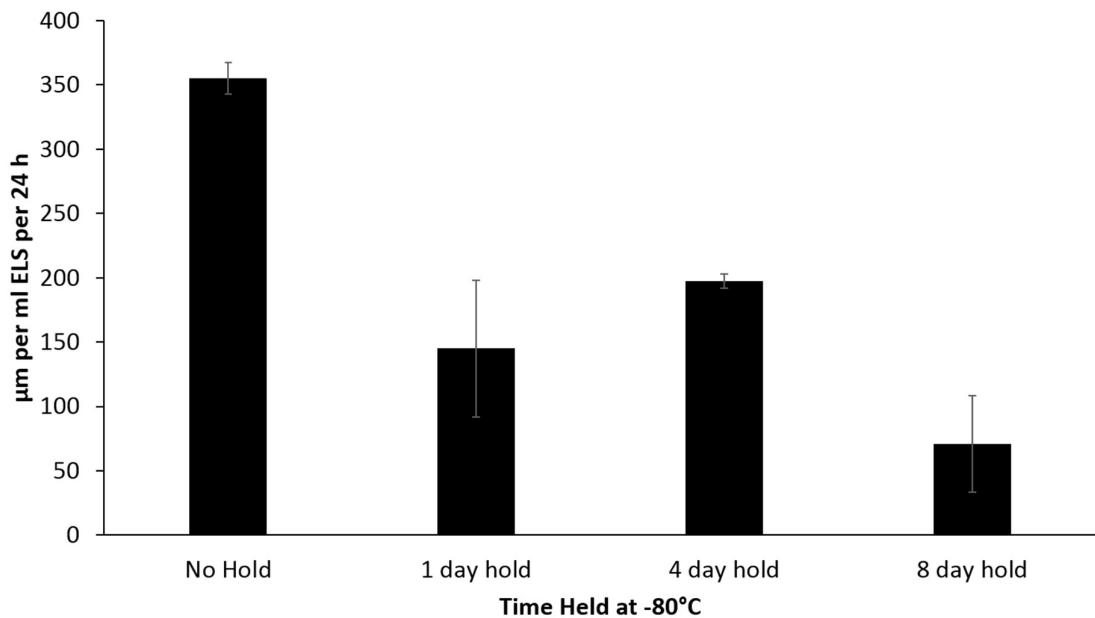


Figure 20 - Glucose consumption levels measured in culture medium 2 days post-thaw of samples experiencing different lengths of storage at  $-80^{\circ}\text{C}$ . The samples with no hold consumed significantly more glucose than those experiencing holds of any duration. Comparing samples with holds, no significant difference was observed.  $P < 0.001$  level using an unpaired student's t-test,  $n = 5 \pm \text{SD}$ .

In the 48 h post-thaw, glucose consumption between sets thawed directly from  $-196^{\circ}\text{C}$  or stored at either  $-80^{\circ}\text{C}$  for 1, 4, or 8 days on thaw was  $355 \pm 12$ ,  $144 \pm 53$ ,  $197 \pm 6$ ,  $71 \pm 37$   $\mu\text{Moles per}$

million cells per 24 h respectively. Any storage time at -80°C post-thaw resulted in significantly lower glucose consumption, as is shown in Figure 20.

ELS consume glucose during the metabolic process, and this data indicates that a direct thaw from -80°C is optimal for cell recovery.

### 5.3.3. Protein synthesis by Alpha-fetoprotein ELISAs

As can be seen from Figure 21, two days post-thaw, cells that had been stored at -196°C and were warmed directly to room temperature exhibited an alpha-1-fetoprotein (AFP) production of  $28.1 \pm 2.7 \mu\text{g}$  of alpha-1-fetoprotein (AFP) per ml ELS per 24 h.

The samples held for 1 day at -80°C after LN<sub>2</sub> storage exhibited a production of  $3.1 \pm 0.3 \mu\text{g}$  of AFP per ml ELS per 24hrs, significantly ( $P < 0.001$ ) lower than those not experiencing a hold.

Sets experiencing a 4 day or 8 day hold at -80°C had negligible AFP production. As AFP is unstable in-vitro, so very low production may decay and be undetectable [449].

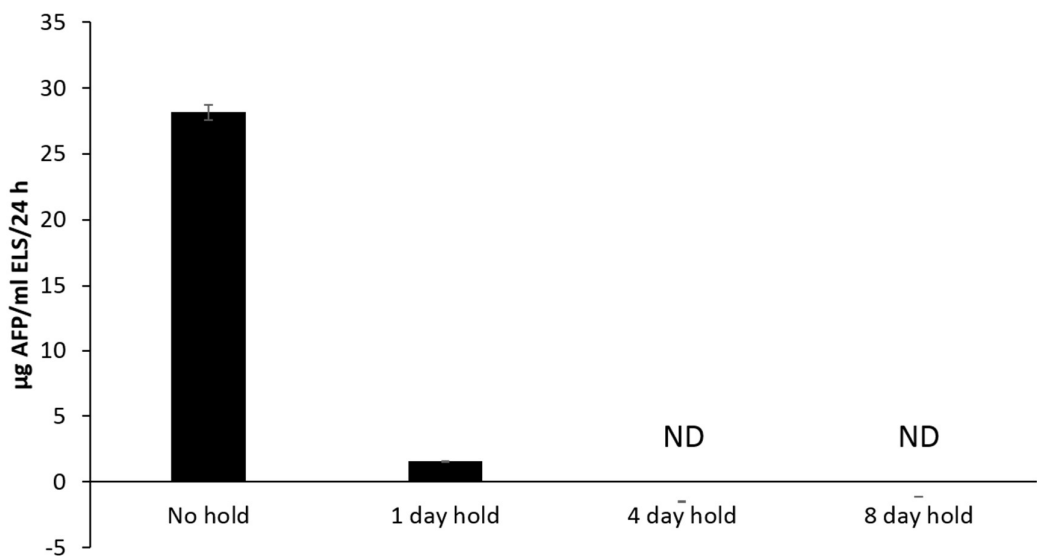


Figure 21 - Alpha-1-fetoprotein (AFP) production per ml ELS per 24 h, of samples experiencing different lengths of hold at -80°C after -196°C storage. These measurements were taken at 2 days post-thaw, with the samples not experiencing any hold at -80°C having a significantly ( $P < 0.001$ ) better AFP production over all other sets. With the exception of samples held for one day at -80°C, all samples that experienced a hold at -80°C on warming had negligible AFP production, with ND indicating none detected.  $n = 5 \pm SD$ .

## 5.4. Discussion

This study shows that for optimal delivery of the BAL device, the biomass will have to be thawed directly from liquid nitrogen storage. Transport and storage at  $-80^{\circ}\text{C}$  is not an option.

The viable cell number data, Figure 18, shows that samples thawed directly from liquid nitrogen recover quickly from cryodamage, which can be explained through cell division and recovery of damage cells. ELS consume glucose during the metabolic process, and this data indicates that a direct thaw from  $-196^{\circ}\text{C}$  is better for cell recovery. These glucose results go in line with the observed decrease in viable cell number.

Non-optimal warming rates can sometimes be blamed for poor cryopreservation outcome [241, 272, 280]. This is not the case in this study – samples held for 1 or 4 h at  $-80^{\circ}\text{C}$  experienced the same interruption in cooling rates at  $-80^{\circ}\text{C}$  as those with longer holds, but showed no additional damage, whereas those with prolonged storage at  $-80^{\circ}\text{C}$  on thawing did.

Storing the cells isothermally at  $-80^{\circ}\text{C}$  for 8 days is no more damaging than for one day at  $-80^{\circ}\text{C}$  following liquid nitrogen storage, Figure 19. Previous work has shown that one month storage at  $-80^{\circ}\text{C}$  (without the cells experiencing liquid nitrogen temperatures) was damaging to cells (drop in viable cell number of around 30%), and two months resulted in a fall in viable cell number of 70% over samples stored below  $-170^{\circ}\text{C}$  [264, 266]. The present data confirms that damage at  $-80^{\circ}\text{C}$  increases non-linearly with time.

The result that short storage at  $-80^{\circ}\text{C}$  after liquid nitrogen storage caused severely reduced post-thaw function was somewhat surprising and an effect isolated to the warming phase. The glass transition temperature for a 12% DMSO solution is  $\sim -120^{\circ}\text{C}$  [59, 264]. Intra-cellular material typically has a higher glass transition temperature than the extra-cellular material consequent of internal proteins, having a higher vitrification temperature [58], although its exact value inside DMSO-permeated mammalian cells is unknown.

The damage is possibly related to the fluidising of the freeze concentrated matrix between the ice crystals on re-warming to  $-80^{\circ}\text{C}$ . While ice crystals develop through our entire system, solutes are preferentially excluded from this ice front and eventually vitrify in channels between the ice [290, 303, 427] and fluidising of these channels may stress ELS via chemical or osmotic effects resulting in poor post-thaw performance. It is possible that the physical changes that occur when the extra cellular material passes through the glass transition point impact the cells resulting in a higher sensitivity to damage at  $-80^{\circ}\text{C}$  when the vitrified channels re-fluidise.

Alternatively, thermal stresses may build in the system due to the large temperature range between  $-196^{\circ}\text{C}$  and  $-80^{\circ}\text{C}$ . As samples stored for 8 days have much lower survival than those stored for 4 days, and that a 4 h hold at  $-80^{\circ}\text{C}$  is not problematic, it is clear that the effect is a longer-term phenomenon, not an instantaneous or very rapid one. Poorer outcomes are not observed with a hold of between 1-4 h on thawing, indicating that the damage is not caused by having a stop in the thermal profile.

FTIR is commonly carried out to determine structure of materials through emission and absorption spectra in the infrared range – this can be used to determine chemical composition [358]. The FTIR data here (measured by J. Molina) show that there is no change in the structure of the alginate component of the ELS that could explain cell death, rather it is a direct effect on the ELS themselves that is in the origin of the damage. While storage at  $-196^{\circ}\text{C}$  is preferable to  $-80^{\circ}\text{C}$  storage, the data shows that damage is not caused by storage only at  $-80^{\circ}\text{C}$  or transitions between  $-80^{\circ}\text{C}$  and  $-196^{\circ}\text{C}$  on the cooling process, rather is an exclusive factor in the warming profile.

Despite its importance to tissue transport, scant research has been published considering challenges of transport and resultant variation of storage temperatures. Publications on samples of arterial and heart valves from the European Homograft Bank state that these tissues cannot be placed back into liquid nitrogen after transfer to  $-80^{\circ}\text{C}$  from  $-196^{\circ}\text{C}$ , but can be stored at  $-80^{\circ}\text{C}$  for 1-3 months after  $-196^{\circ}\text{C}$  storage, although damage here has been related primarily thermal-stress cracking [147, 192].

One group has reported that in studying transportation methods with porcine aortic valves, a dry shipper caused maximal damage, and that only dry ice transportation was possible. However, this was reportedly due to tissue cracking related to variable warming rates [432]. ELS monitored in this study do not seem susceptible to major cracking damage, as the liver spheroids are no larger than about  $100\ \mu\text{m}$ , and morphology of the ELS is generally well preserved after cryopreservation [263]. In addition with many grafts cell survival is not necessary – the scaffold structure is essential and cells can be re-seeded later. Warming rates were shown in this study not to be a factor in cell death after  $-80^{\circ}\text{C}$  storage.

As more tissue engineered constructs become medically feasible, problems in addition to thermal cracking, such as cell function will become crucial, and this study helps address those problems in addition to its direct application to the BAL. This study shows that the BAL system requires transport at either  $-196^{\circ}\text{C}$  or thawed.

Mechanisms have already been developed for BAL short-term ambient temperature storage[361], and post-vitrification storage while transporting has also been reported with

mouse embryos [396]. However, transporting thawed products can be problematic as re-cryopreserving the device if not used will prove difficult, and thus costly products may be wasted.

To summarise, ELS should not be transported and/or stored at  $-80^{\circ}\text{C}$  after liquid nitrogen storage. 8 day storage or transport  $-80^{\circ}\text{C}$  after  $-196^{\circ}\text{C}$  conditions irreversibly damages the biomass in the bioartificial liver device. The BAL must be delivered thawed or thawed on site (from  $-196^{\circ}\text{C}$ ) to be a viable treatment. The former may be preferable as it removes the need for a dedicated GMP facility at each delivery site, and perhaps a system or solution could be developed where a newly-thawed BAL recovers from cryopreservation during the transport phase of the cold-chain delivery.

## 6. Scale Up – Large Scale Biological Freezing

### 6.1. Introduction

#### 6.1.1. Overview

A BAL will require a large number of cells, around  $7 \times 10^{10}$ - $10^{11}$  hepatocytes, likely in a 2 litre volume [101, 213]. Scaling up from a few hundred cells to tens of millions presents issues that must be overcome.

Controlling rates of cooling and heating within a larger space is more difficult – heat energy takes time to travel a finite distance. This leads to difficulties in maintaining a consistent heat profile throughout the BAL, and for creating rapid temperature changes, such as those required for rapid thawing. Literature with hepatocytes suggests that extremely rapid thaw is essential for good post-thaw viability [36, 265, 274, 384, 403]. As the project requires that the BAL cryopreservation chamber can also be used in the FBB and treatment phase of the device, adding more internal components is not feasible due to the effects on the expanded bed culture set-up.

Ice nucleation temperature is also more difficult to manage. Ice nucleates spontaneously, with the cooler the liquid the more probable that it will happen over a shorter time [289]. With a larger volume, and so more water molecules, the chance of a spontaneous event increases, as does the time between ice forming in one section of the BAL to ice being present throughout the BAL [326, 328, 457].

Dehydration of cells takes longer with a larger volume. As individual cells in an ELS may be surrounded completely by other cells, water has further to travel and therefore takes longer to permeate into the inter-ELS space. The resultant reduced rate of water loss in ELS slows the dehydration process, and so the cooling rate must be lowered accordingly, to what may be an otherwise sub-optimal level.

Methods of freezing and thawing individual cells or small groups of cells with high survival rates are well established. Cryopreservation is used widely for the long term storing of embryos, spermatozoa, and oocytes, with protocols being established for many other cell types [84, 106, 150, 175, 402]. The cryopreservation of larger groups of cells or organs is more difficult and there has not been as rapid an improvement over the past few decades in post-thaw viability rates compared to smaller groups of cells. The BAL system represents a ‘halfway house’ – cell

spheroids represent organoids. Progress in this area may have implications for future organ cryopreservation.

This chapter modelled thermal conditions to determine the best material and size for the BAL from a cryopreservation standpoint, and experimentally studied the thermal profiles during large volume cryopreservation.

### **6.1.2. Advantages of Freezing Large Scale Biological Samples**

Donor organs for transplant have only a short window, between 4-24 hours [111, 138, 155, 208, 259, 329], after which point they become non-viable for transplant. More time in which organs remain viable would give hospitals longer to test and match organs to the best effect, reducing the rate of rejection by the recipients. A longer viability time would allow an organ to be transported further, from the places of donation to the places where that organ is most required.

With growth in regenerative medicine, it is also desirable to find methods of preserving created tissue. These can be quite large, and methods of preserving them would enable more common usage in medical settings. Large scale freezing of the BAL will develop techniques useful in this endeavour, as it will consist of a 2 litre volume.

As with single or small groups of cells, there are two different procedures commonly used to achieve tissue survival – vitrification and slow cooling.

### **6.1.3. Vitrification of Large Biological Samples**

Vitrification involves cooling samples rapidly, not allowing the water contained within to freeze. Instead the water enters a glass-like state, where it is very viscous and macroscopically takes the structure of a solid [112, 231, 340, 400, 447].

Although used widely in the cooling of small biological samples, particularly mammalian oocytes and embryos, vitrification becomes more difficult in anything greater than a few millilitres in volume. This difficulty arises from the cooling rates necessary for vitrification to occur. Heat in particular tends to transfer too slowly through an organ to allow for fast enough cooling at the centre of the sample. This results in ice spontaneously nucleating and spreading throughout the sample. As the cooling rate will have been too large to allow for cell dehydration IIF is probable, reducing the viability of the tissue.

Thawing vitrified tissues quickly, above a critical rate, is essential to avoid de-vitrification, in essence the formation of ice crystals [104, 244, 447]. The same heat transfer problems encountered in cooling with larger biological samples also become apparent with rapid warming.

Despite these problems, there has been some limited success in vitrifying small mammalian organs such as rabbit kidneys. Fahy et al. have had some limited success in with kidney preservation [112] and have found solutions to several problems that are faced when trying to vitrify organs.

One method to circumvent the need for rapid freezing and thawing of organs to vitrify is to use a large concentration of CPAs [324]. However, CPAs are often toxic to tissue especially at higher temperatures, and so a large concentration of CPAs can be problematic [447]. Adding more CPAs as a solution cools exposes tissue to the higher concentration of CPAs *only* once the tissue has reached a lower temperature where cell metabolism is lower. The technicalities of this can be difficult. Liquidus tracking, that is cooling to a lower holding temperature just above the ice nucleation temperature for that mixture, where more CPAs are added several times, and then the rapid cooling is initiated is a method developed to try to overcome these technical difficulties [116, 325, 447, 461], albeit with limited success.

The addition of anti-nucleating agents can also be beneficial to vitrification, and to avoid de-vitrification. Research in this area is limited, but Wowk et al. have examined this area [446-448]. Anti-nucleating agents, sometimes called ice-blockers, are chemicals commonly forms of polyvinyl alcohols that in small concentrations can inhibit ice formation. This allows for the vitrification of samples with lower cooling and warming rates, and with lower concentrations of CPAs. There is data on how these ice-blockers interact with human hepatocytes, and this is potentially an area for future research.

#### **6.1.4. Slow Cooling of Large Scale Biological Samples**

The problems associated with slow cooling of biological samples are numerous. As discussed previously, slow cooling is the method by which the organ is cooled at an optimal rate that allows for the cells to dehydrate sufficiently so the cell contents enter a glassy state, thereby reducing the likelihood of IIF, a formation that results in cell death [385].

Extra-cellular ice can damage the usually delicate structure of organs, with ice crystals expanding through areas of least resistance through the tissue. Although this may not damage the individual cells, the larger structure of the organ may be compromised. The viability of cells

cryopreserved in a high cellular density environment, such as an organ, is lower than that of the viability of cells cryopreserved in a low cellular density environment [78]. One reason for this may be that as ice forms, cells are crushed together, damaging the cell membrane and leading to necrosis or apoptosis [303, 427].

The freezing of water releases a large amount of energy (334KJ per Kg [458]). In trying to freeze a large biological sample, energy released from the sample's centre will take a long time to conduct out of the material. This can disrupt cooling curves to a greater degree than smaller groups of, or individual cells. The time taken for freezing to happen can expose the tissue to toxic CPAs at a higher temperature for a longer period of time, thereby damaging viability. Varying warming and cooling rates is not sufficient to compensate for this.

Increasing the pressure to which the organ is exposed while freezing can reduce the concentration of CPAs needed as the nucleation temperature is reduced, and the effects of higher pressure will affect every cell extremely quickly. Currently exposing organs to pressures of above around 70MPa damages them beyond repair [351, 395]. A way to circumvent this damage needs to be established before the exciting prospects of higher pressure cryopreservation are possible.

Despite these issues, there has been some success recently in cryopreserving organs, such as sheep ovaries [46] and claimed success using a directional solidification method with rat livers and sheep ovaries with reasonable viability using slow freezing [14, 138]. Directional solidification is a method where nucleation is triggered at a certain part of the sample. The spread of this ice is controlled by a device that can remove excess heat from the organ effectively, and respond dynamically to temperature readings.

### **6.1.5. Inside the Large Volume**

Having as full as possible an understanding of conditions within the BAL during cryopreservation is essential for optimizing the process. Cooling rates will vary throughout the biomass – biologics are very sensitive to variations in this parameter [241, 271] and so the ranges experienced must be known and tested for acceptability.

The dimensions and construction of the BAL chamber must also be optimized with cooling rates, warming rates, and freezing time in mind. Glass chambers will conduct heat relatively well however they can crack with rapid temperature changes. Plastics are sturdier but have much poorer heat conduction, and metals contract substantially at low temperatures and are expensive to produce. Wall thickness will have a major impact – the thinner the wall the better

the heat conduction but the more fragile the device. The smaller the chamber diameter the greater the surface to area ratio and so thermal variations will be minimized, however the taller and more cumbersome the chamber will be – culture will be more difficult cumbersome and CRF design would have to be adjusted.

The simplest and most accurate method to find the temperature at locations within a tissue is by using thermocouples inside the tissue to give an exact value at certain points – however these only give temperatures at specific points, can move during freezing, and require many hours per experiment. The temperature is assumed to be constant throughout using thermocouples, or the temperature at some specific areas is indicative of the temperature at others. Care must be taken to ensure false readings resulting from heat transfer through the thermocouple wire are not misinterpreted.

Thermal cameras could give a more holistic view of the cryopreservation process thermal profiles, but can only see the surface or wall of a chamber.

Building and testing many different chambers with different materials, wall thicknesses, and sizes – as required for using any experimental method such as thermocouples or thermal cameras - is a costly and time-consuming exercise.

Mathematically modelling the cooling rates at any point within an organ would allow for more detailed information and more accurate cooling profiles to be enacted. Simple modelling has been attempted as a cost and time effective way of understanding the conditions experienced during cooling of the BAL. Modelling can prove difficult due to the non-geometric shapes and the variation in consistency of the material comprising the organ or large cell volume, as will be present in the BAL.

Methods are available that approximate the shape of an organ into geometric constructs for which the thermodynamic properties are easier to calculate and have been studied widely [189], thereby giving estimates of internal heat gradients, based on the surface boundary conditions [351]. Placing organs in cylinders, so giving the organs a geometric shape can more easily approximate the temperature gradients in an organ.

Temperature profiles inside geometric shapes have also been applied historically to cryobiological problems, most notably by Meryman [276]. These have not been developed by various authors specific to their applications, but the basic foundations are the same. A recent review by Xu et al. details various approaches to thermal cooling and ice formation during the cryopreservation process [452]. It is possible to build very advanced models to almost fully characterize a large system on cryopreservation. In this present work the focus is only on the

extremes of the conditions experienced during cryopreservation. If these extremes are acceptable for the biological outcome, then the proposed set-up will allow for acceptable post-thaw outcome in the whole sample. Once an optimized BAL chamber has been established, the modelling can be corroborated with direct experimental measurements – saving laborious trial and error exercises on structures that are completely unacceptable from a cryopreservation standpoint.

## **6.2. Methods**

Several physical large volume samples without biological reagents were cooled in this chapter, the following methods were used:

### **6.2.1. Cryopreserving the 13cm Prototype Chamber with a Planer Controlled Rate Freezer.**

#### **Materials**

2 litre solution of 10% glycerol in water

13cm polycarbonate chamber (3mm wall) with 15cm diameter.

K-type thermocouples

Splint

Picologger software and TC-08 picotechnology unit (Picotechnology, St. Neaots, England, UK).

Laptop

Liquid nitrogen reservoir

Planer controlled rate freezer.

#### **Method**

It had previously been established that 10% glycerol in water has the same thermal properties as 12% DMSO with ELS (unpublished observations), and glycerol has the added advantage of being readily available and translucent.

A small incision was made in the chamber, into which thermocouples were added at set positions, using the splint for support. The freezing mix was then added, and the thermocouples attached to the TC-08 control unit, which was in turn attached to a computer. The Planer freezer's LN<sub>2</sub> reservoir was filled and pressurized, and the freezer set to go to its starting temperature. When the system had reached the start temperature, the chamber with freezing mix and glycerol was loaded into the freezer's compartment and lid sealed. The cooling profile was then run until completion.

### 6.2.1. Cryopreserving the 30cm Prototype Chamber with an Asymptote Large Volume Viafreeze Controlled Rate Freezer.

#### Materials

2 litre solution of 10% glycerol in water

30cm polycarbonate chamber (3mm wall) with 15cm diameter.

K-type thermocouples

Splint

Picologger software and TC-08 picotechnology unit (PicoTechnology, St. Neaots, England, UK).

Laptop

Asymptote Large Volume Viafreeze CRF (Asymptote Ltd. Cambridge, England, UK)

Insulation

#### Method

The thermocouples were set-up as above and added to the chamber. The Viafreeze was lowered to its starting temperature, before the chamber was added, with insulation added on top. The cooling program was then run and temperatures monitored. The set-up can be seen in Figure 22.



Figure 22 - The set-up of the Asymptote Large Volume Viafreeze. On the left is the start of the cooling run, with the cooling plate of the freezer highlighted in yellow, and direction of ice movement noted. The structure in the centre is the thermocouples with their support. On the right is a broader view of the system. For both images, insulation has been removed - normally it would cover the whole set-up. The sample here contained 2 litres of 10% aqueous glycerol solution and the cooling plate was cooled at  $0.3^{\circ}\text{C}/\text{min}$

### 6.3. Modelling for the Bioartificial Liver

Consider any warm solid construct (in the case of the BAL this is a cylinder) placed into a cool water bath. The edges of this construct will cool rapidly and reach an equilibrium temperature

110

with the water bath relatively quickly, while areas further from the edges of the construct will maintain a warmer temperature for longer, as it is insulated by the mass of the construct surrounding it. The most rapid temperature changes will occur around the edges of the construct, while the lowest occur furthest from the edges.

Calculating the central temperature in a mass will give an indication of the extremes of cooling rates in that construct. The central temperature is affected by the distance from the centre to the edge of the object in every direction, as well as the composition and variation in composition of the construct throughout its mass. For an irregular shape with variation in its composition throughout, this proves to be very complex.

For the BAL, several aspects can be controlled or approximated, allowing for easier modelling of the temperature. Firstly the mix to be frozen can be approximated as a homogeneous solution, as the individual components are small and will be mixed thoroughly throughout a large volume. This may lead to inaccuracies over short distances (on the length-scale of the ELS - 500µm and smaller), as local thermal conditions between alginate, liquid, and cells will not be taken into account. Over the whole volume of the BAL however, these differences will be smoothed out. Thermocouples are only accurate to around 1cm in this system, so the homogeneous approximation will not reduce accuracy below the next-best experimental method. The shape of the BAL chamber is also largely under our control.

Take for example a sphere; by definition the centre of the sphere is the exact same distance from every point on the surface in every direction. And if the BAL was made spherical, and based on the assumption that the contents of the sphere are homogenous. Equation ( 1 ) can be used to determine the centreline temperature in this case [189]. Equation ( 1 ) does not take account of any phase changes in the system however, as would occur in the BAL. Equation one is based on - for applied time, size, and temperature - values for the thermal conductance, thermal diffusivity, its density and specific heat. All of these would be taken from experimental values.

$$\theta^* = C_1 \exp(-\varphi^2 F_0)$$

( 1 )

Where  $\theta^*$  is the temperature dependence, defined as  $\theta^* = \frac{T-T_s}{T_i-T_s}$ , With T being the temperature of the centre at time, t.  $T_s$  being the temperature of the surroundings, and  $T_i$  the initial temperature of the object.  $F_0$  is the Fourier number defined as  $F_0 = \frac{\alpha t}{L_c^2}$  where  $L_c$  is the radius of the sphere, and  $\alpha$  is the thermal diffusivity of the material, defined as  $\alpha = \frac{k}{\rho c}$  with k the thermal conductivity of the material,  $\rho$  the material's density, and c its latent heat.  $C_1$  and  $\varphi$  are

constants dependant on the Biot number (a calculable quantity describing heat flow through the material) [189]. These two constants are available for different geometric shapes.

Equation ( 1 ) takes account of all the physical parameters that affect heat transfer. Using it, the central temperature for many geometric shapes can be calculated (namely spheres, long cylinders, and flat planes), so the range of temperature gradients can be approximated.

Sometimes it is beneficial to determine the temperature at any one point inside an object. Take again a geometric object, in this case a long geometric cylinder (closer to the likely shape of the BAL). An adaptation of equation ( 1 ) can be used, as seen below in equation ( 2 )

( 2 ), again not taking account of phase transitions [189]:

$$\theta^* = C_1 \exp(-\varphi^2 F_0) J_0(\varphi r^*)$$

( 2 )

With  $J_0$  being a Bessel Function of the First Kind (a standard mathematical function), and  $r^*$  the relative position of the point chosen in relation to the rest of the object [189]. This becomes more complex and so computer modelling may be easier. Similar adaptations of equation one can be utilized for other shapes. Equation 2 requires no additional experimental information over equation 1. Equation 2 applies to the case on an infinitely long cylinder where thermal conduction only happens radially in the cylinder and not across its length – while the BAL is cylindrical it is not infinite – this will lead to inaccuracies at the wall caps of the BAL chamber which will cool faster than predicted. However as the end caps of the BAL will much thicker than the side walls this inaccuracy can be minimized.

Other factors must also be taken into account, namely the surface conditions. If the organ/cell mass is contained within a skin or container of some kind, the thermal properties of the boundary material must also be considered to determine the heat transfer through the boundary material, before calculating the heat transfer through the mass.

The BAL may also contain some form on internal heating and cooling, the effects of which must be approximated.

#### ***6.4. Simulating the Large Scale Chamber***

Some thermodynamic models of the inside of the BAL had to be created, so that the conditions during cryopreservation were known. If properly calibrated this would allow many test runs to

be carried out theoretically, with only the optimal conditions tested in the large and costly 2 litre set-up. This should also give a picture of conditions everywhere inside the BAL, unlike thermocouples that can only measure specific areas.

### 6.4.1. Modelling

#### Manual Simulation of the Large Scale Chamber

Clearly, with a 15cm diameter chamber (the standard used for the culture phase of the BAL) the centre will be at a different temperature than the edges when cooling, for example as the centre of cooking chicken remains rawer than its edges on heating. Some simple manual modelling was done and tested to quantify the magnitude of this effect.

#### Approximation of a Centrifuge Tube

For practicality, modelling was carried out using the model of a 50ml centrifuge tube containing water in a -80°C freezer. This is a simpler system and easier to define system compared with the BAL and is much quicker and easier to test experimentally.

As only the extremes are of interest (both extremes, and therefore all values must be within an acceptable range [276]), the central temperature of the centrifuge was calculated. The other extreme (the edge), will be close to that of the CRF set-point.

To model the centrifuge tube, the model of an infinite cylinder was used. To attempt this practically, the centrifuge tube was filled with 45ml water and insulated at both ends to reduce edge effects.

After placing the centrifuge tube in the freezer, its cooling takes on three distinct steps. Step one was cooling from its initial temperature (20°C) to the freezing point of water (0°C). Step two was the phase transition, and finally step three - cooling after the water had completely formed ice.

#### Step 1 – Cooling to 0°C

Assuming the water was at a constant temperature as natural convection is much greater than the heat transfer through the sides of the 50ml polypropylene centrifuge tube. If physical properties such as the volume, specific heat capacity, density, and convection characteristics are known, it can be shown that the time taken to cool an infinite cylinder with constant thermal

properties between two temperatures is described by equation ( 3 ) [189]. These physical properties are well defined for water and simple water-solute systems:

$$t = \frac{\rho V c}{h A} \ln \left( \frac{\theta_i}{\theta} \right)$$

( 3 )

Where  $\rho = \text{water density} = 1000 \text{kg/m}^3$

V = Volume of water = 45ml

C = Specific heat capacity of water = 4.18kJ/K

A is the surface area of the tube, calculated to be 0.00754m<sup>2</sup> (sides only, insulated at both ends)

$$\frac{\theta_i}{\theta} = \frac{T_i - T_\infty}{T_{Final} - T_\infty} = \frac{99}{79} \text{ (The } -80^\circ\text{C freezer was actually at } -79^\circ\text{C)}$$

h is the convection coefficient, made from  $h_{\text{air}}$ ,  $h_{\text{water}}$ , and conduction through 1mm sides

$$\frac{1}{h} = \frac{1}{h_{\text{air}}} + \frac{\Delta x}{k_{pp}} + \frac{1}{h_{\text{water}}}$$

$h_{\text{air}} = 10 \text{W/m}^2$  (still conduction)

$\Delta x = 1 \times 10^{-3} \text{m}$

$K_{pp} = 0.12 \text{W/mK}$

$h_{\text{water}} = 500 \text{W/m}^2$

Putting in the values to determine h:

$$\frac{1}{h} = \frac{1}{10} + \frac{1 \times 10^{-3}}{0.12} + \frac{1}{500}, \text{ therefore } \frac{1}{h} = 0.11, \text{ and so } h = 9.06 \text{W/m}^2\text{K}$$

On application of equation ( 3 )

the time taken for the water inside the centrifuge tube to cool from 20°C to 0°C was predicted as 10 mins 22 seconds.

[Step 2 – Freezing](#)

In this step, the water remained at 0°C, changing from a solid to a liquid. It was assumed that liquid remained in contact with the sides of the centrifuge tube throughout this process, and also assumed that in this larger volume there will not be any notable supercooling – the impact of this is discussed below with the experimental data. This is a steady-state problem. To calculate rate of energy loss from the centrifuge tube ( $q_x$ ), equation ( 4 ), heat energy loss for a known temperature gradient below is utilized [189]:

$$q_x = -KA\Delta T$$

( 4 )

Where  $\Delta T = 79^\circ\text{C}$ ,  $A = 0.00754\text{cm}^2$ , and  $K = 9.06$ , giving a heat flux value of  $q_x = 5.4\text{W}$ .

The energy required to freeze 45ml was calculated using equation ( 5 ), the energy required to freeze volume of known mass and known latent heat of freezing.

$$E = m \times E_{freezing}$$

( 5 )

$$= 45 \times 10^{-3} \times 334 \times 10^3 = 15030 \text{ J to freeze.}$$

The time taken was therefore predicted as  $t = \frac{15030}{5.4} = 46 \text{ minutes } 25 \text{ seconds}$  to change phase.

This was of course an approximation. In reality ice will usually form on the outside of the tube and work its way inwards, a process that will lower heat transfer and so this approximation will tend to underestimate the total phase change time, and will also not take into account ice falling below 0°C at some points in the sample while liquid water remains at other points.

### Step 3 – Cooling After Freezing

The temperature inside the centrifuge tube will then asymptotically approach the temperature of the freezer. As theoretically it will never reach it, the time taken to fall below -50°C was chosen.

The Biot Number was calculated to be 0.0065, however the Lumped Capacitance Model (a mathematical simplification) was not used in this case as, although it would be valid for a centrifuge tube, it would not be valid for a 2L mass, which is our final interest. The time taken for the centre of the tube to fall to -50°C can be calculated from Equation ( 6 ) – the time taken for the centreline temperature of an infinitely long tube to fall a certain amount, when there

exists a temperature gradient larger than that amount. Equation ( 6 ) is formed through solving equation ( 1 ) for time.

$$t = \frac{L_c^2}{-\varphi^2 \alpha} \ln \left( \frac{\theta^*}{C} \right)$$

( 6 )

C and  $\varphi$  can be found in the literature for a specific biot number, in this case C=1.016 and  $\varphi = 0.36$  [189].

$$\theta^* = \frac{\theta_i}{\theta} = \frac{T_i - T_\infty}{T_{Final} - T_\infty} = \frac{-50 + 79}{0 + 79}$$

$$\alpha = \text{thermal diffusivity} = \frac{K_{ice}}{\rho_{ice} C_{p_{ice}}} = \frac{2.3}{2 \times 10^3 \times 917} = 1.25 \times 10^{-6}$$

$L_c$  = radius of centrifuge tube = 0.0015m

Entering this into equation ( 6 ) yielded t= 23mins 24seconds to fall from 0°C to -50°C when completely frozen.

To have a complete understanding in this time, a graph of temperature against time was derived from equation (1) and shown in equation ( 7 ) [189] the temperature of the centre at any set time:

$$T = C_1 \exp \left( \frac{-\varphi^2 \alpha t}{L_c^2} \right) \times (-T_\infty + T_1) + T_\infty$$

( 7 )

Where  $T_\infty$  = freezer temperature and  $T_1$  = initial temperature.

This experiment was run with a 50ml centrifuge tube filled with 45ml water and insulated at both ends to compare the theoretical calculated values with experimental data. The graph of equation ( 7 ) for our set-up is shown in Figure 23. As can be seen, a temperature jump was seen in the experimental sample which was not observed in the predicted values, a consequence of supercooling being assumed to be negligible in the model. The effect is short lived however, before the cooling profile 'catches-up' – but means that the model is invalid during supercooling. There is also a deviation particular at lower temperatures. This is a consequence of the measured freezer temperature not being completely accurate – there will be a thermal gradient in the freezer after opening the door to insert the sample which is not taken into account on displayed freezer temperature. Variations in the internal freezer temperature are dampened by the large quantity of ice surrounding the thermometer.

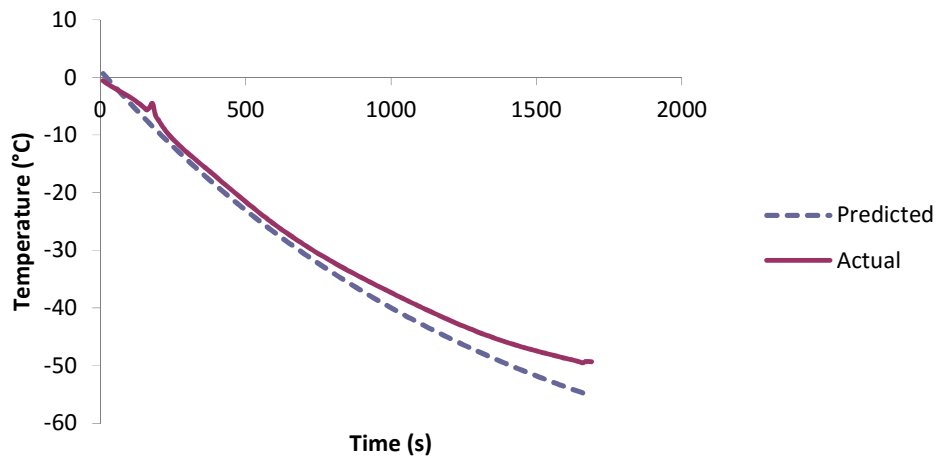


Figure 23 - Comparing the theoretically predicted and actual temperatures inside a centrifuge tube with 45ml distilled water, cooling after the phase transition in a  $-80^{\circ}\text{C}$  freezer. The dashed line is the result from equation ( 7 ), while the solid line is that found by placing a thermocouple in the centreline of the centrifuge tube containing the distilled water. Solid line is average of  $n=5$  experiments.

#### 6.4.2. Calculations for a Large Scale Chamber

The above mathematics was then applied to a larger scale system (up to 15cm diameter). Again, approximations have to be made as the thermal properties of the system were not entirely known or fixed. In time these should become available. Using approximate values, and knowing that the start temperature should be around  $4^{\circ}\text{C}$  but could be reduced closer to the freezing point at  $-4.5^{\circ}\text{C}$  [263].

Using equation ( 5 ) the time taken to freeze should be  $\sim 4$ -5 hours, and the time taken for the centre to fall below  $-50^{\circ}\text{C}$  would then be  $\sim 2$  hours, according to equation ( 6 ).

Of course a larger system will be more complex than this, particularly for the cooling after freezing. As the ice takes such a long time to travel through the system, by the point at which the centre of the chamber solidifies, the edges of that system will already have fallen substantially. This can be overcome with more complex mathematics, which would require a computer program to compute.

#### 6.4.3. Empirical testing of a large scale chamber

Several runs have been carried out with prototype BAL chambers to view the thermal gradients inside. For cooling a smaller 13cm high chamber was used. As very little heat was transferred

through the top and bottom of the chamber this was an acceptable substitute for a taller 30cm chamber. Ultimately, a taller BAL chamber will be cryopreserved on its side. The facilities to do this did not exist at time of writing, but an upright chamber should give broadly similar results, as the materials, walls, and thickness are fairly consistent. Using this system will also allow for a test of the accuracy and calibrate the modelling.

### Temperature Profiles on Cooling

The cooling profile in a large volume was measured using a chamber with heat transfer possible only through its walls. As modelling was very much simplified by only looking at a wall, this can be more easily applied to a model. One factor that needs to be determined to calibrate the model is the heat transfer of the walls. Although the wall thickness and composition is known, there will also be silicone tubing running around the inside of the wall (to help oxygenate the cells when fluidising). The silicone will reduce heat transfer so models will tend to overestimate cooling and should be calibrated with experimental results.

Prior to the addition of silicone tubing, the theoretical value for the heat transfer coefficient of the chamber is  $67 \text{ W/m}^2\text{K}$  at  $20^\circ\text{C}$ . This is based on a polycarbonate chamber with a wall thickness of 3mm. The conductivity of polycarbonate is dependent on the grade of the polycarbonate, and the temperature- higher temperatures resulting in a higher thermal [102].

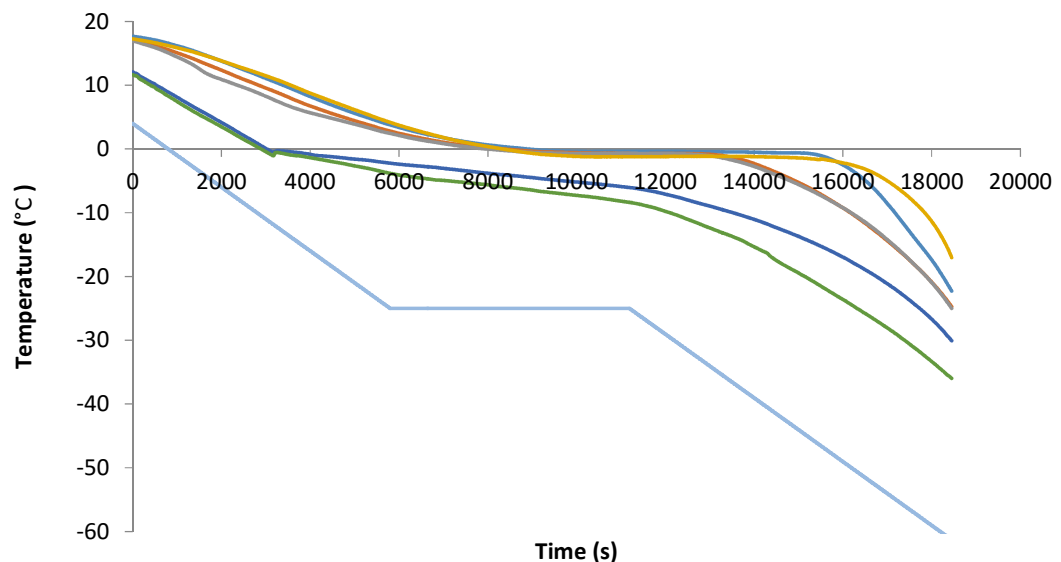


Figure 24 - Temperature profiles inside 2L volume being cryopreserved in a chamber with diameter 15cm and height 13cm. The chamber was filled with 10% aqueous glycerol solution. The lower blue line is the CRF temperature; and the green, dark blue, grey, orange, lighter blue, and yellow lines were the temperatures measured by k-type thermocouples on the internal base of the chamber, 10mm, 20mm, 30mm, 40mm, 50mm, and 70mm from the chamber wall respectively.

The main point to notice from Figure 24 is the long period of time spent in a liquid state (above  $-4.5^{\circ}\text{C}$ ) before the phase transition in the centre of the sample (furthest from the edges). This results in a volume of ELS experiencing a higher DMSO concentration for a longer period of time. The effects of this on post-thaw function are examined in future chapters. Also of note is the long lag time between the CRF and liquid temperatures. While it is ideal to lower the sample temperature below  $-80^{\circ}\text{C}$ , the CRF runs out of liquid nitrogen before this can be achieved – a problem which can be overcome with a Stirling Engine CRF [65, 287].

A thicker wall was also considered. Using the next available thickness of 5mm resulted in a heat transfer coefficient of only  $40 \text{ W/m}^2\text{K}$  at  $20^{\circ}\text{C}$ . This was therefore excluded as a possibility as cooling would take far too long; a thinner wall would be too fragile.

### **The EF600 Stirling engine based controlled rate freezer**

The EF600 is a CRF (controlled rate freezer) developed by Asymptote in Cambridge [65, 265, 287]. It is a revolutionary design as it is powered solely by electricity. No liquid coolant, such as liquid nitrogen is used. This has several advantages; the sample never comes into contact with liquid nitrogen, a substance that is usually non-sterile, with a prohibitively expensive sterile price. Controlled rate freezers also have a finite operating time; they can only run for as long as there is enough liquid nitrogen in the tank to maintain temperature – often these cannot be topped up during the run. Running on electricity, the EF600 can run indefinitely, and so extremely slow and sensitive cooling profiles can be tested. The EF600 is constrained by the maximum power of the Stirling Engines – it cannot cool a very large sample very quickly. This is merely a physical problem – theoretically larger or more engines can be used to increase capacity [65, 287].

## ***6.5. Physical Parameters of the Asymptote Large Volume Liquid Nitrogen Free Large Volume Freezer***

### **6.5.1. Cooling and Equilibrium with 10% Glycerol**

It had been established in the lab that 10% glycerol in water (v/v) was a suitable thermal substitute to ELS in 12% DMSO in Viapsan (v/v), and had the advantage of being inexpensive and translucent.

The thermal profiles were monitored in the full sized 30cm chamber containing 2 litres of 10% glycerol (v/v) when it became available. The chamber was cooled on its side, with a curved cooling plate as can be seen in Figure 22. Although the chamber capacity is a little over 7 litres, 5 litres of this would normally contain culture medium for the culture period as would be removed for cryopreservation, leaving 2 litres biomass and 5 litres air. The chamber was essentially a polycarbonate tube with 3mm wall thickness, sealed at both ends.

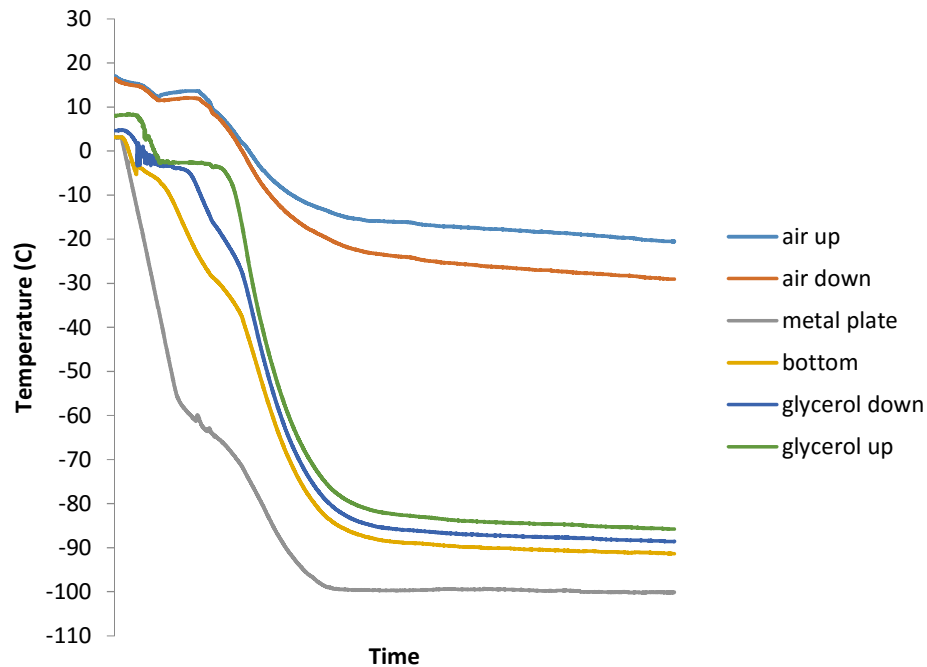


Figure 25 - Thermal profiles in the LVCRF system during cooling and at the equilibrium level. As can be seen, the glycerol substitute has low variation in its final temperature, though the upper section of the chamber only containing air maintains a significantly higher temperature. K-type thermocouples were placed on the metal plate of the CRF (grey), the bottom internal wall of the cryopreservation chamber (yellow), 10mm from the chamber wall (dark blue), 10mm from the glycerol surface – 60mm from the chamber wall (green), 10mm above the glycerol in the air component of the chamber (orange), and 10mm from the upper wall of the chamber in the air component (light blue). The chamber was cooled at approximately 0.3°C/min, slowing to 0.1°C/min between -60°C and -80°C while latent heat of freezing was released. Chart shows data recorded over 20 h.

Thermocouples were attached to the upper section of air in the chamber (air up), the lower part of the air section (air down). The metal cooling plate of the LVCRF (large volume controlled rate freezer), the inner base of the chamber (bottom), 1 cm above the base of the chamber (glycerol down), and the top of the glycerol in the chamber (glycerol up). The LVCRF was cooled at 0.3°C/min, and the system then allowed to thermally equilibrate. The entire run shown in Figure 25 took 20 h.

As can be seen from Figure 25 a large thermal gradients exist during the cooling process, as does a large lag time between the LVCRF plate cooling and the glycerol solution's temperature. After the run had been completed, no large thermal gradients persist in the glycerol (ELS substitute).

While the air temperature in the chamber is much higher, this does not seem to affect the glycerol significantly. This shows that the LVCRF is sufficiently powerful to cool the chamber to below -80°C, and that the chamber is sufficiently insulated to prevent the equilibrium environmental chamber warming the biomass component adversely.

### 6.5.2. Thawing the Chamber with 10% Glycerol Solution

The chamber from Section 6.5.1 was thawed by turning off power to the LVCRF. As can be seen from Figure 26, thawing without using external assistance takes well over an hour – an unacceptable long period of time for a good post thaw outcome based on previous literature where thawing is done in minutes with small volumes. It is clear that new thawing strategies must be developed.

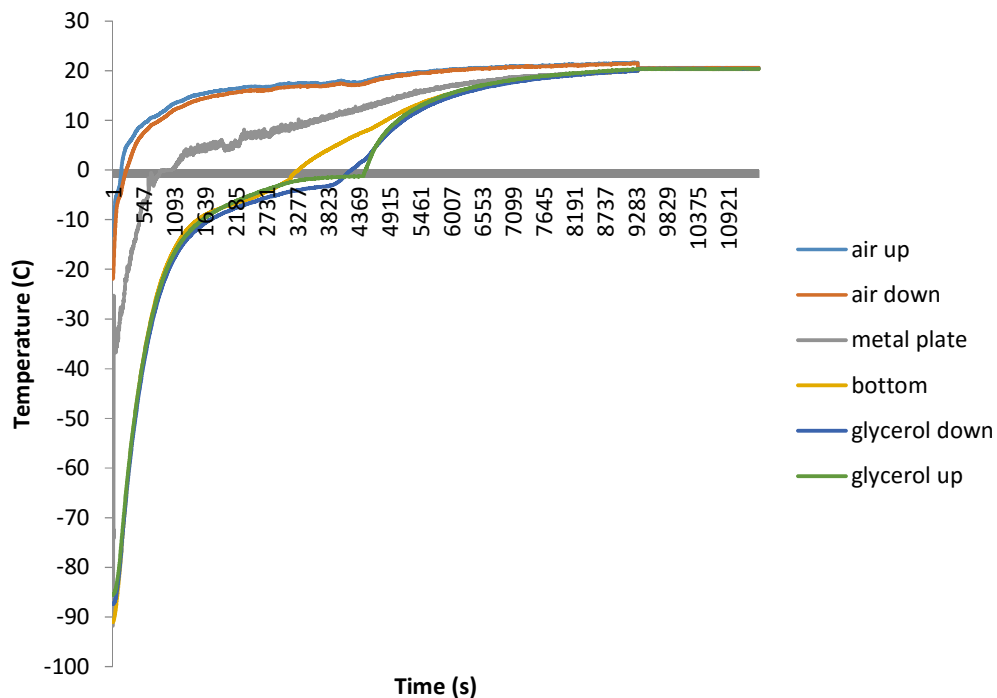


Figure 26 - Thawing of the 30m chamber. As can be seen, thawing is much delayed in the biomass and thawing takes in excess of one hour. This is a continuation of Figure 27, with thermocouples placed in the same locations. The chamber started here cryopreserved, and was left to thaw in air at 20°C. Total thawing time was approximately 90 minutes.

## 6.6. Summary and Conclusions

In this chapter, a simple model was developed to monitor the cooling rate of the 2 litre BAL during cooling. This gave considerable time and resource saving over a purely experimental

approach. The final chosen design for the BAL chamber was a 3mm thick polycarbonate design. While most bioreactors in the literature are made of steel or glass [101, 363], these were excluded as options due to the cost of manufacture for a disposable device, and due to the propensity for glass to shatter while undergoing rapid temperature changes. Polycarbonate is also used widely in the manufacture of biological equipment and so unidentified interactions between the polycarbonate and ELS are unlikely [281].

Experimental data has shown that the cooling and warming are likely to take on the order of 4 and 1.5 hours respectively, with deep local variations in cooling and warming rates. This is in agreement with published work [276]. The model (while simpler than some other similar systems [189, 452]) also showed that cooling time on the order of 4 hours was likely with the BAL, and so the model and experimental results are in agreement.

Meryman conducted a large study on large volume freezing, with similar results to that seen here – ie. a rapid initial cool, a slow phase transition, followed by a relatively rapid cool after the phase transition [276]. The later areas to freeze the faster their subsequent cooling [276]. Rapid cooling rates are typically seen after nucleation on both the large and small scale, and so many cooling profiles hold the temperature of the freezer during this phase transition [150, 289]. This reduces the temperature difference between the biologic and the freezer post-phase transition and so reduces the subsequent cooling rate to ensure it remains at the optimal level.

While cooling profiles with a hold were attempted using a large volume, they were found to be less effective at reducing post-phase transition cooling, particularly far from the wall in the sample, due to the high thermal distances involved in this study. Determining the biological effects and adapting the system to address these spatial variations is considered in later chapters.

The time taken to cool the system is also important for the choice of controlled rate freezer. Liquid nitrogen controlled rate freezers are most commonly used in cryobiology but have many limitations as discussed previously [65, 287]. A key limitation is the amount of coolant required for cooling of a large mass – a larger thermal mass takes more energy to cool directly, but also as a large mass takes longer to cool more liquid nitrogen coolant is required to maintain the system at a lower temperature. As the operating time of the planer controlled rate freezer used in this project is only 3-4 h when loaded with a 2 litre biomass, this chapter also established that a Stirling engine cooler (with indefinite operating time) such as an Asymptote Viafreeze would be more appropriate for this project.

One limitation of the viafreeze system is it has a maximum energy removal rate of a few hundred watts. The theoretical maximum heat transfer rate from the 3mm polycarbonate chamber is 67

W/m<sup>2</sup>K. Using the 30cm length and 15cm diameter dimensions, combined with the desired slow cooling rates of 0.3°C/min this chapter established that a ViaFreeze system can draw enough heat energy out of the system to be a viable controlled rate freezer for large volume cryopreservation.

In conclusion, this chapter modelled the extremes of cooling rates and times likely to be experienced in a BAL used for cryopreservation. When this was found to be acceptable, experimental measurements corroborated these results. The impact of removing excess medium during the freezing process to leave a large air fraction within the BAL during cooling was established experimentally. The heat extraction rates required were also determined, and this was found within the capabilities on a ViaFreeze controlled rate freezer system. This chapter established that moving away from a glass to polycarbonate BAL chamber was optimal for the cryopreservation of the 2 litre biomass.

# 7. A Novel Method to Simulate Large Scale Freezing

## 7.1. Introduction

### 7.1.1. Chapter Overview

Approximate cooling profiles that will be experienced during the cryopreservation of the BAL device were established in chapter 6. This chapter focuses on the biological outcome of these physical characteristics. To reduce time and cost of each experiment, a method to mimic the physical and biological conditions experienced on a 2 litre scale was developed, but using only a 6ml volume [210]. The method, its results, and its justification are the focus of this chapter.

The process of ice formation and propagation during cryopreservation impacts on the post-thaw outcome for a sample. Two processes, here termed network solidification and progressive solidification, can dominate the water-ice phase transition with network solidification typically present in small sample cryo-straws or cryo-vials [210]. Progressive solidification is more often observed in larger volumes or environmental freezing [179]. These different ice phase progressions could have a significant impact on cryopreservation in scale-up and larger volume cryo-banking protocols necessitating their study when considering cell therapy applications [111, 244].

This chapter determines the impact of these different processes on the BAL system during cryopreservation, which should highlight the difference between small-scale and large-scale experiments. This chapter further develops a method to replicate these differences in an economical manner.

It was found that progressive solidification resulted in fewer, but proportionally more viable cells 24 h post-thaw compared with network solidification. The differences between cells cryopreserved using different methods diminished at later time points post-thaw as cells recovered the ability to undertake cell division, with no statistically significant differences seen by either 48 h or 72 h in recovery cultures.

Thus progressive solidification itself should not prove a significant hurdle in the search for successful cryopreservation in large volumes such as the BAL. However, some small but significant differences were noted in total viable cell recoveries and functional assessments between samples cooled with either progressive or network solidification, and these require further investigation.

### **7.1.2. Recap of the Need for Large Volume Cryopreservation**

While the technology for growing an immortalised hepatocyte cell line (HepG2), encapsulation in alginate beads, and proliferating & conditioning of the cell spheroids within the beads has been demonstrated at the large scale with the BAL, storing the BAL long term is not currently possible [63, 101, 361]. This is the general theme of the thesis, which may have been spotted by now, but I'll give a brief recap here with a particular focus on the differences between large and small volume cryopreservation, the theme of this chapter.

Widespread uptake of the BAL technology can only realistically be achieved with cryopreservation as a component of the manufacturing strategy [111, 244]. On demand manufacture of the BAL is not feasible, neither on the basis of cost nor logistics. A single disposable cassette encompassing all processing steps (perfusion, cryopreservation, cell conditioning), would greatly simplify safety and regulatory requirements, provide robust delivery to end users, and facilitate safe delivery in the clinical environment. However, for clinical delivery of a BAL, cryopreservation of up to 2 liters of alginate encapsulated cell spheroids (ELS) are required in a single treatment and these would be ideally contained within a cylindrical cell cassette. This results in a packed product depth of up to 70 mm in a cylindrical chamber of length 30cm held horizontally. Whilst there are reports of the cryopreservation in bags of large volumes (>100 ml) of adult stem cells [379], mammalian tissue culture cells [171, 172, 214] and ELS [265], the geometry of these samples have been those of a thin slab (2d sample) less than 20 mm in thickness. These experience lesser thermal gradients than in our system. The bulk cryopreservation of mammalian cells at a scale and format required for a BAL, or indeed other cell therapies, has not been extensively studied previously.

### **7.1.3. Smaller Volume Cryopreservation**

The physical determinants of the freezing process in either large or small volumes are fundamentally different. In low volume samples (e.g. in straws, or cryovials with volumes <2ml) at the typical cooling rates used in cryopreservation only small temperature gradients tend to occur throughout the sample [210]. The whole volume generally undercools in a uniform way, i.e. cooled below the equilibrium melting point (the highest temperature at which ice and water can co-exist in steady-state) before ice nucleation commences [179, 277, 286, 289, 326]. Following the initial ice nucleation, which can be induced by a nucleating agent (though remains a random process) [167, 170, 263, 289], growth of a continuous ice network throughout the

whole sample occurs rapidly, resulting in a coexisting, continuous phase of freeze concentrated material in which the excluded solutes and cells are distributed [221, 289-291]. As a result of the migration of water from the freeze concentrated matrix, this ice network grows as a coherent entity during subsequent cooling. The structure of the ice network and of the corresponding freeze concentrated matrix is determined by the nucleation temperature [18, 289] and not the rate of cooling [362] – unless material spends considerable time at high subzero temperatures. In materials science this solidification process is called cellular growth [381]; however in order to avoid confusion when considering cell cryopreservation in a biological context, in which cell growth refers to cell proliferation, this mode of ice solidification is referred to here as network (or dendritic) solidification (NS).

#### **7.1.4. Bulk Samples**

In bulk samples, such as the BAL pictured in Figure 27, significant temperature gradients may exist between the cooling interface (often the outer surface of the sample) and the bulk volume unless infinitesimally slow cooling rates are applied [276, 452]. Localized undercooling can easily occur at the container wall whilst there remains a gradient in the bulk sample leading to temperatures remaining above the equilibrium melting point for a significant time [276, 452]. Nucleation of ice will occur at the cold wall and ice will develop into the solution which was initially at a temperature above the equilibrium melting point as seen in chapter 6. As cooling progresses across the sample and the ice nucleation temperature is achieved, an ice front perpendicular to the heat transfer vector front moves through the sample [356]. The structure of the ice front is determined by a number of factors including the nucleation temperature, the rate of heat extraction, and localized inhomogeneities in temperature across the ice front, further complicated by release of latent heat of the ice crystallization process [276, 277, 289, 362]. Depending on the solute composition and the rate of growth of the ice front, solute rejection (including rejection of structures such as cells) can occur ahead of the advancing ice interface [164, 221]. In this configuration, only the small proportion of the sample in contact with the cold wall was initially undercooled to any significant degree. In metallurgy this mode of solidification is referred to as progressive or parallel solidification [381] and here referred to as PS when considering ice formation.

In order to develop protocols rapidly and efficiently for the cryopreservation of large volumes it is necessary to develop and validate a scale down method to emulate the process of ice formation that occurs within a large volume in comparison to that within a standard cryovial. This approach allows multiple samples to be tested within the same run, and also the effects of

thawing to be de-coupled from the freezing step which produces either PS or NS (progressive or network solidification). A technique was also designed to reliably produce PS in small volumes, removing the compounding factor of sample volume on the ice solidification process. In this thesis, I examined the viability and cell function of ELS [101, 210, 265] following either PS or NS. In addition it was determined, by CryoSEM, the structure of the ice crystal networks and the residual freeze concentrated matrix following water to ice phase transition by these two methods.

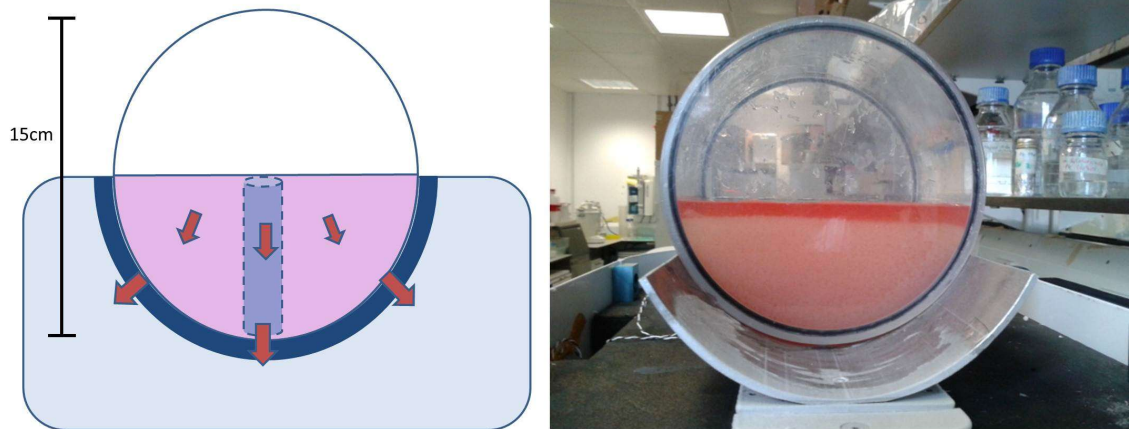


Figure 27 - Schematic and image of the large volume cylindrical chamber. Excess medium is drained out of the prototype chamber prior to cryopreservation and the resulting ELS thermal mimic (10% glycerol) fills the BAL chamber halfway, (the remaining upper volume containing air). The BAL chamber was then placed on a Stirling engine cooled metal plate (dark blue). The arrows indicate heat transfer during cryopreservation, whilst the dashed outline of a vial is overlain, indicating the approximate area modelled with the heat transfer modules in Figure 28. The set-up is also depicted in Figure 22 on page 110.

## 7.2. Materials and Methods

### 7.2.1. Establishment of cooling profiles in a representative large scale volume containing an ELS thermal mimic.

#### Materials

Polycarbonate cylindrical chamber.

Silicone oil ( 85409 Sigma, Dorset, UK)

Large volume VIAfreeze (Asymptote, Cambridge, England, UK)

k-type Thermocouples and recording laptop (Picotechnology, St. Neaots, England, UK)

Glycerol (Sigma, Dorset, UK)

#### Methods

For typical PS (progressive solidification) in a true large volume experiment, a prototype of the cylindrical BAL cassette constructed out of polycarbonate and containing 2000 ml of a 10% glycerol in water (v/v) solution as an ELS thermal mimic was cooled on its side on a modified VIAFreeze controlled rate freezer (Asymptote, Cambridge, UK). Good thermal contact was achieved via a curved plate attached to the cassette (Figure 27). To further enhance thermal contact between the cassette and the sample plate a film of low temperature silicone oil (Sigma, 85409) was applied to the sample plate. Thermocouples were placed throughout the chamber to measure thermal profiles in the ELS thermal mimic, using 10% glycerol which was established previously has equivalent thermal properties to our alginate encapsulated biomass (data not shown).

### 7.2.2. Modification of the Controlled Rate Freezer to Achieve NS or PS in small volumes during cryopreservation

#### Materials

Modified EF600 (Asymptote ltd.)

6m vials (Scintillation vials in this case, chosen for their dimensions, Sigma Z376825, Dorset, England, UK)

Thermocouples and recording laptop

#### Method

Progressive solidification can be readily carried out in a scintillation vial using a controlled rate freezer with an acetal insert. The EF600 cools a metal plate. If a scintillation vial is placed on this plate, heat will be transferred through the vial's base. If this vial is in acetal, a thermal insulator, it will only conduct heat through the base. If the base is taken to be the wall on the BAL, and the top of the vial the centre of the BAL, the scintillation vial can accurately represent a column inside the BAL. Changing the cooling rates can vary the speed of the ice front growth.

A controlled rate freezer (EF600-103, Asymptote, Cambridge, UK) was modified to achieve either NS or PS during cryopreservation by the addition of two modules designed to take polypropylene scintillation vials (Sigma, Z376825, 16 mm x 57 mm). One module was made of aluminium, the other of acetal (Figure 27); these materials are good and poor conductors of heat respectively. These modules were fixed to the flat cooling plate of the EF600-103. Thermocouples (K type) were used to measure the temperature at the base, middle, and upper sample volume inside

the vial, (0 mm, 20 mm, and 40 mm from base respectively) the thermocouples were connected to a Pico Logger (Pico-technology).

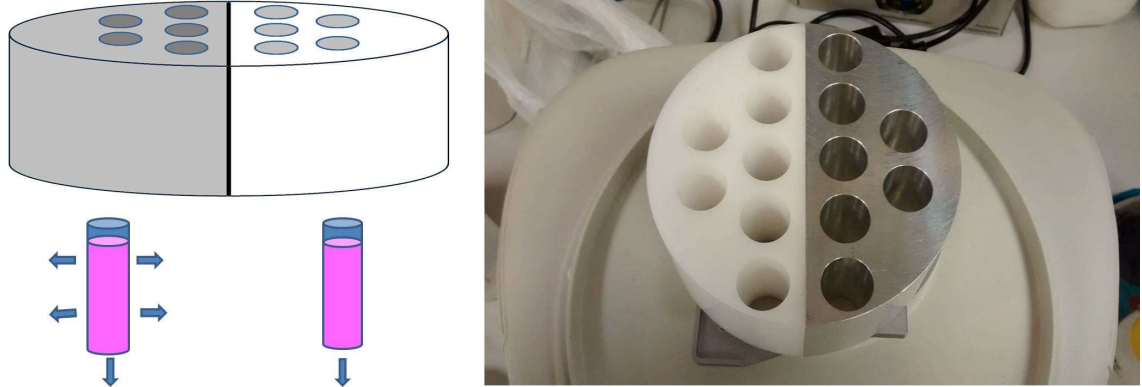


Figure 28 - The two different heat transfer modules designed for the EF600-103 CRF. On the left an aluminum module allowed for maximum heat transfer between the vial and the insert, on the right the acetal insert only allowed for heat transfer between the bottom of the vial and the EF600-103 cooling plate. Both modules operated concurrently during cryopreservation, allowing the study of up to seven replicates in each condition, at identical cooling rates.

### 7.2.3. Cryopreservation Protocol

#### Materials

Freezing solution (DMSO in Viaspan)

Icestart nucleators (Asymptote Ltd. Cambridge, England, UK)

ELS

EF600 CRF

Culture medium

37°C Water bath

#### Method

For small volume PS or NS studies, 5ml aliquots of ELS were harvested and mixed 1:1 with a freezing solution (24% DMSO, 76% Viaspan v/v) precooled to 4°C, and once equilibrated (15 mins), 80% of the excess CPA supernatant was removed, giving a final volume of 6ml of 12% Me<sub>2</sub>SO, 38% Viaspan, and 50% ELS in culture medium, by volume. Icestart beads (1% w/v) (Asymptote) – sterile insoluble granules - which induce ice nucleation close to the equilibrium melting temperature of the mixture, were added and these sank by gravity to the base of the vial. These vials and the CRF were cooled to 4°C before 5 vials (containing 6ml each) were placed in the aluminum module, while 5 were placed into the acetal module (see Figure 27). The EF600-103 was programmed to cool at 1°C/min from 4°C to -80°C. The samples were held in the EF600-

103 at -80°C for 1 hr after the cooling cycle was complete, before being transferred to a -80°C freezer for 7 days.

The samples were warmed rapidly during 330 seconds in a 37°C waterbath until all the ice had melted (yielding an approximate warming rate of 15°C/min). The Me<sub>2</sub>SO was diluted out of solution during a 10 minute stepwise process with prepared chilled culture medium, with residual ice start granules remaining at the bottom of the tube and easily avoided during decanting. The samples were re-cultured in a 5% CO<sub>2</sub> humidified incubator at 37°C.

#### **7.2.4. Cryo Scanning Electron Microscopy (CryoSEM) of samples cooled by PS or NS**

##### **Materials**

Cryo scanning electron microscope

Cryopreserved samples

Water bath

Metal bracket dimensionally appropriate for samples

##### **Method**

To observe physical changes in the structure of the samples, CryoSEM (Cryo electron scanning microscopy) was carried out [64]. Samples recovered from storage at -80°C were warmed slightly (25 seconds in a 37°C waterbath) to loosen the ice matrix from the container wall, allowing the bulk frozen samples to be removed rapidly and transferred onto dry ice (-79°C) without re-warming. These were wrapped in foil and stored on dry ice before being transferred to a -80°C freezer.

Under liquid nitrogen, each sample was held in a metal bracket and split horizontally using a blade, giving a circular cross-section. This was transferred into a cryo scanning electron microscope (FEI XL30 FEGSEM with a Quorum pp2000 cryo-stage) and etched at -80°C, before being coated in a thin layer (~20nm) of gold. The samples in the microscope and images were captured at 5kv using an Everhardt Thornley secondary electron detector. Substantial assistance with cryoSEM was given by Jeremy Skepper of Cambridge University, in whose lab the cryoSEM imaging was undertaken.

### 7.3. Results

#### 7.3.1. Measurement of the Thermal Histories of the Different Cooling Processes in both the Large Volume Prototype Chamber and the Scale-Down Modules

Measured temperatures within the large volume sample (Figure 29) containing 10% glycerol in aqueous solution (v/v) show large temperature gradients between the wall of the cassette (in contact with the cooling plate) and the deeper (more central) layers of the sample. Whilst the sample layer adjacent to the cylinder wall reduced in temperature approximately linearly, the central sample layers experienced delayed cooling, non-linearity of temperature change, and eventual solidification, with a temperature plateau existing in the core of the sample for some considerable time (in the region of 150-180 minutes) at the equilibrium melting temperature before solidification occurred.

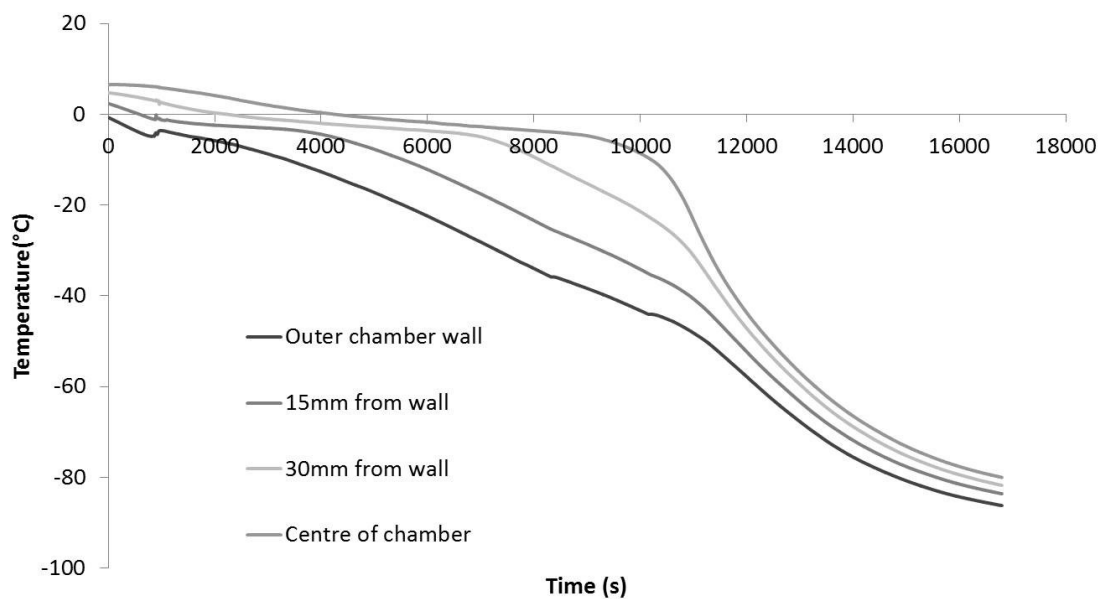


Figure 29 - Measured temperature profiles inside the BAL chamber during cooling of a thermal mimic. Approximately 2000ml of 10% aqueous glycerol solution (having the same thermal properties of ELS) was cooled in the large volume freezer, with pico-logger k-type thermocouples placed at progressively deeper intervals between the wall and the centre of the chamber, at 15mm intervals. Measurements taken at 10 second intervals. The freezer was programmed to cool from 4°C to -80°C at approximately -0.5°C a min. This differs from work in chapter 6 due to a linear CRF profile being used and detailed study of the internal profiles in the Stirling Engine large volume CRF. These data were repeated 3 times, with a typical run presented above. Data here is for the full sized BAL as opposed to those of different sizes in chapter 6.

In the vials processed in the acetal or aluminium modules for the EF600-103, producing either PS or NS (progressive solidification or network solidification) respectively, the monitored

temperature profiles differed between the two processing conditions (Figure 30). With vials in the acetal module, nucleation occurred at the bottom of the cryovial (again, next to the cooling plate of the cryo-cooler) where a small amount of undercooling is evident, whilst the remainder of the sample remained above the melting point of the solution. Ice growth occurred progressively (and in this case – vertically) within the remainder of this sample and no further significant undercooling was evident (see Figure 30) emulating the temperature profile, characteristic of progressive solidification seen in a large volume sample (Figure 29). The whole of the sample volume within a vial in the aluminium module cooled uniformly below the equilibrium melting temperature of the solution before ice nucleation occurred and solidification then progressed instantaneously and in a relatively uniform manner throughout the cryovial, with no large temperature gradients being observed (Figure 30).

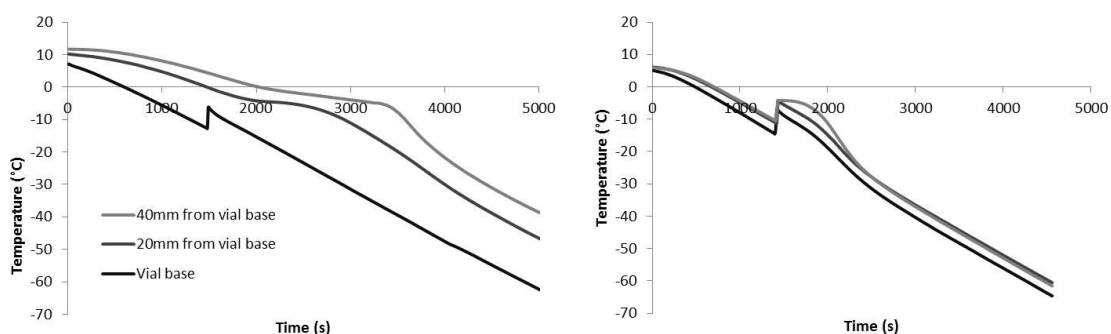
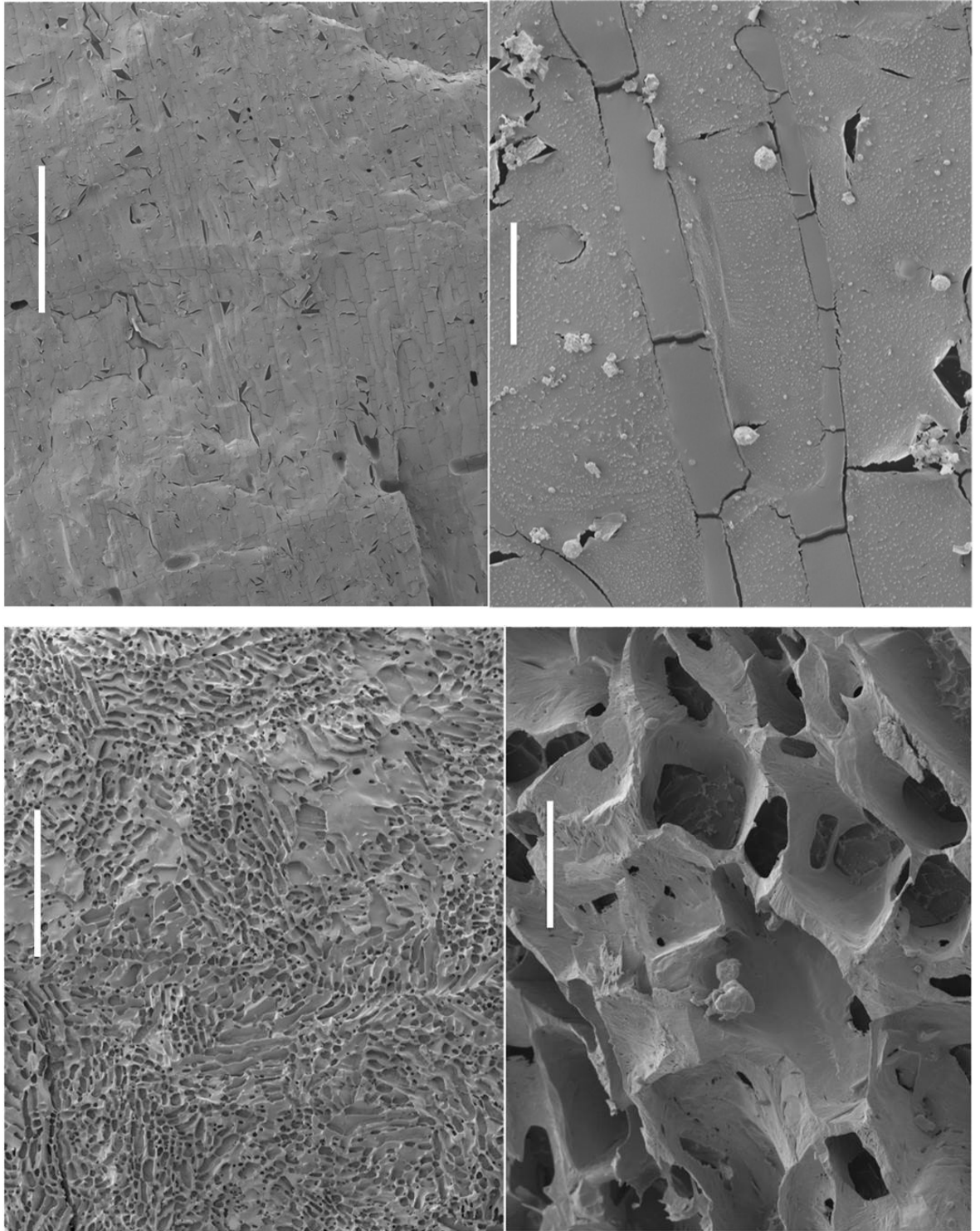


Figure 30 - Temperature profiles in the heat transfer modules measured on the EF600-103 controlled rate freezer. K-type thermocouples were inserted at the base of the sample (which was placed on top of the cooling plate of the freezer) and at progressively deeper intervals. The temperature profiles were recorded in both the acetal module (left) and in the aluminium module (right). The EF600-103 was cooled from 4°C to -80°C at 1°C/min, with samples containing 6ml ELS in 12% DMSO.

The exact timescales and profiles of each of these cooling profiles could be adjusted through the program on the EF600 CRF.

### 7.3.2. Characterization of the Ice Morphologies in the Different Freezing Processes in the Scale-Down Modules

The structure of the ice and the freeze concentrated matrix was very different in samples processed from vials within the two different modules where either NS or PS was developed (Figure 31). A planer ice structure was present under conditions of PS in samples processed in the acetal module (Figure 31), with vertical ice crystals forming in the sample, entrapping ELS between ice crystals. Following NS (cooling in the aluminium module) a multiple dendritic (network) ice structure was apparent, with ice entrapping freeze concentrated matrix including ELS (Figure 31).



*Figure 31 - Cryo-Scanning Electron Microscopy (Cryo-SEM) presenting differences in ice structure between progressive solidification (top) and a network solidification (bottom). The scale bar indicates 1mm on the left hand images, while 50 $\mu$ m on the right hand images in both cases. Progressive solidification exhibits a large and homogeneous ice crystal, indicative of slow growth during formation, while network solidification results in a profoundly separate, disordered dendritic ice structure.*

### 7.3.3. Viability and Viable Cell Number

The cell viabilities, the viable cell numbers were quantified following either NS or PS at 6, 24, 48, and 72 h post-thaw (Figure 32). The samples processed in the aluminium module (NS), displayed a trend towards higher average viability at all time points compared with samples processed in the acetal module; significance was noted for 24 hr ( $p < 0.05$ ,  $n = 5$ ). The viabilities in both sample sets then further recovered and increased significantly ( $p < 0.05$ ) with length of time in culture post-thaw out from 6hr to 72hr, from  $53.2 \pm 11.5\%$  to  $75.8\% \pm 7.1\%$  and from  $41.4 \pm 13.1\%$  to  $72.8\% \pm 5.1\%$  for the samples experiencing either NS or PS respectively. A similar pattern was true for total viable cell numbers (Figure 32) increasing significantly from  $8.1 \pm 1.6$  to  $13.0 \pm 1.7$  million cells/ml following NS. For samples from PS, cell density recovered significantly from a nadir at 24hr -  $5.9 \pm 1.1$  million cells/ml to a maximum of  $12.3 \pm 1.3$  million cells/ml at 72hr post-thaw; thus PS was significantly worse at 24hr ( $p < 0.05$ ,  $n = 5$ ) but not different by 72 hr.

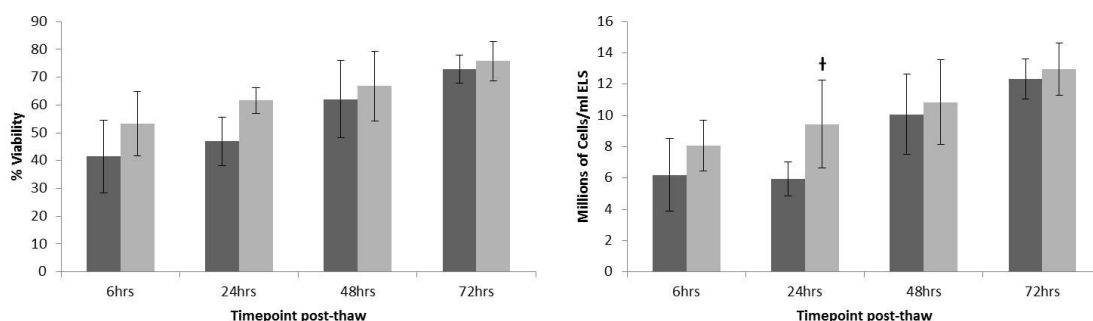


Figure 32 - The cell membrane viability (left) and viable cell number (right) of samples experiencing either progressive solidification or network solidification during cryopreservation. Although network solidification (light grey) produces a better post-thaw outcome at 24hr ( $p < 0.05$ ,  $N = 5 \pm SD$ , marked by \* and + for viability and viable cell number respectively, determined through unpaired student's t-test), these differences disappeared by 48hr and 72hr in post-thaw cultures. Both PS and NS samples' viability and viable cell number increased significantly from 6hrs to 72hrs ( $p < 0.05$ ).

### 7.3.4. Metabolic Activity

Metabolic activity of the samples post-thaw was analysed using MTT. This was related to either the production per unit ELS (Figure 33), or to a viable cell number and so function per cell - at 6, 24, 48, and 72 h post-thaw could be calculated. This is an important comparator to identify differences between cell populations from different culture batches. MTT metabolism per unit ELS (Figure 33), showed no significant difference between either NS or PS samples. When the MTT metabolism was expressed per million viable cells (Figure 33), the mean production per cell

number appeared higher in PS compared with NS at all time points, although not reaching significance ( $p>0.05$ ,  $n=5$ , in each case).

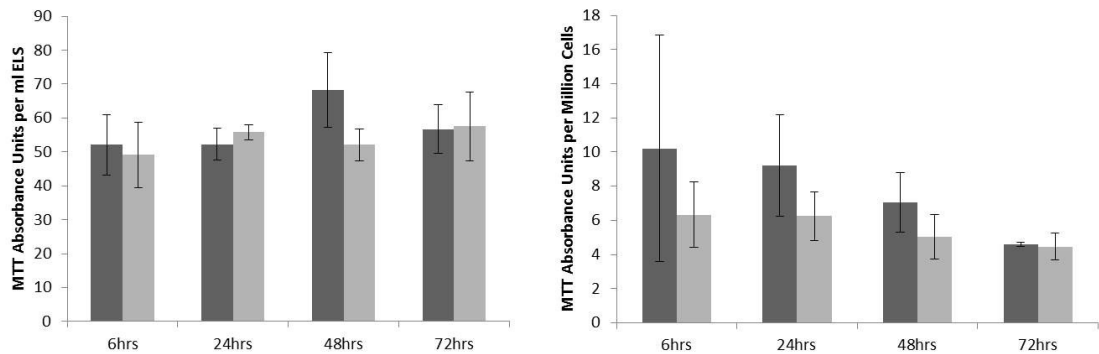


Figure 33 - Metabolic activity in ELS: MTT absorbance units per ml ELS and per million cells, between samples experiencing either progressive solidification (darker) or network solidification (lighter) during cryopreservation. No statistically significant differences between the samples were observed at any time-point. No significant differences in MTT absorbance were observed intra-sample set between 6 and 72 h, using an unpaired student's t-test.  $N=5 \pm SD$

### 7.3.5. Protein Synthesis

Sandwich ELISAs determined protein production per million cells per 24 h in samples collected 1-3 days post thaw. As can be observed in Figure 34, of the three quantified proteins, Alpha-fetoprotein (AFP) did not exhibit a significant difference at any time point.

In contrast, albumin production in the PS samples was significantly higher ( $p<0.05$ ,  $n=5$ ) 24 h post-thaw being measured at  $46.7 \pm 11.5 \mu\text{g}$  per million viable cells per 24 h, compared to  $30.9 \pm 4.4 \mu\text{g}$  per million viable cells per 24 hr following NS.

Alpha-antitrypsin was also significantly improved ( $p<0.05$ ,  $n=5$ ) 24hr post thaw, at  $18.8 \pm 4.8 \mu\text{g}$  per million viable cells per 24 hr, compared to  $12.2 \pm 2.0 \mu\text{g}$  per million viable cells per 24 h following NS.

All protein production capabilities in either NS or PS samples improved significantly from 24 h to 72 h post-thaw, mirroring the recoveries in viable cell numbers during progressive post-thaw culture.

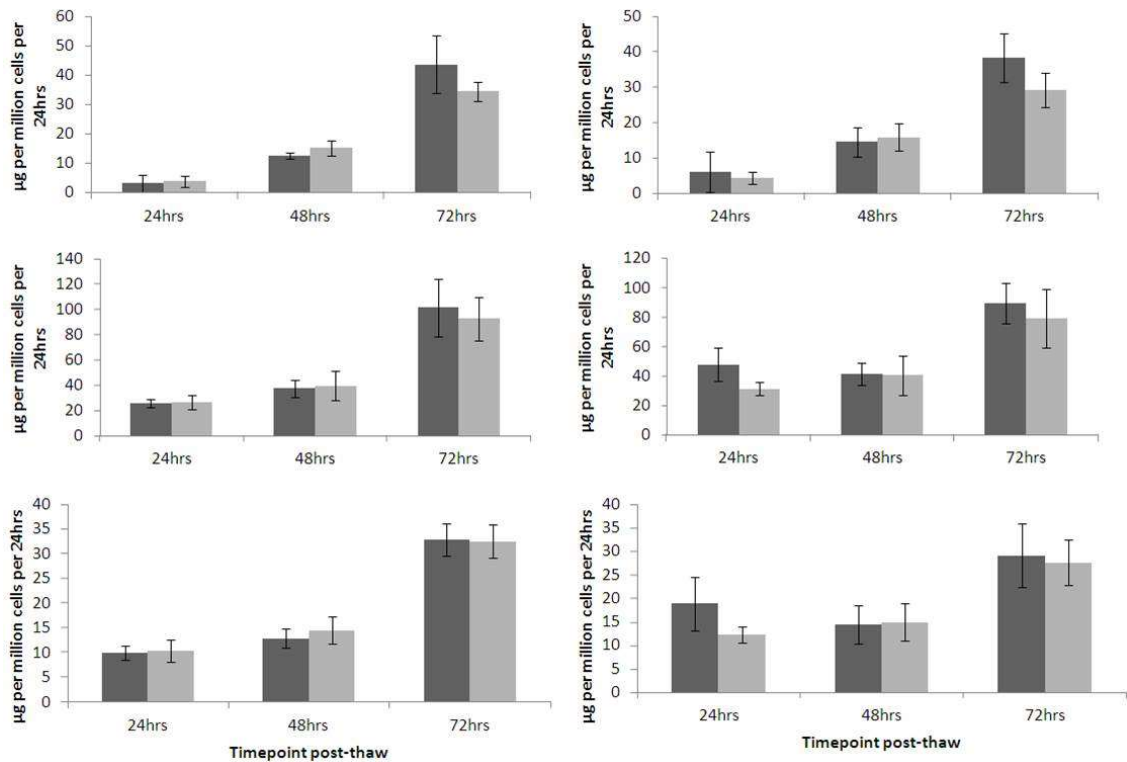


Figure 34 - The production of liver specific proteins by ELS, day 1 to day 3 post-thaw between samples experiencing either progressive solidification (darker) or network solidification (lighter) during cryopreservation - alpha-fetoprotein (top), albumin (middle), and alpha-antitrypsin (bottom). Progressive solidification samples are shown dark in grey with network solidification samples lighter grey. Production was analysed per million viable cells post-thaw per 24hr (right), and normalized per million viable cells pre-thaw that takes account of cells destroyed during the cryopreservation (left). Measurements on the left therefore present the overall outcome per sample cryopreserved - there are no statistically significant differences. Measurements on the right display production per million cells, but take into account that there is now a different cell number between the two sets. Here the progressive solidification samples have significantly improved production of albumin and alpha-antitrypsin in the first 24hr post thaw (at  $p < 0.05$ ). There are no significant differences at other time points or with alpha-fetoprotein  $N=5 \pm SD$ . Intra either NS or PS sample sets, the measured protein production increased significantly from day 1 to day 3 for all measurements ( $p < 0.05$ ). Between different time points intra-sample-set, a paired student's t-test was used, inter samples, an unpaired student's t-test was carried out where statistics are carried out [210].

## 7.4. Discussion

Ice solidification occurs in small and large volumes by two distinct processes. At small volumes network solidification (NS) manifests whilst at large volumes progressive solidification (PS) is the predominant process [210]. These differences in bio-physical events presented as different ice crystal formats in this study. Similar differences in ice matrix ultrastructure have been presented for sperm processed either in straws or bags [348].

With ELS, the observed recovery following these two processes was very similar although the structure of ice and the freeze concentrated residual compartments within the two types of samples are very different. Post-thaw, samples experiencing NS had a higher post-thaw viability and viable cell numbers, significant after 24 h of recovery. When examining the functional

outcomes, samples cryopreserved experiencing PS have an improved outcome per unit of viable cells, although overall differences were small. The results suggest that NS allows more cells to survive cryopreservation, but those surviving cells have greater average damage than those experiencing PS. PS by contract showed a trend to fewer, healthier cells post thaw, especially at the 24 h time point following thawing.

During large scale cryopreservation the potential long exposure to cryoprotectants in the liquid state prior to phase transition, experienced for the central portion of the sample under condition of PS, may be a potential extra stress over and above those which result from cryopreservation in NS conditions. This is in addition to the non-optimal cooling rates experienced in this part of the sample [135, 269, 271, 276]. I had considered the possibility that PS would therefore result in greatly reduced post-thaw recoveries. This was in fact not the case, which is encouraging when planning further work on scaled-up cryopreservation in volumes > 1 litre. It could be hypothesised that under conditions of PS, the extra cryoprotectant stress experienced by part of the sample could act to remove an unhealthy, or poorly performing sub population of cells present before cryopreservation. NS, by reducing the time to which the ELS from the whole sample was exposed to the osmotic and chemical toxicities, where the central mixture was in the liquid state just at the point of nucleation, may avoid injuring this already partially stressed population leading to significantly higher viable cell numbers (although metabolically less productive) by 24 h post-thaw. It is also possible that the temperature discontinuity present when an undercooled sample nucleates damages cells in subtle ways, so they survive cryopreservation though are no longer function effectively. Further studies will need to investigate these mechanisms.

It is important to differentiate the processes described above (NS and PS) from another way to control ice crystal progression – this being the so-called directional solidification (DS) where the sample is moved across a constantly low temperature gradient, sufficiently cold to induce ice nucleation in the portion of the sample in contact with the cold plate [14, 138, 182]. DS allows the morphology of the ice interface to be varied under conditions where the local chemical conditions of the residual solution can be kept constant, which is different to what happens in PS where progressive exclusion of both solutes and cells occurs ahead of the ice front. The technique allowed investigation of whether different ice crystal morphologies (for example, with increasingly complex ice dendrite formation) impacted on cell survival, but this was not generally found to be the case [182]. Differential entrapment or exclusion of cells within the advancing ice front was also noted with DS [183], but the behaviour of larger cell complexes (such as the ELS) has not been investigated as far as I am aware. PS would perhaps be expected to deliver ice fronts moving between and through the alginate capsules containing the ELS, which were used

in relatively high packing density in the current study, but further work will be needed to investigate this aspect [78, 303, 427]. DS also allows better homogeneity of the cooling profile throughout the entire sample [14, 138], whereas, as seen here, PS results in differential thermal profiles towards the sample centre as the excluded solutes, generating areas of local undercooling, result in variable release of latent heat of ice crystal formation. This heat has to be dissipated from the sample core before linear cooling can proceed [276]. This results in a controllable progression of solidification through the specimen dependant on the rate at which the temperature gradient is passed through the sample [15, 182, 183]. DS allows the morphology of the ice interface to be varied under conditions where the local chemical conditions of the residual solution can be kept constant, which is different to what happens in PS where progressive exclusion of both solutes and, in some situations, cells occurs ahead of the ice front [183]. DS also allows better homogeneity of the cooling profile throughout the entire sample, whereas, as seen here, PS results in differential thermal profiles towards the sample centre as the excluded solutes, generating areas of local undercooling, result in variable release of latent heat of ice crystal formation which have to be dissipated from the sample core before controlled cooling can proceed. However, for large cell masses contained within an irregular geometry as investigated here, engineering a DS approach to cryo-cooling would prove to be challenging. In the current work, solidification proceeded only through static surface cooling conditions, with ice growth primarily determined by the thermal properties and 3-dimensional structure of the sample.

Another factor worthy of comment is that the experimental systems used here had little excess cryoprotectant additive and there would be little settling effect of ELS on the ice crystal progression – all the samples were in effect ‘settled’ by removing the extra CPA volume. The process of ice propagation in this system may differ compared with conventional cell and protein suspensions, where sedimentation of cells may occur before initiation of freezing and, secondly, cells and proteins may be pushed ahead of ice fronts during progressive solidification.

While success has been reported with large volumes in flat bag cryopreservation, these have generally been deliberately compressed into a thin wafer or ‘slab’ format with little internal temperature gradients and so often experience NS. It is possible to observe PS in bags however, if the bag temperature is not thermally equilibrated prior to the onset of solidification [171, 265, 379].

Such flat-bag approaches would be very difficult to adapt for BAL cryopreservation due to the geometries involved, where the end-product would ideally reside in a cylindrical fluidised bed format.

The varying temperature profiles throughout the sample when cooling a large cylinder have been recognised for some time [189, 276]. Previous studies have shown that the level of freeze-concentration of solutes is dependent on the cooling rate and this has been studied in detail in cylindrical vessels [220]. In cylindrical configurations, the solutes increased in concentration radially from the edge of the cylinder to the centre, and this was accompanied by aggregation of some proteins within the core layers. Due to the alginate sphere composition of the test BAL, cell aggregation will not occur here as the cells are already immobilised. This increase in solutes centrally (as would be seen in a cylindrical BAL cassette) is a likely cause of lower cell number post thaw when progressive solidification is present in our current scale-down module, and so will be studied in more detail in chapter 8.

Using inserts in the Asymptote EF600-103 to emulate large volume cooling profiles within small samples gave similar thermal histories as were seen in a large volume. This allowed for the study of these thermal profiles as well as longer and variable cryoprotectant exposure and cryo-concentration of solutes in the system, in addition to accurately mimicking the variations in ice structure between the two set-ups. Combining these three effects in a smaller volume format accurately provides more accessible and more economical methods of study of these sample configurations, without the additional variable of differing volume or thawing rate. This equipment modification may have application in studying other large volume freezing problems, such as those encountered with proteins.

Significantly this study informed that PS may be applied to the BAL without major detrimental effects on the bulk ELS product, although there was a low level of early functional attrition seen after PS which requires further study.

## **7.5. Conclusion**

Previously the LG reported good outcome when ELS (cryopreserved in typical small volume format in cryo-vials) experienced network solidification during cryopreservation [263-266]. Good outcomes can now be achieved in a more realistic large scale geometry that necessarily produces progressive solidification, and this can be modelled in an economical way using an adapted head plate for the EF600-103 freezer.

It has been demonstrated that both PS and NS exhibit very different biophysical conditions during ice crystal growth; this is reflected in the ultrastructural observations of the differing ice-matrices during solidification. However these different outcomes of cryo-solidification in reality made only small, mostly non-significant differences to viable cell recovery or function. ELS

cryopreserved under both conditions each showed very good propensity to return to normal cell replication as post-thaw culture extended beyond the first 24 hours. As progressive solidification is almost unavoidable in samples any larger than a few ml, an understanding of the differences between these two conditions may well be necessary for successful larger volume cryopreservation across a wide range of cell therapies.

This chapter has established the biological differences between large and small volumes during traditional, ice-present, cryopreservation – which has not previously been explored in cryobiology. It also allowed for a new technique for cost-effective study of these differences – no widespread have previously been reported. This chapter formed the basis of the paper by Kilbride et al. in *Cryobiology* 2014 [210].

Chapter 8 considers cryoconcentration (also known as freeze-concentration), due to the role it may play in the BAL system during cryopreservation. The spatial location is likely to have an impact during PS due to the non-homogeneous cooling conditions, and so this is studied in detail in chapter 9.

## 8. Cryoconcentration

### 8.1. Overview

This chapter determined the dominant factors involved in cryoconcentration, so that the effect on the BAL could be determined.

The liquid to solid phase transition of an aqueous system, comprising of one or more solutes dissolved in water, does not proceed homogeneously. That is to say while usually liquid water with dissolved solutes naturally proceeds toward an equilibrium state – one in which the concentration of solutes is the same everywhere – this cannot be said for the solid phase.

As ice ‘grows’ through a system, water will be preferentially included in the solid phase, while solutes will be preferentially excluded. This tends to result in a heterogeneous solid phase with solute concentration increasing in the direction of the ice growth [221, 223, 279].

During freezing, three distinct areas exist within the sample – a solid region; a mushy or boundary region where the solidification takes place; and a liquid region ahead of the freezing front [118, 392]. Solute rarely diffuse in the solid phase, and those that do so diffuse at a rate many orders of magnitude lower than would be observed in the liquid state. This is observed in water systems as well as during the solidification of alloys, both of which have been studied in detail [118].

There has been extensive study of this effect, termed cryoconcentration or freeze-concentration, in the food industry as a method to concentrate goods such as milk and fruit juices, so that they can be transported more cheaply before being re-hydrated prior to sale [3]. This method is generally accepted to give a higher re-hydrated quality product over traditional methods such as evaporation-concentration, though it does come with increased economic cost [3, 29, 157, 284].

Freeze-concentration is also used extensively in waste water systems to separate cleaner water from its contaminants. This can be applied to seawater desalination, and other industrial functions [128, 159, 163, 428].

Lesser attention has been paid to this concentration effect in biological systems. As cryopreservation of larger volume tissues and organs becomes widespread, an understanding of cryoconcentration will become essential. Larger volume samples tend to take significantly longer to freeze than their smaller equivalents so will experience extensive cryoconcentration

of salts and cryoprotectants. Biological systems are sensitive to concentrations of these solutes, particularly in the liquid state, and so cryoconcentration could have a significant negative impact on post-thaw outcomes [132, 322].

During cryopreservation of the bioartificial liver, the liquid to solid phase transition takes around 3-4 hours. This may result in significant cryoconcentration in the centre (last section to solidify) of the device, a study of which is essential to mitigate possible damage.

Methods exist to measure the amount of cryoconcentration in a biological system, however these techniques are very advanced and were not available for use in this project [61]. As a consequence, mathematical models were selected from the literature and adapted for the BAL system. These would be able to determine the level of cryoconcentration during the cooling and warming process. Experimental data would then be used to confirm if the models were accurate.

### 8.1.1. Chapter Specific Nomenclature and Abbreviations

A – Avogadro's number ( $6.022 \times 10^{23}$ )

BC – Boundary condition

C;  $C_0$ ;  $C_a$ ;  $C_s$ ;  $C_L$  – Solute concentration; original prior to solidification; at the ice-liquid interface; in the solid; and in the liquid – respectively ( $\text{kg m}^{-3}$ )

$C_L^*$ ; – Relative solute concentrations in the liquid between  $C_0$  and  $C_0/K$  (dimensionless)

D – Diffusion coefficient ( $\text{m}^2 \text{s}^{-1}$ )

$\varepsilon$  – Gradient of Concentration against Density

$\phi$  – Mean free path (m)

F – Melting Rate

g – Gravitational field strength

G – Temperature gradient ( $\text{K m}^{-1}$ )

h – Height of liquid in vial

J – Mass flux ( $\text{kg m}^{-2} \text{s}^{-1}$ )

$K_b$  – Boltzmann Constant ( $1.38 \times 10^{-23} \text{ m}^2 \text{ kg s}^{-2} \text{ K}^{-1}$ )

$K$  ;  $K_0$  ;  $K_e$  ;  $K^*$  - Partition Coefficient; Intrinsic Partition Coefficient; Effective Partition Coefficient; Dimensionless Partition Coefficient – respectively

$\lambda_c$  - Distance between solute channels (m)

$\Lambda$  – Interatomic distance (m)

m – Meters

mt – mass transfer coefficient ( $\text{m s}^{-1}$ )

ml – millilitres =  $\text{cm}^3$

M – Molecular mass (kg)

$\mu$  – Viscosity ( $\text{kg m}^{-1} \text{s}^{-1}$ )

n – Number of molecules

r – Radius (m)

R – Ice front growth speed ( $\text{m s}^{-1}$ )

s – Seconds

T – Temperature (K)

$T_g$  – Glass Transition Temperature (K)

V ;  $V_l$  ;  $V_0$  ;  $V_s$  – Volume; liquid volume; initial volume; solid volume – respectively ( $\text{m}^3$ )

$v_{di}$  – solution diffusive speed (m)

w – Association parameter

x – Distance from start of sample (in direction of ice growth) (m)

$x'$  - Distance from ice front (in direction of ice growth) (m)

Z – Gravitational effect in cryoconcentration.

### 8.1.2. Metallurgy and Inverse Segregation

Perhaps the most studied area of solidification falls in metallurgy [39, 40, 118, 169, 285, 315, 392]. Any variation in concentration of metal components during the casting of alloys has significant impacts on the strength of the final ingot. Therefore redistribution of solutes during casting was one of the earliest areas where freeze concentration was studied. In general when

alloys solidify they display similar properties to water solutions freezing, although with some notable differences:

1. Almost all metal alloys have relatively high melting points, as these are allowed to cool to much lower temperatures extreme heat variations on the order of 100s °C are observed. This has much more significance on solidification rate of the alloy than in freezing of water at its equilibrium melting point, where temperature gradients are minimal.
2. Diffusion coefficients in metals tend to be in the order of a few cm per day [169, 315, 405], as opposed to around 1 m a day for solutes in water, this helps minimise solute redistribution during metallic solidification.
3. Perhaps most significantly, metals contract as they solidify and then further as they cool. This contraction of alloys, both on solidification and during further cooling, results in a fluid flow carrying solutes towards the phase boundary [425, 426]. Water is unusual chemically as it expands on solidification, which will lead to a flow of both solutes and solvent away from the phase boundary (interestingly a phenomenon that has been little studied).

Point 3 can lead to the phenomenon described as inverse segregation, where solute concentration in the solid fraction is greater than that in the liquid fraction [118, 371, 426].

Whereas for metals, solutes can directly be added into the ice structure, for water/solute systems solutes are not included directly into hexagonal ice (in place of water molecules). Rather they are trapped in thin channels between dendrites as the ice front passes.

## ***8.2. Factors Impacting on Magnitude of Cryoconcentration***

### **8.2.1. Effect of Ice Front Speed**

The rate at which the ice front expands through a sample significantly affects the scale of cryoconcentration. Increased cryoconcentration tends to result from decreased ice front speed [41, 52, 223, 284, 285, 302, 347, 433].

In the absence of constitutional supercooling [221] breakdown resulting in rapid solidification, the effect of freezing rate can be simply described. If the ice front is moving faster than solutes rejected from the ice can be transported away through diffusion, then the solutes will be 'captured' by the ice front and the level of cryoconcentration reduced. If solutes are diffused

away more quickly than the ice front is moving, cryoconcentration will be maximised [52, 302]. It is important to note that different solutes will not necessarily diffuse at similar rates, which has a knock on effect for cryoconcentration, larger solutes tend to diffuse more slowly [41, 179, 204, 279, 433].

### **Constitutional Supercooling**

At higher solidification rates, a 'wall' of excluded solutes builds up ahead of the ice front. As solutes generally lower the freezing point, the ice front growth rate will slow on this 'wall' until the system has cooled enough to allow its continued solidification. This effect is known as constitutional supercooling [130, 145, 174, 221, 381, 405].

If an ice crystal can penetrate this wall, the solution beyond the wall with the higher freezing point can solidify rapidly, encasing the solutes in the solid fraction [159, 366].

#### **8.2.2. Effect of pre-freeze Concentration**

The concentration of solutes in the liquid state contributes significantly to the efficiency of freeze concentration [52]. At low concentrations, solutes are excluded from the ice front very effectively. However as the concentration is increased, the osmotic pressure exerted by the solutes increases. This perturbs the ice front and so liquid cavities can more easily become trapped in crevasses in the ice. These combine to increase the proportion of solute included in the ice fraction, and so lowers the relative level of cryoconcentration [128, 154, 157, 159, 179, 204, 284].

#### **8.2.3. Interactions between Solutes**

In a solution of only one solute, a different freeze-concentration profile will be observed than with the same solute in solution with additional solutes [86, 154, 159]. This results from the change in the solutes' diffusion coefficient when mixed solutes are present as a result of the changed properties (viscosity, osmotic pressure etc.) of the system, or direct interactions between separate solutes in solution [86]. If, for example, one solute repels another in solution that has a higher affinity for the solid state, that solute will then exert a higher pressure on the solid phase, and so be more readily absorbed [24].

A solution of multiple different solutes will tend to reduce the difference between each solutes' concentration profile over what would normally be seen when each was considered independently [154, 221]. At low concentrations, solutes can be approximately modelled by considering each solute separately [370].

#### 8.2.4. Effect of Solute Size on Diffusion Rate

The diffusion rate of a particle, in conjunction with the ice front speed, is the primary determinant of cryoconcentration magnitude.

In solutions, molecular weight and diffusion coefficient of a solute follow a linear profile, with increased molecular weight resulting in decreased diffusion rate. This is described by a modified Stokes-Einstein equation [17, 418]. This leads to the prediction that the smaller the solute, the more cryoconcentration should be apparent, as solutes are more likely to 'outrun' the ice-front and concentrate in the liquid phase. This has been observed in equal molecular concentration solutions [179, 204]. The diffusion coefficient of a particle is affected by temperature and viscosity through the Stokes-Einstein equation - equation ( 8 ) - so cannot be considered a constant [221].

$$D = \frac{K_B T}{6\pi\mu r}$$

( 8 )

This is the Stokes-Einstein equation, where D denotes the diffusivity coefficient of a spherical particle at low Reynolds number,  $k_b$  denotes the Boltzmann constant, T the temperature of the system,  $\mu$  its viscosity, and r the radius of the particle. This is generally modified for use at the atomic scale, but is valid on a cellular level [17, 124, 418].

#### 8.2.5. Effect of Temperature

Temperature, diffusion rates, and viscosity are all inter-dependant as defined by the Stokes-Einstein equation. Temperature changes have the added effect of increasing or decreasing the solubility of solutes in solution, which affects nucleation (formation) of new ice crystals, and by affecting the rate of ice growth [124, 130, 181, 330, 419].

With lowering temperature, the viscosity of most liquids increases [291]. This in turn reduces the rates of diffusion of solutes in that liquid and so solutes can be more easily trapped in the

solid phase. A larger temperature gradient in a sample also allows heat to be extracted more quickly, increasing the rate of ice growth and solute capture.

When NaCl is dissolved in water, the temperature of the solution decreases, defining the endothermic energy of solution. This results in a salt-water solution having greater free energy at a given temperature over separate water and salt at the same temperature. Salt therefore becomes less soluble in water with a fall in temperature, as the system naturally tries to minimise free energy [184].

This contrasts with oxygen, which exhibits an exothermic energy of solution, and so becomes more soluble with decreased temperature [143]. DMSO – a commonly used cryoprotectant and the principle agent used with hepatocytes – also exhibits exothermic energy of solution [37, 123]. Little research has been carried out of the freeze concentration of DMSO, but this unusual property will modify its cryoconcentration profile, in particular to other cryoprotectants and salts found in biological systems.

### **8.2.6. Biological Solutes**

Often many biological structures, such as proteins, enzymes, and cells do not truly dissolve in aqueous solution; while they are surrounded by water molecules they remain distinct from it, typically referred to as a 'suspension'. This is in contrast to true solutes such as NaCl which chemically reacts and breaks down into its respective Na<sup>+</sup> and Cl<sup>-</sup> ions. Many proteins do not concentrate significantly during ice formation [41, 52], which may be a consequence of the fact that they generally have very large molecular weights and so low diffusion rates.

Most proteins and biological material have been observed to cryoconcentrate however [41, 233, 279, 347, 433]. Proteins have a wide range of shapes and sizes, and different freezing strategies are used between different proteins. Significant volumes of proteins are manufactured by the pharmaceutical industry and freezing effects such as cryoconcentration can be useful in reducing their transport bulk size, but in some cases can also denature proteins [433].

During the progressive phase transition of a large biological mass, cells in different parts of a sample will experience different solute histories. It is important to understand this, in conjunction with different freezing rates and times, to fully optimise cryopreservation of large samples such as the bio-artificial liver [86].

### 8.2.7. Dissolved Gas

Most environmental liquid includes dissolved gas. As discussed previously, some gases tend to be more soluble in lower temperature water than in higher temperatures, in contrast to most 'solid' solutes. This is due to the exothermic nature of the dissolution reaction, resulting in a lower free energy in the dissolved state. This can be more easily understood through a reaction equation:



If heat is added to the system at equilibrium, the system becomes un-equilibrated. In order to re-establish equilibrium, heat and dissolved oxygen must convert to oxygen and water.

During slow cooling, gas bubbles which form usually re-dissolve in the solvent, so then do not present in the ice structure. Only during rapid freezing where bubbles do not have time to dissipate before being trapped in the ice does dissolved gas become obvious in the ice structure [159, 221, 433].

### 8.2.8. Location of Solute in Ice Matrix

While other structures exist, water-ice most often takes the form of a tightly bound hexagonal matrix at standard pressures. During freezing of an aqueous solution, solute particles tend not to be included in this matrix, rather they reside in channels between the ice crystals and enter a separate vitrified or frozen state [86, 124, 154, 302, 330, 366].

Sometimes there can be limited inclusion in the water-ice matrix, this is preferentially observed with smaller molecules that share similar properties to water molecules. Some larger molecules share an affinity with water and are therefore found in the ice matrix, though this is uncommon [41, 330].

Water can never be totally removed from solutes by freeze concentration. There exists a fraction of bound water that remains in contact with many solutes, particularly those with larger more complex structures. As this water is almost always associated with these particles, it is not generally considered as one with free (un-bound) water [124].

### 8.2.9. Effect on Glass Transition Temperature

Solutes existing in channels enclosed by the ice matrix become vitrified as an amorphous solid once the glass transition temperature  $T_g$  is reached. This transition temperature is not constant; rather it is significantly affected by the composition of the channel, and the interaction between solutes therein [191, 368].

It is possible to measure the glass transition temperature of these channels, and doing so may indicate their composition throughout different channels in the ice matrix.

### 8.2.10. Ice Front Structure

Ice fronts are not naturally smooth and planar – they form a sharp dendritic framework [118, 154, 330], this dendritic framework changing with the freezing rate [285]. When the ice front is moving sufficiently slowly, the protruding leading edge of ice enters the increased solute wall present in front of the expanding ice front, as this higher solute liquid has a lower eutectic point, the edge will melt and perturbations from the ice front will tend to be diminished. This leaves fewer solutes to be trapped between the dendrites. Through solute trapping between dendrites, the morphology of the ice-front affects cryoconcentration [330].

Conversely, during sufficiently rapid ice formation and constitutional supercooling, the leading edge of the ice can pass through the solute wall and then grow rapidly beyond, increasing perturbations and solute inclusion to the solid phase.

It is therefore quite obvious through looking at only solidified ice structure the relative speed of ice formation during freezing [124, 210].

### 8.2.11. Ice Crystal Spacing

As mentioned above, structurally in water ice, as very few solute atoms enter the ice crystal itself the primary crystal will be composed almost exclusively of water molecules, with rare imperfections and solutes trapped within the lattice. The only exception under standard pressures will be molecules who are chemically similar to water, and so can join the water ice matrix with minimal free energy.

The ice crystal will expand into the liquid component dendritically or cellularly, dependant on the growth rate, the shape of the tips identifying a cell or dendrite [187, 256, 419, 424]. Solutes

and impurities will reside in channels between these crystals [86, 221, 290, 302, 419], either being forced out as the channels become consumed by the expanding edge of the ice, naturally diffusing out, or become trapped as the channel is blocked by further crystal growth.

Understanding the morphology of these crystals will determine the effect they have on biological material. Presently it is possible to determine the effects of many parameters on freeze-concentration, however no completely theoretical method exists to determine the level of solute capture as the natural affinity a solute has for the solid phase must be determined experimentally. It seems reasonable to assume that this affinity is related to ice morphology, a study of which would therefore seem prudent.

The primary factor affecting solute trapping would be related to the frequency of these solute channels within the ice matrix, a frequency known to be regular [419]. Samples containing many channels would be expected to contain much more solutes than those where channels are sparse.

Work to determine ice crystal spacing has a long history, both in water based systems and in metallurgy, though no general equation has been accepted [230, 256, 295, 431]. The most commonly proposed relations have channel spacing (or crystal size), as a function of the inverse of the ice growth rate and temperature gradient [187, 256, 278] – which are both generally determined by cooling rate [118], largely independent of initial conditions [205]. This has relevance out with biology and is applied when crystals of a particular size are desirable [209].

It is well established that faster cooling leads to smaller ice crystals, and that a large temperature gradient leads to faster solidification. Faster solidification also leads to increased solute capture in the solid fraction, which would be expected from the channel capture theory.

Historically the following relationships have been proposed for  $\lambda_c$ , the distance between the centre of solute channels, where an ice front growth rate (R) and temperature gradient (G) are imposed [230, 419]:

$$\propto R^{-0.25}G^{-0.5}$$

$$\propto R^{-0.5}G^{-0.5}$$

$$\propto R^{-1}G^{-1}$$

(9)

While more recently van der Sman et. al. [419] have proposed that:

$$\lambda_c \text{ scales as } 50G^{-0.25}$$

(10)

Which agrees with experimental data well. Crystal spacing can be measured in several ways [209, 424], perhaps the most simple is physically looking at a freeze-dried sample under magnification and measuring the gaps [424]. Understanding  $\lambda_c$  more completely will determine the solute structure in the solid and should allow a more theoretical description of the freeze-concentrate process.

### **8.2.12. Rapid Solidification**

A wholly different area of research covers rapid solidification – where the ice front can move at speeds of up to 250m/s [19]. In such systems clearly solute diffusion rates are negligible, and the process is dominated by solute trapping between expanding dendrites [371].

This will be observed in small biological samples, where phase transfer rates in the order of cm/s are typical during snap-freezing or uncontrolled undercooling & nucleation. These rates too are much more rapid than the solutes can diffuse and so enters a different modelling domain.

### **8.2.13. Methods to Increase and Reduce Cryoconcentration**

As most applications of freeze-concentration require the separation of solute and solvent, many techniques have been developed to maximise its efficiency. For a cryopreserved biological system the effect should ideally be dispersed, so the reciprocal of the following methods should be used [433].

A widely used design with freeze-concentration is inclusion of a stirrer, rotating vessel, or vibrating plate to agitate the liquid component during phase transition. This disperses the build-up of solutes on the ice wall as well as generally increasing the motion, so apparent diffusion coefficient, of solutes preventing their capture by the solid phase. Stirring tends to disproportionately mix larger, courser particles over smaller ones [159]. In turn when intending to prevent freeze-concentration samples should be cryopreserved in as calm an environment as possible, well away from possible movements [29, 39, 118, 157, 233, 283].

Partial melting, also known as freeze-thaw processes, improve the yield from cryoconcentration. As the ice fraction expands within a sample, the equilibrium melting point becomes lower, as the solute concentration becomes progressively higher. The final ice crystals will melt first on a

temperature increase, and this melt can be re-frozen to increase the solute and solvent separation further [163, 233, 282, 302].

It is important not to inadvertently allow re-freezing in a biological sample of this nature, as doing so may take parts of the tissue further from their optimal cryopreservation conditions.

### **8.3. Mathematical Modelling**

#### **8.3.1. Determining Diffusivity**

An obvious place to start when considering a cryoconcentration model is the diffusivity of different molecules, proteins, and cells in solution. As this encompasses one of the two established major factors affecting the process (along with ice growth rate that can be measured experimentally easily), a rough estimate will be enough to say whether effects of cryoconcentration need to be considered in any given system.

There are two major ways to determine the diffusivity of solutes in a liquid solvent. For large molecules [93] (solute molecules 5x larger than the solvent molecules), it is common to use the Stokes-Einstein Equation (equation ( 8 )) [70]:

$$D = \frac{K_B T}{6\pi\mu r}$$

Where D is the diffusion coefficient,  $K_B$  is the Boltzmann constant,  $\mu$  is the viscosity of the solvent and r is the radius of the solute molecule – experimental parameters can be measured experimentally, but are generally well known in the literature for common systems. The Stokes-Einstein equation predicts the diffusion with an accuracy of around 20%, as good as current understanding allows. It assumes that molecules are rigid and moving in an infinitely dilute solution (i.e. only one molecule of solute). Clearly in cryoconcentration (and most real-world applications), the solution will not be infinitely dilute, and interactions between solute molecules will reduce accuracy [70, 93].

Young et al. improved the results by modifying the Stokes-Einstein equation for the case of globular proteins (that are always larger than their solvent) [459]:

$$D = 8.43 \times 10^{-8} \left( \frac{T}{\mu M^{1/3}} \right)$$

( 11 )

Where M is the molecular mass of the protein. Of the 143 proteins studied, 75% had a diffusivity within 20% of the value predicted by equation ( 11 ) [459]. Equation 11 was formulated through assuming that proteins are spherical, and assuming a partial specific volume of 0.73cm<sup>3</sup>/g. Inaccuracies may form here when proteins deviate from being spherical and so increase their surface area – this is particularly true for denatured proteins or liver-specific proteins such as albumin that accumulate other compounds as part of their de-toxification role. Partial specific volumes of proteins show a Gaussian distribution of between 0.69cm<sup>3</sup>/g and 0.78m<sup>3</sup>/g, and so this is only accurate ‘normal’ proteins. Proteins with a known partial specific mass different from 0.73 cm<sup>3</sup>/g could use equation 11 with the 8.43x10<sup>-8</sup> factor varied. The full derivation of equation 11 from the Stokes-Einstein equation has been presented by Young et al [459]. The inaccuracies stated in the model underline that for very accurate determination of diffusion, experimental methods such as ultra-centrifuging must be employed.

While numerous variation of the Stokes-Einstein equation are proposed in the literature with slight edits that the authors’ claim make their relationship more accurate than any that have come before, the only one with widespread application for smaller molecules is the Wilke-Chang equation [442]:

$$D = 7.4 \times 10^{-8} \left( \frac{(wM)^{1/2} T}{\mu V^{0.6}} \right)$$

( 12 )

Here w is an association parameter = 2.6 for water, M is the molecular weight of the solvent in daltons, viscosity is measured in centipoises, and V is the volume of the molecule (assuming it’s spherical, in cm<sup>3</sup>/mol). When tested, Equation ( 12 ) gave an accuracy of around 10%, and has widespread use today, primarily for smaller molecules [70, 442]. The Wilke-Chang model was developed through direct experimental studies of a wide range of solutes and solvents, with the V<sup>0.6</sup> factor taken directly from experimental results, not derived. The association factor was added as it was found solvents interacted with themselves in different ways which could impact diffusion, and it’s value for water was determined experimentally. A major assumption and so limitation in the Wilke-Chan model is that it is based on dilute solutions – i.e. interactions between molecules of solute are disregarded. Inaccuracies will then take place at higher concentrations of solutes, or with those with particular attraction or repelling characteristics.

### 8.3.2. Diffusivity of Common Cryoprotectants

All biological systems have water as a base solvent. H<sub>2</sub>O has a molecular weight of 18, which will be the primary determinant when considering what diffusion regime solutes and particles reside.

#### Diffusivity of DMSO

The primary cryoprotectant used with hepatocytes is DMSO, with a molecular weight of 78. Using the Wilke-Chang equation, a diffusion coefficient of  $1.3 \times 10^{-9} \text{m}^2/\text{s}$  is determined at 25°C. The full calculation is detailed in Appendix 2 at the end of this chapter. This is higher than literature values of  $1.03 \times 10^{-9} \text{m}^2/\text{s}$  [55], although this is not surprising based on the number of approximations used during the calculation. Experimental data needs to be obtained to achieve higher accuracy here.

One notable aspect for DMSO's diffusion coefficient is its strong dependence on temperature, most likely an indirect consequence due to changes in water's viscosity rather than a direct affect, and also that it has a strong relation on concentration, something that is not accounted for at all in equations ( 8 ), ( 11 ), or ( 12 ) [55]. There is not an extensive literature on these properties of DMSO despite its widespread use in cryopreservation and also medical settings, and this will be an area of future study.

#### Diffusivity of NaCl

Sodium chloride, regular salt, is essential for cellular life but also very toxic at high concentrations. Limiting its cryoconcentration will lead to higher cryopreservation success. As its molecular weight is 58.44, the Wilke-Chang equation is used as above. This gives a diffusivity coefficient of  $2.3 \times 10^{-5} \text{cm}^2 \text{s}^{-1}$ . Literature values here are much lower, in order  $1.6 \times 10^{-5} \text{cm}^2 \text{s}^{-1}$  [165]. This underlines the need to correlate these values to experimental and literature ones in order to fully describe the system.

## Diffusivity of Glucose

Glucose is commonly used as a cryoprotectant in biological systems, though successful use with hepatocytes has so far been elusive. Nevertheless it is an active area of research and will have different physical effects from DMSO and NaCl. At 180 molecular mass, and assuming it is spherical, the diffusivity can be determined through the Stokes Einstein Equation ( 8 ). As can be seen from Appendix 2, the diffusion coefficient is determined to be  $7.47 \times 10^{-6} \text{cm}^2 \text{s}^{-1}$ . This is only 11% higher than the literature value of  $6.73 \times 10^{-6} \text{cm}^2 \text{s}^{-1}$ , and so quite a good estimate.

## Diffusivity of Hepatocytes and ELS

In the BAL system, cells are immobilised individually due to their growth in clusters of a few hundred cells, and due to their encapsulation in alginate beads. Only the diffusion of ELS (encapsulated liver spheroids) has to be considered.

ELS are not observed to undergo noticeable freeze-concentration during solidification. Using the Stokes Einstein Equation ( 8 ), the estimated diffusion of ELS is  $4.9 \times 10^{-22} \text{m}^2 \text{s}^{-1}$ . During the few hours of freezing, the diffusion of ELS would be vanishingly small.

### 8.3.3. Solute Concentration in Solid and Liquid Phases

The diffusion coefficient on its own does not describe the system, rather it must be related to solute flux. Fick's 1<sup>st</sup> law – Equation ( 13 ) - is used as a basis for this:

$$J = -D\nabla C$$

( 13 )

Where  $J$  is the mass flux, and  $C$  the concentration,  $\nabla$  is the del operator which simplifies when considering ice growth in only the  $x$  dimension:

$$J = -D \frac{\partial C}{\partial x}$$

( 14 )

In the BAL device, ice growth will only be in one direction locally, ie from the edges to the centre. This direction is 'x' in this model. The  $y$  dimension (along the length of the BAL) will be homogeneous – ice growth will be perpendicular to this dimension whereas solutes are excluded

in the direction of ice growth. This assumption will not take into account ice growing from the chamber ends inwards, however as these are relatively insulated very little ice growth here will occur, a fact supported by experimental observations of ice growth such as in figure Figure 22 - The set-up of the Asymptote Large Volume Vialfreezer. On the left is the start of the cooling run, with the cooling plate of the freezer highlighted in yellow, and direction of ice movement noted. The structure in the centre is the thermocouples with their support. On the right is a broader view of the system. For both images, insulation has been removed - normally it would cover the whole set-up. The sample here contained 2 litres of 10% aqueous glycerol solution and the cooling plate was cooled at 0.3°C/min.

Fick's 2<sup>nd</sup> law – Equation ( 15 ) - introduces time-dependence:

$$\frac{\partial C}{\partial t} = D \frac{\partial^2 C}{\partial x^2}$$

( 15 )

The simplest version of this equation valid for non-reversible diffusion is [371]:

$$\frac{\partial C}{\partial t} + \frac{D}{v_{di}} \frac{\partial^2 C}{\partial t^2} = D \nabla^2 C$$

( 16 )

Where  $v_{di}$  is the maximum speed of solute perturbations in the system. This assumes that solutes diffuse in one direction resulting in an entropy increase. Interactions between particles are excluded. With Equation ( 16 ) simplifying to Equation ( 17 ) in the one-dimensional case.

The most complete picture of the solute movement in a cryoconcentrated sample, both in the liquid phase during freezing and the solid phase post freezing was first published by Tiller et al. in 1953 when studying metals [405], and improved upon by Smith et al. (1955) [370], and these will be used as a basis for the current work.

The following assumptions are made:

1. There is an absence of mixing or convection in the system. This would seem the most appropriate model to adopt as the whole sample will be very close to the equilibrium melting point during slow freezing. In systems where convection occurs or mixing is present this model is not valid.

2. A second assumption is that while there is diffusion in the liquid phase, there is none in the solid phase. As diffusion of solutes in water ice is much slower than the liquid state, this would also be reasonable.
3. Finally it is assumed that a local solute equilibrium exists at the solid-liquid interface governed by the partition coefficient K. This is valid for slow freezing, where  $R \leq D$ , although for rapid solidification this would not hold.

Taking equation ( 15 ), with a local equilibrium on the freezing front, and adding in the moving interface boundary of the ice front, the governing relation in a freeze-concentrating system is equation ( 17 ) [39, 370], Fick's law for a moving boundary:

$$D \frac{d^2C}{dx^2} + R \frac{dC}{dx} = 0$$

( 17 )

Where R is the ice growth rate. Solving this (appendix 1) gives [86]:

$$C_L = C_a e^{\left(\frac{-R}{D}x\right)} + C_0$$

( 18 )

Assuming that  $C_L = C_0$  at  $x = \infty$

Where  $C_a$  is the concentration at the ice-solute boundary, and  $C_0$  is the initial solute concentration in the liquid. Solving equation for the boundary conditions that as x tends to infinity the concentration tends to the initial concentration, and that there is a discontinuity at the ice wall where the concentration in the liquid is a factor of K larger than in the ice matrix gives:

$$C_L^* = \left(1 + \frac{1-K}{K} e^{\left(\frac{-R}{D}x\right)}\right)$$

( 19 )

Where  $x'$  is the distance from the ice front and  $C_L$  is the liquid concentration between  $C_0$  and  $C_0/K$ . Plotting equation ( 19 ), it is seen that the concentration rises rapidly, before asymptotically reaching an equilibrium point. This is where the number of solutes being absorbed into the ice phase is equal to the number of solutes entering the boundary layer ahead of the ice front.

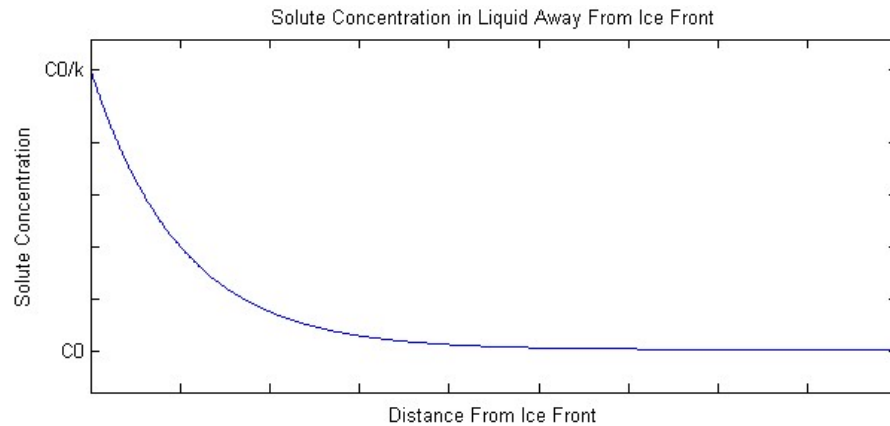


Figure 35 - Solute concentration profile in the liquid phase, for a long sample. This diagram was produced using MATLAB software on equation ( 19 ) – the solute concentration in the liquid component at increasing distance from the advancing ice-liquid interface (at  $x=0$ ). Adapted for Fick's law on a moving boundary. The concentration at the ice wall depends on the partition factor ( $k$ ), and the initial concentration ( $C_0$ ), and declines back to  $C_0$  as distance from the ice wall increases.

The concentration in the solid, up to this equilibrium point, is given by:

$$C_s = C_0 \left( (1 - K) \left[ 1 - e^{\left(-\frac{R}{D} x K\right)} \right] + K \right)$$

( 20 )

The final area to consider is the end of the sample, where solutes cannot physically diffuse away because the liquid zone ends. Applying the boundary conditions again that the concentration in the ice matrix channels is  $K$  lower than in the solute at the boundary condition, and that as the distance to the edge of the chamber falls to zero, the concentration rises to infinity – i.e. as the distance halves the average concentration doubles. In reality at the end of the sample the concentration will increase until a secondary phase transition occurs – either the sample will vitrify or the solution will become super-saturated and solute will precipitate out of the solution.

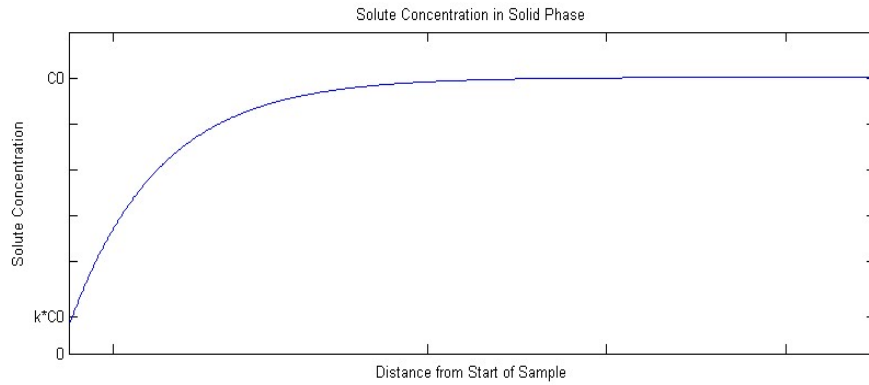


Figure 36 - Solute concentration profile in the solid phase, for a long sample. This diagram was produced using MATLAB software on equation ( 20 ) – the solute concentration in the solid component at increasing distance from the advancing ice-liquid interface (interface at RHS of figure). Adapted for Fick’s law on a moving boundary. The concentration at the ice starts lower than the initial concentration due to solutes being excluded, but increases to the initial liquid concentration as a solute wall builds in the liquid phase. This is for an infinitely long sample.

The simple approximation given in equation ( 20 ) was improved upon by Smith et al. [370], into equation ( 21 ):

$$\frac{C_s(x)}{C_0} = 1/2 \left\{ 1 + \operatorname{erf} \left( \frac{\sqrt{\left(\frac{R}{D}\right)} x}{2} \right) + (2k - 1) e^{-kq\left(\frac{R}{D}\right)x} \operatorname{erfc} \left[ \frac{(2k - 1)}{2} \sqrt{\left(\frac{R}{D}\right)} x \right] \right\}$$

( 21 )

Where erf and erfc are the error function and complementary error function respectively. Smith et al. showed that equation ( 20 ) matches equation ( 21 ) relatively accurately, with no more than 20% deviation [370]. Due to the increased complexity of equation ( 21 ) over equation ( 20 ), for little improved accuracy, equation ( 20 ) is most often used.

Clearly by the end of a sample solutes will start to ‘back-up’ as there is no further sample for them to diffuse into, and so the solid phase solute concentration will increase to remain in equilibrium.

This problem was studied in detail by Smith et al. [370], with the solid concentration (relative to the initial liquid concentration), in the final segment given by equation ( 22 )

$$\begin{aligned} \frac{C_s(x)}{C_0} = & 1 + 3 \left( \frac{1 - k}{1 + k} \right) e^{-2\left(\frac{R}{D}\right)x} + 5 \frac{(1 - k)(2 - k)}{(1 + k)(2 + k)} e^{-6\left(\frac{R}{D}\right)x} + \dots \\ & + (2n - 1) \frac{(1 - k)(2 - k) \dots (n - k)}{(1 + k)(2 + k) \dots (n + k)} e^{-n(n+1)\left(\frac{R}{D}\right)x} + \dots \end{aligned}$$

( 22 )

There then are three distinct regions present in the solid section for a simple single solute solution:

1. – An entry region where the solute increases asymptotically to the equilibrium point.
2. – A central region where the solute concentration remains constant. This should have the same concentration as the initial liquid concentration, though may not exist in relatively short samples [195].
3. – An end region where the solute concentration increases exponentially.

This assumes that  $K$  remains constant throughout the process. This is not strictly speaking true –  $K$  depends on concentration, tending to rise as concentration rises.

Cryoconcentration effectiveness is then not solely dependent on diffusion and ice growth rate, but also sample size – a smaller sample may have no central region at all, while in a large one it may dominate. If a large central region exists then little cryoconcentration will occur. Industrially large samples are cryoconcentrated through mixing of the liquid, which carries solutes away from the phase boundary faster than diffusion.

Samples in our present study are cylindrical, with 1cm diameter and 6cm height, with variations of these dimensions stated when used.

#### **8.3.4. Partition Coefficient**

The principle unknown number that describes a cryoconcentrated system is the partition coefficient,  $K$ , defined as the ratio between solute concentration in the solid phase ( $C_s$ ) and the liquid phase ( $C_l$ ) [39, 169, 392].

$$K = \frac{C_s}{C_l}$$

(23)

If the partition coefficient is assumed to remain constant throughout the freeze-concentration process, the following relation can be proven to describe the phase transfer [154, 337]:

$$(1 - K) \ln \left( \frac{V_L}{V_0} \right) = \ln \left( \frac{C_0}{C_L} \right)$$

(24)

Where  $V_L$  and  $V_0$  are the current liquid volume and the initial volume respectively, and  $C_0$  and  $C_L$  are the initial concentration and current concentration of the liquid respectively. This generally can only be used over smaller ranges in a system as solute concentration, which by definition varies during cryoconcentration, changes  $K$  [39].

Near the boundary, mass balance yields:

$$-D \left( \frac{dC}{dx} \right) + RC = RC_s$$

(25)

An effective partition coefficient – one which is valid over a shorter range and can be related to the intrinsic partition coefficient,  $K$  - can then be found, valid in the boundary layer and that takes account of variation in  $K$  due to the change in solute concentration [39, 337]:

$$K_e = \frac{K_0}{(K_0 + (1 - K_0)e^{-\frac{R}{mt}})}$$

(26)

Where  $mt$  is the mass transfer coefficient. At higher solidification rates, the effects of solute drag may have to be taken into account in particular along the grain boundary (channel between ice crystals) [20, 92]. It has been observed that at low solidification rates solutes with a lower diffusivity tend to dominate, while at higher rates faster diffusing solutes dominate [45, 174].

There are no reliable methods to determine the partition coefficient for a system purely on theoretical grounds, and so they are determined experimentally in the literature.

### 8.3.5. Rapid Solidification

In rapid solidification, where the ice front expands in orders of 10s cm/s to 100s m/s, a more complex picture emerges.

This area has been studied in detail in metallurgy, where very rapid phase transfer is possible and in many cases preferable – extremely rapid solidification can lead to no segregation at all [371, 413].

In previous sections, it has been assumed that a local equilibrium exists at the solid interface, at more rapid solidification this will not be the case [174]. The dominating term is the solution diffusive speed,  $v_{di}$ , the speed at which perturbations propagate in the system [19]. This is defined as the rate of solute diffusivity at the interface to the atomic jump distance:

$$v_{di} = \frac{D_i}{\Lambda}$$

(27)

Where  $\Lambda$  is the interatomic distance. This can typically assume values between 10s of cm and 10s of meters per second [133]. At values of R proportional to  $v_{di}$ , an effective distribution coefficient can be introduced [371, 372]:

$$D^* = D \left( 1 - \frac{R^2}{v_{di}^2} \right)$$

(28)

Equation (17) can then be re-written [371, 372]:

$$D \left( 1 - \frac{R^2}{v_{di}^2} \right) \frac{d^2 C}{dx^2} + R \frac{dC}{dx} = 0$$

(29)

And Equation (18) [372]:

$$C_L = C_a e^{\left( \frac{-R}{D \left( 1 - \frac{R^2}{v_{di}^2} \right)} x' \right)} + C_0$$

(30)

At  $R \ll v_{di}$ , it's clear that these reduce back to their original equations for local equilibrium. The effective partition coefficient where R is of order  $v_{di}$  becomes [133, 371, 372]:

$$K^* = \frac{K \left( 1 - \frac{R^2}{v_{di}^2} \right) + \frac{R}{v_{di}}}{\left( 1 - \frac{R^2}{v_{di}^2} \right) + \frac{R}{v_{di}}} \quad R < v_{di}; \quad K^* = 1 \quad R > v_{di}$$

(31)

Equation 31 can be used to determine the boundary condition at the ice wall at very rapid ice front growth rates (i.e. the relative concentration in the liquid is  $K^*$  the value in the ice matrix at the wall). While at relatively slow ice growth rates (where diffusion is quicker than the ice front growth rate) this value is K, at much more rapid rates (in the order to the maximum solute

movement), an equilibrium cannot be reached and so  $K$  becomes  $K^*$ . This was derived from Fick's laws by Sobolev and is outlined in detail in his paper [371]. For large volume samples with water as the primary solvent, very rapid solidification is rare. Water has a relatively high latent heat of solidification, which works towards bringing the sample back up to the equilibrium melting point and so reducing solidification rate.

These effects may be more noticeable in small volume cryovials or straws that can experience a large degree of undercooling and where ice can nucleate spontaneously.

### Determining $V_{di}$ in Water

To first determine a 'ball-park' figure for  $v_{di}$  in biological systems, first consider pure water. As the density of water is  $10^6 \text{ gm}^{-3}$ , and its molecular mass is 18, the number of molecules in 1 litre is found through Avogadro's number ( $6.022 \times 10^{23}$ ):

$$n = \frac{\text{Avogadro's number} \times 10^6}{18} = 3.35 \times 10^{28} \text{ m}^{-3}$$

The radius of a water molecule is about  $1 \text{ \AA}$  so its cross-sectional area is:

$$A = \pi r^2 = 3.14 \times 10^{-20} \text{ m}^2$$

The mean free path of a particle is given by:

$$\varphi = \frac{1}{nA} = \frac{1}{3.35 \times 10^{28} \times 3.14 \times 10^{-20}} = 9.5 \times 10^{-10} \text{ m} = 9.5 \text{ \AA}$$

Previously in section 8.3.2 I calculated the diffusivity of DMSO to be around  $10 \text{ \AA}^2/\text{s}$ . Using equation ( 27 ),  $v_{di}$  for dilute DMSO in solution is around  $1 \text{ m/s}$ . Rapidly frozen small volume biological samples can achieve solidification rates of  $10 \text{ cm/s}$ , so this factor will become relevant with rapid cooling. When considering more complicated systems with higher fractions of different solutes, these numbers will have to be calculated individually to take account of changes in molar volume and mass density.

## 8.4. Summary of Mathematics

While not regularly considered in detail during cryopreservation, the effects of cryoconcentration are well understood in the fields of food processing and metallurgy.

Biological samples will not solidify homogeneously, they will experience re-distribution of solutes and CPA, and this is likely to be a factor affecting successful cryopreservation of large, delicate, and important samples.

Factors such as temperature, ice growth rate, solute size & concentration, and ice morphology must be considered in detail to fully understand the stresses biological samples will experience when cryopreservation processing occurs.

Cryoconcentration profiles and models have been developed for a wide range of simple and complex systems in metallurgy and food processing, as have the properties of the governing partition coefficient. Adapting these models for biological use is both necessary and possible. Most rely on some experimental data – such as solute diffusion rate and fraction of solutes remaining in ice channels between the ice crystals.

Values in particular for  $K$  are not well known for common cryoprotectants such as DMSO, and so experiments were designed below to determine this to apply the model for non-rapid solidification studied above. Ice growth rate could be measured, diffusion was known approximately from the appendices 8.8.3, and the initial concentration of DMSO could be controlled.

## **8.5. Experimental Measurements**

### **8.5.1. Materials and Methods**

#### **Solidification**

#### **Of Small Volume Vials using the EF600 Freezer**

#### **Materials**

EF600-003 Controlled Rate Freezer (Asymptote Ltd, Cambridge, England, UK)

Aluminium and Acetal Modules (designed to take 6ml vials [210])

Polystyrene modules (designed to take 5ml vials)

6ml vials (Beckman mini poly-Q-vial, Indianapolis, IN, USA)

5ml vials (Greiner, 124263, Kremsmünster, Austria).

Cholesterol (Sigma-Aldrich C8667, Dorset, England, UK)

Picologger thermocouples and reader (TC-08 k-type Picotechnology, St. Neaots, England, UK)

NaCl – Sigma Aldrich (S9888 Dorset, England, UK)

DMSO – Sigma Aldrich (276855 Dorset, England, UK)

Distilled Water

## **Methods**

In the literature, several different methods are used for the study and industrial application of cryoconcentration. Commonly this includes slowly lowering a vial into a cold liquid-bath, thereby inducing a temperature gradient and phase transition at the rate the vial is lowered into the solution [283, 337]. Inducing ice formation on the inner wall of a pipe or cylinder is also practiced, and allows for the easy removal of the liquid component [330], or separately by solidifying a falling film of liquid over a cold surface [342].

The primary experimental set-up consisted of a cold-plate EF600 controlled rate freezer with an attached thermally insulating module. 6ml vials were cooled from their base, and ice developed upward. This allowed a simple, measurable, and reproducible simulation of the cryoconcentration experienced by the bio-artificial liver.

A taller polystyrene module was attached to the EF600 cooling plate for additional measurements in taller & thinner 5ml cryovials.

Unless otherwise stated, all samples contained a small amount to cholesterol to act as an ice nucleator [263].

Samples were prepared and added to the modules on the EF600 freezer. The freezer was cooled to its start temperature, before the pre-defined cooling profile was followed.

To determine ice growth rates, thermocouples (k-type, picotechnology) were placed at four equidistant locations in the sample during a cooling run in duplicate. The time taken for the thermocouples to fall below the freezing point was used to measure ice front speed.

The ice front speed can be controlled and measured quite accurately by modifying the temperature profile of the cold plate.

Very rapid freezing can be induced with the use of a thermally conducting aluminium module, with ice nucleating agents utilized to control the level of supercooling and direction of ice growth.

Samples were stored at -80°C until required.

### **Of Small Volume Vials Cooled Horizontally or Vertically**

#### **Materials**

As above

## Method

It was necessary in some cases to cool vials horizontally or vertically. Vials were placed into their insert used on the EF600 module. After the cholesterol ice nucleator was added, the top of the module was sealed and heavily insulated. The module containing the vials was then placed either on its side or upside-down in either a  $-80^{\circ}\text{C}$  or  $-20^{\circ}\text{C}$  freezer depending on the experimental aims.

Samples were stored at  $-80^{\circ}\text{C}$  until required.

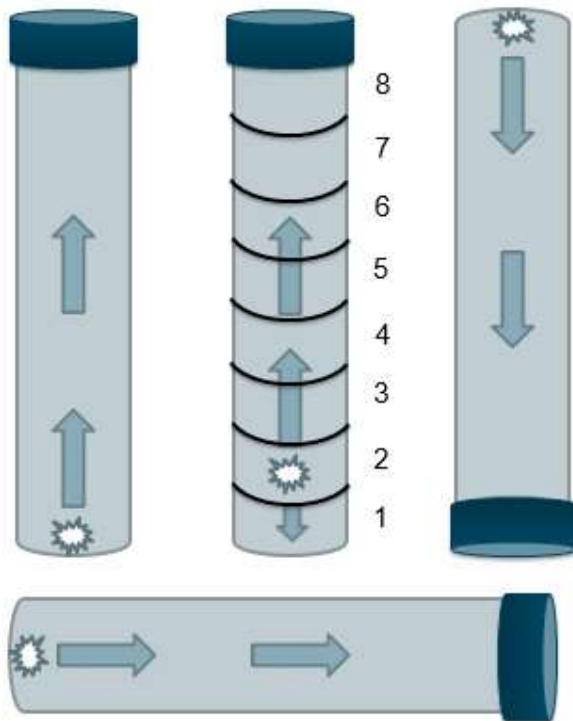


*Figure 37 - Cryoconcentration vial experimental setup. The left vial represents a vial solidified base upwards, with nucleation indicated by the white explosion. The centre vial represents the approximate dissections of the vials, carried out after solidification. The right and bottom vial show ice formation and growth top down and horizontally respectively.*

### Of 1 Litre Samples.

#### Materials

1 litre flask (Corning 490cm<sup>2</sup> roller bottle, sigma, Dorset, England, UK)

Pasteur Pipettes (Sigma Aldrich, Brand, Z331759, Dorset, England, UK)

As above

## Methods

1 litre of the desired solution was added to a 1 litre volume flask. The flask was then placed directly into a -80°C freezer. After a set time, the liquid state (usually located centrally) was mixed, and a sample taken with a pasture pipette.



*Figure 38 - The EF600 freezer (right), with example vial (left). Heat will escape through the base of the vial and ice grow upwards dependant on rate of heat extraction, a method developed in chapter 7 to mimic the large volume BAL during cryopreservation and so these experiments should be directly applicable to the BAL cryopreservation project.*

### Thawing Samples.

#### Of 6ml Vials

#### Materials

20°C water

Scissors

Scalpel (Swann Morton, No. 3 blade, Sheffield, England, UK)

#### Method

6ml vials were removed from cold temperature storage and plunged into 20°C water for 25 seconds. The lid was removed, and a small incision made in the base of the vial. The sample was then forced out of the vial with an implement inserted through this incision.

Samples were then dissected with a scalpel into eight equal disks, and each of these disks allowed to thaw in air separately.

## **Of 5ml Samples**

The taller samples were treated as above, with the following modifications:

Samples were removed from storage and placed into liquid nitrogen. The top of the vials (above the sample) were removed, before the samples were removed from the vials.

This ensured no melting with these smaller samples, and allowed the sample to leave the vial without being hindered by the internal threading used to attach the vial cap.

## **Measuring Concentration Increase**

### **With a Refractometer**

#### **Materials**

Refractometer - (Spec Scientific 300034, Berlin, Germany)

5ml stripettes

Pipette boy

#### **Method**

Refractive index was measured with a refractometer. As the refractive index of water increases with an increase in DMSO (or other solute such as NaCl) concentration can be accurately determined by using a refractometer.

0.25ml thawed samples were placed onto the refractometer reader using a 5ml stripette attached to a pipette boy, and the values produced were related to a standard curve. It was established that cholesterol, the common ice nucleator, did not affect the refractive index.

The refractometer contained a small translucent window, on which the sample to be tested was placed. When the sample was added a cover was placed over the sample – this cover was attached to the refractometer. The refractometer then used light to determine the refractive index which was displayed on a screen.

A standard curve was formed through measuring the refractive index of several known concentrations of DMSO in water.

It should be noted that this will give average concentration of both the pure ice and solute channels together – it will not determine them both individually. Care must also be taken to

measure samples at the same temperature as refractive index is temperature dependent. All samples were warmed to 20C before measurements were taken.

### **Determining Diffusion Coefficients**

As seen in section 8.3.1, models give only an approximate value for the diffusion coefficient for a system that need to be related to an experimental value.

Due to a lack of specialised equipment for this task in the lab, measurements for diffusion coefficients and also for viscosity were taken from published data where stated.

### **8.5.2. Results**

In the first instance, experiments were carried out in 6ml vials with a 1cm diameter in specially designed modules for the EF600 controlled rate freezer. The liquid height in these vials was 4cm, and the freezing times ranged from 5 minutes to several hours.

In order to amplify the effects and measure new parameters, taller and thinner cryovials were also used to measure cryoconcentration. These had a total volume of 5ml, with a liquid height of 6cm.

Unless otherwise stated, vials were placed vertically in the EF600 – its only operable position. This gave rise to the possibility of gravitational effects affecting the results. To measure this, some vials were frozen top-down or horizontally as stated in section (8.5.1)

While it has previously been established that large volumes can be mimicked in smaller sizes, and it is preferable in terms of economics and time, testing cryoconcentration in larger volumes was also carried out for corroboration.

### **DMSO**

The optimal concentration of DMSO for the cryopreservation of ELS is 12%. In view of this, the cryoconcentration of 12% DMSO in distilled was measured in this section.

### **Ice Growth Rates**

The temperature profiles in the EF600 were measured for four different cooling rates in the acetal insert – 5°C/min, 1°C/min, 0.3°C/min, and 0.1°C/min. Further measurements were also

taken for the aluminium insert taken at 5°C/min. The measurements were taken in duplicate equidistant from each other at the top, upper region, lower region, and base of the vials. The rates were used in Figure 39:

Ice growth rates can be found from the timepoint where the thermocouple fell below the equilibrium freezing point, usually accompanied by an increase in the cooling rates,

### Measured Cryoconcentration

The measured concentrations of DMSO in equal volume segments between the base (1) and top (8) of the 6ml samples, for different flow rates was determined by refractive index:

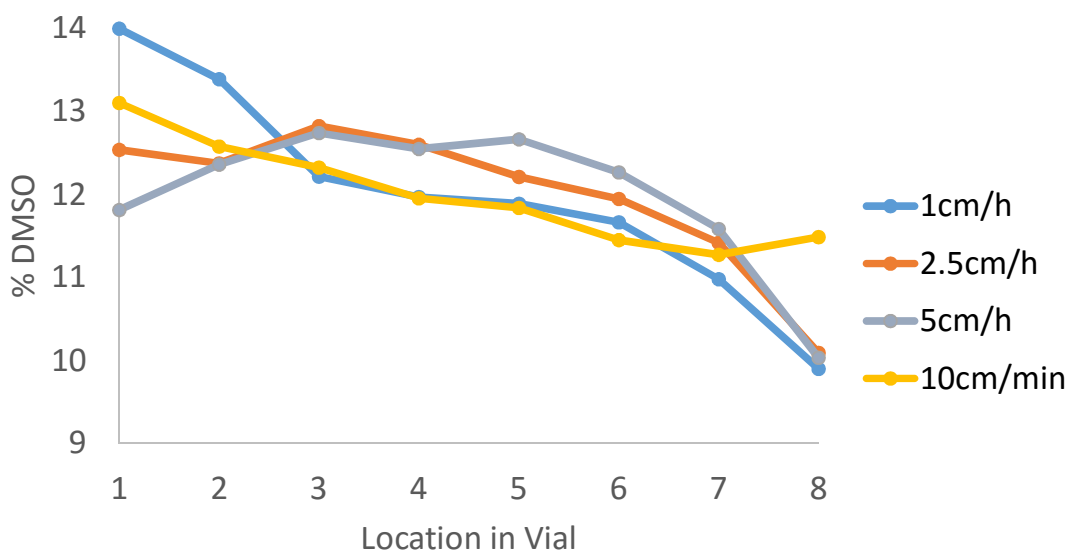


Figure 39 - The levels of DMSO measured in the ice after cryopreservation, in different inserts and at different cooling rates programmed into the EF600. Location one is the bottom 1/8<sup>th</sup> of the sample and location 8 is the top 8<sup>th</sup> of the sample which was dissected into 8 equal segments. Ice formed in location 1 and developed through all segments to location 8. In general, the lower the cooling rates the higher the degree of inverse-cryoconcentration (as the lower the ice growth rates were). Here all samples were cooled in the acetal (Ace) module, except the green line that was in aluminium (Al). n=5.

As can be observed Figure 39, a general decline in DMSO concentration occurred higher in the sample. This became more pronounced for slower cooling rates. The decline between the top and base of the vials is significant ( $P < 0.01$ ) for samples in the acetal insert at the 5, 0.3, and 0.1°C/min cooling rates, and significant at a  $P < 0.05$  level for the aluminium insert using a paired student's t-test.

This was unexpected – the DMSO seems to be preferentially included into the ice front, resulting in a decline in DMSO concentration deeper into the sample. Slower cooling rates would be expected to produce a greater degree of (inverse) cryoconcentration, and that seems to be the case here.

To further 1 dimensionalise the problem, the experiments were repeated in a taller and thinner vial with the y and z dimensions much smaller than the x dimension. Based on the data gathered in section 8.2, the slower and longer cooling should result in a greater degree of inverse cryoconcentration. The temperature profiles and cryoconcentration are displayed in Figure 40 - Measured DMSO concentrations in the taller 5ml vials, each segment representing 5mm in height throughout the height of the 60mm vial. After freezing (ice formation bottom up), samples were extracted from the vials and dissected into 11 equal circular segments. These were separately melted and the refractive index measured which was correlated with a standard. Data is average of  $n=5 \pm SD$ . No statistically significant differences were noted between any location..

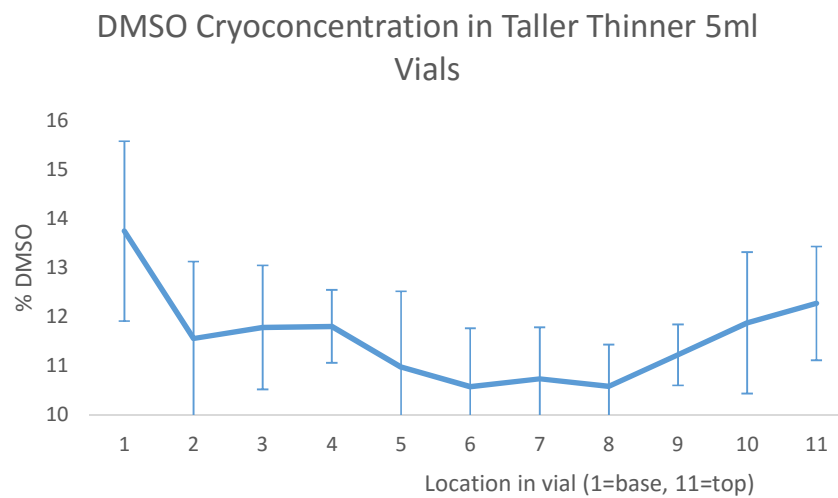


Figure 40 - Measured DMSO concentrations in the taller 5ml vials, each segment representing 5mm in height throughout the height of the 60mm vial. After freezing (ice formation bottom up), samples were extracted from the vials and dissected into 11 equal circular segments. These were separately melted and the refractive index measured which was correlated with a standard. Data is average of  $n=5 \pm SD$ . No statistically significant differences were noted between any location..

Although the beginnings of a trend may be emerging. There is no significance at any location. This is perplexing as a slower cooling rate to resulting in a larger degree of cryoconcentration might be expected. To further investigate the apparent paradox between Figure 39 and Figure 40, a large volume was cooled.

At set timepoints, the samples were removed and the liquid regions' DMSO concentration measured. At later timepoints, the DMSO in the liquid phase became more concentrated (data not shown here).

To further explore the phenomenon, several large translucent 1 litre samples were placed directly into a -80°C freezer, and when partially solidified and then thawed. It was found that higher in the sample had a lower concentration than the base of the sample, indicating that density effects were in play.

A 1 litre sample was also cooled from its base on the cold place of the EF600 freezer. As ice expanded slowly from the base of this volume, plumes were observed to rise from the ice front towards the top of the liquid. The composition of these plumes is not currently known.

It was also noted that on thaw the density components did not mix. A 1 litre volume was frozen and then left to thaw, with the concentration at the top and base of the 11cm vessel measured. 48 h after the thawing was complete, repeat measurements indicated that the top of the chamber had a DMSO concentration of 6%, while the base was at 16%. This was the same as measured on day of thaw. This suggests that diffusion does not play a significant role – density dominates.

Another large volume was also left to thaw. Once all the ice had melted it was shaken vigorously to mix the fractions. After 48 hrs the mixture remained homogeneous at 12% - no spontaneous redistribution of DMSO had taken place.

The experiments with the 5ml vials were repeated, but this time the samples were cryopreserved horizontally. This should have removed the effects of density differences in the sample. Figure 41 shows the measurements.

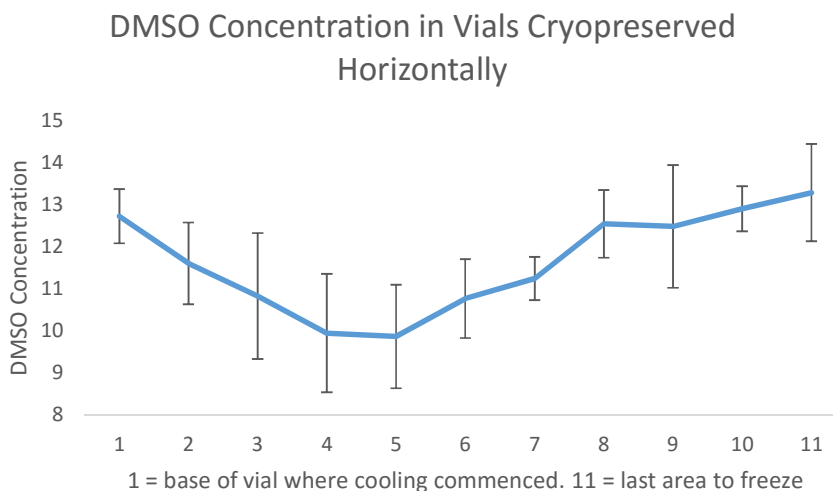


Figure 41 - DMSO concentration in the solid phase after being cooled in a -20°C freezer horizontally.. After freezing samples were extracted from the vials and dissected into 11 equal circular segments. These were separately melted and the refractive index measured which was correlated with a standard. Data is average of  $n=5 \pm SD$ . No statistically significant differences were noted between any locations. No gravitational density effects should exist through the sample in this case.

Figure 41 shows that there was cryoconcentration towards the end of the sample, after a nadir was reached mid-point.

Up to this point, supercooling has not been taken into account. It has been assumed that the supercooled area in the samples is minimal. As part of the sample will solidify quickly prior to the commencement of slow solidification (segments 1 onwards), it could be hypothesised that these were different regimes and the DMSO interacted with ice differently (In a way not predicted by section 8.2.12). Samples were then deliberately supercooled further to examine this regime.

### **Effects of Supercooling**

While trying to minimise supercooling, it can never be completely eliminated [263, 289, 328]. It had a larger effect in samples cooled more rapidly, as the temperature fall is more distinct, and in particular in the aluminium modules as heat is removed much more effectively.

As discussed in 8.3.5 a sample solidifying rapidly – as is the case in the supercooled region – will experience a different dynamic than a slowly cooled PS (progressive solidification) regime. Modelling would suggest that this would reduce cryoconcentration, as it reduces the magnitude of the diffusive term.

The data, particularly in Figure 39, may suggest that during supercooling, DMSO is preferentially included in the ice front, while it is preferentially excluded during subsequent slow cooling. The mechanisms for this are not fully understood and the fact that DMSO becomes more soluble at lower temperatures should be kept in mind.

A sample was cooled from -5°C to -100°C in the aluminium module. As this is closer to the equilibrium melting point than the carried data from 4°C to -100°C, this new data would be expected to show more supercooling. The data is displayed in Figure 42. As can be observed, both data sets follow the same pattern, with no significant difference between the sets, though both sets do display statistically significant ( $p < 0.05$ ) reduction in DMSO concentration from section 1 (first area to solidify) to 8 (last area to solidify).

This could be because supercooling does not have a major effect, or that both samples nucleated at similar temperatures (as both used the same volume of cholesterol as a nucleating agent).

## Measuring supercooling Effects

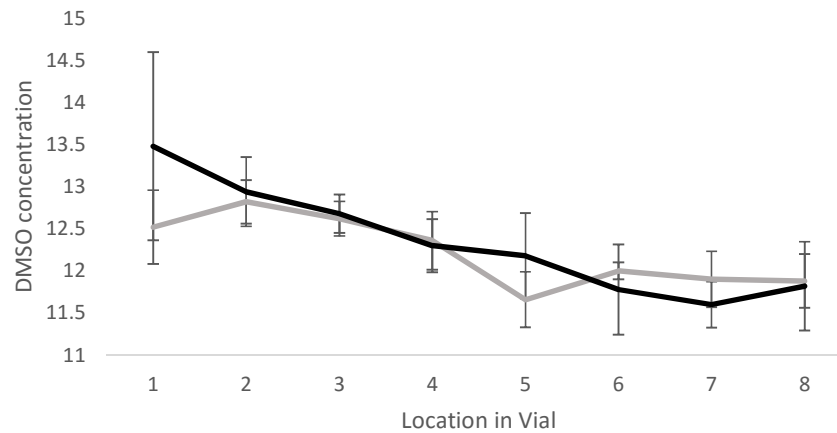


Figure 42 - Data comparing samples cooled to  $-100^{\circ}\text{C}$  at  $5^{\circ}\text{C}/\text{min}$  in the aluminium module of the EF600 controlled rate freezer to investigate the effect of supercooling. After freezing samples were extracted from the vials and dissected into 8 equal circular segments. These were separately melted and the refractive index measured which was correlated with a standard. One set of samples were cooled from  $4^{\circ}\text{C}$  (black), the other from  $-5^{\circ}\text{C}$  (grey) where more supercooling may be expected.  $n=5 \pm \text{SD}$ .

### Gravitational Effects

In consequence of the density gradients observed in 1 litre containers, and the apparent contradiction of data observed between 6ml and 5ml vials, an experiment was carried out to examine the role gravity plays in cryoconcentration. Most biological models do not take account of gravitational effects.

Tall 5ml samples were cooled in a  $-20^{\circ}\text{C}$  freezer, but this time upside down, with ice nucleating at the top of the vial and descending. These results are displayed in Figure 43.

## Cryoconcentration in 5ml Tall Vertically Frozen Samples

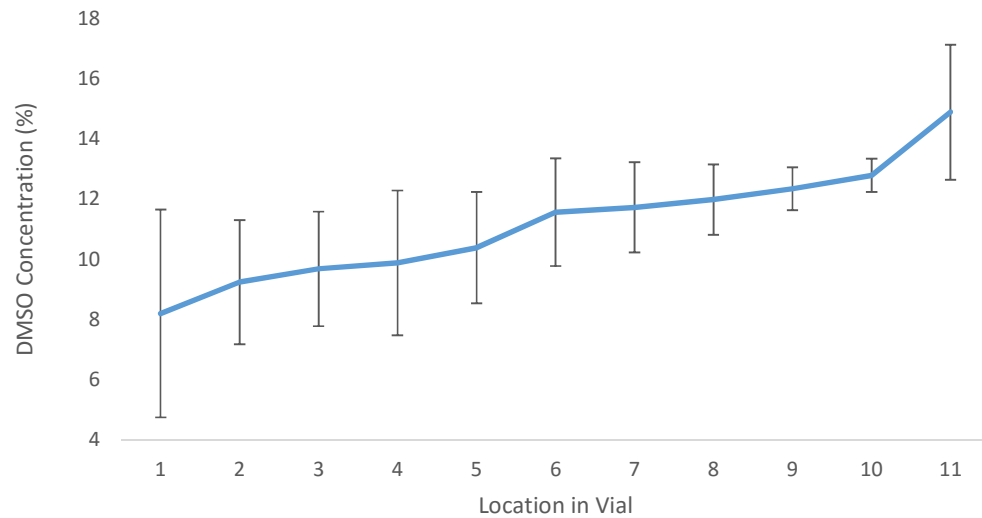


Figure 43 - Cryoconcentration observed in a sample where ice develops downwards in a sample. After freezing samples were extracted from the vials and dissected into 11 equal circular segments. These were separately melted and the refractive index measured which was correlated with a standard. Here gravitational effects are reversed. Ice nucleated near segment 1, and developed downwards to segment 11. Significant ( $p < 0.01$ ) increase in DMSO concentration was observed between segments 1 and 11 using a paired student's t-test  $n = 5 \pm SD$ .

Significant ( $p < 0.01$ ) cryoconcentration is observed. The best explanation that agrees with experimental data is that the dominating factor is gravity. In segments solidified upwards, the wall of solutes (which has a high density), cannot diffuse easily upwards in the sample, retarding cryoconcentration.

In samples solidified top-down, excluded solutes fall to the base of the sample and so cryoconcentration is increased.

It is clear that the orientation of samples must play a significant role in DMSO cryoconcentration damage.

To build an accurate model, gravitational effects must be taken into account, and these would be expected to dominate.

### NaCl

In general, biological systems such as the ELS have NaCl in their environment at 0.15M. To maintain consistency with that, and to not damage ELS unnecessarily, 0.15M NaCl in distilled water was used in this section.

## Ice Growth Rates

Ice growth rates were established as for the solutions with the use of thermocouples and known melting points as in Figure 44 . Ice growth rates of between 1 and 6 cm/h were obtained in the acetal insert, and of 10cm/min in the aluminium insert of the EF600 freezer.

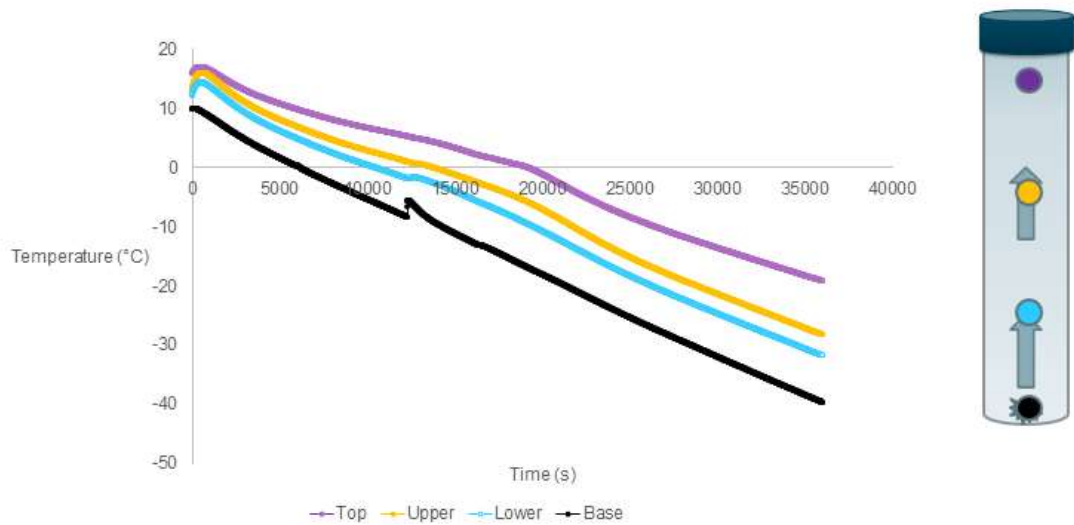


Figure 44 - Typical cooling profiles obtained with thermocouples attached to the pico-logger system. This example is of 0.15M NaCl with a cooling rate of 0.1°C/min, giving an ice front growth speed of approximately 1cm/h, measured by the time taken between thermocouples falling below the freezing point of the solution. The black line related to approximately the black point in the example vial etc. Thermocouples were placed 20mm apart from each other.

### Measured Cryoconcentration

A standard curve was prepared for NaCl in solution as per section 8.5.1 and is displayed in Figure 45, which showed a linear correlation between refractive index and concentration of NaCl.

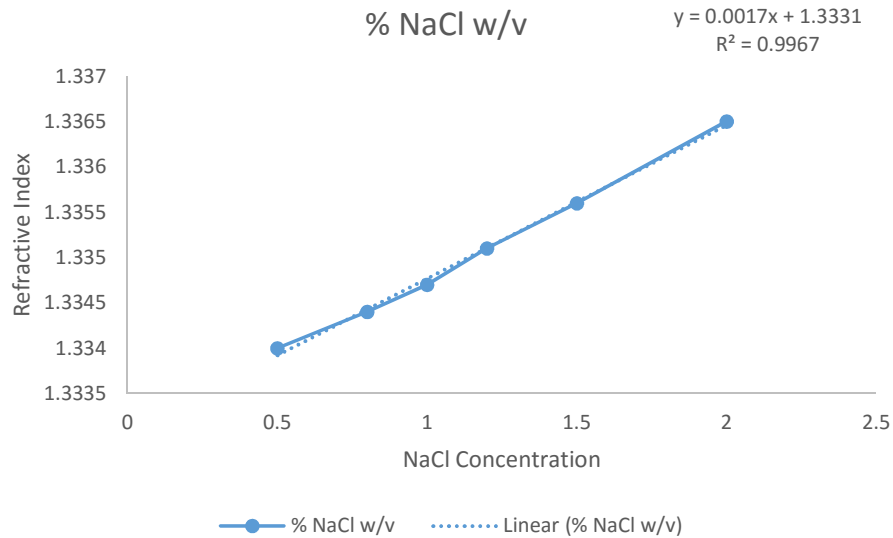


Figure 45 - Standard curve relating the refractive index of NaCl solution to a % weight. A good linear correlation is observed with  $R^2=0.9967$ . For reference, 0.15M NaCl is 0.87% NaCl w/v. Samples were prepared with different concentrations of NaCl and then their refractive index measured at 20°C using a refractometer. Data average of n=5 separate solutions made for each NaCl concentration.

The solute redistribution was first measured vertically in the shorter 6ml vials. The cryoconcentration of NaCl in the samples cooled at 1°C/min showed a significant decline ( $p<0.05$ ) in NaCl concentration throughout the sample. There was no significance in the other sets.

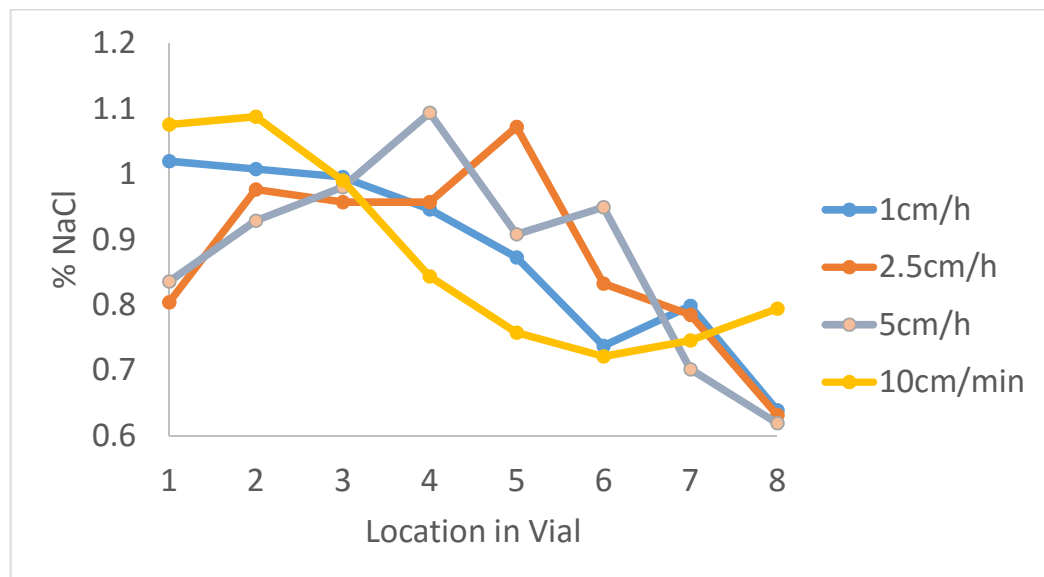


Figure 46 - Cryoconcentration measured in NaCl samples cooled at different ice growth in the acetal module, and at the aluminium module (yellow). After freezing samples were extracted from the vials and dissected into 8 equal circular segments. These were separately melted and the refractive index measured at 20°C which was correlated with a standard. A general trend towards inverse segregation seems to be present.  $n=5 \pm SD$ .

This result was again unexpected, as it has been reported, and is widely accepted that water-ice rejects NaCl. It is also observed in the literature that vertical vials experience solute exclusion, though these literature samples are stirred.

This would seem to add weight to the hypothesis that gravitational effects are dominant during solute redistribution.

At the very top of the sample, there was usually a small 'white' region. On testing, this region was found to contain 21% NaCl – the eutectic point. This implied that this white area was last to freeze and so experienced extreme concentration. Due to the fraction's small size, it could have been missed when sampling the top section.

A second run was carried out using the taller, thinner 5ml samples. For the 0.1°C /min case, (Figure 47), there was no significant variation in the concentration at any timepoint.

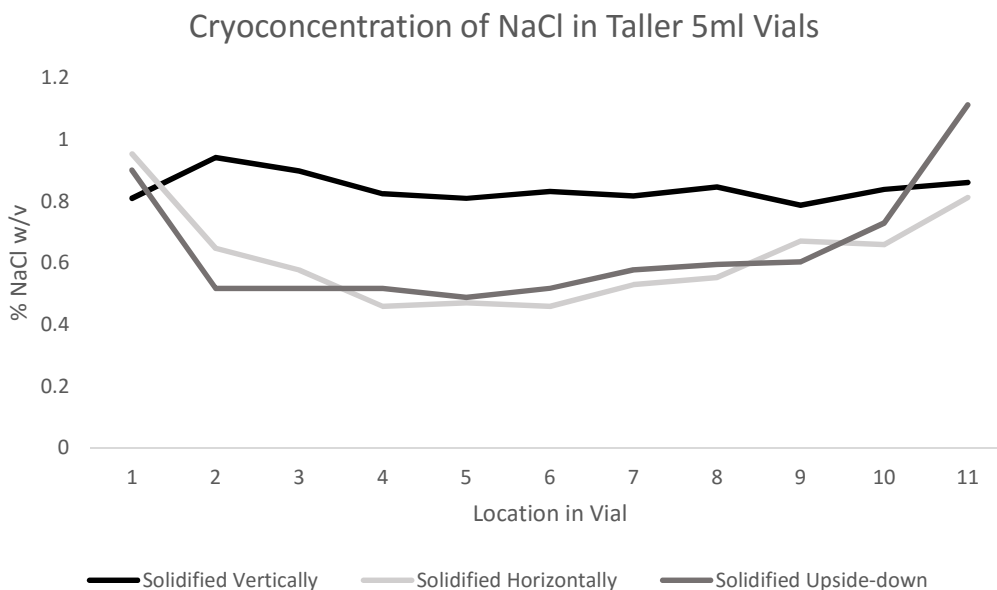


Figure 47 - Cryoconcentration measured in taller 5ml vials, both for samples frozen vertically (bottom up (n=8)), and horizontally or upside down (ice starts at the top and develops downwards) (n=5). . After freezing samples were extracted from the vials and dissected into 11 equal circular segments. These were separately melted and the refractive index measured at 20°C which was correlated with a standard. While horizontally has a lower concentration for most of the sample, notice the large variations at the first and last segments to solidify. Eutectics were noticed in at both edges for all samples, which may have disrupted readings and explains apparent differences in average concentrations in vials.

Cryoconcentration of the tall 5ml vials cooled vertically and horizontally was compared, also in Figure 47. No major differences in the trends were noticed between the two sample sets, though the horizontal sample did show a tendency (not significant) towards increased NaCl concentration at the boundaries (segment 1 and 11), of the sample.

The error bars were high for the NaCl samples, due to difficulties in segmenting samples and lower sensitivities of the refractometer. An in-depth study addressing these problems would be useful before conclusions on the NaCl system can be made.

### ***8.6. Adding Gravity to the Model***

From section 8.5, it is clear that gravitational effects are the dominant factor when it comes to cryoconcentration in our system, and this out-weights the effects of diffusion in our system. If diffusion was the dominant factor, cryoconcentration would be independent of vial orientation (ice growth direction) in this 1-D model. By varying the direction from up-down to down-up and horizontal, the only factor changing is gravity. Gravity therefore has a major impact on the outcome.

Several samples were cooled at different rates, and then allowed to thaw at room temperature. This was done in 5ml vials and 1 litre flasks, with cooling rates varying from 0.1 to 5°C/min. These samples all had a substantial concentration gradient in the system on thaw. It was also observed in all samples that the concentration gradient did not mix when left undisturbed for several days, suggesting that diffusion is almost negligible. Gravity therefore is the dominant factor.

Gravity was not included as a parameter in the models above, and so they cannot be correct in a cryobiological system, indicating that this was a novel contribution to the field. No studies in the literature could be found where the impact of gravity on cryoconcentration was discussed or measured.

Clearly the effect that gravity has will depend on how the density of the solution varies with concentration. This was measured for DMSO and shown in Figure 48. In the base case of 12.5% (v/v) DMSO in aqueous solution the absolute mass density is 1.013 g/ml at 20°C.

## Density of DMSO at Varying Concentrations

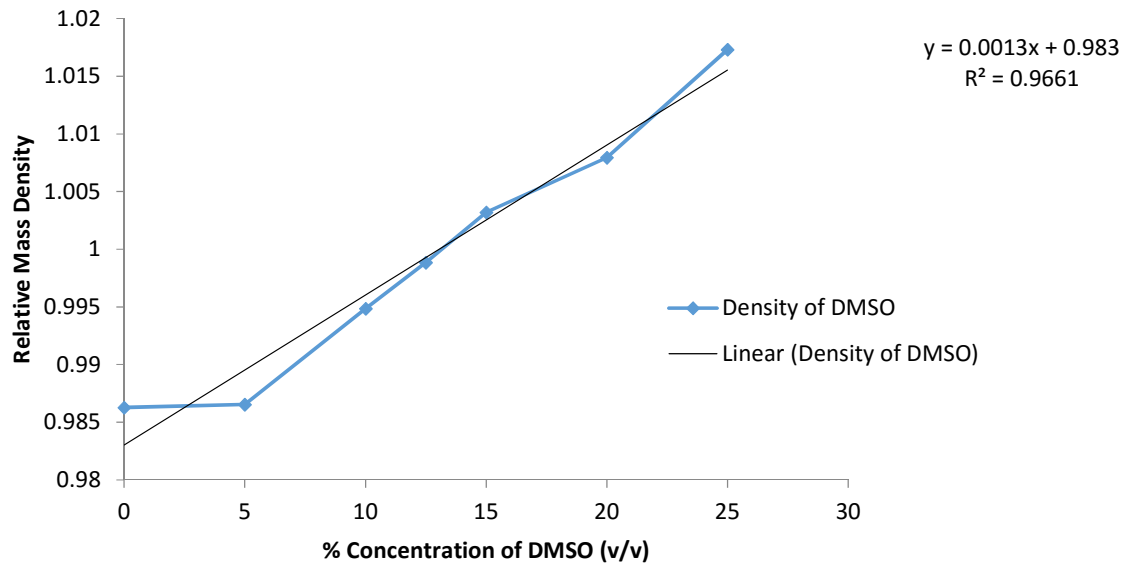


Figure 48 - Figure of relative measured mass density of DMSO at varying concentrations and with a linear line of best fit added. Samples were prepared with different concentrations of DMSO and then their refractive index measured at 20°C using a refractometer. Data average of n=5 separate solutions made for each DMSO concentration, which was then normalized (12.5% = 1). Here 12.5% was assumed to be the 'normal case = 1'. A value of 1.01 indicated that the density of this solution was fractionally 1.01 higher than 12.5% DMSO.

In Figure 39, the concentration of DMSO falls higher in the vial. This is not completely explained by either gravity or standard cryoconcentration – if a solute is being solely excluded from the ice front, areas should not exist in the liquid state prior to freezing below the original concentration. This is clearly happening in our system.

Plumes of liquid have been observed rising from the freezing interface in a DMSO water system being cooled base-up. It is postulated that this happens due to melting on the ice wall. While ice crystals grow globularly, they may melt and shrink locally. If there are more areas of growth than melt the crystal will expand in the globular sense. Small areas of melting crystals (perhaps caused when a dendrite grows into an area of higher solute concentration), could explain how areas of low solute concentration exist. The amount of this melt is important to determine the cryoconcentration picture.

The partition coefficient will determine the difference between the concentration in this melt and the surrounding liquid.

Also, the size and depth of the sample have a significance. The larger the radius of the vial the larger the surface area available for re-melting, and the height of the vial dictated how far this liquid can be carried away from the ice front.

The gravitational term,  $Z$ , will be added to equation ( 17 ) in the following way:

$$(D + Z) \frac{d^2 C}{dx^2} + R \frac{dC}{dx} = 0$$

(32)

Through experimental observations, the form of Z is proposed to be proportional to:

$$\frac{g}{\mu} \times K_L \times F \times \frac{\rho_{increase}}{V_{changing\ state}}$$

(33)

Where g is the gravitational acceleration due to gravity. F is the average number of times each molecule of water solidifies as the ice front passes over (more freeze-thaw of dendrites on the ice wall will increase this value).  $K_L$  is the local partition function,  $\rho_{increase}$  is the change in density of the solution with increasing solute concentration, and V is the volume solidified.

Inserting this into equations ( 19 ) and ( 20 ), gives an updated model.

$$C_L^* = \left( 1 + \frac{1 - K}{K} e^{\left(-\frac{R}{D+Z}x\right)} \right)$$

(34)

$$C_s = C_0 \left( (1 - K) \left[ 1 - e^{\left(-\frac{R}{D+Z}xK\right)} \right] + K \right)$$

(35)

While these two equations ( 34 )( 35 ) are not perfect, in so far as they do not correctly describe the situation for a very large vial or predict the boundary layer of the ice front as accurately, they are more accurate and useful to measure cryoconcentration in biological settings.

## 8.7. Conclusions

Cryoconcentration can cause significant deviation from the optimal concentration of CPAs and other solutes during cryopreservation. The primary factor would appear to be a gravitational term, which has significant impact for large volumes cryopreservation in future. In particular a sample cooled from all sides, as an organ likely would be, will eject a large volume of solutes from its upper edge inwards, resulting in the lower central portion of the biomass experiencing damaging levels of solutes and impacting on cryopreservation success.

No mention of a gravity dependency has been found in the scientific literature after an extensive search, although it is used to make bubble-free ice cubes in the hospitality industry and some

commercial fridge-freezers. This is somewhat surprising due to the dominance of the effect here. Part of the reason for this may be the fact that most models are based on work in metallurgy, where temperature (and so density) changes in metals will be extreme and so the solidification process will be affected by these changes to a greater degree, as well as metal casting carried out quickly to avoid cryoconcentration – solutes will then not have enough time to fall under gravity.

Detailed measurements of viscosity are required for the use of this model in the BAL system to make specific predictions, and equipment for this was not available at time of writing. Future work could explore this to add appropriate scale factors to the BAL system. A simple reading of the model, however, indicates that to minimize cryoconcentration the BAL device must be frozen from the bottom upwards. This is the method already used in the BAL indicating that cryoconcentration is already minimized as much as can be through using gravity.

As one of the primary causes of damage during cryopreservation is related to solute increases, this observation could be applied to many systems to reduce or eliminate solute increase toxicity.

## 8.8. Appendices

### 8.8.1. Appendix 1 –To Equation ( 19 )

See refs [39, 370, 405].

Equation ( 17 ) is a simple second order differential equation with general solution:

$$y = A^{m_1x} + B^{m_2x} \text{ where } m_1 \text{ and } m_2 \text{ are solutions to the auxiliary equation } m^2 + m = 0$$

In our case the specific auxiliary equation is  $Dm^2 + Rm = 0$ , which has solutions  $m_1 = -(R/D)$  and  $m_2 = 0$ . Therefore we have, for the concentration in the liquid  $y = C_L$ :

$$C_L = Ae^{-\frac{R}{D}x'} + B$$

Here  $x'$  is distance from the water-ice interface. For BCs, we know that as  $x' \rightarrow \infty$ ,  $C_L \rightarrow C_0$  (ie. Far away from the ice front the liquid concentration does not change from its original value.) Therefore  $B = C_0$ .

Considering the case at  $x' = 0$  – on the liquid-ice interface -,  $C_L = \frac{C_0}{K}$ , from the definition of the partition coefficient - the ratio of solute preference for the solid phase for the liquid phase. Therefore  $A = \left(\frac{C_0}{k} - C_0\right)$ . Putting this all together gives equation ( 19 ):

$$C_L = \left(1 + \frac{1-K}{K} e^{\left(-\frac{R}{D}x'\right)}\right)$$

### 8.8.2. Appendix 2 – To Equation ( 20 )

Detailed in [405]

Moving from the start of the sample inwards, the concentration of the solid phase will increase from an initial concentration  $C_S = kC_0$  at  $x=0$ , towards  $C_0$ . The rate at which  $C_S$  approaches  $C_0$  will be proportional to the difference between them:

$$\frac{d(C_0 - C_S)}{dx} = -a(C_0 - C_S)$$

Where  $a$  is a constant of proportionality. This has solution:

$$(C_0 - C_S) = Ae^{-ax} + B$$

Where A and B are constants. As  $(C_0 - C_S) \rightarrow 0$  as  $x \rightarrow \infty$ ,  $B=0$ . As  $C_S = kC_0$  at  $x=0$ ,  $A = C_0(1 - k)$ .

Therefore we have  $C_S = C_0 - C_0(1 - k)e^{-ax} = C_0[(1 - k)(1 - e^{-ax}) + k]$

( 36 )

To find  $a$ , we use conservation of mass – the amount of solutes above the  $C_0$  level in the liquid must equal the deficit of solutes in  $C_S$  (below  $C_0$ ).

Integrating equation ( 19 ) w.r.t.  $x$  between 0 and  $\infty$ , yields:

$$\text{Solute excess} = C_0 \frac{D}{R} \left(\frac{K-1}{K}\right)$$

( 37 )

Integrating equation ( 36 ) between 0 and  $\infty$ , yields:

$$\text{Solute deficit} = \frac{1}{a} C_0(1 - k)$$

( 38 )

As equations ( 37 ) and ( 38 ) are equal,  $a = \frac{kR}{D}$

Hence equation ( 20 ):

$$C_s = C_0 \left( (1 - K) \left[ 1 - e^{\left(-\frac{R}{D}xK\right)} \right] + K \right)$$

### 8.8.3. Appendix 3 – Diffusion Coefficients

#### Using the Wilke-Chang equation

DMSO

Using the Wilke-Chang equation as the solute (DMSO, molecular mass = 78) < 5x the size of the solvent (water molecule, molecular mass = 18):

$$D = 7.4 \times 10^{-8} \left( \frac{(wM)^{1/2} T}{\mu V^{0.6}} \right)$$

Here w = 2.6 (constant for water)

M = 18 (of solvent, water)

T = 298k

$\mu$  = 0.8937 cP (centripose)

V = 70.91 molg<sup>-1</sup>cm<sup>3</sup> (calculated from a density of 1.1gcm<sup>-3</sup>)

So diffusivity, D, = 1.31x10<sup>-5</sup>cm<sup>2</sup>s<sup>-1</sup>

NaCl

Here  $w = 2.6$  (constant for water)

$M = 18$

$T = 298\text{K}$

$\mu = 0.8937$  cP (centipoise)

$V = 27 \text{ cm}^3 \text{ mol}^{-1}$  (calculated from a density of  $2.17 \text{ g cm}^{-3}$ )

So diffusivity,  $D$ , =  $2.3 \times 10^{-5} \text{ cm}^2 \text{ s}^{-1}$

### Using the Stokes-Einstein Relationship

ELS

The Stokes-Einstein Equation is:

$$D = \frac{K_B T}{6\pi\mu r}$$

Where  $K_B = 1.38 \times 10^{-23}$  (Boltzmann Constant)

$T = 298\text{K}$

$\mu = 0.8937 \times 10^{-3}$  P (Poise – Pa.s). Note this is of water, the final water-DMSO mix will have a higher viscosity, lowering the diffusion coefficient.

$r = 0.5 \times 10^{-3} \text{ m}$

This gives a value of  $4.9 \times 10^{-22} \text{ m}^2 \text{ s}^{-1}$ . This is well below the limits of detection.

Glucose

Using the Stokes-Einstein Equation,

Where  $K_B = 1.38 \times 10^{-23}$  (Boltzmann Constant)

T = 298K

$\mu = 0.8937 \times 10^{-3}$  P (Poise – Pa.s). Again note this is of water, the final water-glucose mix will have a higher viscosity, lowering the diffusion coefficient.

$r = 3.28 \times 10^{-10}$  m [93].

This gives a value of  $7.47 \times 10^{-10} \text{m}^2 \text{s}^{-1} = 7.47 \times 10^{-6} \text{cm}^2 \text{s}^{-1}$ .

# 9. Spatial Considerations during Cryopreservation of Large Volume Samples.

## 9.1. Introduction

### 9.1.1. Overview of Chapter

Compared with cryopreservation of smaller volumes, typically up to 2ml, there have been relatively few studies on the implications of the physical conditions experienced by cells during large volume (liters) cryopreservation as has been discussed previously. Chapter 7 validated a scale down model to emulate the physical events which occur during large volume cryopreservation, especially relating to the processes of ice crystal nucleation and propagation. In this chapter the spatial effects of ice growth by progressive solidification (PS), generally seen during larger scale cryopreservation, on encapsulated liver hepatocyte spheroids (ELS) have been explored. A method was developed to reliably sample different regions across the frozen cores of samples experiencing PS [210].

This chapter examines the spatial variation in post-thaw outcome of a cryopreserved biomass that experienced PS on cooling, both on the large volume and scale-down system, and considers physical and spatial challenges on thawing a large volume.

Under conditions of progressive solidification (PS), the spatial location of ELS had a strong impact on post-thaw recovery, with cells in areas first and last to solidify demonstrated significantly impaired post-thaw function, whereas areas solidifying through the majority of the process exhibited higher post-thaw outcome. This is likely due to extended exposure to increased concentrations of cryoprotectants redistributed to the remaining small liquid volume towards the end of ice nucleation, and potentially non-optimal cooling rates after the ice front passed.

Spatial significance of warming was also explored, in conditions of non-homogeneous thawing. During warming of a 2-litre volume, it was found that samples where the ice thawed more rapidly had greater post-thaw viability 24 h post-thaw ( $75.7 \pm 3.9\%$  and  $62.0 \pm 7.2\%$  respectively).

### 9.1.2. General Introduction and Large Volume Re-cap

The primary focus of most studies on cryopreservation to date have been of relatively small volumes - these tend to experience minimal spatial variation in their thermal and temporal cryopreservation histories. As covered in earlier chapters, during cooling a cryovial or straw often (depending on the cooling rates and volumes involved) cool below their equilibrium freezing point prior to ice nucleating and passing through the sample rapidly resulting in a dendrite ice structure through the sample [210]. This is a consequence of the morphology of the sample container and its relationship to the source of heat transfer. At low rates of cooling all of the sample is within a few mm of the sample wall, so large inhomogeneous thermal profiles tend to be minimized and disperse relatively quickly. Even in larger cryobags the sample is flattened, with only a few millimetres maximum thickness [171, 265, 379]. The cryopreservation of larger and more complex specimens does not lend itself to such strict morphologies.

With the increased interest in producing bio-artificial and re-cellularized tissue scaffolds in medical settings, the cryopreservation of complex morphologies becomes more significant, hence the PhD. Large replacement and temporary support organs or biomasses can take many months to produce, but are often required urgently. Just in Time Manufacture is not possible – neither logistically nor economically. I need to cryopreserve the BAL so that it can be thawed on demand [173, 186, 377]. This necessitates the further, spatial, study of the physical implications of larger volume cryopreservation and the impact of its physical parameters.

The studies in this chapter have direct applications to the cryopreservation of the 2-litre biomass of alginate encapsulated liver spheroids (ELS) for the BAL, and should help identify where damage occurs spatially in the system, both during cooling and warming, and so used to develop an optimised protocol. Biomass near the chamber wall (within 2-3mm) will undercool before nucleation. As no doubt you will remember from chapter 7, the remainder of the sample will not undercool, rather it will cool asymptotically to the equilibrium freezing point, before solidifying when the ice front 'grows' through its location (the biomass itself being fixed through gravity and alginate encapsulation). After the latent heat of solidification has been liberated, the biomass in that area will cool rapidly towards the external environment temperature [210, 276][4, 5]. Ice structure here tends to be planer and structured [210]. This type of ice formation is termed progressive solidification (PS).

In addition, the last area to solidify during PS will remain exposed to potentially toxic CPA for a greater length of time above the equilibrium freezing temperature [210, 276]. Moreover cryoconcentration may play a role, with solutes excluded from the ice front becoming increasingly concentrated resulting in sub-optimal conditions on solidification and adding to the cryoburden [221, 297], although perhaps less than expected as the BAL is largely cooled base-up and as was shown in chapter 8, due to gravity cryoconcentration is maximised when ice develops top-down.

This chapter examined the effect of location within a PS sample on cell membrane viability and functional outcome. PS was produced in 6ml vials, giving significant cost and time savings [210], with this method being compared to a 2-litre cooling volume to corroborate results independently of sample size.

At larger volumes, with a low surface area to volume ratio, the thawing rates will always be slow. Surface cooling of a cylinder is impractical. Additionally an experimental warming device was constructed which allowed thawing large volumes rapidly and which enabled examination of spatial effects in large volume samples.

This chapter demonstrated that functional outcome of a biomass may vary intra-sample on the large scale, an important consideration for all large volume cryopreservation not just the BAL project. In addition, thawing profiles can be as important as warming profiles, and must be controlled effectively for rapid recovery of large scale cryopreserved biomasses.

## **9.2. *Materials and Methods***

### **9.2.1. *Modification of the Controlled Rate Freezer to Achieve PS in Small Volumes during Cryopreservation***

As previously described in section 7.2.2, a controlled rate freezer (EF600-103, Asymptote, Cambridge, UK) was modified to achieve PS (progressive solidification) during cryopreservation by the addition of a module designed to take 6ml polypropylene vials (Sigma, Z376825, 16 mm x 57 mm, Dorset, England, UK).

## 9.2.2. Modification and Application of 2 Litre Cryopreservation Chamber by Adding Warming Device

### Materials

5 litre volume with special thawing chamber (Asymptote Ltd.)

Water bath

Warming fluid

Heat exchanger

### Methods

The standard large volume cryopreservation chamber consisted of a 5 litre cylindrical polycarbonate chamber with simple polycarbonate end caps, into which 2 litres of alginate beads (alginate without liver spheroids) were added.

For thawing studies, this was modified by adding two larger end caps, with a cavity included in each end that was not in contact with the biomass. Between these end caps ran 25 aluminium tubes with diameter 7mm, through the space occupied by the 2 litre alginate beads.

Between these end caps, tubing was passed that ran through a pump and heat exchanger located in a water bath. A schematic of this chamber is provided on page 191.

To thaw, the chamber was removed from liquid nitrogen and allowed to warm in air for 20 minutes. Ethanol warmed to 30°C was then passed through the chamber tubing at a rate of 4 litres/min. The ethanol did not come into direct contact with the biomass.

When liquid was observed, the whole set-up was shaken on a plate shaker at a rate of 20 rotations/min. When the biomass was observed completely thawed, the ethanol was stopped and the chamber removed to a sterile hood where spatially constrained pouches were sampled.

As the device was completely thawed before sampling, and the ELS contain glass beads to help buoyancy, it was only possible to sample spatially across the device (from one end cap to the other), and not radially (from chamber wall to chamber centre).

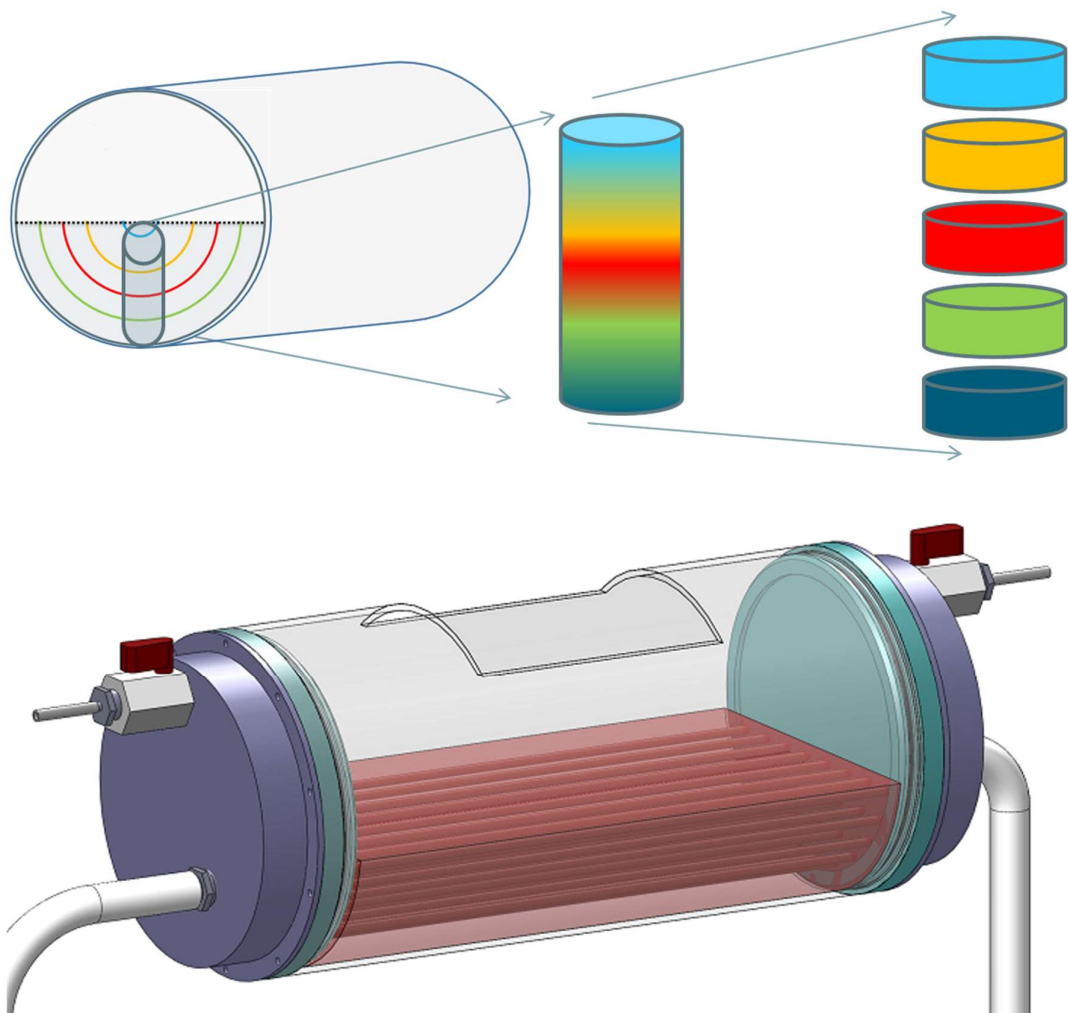


Figure 49 - Top – Schematic of the BAL chamber with representative pouch which contained cells. These pouches were nylon mesh, permeable to culture medium and ice but impermeable to ELS. This chamber was cooled from the edges, and ice developed radially to the central semi-circle, with the semicircles representing areas that solidified at the same time. The biomass fill is represented by the dotted black line. This pouch was extracted and dissected into 5 as shown on the upper right of the figure. These sections were thawed consistently to determine spatial differences in damage on cooling. This approximately replicated conditions in a vial shown in Figure 50.

Bottom – the large chamber used for thawing experiments. This was cooled from the edges as the BAL chamber shown at the top of the figure. 25 warming tubes were passed through the biomass (indicated in red), with ethanol equally distributed through each tube using larger endcaps (purple). The opening at the top was used for addition and removal of vials, and was sealed prior to cryopreservation. Pouches were placed within 5cm of either the inlet or outlet tubes (white), with pouches of cells nearer the warming inlet thawing more rapidly. Pouches were removed for viability studies on thaw. Both BAL set-ups had a diameter of 15cm and length of 30cm.

### 9.2.3. Cryopreservation Protocol for 6ml PS Samples

As section 7.2.2, in the acetal insert.

#### **9.2.4. Cryopreservation Protocol for 2 litre PS Samples without Warming Device.**

As culturing 2 litres of biomass was uneconomical, instead 2L of alginate beads free from cells were produced, and equilibrated to a final concentration of 12% DMSO in UW (University of Wisconsin Solution) solution. These were cooled to 4°C and placed into a cylindrical freezing chamber, with a total volume of 5 litres (including 3L air fraction).

Into this biomass, pouches porous to liquid and ice but not alginate beads were placed, into which alginate beads cultures containing cells (ELS) to a volume of 10ml were added. These pouches were made of a nylon mesh and sealed using a heat sealer. These pouches were 8 cm high with a diameter of 1.25cm and a volume of 10ml. The pouch was adjusted to transcend the entire range of cooling histories in the freezing chamber, and are show in the schematic at the top of Figure 49.

The freezing chamber was then placed onto a specially adapted Asymptote large volume controlled rate freezer, with a cooling plate shaped to the chamber walls [210], and cooled at 0.3°C/min from 4°C to -100°C, the cooling freezer can be seen in Figure 22.

#### **9.2.5. Thawing and Dissection of 6ml Volume PS Samples**

Each sample was removed from liquid nitrogen storage to a sterile hood. There the vial was submerged in 37°C water for 15s. The sample vial lid was opened and an incision made in the vial's base. The frozen sample was pushed out of the vial through its top while still solid. A scalpel was used to dissect the sample into 5 equal circular segments, in a similar manner to section 8.5.1.

Each of these segments were thawed by addition of culture medium in approximately 300s and re-cultured in a T175 flask.

Figure 50 illustrates the morphology of the dissected samples, and how these relate to location in the vial during the cryopreservation cycle.

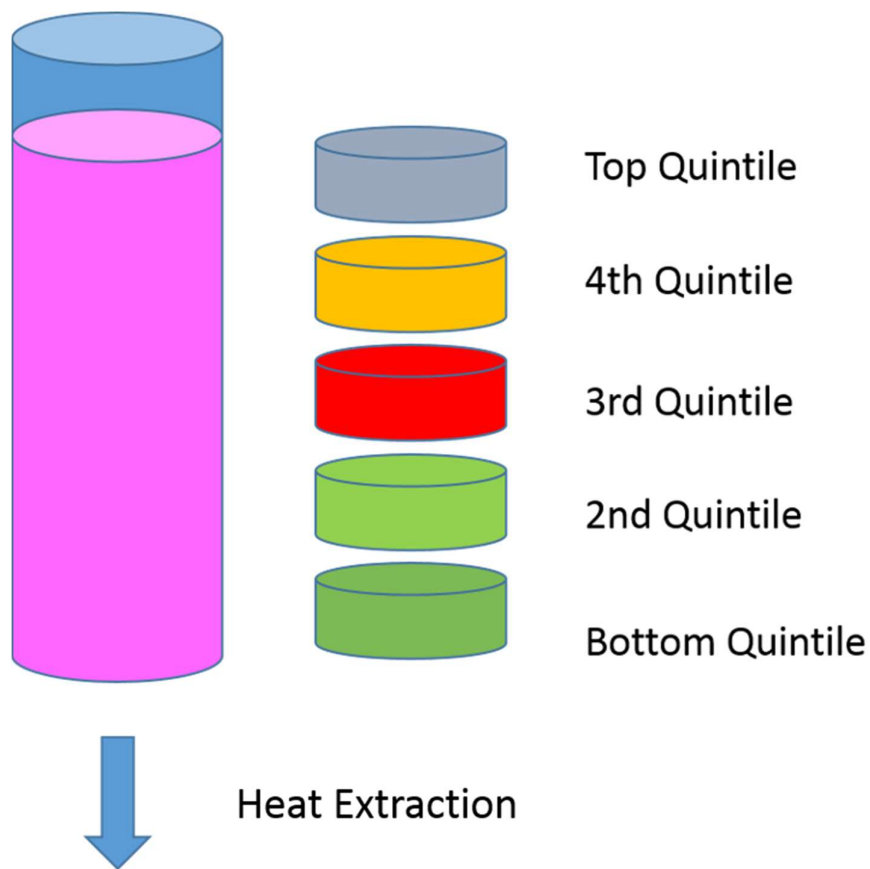


Figure 50 – Right - A schematic of a 6ml vial designed to produce PS. Heat extraction is shown by the arrow, and the sample progressively solidified upwards. Left – A schematic of the samples while still frozen after dissection. Pouches of ELS inside a 2 litre volume of alginate beads (alginate without liver cell spheroids) had a similar appearance, and were extracted while still frozen or after thawing depending on the experimental conditions and are shown in Figure 49.

### 9.2.1. Thawing of 2 Litre PS Sample without Warming Device

#### Materials

37°C water bath

Cryopreserved chamber with cell pouches

Scalpel

Timer

Chisel

## Method

The freezing chamber was removed from LN<sub>2</sub>, and its edges warmed in warm water for 60s. The end caps of the chamber were then removed, and the frozen mass extracted. The pouches containing ELS were removed with a chisel. These were then dissected into 5 components with a scalpel, thawed in 330s, and re-cultured. Post-thaw assays were carried out on thaw as the extraction process could not be carried out under sterile conditions.

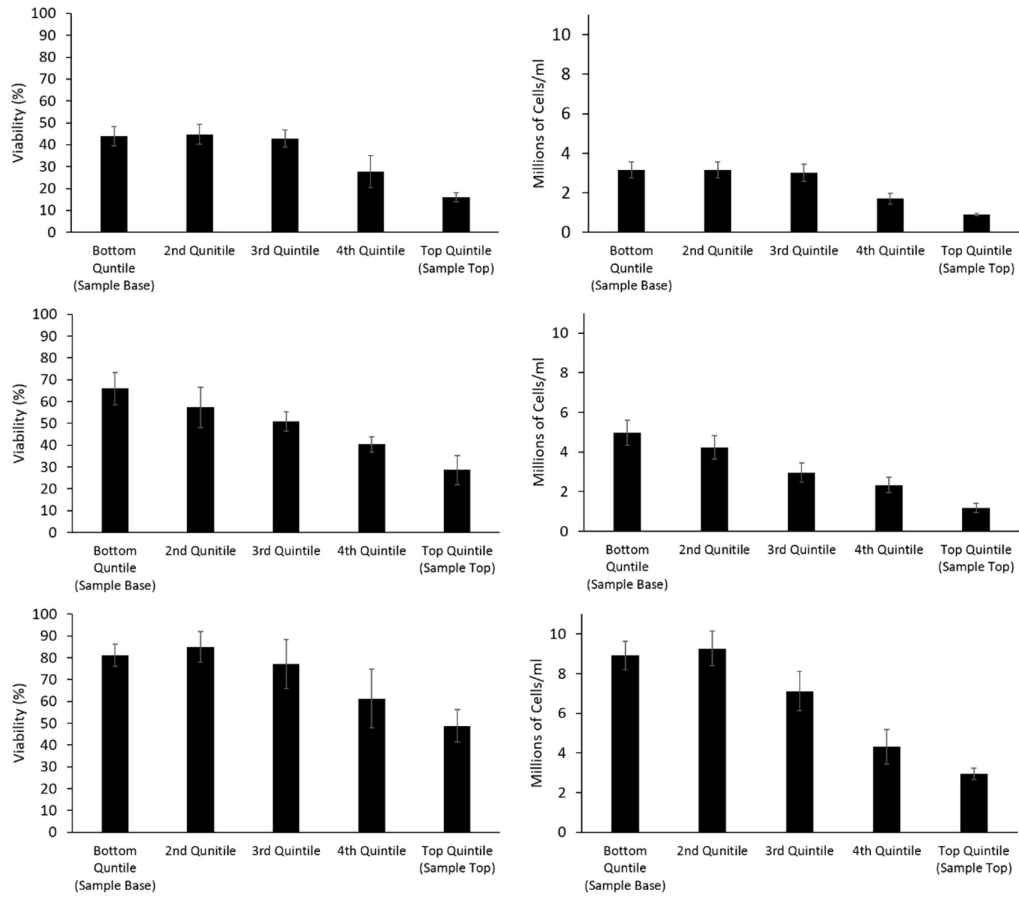


Figure 51 - Viability (left) and viable cell number (right) of samples experiencing PS in 6ml vials, day 1, 2, and 3 post-thaw (top, middle, and bottom respectively). All sets recover from a nadir at 1 day post thaw, By 3 days post-thaw, viability is significantly worse in the top (5<sup>th</sup>) quintile compared to viability in any of 1<sup>st</sup> (bottom) to 3<sup>rd</sup> quintiles. No significant difference in viability is observed between quintiles 1-4, 3 days post thaw. Viable cell number 3 days post thaw is significantly worse in the 5<sup>th</sup> quintile compared to all other locations. All n=5 ± SD. Significance defined as P<0.01 using an unpaired student's t-test.

### 9.3. Results

#### 9.3.1. Progressive Solidification (PS) in 6ml Samples

##### **Viability and Viable Cell Number**

Figure 51 shows viability and viable cell number for samples experiencing PS on cryopreservation from days 1 to 3 post-thaw. There is a trend for highest viability and viable cell number in quintiles 1-3, which falls to a minimum in quintile 5 (top of sample).

Day 1 post-thaw, quintile 3 had a viability and viable cell number of  $42.8 \pm 3.9\%$  and  $3.0 \pm 0.4$  million cells/ml respectively compared to  $15.9 \pm 2.0\%$  and  $0.9 \pm 0.1$  million cells/ml for quintile 5. This improves to  $77.1 \pm 11.3\%$  and  $7.1 \pm 1.0$  million cells/ml for quintile 3 and  $48.8 \pm 7.5\%$  and  $2.9 \pm 0.3$  million cells/ml for 5 day 3 post-thaw. Viable cell number was significantly ( $P < 0.01$ ) lower in the 5<sup>th</sup> quintile compared to all other quintiles at all time points. Viability was significantly ( $P < 0.01$ ) lower in the 5<sup>th</sup> quintile compared with all other quintiles days 2 and 3 post-thaw, and significantly lower than quintiles 1,2, and 3 on day 3 post-thaw.

##### **Protein Production**

Figure 52 shows the production of alpha-antitrypsin and alpha-fetoprotein 2 days post-thaw. These are proteins normally produced by ELS and it is essential that the ELS protein producing functions recover post-thaw in order to make the BAL a viable treatment. Functional data is presented as per ml ELS not per million cells as for the BAL to be a feasible treatment, the total amount of proteins produced must be acceptably high. A fixed volume will be cryopreserved which cannot be changed on thaw. Viable cell count outcomes are presented in Figure 51.

The best results for the tested proteins was observed around quintile 3, with the extremes of the sample (quintile 1 and quintile 5) showing worse outcome. Alpha-antitrypsin production was  $21.5 \pm 0.6$ ,  $33.6 \pm 5.3$ , and  $11.4 \pm 0.4$   $\mu\text{g}$  alpha-antitrypsin per ml ELS per 24 h for the 1<sup>st</sup>, 3<sup>rd</sup> and 5<sup>th</sup> quintiles respectively. AFP production was  $3.6 \pm 0.7$ ,  $4.9 \pm 0.9$ , and  $1.9 \pm 0.2$   $\mu\text{g}$  per ml ELS per 24 h for the 1<sup>st</sup>, 3<sup>rd</sup> and 5<sup>th</sup> quintiles respectively. Alpha-antitrypsin production was significantly higher in the 3<sup>rd</sup> quintile than in both the 5<sup>th</sup> and 1<sup>st</sup> quintile ( $P < 0.01$ ). AFP production was significantly higher in the 3<sup>rd</sup> quintile compared with the 5<sup>th</sup> quintile ( $P < 0.05$ ).

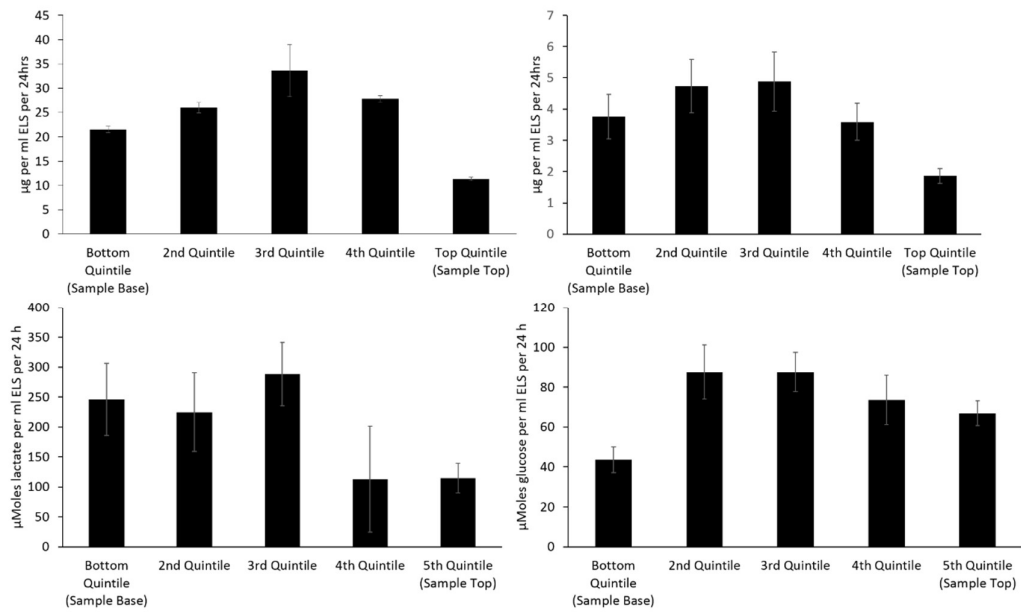


Figure 52 - Functional outcome on ELS experiencing PS on cooling in 6ml vials, 2 days post-thaw (cell counts in Figure 51). Clockwise from top left: Alpha-antitrypsin production per ml ELS per 24 h; Alpha-fetoprotein production per ml ELS per 24 h; Lactate production per ml ELS per 24 h, and glucose consumption per ml ELS per 24 h. In all sets the 3<sup>rd</sup> quintile has significantly increased function over the 5<sup>th</sup> quintile ( $P < 0.05$  AFP,  $P < 0.01$  else). Protein production average of  $n = 3 \pm SD$ , repeated twice. Lactate and glucose average of  $n = 5 \pm SD$ .

### Glucose Consumption and Lactate Production

Figure 52 shows glucose consumption and lactate production in 6ml cryopreserved PS samples 2 days post-thaw. Glucose consumption was  $246 \pm 60$ ,  $288 \pm 53$ , and  $115 \pm 25$   $\mu$ Moles of glucose per ml ELS per 24 h for the 1<sup>st</sup>, 3<sup>rd</sup> and 5<sup>th</sup> quintiles respectively. Lactate production was  $44 \pm 7$ ,  $88 \pm 10$ , and  $67 \pm 6$   $\mu$ Moles of lactate per ml ELS per 24 h for the 1<sup>st</sup>, 3<sup>rd</sup> and 5<sup>th</sup> quintiles respectively.

The 1<sup>st</sup> and 5<sup>th</sup> quintiles have significantly lower ( $P < 0.01$ ) lactate production than the 3<sup>rd</sup> quintile. Glucose consumption in the 5<sup>th</sup> quintile is significantly lower than in the 3<sup>rd</sup> quintile ( $P < 0.01$ )

### 9.3.2. Progressive Solidification in a Pouch in a 2 Litre Volume

#### Viability and Viable Cell Number

Viability in samples cooled as part of a 2 litre mass of alginate beads immediately post-thaw is in the 80-90% range for quintiles 1-4 of the sample. The viability drops significantly ( $P < 0.01$ ) to  $39.8 \pm 18.1\%$  at the biomass top (5th quintile) of the sample as can be seen in Figure 53.

Figure 53 shows that the highest viable cell density is found in the 3<sup>rd</sup> quintile, at  $11.93 \pm 1.61$  million cells/ml ELS. This declines significantly ( $P < 0.01$ ) towards the extremes of the sample, with  $5.91 \pm 0.54$  and  $4.6 \pm 0.95$  million cells/ml recorded in the 1<sup>st</sup> and 5<sup>th</sup> quintiles respectively.

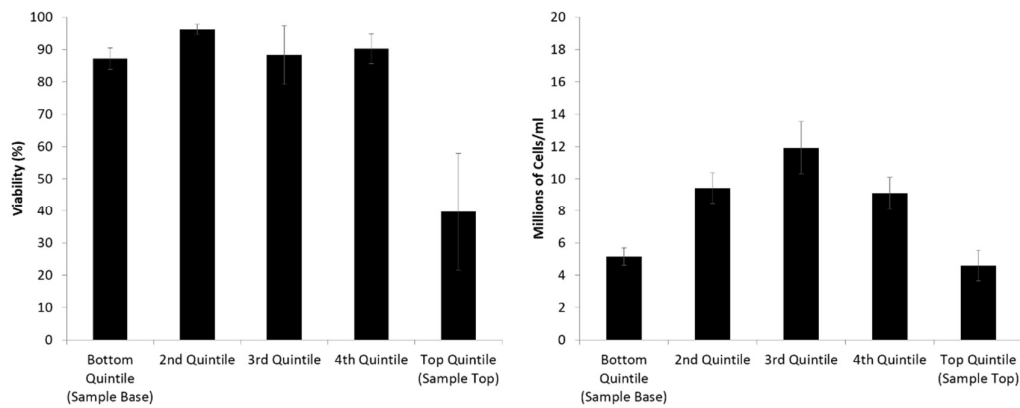


Figure 53 – Viability (left) and viable cell number (right) of samples cryopreserved in porous pouches in a 2 litre mass of alginate beads. Assessments made immediately post-thaw. Viability in the top (5<sup>th</sup>) quintile was significantly lower than in any of quintiles 1-4. No significant difference in viability between any of quintiles 1-4. Viable cell number is significantly lower in the 1<sup>st</sup> and 5<sup>th</sup> quintile compared with the 3<sup>rd</sup> quintile.  $n = 5 \pm SD$ , significance defined as  $p < 0.01$  using an unpaired student's t-test.

## MTT

The pattern for MTT activity showed no significant difference in cell function between the 2<sup>nd</sup>, 3<sup>rd</sup>, and 4<sup>th</sup> quintiles, with function between 0.6 and 0.85 MTT absorbance units per ml ELS of the unfrozen control. Function fell at the edges, with  $0.30 \pm 0.02$  and  $0.20 \pm 0.002$  fractions of the unfrozen control measured (significantly worse than quintiles 2-4,  $P < 0.01$ ); these were both significantly worse than the 2<sup>nd</sup>-4<sup>th</sup> quintiles, with the 1<sup>st</sup> quintile being significantly better than the 5<sup>th</sup> ( $P < 0.01$ ), Figure 54.

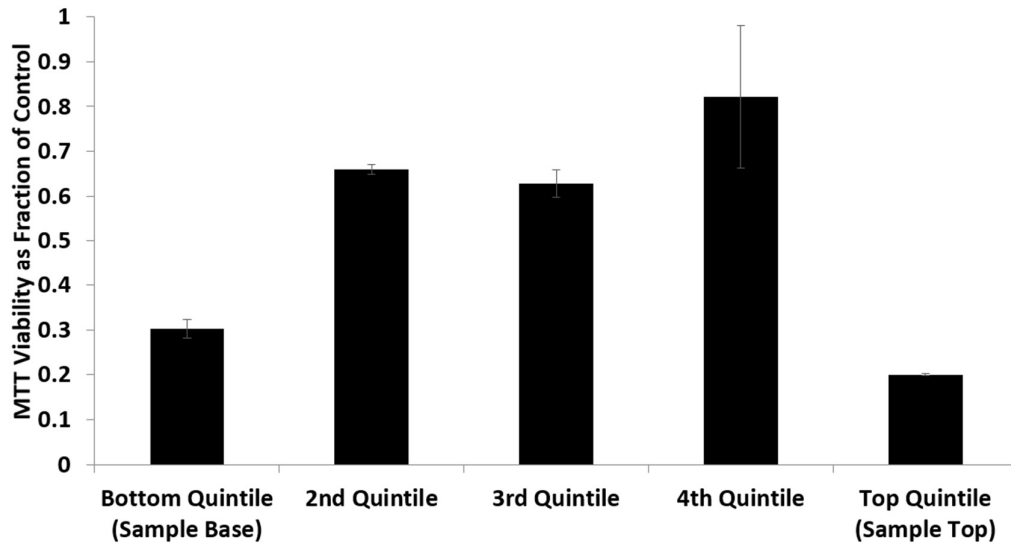


Figure 54 - MTT viability of samples cryopreserved in porous pouches in a 2 litre mass of alginate beads as a fraction of an unfrozen control. Assessments made immediately post-thaw. Quintiles 2-4 has significantly improved MTT viability compared with the top and bottom quintiles.  $n=5 \pm SD$ , significance defined as  $p<0.01$  using an unpaired student's *t*-test.

### 9.3.3. Thawing of a 2 Litre Volume

#### Thermal Profiles

Figure 55 shows thermal profiles in the inlet and outlet tubes of the warming ethanol fluid. The pre-warmed ethanol fluid started to be pumped through the warming device after 900s. The initial temperature difference between the medium going into and coming out of the chamber was 33°C, though rapidly equilibrates to a 10°C difference. After 1700s of ethanol flowing through the device mainly areas near the flow output were observed frozen, the flow direction was reversed for 300s to allow the final frozen biomass to thaw.

The entire thawing process took 50 minutes, 35 of which used ethanol warming.

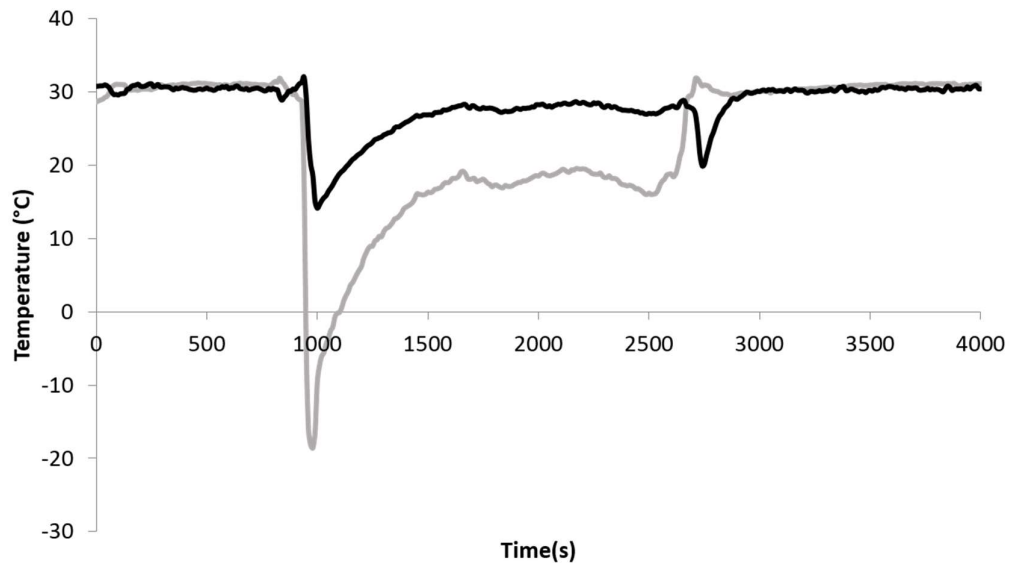


Figure 55 – Temperatures measured in the warming fluid (ethanol) entering (black) and leaving (grey) the thawing tubes of the chamber with warming device. Ethanol is equilibrated to 30°C as the chamber warms in air, after 900s the ethanol is pumped through the thawing tubes at 4 litres/minute. The temperature difference between the grey inlet and black outlet tubes stabilizes at around -10°C (between 1000 and 2500 seconds). This can be used to determine total ethanol energy input into the BAL. The temperature of both the inlet and outlet rises as the biomass warms. Most of the alginate bead and ELS has thawed by 2600s, where the flow was briefly reversed to dislodge remaining ice. The chamber was removed from the warming circuit after 3000s.

#### 9.3.4. Warming Rates Impact on Viability and Viable Cell Number

On thaw, samples were taken from pouches near the inlet of the flow and near the flow outlets and re-cultured, and shown in Figure 56. At 24 h post thaw, ELS thawed near the inlet had viability significantly ( $P < 0.01$ ) higher than the outlet, at  $75.7 \pm 3.9\%$  and  $62.0 \pm 7.2\%$  respectively. The viable cell numbers at the entrance were also significantly ( $P < 0.01$ ) higher, at  $4.7 \pm 0.4$  million cells/ml and  $3.2 \pm 0.4$  million cells/ml for samples near the inlet and outlet respectively.

The combination of three sets of data for the spatial significance during warming are shown in Figure 57. This data was collected together with Stephen Lamb (Asymptote Ltd.), and Aurelie Le Lay (UCL), with the graph itself put together by Stephen Lamb. While the number of repeats per experiment were too low to carry out a robust statistical analysis, the trend towards lower viability on thaw with longer thaw time is apparent.

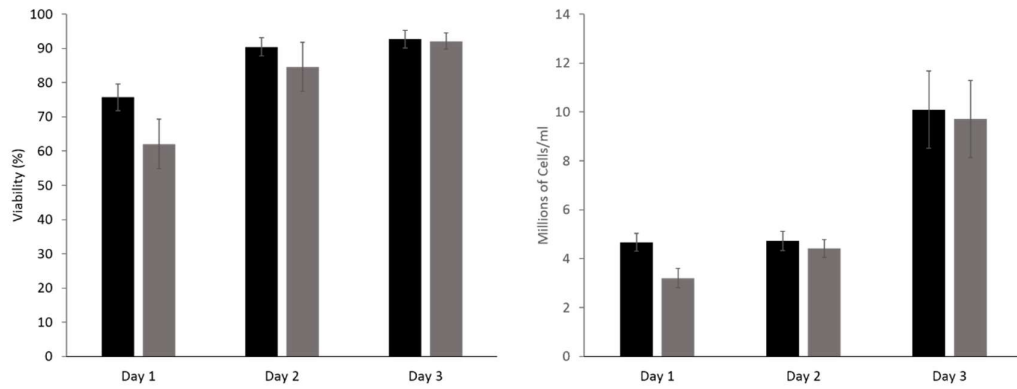


Figure 56 - Viability (left) and viable cell number (right) of samples near the inlet (black), or outlet (grey) days 1-3 post thaw. Both viability and viable cell number are significantly better in samples nearer the warmer inlet 1 day post-thaw. No significant difference is observed in any set at any other time point.  $n=5 \pm SD$ , significance defined as  $p < 0.01$ .

### BAL thawing time v. Day 0 cell viability

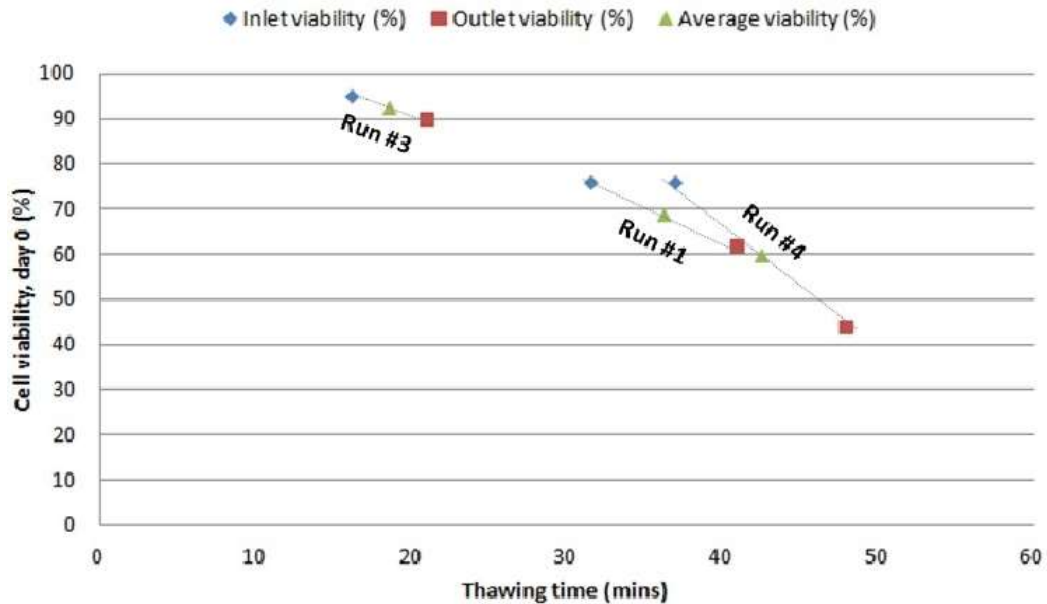


Figure 57 – Relationship between total thawing time of a BAL, and the cell viability on thaw. A clear trend is developing towards lower viability with longer thaw times. Technical difficulties prevented data collection at thaw for run two.  $n=3$  at each data point. Thanks to Stephen Lamb for putting the graph together, and Aurelie Le Lay for data analysis.

## 9.4. Discussion

These data highlight that spatial dimensions become very important when considering successful cryopreservation with PS present. In the present study, cells have been immobilized through their encapsulation in alginate, so localized effects can be studied accurately without mixing of biological material. The same is true for complete organs, where cells rigidly adhere to the intercellular matrix.

#### **9.4.1. 6ml Samples Experiencing Progressive Solidification (PS)**

Our results show that the heterogeneous spatial conditions experienced during the cryopreservation of large volume samples exhibits itself by way of heterogeneous function post-thaw. In terms of viability and viable cell number, there is a general decline in outcome days 1-3 post-thaw from the 1<sup>st</sup> to 5<sup>th</sup> quintile. Functional assessments confirm this, with the exception of the first area to solidify (1<sup>st</sup> quintile) which displays larger damage than those areas solidifying later (2<sup>nd</sup> to 4<sup>th</sup> quintiles) in the process. The 5<sup>th</sup> quintile, the final area to solidify on cooling expressed lowest function of all across the board. This is consistent between samples either cooled in a 6ml or 2 litre volume, each experiencing PS, and between several different post-thaw functional assays, indicating it is a direct consequence of ice formation and not simply volume.

The lower functional outcome in the 1<sup>st</sup> quintile of the samples was expected as biomass in this location experiences undercooling, with subsequent rapid formation of ice (localized to the edge region in a larger volume) on nucleation, and a distinct temperature discontinuity, which tends to be harmful to many cell types [173, 265, 289], and results in a small region of network solidification (NS) in the sample. The discontinuity between simple viability and cell function has been observed before in this system undergoing cryopreservation, and highlights that simple cell counts or viabilities are not sufficient to mark cryopreservation success. The data indicates that cells in the 1<sup>st</sup> area to solidify tend to survive cryopreservation relatively well, but have greater per-cell damage resulting in lower functional outcome. This contrasts with the 3<sup>rd</sup> quintile, which tends to have equally good post-thaw cell viability, but much greater per-cell performance indicative of lower levels of damage.

#### **9.4.2. Comparison of 6ml Samples to 2 Litre Volumes**

Data for the large scale freezing tends to agree with that seen in smaller 6ml PS samples for the central regions (quintiles 2-5). Lower viable cell number is observed – this is likely an artefact of poor warming as the sample edges were warmed slightly to extract the biomass. The overall viability is higher on average, though as these data points were taken on thaw, delayed onset cell death, which plays a large role in this system, will not yet have impacted on viability [26, 27, 263, 377].

### 9.4.3. Spatial Effects of Warming a Large Volume

The impact of small differences in warming rates is distinctly visible, with samples nearer the outlet of the warming tubes having only 2/3 of the viable cell number 1 day post-thaw of those near the inlet. This is surprising as the thawing time was not dissimilar (only 5 minutes in 50 minutes difference), and emphasizes the importance of consistent and rapid thawing for successful post-thaw outcome of large volume cryopreservation. The flow time of the warming fluid through the system was 1.5 seconds, and having faster thaw was difficult to achieve practically. For optimal cryopreservation, this data suggests that novel faster and more consistent thawing methods need to be developed to realize optimal large volume cryopreservation.

The average of the three experiments shown in Figure 57 highlights the need for rapid thawing. It should be noted however, that this chapter has not yet definitively proven the specific significance of the warming profile, only that it is important. It has not been established if the warming rate is important for the whole warming process, or only specific segments. Further work in chapter 10 will help answer this point.

### 9.4.4. Progressive Solidification

The central regions (2<sup>nd</sup> to 4<sup>th</sup> quintile) experienced favourable conditions on cryopreservation, likely due to the combination of optimal cooling rates and ice formation, but without the detrimental effects of undercooling. Studies agree that reducing undercooling is beneficial to post-thaw outcome, hence the inclusion of ice nucleators or manual nucleation in many freezing protocols [156, 210, 263, 289]. As the biomass away from the edge will not experience undercooling, rather a slowly expanding ice front at the equilibrium freezing point, good viability in this central region agrees well with expectations.

Future configurations of large scale cryopreservation could perhaps separate the biomass from the edge of the cooling edge, focusing the sample in this optimal region.

The last region (5<sup>th</sup> quintile) to solidify in the biomass has a much worse post-thaw outcome. It is well reported that the last region to solidify in cylindrical or spherical containers – the most common and efficient approximate shape for large biological samples – experiences a rapid reduction in temperature on freezing [210, 276]. This deviates from the optimum cooling conditions on cryopreservation.

Furthermore, as the cryoprotectant DMSO is toxic at long exposure times and high concentrations in the liquid state [171, 173, 451], the last area to freeze will endure the largest CPA toxicity linked injury. This is before taking into account the effects of solute-redistribution on solidification, which will cause the freezing solution to depart from its optimal freezing concentrations. This solute-redistribution will cause increasing damage with increased distance from the ice nucleation point, and is greater with the slow rate of ice growth seen in our system (Chapter 8) [221, 283]. As the system was being solidified 'bottom up', and solute dense water is heavier than solute sparse, the ELS would remain exposed to damaging CPA as it could not sink below the biomass level due to the freezing set-up and buoyancy of the ELS, forming a solute 'wall' ahead of the ice front. Damage in this section could be mitigated by adding more excess supernatant above the biomass. This will reduce the rapid temperature fall after solidification, and also provide space for freeze concentrated material to dilute into. A balance must be struck between excess volume and acceptable cryopreservation conditions – a larger total volume will reduce practical cooling and warming rates.

For cryopreservation and storage of large volumes with strict anatomy where the phase transition proceeds in the order of mm per minute, the physical impact of freezing varies significantly with cellular location in the biomass. Many large constructs, such as organs or cell scaffolds, cannot be compressed to thin slab or bag geometries without unacceptable damage to the sample.

Under-studied warming may prove to be just as important as cooling rates in developing successful cryopreservation procedures. Rapid warming is generally favoured in protocols, though this can only be readily achieved in small volumes, such as cryo-straws and a water bath, or with compressed cryobags [171, 186]. With the advent and necessity for large volume cryopreservation, this problem is starting to be addressed. Most work focusses on tissue grafts cooled in traditional ice forming cryopreservation where cracking or tearing can occur with non-optimal thawing protocols, and in warming large vitrified samples where cracking must also be avoided but rapid thawing is essential to avoid ice nucleation [103, 104, 192, 353, 432, 451]. Methods such as nanoparticle and dielectric warming may be required for optimal cryopreservation strategies of the bioartificial liver device [103-105, 353, 451].

These physical differences must be fully understood and optimized, perhaps by placing a sample only in certain areas inside a cryopreservation container where possible, with the remainder perhaps containing only freezing solution where ice may start to nucleate or where solutes can concentrate into without additional damage to the biomass.

## **9.5. Conclusion**

This chapter has shown there exists a region in samples experiencing PS on freezing that optimized post-thaw function of ELS.

The last quintile in the sample to solidify displays a significantly worse outcome. While this is not ideal, the cylindrical nature of the bioartificial liver means that the last fifth to solidify (measured by radius) contains less than 4% of the total biomass and so its impact on total outcome is minimal.

For large volume thawing, perfusing warm fluid through a system may not be sufficient, and new methods will have to be utilized to optimize cryopreservation strategies.

# 10. Scaled up – Cryopreservation and Re-Culture of a 2.3 Litre Biomass for Use in a Bioartificial Liver Device

## 10.1. Introduction

### 10.1.1. General Chapter Overview

This chapter optimised parameters such as excess medium concentration and warming rates, combined with earlier data in the thesis, and used the findings to enable the successful cryopreservation of a 2.3 litre biomass consisting of alginate encapsulated liver cell spheroids. This volume of biomass is required for successful treatment of Acute Liver Failure, as have been previously discussed in detail.

Adding 25% extra medium, as well as slow ( $<1^{\circ}\text{C}/\text{min}$ ) warming rates was found to give the best results, so long as the ice melting step was rapid.

After 72 h of re-culture, it was found that viable cell number, glucose consumption, lactate production, and alpha-fetoprotein production had recovered to pre-freeze values in the 2.3 litre biomass ( $1.00 \pm 0.05$ ,  $1.19 \pm 0.10$ ,  $1.23 \pm 0.18$ ,  $2.03 \pm 0.04$  per ml biomass of the control respectively).

It was also shown that further improvements in warming rates of the biomass could result in more rapid recovery of around 48 h.

This is the first example of a biomass of this volume being successfully cryopreserved in a single cassette and re-cultured, demonstrating that a bioartificial liver device can be cryopreserved, and with wider applications to scale-up large volume cryopreservation, and putting a big tick next to the PhD aims.

### 10.1.2. General Introduction and Re-Cap

#### The Problem Re-Visited

Acute Liver Failure (ALF) is a rare but extremely serious condition, where patient death can occur within weeks of diagnosis [31, 239, 306]. The only established treatment for ALF is organ transplant, which comes with the associated problems relating to organ rejection and

immunosuppressant-related illnesses, on top of organ donor shortages [213]. The survival outcome for patients with ALF receiving transplant is lower than for patients receiving an elective liver transplant, and patients presenting with ALF are often not candidates for transplantation [31, 239, 306]. A bioartificial liver device (BAL) may fill this unmet clinical need, by providing extra-corporal liver support allowing a patient's own liver to recover from injury and removes the need for transplant [101, 266].

It takes up to 26 days of cell culture for sufficient biomass required for a BAL to be grown, and this biomass cannot be currently stored viably for more than a few days. ALF can prove fatal within weeks of symptoms first appearing, and so a cryopreservation protocol is essential to ensure on-demand access to BAL treatment [7, 36, 111, 210, 265, 306, 403]. The total biomass of our BAL is just over two litres.

A 2 litre biomass has not previously been cryopreserved successfully in a single cassette and there has been relatively little study involving cryopreservation in anything more than a few ml biological material. Notable exceptions are the cryopreservation of blood, typically in volumes 450-500ml [379], and ELS and other cell types in cryobags. There have also been reports of successful cryopreservation of sheep ovaries, and a noted case of kidney vitrification [46, 110, 329]. I have found no record of biomasses larger than 500ml blood bags (cell suspension), or volumes larger than a few hundred ml for biomasses more complex than a cell suspension being cryopreserved in the frozen state, and these tend to be flattened for cryopreservation in morphologies that would be impractical for larger volumes or rigid constructs [46, 245, 265, 379].

This is despite the growing unmet demand for the preservation of tissue engineered constructs that cannot be produced using Just-In-Time manufacture, neither economically nor logistically [110, 111, 244]. The study of large volume cryopreservation is also essential to improve transplant outcomes. Currently large volume complex tissues such as organs can only be preserved in a chilled state (typically between 0-4°C) for a maximum of between around 4-24 h, depending on the organ [155, 170, 259]. This greatly inhibits successful transplant numbers and outcomes, for example, almost half of donor hearts are discarded, with only 1 in 3 being used for transplant [207], increasing the transportation window through organ banking should increase transplantation rate. Work towards large volume cryopreservation in cell spheroids is an important step towards large scale organ banking, which combined with tissue engineering could ultimately prevent 30-35% of deaths annually in the United States alone [111].

### **Different Ice Structures**

Chapter 7 explored the differences in ice formation between large and small volumes in detail. Small volumes during cooling (up to a few ml), tend to undercool below their equilibrium melting point [210, 263, 289]. Ice then nucleates and spreads rapidly throughout the sample, leading to a dendritic ice structure termed network solidification (NS).

Alternatively, in a larger volume ice tends to nucleate at a higher temperature. As ice starts to form, the latent heat of solidification is released, the sample temperature will rise to the equilibrium melting point, and ice will then form more slowly, demonstrating a larger more structured ice form, in a process known as progressive solidification (PS) [210].

PS can be introduced in smaller volumes such as a cryovial by using slow rates of cooling (not direct plunge into LN<sub>2</sub> for example) and adding a large volume of ice nucleant, that acts as a catalyst for ice formation, and so reduced the relative amount of supercooling [170, 263, 289].

## **Experimental Design**

Initially, two studies were carried out exploring the effects of excess medium and warming rates on ELS cryopreservation.

Three further cryopreservation sets were then carried out. The primary experiment considered the cryopreservation and post-thaw culture of a 2.3 litre biomass consisting of ELS.

Two studies examining the post-thaw outcome of samples cryopreserved in cryovials experiencing network solidification on cooling, and the post-thaw outcome for small samples mimicking the conditions faced during the cooling phase of cryopreservation in a scale down process were carried out in order to localise cooling and warming effects during cryopreservation.

This chapter uses the abbreviations LV (large volume, 2.3 litre biomass), CV (2ml cryovial cryopreservation), and SDP (scale down process cryopreservation) to refer to each of these conditions.

## **10.2. Methods**

### **10.2.1. Large Volume Cell Culture**

#### **Materials**

Applicon Bioreactor (Delft, the Netherlands)

Culture Medium

ELS

207

## Methods

The 2.3 litres of ELS biomass with an initial cell density of  $\sim 2 \times 10^6$  million cells/ml were cultured in a fluidised bed bioreactor (FFB) for 12 days, with partial medium changed every 2-3 days. Culturing this biomass has been published elsewhere in detail, and was carried out by colleagues in the LG [101]. Chapter 12 explored the culture method in detail.

ELS were cultured in alpha-MEM medium, supplemented with 50 U/ml penicillin, 50  $\mu$ g/ml streptomycin (Invitrogen plc. Carlesbad, CA, USA), and 10% FFP (NBTS).

### 10.2.2. Optimised Large Volume Cryopreservation Protocol

#### Materials

DMSO (Sigma, Dorset, England, UK)

UW Solution (Bridge to Life, Columbia, SC, USA)

Icestart (Asymptote, Cambridge, England, UK)

Planer controlled rate freezer (Planer, Sunbury-on-Thames, England, UK)

20cm polycarbonate chamber with end caps (manufactured for project)

#### Methods

A cryopreservation solution consisting of 24% DMSO (Sigma) in 76% UW (University of Wisconsin solution, Bridge to Life) (v/v) was prepared and chilled to 4°C. 0.5g Icestart (Asymptote) was added as ice nucleant.

The 2.3 biomass was removed from the bioreactor, and added to this cryopreservation solution at a 1:1 ratio, mixed, and allowed to equilibrate for 15 minutes. After equilibration, the ELS had settled in the solution, and most of the supernatant removed, leaving 2.3 litres of biomass (equilibrated to 12% DMSO and 38% UW solution) and 0.6 litres excess supernatant, giving a total volume of 2.9 litres.

This 2.9 litres was added to a 20 cm long, 15 cm diameter polycarbonate cylinder, which was sealed with end caps. The cylinder was added to a Planer controlled rate freezer, and cooled at 0.3°C/min from 4 to -100°C. On reaching -100°C the chamber was removed from the freezer and stored for 5 weeks in the vapour phase on a liquid nitrogen reservoir, at approximately -170°C.

### 10.2.3. Scale Down Process Protocol

The method outlined in section 7.2.2 was again used in this chapter.

### 10.2.4. Large Volume Thawing and Re-culture Protocol

#### Materials

-80°C Freezer

-32°C Freezer

Planer controlled rate freezer (Planer, Sunbury-on-Thames, England, UK).

HBSS (Gibco, Paisley, Scotland, UK).

#### Methods

The large volume cryopreservation cylinder was removed from the liquid nitrogen reservoir and placed into a -80°C freezer for 2 hours. It was then transferred to a -30°C freezer for 1 hour, and subsequently moved to the Planer controlled rate freezer, that was set to a constant temperature of -10°C for 1 hour.

The cryopreservation cylinder was then transferred to a large basin sterile hood, where the end caps were removed and 20°C HBSS was added to the system. A total of 10 litres was added over 30 minutes, with the system stirred throughout to dilute out the DMSO and encourage melting. After all the ice had melted, the supernatant was removed and ELS added to the FFB. Approximately 2.1 litres were added to the bioreactor, with 200ml having been lost during the cryopreservation cycle.

### 10.2.5. Thawing and Re-Culture Protocol of Scale Down Process and Cryovial Samples.

As discussed in general methods, with dissections as per section 9.2.5.

### 10.2.6. Temperature Profiles

#### Materials

K-type thermocouples (Picotechnology, St. Neaots, England, UK)

Picologger TC-08 unit (Picotechnology, St. Neaots, England, UK)

Laptop with picotechnology software installed (Picotechnology, St. Neaots, England, UK)

## Methods

To determine temperature profiles during warming of the large volume cylinder, a thermal mimic was set-up using 10% (v/v) glycerol in water, which was previously established has the same thermal properties as ELS in the freezing mix.

As incision was made in the top of the chamber, into which k-type thermocouples (Pico-technology) were added at set depths in the solution. The cylinder was then cooled in a large liquid nitrogen reservoir, before undergoing the warming protocol detailed above for the 2.3 litre biomass. The thermocouples were attached to a picologger unit, and recorded with using picotechnology software.

### 10.3. Results

#### 10.3.1. Warming Rates Significance

Figure 58 indicates that for rapid cell recovery post-thaw, the warming rate need only be controlled in the final phase of the thaw. Samples that were warmed slowly from liquid nitrogen to  $-80^{\circ}\text{C}$ , and then rapidly until thawed exhibited no significance difference in viable cell number 24 h post thaw compared with those warmed slowly from  $\text{LN}_2$  to  $-10^{\circ}\text{C}$ , and then thawed rapidly.

Another set of samples were warmed slowly from  $\text{LN}_2$  and through the phase transition. These samples had significantly lower viable cell number 24 h post-thaw. This indicated that during the warming phase it is the rate of ice melting (how quickly liquid starts forming in the system to the last ice crystal melting) that is significant to post thaw recovery.

This was an encouraging finding as it allowed the chamber to be warmed slowly without damage to the cells, before rapid ice melting. Thawing the 2.9 litre mass rapidly (<30 mins) from  $\text{LN}_2$  to the liquid state would have been difficult to achieve practically.

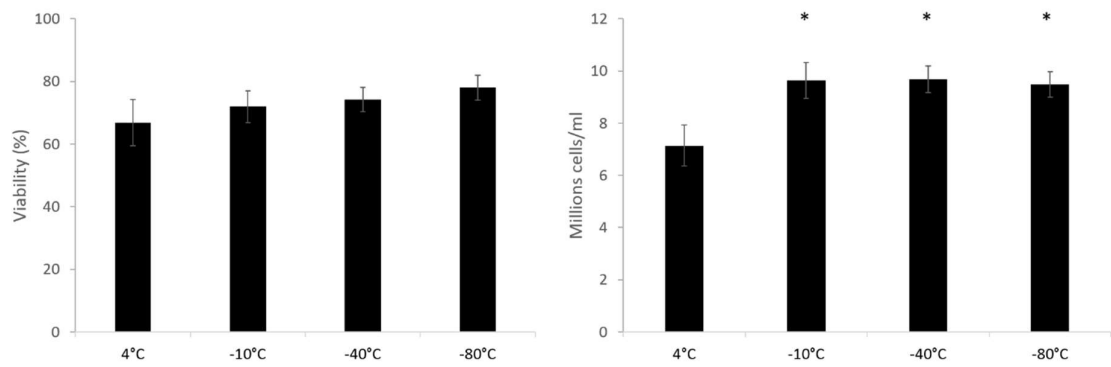


Figure 58 - Viability (left) and viable cell number (right) of samples being warmed at 1°C a minute from -196°C, to the temperatures indicated, before being warmed rapidly to thaw in a water bath. Data 24 h post-thaw. The leftmost sample (4 °C), was warmed slowly until thaw. No significant difference was seen in viabilities, all samples warmed rapidly through the phase transition had significantly increased viable cell number over the sample warmed slowly (4°C sample). n=5 ± SD, significance defined as \*=P<0.001, unpaired student's t-test.

### 10.3.2. Excess Medium Significance

It has previously been reported that with large volume cryopreservation, the last areas to solidify have much reduced cell function post-thaw [210]. It was hypothesised that this was due to cryoconcentration in this areas, as well as rapid cooling after solidification. To test this hypothesis, samples were cryopreserved with 20% of the total volume supernatant (ELS volume + 25%) using the scale-down process.

Figure 59 demonstrates that there was no discernible spatial significance 24 h post-thaw in samples cryopreserved with 20% of the total volume supernatant. While this extra volume would increase the total melting time of large volume samples, this was more than mitigated by improvements intra-sample.

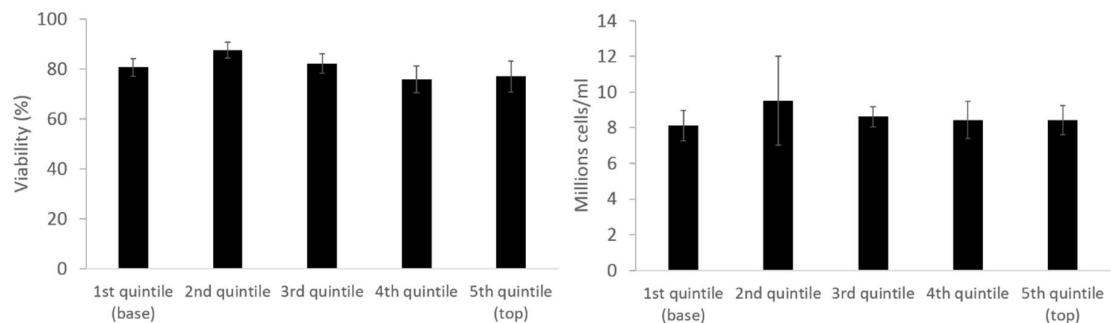


Figure 59 – Viability (left) and viable cell number (right) of samples cryopreserved in cryovials with 20% of the volume excess medium. Samples were thawed rapidly before a viability sample was taken 24 h post-thaw. No significant difference was observed in either viability or viable cell number between any sampling location. . n=5 ± SD

### 10.3.3. Large Volume Warming Profile

The warming data in Figure 60 shows that the 2.9 litre sample volume experienced very little variation intra-sample during the warming phase, indicating that the main barrier to heat transfer was the 3mm polycarbonate wall of the chamber, not the conduction through the solidified mass. The average temperature in storage was  $-173.6 \pm 9.2^{\circ}\text{C}$ , which rose to  $-37.3 \pm 2.1^{\circ}\text{C}$  after the 4 hour warming profile, this approximately halved the energy required to thaw the device.

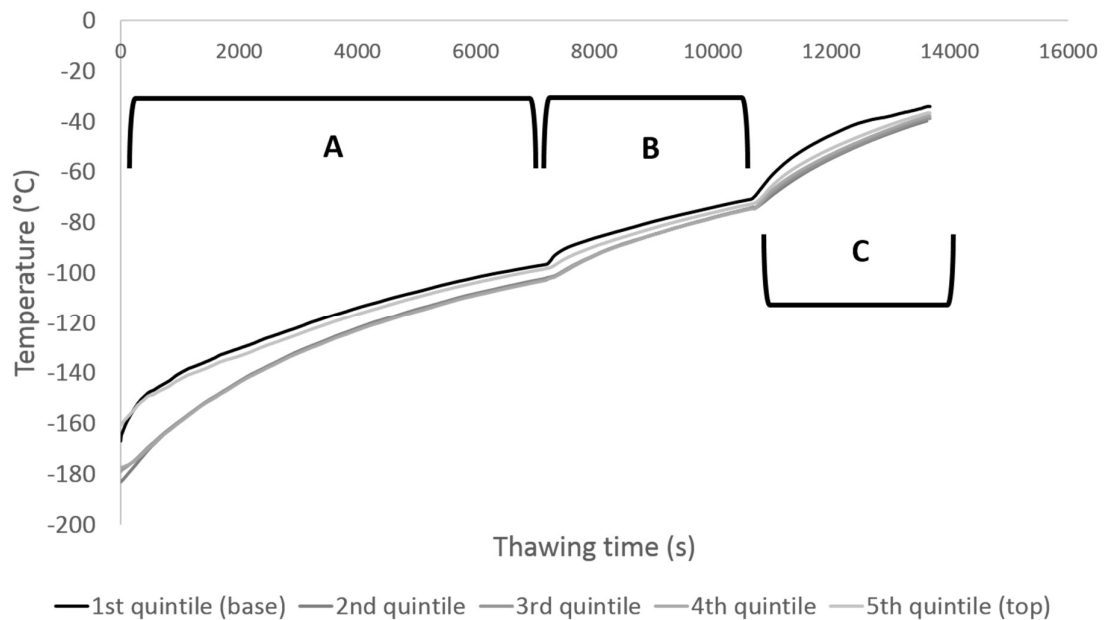


Figure 60 - Warming profiles experienced during warming of the large volume cryopreservation cylindrical chamber. Thermocouples were placed at the bottom of the biomass (black) and the top of the biomass (lightest grey), as well as three others equidistant apart between the bottom and top following a straight line through the deepest part of the sample (dark to lighter grey). Section A demarks thawing in the  $-80^{\circ}\text{C}$  freezer, section B thawing in the  $-30^{\circ}\text{C}$  freezer, and section C  $-10^{\circ}\text{C}$  in the Planer controlled rate freezer. Very little intra-sample temperature variation was observed.

While the  $-80^{\circ}\text{C}$  and  $-30^{\circ}\text{C}$  freezers contained only static air, the Planer freezer at  $-10^{\circ}\text{C}$  has a fan to circulate air, hence the relatively rapid warming in this phase.

### 10.3.4. Viability and Viable Cell Number

Prior to cryopreservation, all samples had a viability of  $99.6 \pm 0.1\%$  and a viable cell number of  $30.9 \pm 1.7$  million cells/ml.

Considering Figure 61, the LV samples recovered to their pre-thaw viable cell number 72 h post-thaw with  $31.0 \pm 1.6$  million cells/ml. Viability by 72 h post thaw was  $91.1 \pm 2.5\%$ , recovering to

99.8 ± 0.1 120 h post-thaw. Viability recovered more slowly due to dead cells being immobilized within the alginate and so being removed from the system slowly. Success post-thaw was defined as a viability >90%. The low nadir of recovery comes 6-24 h post-thaw, an expression of delayed onset cell death.

Samples cryopreserved using either the CV or SDP methods recovered more rapidly, CV samples displayed a viability and viable cell number of 96.3 ± 2.7% and 39.5 ± 7.6 million cells/ml 72 h post-thaw respectively. SDP samples recovered most-rapidly and exhibited 96.2 ± 1.5% and 50.6 ± 4.8 million cells/ml viability and viable cell number respectively, comfortably exceeding the pre-cryopreservation values.

It was noted that while 2.1 litres of ELS was added to the bioreactor, 2.3 litres was recovered at the end of the experiment, indicative of the diameter of the ELS swelling by 4-5% during the culture period.

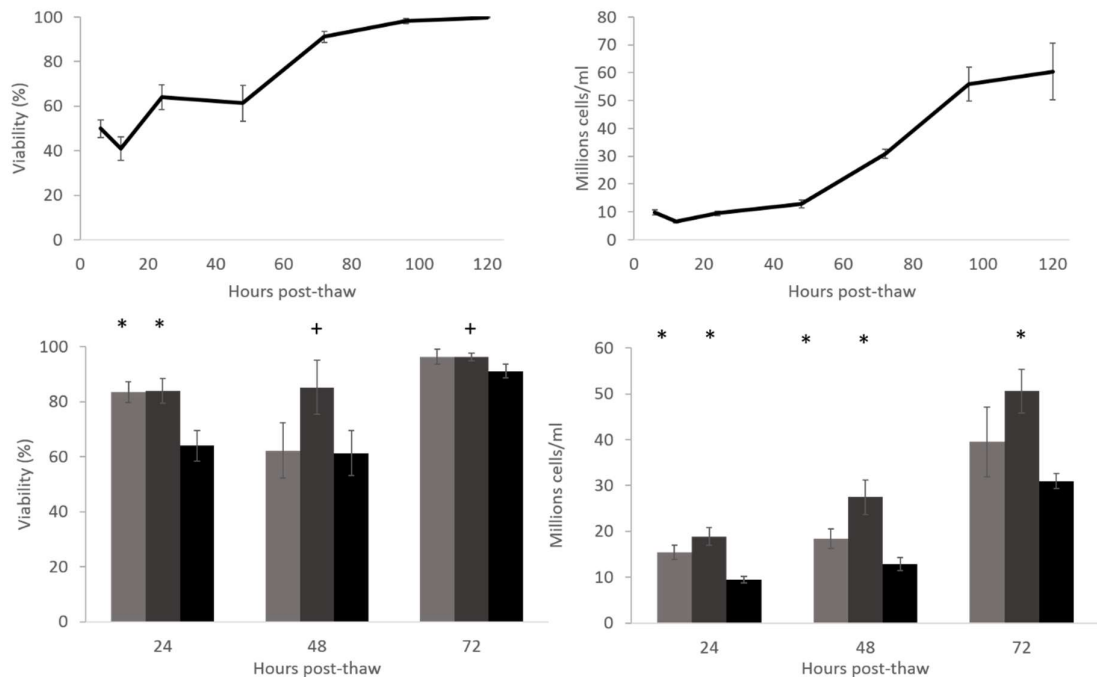


Figure 61 – Top; viability (left) and viable cell number (right) post-thaw of the large volume cryopreservation and; Base: viability (left) and viable cell number (right) of cryopreserved cryovials (CV), scale-down process vials (SDP), and the large volume (LV) (light grey, dark grey, and black respectively). The viability was significantly higher in the scale-down process vials compared to the large volume cryopreservation at all measured timepoints, and was significantly higher in the cryovials over the large volume at 24 h post-thaw. Both the cryovial and scale down process vials samples had significantly higher viable cell number over the biomass at 24 and 48 h post-thaw, the scale-down process vials significantly better also at 72 h post-thaw. n=5 ± SD, significance over large volume cryopreservation defined as \*=P<0.001, +=P<0.005, using an unpaired student’s t-test.

### 10.3.5. Glucose Consumption

Figure 62 shows that 72 h post thaw, samples cryopreserved in all conditions were consuming at least as much glucose per ml ELS as before cryopreservation. No significant difference was observed between the experimental conditions. In the LV condition, the glucose consumption was significantly (95%,  $P < 0.001$ ) higher 120 h post-thaw than pre-cryopreservation per ml ELS. A general decrease in glucose in the culture medium was also observed throughout the re-culture period, falling to a minimum of 13.4mM from 23.6mM from 6 to 120 h post-thaw.

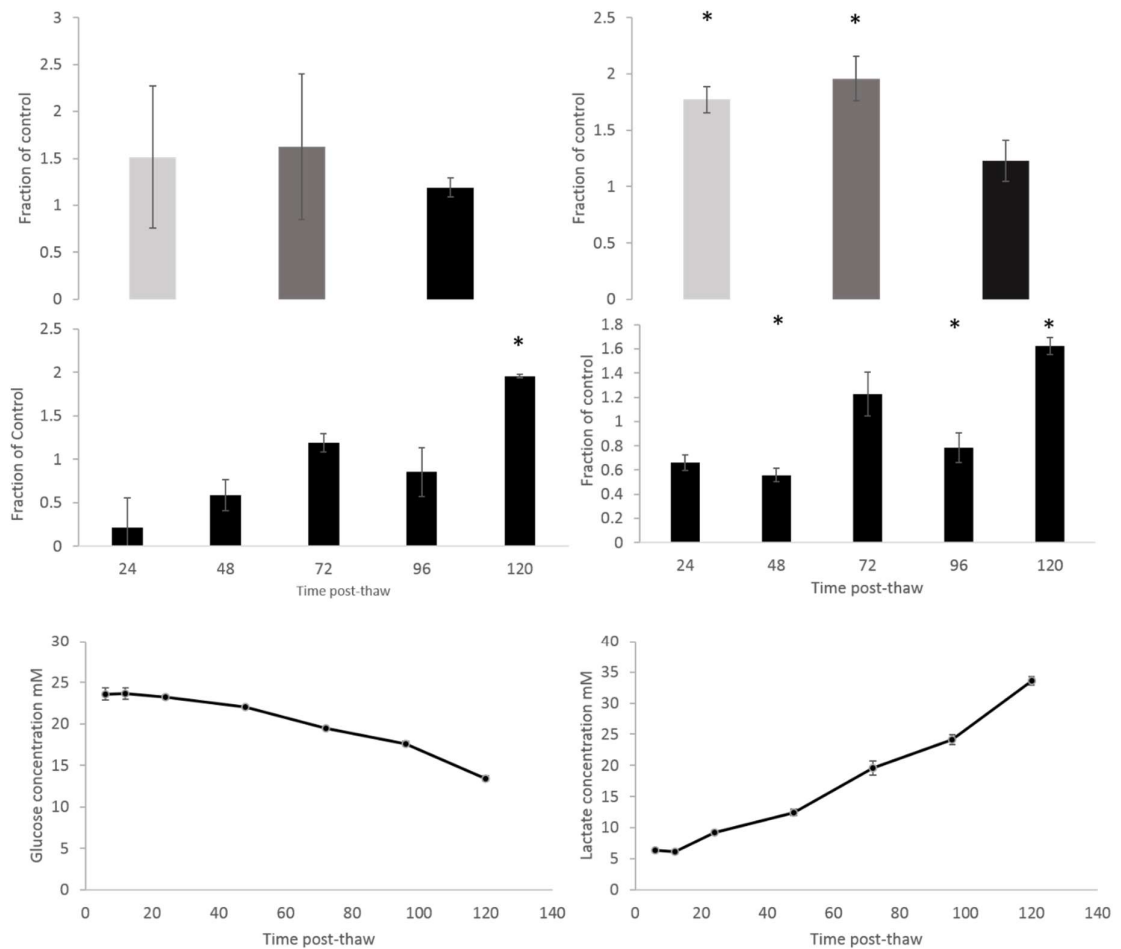


Figure 62 - Glucose consumption (left) and lactate production (right) following cryopreservation. Top – Glucose consumption and lactate production per ml ELS as a fraction of unfrozen control 72 h post-thaw, comparing the cryovial cryopreservation (light grey), scale-down process cryopreservation (dark grey), and large volume cryopreservation (black). No significant difference was observed in glucose consumption. Lactate production was significantly higher in both the cryovial and scale-down process samples over the large volume cryopreservation. Centre – Production at various time points in the large volume cryopreservation per ml ELS over an unfrozen control. Base – Total glucose and lactate measured in the bioreactor at set time points post large volume thaw.  $n = 5 \pm SD$ , significance over large volume cryopreservation (top) or unfrozen control (centre) defined as  $* = P < 0.001$ , using an unpaired student's t-test.

### 10.3.6. Lactate Production

Figure 62 shows that 72 h post-thaw, samples cryopreserved in all conditions were producing at least as much lactate per ml ELS as before cryopreservation, with significantly higher quantities being produced per ml ELS in samples cryopreserved in the CV and SCP experiments, over either LV samples or pre-cryopreservation values. In the LV condition, the lactate production was significantly lower at all time points per ml ELS compared with the pre-cryopreservation values, except at the 72 h time point where no significant difference was observed, and at 120 h post-thaw where lactate production was significantly higher. Lactate concentration in the large volume bioreactor was observed to increase throughout the culture period, from 6.1mM to 33.1mM from 12 to 120 h of re-culture, analogous to the decrease in glucose concentration.

### 10.3.7. Alpha-fetoprotein Production

Alpha-fetoprotein (AFP) production, shown in Figure 63, which is used here as an allegory for wider protein production (that cannot be detected in this system due to the inclusion of human blood fraction in the culture medium), had recovered to pre-cryopreservation levels in the LV set-up 48 h post-thaw when considering either production per ml ELS or per million viable cells.

Per ml ELS, samples in the LV set-up produced significantly ( $P < 0.001$ ) more protein per ml ELS than CV or SDP samples 72 h post-thaw. LV protein production was also significantly increased per million viable cells over CV samples ( $P < 0.005$ ) 72 h post thaw.

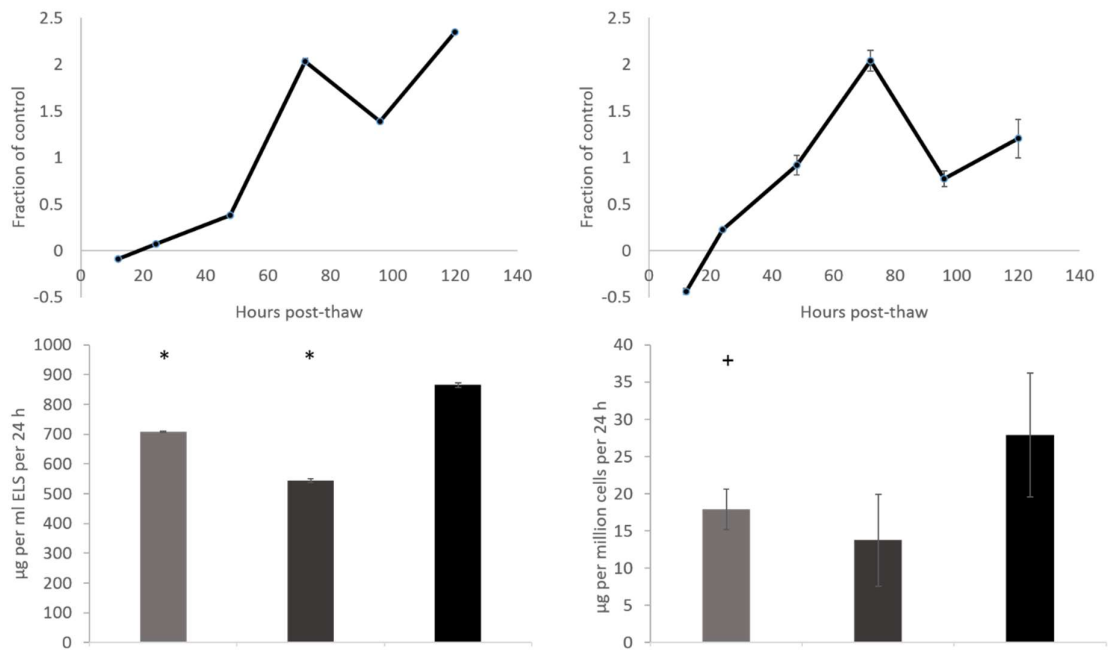


Figure 63 – AFP production of large volume cryopreserved samples, and comparisons with cryovials and scale down process samples. Top: production at time points post-thaw as a fraction of unfrozen control, either per ml ELS (left), or per million viable cells (right). Base: comparison between cryovials (light grey), scale down process samples (dark grey), and large volume samples (black) at 72 h post-thaw. Per ml ELS both conditions produce significantly less AFP than the large volume sample, and per million cells the cryovial production is significantly lower compared with the large volume cryopreservation samples.  $n=5 \pm SD$ , significance compared to large volume cryopreservation (top) defined as  $*=P<0.001$ ,  $+P<0.005$ , using an unpaired student's t-test.

## 10.4. Discussion

### 10.4.1. Warming Rates Significance

This chapter examined three separate conditions, those of samples cryopreserved in cryovials that experience network ice solidification on cooling and were thawed rapidly (CV). Samples cooled using a scale down process that experienced progressive ice solidification on cooling and were thawed rapidly (SDP). Finally a 2.3 litre biomass was cryopreserved that experienced progressive ice solidification on cooling and was thawed relatively slowly (LV).

Previous studies and protocols using hepatocytes indicate that rapid warming is necessary for successful post-thaw outcome [7, 36, 265, 384, 403]. Most of these studies have only focused on small volumes that will experience network solidification on cooling and so damaging recrystallization on warming. As this is not a problem during progressive solidification where samples already have large ice crystals, very slow warming is acceptable. The study indicated that rapid warming is only necessary during the melting phase of ice. Ice does not melt uniformly

on the microscale, rather it will melt in some places and form in others depending on localised heat and mass transfer, and macroscopic thawing occurs where more areas of ice are receding than growing.

I hypothesise that the microscale re-freezing may be damaging during thawing, and therefore this is the critical area to control during the thawing of large scale structures.

This is useful as it allows for slow warming for the majority of the warming cycle (it is difficult to warm large volumes unaided rapidly), and makes the melting phase quicker as the sample interior is warmer at the start of the melting procedure.

While the equilibrium melting point of our solution is  $-4.5^{\circ}\text{C}$  [263, 266], in reality the freeze-concentrated channels will start to thaw prior to that point, and most of the sample will leave the solid phase before this temperature is reached, although this may not be visually apparent on the macroscale [2, 221]. The thaw temperature was therefore chosen as below  $-30^{\circ}\text{C}$ , to mitigate any damage that may occur cellularly to the sample of extended (hours) time in this state.

There has been very little focus on the impact of warming rates of samples cryopreserved using slow rates of freezing ( $<1^{\circ}\text{C}/\text{min}$ ), with ice seeding to induce progressive solidification which is relevant here [5, 241, 265, 272, 273]. They have found mixed results, albeit in different cell types. Faster warming rates were found to be optimal for ELS and blood stem cells, but following slow cooling rates, L-cells were found to have peaks of survival at both high and low warming rates.

In general samples cooled rapidly must be thawed rapidly, while those cooled slowly can be thawed either slowly or rapidly for optimal outcome [272].

It is important to note that, with the exception of some of the blood cell study, the above literature (and much of the cryobiology literature in general exploring warming rates) only looks at average warming rates over the whole process, for example fast warming is induced by placing samples into a  $37^{\circ}\text{C}$  water bath, and slow warming rates by placing the samples in chilled air. Warming rates will not be linear in these situations, rather samples will warm rapidly to start with, with the temperature asymptotically reaching the environment temperatures (with a discontinuity through the phase-transition).

If warming was taken to be a temperature-dominated feature, i.e. the warming rate was defined as the average of the warming rates between each  $1^{\circ}\text{C}$  increment of warming, the average would be found to be much higher than the stated values, as warming through most temperatures (say  $-200$  to  $-50^{\circ}\text{C}$  would be much more rapid than  $-50^{\circ}\text{C}$  to  $0^{\circ}\text{C}$  where slower warming occurs). If the process were taken to be time-dependant, the average warming rate would be much lower than

stated as the majority of the time taken during the warming profile is nearer then environmental temperature, where the warming rate is relatively slow.

The closer to linear the warming rate is, the smaller the difference in these values becomes. Stating an average warming rate for an asymptotic warming profile assumes that time and temperature are equally important during the warming phase, although there is little published data to support this.

#### **10.4.2. Excess Medium Significance**

As ice develops through a volume, solutes will be excluded from the ice front and the last areas to solidify will experience this solute rise after being exposed to CPA for an extended period in the liquid state during the cooling process. As cells are sensitive to cryoprotectant concentration in a system, this leads to a deviation from optimal concentrations and is harmful to biomass solidifying later within a large sample. In addition, the later cells solidify in a larger volume, the greater their rate of cooling post-solidification. This is a consequence of heat transferring through the solid state much more easily than the liquid state, and later solidification requires more 'catching up' to the external controlled rate freezer temperature [210, 276, 289]. Cells are sensitive to cooling rates and so this will also be detrimental to a greater degree in a large sample [5, 226].

To overcome this, 20% total volume of the sample was 'excess' liquid. The ELS are weighted with glass beads so this medium is found above the biomass [101, 210], further from the chamber walls on average, resulting in it solidifying last. While this increased the total energy required to thaw the system, it was more than mitigated by reducing cryoprotectant toxicity and non-optimal cooling rates on cooling. This 20% total volume was found to remove damage observed when only 9% total volume (ELS+ 10%) is medium.

#### **10.4.3. Recovery Timeframe**

The 2.3 litre biomass has recovered lactate production, glucose consumption, viable cell number, and AFP production to pre-cryopreservation values within 72 h of thaw. Lowest viable cell number was observed between 6-24 h post thaw, an indication that delayed onset cell death was occurring [26, 27, 430].

Comparing with CV and SDP samples, it can be seen that the conditions most successful during the cryopreservation cycle are those that experience progressive ice solidification on cooling,

but are thawed rapidly. These are likely better than those cooled in cryovials which will experience a much greater degree of network solidification and so experience supercooling and sharp temperature discontinuities on ice nucleation [210, 289].

In agreement with previously reported particular sensitivity to ELS in the ice melting phase of the cryopreservation cycle, this study established quite clearly the need for more rapid thawing techniques. Slow warming for most of the process helps to reduce this time, but significant energy must be provided for the final thaw step, and the slow warm must stop prior to the equilibrium melting point due to the reduction in ice fraction prior to this point. The melting time was reduced to 30 minutes in this study for the large volume, and further reductions in this time would improve biomass recovery.

If the melting time could be reduced to around 5 minutes, the SDP samples showed that post-thaw viability, viable cell number, lactate production, and AFP per million cells could be significantly improved. Methods such as using radiofrequency warming or dielectric warming are the most promising avenues to explore to further improve post-thaw recovery [104, 105, 353, 451]. The thawing chamber used in Chapter 9 was not available for later studies in this PhD, though such a device would increase ice melting times and so the recovery timeframe.

The field of cryopreservation has largely focused on smaller volumes, which typically undergo different cryostresses relative to larger volumes. Indeed many published studies tend to use the term 'large volume' with samples larger than around 5ml. Large volume cryopreservation, on the order of litres, requires a step change in cryobiology thinking (from cooling patterns only to a combination of cooling and warming profiles) and is required for preservation of organs and tissue engineered constructs, for which Just-In-Time manufacture is not possible [110, 111, 265].

## ***10.5. Conclusions and Future Work***

To summarise, I have demonstrated that adding extra culture medium and having a slow warming phase followed by a rapid thaw allows the cryopreservation and recovery within 72 h of a 2.3 litre bioartificial liver biomass. This is the largest volume cryopreserved and thawed in a single cassette reported in the literature to date, and is a requirement for the bioartificial liver device to be available on demand.

Several aspects could be improved upon in this chapter that could direct future work. Firstly, the system used in this chapter is not compatible with a GMP environment as will be required for a clinical device. Using the same BAL chamber for the culture and cryopreservation phase may assist here. It is also clear that if the melting rate was increased then the system could be fully

re-covered within only 48 h. Using other warming methods such as that employed in chapter 9 could help this (this device was not available at later points in this work), as could other methods such as dielectric warming techniques.

If a molecular method to arrest cell proliferation could be established, this would help clinical delivery of the cryopreserved biomass. The biomass was observed to continue to proliferate even after the viable cell number had recovered – if this could be arrested somehow at the correct cell number the biomass could expend all cellular resources on protein production and other liver specific functions improving clinical outcome.

# 11. Engaging Cold to Increase Cell Proliferation in Alginate Encapsulated Liver Spheroids

## 11.1. Introduction

### 11.1.1. Chapter Overview

This chapter combines two key areas of this thesis – cryopreservation and low temperature biology, with optimising cell culture in the BAL device, with results that were both unexpected and positive.

After around 12 days of culture, ELS stop proliferating, i.e. they have reached their maximum culturable cell density with our current set-up. This is why cryopreservation (for ultimate patient treatment) with the ELS happens at this point. However, while researching cryopreservation an interesting observation can was made. 24 h after thaw ELS had a typical viable cell number around 50% of the pre-thaw value. This recovers rapidly though, usually to 100% by 72 h post-thaw. The experiments usually stopped at that point. It was observed however that cell density did not flatten out at the maximum value achievable pre-thaw, but could continue to a higher value. Perhaps the best example in this thesis is of cryopreserved control ELS in Figure 18 on page 98.

It was hypothesised that perhaps cryopreservation had an effect, either on the cells, the alginate, or a combination of the two, which boosted cell growth. That was the basis for work in this chapter, where it was ultimately discovered that low temperatures above freezing play an important and hitherto unrecognized role.

For many years the negative impact of hyper- and hypo-thermia on mammalian cells has been known, hepatocytes do not deviate from this paradigm. With the exception of short low temperature storage which has uses in areas such as transplantation, positive impacts from low temperature treatment of hepatocytes has not been previously reported.

It has been observed in this chapter that alginate encapsulated hepatocytes which experience a cold reduction in temperature (to 10°C or lower) for periods between 1 and 90 minutes or that are cryopreserved experience greatly enhanced cell proliferation over those cultured at normothermia of 37°C during culture from 7-16 days post-treatment compared with untreated samples. I have termed this effect cryoanaptiksi (cryo – cold; anaptiksi – growth).

8-12 days after treatment ELS experienced a cell density of  $1.71 \pm 0.35$  times that of control samples. The effect has been observed to occur in samples with varying cold-treatment time, with cooling rates between  $0.3^{\circ}\text{C}/\text{min}$  and  $240^{\circ}\text{C}/\text{min}$ , and regardless of cryoprotective agents dimethyl sulphoxide and Viapsan.

For systems requiring extended culture, such as bioartificial liver devices, cryoanaptiksi offers a simple method to rapidly increase cell proliferation rates, allowing manufacture of required biomass more quickly, and increasing cell density thereby reducing final required biomass volume. This will enable bioartificial liver devices to be prepared with greatly reduced cost, making them a more cost effective treatment.

### 11.1.2. Overview of Literature

Alginate encapsulation of cell lines is practised widely for a number of purposes and for various cell types [206, 219, 311, 411, 438]. Encapsulation allows them to proliferate using the alginate polymerized with calcium [76, 101, 219] as a 3 dimensional scaffold, increasing per-cell function over that recorded with a cell monolayer [206, 364].

The culture of a fluidised bed bioreactor, as is the case with all culture methods, is time, cost, and labour intensive, which adds significantly to the cost of the device, hence methods that reduce the culture time required for sufficient biomass to develop is highly desirable.

Separately, many groups have studied cryopreservation of encapsulated or suspensions of cell lines, either to preserve them once a sufficient cell density has been achieved, or to explore if alginate encapsulation may offer some form of cryoprotection [21, 76, 364].

While many studies exist examining the effects of low temperatures or cryopreservation on mammalian cells, the overwhelming majority of studies report negative consequences of low temperature exposure, the extent of negativity ranges from slower cell proliferation through to apoptosis and necrosis [89, 129, 151, 242, 275, 327, 343, 376]. Specific stages of the cell cycle can be disproportionately affected [153], the G1 phase of the cell cycle seems particularly sensitive to the impact of low temperatures, with cells being observed to accumulate in that phase [6, 129, 376]. The only field low temperatures are regularly used on mammalian tissues without freezing are in organ preservation prior to transplant and surgery [72, 129, 343, 417].

To my knowledge, no studies have reported the effects of sub optimal culture temperatures to induce rapid cell proliferation, indeed the consensus is that low temperatures are to be strenuously avoided. In those cases where low temperatures are required, such as for temporary

preservation, protective agents such as found in Viaspan are normally required [25, 236, 258, 275, 382, 417].

In this study, the potential for low temperatures to induce rapid cell proliferation on return to optimal culture conditions have been observed, an observation with wide application to not only HepG2 cell lines but potentially to many systems utilizing cell encapsulation that has been missed in previous studies.

## **11.2. Materials and Methods**

### **11.2.1. Cooling/Warming Methods**

#### **Cold Shock Induction**

##### **Materials**

Ice bucket with ice

Cryovials with ELS and experiment-dependant reagent

Warmed culture medium

Asymptote EF600 CRF

Cooled (0°C culture medium)

#### **Method – General Cooling and Cold Shock**

Unless otherwise stated, cold induced cryoanaptiksi was realized by plunging replicate 1ml ELS with 1ml excess medium in 2ml cryovials centrally into an ice bucket, ensuring that the whole sample was covered in ice. Upon completion of the test time, samples were removed from ice, and 37°C culture medium added prior to re-culture.

For cooling rate studies, samples were cooled as above, or in an EF600 freezer at 0.3°C/min from 20°C to 0°C to study low cooling rates. Alternatively, for extremely rapid cooling 1ml ELS samples were pipetted directly to 9ml pre-cooled (0°C) culture medium, which would induce a classical cold-shock.

#### **Method - Studies of Reagents**

In experimental conditions where the impact of reagents on cooling were explored, required reagent mix was prepared to 1ml at 2x concentration in culture medium, before addition 1:1 to 1ml sample resulting in a 2ml final volume. Samples then immediately underwent test conditions.

### **11.2.2. Cryopreservation Protocol – DMSO with Viaspan**

As per sections 3.2.3 and 3.2.6.

### **11.2.3. Cell Culture**

All data in this chapter was carried out on ELS cultures in static culture flasks, outlined in section 3.1.5. This is with the exception of data in Figure 64 and Figure 70, which used RCCS culture as outlined in section 3.1.6, where RCCS were used, this is also stated in the figure legends. No direct comparisons were made between RCCS and static cultures.

## **11.3. Results**

### **11.3.1. Comparing ELS Cryopreserved on Encapsulation with those Cultured in a FBB Directly.**

Figure 64 presents a comparison between cells cryopreserved on encapsulation, and those cultured directly without any chilling. Day 1 of culture, the viable cell number in the cryopreserved samples has declined significantly ( $P < 0.01$ ) their values on encapsulation, likely due to cryopreservation stresses that have been well documented in this thesis. At all comparable time points days 5 and onwards, cell density in the cryopreserved set was significantly ( $P < 0.01$ ) higher than the standard, untreated set.

The maximum cell density achieved with the cryopreserved samples is 95 million cells/ml, more than double that achieved without treatment. Considering that the cryopreserved sets lost approximately half of their cells during the cryopreservation process, the later increase in cell proliferation is striking.

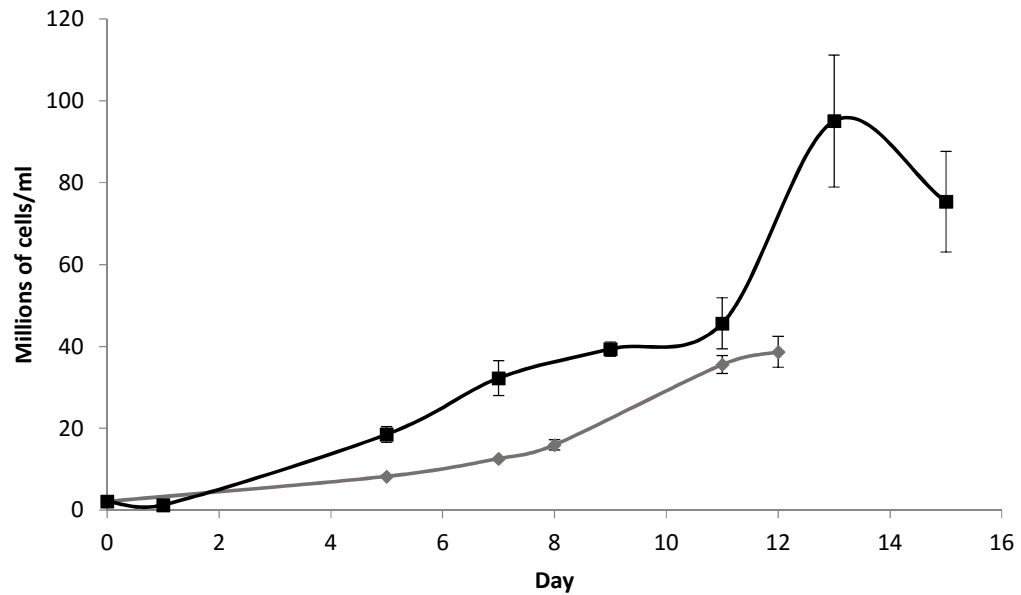


Figure 64 – Comparison between ELS encapsulated and cultured directly in an FBB environment (grey), with ELS cryopreserved and thawed before RCCS culture (black). RCCS culture mimics FBB conditions on the smaller scale and so is not responsible for differences. Data in black in this figure measured by the author, which was compared with data in grey, an experiment carried out by and data points measured by James Bundy and Eloy Erro, who also carried out the cell encapsulation (same encapsulation for both sets)  $N=5 \pm SD$ , comparisons in text used an unpaired student's t-test.

### 11.3.2. Spheroid breakout from Alginate

At cell densities of around 50 million cells/ml, spheroids were observed to break-out of the alginate which affects further culture. Spheroids which have broken free from alginate will not be useful for treatment (they will not be fluidised or receive nutrients properly) [312]. They also have the risk of attaching to the culture vessel and flow distributor at the base of the vessel, which may block flow. Additionally, these spheroids that start to die will release unwanted chemicals into the medium, potentially damaging ELS and increasing the bioburden that must be removed prior to patient re-entry.

Cell-breakout also makes cell counts less accurate, as can be observed from the later time points in Figure 64. Figure 65 shows microscope images of cell break-out, from the same experiment as Figure 64. With increasing cell density new methods to reduce cell breakout must be devised, or cell culture deemed complete around 50 million cells/ml (higher than currently achievable without treatment).

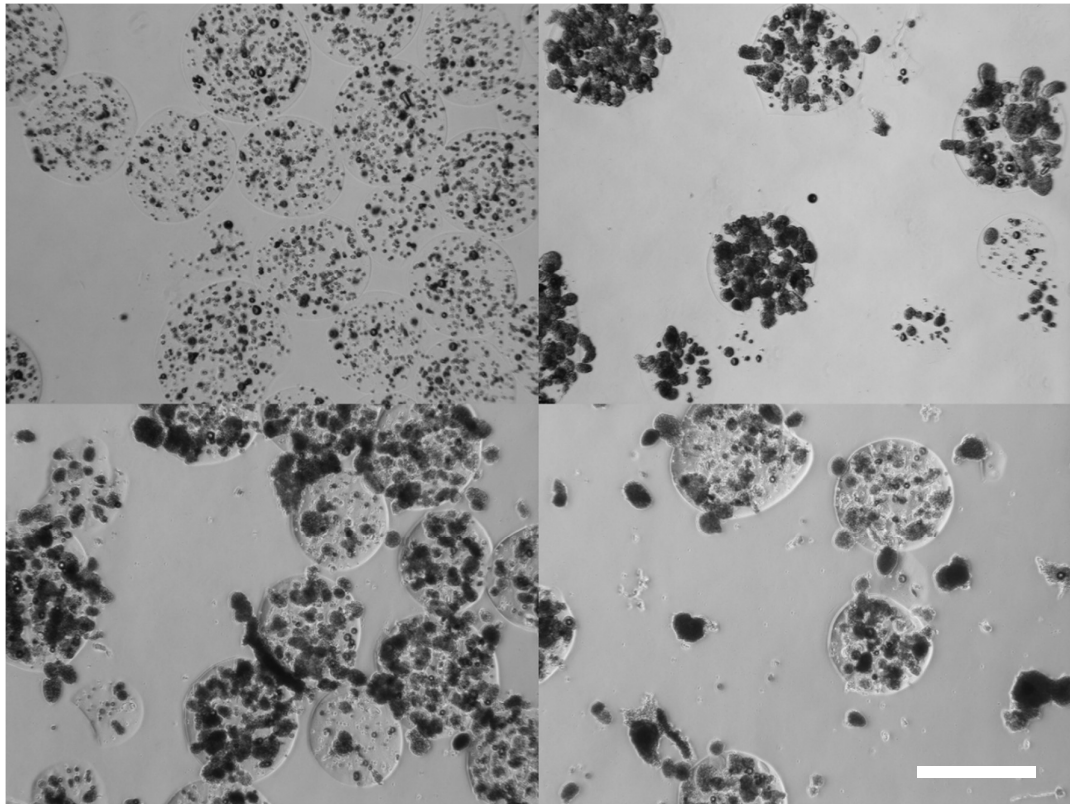


Figure 65 – Images of cell breakout at high cell densities, from the cryopreserved cells counted for Figure 64. Top left shows ELS after one day of culture; top right after 9 days; bottom left after 13 days; and bottom right after 15 days. Images acquired at 4x magnification using a phase contrast black-and-white image. Scale bar of 0.5mm.

### 11.3.3. Cold Treatment in Culture Medium

Figure 66 shows a summary of 6 different experiments. For ELS experiencing cryoanaptiksi induced on the day of encapsulation, viable cell density after 8 days (set C), or 12 days (sets A,B,D,E,F) of culture is on average  $171\% \pm 35\%$  of those controls (not experiencing lower temperatures), entering 37°C culture directly. Inter-experimental variation in cell density occurs due to natural variation in the system, hence variations in control values, as has been noted previously [101].

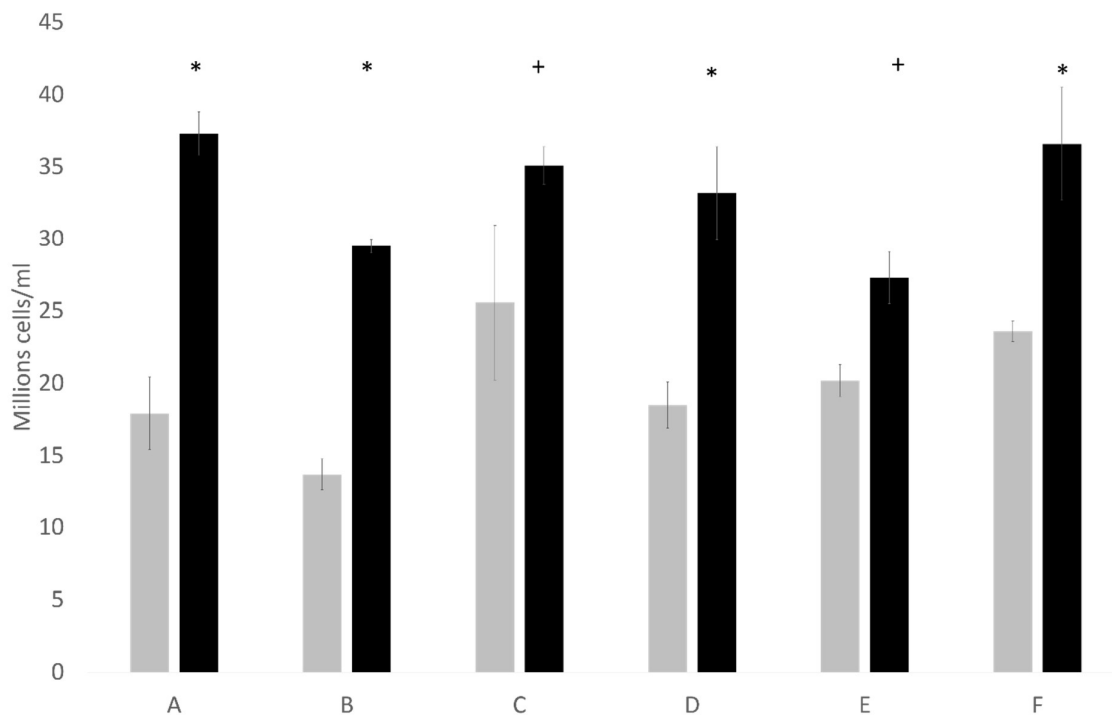


Figure 66 - Comparison in viable cell number between samples experiencing cryoanaptiksi induced by either simple chilling or cryopreservation (black), and untreated control samples (grey). Data is presented as average of 5 samples  $\pm$  one SD, except set C where the control is average of  $n=10$ . Set A, B, and F experienced cryopreservation induced cryoanaptiksi, sets C, D, and E cryoanaptiksi was induced through chilling samples to  $0^{\circ}\text{C}$ . All data is 12 days after treatment, except for set C which is 8 days. All sets experience a significant improvement in performance, \* indicated  $P<0.001$ , + denotes  $P<0.005$ , using an unpaired student's t-test. Combination of all sets A-F is significant at  $P<0.001$ , using a paired student's t-test.

### 11.3.4. Time and Temperature Dependence of Low Temperature

Figure 67 demonstrated that varying the time of the low temperature to induce chill induced cryoanaptiksi from 30 to 90 minutes does not significantly change the outcome between sets. All sets were significantly improved over control ( $P<0.001$ ). Data for 8 days of culture show a cell number of  $19.1 \pm 1.6$ ,  $30.7 \pm 4.0$ ,  $34.6 \pm 3.2$ , and  $38.3 \pm 3.5$  million cells/ml for ELS samples experiencing no low temperatures, a 30 minute hold at  $0^{\circ}\text{C}$ , a 45 minute at  $0^{\circ}\text{C}$ , and a 90 minute at  $0^{\circ}\text{C}$  respectively.

Viability was recorded at  $96.5 \pm 0.7\%$ ,  $96.1 \pm 0.5\%$ ,  $95.9 \pm 1.1\%$ , and  $94.3 \pm 1.4\%$  for ELS samples experiencing no low temperatures, 30 minute hold at  $0^{\circ}\text{C}$ , 45 minutes at  $0^{\circ}\text{C}$ , and 90 minutes at  $0^{\circ}\text{C}$  respectively, resulting in a viable cell density of  $18.5 \pm 1.6$ ,  $29.5 \pm 3.8$ ,  $33.2 \pm 3.2$ , and  $36.1 \pm 3.5$  million cells/ml respectively.

While the encapsulation process takes place at room temperature, Figure 67 demonstrates that cooling samples to only  $10^{\circ}\text{C}$  for 45 minutes is sufficient to induce rapid cell growth, with a day 8 viable cell number  $2.13 \pm 0.22$  times that of the control ( $P<0.001$ ), with cell density  $19.1 \pm 1.6$

and  $41.6 \pm 4.3$  million cells/ml for the control and samples cooled to  $10^{\circ}\text{C}$  for 45 minutes respectively.

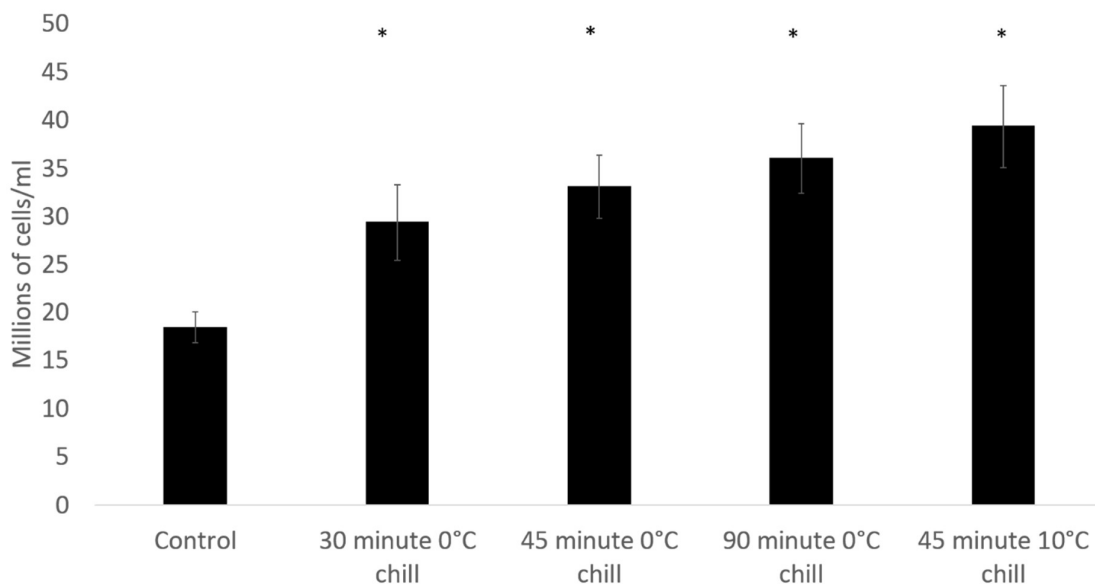


Figure 67 - Viable cell number of samples experiencing various chilling times and chilling temperatures to induce cryoanaptiksi. All conditions (\*) showed significant improvement over the control at  $P < 0.001$ , though no significance between sets was observed at that threshold. Data is displayed as average of  $5 \pm$  one SD, significance determined using an unpaired student's t-test.

### 11.3.5. Cooling Rate Dependency of Low Temperature Treatment

To determine whether the rate of initial cooling was significant for the cryoanaptiksi effect, five conditions were tested:

Plunging 2ml samples in cryovials into an ice bucket, and holding them there for either 30 or 60 minutes prior to re-warming. Pipetting 1ml ELS into pre-cooled  $0^{\circ}\text{C}$  culture medium to induce immediate cooling, and re-warming after either 1 minute or 30 minutes, or cooling samples linearly from  $20^{\circ}\text{C}$  to  $0^{\circ}\text{C}$  at  $0.3^{\circ}\text{C}/\text{min}$  in cryovials in an EF600 controlled rate freezer. The results are shown in Figure 68.

Viabilities of  $98.5 \pm 0.4\%$ ,  $98.8 \pm 0.2\%$ ,  $98.0 \pm 1.5\%$ ,  $98.9 \pm 0.2\%$ , and  $98.4 \pm 1.0\%$  resulted in a viable cell number of  $27.3 \pm 1.8$ ,  $24.6 \pm 1.8$ ,  $31.9 \pm 2.4$ ,  $29.0 \pm 0.9$ , and  $30.9 \pm 2.2$  million cells/ml for 2ml samples (1ml ELS, 1ml excess medium) in cryovials plunged into an ice bucket, and held for either 30 or 60 minutes prior to re-warming, 1ml cooled immediately, and re-warming after either 1 minute or 30 minutes, or samples cooled linearly from  $20^{\circ}\text{C}$  to  $0^{\circ}\text{C}$  at  $0.3^{\circ}\text{C}/\text{min}$  in cryovials in an EF600 controlled rate freezer respectively. The viable cell number data is displayed in Figure 68.

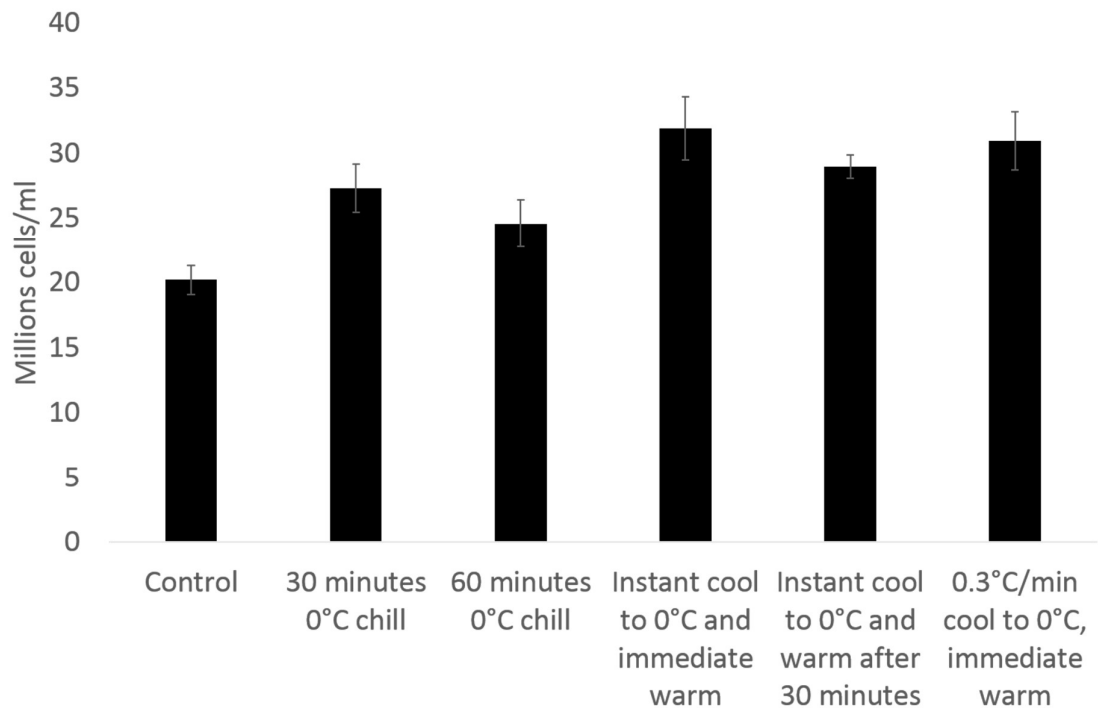


Figure 68 - Viable cell number after 12 days of culture following cryoanaptiksi induced through various cooling conditions. Samples marked 30 and 60 minutes 0°C chill were 2ml samples containing 1ml ELS in cryovials that were plunged directly into an ice bucket. All 5 tested conditions show significant improvement over control at  $P < 0.001$ , except 30 and 60 minutes 0°C chilled samples which were significant at  $P < 0.002$ . Samples cooled and warmed instantly showed significant improvement over samples held at 0°C for 60 minutes, at  $P < 0.001$  significance level. All data is average of  $n=5 \pm$  one SD.

Cryoanaptiksi has been observed in samples treated on day 0 of encapsulation at cell densities between 1.50 and 2.13 million cells/ml (day 0 cell counts not shown).

Figure 69 shows the impact of cryoanaptiksi on samples where chilling was induced at day 12 post-encapsulation, at a cell density, viability, and viable cell density of  $20.5 \pm 1.1$  million cells/ml,  $98.6 \pm 0.5\%$ , and  $20.2 \pm 1.1$  million cells/ml respectively. Figure 5 also shows the effect of cell-break out, commented on earlier and which makes isolating the effect at higher cell densities more difficult.

In samples experiencing chilling on day 12, no significance in cell density is observed at any time point.

Another pair of sets were cryopreserved with different levels of cryostress, as can be observed in Figure 70. Here one set underwent optimized cryopreservation, while another underwent cryopreservation using sub-optimal CPAs to increase damage. While the set with more extreme damage has significantly ( $P < 0.01$ ) lower viable cell number at all time points, the average daily proliferation rate between days 7 and 11 post-thaw is not significantly different between the sets, at 46% and 47% growth per day for optimized and non-optimized samples respectively. As cells will have recovered from cryodamage 7 days post-thaw, the data demonstrated that the

rapid cell proliferation was not cell density dependent below 50 million cells/ml where breakout starts to occur.

As ELS are encapsulated as single cells, which proliferate into cell spheroids, this data also indicated that the number of individual spheroids did not seem to be a factor.

### 11.3.6. Effect of Cell Density

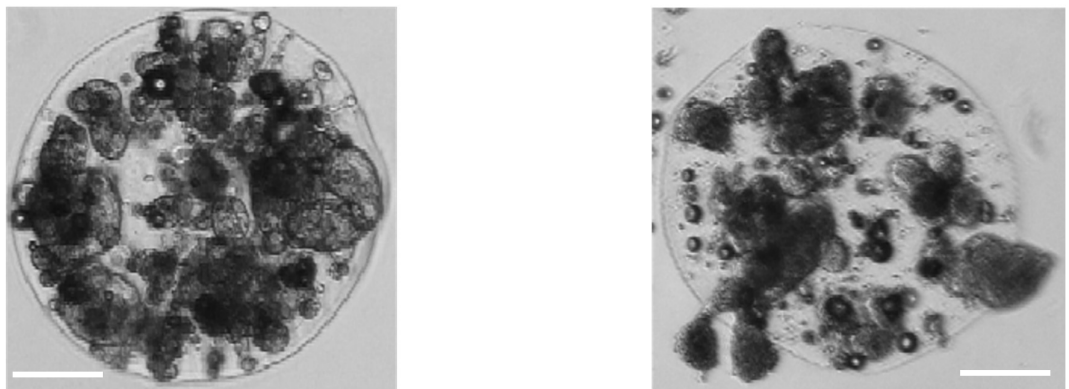
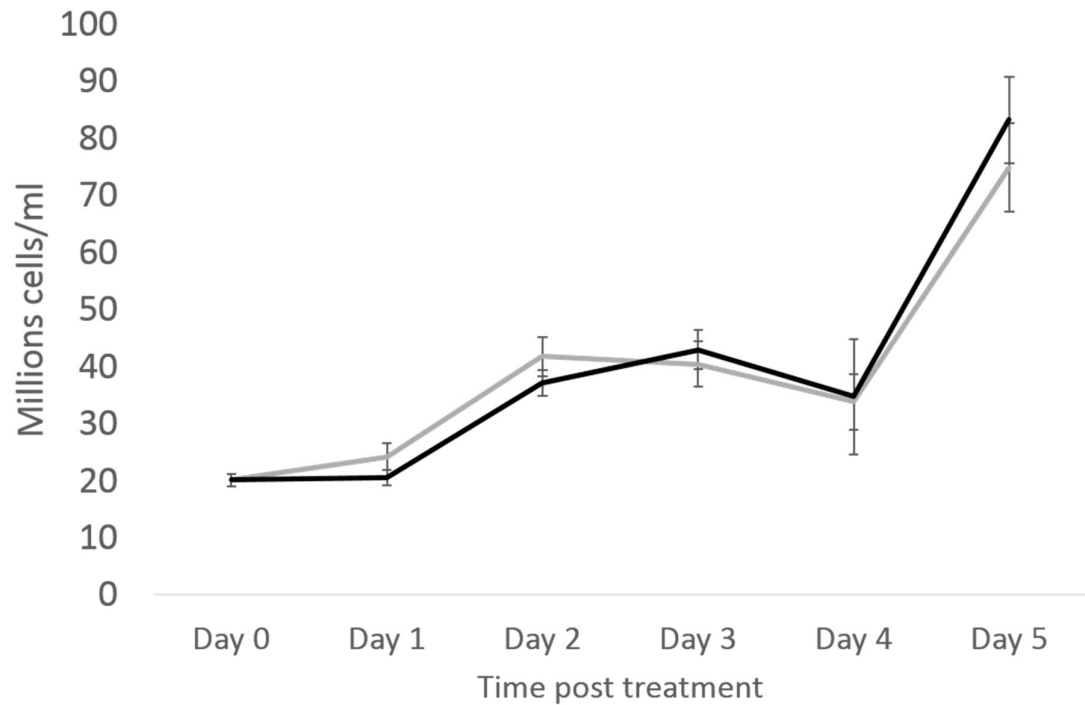


Figure 69 - Top shows effect of 0°C chill at a high cell density, after 12 days prior culture. No significant difference is observed at any time point between chilled samples (black) and the control (grey). Average of  $n=5 \pm$  one SD. The bottom left shows a single typical cell-dense ELS bead without cell breakout. The bottom right shows break-out occurring – an increasingly common occurrence above around 50 million cells/ml. Cell spheroids eventually detach completely from the beads. Scale bar indicates 100 $\mu$ m.

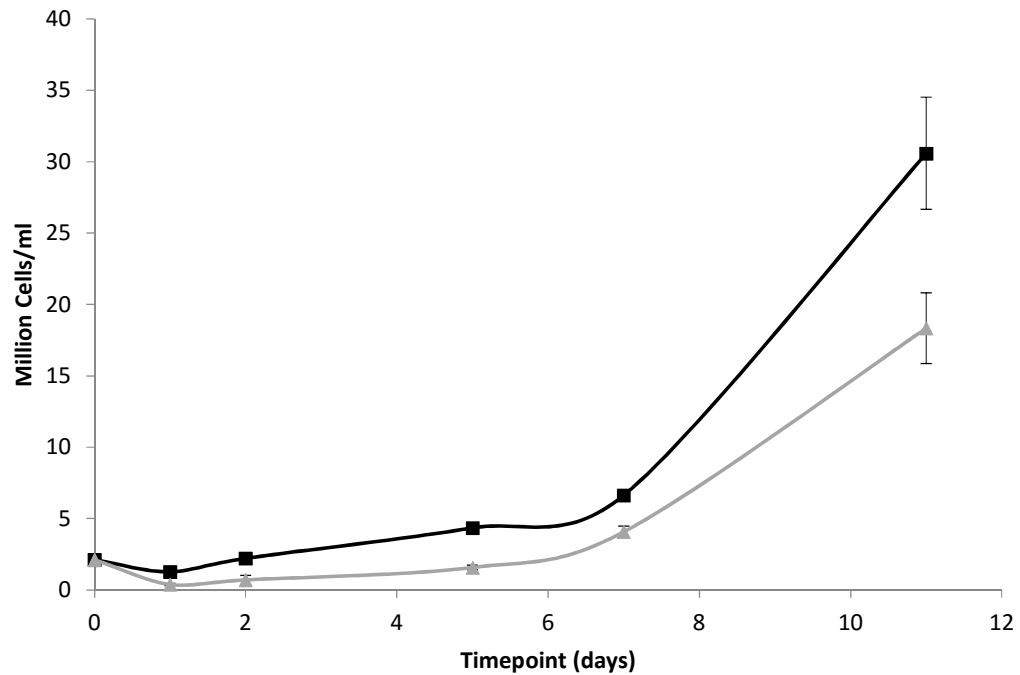


Figure 70 – Comparison of viable cell number between ELS sets experiencing different levels of cryodamage, ELS cultured in RCCS. Optimized cryopreservation was carried out on one set (black), resulting in a viable cell number of  $1.27 \pm 0.12 \times 10^6$  million cells/ml day 1 post thaw. A non-optimal profile was used in another set (grey), resulting in a viable cell number of  $0.38 \pm 0.08 \times 10^6$  million cells/ml 24 h post-thaw. % growth rates are not significantly different between the sets days 7-11 post thaw. Average of 5  $\pm$  SD.

To determine if cryoanaptiksi induced by different methods – simple chilling at 0°C for 45 minutes on manufacture or cryopreservation and storage at -196°C on manufacture before rapid thaw – has an effect on the magnitude of cryoanaptiksi, results were compared. Figure 71 shows the effect on 12 days after re-culture, for two separate experiments with 5 sets per each of three experimental condition per experiment.

Set A showed chilled and cryopreserved samples with a viable cell number of  $35.1 \pm 1.3$  and  $32.9 \pm 1.6$  million cells/ml respectively compared with  $25.6 \pm 5.4$  million cells/ml for non-chilled or cryopreserved cells.

Set B showed chilled and cryopreserved samples with a viable cell number of  $25.5 \pm 2.3$  and  $29.3 \pm 0.5$  million cells/ml respectively compared with  $13.7 \pm 1.1$  million cells/ml for non-chilled or cryopreserved cells.

### 11.3.7. Effect of Cryopreservation over Simple Chilling.

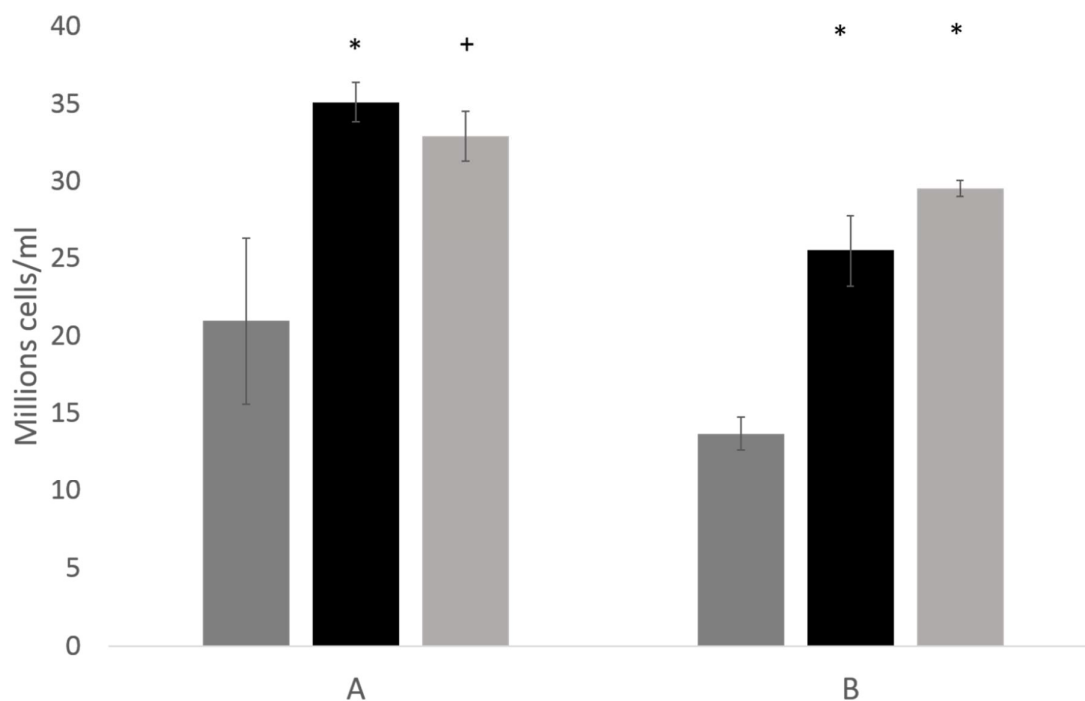


Figure 71 - Comparison between viable cell number 12 days after cryoanaptiksi induced by either simple chilling (centre, black), or cryopreservation (light grey, right) of two separate tests. All tested conditions show significant improvement over control (\* =  $P < 0.001$ , + =  $P < 0.02$ ) using an unpaired student's t-test. No significant difference was seen between samples experiencing either chill induced or cryopreservation induced cryoanaptiksi at  $P < 0.01$  level. All data is average of  $n=5 \pm$  one SD except set A where the control is average of  $n=10$ .

### 11.3.8. Effect of Cryopreservation Reagents.

Cryopreservation induced cryoanaptiksi brings the additional challenge related to cryoprotectants added during the cryopreservation process, in the case of ELS Viaspan and DMSO. Figure 72 shows the effect of chilling with and without these reagents, both individually and together. In addition, the addition of Viaspan with no chilling, instead a 45 minute culture at 37°C is demonstrated.

At 12 days post-treatment, viable cell density was  $25.6 \pm 5.4$ ,  $30.2 \pm 2.9$ ,  $35.9 \pm 2.7$ ,  $35.1 \pm 1.3$ ,  $27.8 \pm 0.9$ ,  $36.7 \pm 3.4$ ,  $32.9 \pm 1.6$  for the control, samples chilled in 12% DMSO, samples chilled in 12% DMSO and 38% Viaspan, samples chilled in only culture medium, incubated in 38% Viaspan at 37°C or chilled in Viaspan, and samples thawed after cryopreservation respectively.

Samples incubated in Viaspan at 37°C showed no significant improvement in cell density over the control. All chilled and cryopreserved samples were significantly better than the control ( $P < 0.001$ ), except for samples chilled in only DMSO. Between samples treated only with Viaspan, chilled samples were significantly better than incubated samples ( $P < 0.001$ ).

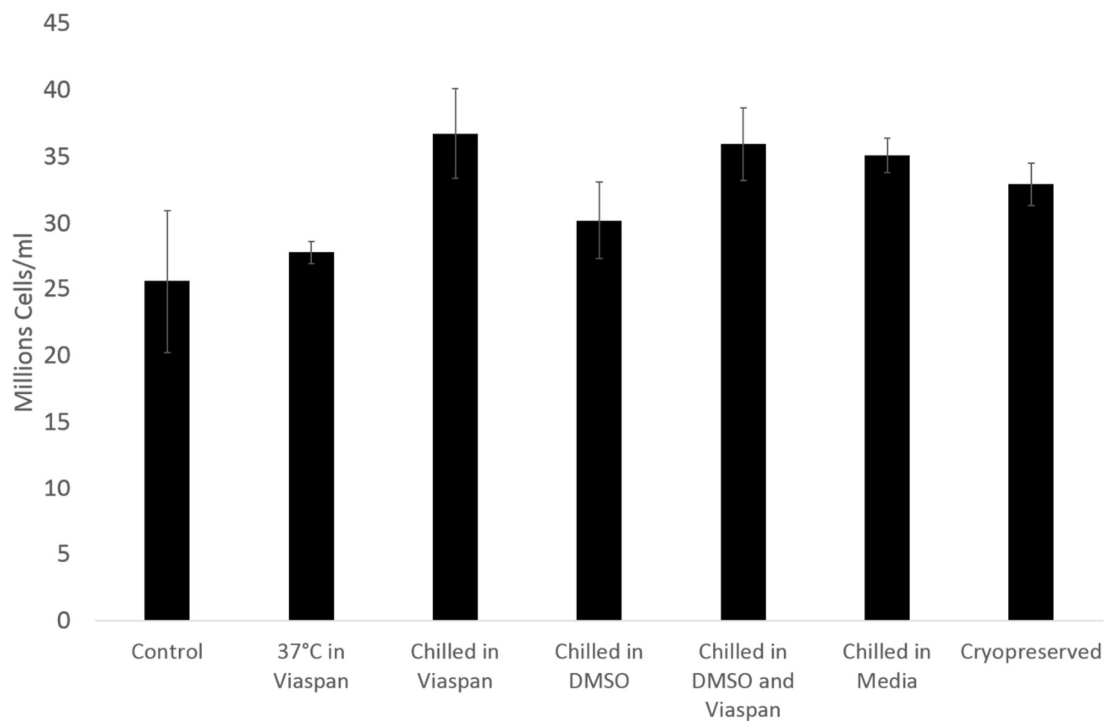


Figure 72 - Viable cell number of samples experiencing different reagents when undergoing cryoanaptiksi. All samples are significantly improved at  $P < 0.001$  levels (cryopreserved  $P < 0.02$ ) over control levels except those experiencing only DMSO or Viaspan at 37°C. Samples experiencing only Viaspan and chilled are significantly improved over those experiencing Viaspan at 37°C. All data is average of  $n=5 \pm$  one SD except the control which is average of  $n=10$ .

### 11.3.9. Time-course of Cryoanaptiksi Cell Proliferation.

Figure 73 shows the impact on cell number of cryopreservation induced cryoanaptiksi on cell growth, from Day 1 to Day 12. Cells were encapsulated at a density of  $1.92 \pm 0.2$  million cells/ml. Unlike the data in Figure 64 at the start of this chapter, culture conditions and measurement time points were identical between sets, allowing for more detailed direct analysis.

For the first 7 days of culture, cryoanaptiksi experiencing samples have a lower viable cell number than control samples, but have overtaken by day 8. Viable cell numbers were  $9.0 \pm 1.6$  million cells/ml for the control versus  $6.9 \pm 1.0$  for cryoanaptiksi samples at day 5. Viable cell numbers were  $11.5 \pm 1.0$  million cells/ml for the control versus  $12.8 \pm 1.0$  for cryoanaptiksi samples at day 8, and  $17.9 \pm 2.5$  million cells/ml for the control versus  $37.3 \pm 1.5$  million cells/ml for cryoanaptiksi samples at day 12.

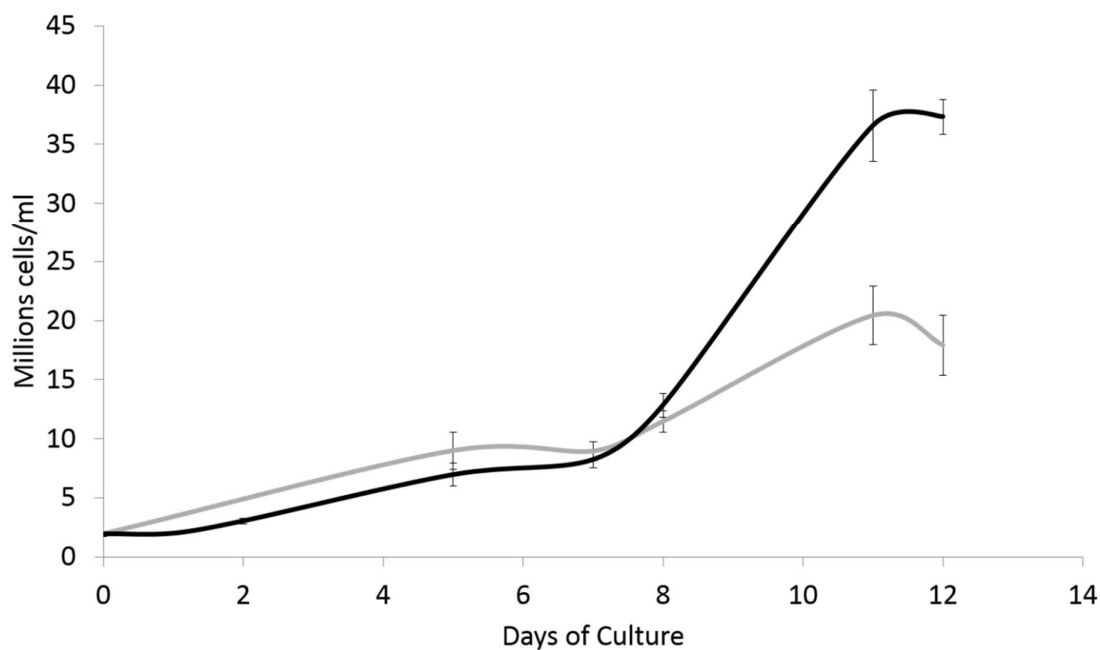


Figure 73 - Comparing temporal cell growth between samples undergoing cryoanaptiksi (black) and an untreated control (grey). Cryopreservation induced cryoanaptiksi samples show a lower viable cell number for the first 7 days of culture, a consequence of damage induced during the cryopreservation cycle, however by the end of the 12 day culture the cell count is significantly higher ( $P < 0.001$ ) in the cryopreserved samples.  $N = 5 \pm$  one SD,  $P < 0.001$ , using an unpaired student's  $t$ -test.

### 11.3.10. Impact on Cell Function and Extended Culture

MTT viability data (image A) in Figure 74 shows samples experiencing cryoanaptiksi maintain their MTT viability, and that it is significantly improved over control samples days 5, 7, and 11 post-treatment.

Glucose consumption per ml biomass per 24 h, indicative of cell metabolism, shows no significant difference between the ELS at any measured time point (days 7, 8, and 12, image B), glucose consumption increased through this period as cells numbers in both sets become greater.

AFP production per ml biomass per 24 h was significantly better in fresh samples over cryopreserved samples.

The right of Figure 74 shows cell performance of separate samples examined days 13-15 post-treatment, with viable cell numbers displayed in image D. Cryoanaptiksi samples had significantly higher viable cell numbers at all measured time points ( $P < 0.001$ ). Glucose consumption per ml ELS per 24 h (Image E) was significantly better ( $P < 0.001$ ) at all time points day 13 to day 15 for samples experiencing cryoanaptiksi over the control.

Day 13 AFP production (Image F) per ml ELS per 24 h was significantly worse in samples experiencing cryoanaptiksi over the control ( $P<0.002$ ). Cryoanaptiksi experiencing samples exhibited significantly improved performance per ml ELS per 24 at days 14 and 15 ( $P<0.001$ ).

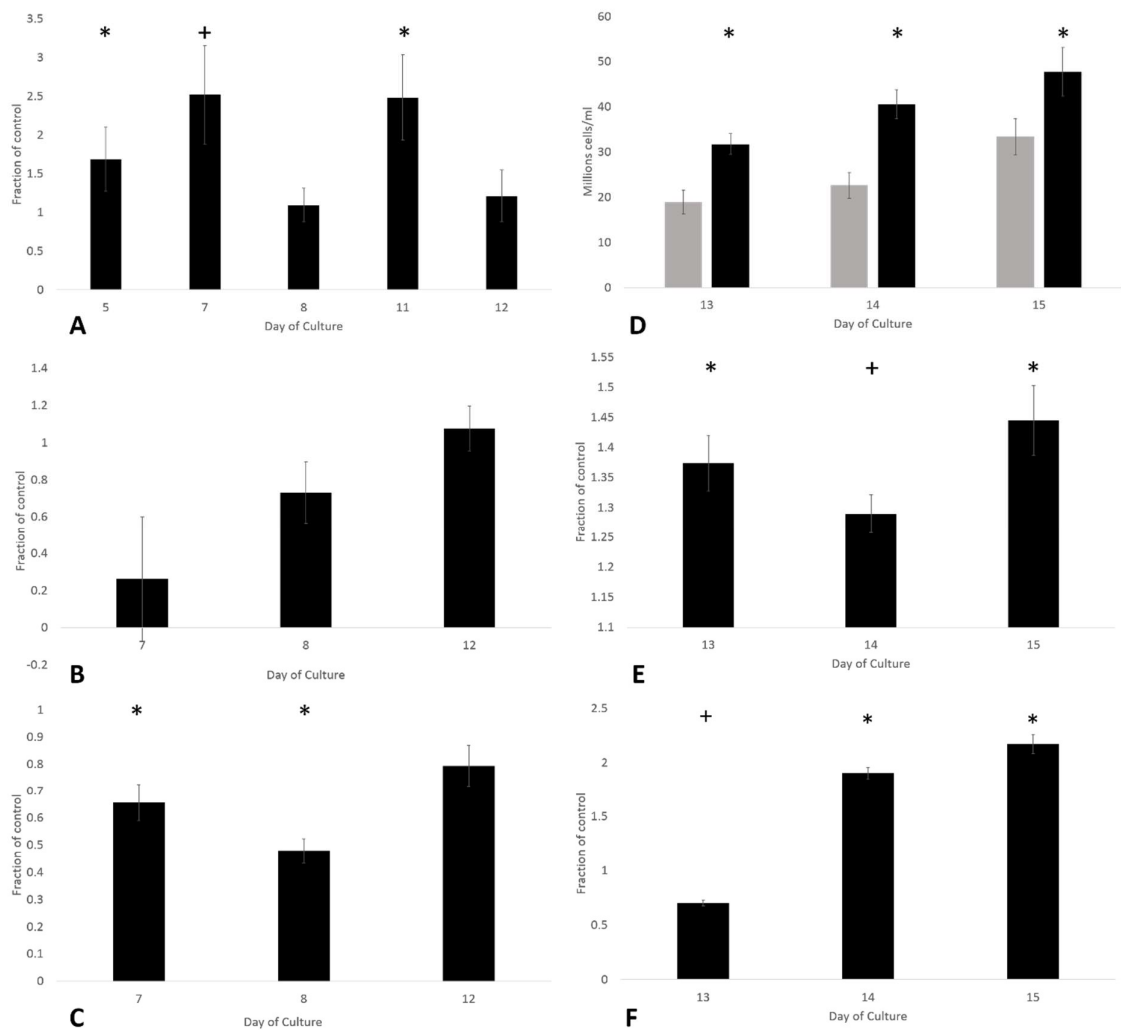


Figure 74 – Functional assays of ELS having undergone cryoanaptiksi. Cell number for images A-C is shown in Figure 7. Image A shows MTT viability of ELS having undergone cryoanaptiksi as a fraction of control samples as chosen time points post treatment. Image B shows relative glucose consumption per ml ELS per 24 h, while image C shows alpha-1-fetoprotein production per ml ELS per 24 h as a fraction of control. Images D-F show functionality for ELS days 13-15 post treatment (potential BAL usage time). Image D shows viable cell number of cryoanaptiksi samples (black) compared to an untreated control (grey). Image E shows relative glucose consumption and F relative alpha-1-fetoprotein production. Significance from control is indicated as \* for  $P<0.001$ , and + for  $P<0.002$  where unpaired student t-tests are used. All data points are average of  $n=5 \pm$  one combined SD.

## 11.4. Discussion

While heat shock has been widely studied in biological systems, the effects of cold shock and low temperatures have been relatively neglected. Almost all studies report on damaging effects of sub optimal temperature and report reduced cell proliferation, although many activated cold-

shock proteins and responses are known [6, 72, 129, 151, 275, 309, 331]. Mechanisms of damage related to cold shock can be grouped into several categories – membrane phase changes; interruption of the cell cycle; and sensitivity to intracellular  $\text{Ca}^{2+}$  ion concentration; lipid peroxidation; cell swelling; blebbing; and cold induced ischemia. This list is not exhaustive and significance of each mechanism is an open question [25, 89, 129, 153, 242, 258, 275, 327, 331, 343, 376, 382, 417].

Two types of low temperature damage to cells have been classified, chilling injury which is time dependent and cold shock which occurs immediately following rapid cooling [153]. Chilling injury is time-dependant, and many studies focus on longer term (greater than several hours) sub optimal culture [129, 153, 258, 309, 343, 417], and only observe cells up to a maximum of a few days post-treatment, and often much shorter [25, 129, 151, 242, 258, 327, 343, 417]. This perhaps explains why this effect has not been recognized before – our data confirms lower cell number and proliferation for several days post-treatment.

Proliferation is observed to be reduced 24 h post-treatment, likely as a consequence of factors widely reported on. The encapsulation may mitigate cell damage somewhat as the alginate is rich in  $\text{Ca}^{2+}$  ions that will maintain the calcium gradient, but not migrate into cells due to its binding with the alginate.

Indeed, inducing cryoanaptiksi reduces their proliferation relative to the control for several days, agreeing with previous literature. It can take up to 7 days for the cell spheroids to recover from cold induced damage and overtake the control values. While in many systems cell cultures will be disposed before this time, systems such as bioartificial livers generally culture for periods of up to two weeks making cryoanaptiksi a useful tool.

Membrane phase transitions occur to a greater degree at increasingly lower temperatures [129, 153]. The observed data with a  $10^{\circ}\text{C}$  hold indicates that the significant changes for cryoanaptiksi our HepG2 cells occur between  $10^{\circ}\text{C}$  and room temperature at  $20^{\circ}\text{C}$ . While studies have observed changes at high sub optimal culture (above  $20^{\circ}\text{C}$ ), and some recombinant protein functions have been observed to increase at these high sub-optimal temperatures [6], these are not dominant in our system as samples prepared at  $20^{\circ}\text{C}$  are not increased compared with chilled or cryopreserved sets. Previous work on pig and boar sperm indicate membrane phase changes occur between  $30^{\circ}\text{C}$  and  $5^{\circ}\text{C}$ , with peak variation at  $18^{\circ}\text{C}$  [89], and it may be that a side effect of these changes induces delayed rapid proliferation. Extended culture of HepG2 cells at  $17^{\circ}\text{C}$  results in only non-fatal damage so cryoanaptiksi induction around this temperature may be optimal, although confirmation requires further study [309].

The effect has little time dependence, with samples cooled and warmed over the space of a minute displaying increased cell proliferation indicating that the mechanism for cryoanaptiksi is triggered very rapidly. While many cell types cannot survive rapid temperature fluctuations [89, 153], our HepG2 cells seem largely immune to above zero temperature fluctuations. This combined with good cryoanaptiksi for cold storage times between 1-90 minutes will allow this method to be used robustly in large volumes, where consistent cooling and warming times and rates are difficult to obtain.

Observing that cryopreserved samples display this effect to the same degree as chilled-only samples is encouraging. Manufacturing a large quantity of ELS and immediately cryopreserving allows for rapid delivery on demand, and cryopreservation is necessary for most BAL or tissue engineered constructs to be viable [236, 275]. Viaspan contains potassium lactobionate and as lactobionate is a strong chelator of calcium [180] it will remove calcium from ELS and thereby weaken their structure and may allow more rapid proliferation, however, this was not observed to be a dominant factor. Indeed this weakening is to be prevented as it may result in spheroid breakout from ELS occurring at a lower cell density. Extra calcium ions have been added to culture medium to reduce this effect.

Cryopreservation will induce a large stress on the hepatocytes, as will cryoprotectant toxicity. Processes will not be uniform due to variations in undercooling of samples [289]. Despite this the low temperatures experienced during the process more than make up this damage at later time points, indicating the robustness of cryoanaptiksi.

Previous work carried out by a colleague in the LG using Fourier-Transform Infrared Spectroscopy on ELS pre- and post- cryopreservation detected no difference in alginate structure. A study was also carried out on cell suspensions experiencing cryoanaptiksi before being seeded as a monolayer. No difference in proliferation between the sets was observed (data not shown). This effect therefore only seems to impact on alginate encapsulated cells, and not monolayers. However, as monolayer cells need passaged every 5-7 days (a process that disrupts the growth cycle), and are usually confluent by this stage, any effect may be masked and so the behaviour on monolayer cultures is not completely closed by this study. Seeding cells at very low cell density in monolayers results in cell clumping and so cannot be used to effectively study the effect.

Alpha-1-fetoprotein (AFP) production tended to be reduced post treatment. In these data, the overall performance was slightly reduced in the cryo-treated samples. As cell density was higher in the cryoanaptiksi experiencing sample, this indicates a large reduction of around 50% in per-cell performance during the 12 day growth period. However, protein production tends to be

inversely proportional to cell proliferation, as during the growth cycle cellular resources are directed to proliferation and not protein production. A previous study examining the effects of low temperatures on hepatocytes found that after 30 minutes at 4°C, albumin production was reduced until around 7 days post-thaw, agreeing with our AFP observations, and could be mitigated with addition of polyethylene glycol [382]. Due to the presence of human plasma in our culture medium, albumin quantification cannot be done and AFP is instead used as an indicative protein.

MTT and glucose consumption was maintained after cryoanaptiksi indicating that the cell spheroids were healthy. Viability tended to be slightly lower in cryoanaptiksi experiencing samples, this is due to the higher cell density making nutrient transfer more difficult. In most cases the effect was <3%, and was taken into account in viable cell numbers. Viability remained suitably high throughout, above 90% in all test conditions.

The BAL is intended for use after this 12 day initial FBB growth period, between approximately 12-15 days post-encapsulation. Cell function here shows increased protein production as cell growth rate slows. For effective delivery of these treatments, it would be beneficial to develop a method to arrest cell proliferation once a desired cell number is achieved to increase protein production. This would also eliminate the risk of spheroid break-out observed above around 50 million cells/ml. Methods such as adding a small extra layer to the outside of alginate beads has been shown to stop cell proliferation when the alginate bead is full and prevent cell break-out [219].

A major consideration when developing bioartificial organs is the prolonged cell culture time required to achieve sufficient cell number. By employing low temperature treatment to ELS, I've have shown that cell proliferation can be greatly increased, allowing a more economical cell-growth regime.

This observation has never been published in mammalian cells before, and could result in a greater cell density for encapsulated cell lines, reducing biomass volume required for treatment, and substantially reducing costs, making these devices cheaper to culture, quicker to prepare, and more practical.

This upregulation is particularly impressive when considering that the cryostress experienced during cryoanaptiksi inducement delays cell growth for several days at the start of the culture period.

This can rapidly improve FBB cultures of encapsulated cell lines on several fronts sufficient cell numbers can be achieved in a smaller total biomass volume, due to the increased cell density, with proportional reductions in labour, consumables, and equipment costs.

This could also allow for the possibility of very large volumes of ELS being prepared at the same encapsulation, with thaw on demand and treatment commencing within 8-9 days as opposed to 26 days with our current set-up – exact volumes dependant on patient needs could also be determined prior to thaw, removing the one-size-fits-all of many BAL systems, and instead tailoring to specific patient needs without the requirement of an additional thaw.

For LG ELS, optimal growth is generally observed when the ELS have a cell density of 2 million cells/ml at the start of the FBB culture period. For cell types that experience a reduced viable cell number post-thaw, it would be feasible to have a pre-freeze cell density proportionally above the optimal level, which reduces to the optimum on thaw, resulting in ideal cell growth conditions.

While the biological mechanism for this effect has not yet been established, there are several possibilities. Hibernating animals are known to go through phases of cooling and warming of core body temperature prior to entering, and after emerging from hibernation [188, 222]. After hibernation cell growth increases [454] in these animals to make up for damage caused during hibernation – the cold temperatures (or temperature fluctuations) may trigger an old gene to activate causing the hepatocytes to increase proliferation – hibernation is shown to impact huge numbers of genes which regular cell growth and metabolism, including in the liver [97, 260, 454]. A second possibility is that lowering temperatures causes damage to cells and so recovery processes are initiated which stay active for longer than is required to repair any damage caused. Future work can establish what mechanism causes cryoanaptiksi, what are the optimal temperatures and storage times to induce it (perhaps more than one chilling step is optimal), if warming is of benefit, and what other systems display this characteristic.

I enthusiastically await results using this method in different cell lines and types, and believe it to be an exciting and promising avenue for bioartificial liver development, and to offer potential for other devices.

## 12. Fluidisation

### 12.1. Introduction

This chapter determined the significant parameters to be considered and best models to use when considering fluidization of the bio-artificial liver device.

Fluidisation has found numerous industrial applications over the past century as a result of its ability to ensure highly efficient mixing and fluid-particle contact in a controllable manner. It is founded on the principle that as a fluid passes up through a layer (particle bed) of many discrete solid particles, the particle bed will expand with increased fluid flow, due to the upward pressure on the particles from the fluid. Within the bed, individual particles vibrate and rotate relative to one another, this movement increasing as the height of the bed increases.

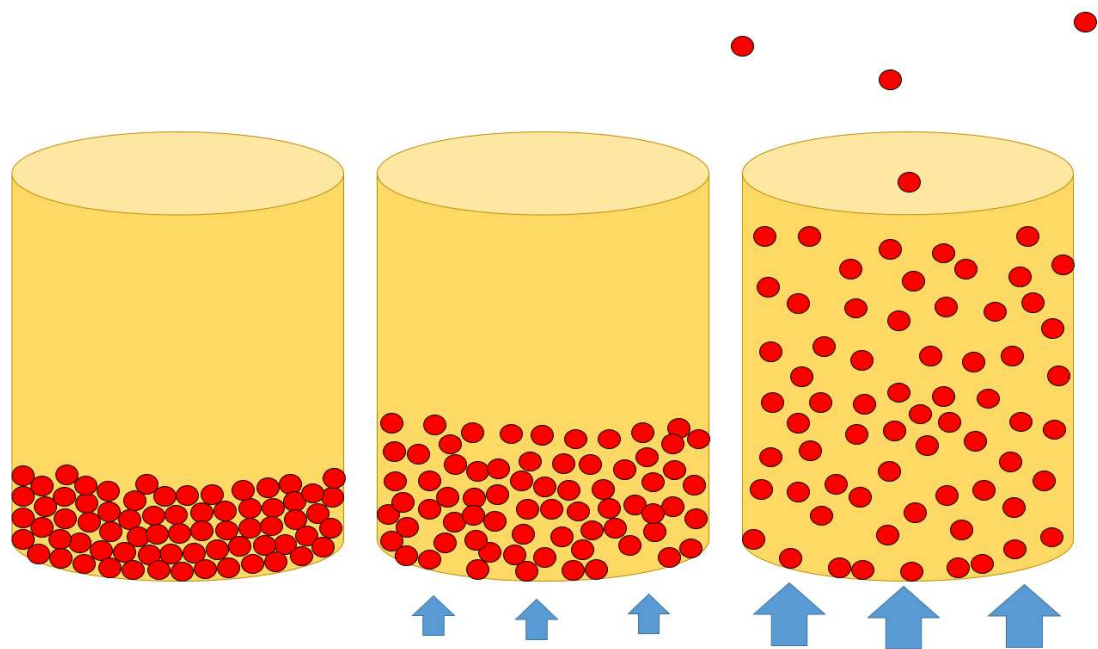


*Figure 75 - Example of a solid-liquid fixed bed of particles (left), an expanded (fluidised) bed (centre) and an over fluidised bed (right). Fluid flow direction and speed are denoted with blue arrows. As fluid linear flow rate is increased, the system will develop from a packed bed with no flow (left), to an expanded bed with some flow (centre) to a fluidised bed with increased flow (right). The fluidised bed bioreactor in this project uses a set-up similar to the middle image.*

More recently the biological benefits of fluidised beds have been realised – the increased contact between a culture medium and cells can give better cell performance over a standard culture flask, resulting in higher cell performance [240]. A fluidised bed bio-reactor is the primary culture method for the bioartificial liver device, and so a fuller understanding of fluidisation will

be explored here, before determining critical fluidisation parameters in the BAL system and characterizing scale down processes for the BAL culture regime.

## **12.2. Types of Fluidisation**

### **12.2.1. Gas-Solid**

The most common form of fluidised beds is that of a gas-solid system in which gas is passed through a bed of solids. This was the earliest fluidisation performed on an industrial scale, and is widespread today. Fluidisation of this type can often appear like a water boiling in a kettle, with bubbles of gas passing through a turbulent regime of numerous small particles moving together as a liquid. This turbulent and unstable fluidisation is known as aggravated fluidisation [62, 345].

Gas-Solid fluidisation is perhaps most commonly seen in hot-air popcorn makers. Hot air is passed through the kernels, fluidising and so mixing them, effectively homogenising their temperatures. When a kernel pops, its increased surface area causes it to be removed by the hot air as a finished product, preventing burning [339].

### **12.2.2. Liquid-Solid**

A little later than gas-solid fluidisation became widespread, the benefits of solid-liquid fluidisation were recognised in many other systems - to fluidised bed nuclear reactors, to particle washing, and to bio-reactors amongst many other uses [98, 455]. Liquid-solid fluidisation of bioreactors is of particular interest here as it is the method used in the bio-artificial liver device. When a liquid-solid system fluidises, the particles tend to move further apart from each other with an increase in velocity, in a consistent and non-turbulent regime. Bubbles (large upward moving chasms of liquid in this case) rarely form except at very high flow rates. This is distinctly different than aggravated fluidisation and is named particulate fluidisation [62, 134, 345]. This particulate fluidisation tends to be cheaper, simpler, and more effective than mechanical shaking in industrial applications [464].

Importantly, while bed depth affects the fluid flow rates required for solid-gas fluidisation, bed expansion is independent of bed depth for solid-liquid systems [193, 232, 247, 455].

Liquid-solid systems are now used for many biological purposes including wastewater treatment and the production of penicillin. These bioreactors are very efficient both on the smaller scale and when scaled up [88, 235, 240].

### **12.2.3. Gas-Liquid-Solid**

Applications of a mixture of the above, gas-liquid-solid fluidised beds, additionally have widespread uses. Historically this included the liquefaction of coal. Coal and oil mixes can be fluidised at high pressures with hydrogen, resulting in a liquid product that has been used as fuel. Fluidisation in this system will tend to result in aggregated dynamics, with bubbles of gas passing through a solid-liquid mix [113].

### **12.2.4. Circulating Fluidised Bed Reactors**

Most fluidisers consist of a large column where the fluidised particles are isolated. Other systems do exist such as circulating fluidised bed reactors, these work by completely fluidising a system and allowing particles to reach the top of the fluidisation chamber. When the particles reach the top, a condenser collects them and re-introduces them at the fluidiser's base; hence a continuous circulation of fluidised particles is achieved [69, 142, 422].

These circulating fluidised bed bioreactors achieve greater flow rates and liquid-solid contact over traditional liquid-solid fluidised beds along with very effective mixing [142, 466]. These beds tend to be more unstable than a standard fluidiser, with very rapid re-circulation through the condenser required especially at high flow rates [228, 466].

### **12.2.5. Inverse Fluidisation**

It is not uncommon, particularly in liquid-solid fluidised beds, to have solid particles less dense than the liquid component. The particles then float in the fluidiser, with liquid passed downwards for fluidisation. This is termed an inverse fluidised bed [200, 232, 344], and operates in the same way as a standard fluidised bed, but with the gravity and flow direction properties reversed [235]. This form of fluidisation is particularly useful for biological wastewater treatment [6]. Interestingly they will have different critical values of Reynolds Number, which dictate flow characteristics, as a result of lower inertia for less dense particles [200].

### **12.2.6. Semi-Fluidised Beds**

Another variation on the theme is a semi-fluidised bed – a bed where the base is fluidised but the top is fixed (usually by means of an upper restraint on the particles). These beds have the advantages of both fixed and fluidised beds, but suffer from drawbacks such as larger mechanical stress of the individual particles [193].

## **12.3. Applications of Fluidisation**

### **12.3.1. Mixing**

Fluidisation is particularly effective at heat and mass transfer. In a fluidised system particles follow a random and rapid (with respect to natural diffusion) path throughout the whole fluidised bed. Extensive mixing therefore takes place and so all products in the bed experience the same conditions, without the same level of shear that can be experienced if using a mechanical stirrer.

Mixing is not usually possible in liquid-solid fluidised beds with non-homogenous particles. If a binary mixture of particles is fluidised liquid-solid, the phenomenon of inversion is often observed, that is the larger particles will form a distinct layer at the base of the bed and smaller particles will form a separate layer of particles on top [16].

### **12.3.2. Particle Separation**

Perhaps one of the simplest and most common uses for fluidisation is to separate particles of different sizes, shapes, or composition [98, 134, 294]. First consider particles equal except in size; as fluid passes through the system larger grains will sink in the bed while smaller ones tend to rise, this being a consequence of volume, and therefore mass, increasing cubically while the surface area only increases as the square of the radius, reducing the surface area to volume ratio.

Fluidisation can even be imposed where the smaller particles achieve full fluidisation and leave the top of the system to be collected, and larger ones sink and are collected at the base of the fluidiser, where they're collected. Systems can be constructed where mixed-size particles are continually inserted and separated-sized particles are concurrently removed.

Fluidised beds are used extensively in industry for particle separation, such as in necessary for the beneficiation (separation of useful minerals from surrounding gangue) of ores [412].

### **12.3.3. Particle coating**

A more advanced use of particle separation can be applied to particle coating. Un-treated particles can be added to the fluidised system, in which there they are coated with the desired material. As the size and density of the particles will change, the system can be designed so that when sufficient coating has been added the finished products are removed from the fluidiser [456].

### **12.3.4. Biomass Combustion**

The burning of biomass for energy requires the use of a gas-solid fluidised bed reactor. The dynamics of the fluidiser allows the fuel to be burnt faster, more completely, and at a higher temperature than is possible in a conventional furnace, where typically there is only burning at the surface. This usually requires high fluidisation rates and few models are available to describe the process due to the varied and irregular fuel material topography [69, 320].

Often when burning biomass, and in other industrial applications, adding small particles such as sand or glass improves the fluidisation, though the mechanism is not fully understood [69, 320]. Generally, by adding smaller finer particles, the minimum fluidisation velocity of the larger ones will be reduced [16].

### **12.3.5. Application to the Bioartificial Liver**

Prior to and post cryopreservation, the ELS (alginate encapsulated liver spheroids) will be maintained in a culture chamber; a cylindrical vessel in which the ELS sit with a flow through of culture medium. To ensure maximum health and proliferation of the hepatocytes (liver cells), this culture chamber will be fluidised.

The fluidising chamber itself will be a glass cylinder, approximately 30cm high and with a 15cm inner diameter, with approximately 2 litres of ELS, each with a diameter of around 0.5mm.

During the growth phase, culture medium supplemented with plasma will be used as fluidisation liquid. For the treatment phase (where the bioartificial liver will be used in a patient) blood plasma – which has a higher viscosity – will be used. The circulation in the chamber leads to maximum contact between the beads and the growth medium, resulting in hepatocytes that proliferate more readily and have higher function per cell. Determining the correct flow rates and physics of fluidisation is therefore necessary for the bio-artificial liver project [101, 240, 363].

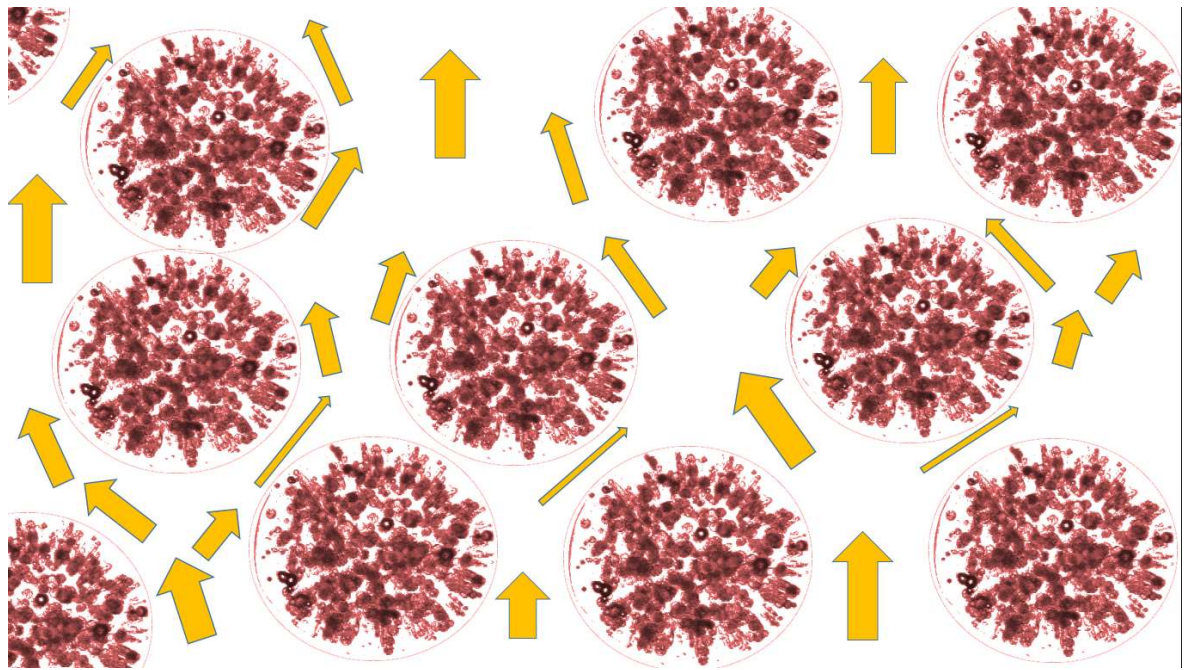


*Figure 76 - A false colour representation of possible fluid flow through the bioartificial liver device at any particular moment. The red spheres represent encapsulated liver spheroids, while the arrows represent fluid flow. The length of the arrow denoted speed of flow and thickness denotes volume.*

It was out with the remit of this thesis to determine whether improved cell function in a fluidised bed system was due to the fluidised bed per-se, or was a consequence of culture medium movement relative to ELS.

## **12.4. Mechanical Considerations during Fluidisation (solid-liquid)**

As the bioartificial liver device uses a solid-liquid fluidised bed, this will be examined preferentially over gas-solid fluidisation in this chapter.

### **12.4.1. Linalising Flow**

It is important to have a linear homogenous flow for good quality fluidisation. The first tool to ensure this is a distributor found at the base of the fluidiser, this is usually a solid component with many holes in it which breaks up liquid flow homogeneously throughout the fluidiser [62, 247]. It is used to prevent channelling – the preferential movement of fluid in a few arteries.

A plenum chamber (an area filled with spherical weights below the fluidiser) or homogenising section is often incorporated in a fluidiser to start homogenising flow before it reaches the distributor [62, 412].

Occasionally, particularly with very fine particles in a liquid-solid system, channelling can still occur damaging the quality of the fluidisation. This can be overcome with the use of a mixer or vibrator located near the base of the device. The mixer will force particles into the channels, effectively destroying them. Once good fluidisation is achieved, the mixer can be removed without the recurrence of channelling [345].

As with all liquid passing through an enclosed cylinder, wall effects will start to disrupt the linearised fluid flow. This is a major determinant of particulate movement inside a fluidiser, with particles more likely to rise centrally and fall near the walls. Fluidisers therefore should not be excessively tall relative to their inner diameter.

#### **12.4.2. Effect of Particle Size and Shape**

On the microscopic level, the primary interaction in a FB (fluidised bed) is the drag exerted by the fluid on individual particles. This is highly dependent on the form of particles – for spherical particles experiencing laminar flow the dominating factor is the particles relative size and density, outlined by Stokes. For particles of irregular shapes such as stems of plants the picture becomes more complicated and fluidisation characteristics can only be determined experimentally.

In general larger particles require a greater fluid flow rate to experience fluidisation than similar smaller ones [99, 193, 232, 344].

#### **12.4.3. Collisions between Particles**

Particles in a fluidised bed will continually interact and collide with each other. This significantly impacts on the particle path for individual particles, and is highly complicated to model. Not all collisions are created equally, with inelastic ones increasing mixing in the system, however

elastic collisions remove kinetic energy and can interrupt fluidisation on the microscopic and macroscopic scale. These collisions thereby affect the parameters for fluidisation [79, 193].

Collisions can also be detrimental in systems undergoing fluidisation for extended periods, complex particles may be damaged or destroyed as a result of many collisions over long periods of time.

Relatively little data has been published on the effects and frequency of particle-particle collisions in fluidised beds. It is also difficult to measure experimentally, though several computer models can be used in lieu [79]. One method used by Del Pozo and Briens [80] uses tethered electrodes which discharge as a result of collisions. It was reported that this method was more accurate in detecting collisions than a fixed electrode, but suffered from some drawbacks such as the tether becoming tangled and electrode being localised to its anchorage point.

It was found that the collision rate was at a maximum when the system was just fluidised, and then decreased with increasing bed expansion [80]. This might be expected as particles are closer together with minimum fluidisation. It is possible that at higher bed expansions the collisions involve more energy, even if they are less frequent.

### ***12.5. Modelling System Parameters***

This chapter focuses on determining approximate models of fluidization in the system and then replicating them on the smaller scale experimentally. There are two main advantages of doing so. The first is consistency between different experiments where the BAL is used. Prior to this chapter, bed expansion is established through a trial and error exercise. This necessarily results in variation between liver group BALs cultured at different times. If a simple model was created where known inputs are added and the output gave the flow rate throughout the system required for a certain bed expansion, these inter-BAL differences would be reduced. This is a necessary step for clinical delivery where consistency is required.

A second large advantage would be to fully understand how changes in the makeup and culture of ELS will impact fluidization. ELS experience a flow throughout the culture and usage phase using a fluidized bed bioreactor. This causes some problems not seen in other bioreactors such as a hollow fibre bioreactor such as disintegration of the alginate. This disintegration is caused by the flow of liquid past the ELS for several weeks. Ideally, ELS would be cultured with a density very similar to that of the culture medium to reduce this stress however too low a density will result in insufficient nutrient exchange. The treatment phase also used blood plasmas which has

a density and viscosity much greater than culture medium. If the density of the ELS is too low these will flow out of the BAL chamber during the treatment phase. It is therefore desirable to fully understand how each parameter impacts ELS-plasma/medium interactions, so that the optimal size, density, and nutrient exchange rate can be found.

While the Navier-Stokes equations should theoretically be able to describe all parameters in a fluid-solid system, the sheer complexity of a fluidised bed and number of particles makes solving this system undoable practically [12].

An extensive number of models exist to try and predict and describe the behaviour of all or some aspects of every imaginable design of fluidised beds [12, 62, 80, 91, 114, 142, 161, 178, 200, 215, 228, 235, 350, 412, 464, 466]. Many of these models are useful only for the system that they were designed to model, and reviewing them all in detail would be impractical and of little use. Several of the main parameters and methods common to many models are discussed below, by doing so the key factors in fluidisation of the BAL should be identified.

Often systems incorporate non-spherical particles. Generally this involves finding what size of spherical particle best describes the non-spherical particle in terms of a sphericity factor  $\varphi$  [166]. In the bioartificial liver system, the particles are approximately spherical so this sphericity factor is ignored.

### 12.5.1. Nomenclature

$Ar$  – Archimedes Number (dimensionless)

$C_D$  – Drag Coefficient (dimensionless)

$d$  – diameter of particles (m)

$D$  – diameter of fluidiser (m)

$\varepsilon$  – voidage (dimensionless)

$F_D$  – Drag Force ( $\text{kg m s}^{-2}$ )

$g$  – gravitational force ( $\text{m s}^{-2}$ )

$l$  – characteristic length (dimensionless)

$n$  – Exponent of the Richardson-Zaki equation (dimensionless)

$\rho$  – Density ( $\text{kg m}^{-3}$ )

Re – Reynolds Number (dimensionless)

$U_{mf}$  - Minimum Fluidisation Velocity ( $\text{m s}^{-1}$ )

$\mu$  – Viscosity ( $\text{Pa s} = \text{kg m}^{-1} \text{s}^{-1}$ )

v – velocity ( $\text{m s}^{-1}$ )

w – weight (kg)

### Subscripts

p – particle

l – liquid

t – terminal (velocity)

' – relative

\* - dimensionless

## 12.5.2. Reynolds Number

In almost all physical fluid systems, fluid behaviour is highly dependent on the Reynolds Number (Re) [91] the ratio of inertial forces to viscous forces. This essentially dictates the flow regime around an object. In systems with a low Reynolds number, flow can be described as laminar, essentially moving slowly and smoothly around obstacles for spheres this laminar flow is seen for Reynolds numbers approximately  $< 10$ , although the change from laminar to more complicated flow regimes is a continual process so no special significance should be attributed to a Reynolds value of 10. At higher Reynolds numbers, flow transitions into a more turbulent and complex regime. This transition takes place up to a Reynolds number of approximately 1000 for a sphere in a fluid, after which the fluid flow is normally described as turbulent [24]. The Reynolds number for a sphere moving relative to a fluid is [440]:

$$\text{Re} = \frac{\rho v l}{\mu}$$

(39)

Where  $\rho$  is the density of the particle, v is the relative velocity, l is the characteristic length (in this case the diameter of the sphere), and  $\mu$  is the liquid viscosity.

At sufficiently low Reynolds numbers where smooth laminar flow dominates Stokes' law can be used to characterise the system. With increasing Reynolds number turbulence becomes significant around the particle, and so an additional drag terms are required when fluid-solid interactions are studied.

In the bio-artificial liver, the alginate spheroids are 0.5mm in diameter, with a density of around 1020kg/m<sup>3</sup>, in medium with a viscosity of approximately 3Cp. The linear flow rate is <1mm/s, giving a Reynolds number <<1. Laminar flow will dominate in the bioartificial liver system.

Several modifications of the Reynolds number have been proposed for packed and fluidised beds. The Reynolds number is crucially important when considering fluidisation problems, as different models are designed only for finite ranges of Reynolds number [91].

### 12.5.3. Archimedes Number

Commonly, finding the free-fall velocity of a particle and its general flow characteristics relies on the Archimedes number [200, 232, 294, 344, 455]. This number summarized how important density differences between ELS in the system are compared with the viscosity of the medium – at higher viscosities ELS free-fall viscosity will decreased, while the velocity will increase with a greater density difference between the ELS and the culture medium. The Archimedes' number is interesting to determine for the BAL system as it will indicate how much the flow characteristics of the system change when culture medium is replaced with denser, more viscous, human blood plasma for the treatment phase. This is a dimensionless constant dependant on the physical parameters of the system and is defined as:

$$Ar = \frac{d^3 g (\rho_l - \rho_p)}{\mu_l^2} = \frac{3Re^2 C_D}{4}$$

(40)

Where  $C_D$  is the drag coefficient (Section 12.5.4). This is based on Archimedes' principle - the downward force of a spherical particle in a liquid is equal to the weight of that particle minus its buoyancy. In general the higher the Archimedes number of a particle increases at Re at  $U_{mf}$  increases [235]. While the above equation is the most common form of the relation between Re and Archimedes number, other correlations are proposed [24, 25]. For  $Re < 0.2$ , a linear relationship holds:  $Ar = 18Re_t$  [455].

#### 12.5.4. Drag Coefficient

The drag coefficient is a dimensionless quantity used to determine total drag force  $F_D$  in a system, which changes dependent on the system's topography, relative speed, and density of fluid – essentially it is caused by the force required for fluid to flow past a particle. Perfect fluidisation will occur when the drag caused by culture medium flowing upwards through the system is balanced by the relative weight of the ELS. The inertial form of the drag equation is [54]:

$$C_D = \frac{2F_D}{\rho v^2 A}$$

(41)

There are bountiful different methods used to relate this drag coefficient to the Reynolds number (and so the terminal velocity) in the literature [69, 158, 166, 227, 416]. It is possible to directly determine terminal velocity from the drag coefficient using equation (42) [158, 200]:

$$U_t = \sqrt{\frac{4(\rho_s - \rho_l)gd}{3\rho_l C_D}}$$

(42)

Where  $C_D$  is the drag coefficient, with  $\ln(C_D) \propto \ln(Re)$ .

For regions of  $Re < 0.2$ , equation (43) has been proposed to link  $Re$ ,  $Ar$ , and  $C_D$  with voidage (empty space in the system) [455]:

$$\frac{3}{4} C_D \frac{Re^2}{Ar} = \varepsilon^{4.78}$$

(43)

Haider and Levenspeil highlighted a commonly used relationship for drag coefficient has been determined directly through experimental measurements, and has the advantage of being valid at both high and low Reynolds number for spherical particles [158]:

$$C_D = \frac{24}{Re} (1 + 0.1806 Re^{0.6457}) + \frac{0.4251}{1 + \frac{6880.95}{Re}}$$

(44)

This could be related to the terminal velocity through [158]:

$$U_* = \left[ \frac{18}{d_*^2} + \frac{(2.3348 - 1.7439)}{d_*^{0.5}} \right]^{-1}$$

(45)

Where  $U_*$  is the dimensionless terminal velocity  $= u_t \left[ \frac{\rho_l^2}{g\mu(\rho_s - \rho_l)} \right]^{0.33}$  and  $d_*$  is the dimensionless particle diameter  $d \left[ \frac{g\rho_l(\rho_s - \rho_l)}{\mu^2} \right]^{0.33}$ . The drag coefficient equation was found to be more accurate than the equation previously proposed by Turton and Levenspeil, though for the final calculation of terminal velocity, Turton and Clark's equation ( 44 ) was slightly more accurate [158, 416]:

$$u_* = \left[ \frac{1}{\left(\frac{18}{d_*^2}\right)^{0.824} + \left(\frac{18}{d_*}\right)^{1.214}} \right]^{1.214}$$

( 46 )

Almost all of the above equations have been developed through some experimental measurements, and so are very accurate in those specific systems but less useful in a general case. Many have excessive terms as they attempt to operate at both high and low Reynolds number. Perhaps the simplest method is based on Stokes' work. Stokes proved that the total drag on a sphere during laminar flow is [386]:

$$F_D = 6\pi\mu r v$$

( 47 )

Which agrees with experimental data as high as  $Re = 1$  [441]. As this is well within the flow regime of the BAL ELS and has been established to be accurate in these regimes since it was first proposed in the 19<sup>th</sup> century. Equation 47 combines all the fundamental aspects of drag – velocity, particle size and shape, and viscosity of the medium. Combining equations ( 41 ) and ( 47 ) , and that the maximum cross sectional area of a sphere is  $A = \pi r^2$ :

$$C_D = \frac{12\pi\mu r v}{\rho v^2 \pi r^2} = \frac{12\mu}{\rho v r}$$

( 48 )

So relating the total drag coefficient to drag force [82, 441]:

$$C_D = \frac{24}{Re}$$

( 49 )

It is clear that many methods can be used to determine the drag of a particle, all that apparently agree well with experimental data. Many of these give very similar results, though experimental determination will have to be carried out too as no generalised formula has been proven. This experimental value can then be related back to theoretical values and the most appropriate model chosen.

### 12.5.5. Minimum Fluidisation Velocity and Pressure Drop

During fluidisation, as a liquid passes through the matrix of channels created between particles, the pressure drop through that matrix is proportional to the resistance presented by the matrix. A packed bed of particles normally results in a large pressure drop. As liquid flow rate is increased in a fixed system, the pressure drop increases lineally. This continues until the pressure drop over the system equals the total weight of particles in the system.

At this point the particles are fully supported by the liquid and the bed starts to expand. The linear flow rate at this point is termed the minimum fluidisation velocity,  $U_{mf}$ . Increasing the fluid flow rate past this point results in the bed becoming increasingly expanded, but with the pressure drop remaining constant.  $U_{mf}$  is one of the most important values, the lower boundary condition, for any fluidised bed.

$U_{mf}$  can be measured experimentally through the pressure drop; normally a plot of pressure drop over the bed against linear flow rate is determined for a given system. The point where the pressure stops increasing can then be used to determine  $U_{mf}$ . In an ideal system the pressure will stop increasing abruptly, however in reality this will occur over a range of linear flow rates as a consequence of small perturbations in the system that may be caused by channelling, circulation in the system, non-equal particle size, an imperfect distributor etc. all of which prevent 'perfect' fluidisation experimentally [121, 345].

To overcome this a second dataset is usually added to the plot, this time during defluidisation. The flow rate in an initially fluidised system is slowly reduced, until the bed becomes fixed. This plot usually differs slightly from the fluidisation plot, as the particles vibrate more during defluidisation so the bed does not readily enter its most compact state.  $U_{mf}$  can be determined by the intersection of the projected linear component of these plots [62, 163].

### 12.5.6. Mathematically Modelling Pressure Drops and Minimum Fluidisation Velocity

While it is straightforward to measure  $U_{mf}$  empirically, it is preferable to have a quicker and easier method of determining it theoretically.

A seemingly endless list of equations for calculating  $U_{mf}$  is proposed in the literature, each one claiming to be more accurate for specific systems than any other, but no generalised or widely agreed formula exists [62, 69, 121]. This is due to the same reasons that there are many different formulae for drag coefficient/Reynolds number relationships.

Most proposals are based on one of two separate foundations – the Ergun equation [99, 149, 200, 235, 240, 249] or the Carman-Kozeny equation [49, 121]. The Ergun equation has been studied extensively but its validity starts to be questioned at low Reynolds numbers and so is not reviewed here [35]. In contrast the Carman-Kozeny Equation tends only to be valid during laminar flow and so cannot be used at high Reynolds numbers [99]. As the bioartificial liver system is fluidised at low Reynolds number, the Carman-Kozeny Equation will be used as a basis for our model. The Carman-Kozeny equation was developed through experimental measurements of flow through small particle beds such as sand at low rates of velocity, where the porosity of systems was high. Porosity was found to have a major impact experimentally by Carman. This is a similar regime to the BAL fluidised bed system, another reason for choosing it to examine here, as well as it being studied with success since the 1930s [49].

For the case of flow around spherical particles with low Reynolds numbers, a formula can be obtained from the Carman-Kozeny equations to determine  $U_{mf}$  [163]:

$$U_{mf} = 0.0055 \left( \frac{\varepsilon_{mf}^3}{1 - \varepsilon_{mf}} \right) \frac{d^2(\rho_s - \rho_l)g}{\mu}$$

(50)

Where  $\varepsilon$  is the voidage of the system,  $d$  is the diameter of the spherical particles,  $g$  is acceleration due to gravity,  $\mu$  is the viscosity of the liquid,  $\rho_s$  is the density of the particles, and  $\rho_l$  is the density of the liquid. Many other equations have been proposed [416], based on a wide range of starting points.

### 12.5.7. Maximum Fluidisation Velocity

As discussed in section 12.5.5, when a liquid starts to pass through a packed bed of particles, it follows an erratic path through gaps in the bed and exerts an upward pressure on the bed particles. At  $U_m$ , the upward pressure exerted by the liquid equals the particles apparent weight, here the bed will start to expand and particles re-orientate themselves to present the smallest surface area to the liquid [346]. A further increase in flow rate results in a further linear increase in bed height, until the particles become fully fluidised and spatially unrestricted in the

fluidiser at flow rates greater than the maximum fluidisation rate (equal to the free fall speed of the particles).

Using Equation ( 47 ), force exerted by a falling sphere (  $F_D = 6\pi\mu rv$  ) [5, 51] where  $F_D$  is the drag on the sphere, and  $r$  is the particle's radius, that apparent weight of a particle in a fluid can be related to  $F_D$  using 1<sup>st</sup> principles of buoyancy and weight:

$$W = mg = \frac{4}{3}\pi r^3 \rho' g$$

( 51 )

Where  $\rho'$  is the relative density of the particle (particle density - fluid density).

As the particle falls it will accelerate under gravity until the drag force equals the apparent weight, at the terminal or settling velocity. Equations ( 47 ) and ( 51 ) can be easily solved to show:

$$v_t = \frac{2}{9\mu} r^2 \rho' g$$

( 52 )

This method only considers a sphere falling in an infinite medium, and neglects interactions between other particles and the wall of the chamber, so will not be completely accurate. In the bioartificial liver, the relative density is around 40kg/m<sup>3</sup> (bead density falls with temperature, but is still to be determined experimentally), giving a settling velocity of 0.5cm/sec.

Foscolo has used a slightly different method still based on stokes flow and found for laminar flow that voidage and drag can be related through [122]:

$$F_D = 3\pi\mu dv \left( \frac{4(1-\varepsilon)}{\varepsilon^3} + 1 \right)$$

( 53 )

Equation 53 takes account of the fact that the drag may be higher at low voidages as fluid will continually change direction and pass over particles as it passes through a system – fluid flow will not be in a straight line. As can be seen as the voidage tends to 1 the term will simplify to the Stokes relation. When the linear flow rate reaches this level, the bed will become fully fluidised, and any further increase in fluid flow will cause particles to be removed from the system.

### 12.5.8. Bed Expansion and Voidage

Between the minimum and maximum fluidisation levels, the bed will expand based on the extensively studied Richardson-Zaki equation or an adaptation of it [114, 122, 142, 161, 163, 178, 200, 247, 344, 350, 455], which relates the fluid velocity, the terminal velocity of the particle, and the voidage (empty space) of the bed:

$$\frac{v_l}{v_t} = \varepsilon^n$$

(54)

Where  $v_l$  is the liquid velocity. While other models exist [134], Richardson and Zaki's is by far the most common in solid-liquid fluidisation.

The voidage of a layer of packed particles is a measure of how much empty space exists between the solid components. This depends on the topography of the particles through the shape or sphericity factor, which also takes into account the variation of sizes in the bed and the pattern of particle packing - a bed of equally sized cubes stacked one on top of another will have a voidage of zero while if the cubes are imperfectly stacked, such as some having been stacked diagonally, the voidage will change completely. Clearly spherical particles will always have some space between them.

A variation in size of the particles will also have an effect on voidage – small particles tend to fill in spaces between large particles where large size variations exist.

As fluidisation takes hold and the particles move apart from each other, the voidage must decrease. This change is easily measureable by the increase in bed height and is used for an insight to the new fluid-flow regime in the system. The bed height has been observed to increase linearly with increased velocity beyond  $U_{mf}$  [235].

Determining the exponent  $n$  in the Richardson-Zaki equation, and combining it with the minimum fluidisation velocity, the terminal velocity, and the initial voidage should give a complete description of the FB system.

Richardson and Zaki determined experimentally that  $n$  was independent of  $Re$  for  $Re < 0.2$ , instead being a function solely of  $d/D$ , that is the individual particle diameter to the diameter of the fluidiser:

$$n = 4.65 + 19.5 \times \frac{d}{D}$$

(55)

And dependant only on Reynolds number for  $0.2 < Re < 500$ , assuming that  $d/D \ll 1$ :

$$n = 4.35Re^{-0.03} \text{ For } 0.2 < Re < 1$$

$$n = 4.45Re^{-0.1} \text{ For } 1 < Re < 500$$

(56)

At  $Re > 500$   $n$  is independent of both  $Re$  and  $d/D$ , found through experimental designs.

In fluidisers which are narrow compared to the width of the particles, the terminal velocity of the particles will be lower than if the particles were in an infinite fluid. Richardson and Zaki proposed a correction where  $U_{ti}$ , the terminal velocity of a particle in an infinite medium, could be related to  $U_t$ , the free fall velocity in the fluidiser, when  $d/D \ll 1$  [163].

$$\log\left(\frac{U_{ti}}{U_t}\right) = \frac{d}{D}$$

(57)

Updated values for  $n$  have been widely suggested [200, 247, 344, 455], through many do not differ hugely from those initially proposed. Rowe [350] formulated a model for all values of Reynolds numbers, when  $d/D \ll 1$ , which matches experimental observations:

$$n = \frac{2(2.35 + 0.175Re_t^{0.75})}{(1 + 0.175Re_t^{0.75})}$$

(58)

Equation 55 is most useful for the BAL due to its simplicity and its validity in the low Reynolds number regime of the system.

### 12.5.9. Particle distribution

Individual particles in a fluidised bed will move in a largely random path [161, 247]. Many methods have been used to try and follow particle paths in a fluidiser; either by tagging individual particles or by constructing stochastic models.

One experimental model involves introducing radioactive particles into the system that have the same size, weight, and shape as the fluidised particles. These radionuclides should therefore have the same flow characteristics as the fluidised elements. Detectors can be placed around the fluidiser and detect these particles, giving an overview of flow characteristics [247]. While

reliable and accurate, this method requires expensive and sophisticated equipment, and a very careful choice of radioactive particle must be made.

Particle distribution is dependent on the porosity of the system. At low porosities, such as with a fluid velocity very close to  $U_{mf}$ , particles are restricted in their movement by their neighbours. As porosity increases ( $> \sim 0.55$ ), so too does the movement of individual particles. Particles can clump together and voids become apparent in the system [141, 215]. Particles with larger size variations show larger fluctuations spatially with solid concentration [227].

Noticeable spatial and wall effects may also become apparent. Particles nearer the centre of the fluidiser will move more quickly, usually upwards. Nearer the walls particles tend to cluster more readily (though the literature is not conclusive on this point) – with an oscillatory distribution extending inwards. Particles are more likely to descend near the wall, sometimes with a speed greater than  $U_t$ , indicative of local regions of back-flow [141, 215]. This can result in a large circulation, rising through the centre and descending in the edges [247].

#### **12.5.10. Usefulness of Theory to Practice**

The bioartificial liver will consist of a volume of around 2 litres of ELS. Once fluidised, this volume will increase up to 2-fold. It is important to determine this level of increase in the volume so that the bio-reactor is large enough to cope, and also so that liquid pumping rates can be established [101, 363].

Although a fluidised bed is theoretically the ideal state for the hepatocytes to grow in, there are some other factors that must be taken into account before the reactor is optimised for cell growth. One such factor is localised flow rate – how much circulation is present in the system and how this impacts the ELS.

The ELS can be leached and strained over time if they are in a fast flowing current. It may be the case that 10+ days of growth at even the minimum fluidisation velocity is could be damaging if these effects are taken into account, especially when combined with the stresses of cryopreservation which the system also experiences.

With this in mind it is important to understand as fully as possible the physical and biological impact of fluidising behaviour on the ELS. It is clear that in order to have a full picture a combination of experimental measurements and theoretical analysis must be undertaken.

## **12.6. Materials and Methods**

Most fundamental parameters of the BAL system must be determined experimentally before the values can be inserted into any model. The viscosity of plasma and its dependence on temperature is essential for accurate modelling, both inside the bioreactor and in a scale-down physical model. So too does the density of the ELS. It will be important to visually inspect flow regimes inside the fluidiser, and to determine any effects that non-spherical ELS and variations in ELS size has on fluidisation.

### **12.6.1. The Bioartificial Liver Vessel**

#### **Materials**

45 cm glass cylindrical chamber

Culture Medium

ELS

#### **Method**

The BAL vessel chamber itself consists of a glass cylinder of diameter 15cm and an effective height of 30cm (taking into account area of lid, area between the flow separator etc.). Liquid is introduced at the base at a flow rate of around 330ml/min. Into this chamber approximately 2 litres of ELS are added, which are then fluidised to the desired level (usually 1.67x during culture, 2x during the treatment phase).

The chamber interior does not consist of only liquid and ELS as is assumed in the models. There were also tubing and probes present to optimise cell growth. These models assume that these had minimal effect on fluidisation.

The BAL chamber is used for culturing the ELS to approximately  $7 \times 10^{10}$  cells, and the full procedure has been detailed by Erro et al. [101]. While this chamber was used for the culture of a full sized-BAL, it was not possible to use for experiments in this chapter – a scale down process was used instead.

## 12.6.2. Mini-columns



*Figure 77 - The mini-column set up with 6 circuits in series (not filled with ELS here). This set up allowed many replicates to be carried out in an identical and easily manipulatable manner. Many columns were set up and filled with ELS and culture medium as is done in the full scale bioreactor. A single multi-channel pump was used to ensure that equal flow existed between all columns. This was used to mimic conditions in the bioreactor in an economical and less labour intensive scale down process.*

### **Materials**

Watson Marlow multi-channel pump (Watson-Marlow, Falmouth, England, UK)

Silicone Tubing (Altec, Birmingham, AL, USA)

3cm Glass Columns (manufactured for project)

ELS

Culture Medium

### **Method**

As the bioartificial chamber was not a perfect fluidiser, and due to practical and economic considerations, experiments were done with especially designed fluidisers.

These were 3cm diameter glass columns. There was a double inlet port, followed by a sintered glass distributor – this was manufactured especially for the project. There was a maximum height of 15 cm above this distributor, before the flow exited the column back to the medium reservoir.

Up to 6 of these minicolumns could be run concurrently, with the use of a Watson-Marlow multi-channel pump.

These minicolumns are filled with the desired ELS volume, and the height of bed expansion measured with use of a ruler, allowing for effects of flow rates, ELS volume, viscosity, etc. all to be measured separately. The set-up can be seen in figures Figure 77Figure 78.

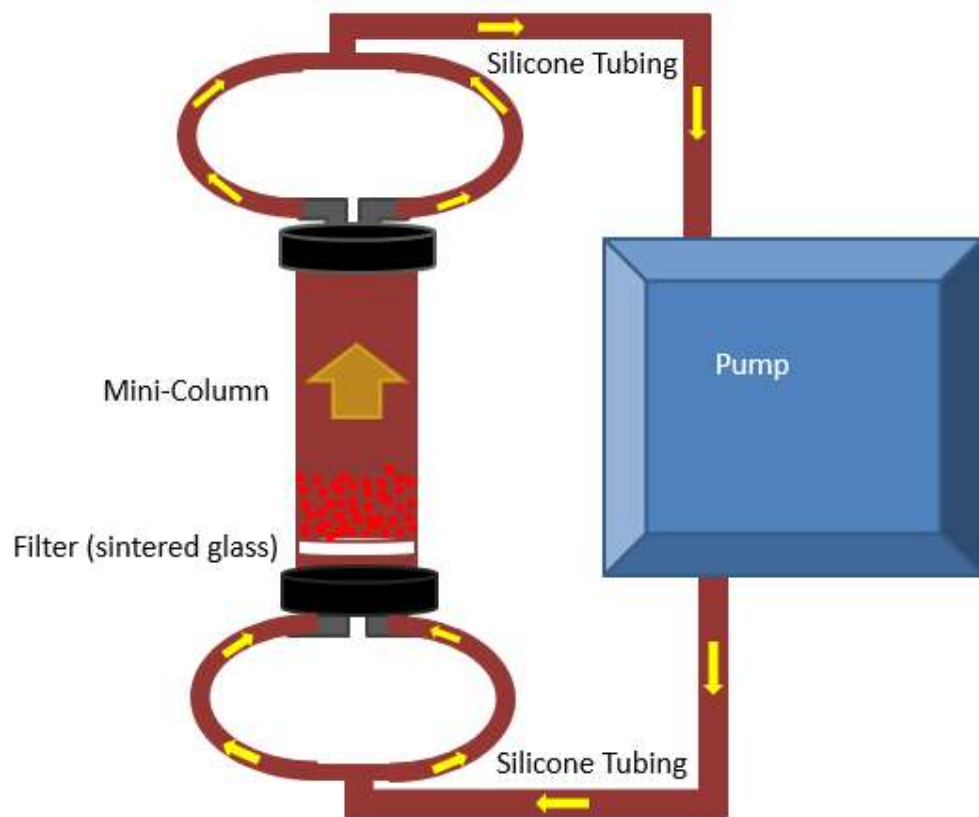


Figure 78 - The mini-column set-up. Medium is pumped into minicolumns at selected flow rates. Up to 6 mini-columns can be run concurrently, through the use of a Watson-Marlow multi-channel pump. A sintered glass filter was used to linearise the flow, and two equal inlets and outlet ports were employed per mini-column in order to further homogenise the medium flow.

### 12.6.3. Viscosity

Due to LG budget constraints, it was not possible to acquire a viscometer and so the viscosity of the system was not studied, or to very accurately determine the density of ELS, taking developing an accurate theoretical model out of the remit of this chapter, a situation that I was 'less than pleased' with. The chapter focuses on direct experimental measurements to form an understanding of the system. It seems that the most accurate models and most widely accepted are still those developed by Stokes in 1851 and Richardson-Zaki 1952 [346, 386].

## 12.7. Results

### 12.7.1. Construction and Operation of the System.



*Figure 79 - One minicolumn during use of a fluidisation experiment. The alginate beads (cell free ELS) can be seen between the sintered glass flow distributor and the 2.7cm mark. This is a close up of the system shown in figures Figure 77Figure 78 and shows what was monitored during experiments. The medium used in the image contains fetal calf serum in place of human plasma (both 10% v/v) to increase contrast.*

In order to set-up the circuit, end caps were added with a double inlet-outlet, which would help to distribute the flow more evenly past the distributor. This was found to work quite effectively, and while there is always room for improvement, it was effective enough to study the fluidisation of ELS in scale down manner.

An incision was made in the top cap, with some tubing attached. This was secured in place and sealed securely using silicone glue. This allowed for sterile sampling of the system during use, increasing efficiency over having to remove the tubing from the stem to a sterile hood for sampling.

The system was autoclaved, and sterile alginate beads (ELS without cells) added to the column. The system was run at a linear flow rate for a total of 14 days in a 37°C incubator. Medium samples were taken every 2-3, and no infections were found through the culture period, indicating that the cells could be cultured sterily in the system. Some channelling was apparent on days 1 and 2, though this was resolved by giving the tube a sharp knock, and no further

channelling past day 2 was noted.

### 12.7.2. Effect of Volume of Encapsulated Liver Spheroids

Up to 6 mini-columns could be run at any one time. A multi-channel Watson Marlow pump could drive fluid around all circuits concurrently.

With a larger volume of ELS, it was expected that a larger pump rate would be required to maintain a consistent flow rate, as the frictional forces were greater. Data was collected and a graph was drawn of flow rate versus pump rate for different volumes of ELS (Figure 80).

## Rotation Rate Versus Linear Flow Rate

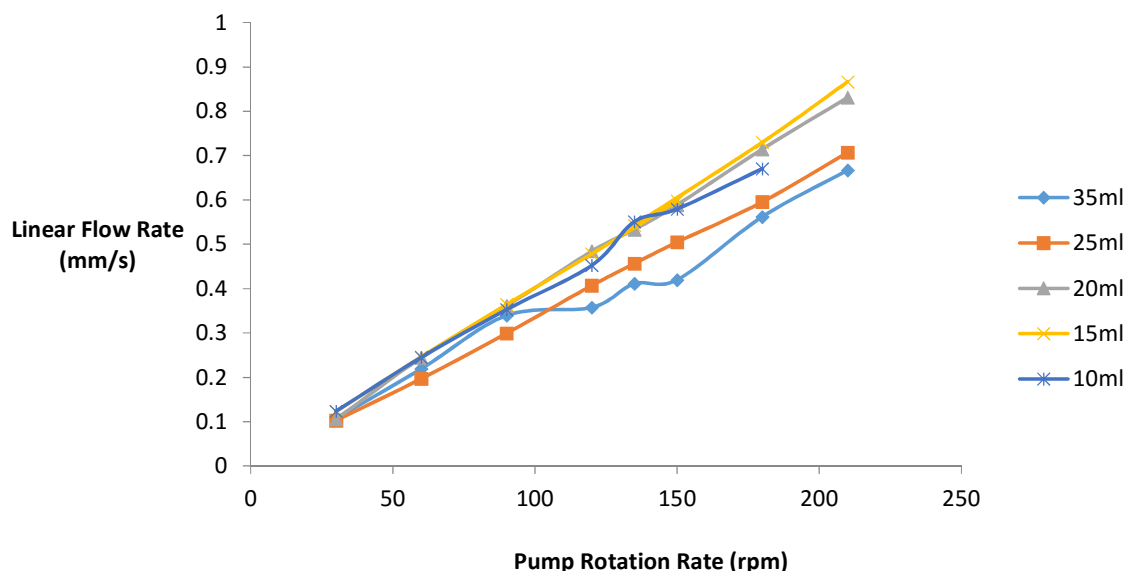


Figure 80 - Flow rate versus pump rotation rate for different volumes of ELS. The circuits are identical in all other respects. Minicolumns were set-up in the manner described above. With the figure showing the average linear flow rates recorded with different flow rates and ELS volume. Data is average of  $n=6$  experiments.

Figure 80 shows the expected tendency for slower linear flow rates with greater volumes of ELS, though encouragingly the effect is very mild. Above 100 rpm the largest volume, the largest 35ml test condition linear flow rate is significantly ( $P<0.01$ ) lower than for all other volumes. For the second largest volume, 25ml, the linear flow rate is significantly ( $P<0.01$ ) slower than all other sets except 35ml. No difference was observed between volumes 10-20ml. It is also apparent that the increases in flow rate are largely linear with increase in pump rotation rates, establishing the robustness of the system.

### 12.7.3. Flow Rates required for Fluidisation

None of the formulae used to measure minimum fluidisation velocity, bed expansion, or maximum fluidisation velocity contain a term dependant on bed height – i.e. Fluidisation should be independent of volume of ELS. To fully test the system and to ensure that there were no anomalous factors affecting the mini-column circuit, several fluidisation experiments were carried out in the mini-columns with different volumes of ELS. The bed expansion was noted at different flow rates, and these plotted on a graph.

## Bed Expansion in the mini-columns with Different ELS Volume

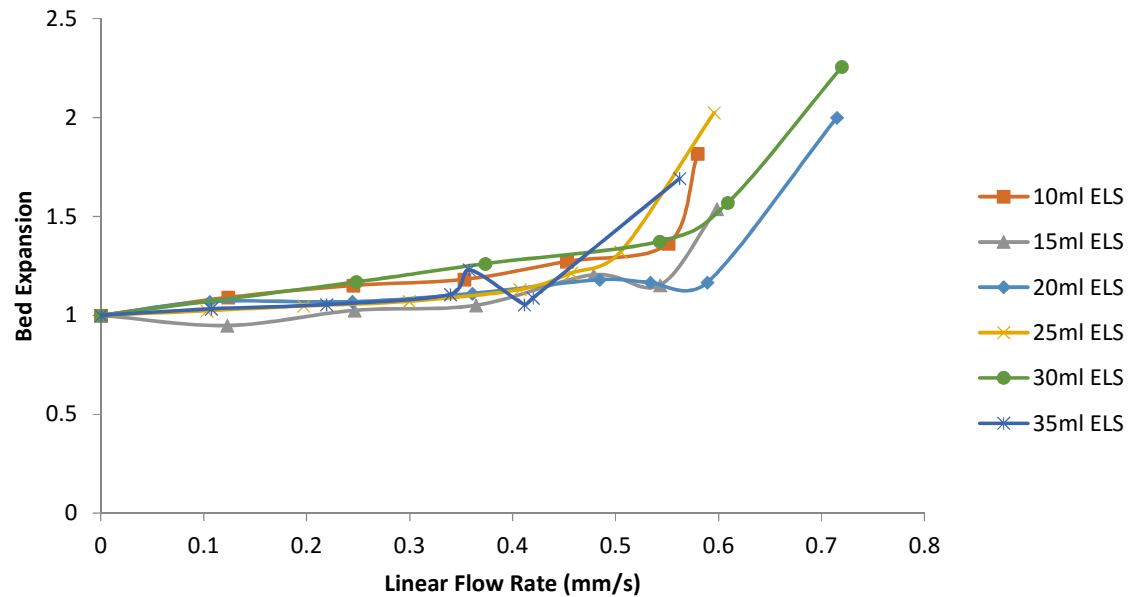


Figure 81 – Level of bed expansion compared to linear flow rate of different volumes of ELS in identical minicolumns. Here ELS without cell beads were used, and FCS culture medium. Fluidisation becomes prominent in all samples at around 0.5mm/sec – visible by the increase in bed expansion in the figure. Data is average of n=6.

As can be seen from Figure 81, fluidisation in our system was indeed independent of ELS volume. Ideal fluidisation for cell growth (around 1.5-2 x expansion) occurs between 0.5 and 0.7 mm/sec. It is clear that the crucial linear flow rates fall over a very tight band, and so sensitive equipment is required to optimise the flow rate in small volumes.

As the data from Figure 81 was collected from FCS medium, which is less viscous than FFP medium, the linear flow rates in the BAL system which used FFP medium should be lower for the same level of fluidisation.

### 12.8. Discussion, Conclusions, and Future Work

Fluidisation has been studied widely in industry, and its understanding is crucial to optimize the BAL device. In order for this optimization to happen, the key parameters affecting the process must be identified in the BAL system. These have found to be bead size and density, along with density and viscosity of the culture medium. This ELS system is particularly sensitive to changes in these parameters, as the minimum fluidization velocity was found to be very close to the linear flow velocity that would result in total fluidization. This is in agreement with other groups that use fluidized bed bioreactors for encapsulated systems where the size of alginate beds has to be very closely controlled.

It was also determined that no general models exist for fluidization of encapsulated bioreactors exist, necessitating this study and future work.

A major drawback of a fluidized bed bioreactor is the lack of oxygen zonation seen in vivo and other bioreactor systems [8, 73, 139, 199]. A second drawback is the change in culture conditions between the culture and treatment phase. Culture medium is relatively fluid and light, while the 100% human plasma used during the treatment phase is much more dense and viscous – this requires the bioreactor to be very tall to prevent ELS escaping the culture chamber. A tall chamber requires the BAL circuit to have a volume of up to 10 liters. As the average human has only 2-3 litres of blood plasma fraction, the system will require an excessive number of blood transfusions to operate. Potential solutions include having a sink whereby ELS escaping from the system are re-circulated – this is done in many industrial applications. Alternatively the ELS could be made denser to reduce the risk of removal from the system, and a coating could be applied to the alginate to make them more robust as has been done in other systems.

This chapter has shown that mini-columns can provide an accurate method of simulating fluidization in the BAL, which can be used in future to calibrate any mathematical model of fluid flow. This is on a much smaller and cost-effective scale than the full scale BAL.

Moving forward, it will be important to test the system with ELS containing cells, which will give an accurate understanding of the system as the cell (and so mass) density of the ELS increases during the culture period. If a detailed mathematical system is required, determining parameters such as viscosity of different combinations of medium and accurately determining the density of the ELS will be essential, and this is how the mathematical section here should be brought forward. Channeling could be prevented in the system by adding spheres or particles below the flow distributor, making the flow more even before it reaches the ELS.

Different designs of BAL chamber could be considered as part of future work. Wall effects have a major impact on fluidisation and so most systems carry out fluidisation in a chamber free from impediment. The BAL chamber contains layers of silicone tubing (used for oxygen supply) in the main chamber [101]. ELS often get caught between these tubes and they will negatively impact on smooth fluidisation. The chamber also contains various pH and temperature probes. Designing a new way to take measurements and deliver oxygen to the ELS that does not involve physical additions to the BAL chamber would improve fluidisation outcome. However such changes may be impractical and have other, as yet unforeseen, consequences.

# 13. Oxygenation of the Bioartificial Liver Device (BAL) as a Diagnostic Tool.

## 13.1. Introduction

### 13.1.1. Chapter Outline

The BAL system studied in this thesis is cultured using medium containing 10% human blood plasma [101]. This boosts growth rates and cell functions but comes with a drawback – proteins produced by a healthy human liver and ELS cannot be detected as the levels are too low to pick up over those in the human plasma [101]. It is therefore desirable to find new additional tools to determine the impact cryopreservation has on ELS. One of these is cell oxygen consumption rates [369]. HepG2 cells consume oxygen under normal conditions and other cell types have linked oxygen consumption to cell viability and cell density [198]. Oxygen measurements are taken as standard during the culture of a BAL, and so this chapter focuses on relating these measurements to cell oxygen consumption. In addition measuring oxygen consumption may be useful to optimise the culture phase of the system [369].

This chapter is arranged into three sections.

1. Developing a model of the FBB culture phase of the BAL from 1<sup>st</sup> principles.
2. Calculation of the oxygenation of the FBB culture phase of the BAL system from existing data.
3. Development of an oxygen diagnostic tool and application to post-thaw culture.

### 13.1.2. Oxygenation

Oxygen consumption rates of cell cultures are used in many applications to determine the system's health [198, 293, 369]. It has many direct applications in the culturing and cryopreservation of BAL devices as a tool to measure how quickly the biomass recovers post-thaw, and in addition to monitor the efficiency of the cell culturing conditions and cell activity [369]. While cell activity can in some situation be measured accurately by protein analysis (ELISA), cell protein production tends to fall while rapid cell division is taking place, however the oxygen consumption is less affected.

Several techniques are used to measure oxygen consumption rates of BAL devices or cell spheroids in the literature [127, 198, 293, 369, 435], though the one developed here is specific to our system which not only models oxygen consumption, it can be used to as a diagnostic tool to determine problems during the FBB culture phase of the ELS, identifying problems more quickly than presently possible and so allowing rapid remedial action, potentially saving BALs from failing, and more rapidly identifying and solving non-lethal problems. Together these tools will make the BAL device both more economic and more reliable to manufacture.

### **13.1.3. Overview**

The Liver Group's BAL is cultured in a fluidised bed bioreactor for a total of 12 days during its culture. In this time, the biomass increases significantly and the oxygen requirement of the cells rises in tandem [101].

The oxygen already dissolved in the culture medium naturally is not sufficient to maintain the liver cells at later time points, as culture medium is typically 50 times less efficient at oxygen transport than blood [435], and so additional oxygen must be provided to the system. This is done in the form of silicone tubing inside the BAL. Through this silicone, which is porous to oxygen, 100 % O<sub>2</sub> gas is passed.

Theoretical oxygen increases in the absence of a biomass have been calculated. The oxygen flow rates and pressured have also been measured, as has the increase in oxygen concentration between the base and top of the BAL chamber, and this related to the theoretical values.

In this chapter this theoretical oxygen perfusion through the tubing and into the biomass is related successfully to some experimental measurements. This is then applied to large scale culture experiments, and hence oxygen consumption of the biomass is calculated.

The modelling has two primary focuses – firstly the simple oxygenation of the system where there is no external oxygen flow through the silicone tubing so oxygen is provided through only what is dissolved in culture medium. The second focus is where oxygen is provided both through the medium and externally through the silicone tubing. Each of these represent a different regime.

#### 13.1.4. Design of the BAL Culture Chamber

The bioartificial liver device (BAL) consists of a cylindrical glass chamber, with an inner diameter of 15cm, a schematic is shown in Figure 82. Through 30cm of the chamber height, silicone tubing is spiralled around the inner wall of the BAL chamber. During culture and operation of the BAL, pure oxygen is passed through this tubing in order to oxygenate the culture medium and so supply oxygen to the encapsulated liver spheroids (ELS) component of the BAL while culture medium is circulated throughout the system, this does not contain sufficient oxygen for the biomass without additional support.

The silicone tubing is supplied by Altec, and has a permeability to oxygen of  $170 \text{ cm}^3\text{mm}/\text{hm}^2\rho$  (as stated by Altec).

The layout of the silicone tubing gives rise to two distinct sections. As the silicone enters the BAL, it splits into two. The first area passes around the inner side of the exterior wall of the BAL chamber, while the second length forms an inner coil, with radius of 7cm largely supporting itself. The exact proportions of gas passing through these two coils is beyond the scope of this study.

There are 59 silicone coils on the inner wall of the chamber and 49 coils in the central silicone spiral, presenting a total length of approximately 38.58m. The silicone tubing has a bore of 2.5mm, and wall thickness of 0.5 mm. The oxygen content of the medium can be measured at the entry and exit of the BAL chamber, and the gas pressure in the silicone tubing can be recorded at the start and end of the oxygenation area. Figure 82 displays a diagrammatic description of the experimental set-up.

#### 13.1.5. Converting % Measurements to Molar Consumption

While it is difficult to find the oxygen solubility in human plasma and culture medium precisely, I have approximated a value of 5.2ml/litre. This has been selected by comparing the values for fresh and salt water between 35°C and 40°C (in air with a 21% oxygenation), and looking at previous work in the LG. A higher estimate (around 10%) is chosen due so as to remain consistent with previous work and to take account of mixing in the bioreactor, and residual haemoglobin that may have entered the blood plasma fraction used during culture [299, 436].

Considering that the molar volume of oxygen is 22.414 litres [458], a 1% change in the oxygen level would represent a  $1.1047 \times 10^{-5}$  M/L change in the oxygen levels. This is 0.2476 ml O<sub>2</sub> per litre of culture medium.

## 13.2. Materials and Methods

### 13.2.1. Measuring Oxygen Pressure in Silicone Tubing

#### Materials

The BAL Chamber

Culture Medium

Oxygenator

ADI Instruments Control Unit and Software (ADI Instruments, Oxford, England, UK)

Pressure Transducers (LogiCal, Smiths Medical, Ashford, England, UK)

#### Methods

The system is set-up as in Figure 82, with all ELS removed so the BAL contains only culture medium. The oxygenator is activated and the gas flow rate varied. For each of these variations the pressure at the start and end of the silicone tubing is measured. At the end of the BAL chamber, oxygen is vented to the environment.

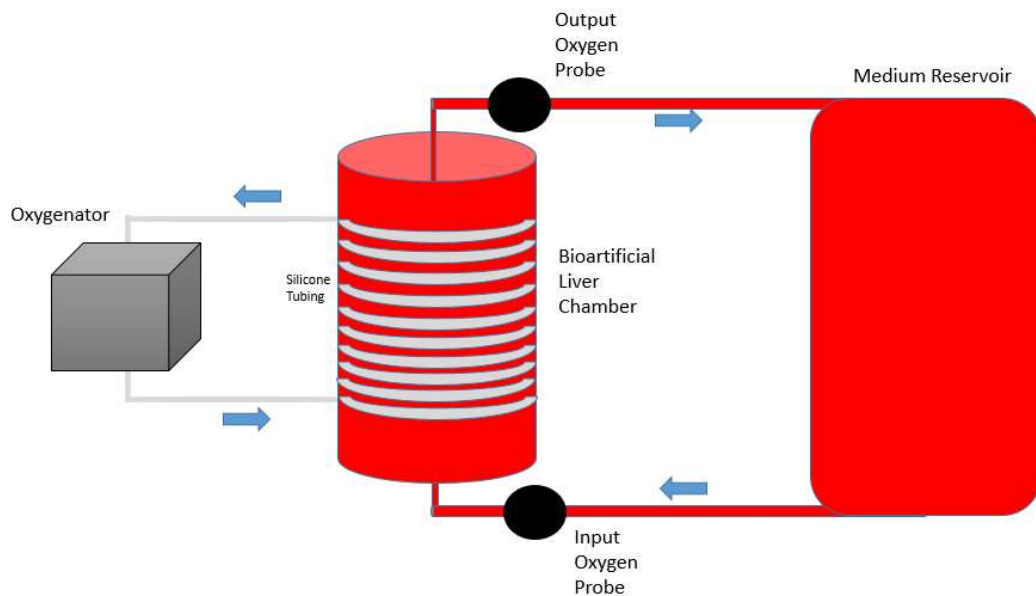


Figure 82 - A Schematic of the BAL device during oxygenation tests.. The culture medium and oxygenation are run on separate circuits. The inner coil of silicone tubing is not visible here. ELS would normally sit halfway-up the BAL chamber during culture, with oxygen pressure varied depending on cellular requirements.

Filters can be added to the silicone tubing outlet to increase the pressure in the tubing. For each additional filter, the experiment was repeated. These were then plotted on a graph.

### **13.2.1. Measuring Oxygen Levels in the BAL Chamber without ELS**

#### **Materials**

Oxygen probes

Watson-Marlow pump (Watson-Marlow, Falmouth, England, UK)

BAL chamber set up as per Figure 82

External hydrophobic filters (Sigma, Gillingham, England, UK)

#### **Methods**

At the end of a culture period, all the cell beads were removed from the culture chamber but the culture medium (with FFP (human blood plasma)) remained. The input medium oxygen level was set to 21% O<sub>2</sub>, chosen as it would be consistent with atmospheric pressure and so no net change in oxygen would occur between the medium reservoir and the culture chamber.

The oxygen flow rate in the silicone tubing was set various defined set-points to monitor the system. The system was left to equilibrate and reach a steady state at each set-point, with the medium temperature, the oxygen levels at the entrance and exit of the chamber (before and after the silicone tubing), and the pressure in the silicone tubing recorded.

This was repeated later at different culture medium flow rates and at the end of different culture periods to add robustness to the system, and also for either 0, 1, or 2 exit filters (at the end of the silicone tubing). These filters increase the pressure in the tubing. This allowed the rate of oxygen transfer from the silicone tubing to the medium over the whole BAL chamber when no cells were present to be established.

## **13.3. Mathematical Approximations**

### **13.3.1. Determining Oxygen Diffusion through the Silicone Tubing**

In many physical applications, heat transfer is analogous to mass transfer, hence why the two fields are often lumped together. This was used to determine an approximate model for oxygen

transfer through the silicone tubing in the BAL system. In our system, oxygen flux through the silicone tubing follows the same laws as heat transfer.

The heat flux from a pipe containing a hot material in steady state is covered by Equation ( 59 ) [1]:

$$q'' = \frac{k\Delta T}{r_o \ln(r_o/r_i)}$$

( 59 )

Where  $q''$  is heat flux ( $W/m^2$ ),  $k$  is the heat transfer coefficient,  $\Delta T$  is the temperature difference, and  $r_o$  &  $r_i$  are the outer and inner diameters of the pipe respectively.

This is directly analogous to our mass transfer system, Equation ( 60 ) where:

$$M'' = \frac{P\Delta\rho}{r_o \ln(r_o/r_i)}$$

( 60 )

Where  $M''$  is the mass flux,  $P$  is the membrane permeability, and  $\Delta\rho$  is the absolute oxygen pressure difference.

To determine total flux per unit time we have to multiply by the area of the tubing =  $2 \times \pi \times r \times L$ , where  $L$  is the length of tubing. This gives Equation ( 61 ).

$$M' = \frac{2\pi \times r_o \times LP\Delta\rho}{r_o \ln(r_o/r_i)}$$

( 61 )

### Dimensional Analysis

The permeability of silicone to oxygen has been given by Altec in unusual units ( $cm^3mm/hm^2\rho$ ), and this must be factored in so that the model is dimensionally correct (the units are legitimate).

The surface area of the silicone is  $\pi 2rL$ .  $r$  and  $L$  in the numerator must be measured in meters to agree with the  $m^2$  term and  $r_o$  in the denominator must similarly be measured in mm.

To take account of the radial transfer of mass through the silicone, I include the dimensionless  $\ln(r_o/r_i)$  term.

### 13.3.2. Determining the Partial Pressures between the Silicone and the Culture Medium

To calculate the pressure differences, calculating the partial pressures of oxygen at the entrance and exit of the system was required. This was done here for the specific case of values measured as per Sections 13.2.1 at a 0.5 L/min flow rate with no external filters, before a general strategy for the general case at low flow rates (<1 litre a minute) is presented. This makes it clearer to follow.

In the (pre-silicone) entrance to the chamber, the partial pressure of oxygen in the culture medium was approximately 0.21 bar, as air at atmospheric pressure is 21%. After the silicone tubing the DO<sub>2</sub> probe recorded a steady state value of 40% O<sub>2</sub>, which equates to 0.4 bar partial pressure. Partial pressure = the fraction of a particular gas at atmospheric pressure.

At the beginning of the silicone tubing, the pressure measured by the pressure transducers was 13mmHg over and above standard atmospheric pressure (1 bar = 750mmHg). As the silicone tubing contained pure oxygen the pressure here was 763mmHg. At the exit, the pressure reading had dropped to 10.5mmHg, giving an exit pressure of 760.5 mmHg.

Considering only 'additional pressure', that is pressure above atmospheric, the pressure in the silicone tubing will likely fall with distance through the tubing asymptotically to standard atmospheric pressure (750mmHg). In the 38.58m of tubing the pressure had fallen 19.25%, which was 0.552% per meter. The pressure (in mmHg) profile in the silicone tubing (over and above standard pressure) was therefore as Equation ( 62 ).

$$p = 13 \times 0.9945^L$$

( 62 )

Where  $L$  is length of silicone tubing in meters from its entry point in the chamber.

To calculate the partial pressures (and so concentration) of oxygen in the chamber, I considered the fact that the oxygen pressure in the chamber will asymptotically approach that in the tubing, will start at 157mmHg (0.21bar), and rises to 300mmHg (0.4bar) in 0.3m of chamber height. The total pressure difference and the entrance and exit of the tubing is therefore 605.5mmHg and 460.5 mmHg respectively.

As the pressure difference in the chamber fell 24% in 0.3m of chamber height, it was determined that it fell at a rate of 60% per metre, as per Equation ( 63 ).

$$\Delta\rho = 605.5 \times 0.4^h$$

( 63 )

Where  $h$  is the height in the chamber above the first coil of silicone tubing below the silicone tubing top. Care must be taken not to confuse  $h$ , the chamber height used for oxygen profiles in the chamber, to  $L$ , the length of tubing, used for the pressure profiles in the silicone tubing.

As oxygen transfer is directly proportional to pressure, I determined an average pressure for the system. This was done by determining the pressure difference between the silicone tubing =  $605.5 \times 0.4^h$ , and integrating this between the top and bottom of the tubing gives an average value of 529mmHg = 0.705 bar as per Equation ( 64 ).

$$\frac{1}{h} \int_0^{0.3} 605.5 \times 0.4^h dh$$

( 64 )

This gave the average pressure difference that was then placed into Equation ( 61 ), which will give an estimated oxygen transfer rate for the specific case examined:

$$M_{transfer} = \frac{170 \times \pi \times 2 \times 0.00175 \times 38.58 \times 0.705}{1.75 \ln(1.75/1.25)}$$

( 65 )

Showing that the rate of oxygen diffusion to the medium is  $86.34\text{cm}^3/\text{h} = 1.44\text{cm}^3/\text{min}$ .

As the system was being fluidised at 330ml/min, each ml of medium was expected to absorb  $4.36 \times 10^{-3} \text{cm}^3$ .

This is  $1.78 \times 10^{-7}$  Moles/ml. As a 1% increase in measured  $\text{O}_2$  is  $1.0476 \times 10^{-8}$  moles. An oxygen increase of 16.5% would be expected. The actual measured increase was 19%. This is a reasonable accuracy.

### ***13.4. Modelling oxygenation of ELS during low external oxygen flow rates during FBB culture – Steps***

The following protocol can be used to determine the oxygen consumption of ELS during FBB culture, when flow rates of <1 litre a minute and no pressure-increasing filters are used.

1. Determine the entry and exit pressures in the silicone tubing at the time in question.
2. Determine the entry and exit % oxygenations in the BAL.
3. Find the pressure differences through integration.
4. Add values into equation ( 65 ).
5. Convert into expected % increase in oxygen.
6. Compare this expected oxygen increase to actual oxygen increase. This 'deficit' will be the amount absorbed by the cells.

### **13.5. Higher Oxygen Flow Rates**

A test was carried out at a higher flow regime - flow rate of 5 litres/min. In this set-up the outlet oxygen measurement increased from 21% to 80%. At this high flow rate, taking into account the fact that oxygen could take two paths through the tubing (either the inner or outer coils), the speed of oxygen flow in the tubes was around 53cm/sec, so completing full loop of the outer tubing in 0.88 seconds. This is a lower estimate, as the path length of one coil is much less in the inner tubing, and as the % splits of flow between the inner and outer tubing is not known and are beyond the scope of this study.

Such a rapid flow rate will result in a higher pressure on the outer wall of the silicone over the inner wall. This extreme turbulence seemed to decrease the efficiency of the silicone tubing to oxygenate the biomass substantially. This could not be measured experimentally. The mathematical model developed above, which held for low flow rates, did not hold for higher flow rates without more detailed experimental analysis. For this reason, explicit correlations were then examined to determine cell oxygenation, without the use of first principle mathematical models.

### **13.6. General System**

#### **13.6.1. Oxygen Pressures at Specific Flow Rates**

In the BAL chamber, it is usually impractical to measure the oxygen pressures in the silicone tubing during the culture phase of the BAL. However, the system should be reproducible and so

the pressures should be equal at every time with the same flow rates. Making a standard curve of these flow rates will allow the pressures to be known from only the flow rates.

As outlined above, the oxygenation apparatus had three settings, each defined by the conditions of the exit valve. One condition had no exit filter, another had one filter, and a third had two filters. These filters are added at later time points to increase the pressure, and so oxygenation, in the system. This data for average pressures in the tubing is plotted in Figure 83.

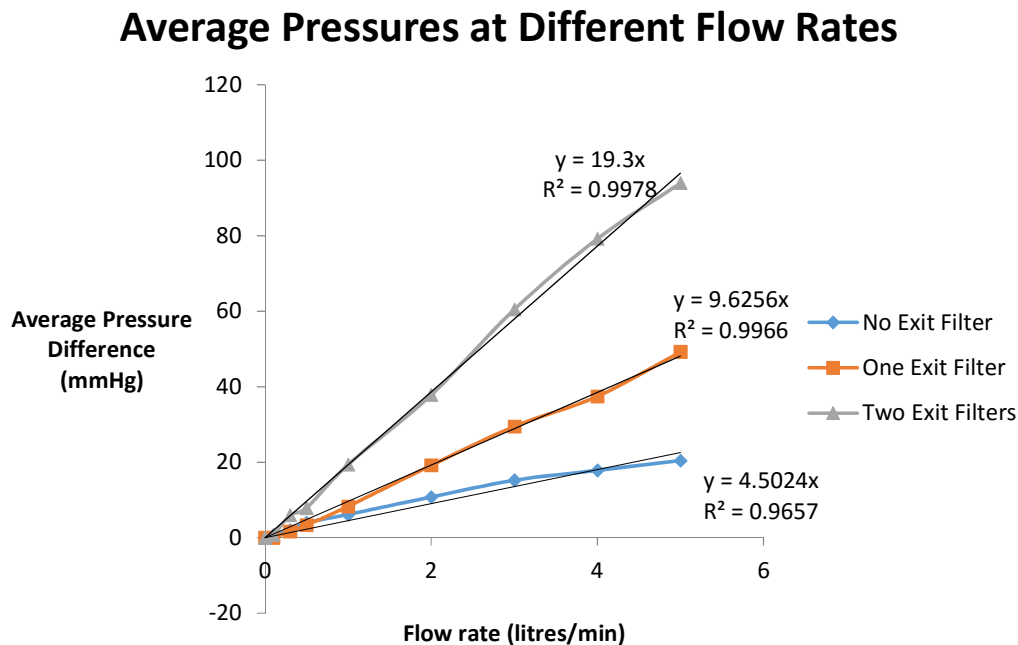


Figure 83 - Standard curves of oxygen pressure related to flow rate at different exit conditions. The straight lines of best fit were added with their respective R values. When no external hydrophilic filters were present, pressure was relatively low for all oxygen flow rates (blue). Add in one (orange) or two (grey) hydrophobic filters significantly increased average pressure difference between the medium and the tubing. Data is average of 5 experimental measurements.

As can be seen from Figure 83, the plots are approximately linear, with low values for  $R^2$ . This allows the average pressure to be found using only the programmed flow rate and exit condition. It has been noted that at flow rates  $> 6L/min$ , these pressures flatten out, and so no further increase is observed. This was also true for the pressures only at the start of the silicone tubing as can be seen in Figure 84.

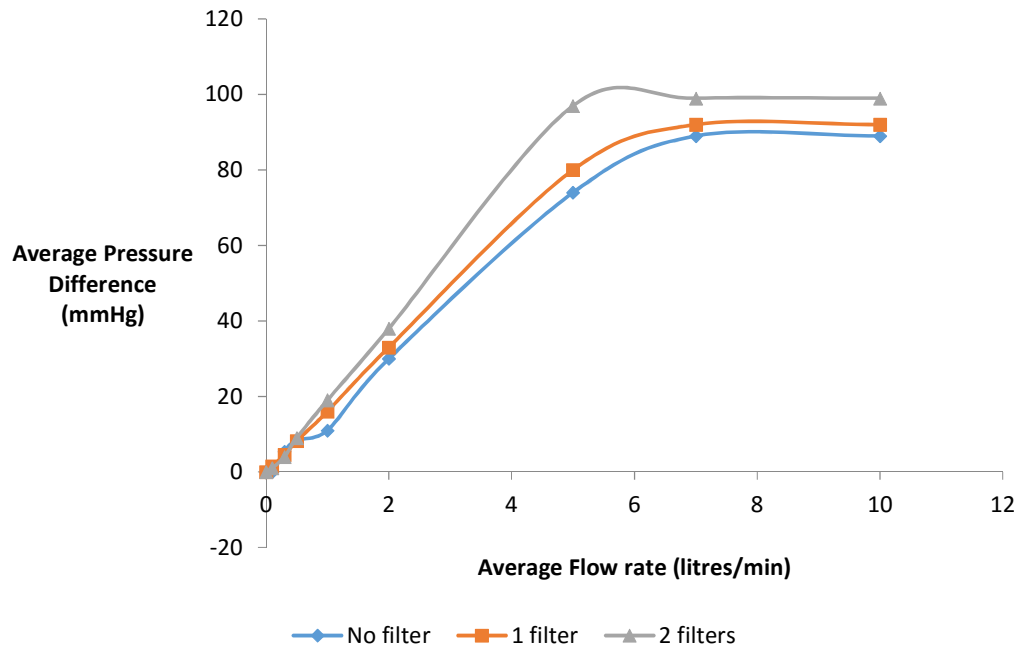


Figure 84 – Average pressure measured in the inlet pressure transducer at different oxygen flow rates. Below 6 litres/min, pressure increases linearly with oxygen flow rates. Above 6 litres/min, the pressure remains constant, indicating that the oxygen generator may have reached maximum capacity. Data is plotted for conditions where no exit hydrophobic filters existed (blue), one filter existed in the system (orange), or two filters added (grey). Data is average on 5 separate experiments.

A good correlation has been found between the (additional) pressure in the silicone tubing, and the total increase in O<sub>2</sub> observed in the absence of cells, shown in Figure 85. The equations of these lines can be used to estimate the level of oxygenation in the BAL system.

This correlation between additional pressure increase at the entrance of the silicone tubing was used as a basis for determining expected oxygen increase in the system.

To determine oxygenation, the average pressure in the silicone tubing was determined by using the appropriate line of best fit in Figure 83. This is then determined to the theoretical increase in oxygen, through the line of best fit in Figure 85. Finally, the amount of oxygen initially at the system entrance and the amount at the exit of the system is recorded. The deficit between what the exit pressure is and what it would be without cells gives oxygenation values.

## Additional Pressure at Entrance vs. Measured Oxygen Increase

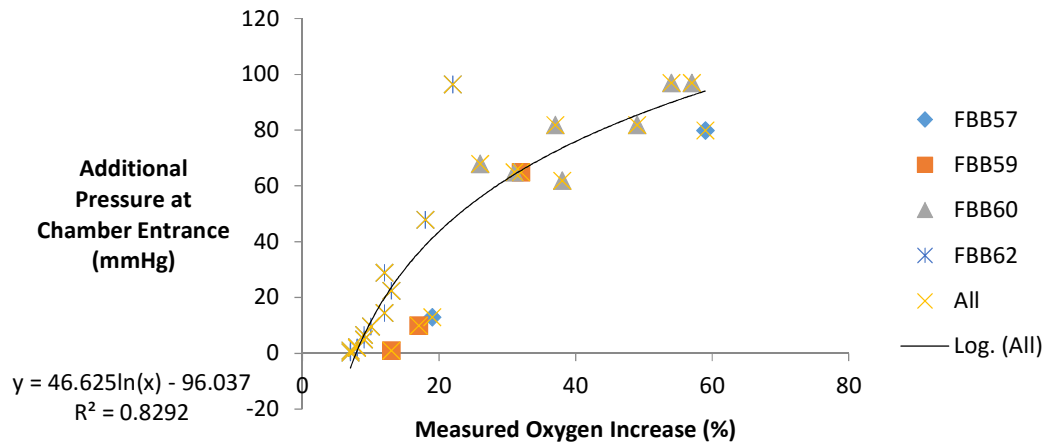


Figure 85 - The additional pressure supplied by the silicone tubing related to the measured increase in oxygen levels for four different experiments, at a variety of pressures measured at the silicone entrance. (FBB is used to define different experiments, number is an internal LG numbering system). A line of best fit is added with an  $R^2$  value of 0.8702, indicative of variation in the system. Good correlation was found between measurements taken between different experiments, indicated by different icons in the figure.

### 13.7. Estimating Oxygen Consumption during the FBB Culture

During the FBB, system parameters such as oxygen flow rates, number of filters, medium flow rates and oxygenation, as well as cell number are either recorded as standard with the Applicon software (Applicon, Delft, the Netherlands), or are measured by default as the process continues. Using these readily available values it should be possible to estimate the oxygen consumption at any time point during the culture of the BAL.

The oxygen consumption has been estimated below explicitly for the specific case of FBB60 (internally numbered experiment where a BAL was cultured in the bioreactor), before the results of a full study are presented.

At the start of the FBB experiment, the recorded difference between the entrance and exit oxygen levels in the medium was 4.2%, and no external oxygenation took place. As 1% oxygenation is equal to  $1.1047 \times 10^5$  M/L, the total oxygen difference was  $4.2 \times 1.1047 \times 10^{-5} = 0.464 \times 10^{-4}$  M/L.

The medium flow rate was 0.42L/min, so the total oxygen consumption at this time point was  $0.42 \times 0.464 \times 10^{-4} = 1.95 \times 10^{-5}$  M/min =  $3.25 \times 10^{-7}$  M/s.

At this time point, the cell density in the ELS was around 2.1 million cells/ml, and there was 2.5 L in total, giving  $5.25 \times 10^9$  cells at that point in the FBB. Dividing this through by the oxygen consumption rate gives  $0.52 \times 10^{-16}$  moles per cell per second. This is 0.052 nM/million cells sec.

At 8 days into the FBB culture, there was external oxygenation - the oxygen flow rate was 10 L/min with two exit filters. No change was made to the oxygen flow rates. This as per section 13.6.1 means there was 115 mmHg of extra pressure at the in the silicone tubing, which as per section 13.6 results in 73% additional oxygenation, on top of the 20% measured in the FBB. The total oxygen deficit is therefore 93% - which must have been consumed by the cells.

$93 \times 1.1047 \times 10^5 \text{ M/L} = 9.7 \times 10^{-4} \text{ M/L}$  as the total oxygen deficit. The total medium flow rate was 0.42 litres per minute, and the cell density was now 16 million cells/ml. The same analysis as above yields an oxygen consumption rate of 0.18 nM/million cell seconds.

This was repeated for all time points, and for several FBBs with the values plotted in Figure 86.

The data in Figure 86 shows the calculated oxygen consumption of the BAL system, for 5 separate experiments. The black line is extrapolated from data previously published by the LG [101]. While this previous data was collected using a different culture chamber, lower total volume, and higher average cell density, there is good agreement between the sets, confirming this work with a previous study. The previous study, while using an FBB did not have an identical culture condition and hence the comparison being made here was between the approximate average values for ELS oxygen consumption, not a time-specific comparison.

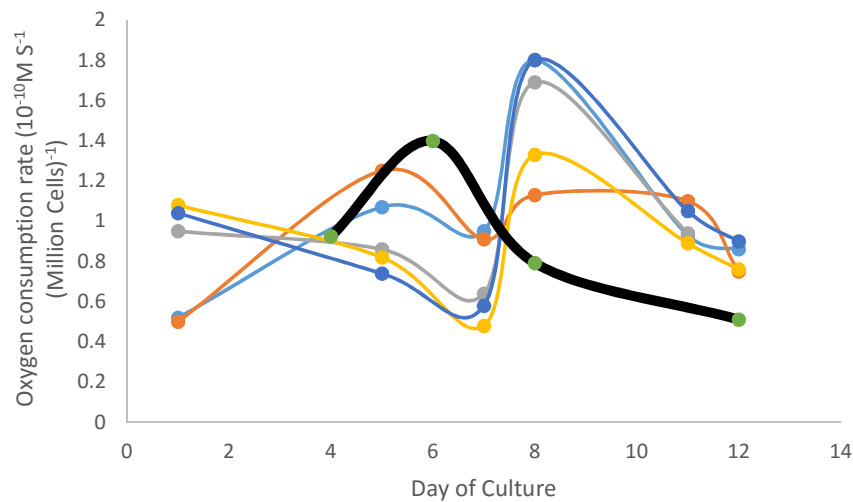


Figure 86 - Measured oxygen consumption rates of the BAL during 5 different experiments, and comparing to LG published data (thick black line). General numbers were found to be similar, however the different pattern is indicative of scaling up culturing from 800ml (black) to 2300ml volume (colours).

Each FBB experiment had a different starting and ending cell density (within set-limits), as well as different total ELS volume and supplied oxygen due to natural variations in the system. Despite this, there is a consistent and significant trend. There was a significant (defined in this chapter as  $P < 0.01$ ) decline in per cell oxygen consumption between days 5 and 7, significant increase between days 7 and 8, and significant decrease between days 8 and 11, and days 11 and 12. Statistics for oxygen consumption rate in this chapter are determined for a binary system (either an increase or a decrease between two points) at each point.

Filters in the oxygen were added between days 7-8 of the culture period, increasing the oxygen pressure in the silicone tubing and so oxygen transfer to medium. The increase in oxygen consumption in this period coincided with an increase in the average cell proliferation rates between days 7 and 8 (data out with remit of this thesis). It may be the case that ELS become starved of oxygen towards day 7 of the culture period, and with the increase of pressures relieves this starvation. It may improve the culture of the system if extra filters were to be added at the start of the culture period [435].

The decline in oxygen consumption after day 8 of the culture period may indicate increased starvation past this point. The oxygen levels by days 11-12 of the culture period have been observed to fall as low as 3% in the culture medium. It seems likely that HepG2 cells cannot metabolise concentrations this low at maximum efficiency, and having a more effective oxygenation system, such as a tubing with a higher oxygen permeability, a larger tubing surface

area, or higher pressures, may improve culture outcomes. It should be noted at this stage that HepG2 cells can operate anaerobically for a time, so this low oxygen concentration would not be expected to lower viability over the short term. The ELS are not static in the FBB system, they experienced large variations from 35% to 3% for several days during the culture period, and there is no reason to believe that this is beneficial for hepatocytes. Even with full oxygenation however, a decline in per cell oxygen consumption would be expected to fall during the culture period, as higher cell densities result in a decline in per-cell oxygenation in many (but not all) systems [71, 319, 435].

### 13.7.1. Problems with the Model

This data approximately agreed with previous oxygen consumption levels published, both in the LG and separate organisations [101, 319, 369, 435], which indicate that oxygen consumption levels around  $10^{-10}\text{M S}^{-1}$  (million cells) $^{-1}$  for monolayer cells. As the ELS system up-regulates cell function, it seems counter-intuitive that the oxygen consumption would be lower in an upregulated system although published work does show that lower per-cell oxygen consumption is common at higher cell densities.

Only existing lab equipment and used reagents could be applied to this work, a situation that I was 'less than pleased' with.

To have a fully characterized model, it is essential to know the oxygen profile within the BAL during FBB culture. In the current model where culture medium was oxygenated without cells was examined, oxygen concentration would necessarily always increase as it passed through the chamber (inlet < outlet), however, this is markedly different to the system with cells to which the model is applied, where the oxygen always declines through the culture chamber (inlet > outlet). Knowing this profile is essential to validate this work. It is probable that in this case the entry pressure is the dominating factor as it is here where the pressure difference is greatest. In a cell system it is lowest at this point. This is likely a major source of error. A second source of error falls within the permeability of the silicone tubing. Altec were unable to quantify the temperature dependence of the permeability, and also effect that other gas and liquid molecules in this system. Future work should consider this factor.

Despite these approximations, the data agrees with previous results, indicating that the error in the approximations made are not substantially deleterious to the model.

## 13.8. Oxygenation as a Diagnostic Tool

### 13.8.1. Experimental Design

To determine if the calculated oxygen consumption rates could be used as a diagnostic tool during the culture of the FBB system, an experiment was set up where 10 consecutive FBBs were monitored between October 2014 and August 2015. The 5 of these that went completely according to plan (Figure 86) were averaged so that the trend of oxygen consumption between the data points was clear. As discussed above, the trend between each consecutive point was significant ( $P > 0.01$ ) after day 5. 3 of the FBB cultures experienced adverse conditions that did not result in the loss of the BAL. These are examined below in Figure 87, Figure 88, and Figure 89.

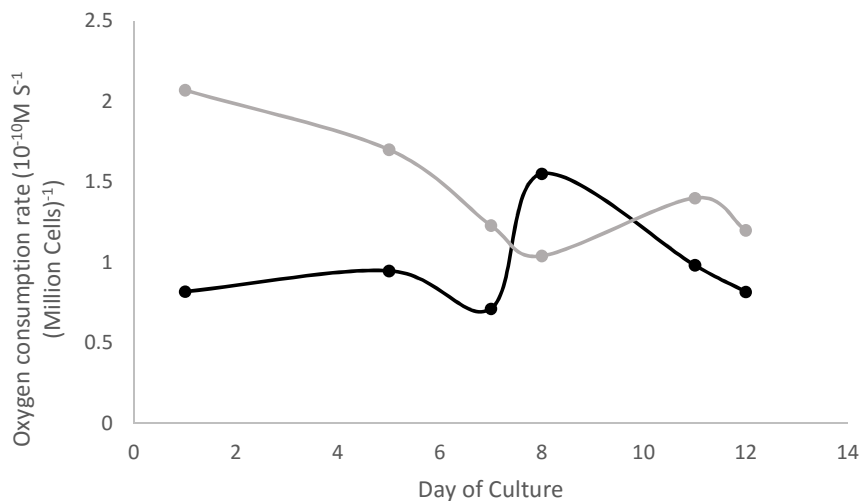


Figure 87 - Comparing the oxygen consumption rates of an FBB experiment where poor cell growth was seen (grey) compared with the average of the 5 gathered FBB data in Figure 86 (black). While similar consumption rates are seen, the pattern of oxygen consumption throughout the culture period is different. Each point represents one data point taken from each of 5 separate experiments.

Figure 87 shows an FBB where poor cell proliferation was observed during the culture cycle, resulting in a final cell density around 2/3 of average. The reason for this poor proliferation was not established, however observing the pattern of oxygen consumption, it can be seen that between days 7 and 8 of culture the oxygen consumption does not increase on a per-cell basis, and it is possible that an event resulting in the slower cell proliferation happened around this time. While cell counts were lower than average by day 8, it was not substantially so. Using this

mechanism would have highlighted a problem earlier than other mechanisms, and therefore more time to identify and solve the problem would have been available.

I note the gross value is not being considered as a diagnostic tool, rather the  $\pm$  of the line differential.

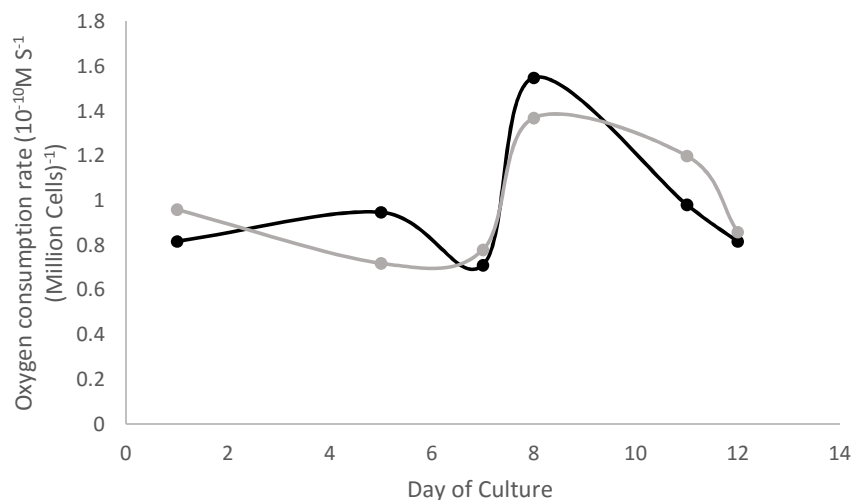


Figure 88 - Comparing the oxygen consumption rates of an FBB experiment where an overheating event occurred (grey) between days 5-7 compared with the average of the 5 gathered FBB data in Figure 86 (black). The overheating event occurred early in the process and can be seen in the graph by the fall in per cell oxygen consumption between days 1 and 5 of culture. The average consumption shown in black is the average of 5 different FBBs at each timepoint, while the grey line represents one FBB experiment where overheating occurred.

Figure 88 shows a separate problem where an FBB experienced a short heat shock between days 5-7 of the culture period, where the medium entering the chamber was heated above 41°C. While this was spotted and resolved quickly as it occurred during working hours, there was an arrest of cell proliferation between days 5-8 of the culture period. The cells recovered after this point, as can be seen by the return of the line differential to normal polarity after day 8. This problem was spotted and resolved quite quickly, however if it had happened over a weekend, for example, it may have been left for many more hours resulting in loss of the BAL associated with the FBB experiment. As oxygen data is recorded by the Applicon culture software by default in the LG set-up, constructing a program to monitor it remotely (even without cell counts), could prevent future FBB experiment failures, making the system more reliable and cost-effective.



Figure 89 - Comparing the oxygen consumption rates of an FBB experiment where the external oxygen tubing started to leak, bubbling oxygen directly into the culture chamber (grey) compared with the average of the 5 gathered FBB data in Figure 86 (black). Unlike the FBBs displayed in Figure 87 and Figure 88, this event did not lead to any noticeable decline in cell proliferation. The average consumption shown in black is the average of 5 different FBBs at each timepoint, while the grey line represents one FBB experiment where leaking of the oxygen tubing occurred. .

Figure 89 examined an FBB during the study where the oxygen tubing started to leak at some point in the culture period. This was not noticed as the culture chamber is opaque when in use, and so continued for most of the culture period. This was not detrimental to the ELS. It can be seen, between days 7-8 of the culture there is a deviation from the trend, indicating a problem. The predicted oxygenation values continued to decline through the remainder of the culture period. The explanation of this trend is likely due to the design of the BAL chamber – there is a gap above the ELS to prevent over-fluidised ELS escaping from the BAL chamber. This gap comes before the oxygen probe measuring the outlet oxygen concentration of the system. As gas bubbles rise, the oxygen may have dissolved in the culture medium downstream from the ELS and upstream from the probe monitor. This would give the impression that the cells consumed less oxygen than they had, and as the cell number increased the per-cell apparent consumption would decline.

While the leaking oxygen did not have an apparent effect on cell proliferation, if the leak that developed happened to be worse than above, the tubing may have failed entirely which would have a serious impact on the culture, and so this diagnostic tool can be used to identify that there is a problem, which can then be fixed before becoming more serious.

To conclude, a diagnostic tool has been established, with our study showing that it correctly identified ( $P < 0.01$ ) the state of the culture system, over a wide range of problems.

### 13.8.1. Oxygen Consumption after Cryopreservation

A primary advantage of this work is the extra information that can be extracted from the system post large volume cryopreservation. The above techniques were applied to the large volume cryopreservation carried out in chapter 10 to determine the impact of cryopreservation on oxygen consumption.

Predicted oxygen values are shown in Figure 90. Here the initial culture is shown, before the cryopreservation takes place on day 12 (indicated by the black line). Day 1 post-thaw (day 13 of total culture time), oxygen consumption was equivalent to that pre-cryopreservation. A nadir of consumption was reached 3 days post-thaw, at  $0.32 \times 10^{-10}$  moles oxygen per million cell seconds, before increasing consumption to  $0.42 \times 10^{-10}$  5 days post thaw (17 days of total culture).

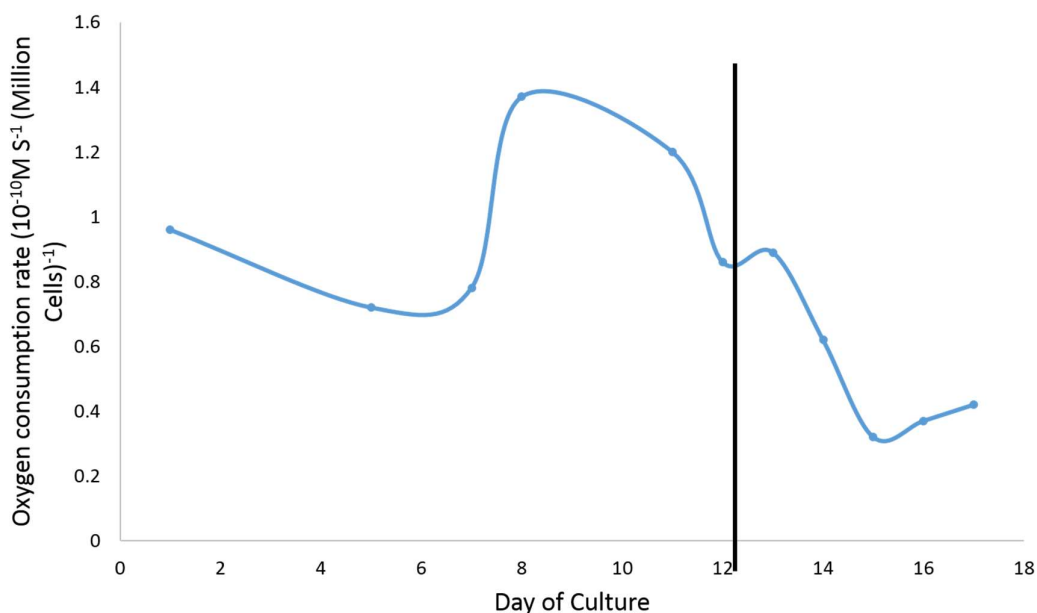


Figure 90 - Oxygen consumption measured during the pre-cryopreservation culture phase of the large volume compared with values post-thaw. The black line indicates the cryopreservation, with day of culture referring to total number of days in FBB culture since encapsulation. The cell count, viability, and other system parameters were discussed in chapter 10. Data is average of 5 measurements taken on one large volume experiment.

Oxygen consumption did not seem substantially affected by the freezing process, with recovery in < 24 h to pre-cryopreservation values. The oxygen consumption per cell fell substantially at later time points, with an approximate inverse correlation to cell number. The HepG2 cell line can function anaerobically for periods of time, and likely switched into this mode of operation, as proliferation and viability continued in the system as discussed in chapter 10.

### ***13.9. Discussion and Conclusions***

In this chapter, a theoretical model of oxygen consumption has been attempted, both from a theoretical and practical perspective. The oxygen consumption found agreed with previously published data [101].

A diagnostic tool has been developed which highlights deviations in oxygen consumption of the cells, which has been shown to successfully identify that a problem has developed rapidly ( $P < 0.01$ ) using statistics for a binary system. This tool is non-invasive, and as it used data already collected as standard it is cost-free, and if implemented, will be able to increase the reliability and reduce the cost of the BAL culture phase.

While other more accurate systems to measure oxygenation exist [8, 127, 198, 293, 369, 435], the advantage of the work here is that no further equipment is required and extra information can be collected from existing data.

The diagnostic system could be improved if a total oxygen consumption model could be developed independently of cell number, although as this would remove information, the system just may be overwhelmed by noise. If successful, changes in oxygen consumption rates could be measured in real-time giving a very rapid indication of developing problems, and robustly identifies problems over a wide range of independent causes. Explicitly measuring the oxygen capacity of the LG culture medium would also improve the accuracy of the tool.

If this cannot be developed, having an earlier cell count could allow for monitoring pre-day 7 of the culture process.

All medical devices and cell cultures must remain sterile. In the LG BAL system, sterility samples are taken at set points in the process and monitored for infection, a process which takes around 3 days. This system may identify a problem earlier, and so a sterility test sample could be taken and so analysed earlier than planned. This may marginally reduce time to identify an infection, and so containment can start earlier. As it is not possible to 'cure' most cell culture systems with an infection, the indicator would not prevent a BAL becoming infected, or recover one from infection.

A major finding of this chapter is that the oxygen consumption per cell displays a trend to be inversely proportional to cell number – something not seen in other cell lines such as CHO cells [198], although spheroid systems have been seen to experience less per-cell oxygen

consumption in larger spheroids after the growth phase [127]. This may suggest that the cells become starved of oxygen during the culture phase – an observation supported by the fact that cell proliferation increases when more oxygen is supplied to the system [435]. HepG2 cells are able to operate anaerobically for periods, and it's been reported that they prefer to do so at higher cell densities supporting this work [308]. Developing methods to increase oxygen delivery to the ELS in the BAL may be a tool to improve cell growth [435].

A clear gradient of oxygen exists within the BAL, however this changes with cell density, from 21% to around 17% at the start of culture to 30% to 4% by the end of the culture phase. Zonation is in general a feature of healthy livers and some bioreactors [8, 73, 139, 199], however in *in vivo* livers and hollow-fibre bioreactors cells are fixed [50, 213] and so receive a constant concentration of oxygen – this concentration dependent on location [319]. In this fluidised bed system the oxygen concentration will vary widely and rapidly as ELS move throughout a chamber. This zonation has been shown to be important to cell functions such as toxin metabolism in the liver [8, 139, 199]. A possible reason for the very low levels of protein production by HepG2 cells in this BAL device compared with hepatocyte function *in vivo* is this rapid fluctuation in oxygen levels. While the fluidised bed system by design makes zonation difficult, improved oxygen delivery should reduce fluctuations in the BAL chamber.

Oxygen consumption per cell is seen to fall post-cryopreservation, however this may be due to increased cell density rather than a cryopreservation induced effect.

## 14. Concluding Remarks, Thoughts, and Potential Future Directions

The two primary hypotheses of this thesis, as outlined in section 2.5.1, were:

1. The 2-litre bioartificial liver device can be successfully cryopreserved, and fully recovered within 72 h of thaw.
2. Parameters of the biomass culture system can be optimised to increase culture effectiveness.

The first hypothesis has been proven in this thesis, in Chapter 10, using the protocols developed and knowledge gained in chapters 4, 5, 6, 7, and 8.

While many factors played a part in this success, the main innovation to carry out this 2.3 litre volume was the observation that the melting rate was the dominant factor in the whole cryopreservation, and specifically warming process. Future work in determining why the melting rate is so important, and work exploring thawing rates in general, are good places to continue with this research.

Chapter 10 also demonstrated a method to rapidly improve recovery of large volume cryopreservation, from around 72 h to 48 h. This can be done through having more rapid melting rates, and developing new or adapting existing protocols in the literature.

The work in this chapter will enable cold-chain delivery of the BAL device, which is further enhanced by the data in chapter 5.

The second primary hypothesis, to improve and optimize culture conditions for the BAL has been successfully demonstrated through chapters 12 and 13, which both have large potential for future work.

Perhaps the most interesting chapter is, along with chapter 10, where culture methods and cryopreservation were combined to unexpectedly positive success in chapter 11.

When ELS are cultured, the cell density is very often observed to plateau after around 12 days of culture. On optimized cryopreservation and thaw, the cell density usually falls substantially

24 h post-thaw, and recovered around 72 h after a sharp growth period. While this had been observed for many years, focus had been placed on reducing the recovery time. Determining experimentally from this that chilling encapsulated liver spheroids for a short time before culture boosted cell growth may lead to quicker and more cost efficient delivery of devices in regenerative medicine.

To my knowledge, this has not been explicitly identified in any mammalian cell system, encapsulated or otherwise, although no papers were found that looked at such extended culture after short chilling durations.

Future work will here need to focus determining if the effect is a cellular or an alginate related, and determine methods to arrest cell growth once sufficient density has been reached to prevent cell break-out. Examining this effect in other cell types would be an exciting and worthwhile avenue to explore.

Future work could also explore if ice-present cryopreservation is optimal for BAL cryopreservation. Methods to vitrify biological volumes have so far been unsuccessful, but perhaps with the advent of new concepts for vitrification such as I outlined in Cryobiology [ref], or other ice free methods, the system could be further optimized.

I briefly summarize the main conclusions from each chapter, highlighting the novel contributions in this work.

**Chapter 4** looked at new CPA combinations, though 12% DMSO was found to be the ideal cryoprotectant, in agreement with previous work. The effects of cooling and warming rates and cell density was also noted. The main contribution here was that different cell densities have different optimal cooling rates.

**Chapter 5** looked at practical aspects of the cold-chain delivery process, namely at what temperatures can ELS be transported. Either thawed or at  $-196^{\circ}\text{C}$ . It was determined that storage at  $-80^{\circ}\text{C}$  after liquid nitrogen storage was very damaging, and a factor only of the warming process. This work may contribute to transport of regenerative medicine devices.

**Chapter 6** explored practical methods from scaling up to a larger volume, looking at thermal profiles and testing new Asymptote Viafreeze systems, which were shown to work well with the BAL set-up. Simple models were reviewed, and the optimal BAL dimension, within culture constraints, chosen.

**Chapter 7** explored the impact that these different cooling patterns had on ice structure and post-thaw outcome, and developed a novel scale-down process method where conditions experienced by ELS on large scale cooling could be mimicked on a smaller scale, making optimization and experimentation much more cost effective, time effective, and practical.

**Chapter 8** explored the phenomenon of cryoconcentration (freeze-concentration). The main breakthrough in this chapter was discovering that gravity played such a significant role in samples where ice grew slowly, and this may have many uses in a wide range of large scale cryopreservation projects. Extra supernatant was added during the 2.3 litre cryopreservation to minimise the effect of cryoconcentration on our system.

**Chapter 9** explored how the non-homogeneous thermal histories on cryopreservation, whether it temporal, thermal, or related to cryoconcentration, affected the outcome of ELS on a spatial basis, finding that the last areas in a sample had the worst post-thaw outcome – this has implications for many cellular systems being cryopreserved on the order of litres.

**Chapter 10** described the 2.3 litre cryopreservation, discussed above, and determined a way to cryopreserve large volumes required for a bioartificial liver device.

**Chapter 11** developed the cryoanaptiksi discovery. It was found that chilling cells before culture can be used to increase their cell growth rates substantially.

**Chapter 12** studied the technique of fluidisation, and defined its parameters in the LG BAL system. Fluidisation was determined to occur over quite a tight linear flow rate, around 0.5mm/s for ELS without cells (alginate beads) in medium. Further work here could establish the viscosity of different types of culture medium and at different temperatures to apply to the full size BAL system. As the full sized system uses 10% human blood fraction, which is likely to be more viscous than medium without it, it seems probable that for optimized fluidisation lower linear flow rates will be required.

**Chapter 13** approximated oxygen consumption rates of ELS in the BAL system which agreed with previous data. A new diagnostic tool for the BAL was also developed, and building this into current protocols would be a worthwhile future step.

In summary, at the outset of this project the cryopreservation of a 2 litre BAL device showed viability of only 4% 48 h post thaw, with no viability recorded 72 h post-thaw [266]. At the conclusion of the project, the 2.3 litre biomass of a bioartificial liver device can be completely recovered within 72 h of thaw.

**The End.**

## 15. References

- [1] F. AbdelHafez, J. Xu, J. Goldberg, N. Desai, Vitrification in Open and Closed Carriers at Different Cell Stages: Assessment of Embryo Survival, Development, DNA Integrity and Stability during Vapor Phase Storage for Transport, *Bmc Biotechnol*, 11 (2011).
- [2] S. Ablett, M.J. Izzard, P.J. Lillford, Differential Scanning Calorimetric Study of Frozen Sucrose and Glycerol Solutions, *J Chem Soc Faraday T*, 88 (1992) 789-794.
- [3] M. Aider, D. De Halleux, Cryoconcentration technology in the bio-food industry: Principles and applications, *LWT-Food Science and Technology*, 42 (2009) 679-685.
- [4] M. Akhoondi, H. Oldenhof, C. Stoll, H. Sieme, W.F. Wolkers, Membrane hydraulic permeability changes during cooling of mammalian cells, *Biochimica et Biophysica Acta (BBA)-Biomembranes*, 1808 (2011) 642-648.
- [5] T. Akhtar, D.E. Pegg, J. Foreman, Effect of Cooling and Warming Rates on the Survival of Cryopreserved L-Cells, *Cryobiology*, 16 (1979) 424-429.
- [6] M.B. Al-Fageeh, R.J. Marchant, M.J. Carden, C.M. Smales, The cold-shock response in cultured mammalian cells: Harnessing the response for the improvement of recombinant protein production, *Biotechnol Bioeng*, 93 (2006) 829-835.
- [7] E. Alexandre, C. Viollon-Abadie, P. David, A. Gandillet, P. Coassolo, B. Heyd, G. Manton, P. Wolf, P. Bachellier, D. Jaeck, L. Richert, Cryopreservation of adult human hepatocytes obtained from resected liver biopsies, *Cryobiology*, 44 (2002) 103-113.
- [8] J.W. Allen, S.N. Bhatia, Formation of steady-state oxygen gradients in vitro: Application to liver zonation, *Biotechnol Bioeng*, 82 (2003) 253-262.
- [9] J.W. Allen, T. Hassanein, S.N. Bhatia, Advances in bioartificial liver devices, *Hepatology*, 34 (2001) 447-455.
- [10] K. Almansoori, V. Prasad, J. Forbes, G. Law, L. McGann, J. Elliott, N. Jomha, Cryoprotective agent toxicity interactions in human articular chondrocytes, *Cryobiology*, 64 (2012) 185-191.
- [11] S.A. Altman, L. Randers, G. Rao, Comparison of trypan blue dye exclusion and fluorometric assays for mammalian cell viability determinations, *Biotechnol Progr*, 9 (1993) 671-674.
- [12] T.B. Anderson, R. Jackson, Fluid mechanical description of fluidized beds. Equations of motion, *Industrial & Engineering Chemistry Fundamentals*, 6 (1967) 527-539.
- [13] T. Arakawa, J.F. Carpenter, Y.A. Kita, J.H. Crowe, The basis for toxicity of certain cryoprotectants: a hypothesis, *Cryobiology*, 27 (1990) 401-415.
- [14] A. Arav, Z. Gavish, A. Elami, Y. Natan, A. Revel, S. Silber, R.G. Gosden, P. Patrizio, Ovarian function 6years after cryopreservation and transplantation of whole sheep ovaries, *Reproductive biomedicine online*, 20 (2010) 48-52.
- [15] A. Arav, J. Saragusty, Directional freezing of spermatozoa and embryos, *Reproduction, Fertility and Development*, 26 (2014) 83-90.

- [16] M. Asif, A.A. Ibrahim, Minimum fluidization velocity and defluidization behavior of binary-solid liquid-fluidized beds, *Powder technology*, 126 (2002) 241-254.
- [17] I. Avramov, Relationship between diffusion, self-diffusion and viscosity, *Journal of Non-Crystalline Solids*, 355 (2009) 745-747.
- [18] V. Ayel, O. Lottin, M. Faucheux, D. Sallier, H. Peerhossaini, Crystallisation of undercooled aqueous solutions: Experimental study of free dendritic growth in cylindrical geometry, *International journal of heat and mass transfer*, 49 (2006) 1876-1884.
- [19] M.J. Aziz, Non-equilibrium interface kinetics during rapid solidification, *Materials Science and Engineering: A*, 178 (1994) 167-170.
- [20] M.J. Aziz, T. Kaplan, Continuous growth model for interface motion during alloy solidification, *Acta metallurgica*, 36 (1988) 2335-2347.
- [21] Y. Bachiri, C. Gazeau, J. Hansz, C. Morisset, J. Dereuddre, Successful cryopreservation of suspension cells by encapsulation-dehydration, *Plant Cell Tiss Org*, 43 (1995) 241-248.
- [22] R. Bañares, F. Nevens, F.S. Larsen, R. Jalan, A. Albillos, M. Dollinger, F. Saliba, T. Sauerbruch, S. Klammt, J. Ockenga, A. Pares, J. Wendon, T. Brännler, L. Kramer, P. Mathurin, M. de la Mata, A. Gasbarrini, B. Müllhaupt, A. Wilmer, W. Laleman, M. Eefsen, S. Sen, A. Zipprich, T. Tenorio, M. Pavesi, H.H.J. Schmidt, S. Mitzner, R. Williams, V. Arroyo, R.s.g. on behalf of the, Extracorporeal albumin dialysis with the molecular adsorbent recirculating system in acute-on-chronic liver failure: The RELIEF trial, *Hepatology*, 57 (2013) 1153-1162.
- [23] H. Barle, B. Nyberg, P. Essén, K. Andersson, M.A. McNurlan, J. Wernerman, P.J. Garlick, The synthesis rates of total liver protein and plasma albumin determined simultaneously in vivo in humans, *Hepatology*, 25 (1997) 154-158.
- [24] T. Battle, Mathematical modelling of solute segregation in solidifying materials, *International materials reviews*, 37 (1992) 249-270.
- [25] C. Baumstark, M. Schenk, H.D. Becker, M.J. Sessler, Intracellular Ca<sup>2+</sup> regulation in hepatocytes under experimental transplantation conditions, *Transplant international : official journal of the European Society for Organ Transplantation*, 15 (2002) 233-239.
- [26] J.M. Baust, K.K. Snyder, R.G. VanBuskirk, J.G. Baust, Changing paradigms in biopreservation, *Biopreservation and biobanking*, 7 (2009) 3-12.
- [27] J.M. Baust, R. Van Buskirk, J.G. Baust, Cell viability improves following inhibition of cryopreservation-induced apoptosis, *In Vitro Cellular & Developmental Biology-Animal*, 36 (2000) 262-270.
- [28] J.M. Baust, R. Van Buskirk, J.G. Baust, Modulation of the cryopreservation cap: elevated survival with reduced dimethyl sulfoxide concentration, *Cryobiology*, 45 (2002) 97-108.
- [29] L. Bayindirli, M. Özilgen, S. Urgan, Mathematical analysis of freeze concentration of apple juice, *Journal of Food Engineering*, 19 (1993) 95-107.
- [30] W. Bernal, G. Auzinger, A. Dhawan, J. Wendon, Acute liver failure, *The Lancet*, 376 (2010) 190-201.

- [31] W. Bernal, J. Wendon, Acute Liver Failure, *New Engl J Med*, 369 (2013) 2525-2534.
- [32] M. Bernardi, C. Maggioli, G. Zaccherini, Human albumin in the management of complications of liver cirrhosis, *Critical Care*, 16 (2012) 211-211.
- [33] A. Bielanski, Non-transmission of bacterial and viral microbes to embryos and semen stored in the vapour phase of liquid nitrogen in dry shippers, *Cryobiology*, 50 (2005) 206-210.
- [34] A. Bielanski, H. Bergeron, P.C.K. Lau, J. Devenish, Microbial contamination of embryos and semen during long term banking in liquid nitrogen, *Cryobiology*, 46 (2003) 146-152.
- [35] A. Biń, Prediction of the minimum fluidization velocity, *Powder technology*, 81 (1994) 197-199.
- [36] I.H. Borel Rinkes, M. Toner, S.J. Sheeha, R.G. Tompkins, M.L. Yarmush, Long-term functional recovery of hepatocytes after cryopreservation in a three-dimensional culture configuration, *Cell transplantation*, 1 (1992) 281-292.
- [37] I.A. Borin, M.S. Skaf, Molecular association between water and dimethyl sulfoxide in solution: a molecular dynamics simulation study, *The Journal of chemical physics*, 110 (1999) 6412-6420.
- [38] K.G. Brockbank, M.J. Taylor, 8 Tissue Preservation, *Advances in biopreservation*, DOI (2006) 157.
- [39] J. Burton, R. Prim, W. Slichter, The distribution of solute in crystals grown from the melt. Part I. Theoretical, *The journal of chemical physics*, 21 (1953) 1987-1991.
- [40] J.A. Burton, E.D. Kolb, W.P. Slichter, J.D. Struthers, DISTRIBUTION OF SOLUTE IN CRYSTALS GROWN FROM THE MELT .2. EXPERIMENTAL, *J. Chem. Phys.*, 21 (1953) 1991-1996.
- [41] M.F. Butler, Freeze concentration of solutes at the ice/solution interface studied by optical interferometry, *Crystal growth & design*, 2 (2002) 541-548.
- [42] R.F. Butterworth, Complications of cirrhosis III. Hepatic encephalopathy, *J Hepatol*, 32, Supplement 1 (2000) 171-180.
- [43] R.F. Butterworth, J.-F. Giguère, J. Michaud, J. Lavoie, G.P. Layrargues, Ammonia: Key factor in the pathogenesis of hepatic encephalopathy, *Neurochemical Pathology*, 6 (1987) 1-12.
- [44] S. C. M. S, C. Steiner, S. Mitzner, Experiences with MARS liver support therapy in liver failure: analysis of 176 patients of the International MARS Registry, *Liver*, 22 (2002) 20-25.
- [45] J.W. Cahn, The impurity-drag effect in grain boundary motion, *Acta metallurgica*, 10 (1962) 789-798.
- [46] B.K. Campbell, J. Hernandez-Medrano, V. Onions, C. Pincott-Allen, F. Aljaser, J. Fisher, A.S. McNeilly, R. Webb, H.M. Picton, Restoration of ovarian function and natural fertility following the cryopreservation and autotransplantation of whole adult sheep ovaries, *Human reproduction*, 29 (2014) 1749-1763.
- [47] L.H. Campbell, K.G. Brockbank, Culturing with trehalose produces viable endothelial cells after cryopreservation, *Cryobiology*, 64 (2012) 240-244.

- [48] A. Capes-Davis, G. Theodosopoulos, I. Atkin, H.G. Drexler, A. Kohara, R.A. MacLeod, J.R. Masters, Y. Nakamura, Y.A. Reid, R.R. Reddel, Check your cultures! A list of cross-contaminated or misidentified cell lines, *Int J Cancer*, 127 (2010) 1-8.
- [49] P.C. Carman, Permeability of saturated sands, soils and clays, *The Journal of Agricultural Science*, 29 (1939) 262-273.
- [50] B. Carpentier, A. Gautier, C. Legallais, Artificial and bioartificial liver devices: present and future, *Gut*, 58 (2009) 1690-1702.
- [51] J.L. Chaytor, J.M. Tokarew, L.K. Wu, M. Leclère, R.Y. Tam, C.J. Capicciotti, L. Guolla, E. von Moos, C.S. Findlay, D.S. Allan, Inhibiting ice recrystallization and optimization of cell viability after cryopreservation, *Glycobiology*, 22 (2012) 123-133.
- [52] P. Chen, X.D. Chen, K.W. Free, Solute inclusion in ice formed from sucrose solutions on a sub-cooled surface—an experimental study, *Journal of Food Engineering*, 38 (1998) 1-13.
- [53] G. Chong, S. Tsai, L.-H. Wang, C.-Y. Huang, C. Lin, Cryopreservation of the gorgonian endosymbiont *Symbiodinium*, *Scientific reports*, 6 (2016).
- [54] N.S. Choudhary, S. Saigal, R. Shukla, H. Kotecha, N. Saraf, A.S. Soin, Current Status of Immunosuppression in Liver Transplantation, *Journal of Clinical and Experimental Hepatology*, 3 (2013) 150-158.
- [55] S. Chowdhuri, S.K. Pattanayak, Pressure dependence on the single-particle dynamics and hydrogen-bond structural relaxation of water–DMSO mixtures under ambient and cold conditions, *Molecular Physics*, 111 (2013) 135-146.
- [56] M.S. Clark, M.R. Worland, How insects survive the cold: molecular mechanisms—a review, *Journal of Comparative Physiology B*, 178 (2008) 917-933.
- [57] A. Clarke, K. Fraser, Why does metabolism scale with temperature?, *Functional Ecology*, 18 (2004) 243-251.
- [58] A. Clarke, G.J. Morris, F. Fonseca, B.J. Murray, E. Acton, H.C. Price, A Low Temperature Limit for Life on Earth, *PloS one*, 8 (2013).
- [59] G.N. Clarke, Sperm cryopreservation: is there a significant risk of cross-contamination?, *Human reproduction*, 14 (1999) 2941-2943.
- [60] M. Clugston, R. Flemming, *Advanced Chemistry*, OUP Oxford 2000.
- [61] A. Corral, M. Balcerzyk, Á. Parrado-Gallego, I. Fernández-Gómez, D.R. Lamprea, A. Olmo, R. Risco, Assessment of the cryoprotectant concentration inside a bulky organ for cryopreservation using X-ray computed tomography, *Cryobiology*, 71 (2015) 419-431.
- [62] J. Couderc, Incipient fluidization and particulate systems, *Fluidization*, 2 (1985) 2.
- [63] S.M. Coward, C. Selden, A. Mantalaris, H.J.F. Hodgson, Proliferation rates of HepG2 cells encapsulated in alginate are increased in a microgravity environment compared with static cultures, *Artif Organs*, 29 (2005) 152-158.

- [64] S. Craig, C.D. Beaton, A simple cryo-SEM method for delicate plant tissues, *Journal of Microscopy*, 182 (1996) 102-105.
- [65] E. Creemers, M. Nijs, E. Vanheusden, W. Ombelet, Cryopreservation of human sperm: efficacy and use of a new nitrogen-free controlled rate freezer versus liquid nitrogen vapour freezing, *Andrologia*, 43 (2011) 392-397.
- [66] J.H. Crowe, J.F. Carpenter, L.M. Crowe, T.J. Anchordoguy, Are freezing and dehydration similar stress vectors? A comparison of modes of interaction of stabilizing solutes with biomolecules, *Cryobiology*, 27 (1990) 219-231.
- [67] J. Crowther, Enzyme Linked Immunosorbent Assay (ELISA), in: J.M. Walker, R. Rapley (Eds.) *Molecular Biomethods Handbook*, Humana Press, Totowa, NJ, 2008, pp. 657-682.
- [68] J.R. Crowther, *The ELISA Guidebook*, Humana Press 2000.
- [69] H. Cui, J.R. Grace, Fluidization of biomass particles: A review of experimental multiphase flow aspects, *Chemical Engineering Science*, 62 (2007) 45-55.
- [70] E.L. Cussler, *Diffusion: Mass Transfer in Fluid Systems*, Cambridge University Press 2009.
- [71] L.H. Damelin, S. Coward, S.F. Choudhury, S.-A. Chalmers, I.J. Cox, N.J. Robertson, G. Revial, M. Miles, R. Tootle, H.J. Hodgson, Altered mitochondrial function and cholesterol synthesis influences protein synthesis in extended HepG2 spheroid cultures, *Archives of biochemistry and biophysics*, 432 (2004) 167-177.
- [72] S. Danno, H. Nishiyama, H. Higashitsuji, H. Yokoi, J.H. Xue, K. Itoh, T. Matsuda, J. Fujita, Increased transcript level of RBM3, a member of the glycine-rich RNA-binding protein family, in human cells in response to cold stress, *Biochemical and biophysical research communications*, 236 (1997) 804-807.
- [73] A.J. Davidson, M.J. Ellis, J.B. Chaudhuri, A theoretical approach to zonation in a bioartificial liver, *Biotechnol Bioeng*, 109 (2012) 234-243.
- [74] P.L. Davies, C.L. Hew, Biochemistry of fish antifreeze proteins, *The FASEB Journal*, 4 (1990) 2460-2468.
- [75] P.L. Davies, B.D. Sykes, Antifreeze proteins, *Current opinion in structural biology*, 7 (1997) 828-834.
- [76] J.G. Day, R.A. Fleck, E.E. Benson, Cryopreservation-recalcitrance in microalgae: novel approaches to identify and avoid cryo-injury, *Journal of Applied Phycology*, 12 (2000) 369-377.
- [77] J.G. Day, G. Stacey, *Cryopreservation and freeze-drying protocols*, 2nd ed., Humana Press, Totowa, N.J., 2007.
- [78] W. De Loecker, V.A. Koptelov, V.I. Grischenko, P. De Loecker, Effects of cell concentration on viability and metabolic activity during cryopreservation, *Cryobiology*, 37 (1998) 103-109.
- [79] N. Deen, M.V.S. Annaland, M. Van der Hoef, J. Kuipers, Review of discrete particle modeling of fluidized beds, *Chemical Engineering Science*, 62 (2007) 28-44.

- [80] M. Del Pozo, C. Briens, G. Wild, Particle—particle collisions in liquid—solid and gas—liquid—solid fluidized beds, *Chemical engineering science*, 48 (1993) 3313-3319.
- [81] A.A. Demetriou, R.S. Brown Jr, R.W. Busuttill, J. Fair, B.M. McGuire, P. Rosenthal, I. Jan Schulte Am Esch, J. Lerut, S.L. Nyberg, M. Salizzoni, Prospective, randomized, multicenter, controlled trial of a bioartificial liver in treating acute liver failure, *Ann Surg*, 239 (2004) 660-670.
- [82] M.M. Denn, *Process Fluid Mechanics*, Prentice-Hall 1980.
- [83] A. Dhawan, Clinical human hepatocyte transplantation: Current status and challenges, *Liver Transplant*, 21 (2015) S39-S44.
- [84] B. Diener, D. Utesch, N. Beer, H. Dürk, F. Oesch, A method for the cryopreservation of liver parenchymal cells for studies of xenobiotics, *Cryobiology*, 30 (1993) 116-127.
- [85] K.R. Diller, The influence of controlled ice nucleation on regulating the thermal history during freezing, *Cryobiology*, 22 (1985) 268-281.
- [86] J. Dong, A. Hubel, J.C. Bischof, A. Aksan, Freezing-induced phase separation and spatial microheterogeneity in protein solutions, *The Journal of Physical Chemistry B*, 113 (2009) 10081-10087.
- [87] R.F. Doolittle, Fibrinogen and fibrin, eLS, DOI (2001).
- [88] E. Dore, C. Legallais, A new concept of bioartificial liver based on a fluidized bed bioreactor, *Therapeutic Apheresis*, 3 (1999) 264-267.
- [89] E.Z. Drobnis, L.M. Crowe, T. Berger, T.J. Anchordoguy, J.W. Overstreet, J.H. Crowe, Cold Shock Damage Is Due to Lipid Phase-Transitions in Cell-Membranes - a Demonstration Using Sperm as a Model, *J Exp Zool*, 265 (1993) 432-437.
- [90] J.G. Duman, Antifreeze and ice nucleator proteins in terrestrial arthropods, *Annual Review of Physiology*, 63 (2001) 327-357.
- [91] P.N. Dwivedi, S. Upadhyay, Particle-fluid mass transfer in fixed and fluidized beds, *Industrial & Engineering Chemistry Process Design and Development*, 16 (1977) 157-165.
- [92] K. Eckler, D. Herlach, M. Aziz, Search for a solute-drag effect in dendritic solidification, *Acta metallurgica et materialia*, 42 (1994) 975-979.
- [93] J.T. Edward, Molecular volumes and the Stokes-Einstein equation, *Journal of Chemical Education*, 47 (1970) 261.
- [94] C. Ellerström, R. Strehl, K. Noaksson, J. Hyllner, H. Semb, Facilitated expansion of human embryonic stem cells by single-cell enzymatic dissociation, *Stem Cells*, 25 (2007) 1690-1696.
- [95] A.J. Ellis, R.D. Hughes, J.A. Wendon, J. Dunne, P.G. Langley, J.H. Kelly, G.T. Gislason, N.L. Sussman, R. Williams, Pilot-controlled trial of the extracorporeal liver assist device in acute liver failure, *Hepatology*, 24 (1996) 1446-1451.
- [96] S. Enosawa, T. Miyashita, Y. Fujita, S. Suzuki, H. Amemiya, T. Omasa, S. Hiramatsu, K. Suga, T. Matsumura, In vivo estimation of bioartificial liver with recombinant HepG2 cells using pigs with ischemic liver failure, *Cell transplantation*, 10 (2001) 429-433.

- [97] L.E. Epperson, J.C. Rose, H.V. Carey, S.L. Martin, Seasonal proteomic changes reveal molecular adaptations to preserve and replenish liver proteins during ground squirrel hibernation, *American Journal of Physiology-Regulatory, Integrative and Comparative Physiology*, 298 (2010) R329-R340.
- [98] N. Epstein, Applications of liquid-solid fluidization, *International Journal of Chemical Reactor Engineering*, 1 (2003).
- [99] S. Ergun, Fluid flow through packed columns, *Chem. Eng. Prog.*, 48 (1952) 89-94.
- [100] A. Eroglu, M.J. Russo, R. Bieganski, A. Fowler, S. Cheley, H. Bayley, M. Toner, Intracellular trehalose improves the survival of cryopreserved mammalian cells, *Nature biotechnology*, 18 (2000) 163-167.
- [101] E. Erro, J. Bundy, I. Massie, S.A. Chalmers, A. Gautier, S. Gerontas, M. Hoare, P. Sharratt, S. Choudhury, M. Lubowiecki, I. Llewellyn, C. Legallais, B. Fuller, H. Hodgson, C. Selden, Bioengineering the liver: scale-up and cool chain delivery of the liver cell biomass for clinical targeting in a bioartificial liver support system, *BioResearch open access*, 2 (2013) 1-11.
- [102] U. Escher, F.v. Schoenebeck, M. Jäckel, A. Gladun, Experimental investigation of thermal properties and Grueneisen parameter of aligned polycarbonate at low temperatures, *Cryogenics*, 38 (1998) 109-112.
- [103] M.L. Etheridge, K.R. Hurley, J. Zhang, S. Jeon, H.L. Ring, C. Hogan, C.L. Haynes, M. Garwood, J.C. Bischof, Accounting for biological aggregation in heating and imaging of magnetic nanoparticles, *Technology*, 2 (2014) 214-228.
- [104] M.L. Etheridge, Y. Xu, L. Rott, J. Choi, B. Glasmacher, J.C. Bischof, RF heating of magnetic nanoparticles improves the thawing of cryopreserved biomaterials, *Technology*, 2 (2014) 229-242.
- [105] S. Evans, Electromagnetic rewarming: the effect of CPA concentration and radio source frequency on uniformity and efficiency of heating, *Cryobiology*, 40 (2000) 126-138.
- [106] R. Fadini, F. Brambillasca, M.M. Renzini, M. Merola, R. Comi, E. De Ponti, M. Dal Canto, Human oocyte cryopreservation: comparison between slow and ultrarapid methods, *Reproductive biomedicine online*, 19 (2009) 171-180.
- [107] G.M. Fahy, B. Khirabadi, Y. Okouchi, T. Maciag, Method of preparing organs for vitrification, *Google Patents*, 1998.
- [108] G.M. Fahy, T.H. Lilley, H. Linsdell, M.S.J. Douglas, H.T. Meryman, Cryoprotectant toxicity and cryoprotectant toxicity reduction: in search of molecular mechanisms, *Cryobiology*, 27 (1990) 247-268.
- [109] G.M. Fahy, D. MacFarlane, C.A. Angell, H. Meryman, Vitrification as an approach to cryopreservation, *Cryobiology*, 21 (1984) 407-426.
- [110] G.M. Fahy, B. Wowk, R. Pagotan, A. Chang, J. Phan, B. Thomson, L. Phan, Physical and biological aspects of renal vitrification, *Organogenesis*, 5 (2009) 167-175.
- [111] G.M. Fahy, B. Wowk, J. Wu, Cryopreservation of complex systems: The missing link in the regenerative medicine supply chain (vol 9, pg 279, 2006), *Rejuv Res*, 9 (2006) 509-509.

- [112] G.M. Fahy, B. Wowk, J. Wu, J. Phan, C. Rasch, A. Chang, E. Zendejas, Cryopreservation of organs by vitrification: perspectives and recent advances, *Cryobiology*, 48 (2004) 157-178.
- [113] L.-S. Fan, Gas-liquid-solid fluidization engineering, DOI (1989).
- [114] L.T. Fan, J.A. Schmitz, E.N. Miller, Dynamics of liquid-solid fluidized bed expansion, *AIChE Journal*, 9 (1963) 149-153.
- [115] W.-X. Fan, X.-H. Ma, D. Ge, T.-Q. Liu, Z.-F. Cui, Cryoprotectants for the vitrification of corneal endothelial cells, *Cryobiology*, 58 (2009) 28-36.
- [116] J. Farrant, Mechanism of cell damage during freezing and thawing and its prevention, *Nature*, 205 (1965) 1284-1287.
- [117] M. Fireman, A.F. DiMartini, S.C. Armstrong, K.L. Cozza, Immunosuppressants, *Psychosomatics*, 45 (2004) 354-360.
- [118] M.C. Flemings, Solidification processing, *Metallurgical transactions*, 5 (1974) 2121-2134.
- [119] G.L. Fletcher, C.L. Hew, P.L. Davies, Antifreeze proteins of teleost fishes, *Annual review of physiology*, 63 (2001) 359-390.
- [120] F. Fonseca, J. Meneghel, S. Cenard, S. Passot, G.J. Morris, Determination of Intracellular Vitrification Temperatures for Unicellular Micro Organisms under Conditions Relevant for Cryopreservation, *PloS one*, 11 (2016) e0152939.
- [121] B. Formisani, Packing and fluidization properties of binary mixtures of spherical particles, *Powder technology*, 66 (1991) 259-264.
- [122] P. Foscolo, L. Gibilaro, S. Waldram, A unified model for particulate expansion of fluidised beds and flow in fixed porous media, *Chemical Engineering Science*, 38 (1983) 1251-1260.
- [123] M.F. Fox, K. Whittingham, Component interactions in aqueous dimethyl sulphoxide, *Journal of the Chemical Society, Faraday Transactions 1: Physical Chemistry in Condensed Phases*, 71 (1975) 1407-1412.
- [124] F. Franks, The properties of aqueous solutions at subzero temperatures, Springer1982.
- [125] B.A. Freeman, J.D. Crapo, Biology of disease: free radicals and tissue injury, *Laboratory investigation; a journal of technical methods and pathology*, 47 (1982) 412-426.
- [126] R.B. Freeman, E.B. Edwards, Liver transplant waiting time does not correlate with waiting list mortality: implications for liver allocation policy, *Liver Transplant*, 6 (2000) 543-552.
- [127] J. Freyer, E. Tustanoff, A. Franko, R. Sutherland, In situ oxygen consumption rates of cells in V-79 multicellular spheroids during growth, *Journal of cellular physiology*, 118 (1984) 53-61.
- [128] R. Fujioka, L.P. Wang, G. Dodbiba, T. Fujita, Application of progressive freeze-concentration for desalination, *Desalination*, 319 (2013) 33-37.
- [129] J. Fujita, Cold shock response in mammalian cells, *Cold Shock Response and Adaptation*, DOI (2000) 113-142.

- [130] K. Fukui, K. Maeda, Distribution of solute at solid–liquid interface during solidification of melt, *The Journal of chemical physics*, 109 (1998) 7468-7473.
- [131] B.J. Fuller, Cryoprotectants: the essential antifreezes to protect life in the frozen state, *CryoLetters*, 25 (2004) 375-388.
- [132] B.J. Fuller, N. Lane, E.E. Benson, *Life in the frozen state*, CRC Press, Boca Raton, Fla., 2004.
- [133] P. Galenko, Solute trapping and diffusionless solidification in a binary system, *Physical Review E*, 76 (2007) 031606.
- [134] U. Ganguly, An improved relationship to predict expanded bed height in particulate fluidization, *International journal of mineral processing*, 34 (1992) 243-251.
- [135] D. Gao, J. Critser, Mechanisms of cryoinjury in living cells, *ILAR journal*, 41 (2000) 187-196.
- [136] M. Garcovich, M.A. Zocco, A. Gasbarrini, Clinical use of albumin in hepatology, *Blood Transfusion*, 7 (2009) 268-277.
- [137] A. Gautier, B. Carpentier, M. Dufresne, Q. Vu Dinh, P. Paullier, C. Legallais, Impact of alginate type and bead diameter on mass transfers and the metabolic activities of encapsulated C3A cells in bioartificial liver applications, *Eur Cell Mater*, 21 (2011) 94-106.
- [138] Z. Gavish, M. Ben-Haim, A. Arav, Cryopreservation of whole murine and porcine livers, *Rejuv Res*, 11 (2008) 765-772.
- [139] R. Gebhardt, Metabolic zonation of the liver: regulation and implications for liver function, *Pharmacology & therapeutics*, 53 (1992) 275-354.
- [140] M. George, M. Johnson, Use of fetal bovine serum substitutes for the protection of the mouse zona pellucida against hardening during cryoprotectant addition, *Human reproduction (Oxford, England)*, 8 (1993) 1898-1900.
- [141] F. Gevrin, O. Masbernat, O. Simonin, Numerical study of solid–liquid fluidization dynamics, *AIChE journal*, 56 (2010) 2781-2794.
- [142] L. Gibilaro, R. Di Felice, P. Foscolo, A circulating liquid fluidised bed, *Chemical engineering science*, 43 (1988) 2901-2903.
- [143] S. Gill, I. Wadsö, Flow-microcalorimetric techniques for solution of slightly soluble gases. Enthalpy of solution of oxygen in water at 298.15 K, *The Journal of Chemical Thermodynamics*, 14 (1982) 905-919.
- [144] R. Girlanda, M. Rela, R. Williams, J.G. O'Grady, N.D. Heaton, Long-Term Outcome of Immunosuppression Withdrawal After Liver Transplantation, *Transpl P*, 37 (2005) 1708-1709.
- [145] M.E. Glicksman, *Principles of Solidification: An Introduction to Modern Casting and Crystal Growth Concepts*, Springer New York 2010.
- [146] S.A. Glynn, A.E. Williams, C.C. Nass, J. Bethel, D. Kessler, E.P. Scott, J. Fridey, S.H. Kleinman, G.B. Schreiber, Attitudes toward blood donation incentives in the United States: implications for donor recruitment, *Transfusion*, 43 (2003) 7-16.

- [147] Y.A. Goffin, B. Van Hoeck, R. Jashari, G. Soots, P. Kalmar, Banking of cryopreserved heart valves in Europe: Assessment of a 10-year operation in the European Homograft Bank (EHB), *J Heart Valve Dis*, 9 (2000) 207-214.
- [148] M. Gomez-Lechon, A. Lahoz, N. Jimenez, J. Vicente Castell, M. Donato, Cryopreservation of rat, dog and human hepatocytes: influence of preculture and cryoprotectants on recovery, cytochrome P450 activities and induction upon thawing, *Xenobiotica*, 36 (2006) 457-472.
- [149] W.R. Goossens, Classification of fluidized particles by Archimedes number, *Powder technology*, 98 (1998) 48-53.
- [150] R. Gosden, Cryopreservation: a cold look at technology for fertility preservation, *Fertility and sterility*, 96 (2011) 264-268.
- [151] C.D. Gregory, A.E. Milner, Regulation of Cell-Survival in Burkitt-Lymphoma - Implications from Studies of Apoptosis Following Cold-Shock Treatment, *Int J Cancer*, 57 (1994) 419-426.
- [152] B.W.W. Grout, G.J. Morris, Contaminated liquid nitrogen vapour as a risk factor in pathogen transfer, *Theriogenology*, 71 (2009) 1079-1082.
- [153] B.W.W. Grout, G.J. Morris, *The Effects of low temperatures on biological systems*, E. Arnold, London, 1987.
- [154] X. Gu, T. Suzuki, O. Miyawaki, Limiting Partition Coefficient in Progressive Freeze-concentration, *J Food Sci*, 70 (2005) E546-E551.
- [155] E.E. Guibert, A.Y. Petrenko, C.L. Balaban, A.Y. Somov, J.V. Rodriguez, B.J. Fuller, Organ Preservation: Current Concepts and New Strategies for the Next Decade, *Transfus Med Hemoth*, 38 (2011) 125-142.
- [156] K.T. Gunasena, P.M. Villines, E.S. Critser, J.K. Critser, Live births after autologous transplant of cryopreserved mouse ovaries, *Human reproduction*, 12 (1997) 101-106.
- [157] M. Gunathilake, K. Shimmura, O. Miyawaki, Analysis of solute distribution in ice formed in progressive freeze-concentration, *Food Science and Technology Research*, 19 (2013) 369-374.
- [158] A. Haider, O. Levenspiel, Drag coefficient and terminal velocity of spherical and nonspherical particles, *Powder technology*, 58 (1989) 63-70.
- [159] R. Halde, Concentration of impurities by progressive freezing, *Water Research*, 14 (1980) 575-580.
- [160] D.L. Hall, S.M. Sterner, R.J. Bodnar, Freezing point depression of NaCl-KCl-H<sub>2</sub>O solutions, *Economic Geology*, 83 (1988) 197-202.
- [161] I.S. Han, H.O. Lim, K.T. Kim, Y. Kang, K.W. Jun, Particle dispersion and fluctuations in viscous liquid–solid fluidised Beds, *The Canadian Journal of Chemical Engineering*, 91 (2013) 542-549.
- [162] X. Han, J.K. Critser, Measurement of the size of intracellular ice crystals in mouse oocytes using a melting point depression method and the influence of intracellular solute concentrations, *Cryobiology*, 59 (2009) 302-307.
- [163] J.H. Harker, J.R. Backhurst, J.F. Richardson, *Chemical Engineering*, Elsevier Science 2013.

- [164] H.R. Harmison, K.R. Diller, J.R. Walsh, C.M. Neils, J.J. Brand, Measurement of Cell Volume Loss in the Liquid Region Preceding an Advancing Phase Change Interface, *Annals of the New York Academy of Sciences*, 858 (1998) 276-283.
- [165] H.S. Harned, C.L. Hildreth Jr, The differential diffusion coefficients of lithium and sodium chlorides in dilute aqueous solution at 25, *Journal of the American Chemical Society*, 73 (1951) 650-652.
- [166] M. Hartman, J.G. Yates, Free-fall of solid particles through fluids, *Collection of Czechoslovak chemical communications*, 58 (1993) 961-982.
- [167] S. Hartmann, D. Niedermeier, J. Voigtländer, T. Clauss, R. Shaw, H. Wex, A. Kiselev, F. Stratmann, Homogeneous and heterogeneous ice nucleation at LACIS: operating principle and theoretical studies, *Atmospheric Chemistry and Physics*, 11 (2011) 1753-1767.
- [168] T.I. Hassanein, R.R. Schade, I.S. Hepburn, Acute-on-chronic liver failure: extracorporeal liver assist devices, *Current opinion in critical care*, 17 (2011) 195-203.
- [169] Z. He, H.B. Zhou, Z.Y. Zhang, L.Y. Li, The Solute Redistribution during Solidification of Al-Si-Mg Alloys, *Advanced Materials Research*, Trans Tech Publ, 2012, pp. 979-982.
- [170] R.B. Head, Steroids as Ice Nucleators, *Nature*, 191 (1961) 1058-&.
- [171] R. Heidemann, S. Lunse, D. Tran, C. Zhang, Characterization of Cell-Banking Parameters for the Cryopreservation of Mammalian Cell Lines in 100-ML Cryobags, *Biotechnol Progr*, 26 (2010) 1154-1163.
- [172] R. Heidemann, M. Mered, D. Wang, B. Gardner, C. Zhang, J. Michaels, H.-J. Henzler, N. Abbas, K. Konstantinov, A new seed-train expansion method for recombinant mammalian cell lines, *Cytotechnology*, 38 (2002) 99-108.
- [173] J.G. Hengstler, D. Utesch, P. Steinberg, K. Platt, B. Diener, M. Ringel, N. Swales, T. Fischer, K. Biefang, M. Gerl, T. Bottger, F. Oesch, Cryopreserved primary hepatocytes as a constantly available in vitro model for the evaluation of human and animal drug metabolism and enzyme induction, *Drug Metab Rev*, 32 (2000) 81-118.
- [174] D.M. Herlach, Non-equilibrium solidification of undercooled metallic metals, *Materials Science and Engineering: R: Reports*, 12 (1994) 177-272.
- [175] L. Herrero, M. Martínez, J.A. Garcia-Velasco, Current status of human oocyte and embryo cryopreservation, *Current Opinion in Obstetrics and Gynecology*, 23 (2011) 245-250.
- [176] N.J. Hewitt, A.P. Li, Cryopreservation of Hepatocytes, *Protocols in In Vitro Hepatocyte Research*, DOI (2015) 13-26.
- [177] D. Hirai, K. Shirai, S. Shirai, A. Sakai, Cryopreservation of in vitro-grown meristems of strawberry (*Fragaria x ananassa* Duch.) by encapsulation-vitrification, *Euphytica*, 101 (1998) 109-115.
- [178] A. Hirata, F.B. Bulos, Predicting bed voidage in solid-liquid fluidization, *Journal of Chemical Engineering of Japan*, 23 (1990) 599-604.
- [179] P.V. Hobbs, *Ice Physics*, OUP Oxford 2010.

- [180] E.M. Hoenicke, D.S. Peterseim, C.T. Ducko, X.W. Sun, R.J. Damiano, Donor heart preservation with the potassium channel opener pinacidil: Comparison with University of Wisconsin and St. Thomas' solution, *J Heart Lung Transpl*, 19 (2000) 286-297.
- [181] M. Holz, S.R. Heil, A. Sacco, Temperature-dependent self-diffusion coefficients of water and six selected molecular liquids for calibration in accurate <sup>1</sup>H NMR PFG measurements, *Physical Chemistry Chemical Physics*, 2 (2000) 4740-4742.
- [182] A. Hubel, E. Cravalho, B. Nunner, C. Körber, Survival of directionally solidified B-lymphoblasts under various crystal growth conditions, *Cryobiology*, 29 (1992) 183-198.
- [183] A. Hubel, T. Darr, A. Chang, J. Dantzig, Cell partitioning during the directional solidification of trehalose solutions, *Cryobiology*, 55 (2007) 182-188.
- [184] N. Hubert, R. Solimando, A. Pere, L. Schuffenecker, Dissolution enthalpy of NaCl in water at 25° C, 45° C and 60° C. Determination of the Pitzer's parameters of the {H<sub>2</sub>O · NaCl} system and the molar dissolution enthalpy at infinite dilution of NaCl in water between 25° C and 100° C, *Thermochimica acta*, 294 (1997) 157-163.
- [185] P. Hughes, D. Marshall, Y. Reid, H. Parkes, C. Gelber, The costs of using unauthenticated, over-passaged cell lines: how much more data do we need?, *Biotechniques*, 43 (2007) 575.
- [186] R.D. Hughes, R.R. Mitry, S.C. Lehec, Cryopreservation of human hepatocytes for clinical use, *Hepatocytes: Methods and Protocols*, DOI (2010) 107-113.
- [187] J. Hunt, S.-Z. Lu, Numerical modeling of cellular/dendritic array growth: spacing and structure predictions, *Metallurgical and Materials Transactions A*, 27 (1996) 611-623.
- [188] R. Hut, B. Barnes, S. Daan, Body temperature patterns before, during, and after semi-natural hibernation in the European ground squirrel, *Journal of Comparative Physiology B*, 172 (2002) 47-58.
- [189] F.P. Incropera, *Fundamentals of heat and mass transfer*, John Wiley 2007.
- [190] V. Isachenko, E. Isachenko, J. Reinsberg, M. Montag, F. Braun, H. van der Ven, Cryopreservation of human ovarian tissue: effect of spontaneous and initiated ice formation, *Reproductive biomedicine online*, 16 (2008) 336-345.
- [191] K.-i. Izutsu, S. Kojima, Freeze-concentration separates proteins and polymer excipients into different amorphous phases, *Pharmaceutical research*, 17 (2000) 1316-1322.
- [192] R. Jashari, B. Van Hoeck, R. Ngakam, Y. Goffin, Y. Fan, Banking of cryopreserved arterial allografts in Europe: 20 years of operation in the European Homograft Bank (EHB) in Brussels, *Cell and tissue banking*, 14 (2013) 589-599.
- [193] H. Jena, G. Roy, B. Meikap, Hydrodynamics of regular particles in a liquid–solid semi-fluidized bed, *Powder Technology*, 196 (2009) 246-256.
- [194] L. Jiang, C. Shen, J. Dai, Q. Meng, Di-rhamnolipids improve effect of trehalose on both hypothermic preservation and cryopreservation of rat hepatocytes, *Applied microbiology and biotechnology*, 97 (2013) 4553-4561.

- [195] W. Jie, D. Ma, An approximate method to calculate the solute redistribution in directional solidification specimen with limited length, *Journal of crystal growth*, 156 (1995) 467-472.
- [196] N.M. Jomha, A.D. Weiss, J.F. Forbes, G.K. Law, J.A. Elliott, L.E. McGann, Cryoprotectant agent toxicity in porcine articular chondrocytes, *Cryobiology*, 61 (2010) 297-302.
- [197] K.H. Jones, J.A. Senft, An improved method to determine cell viability by simultaneous staining with fluorescein diacetate-propidium iodide, *Journal of Histochemistry & Cytochemistry*, 33 (1985) 77-79.
- [198] P. Jorjani, S.S. Ozturk, Effects of cell density and temperature on oxygen consumption rate for different mammalian cell lines, *Biotechnol Bioeng*, 64 (1999) 349-356.
- [199] K. Jungermann, T. Kietzmann, Oxygen: Modulator of metabolic zonation and disease of the liver, *Hepatology*, 31 (2000) 255-260.
- [200] D. Karamanev, L. Nikolov, Bed expansion of liquid-solid inverse fluidization, *AIChE journal*, 38 (1992) 1916-1922.
- [201] A.M. KAROW, Cryoprotectants—a new class of drugs, *Journal of Pharmacy and Pharmacology*, 21 (1969) 209-223.
- [202] E. Katenz, F.W.R. Vondran, R. Schwartlander, G. Pless, X. Gong, X. Cheng, P. Neuhaus, I.M. Sauer, Cryopreservation of primary human hepatocytes: the benefit of trehalose as an additional cryoprotective agent, *Liver Transplant*, 13 (2007) 38-45.
- [203] N.R. Katz, Metabolic Heterogeneity of Hepatocytes across the Liver Acinus<sup>1</sup>, *The Journal of nutrition*, 122 (1992) 843.
- [204] K. Kawasaki, A. Matsuda, H. Kadota, Freeze concentration of equal molarity solutions with ultrasonic irradiation under constant freezing rate: effect of solute, *Chemical Engineering Research and Design*, 84 (2006) 107-112.
- [205] D.A. Kessler, J. Koplik, H. Levine, Steady-state dendritic crystal growth, *Physical Review A*, 33 (1986) 3352.
- [206] M. Khalil, A. Shariat-Panahi, R. Tootle, T. Ryder, P. McCloskey, E. Roberts, H. Hodgson, C. Selden, Human hepatocyte cell lines proliferating as cohesive spheroid colonies in alginate markedly upregulate both synthetic and detoxificatory liver function, *J Hepatol*, 34 (2001) 68-77.
- [207] K.K. Khush, J. Zaroff, J. Nguyen, R. Menza, B.A. Goldstein, National Decline in Donor Heart Utilization With Regional Variability: 1995–2010, *Am J Transplant*, 15 (2015) 642-649.
- [208] K.K. Khush, J.G. Zaroff, J. Nguyen, R. Menza, B.A. Goldstein, National Decline in Donor Heart Utilization With Regional Variability: 1995-2010, *Am J Transplant*, 15 (2015) 642-649.
- [209] H. Kiani, D.-W. Sun, Water crystallization and its importance to freezing of foods: A review, *Trends in Food Science & Technology*, 22 (2011) 407-426.
- [210] P. Kilbride, G.J. Morris, S. Milne, B. Fuller, J. Skepper, C. Selden, A scale down process for the development of large volume cryopreservation, *Cryobiology*, 69 (2014) 367-375.

- [211] P. Kilbride, J. Morris, B. Fuller, C. Selden, 006 The importance of spatial location of cells during large volume cryopreservation and contrast between larger and smaller cryopreservation volumes, *Cryobiology*, 67 (2013) 400.
- [212] P. Kilbride, H.J. Woodward, K.B. Tan, N.T. Thanh, K.E. Chu, S. Minogue, M.G. Waugh, Modeling the effects of cyclodextrin on intracellular membrane vesicles from Cos-7 cells prepared by sonication and carbonate treatment, *PeerJ*, 3 (2015) e1351.
- [213] Y. Kim, S. Ozer, B.E. Uygun, Chapter 24 - Liver Regeneration: The Bioengineering Approach A2 - Orlando, Giuseppe, in: J. Lerut, S. Soker, R.J. Stratta (Eds.) *Regenerative Medicine Applications in Organ Transplantation*, Academic Press, Boston, 2014, pp. 333-352.
- [214] M.I. Kleman, K. Oellers, E. Lullau, Optimal conditions for freezing CHO-S and HEK293-EBNA cell lines: Influence of Me<sub>2</sub>SO, freeze density, and PEI-mediated transfection on revitalization and growth of cells, and expression of recombinant protein, *Biotechnol Bioeng*, 100 (2008) 911-922.
- [215] A. Kmieć, Particle distributions and dynamics of particle movement in solid—liquid fluidized beds, *The Chemical Engineering Journal*, 15 (1978) 1-12.
- [216] B. Knowles, C. Howe, D. Aden, Human hepatocellular carcinoma cell lines secrete the major plasma proteins and hepatitis B surface antigen, *Science*, 209 (1980) 497-499.
- [217] N. Kobayashi, T. Okitsu, S. Nakaji, N. Tanaka, Hybrid bioartificial liver: establishing a reversibly immortalized human hepatocyte line and developing a bioartificial liver for practical use, *Journal of Artificial Organs*, 6 (2003) 236-244.
- [218] N. Kobayashi, T. Okitsu, N. Tanaka, Cell choice for bioartificial livers, *The Keio journal of medicine*, 52 (2003) 151-157.
- [219] S. Koch, C. Schwinger, J. Kressler, C. Heinzen, N.G. Rainov, Alginate encapsulation of genetically engineered mammalian cells: comparison of production devices, methods and microcapsule characteristics, *J Microencapsul*, 20 (2003) 303-316.
- [220] P. Kolhe, A. Badkar, Protein and solute distribution in drug substance containers during frozen storage and post-thawing: A tool to understand and define freezing—thawing parameters in biotechnology process development, *Biotechnol Progr*, 27 (2011) 494-504.
- [221] C. Korber, Phenomena at the Advancing Ice Liquid Interface - Solutes, Particles and Biological Cells, *Q Rev Biophys*, 21 (1988) 229-298.
- [222] G. Körtner, F. Geiser, The temporal organization of daily torpor and hibernation: circadian and circannual rhythms, *Chronobiology international*, 17 (2000) 103-128.
- [223] A. KRAMER, K. WANI, J.H. SULLIVAN, I. SHOMER, Freeze concentration by directional cooling, *J Food Sci*, 36 (1971) 320-322.
- [224] P. Krisper, R.E. Stauber, Technology Insight: artificial extracorporeal liver support—how does Prometheus® compare with MARS®?, *Nature Clinical Practice Nephrology*, 3 (2007) 267-276.
- [225] P. Kumar, M.L. Clark, Kumar and Clark's Clinical Medicine, Saunders Elsevier 2012.

- [226] S. Kumar, J.D. Millar, P.F. Watson, The effect of cooling rate on the survival of cryopreserved bull, ram, and boar spermatozoa: a comparison of two controlled-rate cooling machines, *Cryobiology*, 46 (2003) 246-253.
- [227] P.K. Kundu, I.M. Cohen, D.R. Dowling, *Fluid Mechanics*, Elsevier Science 2015.
- [228] D. Kunii, O. Levenspiel, Circulating fluidized-bed reactors, *Chemical Engineering Science*, 52 (1997) 2471-2482.
- [229] E. Kuntz, H.D. Kuntz, *Hepatology: Textbook and Atlas*, Springer Berlin Heidelberg 2009.
- [230] W. Kurz, D. Fisher, Dendrite growth at the limit of stability: tip radius and spacing, *Acta Metallurgica*, 29 (1981) 11-20.
- [231] M. Kuwayama, G. Vajta, O. Kato, S.P. Leibo, Highly efficient vitrification method for cryopreservation of human oocytes, *Reproductive BioMedicine Online*, 11 (2005) 300-308.
- [232] A.V. Lakshmi, M. Balamurugan, M. Sivakumar, T.N. Samuel, M. Velan, Minimum fluidization velocity and friction factor in a liquid-solid inverse fluidized bed reactor, *Bioprocess Engineering*, 22 (2000) 461-466.
- [233] U. Lashmar, M. Vanderburgh, S. Little, Bulk freeze-thawing of macromolecules: Effects of cryoconcentration on their formulation and stability, *BioProcess International*, 5 (2007) 44.
- [234] A. Lawson, H. Ahmad, A. Sambanis, Cytotoxicity effects of cryoprotectants as single-component and cocktail vitrification solutions, *Cryobiology*, 62 (2011) 115-122.
- [235] D.H. Lee, Transition velocity and bed expansion of two-phase (liquid-solid) fluidization systems, *Korean Journal of Chemical Engineering*, 18 (2001) 347-351.
- [236] J.H. Lee, D.H. Jung, D.H. Lee, J.K. Park, S.K. Lee, Effect of Spheroid Aggregation on Susceptibility of Primary Pig Hepatocytes to Cryopreservation, *Transpl P*, 44 (2012) 1015-1017.
- [237] K. Lee, J. Park, J. Yoon, J. Lee, S. Kim, H. Jung, S. Lee, S. Kim, H. Lee, D. Lee, The viability and function of cryopreserved hepatocyte spheroids with different cryopreservation solutions, *Transpl P*, Elsevier, 2004, pp. 2462-2463.
- [238] K.C. Lee, L.A. Baker, G. Stanzani, H. Alibhai, Y.M. Chang, C.J. Palacios, P.J. Leckie, P. Giordano, S.L. Priestnall, D.J. Antoine, Extracorporeal liver assist device to exchange albumin and remove endotoxin in acute liver failure: Results of a pivotal pre-clinical study, *J Hepatol*, 63 (2015) 634-642.
- [239] W.M. Lee, Acute Liver Failure, *Semin Resp Crit Care*, 33 (2012) 36-45.
- [240] C. Legallais, E. Doré, P. Paullier, Design of a Fluidized Bed Bioartificial Liver, *Artif Organs*, 24 (2000) 519-525.
- [241] S. Leibo, J. Farrant, P. Mazur, j.M. Hanna, L. Smith, Effects of prefreezing on marrow stem cell suspensions: Interactions of cooling and warming rates in the presence of pvp, sucrose, or glycerol, *Cryobiology*, 6 (1970) 315-332.

- [242] J.J. Lemasters, J. Diguseppi, A.L. Nieminen, B. Herman, Blebbing, Free Ca-2+ and Mitochondrial-Membrane Potential Preceding Cell-Death in Hepatocytes, *Nature*, 325 (1987) 78-81.
- [243] C.R. Leric, M. Piva, M.D. Rosa, Water Activity and Freezing Point Depression of Aqueous Solutions and Liquid Foods, *J Food Sci*, 48 (1983) 1667-1669.
- [244] J.K. Lewis, J.C. Bischof, I. Braslavsky, K.G. Brockbank, G.M. Fahy, B.J. Fuller, Y. Rabin, A. Tocchio, E.J. Woods, B.G. Wowk, J.P. Acker, S. Giwa, The Grand Challenges of Organ Banking: Proceedings from the first global summit on complex tissue cryopreservation, *Cryobiology*, DOI 10.1016/j.cryobiol.2015.12.001(2015).
- [245] Y. Li, T. Ma, Bioprocessing of cryopreservation for large-scale banking of human pluripotent stem cells, *BioResearch open access*, 1 (2012) 205-214.
- [246] P.J. Lillford, C.B. Holt, In vitro uses of biological cryoprotectants, *Philosophical Transactions of the Royal Society of London B: Biological Sciences*, 357 (2002) 945-951.
- [247] S. Limtrakul, J. Chen, P.A. Ramachandran, M.P. Duduković, Solids motion and holdup profiles in liquid fluidized beds, *Chemical Engineering Science*, 60 (2005) 1889-1900.
- [248] K.B. Lintern, Immobilisation of Lactate Oxidase and Deoxyribonuclease I for use within a Bio-Artificial Liver Assist Device for the Treatment of Acute Liver Failure, UCL (University College London), 2013.
- [249] B.C. Lippens, J. Mulder, Prediction of the minimum fluidization velocity, *Powder technology*, 75 (1993) 67-78.
- [250] T.D. Lloyd, S. Orr, P. Skett, D.P. Berry, A.R. Dennison, Cryopreservation of hepatocytes: a review of current methods for banking, *Cell and tissue banking*, 4 (2003) 3-15.
- [251] J.F. Lock, M. Malinowski, D. Seehofer, S. Hoppe, R.I. Röhl, S.M. Niehues, P. Neuhaus, M. Stockmann, Function and volume recovery after partial hepatectomy: influence of preoperative liver function, residual liver volume, and obesity, *Langenbeck's Archives of Surgery*, 397 (2012) 1297-1304.
- [252] M.-C. Londoño, A. Rimola, J. O'Grady, A. Sanchez-Fueyo, Immunosuppression minimization vs. complete drug withdrawal in liver transplantation, *J Hepatol*, 59 (2013) 872-879.
- [253] O. Loreal, F.o. Levavasseur, C. Fromaget, D. Gros, A. Guillouzo, B. Clement, Cooperation of Ito cells and hepatocytes in the deposition of an extracellular matrix in vitro, *The American journal of pathology*, 143 (1993) 538.
- [254] J. Lovelock, The haemolysis of human red blood-cells by freezing and thawing, *Biochimica et biophysica acta*, 10 (1953) 414-426.
- [255] J. Lovelock, The protective action of neutral solutes against haemolysis by freezing and thawing, *Biochemical Journal*, 56 (1954) 265.
- [256] S.-Z. Lu, J. Hunt, A numerical analysis of dendritic and cellular array growth: the spacing adjustment mechanisms, *Journal of crystal growth*, 123 (1992) 17-34.

- [257] R. Malpique, L.M. Osório, D.S. Ferreira, F. Ehrhart, C. Brito, H. Zimmermann, P.M. Alves, Alginate encapsulation as a novel strategy for the cryopreservation of neurospheres, *Tissue Engineering Part C: Methods*, 16 (2010) 965-977.
- [258] M.E. Mamprin, S. Petrocelli, E. Guibert, J. Rodriguez, A novel BES-gluconate-sucrose (BGS) solution for cold storage of isolated hepatocytes, *Cryo letters*, 29 (2008) 121-133.
- [259] S.F. Marasco, M. Bailey, D. McGlade, G. Snell, G. Westall, T. Oto, D. Pilcher, Effect of donor preservation solution and survival in Lung transplantation, *J Heart Lung Transpl*, 30 (2011) 414-419.
- [260] S. Martin, T. Dahl, L. Epperson, Slow loss of protein integrity during torpor: a cause for arousal, *Life in the Cold. Evolution, Mechanisms, Adaptation, and Application*, 27 (2004) 199-208.
- [261] J. Mase, H. Mizuno, K. Okada, K. Sakai, D. Mizuno, K. Usami, H. Kagami, M. Ueda, Cryopreservation of cultured periosteum: effect of different cryoprotectants and pre-incubation protocols on cell viability and osteogenic potential, *Cryobiology*, 52 (2006) 182-192.
- [262] I. Massie, J. Ross, N. Mallorqui-Fernandez, E. Gherardi, H. Hodgson, C. Selden, B. Fuller, 93. Reducing apoptosis following cryopreservation in encapsulated liver cell spheroids, *Cryobiology*, 61 (2010) 390.
- [263] I. Massie, C. Selden, H. Hodgson, B. Fuller, Cryopreservation of encapsulated liver spheroids for a bioartificial liver: reducing latent cryoinjury using an ice nucleating agent, *Tissue engineering. Part C, Methods*, 17 (2011) 765-774.
- [264] I. Massie, C. Selden, H. Hodgson, B. Fuller, Storage Temperatures for Cold-Chain Delivery in Cell Therapy: A Study of Alginate-Encapsulated Liver Cell Spheroids Stored at -80 degrees C or -170 degrees C for Up to 1 Year, *Tissue Eng Part C-Me*, 19 (2013) 189-195.
- [265] I. Massie, C. Selden, H. Hodgson, B. Fuller, S. Gibbons, G.J. Morris, GMP cryopreservation of large volumes of cells for regenerative medicine: active control of the freezing process, *Tissue engineering. Part C, Methods*, 20 (2014) 693-702.
- [266] I.R. Massie, Development of optimised cryopreservation protocol for encapsulated liver cell spheroids: towards delivery of a bioartificial liver, UCL (University College London), 2012.
- [267] D. Mavri-Damelin, S. Eaton, L.H. Damelin, M. Rees, H.J. Hodgson, C. Selden, Ornithine transcarbamylase and arginase I deficiency are responsible for diminished urea cycle function in the human hepatoblastoma cell line HepG2, *The international journal of biochemistry & cell biology*, 39 (2007) 555-564.
- [268] P. Mazur, Freezing of living cells: mechanisms and implications, *American Journal of Physiology-Cell Physiology*, 247 (1984) C125-C142.
- [269] P. Mazur, The role of intracellular freezing in the death of cells cooled at supraoptimal rates, *Cryobiology*, 14 (1977) 251-272.
- [270] P. Mazur, K.W. Cole, Influence of cell concentration on the contribution of unfrozen fraction and salt concentration to the survival of slowly frozen human erythrocytes, *Cryobiology*, 22 (1985) 509-536.

- [271] P. Mazur, S.P. Leibo, E.H.Y. Chu, A two-factor hypothesis of freezing injury, *Experimental Cell Research*, 71 (1972) 345-355.
- [272] P. Mazur, S.P. Leibo, J. Farrant, E. Chu, M. Hanna, L. Smith, Interactions of cooling rate, warming rate and protective additive on the survival of frozen mammalian cells, *Ciba Foundation Symposium-The Frozen Cell*, Wiley Online Library, 1970, pp. 69-88.
- [273] L.E. McGann, Differing actions of penetrating and nonpenetrating cryoprotective agents, *Cryobiology*, 15 (1978) 382-390.
- [274] L.E. McGann, A.R. Turner, M.J. Allalunis, J.M. Turc, Cryopreservation of Human Peripheral-Blood Stem-Cells - Optimal Cooling and Warming Conditions, *Cryobiology*, 18 (1981) 469-472.
- [275] Q. Meng, Hypothermic preservation of hepatocytes, *Biotechnol Prog*, 19 (2003) 1118-1127.
- [276] H.T. Meryman, *Cryobiology*, Academic P., London, New York,, 1966.
- [277] H.T. Meryman, Cryopreservation of living cells: principles and practice, *Transfusion*, 47 (2007) 935-945.
- [278] E.S. Meza, F. Bertelli, P.R. Goulart, N. Cheung, A. Garcia, The effect of the growth rate on microsegregation: Experimental investigation in hypoeutectic Al-Fe and Al-Cu alloys directionally solidified, *Journal of Alloys and Compounds*, 561 (2013) 193-200.
- [279] M.A. Miller, M.A. Rodrigues, M.A. Glass, S.K. Singh, K.P. Johnston, J.A. Maynard, Frozen-state storage stability of a monoclonal antibody: Aggregation is impacted by freezing rate and solute distribution, *Journal of pharmaceutical sciences*, 102 (2013) 1194-1208.
- [280] R.H. Miller, P. Mazur, Survival of frozen-thawed human red cells as a function of cooling and warming velocities, *Cryobiology*, 13 (1976) 404-414.
- [281] R. Mitteregger, G. Vogt, E. Rossmannith, D. Falkenhagen, Rotary cell culture system (RCCS): a new method for cultivating hepatocytes on microcarriers, *The International journal of artificial organs*, 22 (1999) 816-822.
- [282] O. Miyawaki, S. Kato, K. Watabe, Yield improvement in progressive freeze-concentration by partial melting of ice, *Journal of Food Engineering*, 108 (2012) 377-382.
- [283] O. Miyawaki, L. Liu, K. Nakamura, Effective partition constant of solute between ice and liquid phases in progressive freeze-concentration, *J Food Sci*, 63 (1998) 756-758.
- [284] O. Miyawaki, L. Liu, Y. Shirai, S. Sakashita, K. Kagitani, Tubular ice system for scale-up of progressive freeze-concentration, *Journal of Food Engineering*, 69 (2005) 107-113.
- [285] M. Mizumoto, N. Mori, K. Ogi, Primary Dendrite Growth of Al-Cu Alloy Films between Solid Plates, *Materials Transactions, JIM*, 40 (1999) 248-253.
- [286] E.B. Moore, V. Molinero, Structural transformation in supercooled water controls the crystallization rate of ice, *Nature*, 479 (2011) 506-508.
- [287] G. Morris, E. Acton, K. Faszler, A. Franklin, H. Yin, R. Bodine, J. Pareja, N. Zaninovic, R. Gosden, Cryopreservation of murine embryos, human spermatozoa and embryonic stem cells

using a liquid nitrogen-free, controlled rate freezer, *Reproductive biomedicine online*, 13 (2006) 421-426.

[288] G. Morris, B. Grout, *The Effects of Low Temperatures on Biological Systems*, Edward Arnold 1987.

[289] G.J. Morris, E. Acton, Controlled ice nucleation in cryopreservation--a review, *Cryobiology*, 66 (2013) 85-92.

[290] G.J. Morris, E. Acton, B.J. Murray, F. Fonseca, Freezing injury: the special case of the sperm cell, *Cryobiology*, 64 (2012) 71-80.

[291] G.J. Morris, M. Goodrich, E. Acton, F. Fonseca, The high viscosity encountered during freezing in glycerol solutions: effects on cryopreservation, *Cryobiology*, 52 (2006) 323-334.

[292] E. Morsiani, P. Pazzi, A. Puviani, M. Brogli, L. Valieri, P. Gorini, P. Scoletta, E. Marangoni, R. Ragazzi, G. Azzena, Early experiences with a porcine hepatocyte-based bioartificial liver in acute hepatic failure patients, *The International journal of artificial organs*, 25 (2002) 192-202.

[293] W. Mueller-Klieser, Method for the determination of oxygen consumption rates and diffusion coefficients in multicellular spheroids, *Biophysical journal*, 46 (1984) 343-348.

[294] A. Mukherjee, B. Mishra, R.V. Kumar, Application of liquid/solid fluidization technique in beneficiation of fines, *International Journal of Mineral Processing*, 92 (2009) 67-73.

[295] W.W. Mullins, R. Sekerka, Stability of a planar interface during solidification of a dilute binary alloy, *Journal of applied physics*, 35 (1964) 444-451.

[296] C. Mullan, Z. Pitkin, The HepatAssist® Bioartificial Liver Support System: clinical study and pig hepatocyte process, *Expert opinion on investigational drugs*, 8 (1999) 229-235.

[297] N. Murase, F. Franks, Salt Precipitation during the Freeze-Concentration of Phosphate Buffer Solutions, *Biophys Chem*, 34 (1989) 293-300.

[298] B.M. Murphy, S. Swarts, B.M. Mueller, P. van der Geer, M.C. Manning, M.I. Fitchmun, Protein instability following transport or storage on dry ice, *Nature methods*, 10 (2013) 278-279.

[299] C. Murray, J. Riley, The solubility of gases in distilled water and sea water—II. Oxygen, *Deep Sea Research and Oceanographic Abstracts*, Elsevier, 1969, pp. 311-320.

[300] S. Nadalin, G. Testa, M. Malagó, M. Beste, A. Frilling, T. Schroeder, C. Jochum, G. Gerken, C.E. Broelsch, Volumetric and functional recovery of the liver after right hepatectomy for living donation, *Liver Transplant*, 10 (2004) 1024-1029.

[301] Y. Nagahara, H. Sekine, M. Otaki, M. Hayashi, N. Murase, Use of high concentrations of dimethyl sulfoxide for cryopreservation of HepG2 cells adhered to glass and polydimethylsiloxane matrices, *Cryobiology*, DOI (2015).

[302] K. Nakagawa, S. Maebashi, K. Maeda, Freeze-thawing as a path to concentrate aqueous solution, *Separation and Purification Technology*, 73 (2010) 403-408.

[303] T. Nei, Mechanism of hemolysis of erythrocytes by freezing at near-zero temperatures: II. Investigations of factors affecting hemolysis by freezing, *Cryobiology*, 4 (1968) 303-308.

- [304] F. Nevens, W. Laleman, Artificial liver support devices as treatment option for liver failure, *Best Practice & Research Clinical Gastroenterology*, 26 (2012) 17-26.
- [305] G.A.A. Nibourg, M.T. Huisman, T.V. van der Hoeven, T.M. van Gulik, R.A.F.M. Chamuleau, R. Hoekstra, Stable overexpression of Pregnane X receptor in HepG2 cells increases its potential for bioartificial liver application, *Liver Transplant*, 16 (2010) 1075-1085.
- [306] S.L. Nyberg, S.A. Mao, J.M. Glorioso, Bioartificial Liver, in: L.M.M.N. Mitchell (Ed.) *Pathobiology of Human Disease*, Academic Press, San Diego, 2014, pp. 1800-1808.
- [307] S.L. Nyberg, M.V. Peshwa, W.D. Payne, W.-S. Hu, F.B. Cerra, Evolution of the bioartificial liver: The need for randomized clinical trials, *The American Journal of Surgery*, 166 (1993) 512-521.
- [308] S.L. Nyberg, R.P. Remmel, H.J. Mann, M.V. Peshwa, W.S. Hu, F.B. Cerra, Primary hepatocytes outperform Hep G2 cells as the source of biotransformation functions in a bioartificial liver, *Ann Surg*, 220 (1994) 59-67.
- [309] Y. Ohsaka, S. Ohgiya, T. Hoshino, K. Ishizaki, Mitochondrial genome-encoded ATPase subunit 6+8 mRNA increases in human hepatoblastoma cells in response to nonfatal cold stress, *Cryobiology*, 40 (2000) 92-101.
- [310] M. Okamoto, N. Nakagata, Y. Toyoda, Cryopreservation and transport of mouse spermatozoa at -79 degrees C, *Exp Anim Tokyo*, 50 (2001) 83-86.
- [311] G. Orive, R.M. Hernandez, A.R. Gascon, M. Igartua, J.L. Pedraz, Survival of different cell lines in alginate-agarose microcapsules, *Eur J Pharm Sci*, 18 (2003) 23-30.
- [312] G. Orlando, *Regenerative Medicine Applications in Organ Transplantation*, Elsevier Science 2013.
- [313] G. Ostapowicz, R.J. Fontana, F.V. Schiødt, A. Larson, T.J. Davern, S.H.B. Han, T.M. McCashland, A.O. Shakil, J.E. Hay, L. Hynan, J.S. Crippin, A.T. Blei, G. Samuel, J. Reisch, W.M. Lee, Results of a Prospective Study of Acute Liver Failure at 17 Tertiary Care Centers in the United States, *Annals of Internal Medicine*, 137 (2002) 947-954.
- [314] A. Ostróзка-Cieslik, B. Dolinska, M. Krzysztofik, A. Caban, F. Ryszka, Z. Smorag, Influence of the selected antioxidants on the stability of the ViaSpan solution used for perfusion and organ preservation purposes, *Latin American Journal of Pharmacy*, 30 (2011).
- [315] T. Owadano, Redistribution of Solute during Cellular Solidification of Single Phase Alloys, *Materials transactions*, 51 (2010) 969-976.
- [316] A.A. Palakkan, D.K. Raj, J. Rojan, S. Raj R.G, P.R. Anil Kumar, C.V. Muraleedharan, T.V. Kumary, Evaluation of Polypropylene Hollow-Fiber Prototype Bioreactor for Bioartificial Liver, *Tissue Engineering Part A*, 19 (2012) 1056-1066.
- [317] J. Parks, J. Graham, Effects of cryopreservation procedures on sperm membranes, *Theriogenology*, 38 (1992) 209-222.
- [318] A. Partyka, E. Łukaszewicz, W. Nizański, Effect of cryopreservation on sperm parameters, lipid peroxidation and antioxidant enzymes activity in fowl semen, *Theriogenology*, 77 (2012) 1497-1504.

- [319] J.F. Patzer, Oxygen consumption in a hollow fiber bioartificial liver—revisited, *Artif Organs*, 28 (2004) 83-98.
- [320] B. Paudel, Z.-G. Feng, Prediction of minimum fluidization velocity for binary mixtures of biomass and inert particles, *Powder technology*, 237 (2013) 134-140.
- [321] P. Pedotti, M. Cardillo, P. Rigotti, G. Gerunda, R. Merenda, U. Cillo, G. Zanus, U. Bacarani, M.L. Berardinelli, L. Boschiero, A comparative prospective study of two available solutions for kidney and liver preservation, *Transplantation*, 77 (2004) 1540-1545.
- [322] D. Pegg, The history and principles of cryopreservation, *Seminars in reproductive medicine*, 2002, pp. 5-13.
- [323] D.E. Pegg, Principles of cryopreservation, *Cryopreservation and freeze-drying protocols*, DOI (2007) 39-57.
- [324] D.E. Pegg, The relevance of ice crystal formation for the cryopreservation of tissues and organs, *Cryobiology*, 60 (2010) S36-S44.
- [325] D.E. Pegg, L. Wang, D. Vaughan, Cryopreservation of articular cartilage. Part 3: the liquidus-tracking method, *Cryobiology*, 52 (2006) 360-368.
- [326] R.G. Pereyra, I. Szleifer, M.A. Carignano, Temperature dependence of ice critical nucleus size, *The Journal of chemical physics*, 135 (2011) 034508.
- [327] M. Perotti, F. Toddei, F. Mirabelli, M. Vairetti, G. Bellomo, D.J. Mcconkey, S. Orrenius, Calcium-Dependent DNA Fragmentation in Human Synovial-Cells Exposed to Cold Shock, *Febs Lett*, 259 (1990) 331-334.
- [328] A. Petersen, H. Schneider, G. Rau, B. Glasmacher, A new approach for freezing of aqueous solutions under active control of the nucleation temperature, *Cryobiology*, 53 (2006) 248-257.
- [329] H. Petrowsky, P.-A. Clavien, Chapter 44 - Principles of Liver Preservation, in: R.W.B.B.G. Klintmalm (Ed.) *Transplantation of the Liver (Third Edition)*, W.B. Saunders, Philadelphia, 2015, pp. 582-599.
- [330] G. Petzold, J.M. Aguilera, Ice morphology: fundamentals and technological applications in foods, *Food Biophysics*, 4 (2009) 378-396.
- [331] S. Phadtare, J. Alsina, M. Inouye, Cold shock response and cold-shock proteins, *Curr Opin Microbiol*, 2 (1999) 175-180.
- [332] B.P. Piasecki, K.R. Diller, J.J. Brand, Cryopreservation of *Chlamydomonas reinhardtii*: A cause of low viability at high cell density, *Cryobiology*, 58 (2009) 103-109.
- [333] Z. Pitkin, C. Mullon, Evidence of absence of porcine endogenous retrovirus (PERV) infection in patients treated with a bioartificial liver support system, *Artif Organs*, 23 (1999) 829-833.
- [334] G. Pless, Artificial and bioartificial liver support, *Organogenesis*, 3 (2007) 20-24.
- [335] A.S. Podoll, A. DeGolovine, K.W. Finkel, Liver support systems—a review, *Asaio Journal*, 58 (2012) 443-449.

- [336] A. Polge, A. Smith, A. Parks, Survival of spermatozoa after dehydration and vitrification at low temperature, *Nature*, 164 (1949) 666.
- [337] C. Pradistsuwana, P. Theprugsa, O. Miyawaki, Measurement of limiting partition coefficient in progressive freeze-concentration, *Food science and technology research*, 9 (2003) 190-192.
- [338] J.A. Preciado, B. Rubinsky, Isochoric preservation: A novel characterization method, *Cryobiology*, 60 (2010) 23-29.
- [339] S. Rahman, J. Ahmed, *Handbook of Food Process Design*, Wiley 2012.
- [340] W.F. Rall, G.M. Fahy, Ice-free cryopreservation of mouse embryos at -196 C by vitrification, *DOI* (1985).
- [341] D. Rasmussen, A. MacKenzie, Phase diagram for the system water-dimethylsulphoxide, *DOI* (1968).
- [342] S.K. Ratkje, O. Flesland, Modelling the freeze concentration process by irreversible thermodynamics, *Journal of food engineering*, 25 (1995) 553-568.
- [343] U. Rauen, B. Polzar, H. Stephan, H.G. Mannherz, H. de Groot, Cold-induced apoptosis in cultured hepatocytes and liver endothelial cells: mediation by reactive oxygen species, *Faseb J*, 13 (1999) 155-168.
- [344] T. Renganathan, K. Krishnaiah, Voidage characteristics and prediction of bed expansion in liquid-solid inverse fluidized bed, *Chemical engineering science*, 60 (2005) 2545-2555.
- [345] J. Richardson, Incipient fluidization and particulate systems. *Fluidization*, editors: Davidson IF, Harrison D., Chapt. 2, Academic Press, London and New York, 1971.
- [346] J.t. RICHARDSON, Sedimentation and fluidisation: Part I, *Trans. Inst. Chem. Eng.*, 32 (1954) 35-53.
- [347] M.A. Rodrigues, M.A. Miller, M.A. Glass, S.K. Singh, K.P. Johnston, Effect of freezing rate and dendritic ice formation on concentration profiles of proteins frozen in cylindrical vessels, *Journal of pharmaceutical sciences*, 100 (2011) 1316-1329.
- [348] H. Rodriguez-Martinez, Cryopreservation of porcine gametes, embryos and genital tissues: state of the art, *INTECH Open Access Publisher* 2012.
- [349] T.L. Roth, L.M. Bush, D.E. Wildt, R.B. Weiss, Scimitar-horned oryx (*Oryx dammah*) spermatozoa are functionally competent in a heterologous bovine in vitro fertilization system after cryopreservation on dry ice, in a dry shipper, or over liquid nitrogen vapor, *Biol Reprod*, 60 (1999) 493-498.
- [350] P. Rowe, A convenient empirical equation for estimation of the Richardson-Zaki exponent, *Chemical Engineering Science*, 42 (1987) 2795-2796.
- [351] B. Rubinsky, E.G. Cravalho, An analytical method to evaluate cooling rates during cryopreservation protocols for organs, *Cryobiology*, 21 (1984) 303-320.

- [352] B. Rubinsky, P.A. Perez, M.E. Carlson, The thermodynamic principles of isochoric cryopreservation, *Cryobiology*, 50 (2005) 121-138.
- [353] P.S. Ruggera, G.M. Fahy, Rapid and uniform electromagnetic heating of aqueous cryoprotectant solutions from cryogenic temperatures, *Cryobiology*, 27 (1990) 465-478.
- [354] A. Sakai, F. Engelmann, Vitrification, encapsulation-vitrification and droplet-vitrification: a review, *CryoLetters*, 28 (2007) 151-172.
- [355] M. Saliem, F. Holm, R.B. Tengzelius, C. Jorns, L.-M. Nilsson, B.-G. Ericzon, E. Ellis, O. Hovatta, Improved cryopreservation of human hepatocytes using a new xeno free cryoprotectant solution, *World journal of hepatology*, 4 (2012) 176.
- [356] J. Saragusty, H. Gacitua, I. Rozenboim, A. Arav, Do physical forces contribute to cryodamage?, *Biotechnol Bioeng*, 104 (2009) 719-728.
- [357] S. Sargent, *Liver Diseases: An Essential Guide for Nurses and Health Care Professionals*, Wiley 2009.
- [358] J. Schmitt, H.-C. Flemming, FTIR-spectroscopy in microbial and material analysis, *International Biodeterioration & Biodegradation*, 41 (1998) 1-11.
- [359] D. Schuppan, N.H. Afdhal, Liver cirrhosis, *The Lancet*, 371 (2008) 838-851.
- [360] M. Schwaiblmair, C. Vogelmeier,  $\alpha$ 1-Antitrypsin, *Drugs & Aging*, 12 (1998) 429-440.
- [361] D.L. Scroggie, E. Erro, J.T. Bundy, A. Le Lay, D. Davis, S.R. Modi, B. Fuller, C. Selden, Ambient temperature short-term preservation of liver cells for bioengineering applications using perfluorodecalin as an oxygen source, *Hepatology*, 60 (2014) 557a-557a.
- [362] J.A. Searles, J.F. Carpenter, T.W. Randolph, The ice nucleation temperature determines the primary drying rate of lyophilization for samples frozen on a temperature-controlled shelf, *Journal of pharmaceutical sciences*, 90 (2001) 860-871.
- [363] C. Selden, C.W. Spearman, D. Kahn, M. Miller, A. Figaji, E. Erro, J. Bundy, I. Massie, S.-A. Chalmers, H. Arendse, Evaluation of encapsulated liver cell spheroids in a fluidised-bed bioartificial liver for treatment of ischaemic acute liver failure in pigs in a translational setting, *PloS one*, 8 (2013) e82312.
- [364] M. Serra, C. Correia, R. Malpique, C. Brito, J. Jensen, P. BJORQUIST, M.J.T. Carrondo, P.M. Alves, Microencapsulation Technology: A Powerful Tool for Integrating Expansion and Cryopreservation of Human Embryonic Stem Cells, *PloS one*, 6 (2011).
- [365] D. Shah, M. Naciri, P. Clee, M. Al-Rubeai, NucleoCounter—an efficient technique for the determination of cell number and viability in animal cell culture processes, *Cytotechnology*, 51 (2006) 39-44.
- [366] J. Shapiro, Freezing-out, a safe technique for concentration of dilute solutions, *Science*, 133 (1961) 2063-2064.
- [367] B.J. Sinclair, D. Renault, Intracellular ice formation in insects: Unresolved after 50 years?, *Comparative Biochemistry and Physiology Part A: Molecular & Integrative Physiology*, 155 (2010) 14-18.

- [368] K.J. Singh, Y.H. Roos, State transitions and freeze concentration in trehalose–protein–cornstarch mixtures, *LWT-Food Science and Technology*, 39 (2006) 930-938.
- [369] M. Smith, A. Smirthwaite, D. Cairns, R. Cousins, J. Gaylor, Techniques for measurement of oxygen consumption rates of hepatocytes during attachment and post-attachment, *The International journal of artificial organs*, 19 (1996) 36-44.
- [370] V.G. Smith, W.A. Tiller, J. Rutter, A mathematical analysis of solute redistribution during solidification, *Canadian Journal of Physics*, 33 (1955) 723-745.
- [371] S. Sobolev, Effects of local non-equilibrium solute diffusion on rapid solidification of alloys, *physica status solidi (a)*, 156 (1996) 293-303.
- [372] S. Sobolev, Local non-equilibrium diffusion model for solute trapping during rapid solidification, *Acta materialia*, 60 (2012) 2711-2718.
- [373] A.-K. Sohlenius-Sternbeck, Determination of the hepatocellularity number for human, dog, rabbit, rat and mouse livers from protein concentration measurements, *Toxicology in Vitro*, 20 (2006) 1582-1586.
- [374] A.-K. Sohlenius-Sternbeck, Response to comment on “Determination of the hepatocellularity number for human, dog, rabbit, rat and mouse livers from protein concentration measurements”, *Toxicology in Vitro*, 21 (2007) 1694.
- [375] E. Sokolov, A.L. Eheim, W.A. Ahrens, T.L. Walling, J.H. Swet, M.T. McMillan, K.A. Simo, K.J. Thompson, D. Sindram, I.H. McKillop, Lysophosphatidic acid receptor expression and function in human hepatocellular carcinoma, *Journal of Surgical Research*, 180 (2013) 104-113.
- [376] L.A. Sonna, J. Fujita, S.L. Gaffin, C.M. Lilly, Invited review: Effects of heat and cold stress on mammalian gene expression, *Journal of applied physiology*, 92 (2002) 1725-1742.
- [377] M.N. Sosef, J.M. Baust, K. Sugimachi, A. Fowler, R.G. Tompkins, M. Toner, Cryopreservation of isolated primary rat hepatocytes - Enhanced survival and long-term hepatospecific function, *Ann Surg*, 241 (2005) 125-133.
- [378] A. Soto-Gutierrez, N. Navarro-Alvarez, J.D. Rivas-Carrillo, K. Tanaka, Y. Chen, H. Misawa, T. Okitsu, H. Noguchi, N. Tanaka, N. Kobayashi, Construction and transplantation of an engineered hepatic tissue using a polyaminourethane-coated nonwoven polytetrafluoroethylene fabric, *Transplantation*, 83 (2007) 129-137.
- [379] A. Sputtek, M. Lioznov, N. Kroger, A.W. Rowe, Bioequivalence comparison of a new freezing bag (CryoMACS (R)) with the Cryocyte (R) freezing bag for cryogenic storage of human hematopoietic progenitor cells, *Cytotherapy*, 13 (2011) 481-489.
- [380] J. Stange, S. Mitzner, T. Risler, C. Erley, W. Lauchart, H. Goehl, S. Klammt, P. Peszynski, J. Freytag, H. Hickstein, Molecular adsorbent recycling system (MARS): clinical results of a new membrane-based blood purification system for bioartificial liver support, *ARTIFICIAL ORGANS-OHIO-*, 23 (1999) 319-330.
- [381] D. Stefanescu, *Science and Engineering of Casting Solidification*, Springer International Publishing 2015.

- [382] P. Stefanovich, R. Ezzell, S. Sheehan, R. Tompkins, M. Yarmush, M. Toner, Effects of hypothermia on the function, membrane integrity, and cytoskeletal structure of hepatocytes, *Cryobiology*, 32 (1995) 389-403.
- [383] V. Stensvaag, T. Furmanek, K. Lønning, A. Terzis, R. Bjerkvig, T. Visted, Cryopreservation of alginate-encapsulated recombinant cells for antiangiogenic therapy, *Cell transplantation*, 13 (2004) 35-44.
- [384] X. Stephenne, M. Najimi, E.M. Sokal, Hepatocyte cryopreservation: is it time to change the strategy?, *World J Gastroentero*, 16 (2010) 1-14.
- [385] D. Stevenson, C. Morgan, E. Goldie, G. Connel, M. Grant, Cryopreservation of viable hepatocyte monolayers in cryoprotectant media with high serum content: metabolism of testosterone and kaempherol post-cryopreservation, *Cryobiology*, 49 (2004) 97-113.
- [386] G.G. Stokes, On the effect of the internal friction of fluids on the motion of pendulums.
- [387] A. Stolzing, Y. Naaldijk, V. Fedorova, S. Sethe, Hydroxyethylstarch in cryopreservation—Mechanisms, benefits and problems, *Transfusion and Apheresis Science*, 46 (2012) 137-147.
- [388] K.B. Storey, J.M. Storey, Natural freezing survival in animals, *Annual Review of Ecology and Systematics*, DOI (1996) 365-386.
- [389] A.J. Strain, J.M. Neuberger, A Bioartificial Liver--State of the Art, *Science*, 295 (2002) 1005-1009.
- [390] W. Strober, Trypan Blue Exclusion Test of Cell Viability, *Current Protocols in Immunology*, John Wiley & Sons, Inc.2001.
- [391] M. Swain, R.F. Butterworth, A.T. Blei, Ammonia and related amino acids in the pathogenesis of brain edema in acute ischemic liver failure in rats, *Hepatology*, 15 (1992) 449-453.
- [392] C. Swaminathan, V. Voller, Towards a general numerical scheme for solidification systems, *International Journal of Heat and Mass Transfer*, 40 (1997) 2859-2868.
- [393] S.A. Szobota, B. Rubinsky, Analysis of isochoric subcooling, *Cryobiology*, 53 (2006) 139-142.
- [394] J. Szein, K. Noble, J. Farley, L. Mobraaten, Comparison of permeating and nonpermeating cryoprotectants for mouse sperm cryopreservation, *Cryobiology*, 42 (2001) 28-39.
- [395] T. Takahashi, A. Kakita, Y. Takahashi, K. Yokoyama, I. Sakamoto, S. Yamashina, Preservation of rat livers by supercooling under high pressure, *Transpl P*, Elsevier, 2001, pp. 916-919.
- [396] T. Takeo, T. Kaneko, Y. Haruguchi, K. Fukumoto, H. Machida, M. Koga, Y. Nakagawa, Y. Takeshita, T. Matsuguma, S. Tsuchiyama, N. Shimizu, T. Hasegawa, M. Goto, H. Miyachi, M. Anzai, E. Nakatsukasa, K. Nomaru, N. Nakagata, Birth of mice from vitrified/warmed 2-cell embryos transported at a cold temperature, *Cryobiology*, 58 (2009) 196-202.
- [397] N.J. Talley, K.D. Lindor, H.E. Vargas, *Practical Gastroenterology and Hepatology: Liver and Biliary Disease*, Wiley2011.

- [398] K. Tanikawa, T. Ueno, *Liver Diseases and Hepatic Sinusoidal Cells*, Springer Japan 2012.
- [399] K. Taylor, P. Roberts, K. Sanders, P. Burton, Effect of antioxidant supplementation of cryopreservation medium on post-thaw integrity of human spermatozoa, *Reproductive biomedicine online*, 18 (2009) 184-189.
- [400] M.J. Taylor, Y. Song, B. Kheirabadi, F. Lightfoot, K. Brockbank, Vitrification fulfills its promise as an approach to reducing freeze-induced injury in a multicellular tissue, *ASME-PUBLICATIONS-HTD*, 363 (1999) 93-102.
- [401] R. Taylor, G. Adams, C. Boardman, R. Wallis, Cryoprotection—permeant vs nonpermeant additives, *Cryobiology*, 11 (1974) 430-438.
- [402] C. Terry, A. Dhawan, R.R. Mitry, R.D. Hughes, Cryopreservation of isolated human hepatocytes for transplantation: State of the art, *Cryobiology*, 53 (2006) 149-159.
- [403] C. Terry, A. Dhawan, R.R. Mitry, S.C. Lehec, R.D. Hughes, Optimization of the Cryopreservation and Thawing Protocol for Human Hepatocytes for Use in Cell Transplantation, *Liver Transplant*, 16 (2010) 229-237.
- [404] C. Terry, A. Dhawan, R.R. Mitry, S.C. Lehec, R.D. Hughes, Preincubation of rat and human hepatocytes with cytoprotectants prior to cryopreservation can improve viability and function upon thawing, *Liver Transplant*, 12 (2006) 165-177.
- [405] W. Tiller, K. Jackson, J. Rutter, B. Chalmers, The redistribution of solute atoms during the solidification of metals, *Acta metallurgica*, 1 (1953) 428-437.
- [406] H. Tominaga, M. Ishiyama, F. Ohseto, K. Sasamoto, T. Hamamoto, K. Suzuki, M. Watanabe, A water-soluble tetrazolium salt useful for colorimetric cell viability assay, *Analytical Communications*, 36 (1999) 47-50.
- [407] M. Toner, E. Cravalho, D. Armant, Water transport and estimated transmembrane potential during freezing of mouse oocytes, *The Journal of membrane biology*, 115 (1990) 261-272.
- [408] M. Toner, E.G. Cravalho, M. Karel, Thermodynamics and kinetics of intracellular ice formation during freezing of biological cells, *Journal of Applied Physics*, 67 (1990) 1582-1593.
- [409] M. Toner, R.G. Tompkins, E.G. Cravalho, M.L. Yarmush, Transport phenomena during freezing of isolated hepatocytes, *AIChE journal*, 38 (1992) 1512-1522.
- [410] F.S. Trad, M. Toner, J.D. Biggers, Effects of cryoprotectants and ice-seeding temperature on intracellular freezing and survival of human oocytes, *Human reproduction*, 14 (1999) 1569-1577.
- [411] N.M. Tran, M. Dufresne, F. Helle, T.W. Hoffmann, C. Francois, E. Brochot, P. Paullier, C. Legallais, G. Duverlie, S. Castelain, Alginate hydrogel protects encapsulated hepatic HuH-7 cells against hepatitis C virus and other viral infections, *PLoS one*, 9 (2014) e109969.
- [412] A. Tripathy, A. Sahu, S. Biswal, B. Mishra, A model for expansion ratio in liquid–solid fluidized beds, *Particuology*, 11 (2013) 789-792.

- [413] R. Trivedi, J. Lipton, W. Kurz, Effect of growth rate dependent partition coefficient on the dendritic growth in undercooled melts, *Acta Metallurgica*, 35 (1987) 965-970.
- [414] B.F. Trump, D.E. Young, E.A. Arnold, R.E. Stowell, Effects of freezing and thawing on the structure, chemical constitution, and function of cytoplasmic structures, DTIC Document, 1965.
- [415] M. Tsujimoto, S. Imura, H. Kanda, Recovery and reproduction of an Antarctic tardigrade retrieved from a moss sample frozen for over 30 years, *Cryobiology*, DOI (2015).
- [416] R. Turton, N. Clark, An explicit relationship to predict spherical particle terminal velocity, *Powder technology*, 53 (1987) 127-129.
- [417] K. Umeshita, M. Monden, T. Fujimori, H. Sakai, M. Gotoh, J. Okamura, T. Mori, Extracellular calcium protects cultured rat hepatocytes from injury caused by hypothermic preservation, *Cryobiology*, 25 (1988) 102-109.
- [418] D.P. Valencia, F.J. González, Understanding the linear correlation between diffusion coefficient and molecular weight. A model to estimate diffusion coefficients in acetonitrile solutions, *Electrochemistry Communications*, 13 (2011) 129-132.
- [419] R. Van der Sman, A. Voda, G. van Dalen, A. Duijster, Ice crystal interspacing in frozen foods, *Journal of Food Engineering*, 116 (2013) 622-626.
- [420] A. Van Herwaarden, P. Sarro, Thermal sensors based on the Seebeck effect, *Sensors and Actuators*, 10 (1986) 321-346.
- [421] J. van Meerloo, G.J.L. Kaspers, J. Cloos, Cell Sensitivity Assays: The MTT Assay, in: A.I. Cree (Ed.) *Cancer Cell Culture: Methods and Protocols*, Humana Press, Totowa, NJ, 2011, pp. 237-245.
- [422] S. Vidyasagar, K. Krishnaiah, P. Sai, Macroscopic properties of liquid–solid circulating fluidized bed with viscous liquid medium, *Chemical Engineering and Processing: Process Intensification*, 50 (2011) 42-52.
- [423] R. Viskanta, M. Bianchi, J. Critser, D. Gao, Solidification processes of solutions, *Cryobiology*, 34 (1997) 348-362.
- [424] A. Voda, N. Homan, M. Witek, A. Duijster, G. van Dalen, R. van der Sman, J. Nijse, L. van Vliet, H. Van As, J. van Duynhoven, The impact of freeze-drying on microstructure and rehydration properties of carrot, *Food Research International*, 49 (2012) 687-693.
- [425] V. Voller, A. Mouchmov, M. Cross, An explicit scheme for coupling temperature and concentration fields in solidification models, *Applied Mathematical Modelling*, 28 (2004) 79-94.
- [426] V.R. Voller, A numerical scheme for solidification of an alloy, *Canadian metallurgical quarterly*, 37 (1998) 169-177.
- [427] C.T. Wagner, M.B. Burnett, S.A. Livesey, J. Connor, Red blood cell stabilization reduces the effect of cell density on recovery following cryopreservation, *Cryobiology*, 41 (2000) 178-194.
- [428] M. Wakisaka, Y. Shirai, S. Sakashita, Ice crystallization in a pilot-scale freeze wastewater treatment system, *Chemical Engineering and Processing: Process Intensification*, 40 (2001) 201-208.

- [429] T. Wang, G. Zhao, X.M. Liang, Y. Xu, Y. Li, H. Tang, R. Jiang, D. Gao, Numerical simulation of the effect of superparamagnetic nanoparticles on microwave rewarming of cryopreserved tissues, *Cryobiology*, 68 (2014) 234-243.
- [430] X. Wang, Y. Wang, Apoptosis-like death was involved in freeze-drying-preserved fungus *Mucor rouxii* and can be inhibited by l-proline, *Cryobiology*, DOI (2015).
- [431] J.A. Warren, J. Langer, Prediction of dendritic spacings in a directional-solidification experiment, *Physical Review E*, 47 (1993) 2702.
- [432] C. Wassenaar, E.G. Wijsmuller, L.A. Van Herwerden, Z. Aghai, C.L. Van Tricht, E. Bos, Cracks in cryopreserved aortic allografts and rapid thawing, *The Annals of thoracic surgery*, 60 (1995) S165-167.
- [433] S.D. Webb, J.N. WEBB, T.G. HUGHES, D.F. SESIN, A.C. KINCAID, Freezing bulk-scale biopharmaceuticals using common techniques: and the magnitude of freeze-concentration, *Biopharm*, 15 (2002) 22-34.
- [434] J. Wegener, K. Bienefeld, Toxicity of cryoprotectants to honey bee semen and queens, *Theriogenology*, 77 (2012) 600-607.
- [435] F. Weise, U. Fernekorn, J. Hampl, M. Klett, A. Schober, Analysis and comparison of oxygen consumption of HepG2 cells in a monolayer and three-dimensional high density cell culture by use of a matrigrid®, *Biotechnol Bioeng*, 110 (2013) 2504-2512.
- [436] R. Weiss, The solubility of nitrogen, oxygen and argon in water and seawater, *Deep Sea Research and Oceanographic Abstracts*, Elsevier, 1970, pp. 721-735.
- [437] R.A. Weiss, The Leeuwenhoek Lecture 2001. Animal origins of human infectious disease, *Philosophical Transactions of the Royal Society of London B: Biological Sciences*, 356 (2001) 957-977.
- [438] T.P. West, M.B. Ravindra, J.E. Preece, Encapsulation, cold storage, and growth of *Hibiscus moscheutos* nodal segments, *Plant Cell Tiss Org*, 87 (2006) 223-231.
- [439] P. Westh, Preferential interaction of dimethyl sulfoxide and phosphatidyl choline membranes, *Biochimica et Biophysica Acta (BBA)-Biomembranes*, 1664 (2004) 217-223.
- [440] F. White, *Fluid Mechanics*, McGraw-Hill Education 2015.
- [441] F. White, *Viscous Fluid Flow*, McGraw-Hill Education 2005.
- [442] C. Wilke, P. Chang, Correlation of diffusion coefficients in dilute solutions, *AIChE Journal*, 1 (1955) 264-270.
- [443] D.P. Williams, R. Shipley, M.J. Ellis, S. Webb, J. Ward, I. Gardner, S. Creton, Novel in vitro and mathematical models for the prediction of chemical toxicity, *Toxicology Research*, 2 (2013) 40-59.
- [444] R. Williams, S.W. Schalm, J.G. O'Grady, Acute liver failure: redefining the syndromes, *The Lancet*, 342 (1993) 273-275.

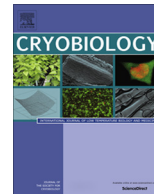
- [445] Z. Wilson, A. Rostami-Hodjegan, J. Burn, A. Tooley, J. Boyle, S. Ellis, G. Tucker, Inter-individual variability in levels of human microsomal protein and hepatocellularity per gram of liver, *British journal of clinical pharmacology*, 56 (2003) 433-440.
- [446] B. Wowk, Anomalous high activity of a subfraction of polyvinyl alcohol ice blocker, *Cryobiology*, 50 (2005) 325-331.
- [447] B. Wowk, Thermodynamic aspects of vitrification, *Cryobiology*, 60 (2010) 11-22.
- [448] B. Wowk, E. Leitel, C.M. Rasch, N. Mesbah-Karimi, S.B. Harris, G.M. Fahy, Vitrification enhancement by synthetic ice blocking agents, *Cryobiology*, 40 (2000) 228-236.
- [449] J.T. Wu, J.A. Knight, In-vitro stability of human alpha-fetoprotein, *Clinical chemistry*, 31 (1985) 1692-1697.
- [450] Y. Wu, H. Yu, S. Chang, R. Magalhães, L.L. Kuleshova, Vitreous cryopreservation of cell-biomaterial constructs involving encapsulated hepatocytes, *Tissue engineering*, 13 (2007) 649-658.
- [451] M. Wusteman, M. Robinson, D. Pegg, Vitrification of large tissues with dielectric warming: biological problems and some approaches to their solution, *Cryobiology*, 48 (2004) 179-189.
- [452] F. Xu, S. Moon, X. Zhang, L. Shao, Y.S. Song, U. Demirci, Multi-scale heat and mass transfer modelling of cell and tissue cryopreservation, *Philosophical Transactions of the Royal Society of London A: Mathematical, Physical and Engineering Sciences*, 368 (2010) 561-583.
- [453] T. Yagi, J.A. Hardin, Y.M. Valenzuela, H. Miyoshi, G.J. Gores, S.L. Nyberg, Caspase inhibition reduces apoptotic death of cryopreserved porcine hepatocytes, *Hepatology*, 33 (2001) 1432-1440.
- [454] J. Yan, B.M. Barnes, F. Kohl, T.G. Marr, Modulation of gene expression in hibernating arctic ground squirrels, *Physiological genomics*, 32 (2008) 170-181.
- [455] J. Yang, A. Renken, A generalized correlation for equilibrium of forces in liquid–solid fluidized beds, *Chemical Engineering Journal*, 92 (2003) 7-14.
- [456] W.C. Yang, *Handbook of Fluidization and Fluid-Particle Systems*, Taylor & Francis 2003.
- [457] P. Yi, G.C. Rutledge, Molecular origins of homogeneous crystal nucleation, *Annual review of chemical and biomolecular engineering*, 3 (2012) 157-182.
- [458] H.D. Young, R.A. Freedman, *Sears and Zemansky's University Physics*, Addison-Wesley 2008.
- [459] M. Young, P. Carroad, R. Bell, Estimation of diffusion coefficients of proteins, *Biotechnol Bioeng*, 22 (1980) 947-955.
- [460] I. Yu, N. Songsasen, R. Godke, S. Leibo, Differences among dogs in response of their spermatozoa to cryopreservation using various cooling and warming rates, *Cryobiology*, 44 (2002) 62-78.

- [461] X. Yu, G. Chen, S. Zhang, A model for predicting the permeation of dimethyl sulfoxide into articular cartilage, and its application to the liquidus-tracking method, *Cryobiology*, 67 (2013) 332-338.
- [462] K.E. Zachariassen, Physiology of cold tolerance in insects, *Physiological reviews*, 65 (1985) 799-832.
- [463] K.E. Zachariassen, E. Kristiansen, Ice nucleation and antinucleation in nature, *Cryobiology*, 41 (2000) 257-279.
- [464] K. Zhang, Y. Guan, X. Yao, Y. Li, X. Fan, S. Brandani, Two-and three-dimensional computational studies of liquid–solid fluidization, *Powder technology*, 235 (2013) 180-191.
- [465] W. Zhang, K. Yi, C. Chen, X. Hou, X. Zhou, Application of antioxidants and centrifugation for cryopreservation of boar spermatozoa, *Animal reproduction science*, 132 (2012) 123-128.
- [466] Y. Zheng, J.-X.J. Zhu, Overall pressure balance and system stability in a liquid–solid circulating fluidized bed, *Chemical Engineering Journal*, 79 (2000) 145-153.



Contents lists available at ScienceDirect

## Cryobiology

journal homepage: [www.elsevier.com/locate/ycryo](http://www.elsevier.com/locate/ycryo)

## A scale down process for the development of large volume cryopreservation <sup>☆</sup>



Peter Kilbride <sup>a,\*</sup>, G. John Morris <sup>b</sup>, Stuart Milne <sup>b</sup>, Barry Fuller <sup>c</sup>, Jeremy Skepper <sup>d</sup>, Clare Selden <sup>a</sup>

<sup>a</sup> Institute of Liver and Digestive Health, Royal Free Hospital Campus, UCL, London NW3 2PF, UK

<sup>b</sup> Asymptote Ltd., St. John's Innovation Centre, Cowley Road, Cambridge CB4 0WS, UK

<sup>c</sup> Department of Surgery, Royal Free Hospital Campus, UCL, London NW3 2PF, UK

<sup>d</sup> Multi Imaging Centre, Anatomy Building, Downing Site, Cambridge University, CB2 3DY, UK

### ARTICLE INFO

#### Article history:

Received 23 June 2014

Accepted 2 September 2014

Available online 16 September 2014

#### Keywords:

Large volume cryopreservation

Bioartificial liver

Undercooling

Network solidification

Progressive solidification

### ABSTRACT

The process of ice formation and propagation during cryopreservation impacts on the post-thaw outcome for a sample. Two processes, either network solidification or progressive solidification, can dominate the water–ice phase transition with network solidification typically present in small sample cryo-straws or cryo-vials. Progressive solidification is more often observed in larger volumes or environmental freezing. These different ice phase progressions could have a significant impact on cryopreservation in scale-up and larger volume cryo-banking protocols necessitating their study when considering cell therapy applications.

This study determines the impact of these different processes on alginate encapsulated liver spheroids (ELS) as a model system during cryopreservation, and develops a method to replicate these differences in an economical manner.

It was found in the current studies that progressive solidification resulted in fewer, but proportionally more viable cells 24 h post-thaw compared with network solidification. The differences between the groups diminished at later time points post-thaw as cells recovered the ability to undertake cell division, with no statistically significant differences seen by either 48 h or 72 h in recovery cultures.

Thus progressive solidification itself should not prove a significant hurdle in the search for successful cryopreservation in large volumes. However, some small but significant differences were noted in total viable cell recoveries and functional assessments between samples cooled with either progressive or network solidification, and these require further investigation.

© 2014 The Authors. Published by Elsevier Inc. This is an open access article under the CC BY license (<http://creativecommons.org/licenses/by/3.0/>).

### Introduction

A bioartificial liver (BAL) machine can temporarily replace the functions of the liver, allowing a damaged liver to regenerate while protecting the patient's other organs from the life-threatening damage that ensues during liver failure. The technology for growing an immortalised hepatocyte cell line (HepG2), encapsulation in alginate beads and proliferating and conditioning of the cell spheroids within the beads has been demonstrated at the large scale. However, widespread uptake of the BAL technology can only

realistically be achieved with cryopreservation as a component of the manufacturing strategy. On demand manufacture of the BAL is not feasible, neither on the basis of cost nor logistics. A single disposable cassette encompassing all processing steps (perfusion, cryopreservation, cell conditioning), would greatly simplify safety and regulatory requirements, provide robust delivery to end users, and facilitate safe delivery in the clinical environment. However, for clinical delivery of a BAL, cryopreservation of up to 2 l of alginate encapsulated cell spheroids (ELS) are required in a single treatment and these would be ideally contained within a cylindrical cell cassette resulting in a packed product depth of up to 70 mm in a cylindrical chamber of length 30 cm held horizontally. While there are reports of the cryopreservation in bags of large volumes (>100 ml) of adult stem cells [25], mammalian tissue culture cells [8,9,12] and ELS [15], the geometry of these samples have been those of a thin slab (2d sample) less than 20 mm in thickness. These experience lesser thermal gradients than in our system.

*Abbreviations:* ELS, encapsulated liver spheroids; PS, progressive solidification; NS, network solidification; BAL, bioartificial liver device.

*\* Statement of funding:* Funding for this work was provided through an MRC (UK) Industrial Case PhD Studentship and through a Technology Strategy Board (UK) funding.

\* Corresponding author. Fax: +44 (0) 207 433 2852.

E-mail address: [peter.kilbride.11@ucl.ac.uk](mailto:peter.kilbride.11@ucl.ac.uk) (P. Kilbride).

<http://dx.doi.org/10.1016/j.cryobiol.2014.09.003>

0011-2240/© 2014 The Authors. Published by Elsevier Inc.

This is an open access article under the CC BY license (<http://creativecommons.org/licenses/by/3.0/>).

The bulk cryopreservation of mammalian cells at a scale and format required for a BAL, or indeed other cell therapies, has not been extensively studied previously.

The physical determinants of the freezing process in either large or small volumes are fundamentally different. In low volume samples (e.g. in straws, or cryovials with volumes <2 ml) at the typical cooling rates used in cryopreservation only small temperature gradients tend to occur throughout the sample. The whole volume generally undercool in a uniform way, i.e. cooled below the equilibrium melting point (the highest temperature at which ice and water can co-exist in steady-state) before ice nucleation commences [18,20,21]. Following the initial ice nucleation, which can be induced by a nucleating agent [6,7], growth of a continuous ice network throughout the whole sample occurs rapidly, resulting in a coexisting, continuous phase of freeze concentrated material in which the excluded solutes and cells are distributed [20]. As a result of the migration of water from the freeze concentrated matrix, this ice network grows as a coherent entity during subsequent cooling. The structure of the ice network and of the corresponding freeze concentrated matrix is determined by the nucleation temperature [3] and not the rate of cooling [24]. In materials science this solidification process is called cellular growth [26]; however in order to avoid confusion when considering cell cryopreservation in a biological context, in which cell growth refers to cell proliferation, we will refer to this mode of ice solidification as network (or dendritic) solidification (NS).

In bulk samples significant temperature gradients may exist between the cooling interface (often the outer surface of the sample) and the bulk volume unless infinitesimally slow cooling rates are applied. Localized undercooling can easily occur at the container wall while there remains a gradient in the bulk sample leading to temperatures remaining above the equilibrium melting point for a significant time [19]. Nucleation of ice will occur at the cold wall and ice will develop into the solution which was initially at a temperature above the equilibrium melting point. As cooling progresses across the sample and the ice nucleation temperature is achieved, an ice front perpendicular to the heat transfer vector front moves through the sample [23]. The structure of the ice front is determined by a number of factors including the nucleation temperature, the rate of heat extraction, and localized inhomogeneities in temperature across the ice front, further complicated by release of latent heat of the ice crystallization process [18]. Depending on the solute composition and the rate of growth of the ice front, solute rejection (including rejection of structures such as cells) can occur ahead of the advancing ice interface [5,14]. In this configuration, only the small proportion of the sample in contact with the cold wall was initially undercooled to any significant degree. In metallurgy this mode of solidification is referred to as progressive or parallel solidification [26] and we shall refer to this as PS when considering ice formation.

In order to develop protocols rapidly and efficiently for the cryopreservation of large volumes it is necessary to develop and validate a scale down method to emulate the process of ice formation that occurs within a large volume in comparison to that within a standard cryovial. This approach allows multiple samples to be tested within the same run, and also the effects of thawing to be decoupled from the freezing step which produces either PS or NS. We also designed a technique to reliably produce PS in small volumes, removing the compounding factor of sample volume on the ice solidification process. In this study, we examined the viability and cell function of ELS (where we have extensive previous experience of post-cryopreservation functional assessment) [15–17] following either PS or NS. In addition we determined, by CryoSEM, the structure of the ice crystal networks and the residual freeze concentrated matrix following water to ice phase transition by these two methods.

## Materials and methods

### Cell culture and encapsulation

The techniques for producing ELS have been described previously in detail [4]. HepG2 cells (human-derived hepatocyte cell-line) were grown in monolayer culture for 7 days and passaged at 80–90% confluence. Culture medium composed of alpha-MEM medium, supplemented with 50 U/ml penicillin, 50 µg/ml streptomycin (Invitrogen plc.), and 10% FCS (Hyclone Thermo Scientific). A suspension of  $3.5 \times 10^6$  cells/ml in culture medium mixed 1:1 with 2% aqueous alginate solution (FMC bio-polymers), was passed through a jetcutter system (GeniaLab), resulting in spherical droplets with a diameter of 500–550 µm, which were polymerised by ejection into a buffer with 0.204 M CaCl<sub>2</sub>. These (ELS) were grown in culture medium at a ratio of beads to medium of 1:32 in static culture (T175 flasks) in a 5% CO<sub>2</sub> humidified incubator at 37 °C for 11 days, with medium changed every 2–3 days, where they proliferated to approximately  $1 \times 10^7$  cells/ml.

### Establishment of cooling profiles in a representative large scale volume containing an ELS thermal mimic

For typical PS in a true large volume experiment, a prototype of the cylindrical BAL cassette constructed out of polycarbonate and containing 2000 ml of a 10% glycerol in water (v/v) solution as an ELS thermal mimic was cooled on its side on a modified VIAFreeze controlled rate freezer (Asymptote, Cambridge, UK). Good thermal contact was achieved via a curved plate attached to the cassette (Fig. 2). To ensure good thermal contact between the cassette and the sample plate a film of low temperature silicone oil (Sigma, 85409) was applied to the sample plate. Thermocouples were placed throughout the chamber to measure thermal profiles in the ELS thermal mimic, using 10% glycerol which we have established previously has equivalent thermal properties to our alginate encapsulated biomass (data not shown).

### Modification of the controlled rate freezer to achieve NS or PS in small volumes during cryopreservation

A controlled rate freezer (EF600-103, Asymptote, Cambridge, UK) was modified to achieve either NS or PS during cryopreservation by the addition of two modules designed to take polypropylene scintillation vials (Sigma, Z376825, 16 mm × 57 mm). One module was made of aluminum, the other of acetal (Fig. 1); these materials are good and poor conductors of heat respectively. These modules were fixed to the flat cooling plate of the EF600-103. Thermocouples (K type) we used to measure the temperature at the base, middle, and upper sample volume inside the vial, (0 mm, 20 mm, and 40 mm from base respectively) the thermocouples were connected to a Pico Logger (Pico-technology).

### Cryopreservation protocol

For small volume PS or NS studies, 5 ml aliquots of ELS were harvested and mixed 1:1 with a freezing solution (24% Me<sub>2</sub>SO, 76% Viaspan v/v) precooled to 4 °C, and once equilibrated (15 min), 80% of the excess CPA supernatant was removed, giving a final volume of 6 ml of 12% Me<sub>2</sub>SO, 38% Viaspan, and 50% ELS in culture medium, by volume. Icestart beads (1% w/v) (Asymptote) – sterile insoluble granules – which induce ice nucleation close to the equilibrium melting temperature of the mixture, were added and these sank by gravity to the base of the vial. These vials and the CRF were cooled to 4 °C before 5 vials (containing 6 ml each) were placed in the aluminum module, while 5 were placed

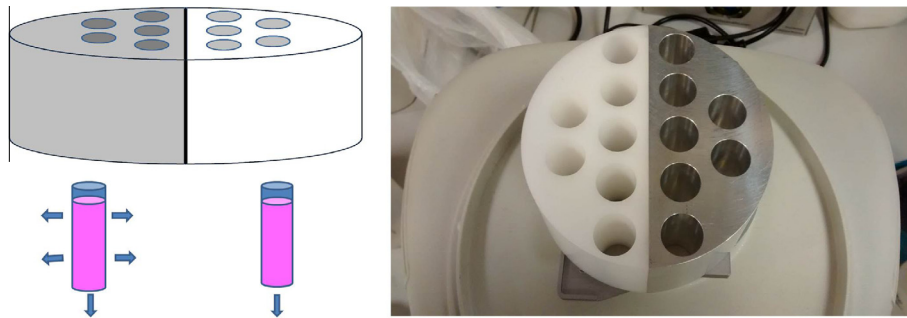


**Fig. 1.** The two different heat transfer modules designed for the EF600-103 CRF. On the left an aluminum module allowed for maximum heat transfer between the vial and the insert, on the right the acetal insert only allowed for heat transfer between the bottom of the vial and the EF600-103 cooling plate. Both modules operated concurrently during cryopreservation, allowing the study of up to seven replicates in each condition, at identical cooling rates.

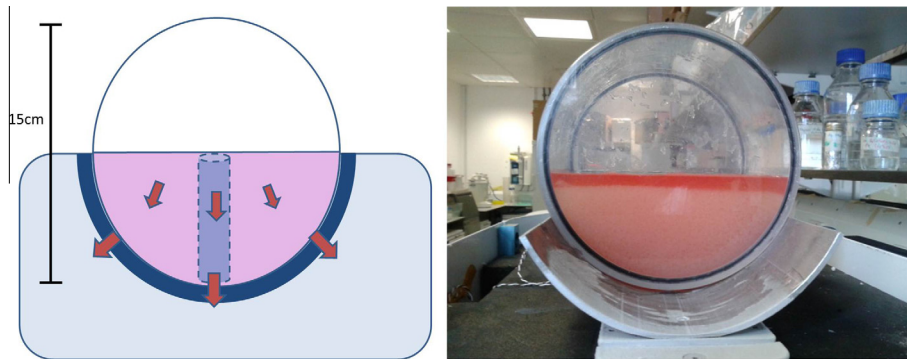


**Fig. 2.** Schematic and image of the large volume cylindrical chamber. Excess media is drained out of the prototype chamber prior to cryopreservation and the resulting ELS thermal mimic (10% glycerol) fills the BAL chamber halfway, (the remaining upper volume containing air). The BAL chamber was then placed on a Stirling engine cooled metal plate (dark blue). The arrows indicate heat transfer during cryopreservation, while the dashed outline of a vial is overlain, indicating the approximate area modeled with the heat transfer modules in Fig. 1. (For interpretation of the references to color in this figure legend, the reader is referred to the web version of this article.)

into the acetal module (see Fig. 1). The EF600-103 was programmed to cool at 1 °C/min from 4 °C to –80 °C. The samples were held in the EF600-103 at –80 °C for 1 h after the cooling cycle was complete, before being transferred to a –80 °C freezer for 7 days.

The samples were warmed rapidly during 330 s in a 37 °C water bath until all the ice had melted (yielding an approximate warming rate of 15 °C/min). The Me<sub>2</sub>SO was diluted out of solution during a 10 min stepwise process with prepared chilled culture medium, with residual ice start granules remaining at the bottom of the tube and easily avoided during decanting. The samples were re-cultured in a 5% CO<sub>2</sub> humidified incubator at 37 °C.

#### *Cryo scanning electron microscopy (CryoSEM) of samples cooled by PS or NS*

To observe physical changes in the structure of the samples, CryoSEM was carried out. Samples recovered from storage at –80 °C were warmed slightly (25 s in a 37 °C water bath) to loosen the ice matrix from the container wall, allowing the bulk frozen samples to be removed rapidly and transferred onto dry ice (–78 °C) without re-warming. These were wrapped in foil and stored on dry ice before being transferred to a –80 °C freezer.

Under liquid nitrogen, each sample was held in a metal bracket and split horizontally using a blade, giving a circular cross-section. This was transferred into a cryo scanning electron microscope (FEI XL30 FEGSEM with a Quorum pp2000 cryo-stage) and etched at –80 °C, before being coated in a thin layer (~20 nm) of gold. The samples in the microscope and images were captured at 5 kV using an Everhardt Thornley secondary electron detector.

#### *Post-thaw functional tests after either PS or NS cryopreservation*

##### *Viability assay*

A viability assay was carried out using PI/FDA staining. 20 µl PI (propidium iodine solution, 1 mg/ml, Sigma) and 10 µl FDA (fluorescein diacetate solution 1 mg/ml, Sigma) were added to ELS and incubated at room temperature for 90 s. The ELS were washed once in PBS (Invitrogen) and then fluorescence at 617 nm (excitation) and 520 nm (emission) measured, with 1 s and 150 ms exposure respectively. The total FDA intensity was compared to the total PI plus FDA intensity using Nikon imaging software, giving both a cell membrane integrity and metabolic viability read-out. This was carried out at 6, 24, 48, and 72 h post-thaw. The 6 h time-point was chosen as this was the minimum time required to fully remove residual (pre-freeze) FDA-sensitive enzymes from non-viable cells.

##### *Total cell counts*

A known volume of ELS were removed from alginate post-cryopreservation in 16 mM EDTA (Applichem) solution before the ELS were dis-aggregated and a nucleic count carried out using the nucleocounter system. Since HepG2 cells are mononuclear this equates to cell number.

##### *MTT assay*

Further standardized samples of ELS were liberated from alginate and 0.75% w/v MTT solution (tetrazolium salt, invitrogen) added to the ELS. After 3 h incubation the MTT was removed and the crystal product dissolved using acidified isopropanol (10% acetic acid in propan-2-ol). Total absorbance was measured at 570 nm

on an Anthos III microplate reader, and quantified using MANTA software.

#### Enzyme-linked-immuno-sorbent-assays (ELISA)

Albumin, alpha-anti-trypsin and alpha-fetoprotein protein production were quantified by ELISA in ELS conditioned media collected 1–3 days post-thaw, and normalized with cell counts. The normalization took two separate forms, one related to cell count post-thaw which showed the average function of the cells surviving cryopreservation. A second normalization determined average production based on number of cells cryopreserved – therefore even cells that were destroyed during cryopreservation were accounted for here.

#### Statistics

To determine significance between samples cryopreserved either through NS or PS, a Welch's *t*-test was performed. To determine significance between samples experiencing the same conditions during cryopreservation at different time points, a Student's *t*-test was performed. Significance was determined as  $p < 0.05$ . Samples for cell functional analysis contained five replicates unless otherwise stated.

## Results

#### Measurement of the thermal histories of the different cooling processes in both the large volume prototype chamber and the scale-down modules

Measured temperatures within the large volume sample (Fig. 3) containing 10% glycerol in aqueous solution (v/v) show large temperature gradients between the wall of the cassette (in contact with the cooling plate) and the deeper (more central) layers of the sample. While the sample layer adjacent to the cylinder wall reduced in temperature approximately linearly, the central sample layers experienced delayed cooling, non-linearity of temperature change, and eventual solidification, with a temperature plateau existing in the core of the sample for some considerable time (in the region of 150–180 min) at the equilibrium melting temperature before solidification occurred.

In the vials processed in the acetal or aluminum modules for the EF600-103, producing either PS or NS respectively, the monitored

temperature profiles differed between the two processing conditions (Fig. 4). With vials in the acetal module, nucleation occurred at the bottom of the cryovial (again, next to the cooling plate of the cryo-cooler) where a small amount of undercooling is evident, while the remainder of the sample remained above the melting point of the solution. Ice growth occurred progressively (and in this case – vertically) within the remainder of this sample and no further significant undercooling was evident (see Fig. 4 – left) emulating the temperature profile, characteristic of progressive solidification seen in a large volume sample (Fig. 3). The whole of the sample volume within a vial in the aluminum module cooled uniformly below the equilibrium melting temperature of the solution before ice nucleation occurred and solidification then progressed instantaneously and in a relatively uniform manner throughout the cryovial, with no large temperature gradients being observed (Fig. 4 – right).

#### Characterization of the ice morphologies in the different freezing processes in the scale-down modules

The structure of the ice and the freeze concentrated matrix is very different in samples processed from vials within the two different modules where either NS or PS was developed (Fig. 5). A planer ice structure is present under conditions of PS in samples processed in the acetal module (Fig. 5A), with vertical ice crystals forming in the sample, entrapping ELS between ice crystals. Following NS (cooling in the aluminum module) a multiple dendritic (network) ice structure is apparent, with ice entrapping freeze concentrated matrix including ELS (Fig. 5B).

#### Viability and viable cell number

The cell viabilities, the viable cell numbers were quantified following either NS or PS at 6, 24, 48, and 72 h post-thaw (Fig. 6). The samples processed in the aluminum module (NS), displayed a trend towards higher average viability at all time points compared with samples processed in the acetal module; significance was noted for 24 h ( $p < 0.05$ ,  $n = 5$ ). The viabilities in both sample sets then further recovered and increased significantly ( $p < 0.05$ ) with length of time in culture post-thaw out from 6 h to 72 h, from  $53.2 \pm 11.5\%$  to  $75.8 \pm 7.1\%$  and from  $41.4 \pm 13.1\%$  to  $72.8 \pm 5.1\%$  for the samples experiencing either NS or PS respectively. A similar pattern was true for total viable cell numbers (Fig. 6 – right) increasing significantly from  $8.1 \pm 1.6$  to  $13.0 \pm 1.7$  million cells/

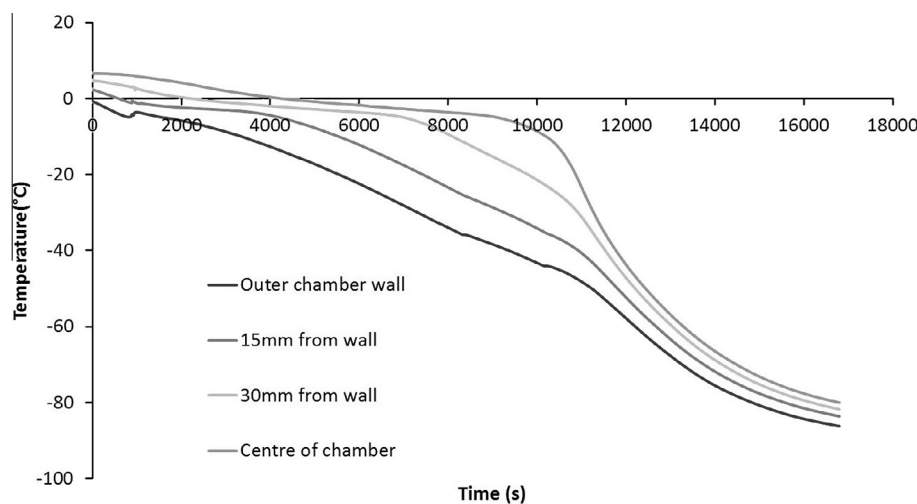


**Fig. 3.** Measured temperature profiles inside the BAL chamber during cooling of a thermal mimic. Approximately 2000 ml of 10% aqueous glycerol solution (having the same thermal properties of ELS) was cooled in the large volume freezer, with pico-logger k-type thermocouples placed at progressively deeper intervals between the wall and the centre of the chamber, at 15 mm intervals. The freezer was programmed to cool from 4 °C to –80 °C at approximately –0.5 °C a min.

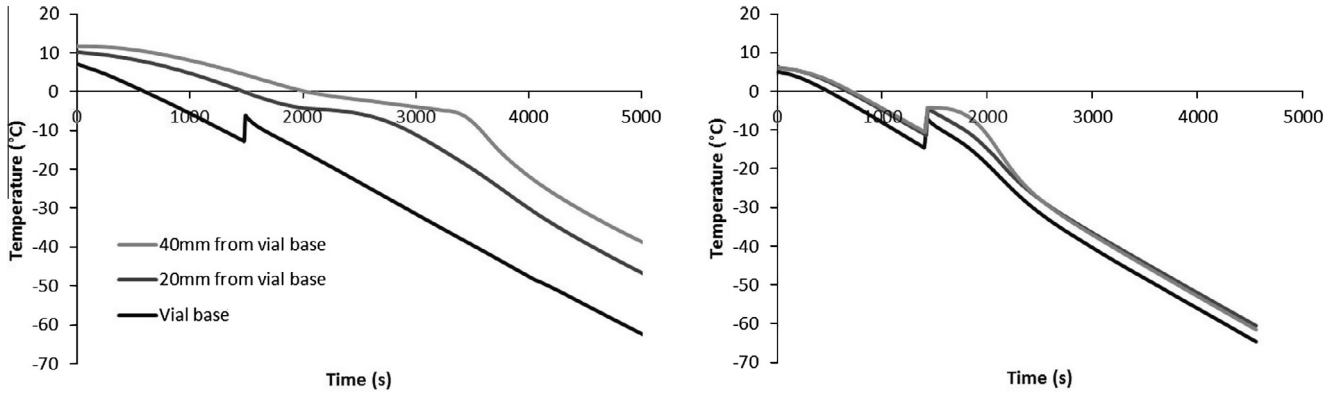


**Fig. 4.** Temperature profiles in the heat transfer modules measured on the EF600-103 controlled rate freezer. K-type thermocouples were inserted at the base of the sample (which was placed on top of the cooling plate of the freezer) and at progressively deeper intervals. The temperature profiles were recorded in both the acetal module (left) and in the aluminum module (right). The EF600-103 was cooled from 4 °C to -80 °C at 1 °C/min, with samples containing 6 ml ELS in 12% Me<sub>2</sub>SO.

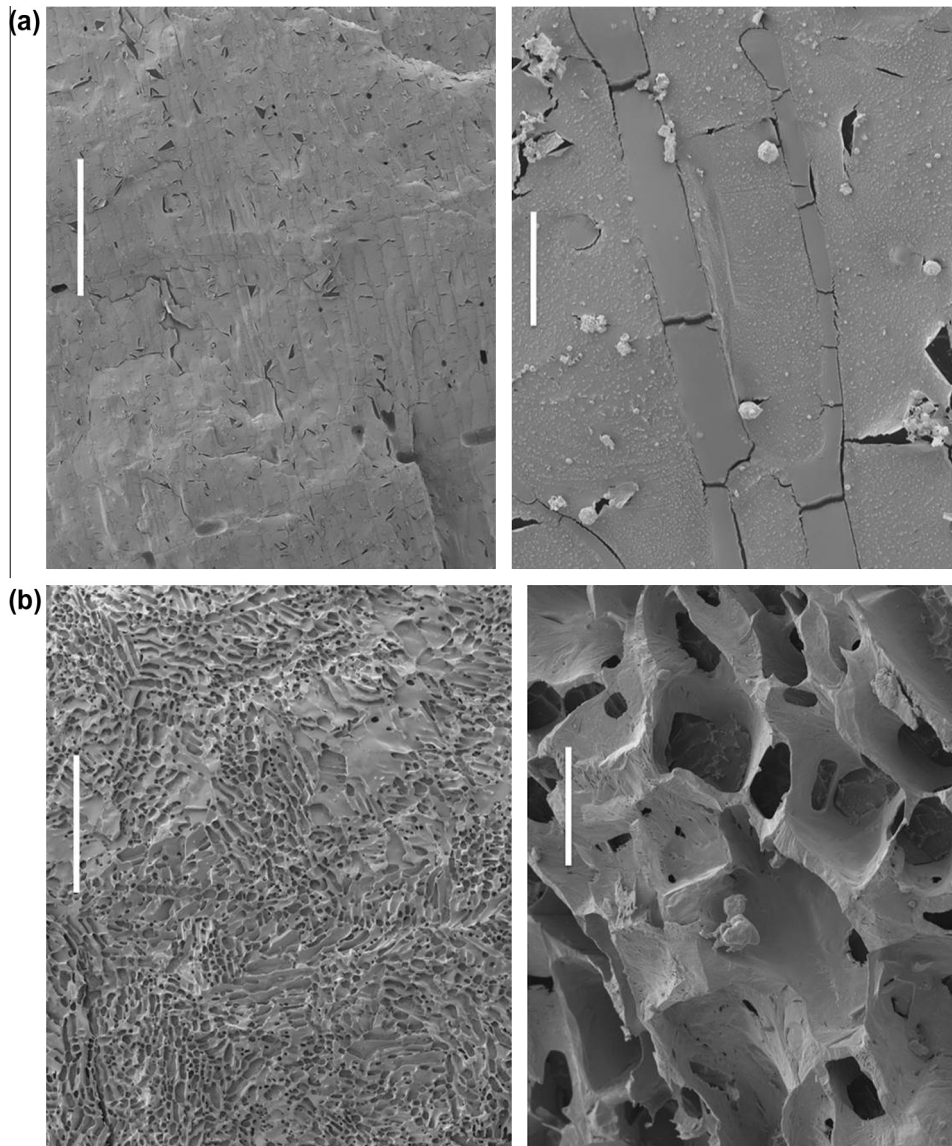


**Fig. 5.** Cryo-scanning electron microscopy (Cryo-SEM) presenting differences in ice structure between progressive solidification (a) and a network solidification (b). The scale bar indicates 1 mm on the left hand images, while 50 μm on the right hand images in both cases. Progressive solidification exhibits a large and homogeneous ice crystal, indicative of slow growth during formation, while network solidification results in a profoundly separate, disordered dendritic ice structure.

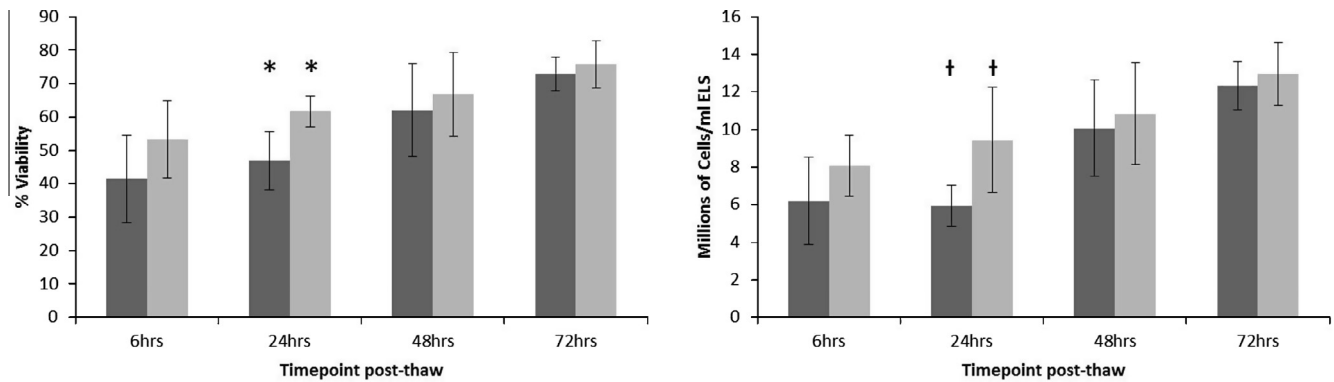


**Fig. 6.** The cell membrane viability (left) and viable cell number (right) of samples experiencing either progressive solidification or network solidification during cryopreservation. Although network solidification (light gray) produces a better post-thaw outcome at 24 h ( $p < 0.05$ ,  $N = 5 \pm SD$ , marked by \* and † for viability and viable cell number respectively), these differences disappeared by 48 h and 72 h in post-thaw cultures. Both PS and NS samples' viability and viable cell number increased significantly from 6 h to 72 h ( $p < 0.05$ ).

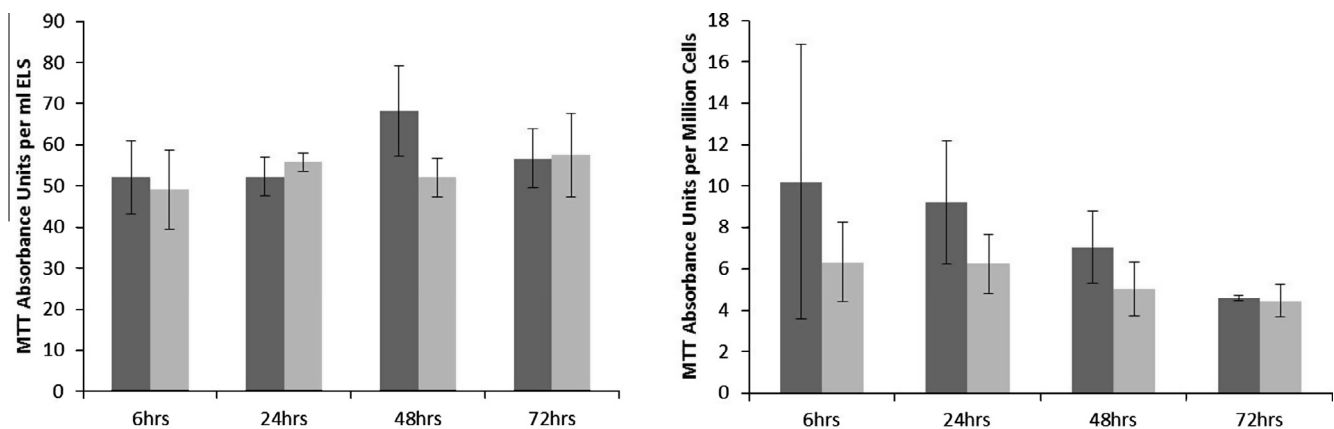


**Fig. 7.** Metabolic activity in ELS: MTT absorbance units per ml ELS (left), and per million cells (right), between samples experiencing either progressive solidification or network solidification during cryopreservation. No statistically significant differences between the samples were observed at any time-point. No significant differences in MTT absorbance were observed intra-sample set between 6 and 72 h.  $N = 5 \pm SD$ .

ml following NS. For samples from PS, they recovered significantly from a nadir at 24 h –  $5.9 \pm 1.1$  million cells/ml to a maximum of  $12.3 \pm 1.3$  million cells/ml at 72 h post-thaw; thus PS was significantly worse at 24 h ( $p < 0.05$ ,  $n = 5$ ) but not different by 72 h.

#### Metabolic activity

Metabolic activity of the samples post-thaw was analyzed using MTT. This was related to either the production per unit ELS (Fig. 7 – left), or to a viable cell number (Fig. 7 – right) and so function per cell – at 6, 24, 48, and 72 h post-thaw could be calculated. This is an important comparator to identify differences between cell populations from different culture batches. MTT metabolism per unit ELS (Fig. 7 – left), showed no significant difference between either NS or PS samples. When the MTT metabolism was expressed per million viable cells (Fig. 7 – right), the mean production per cell number appeared higher in PS compared with NS at all time points, although not reaching significance ( $p > 0.05$ ,  $n = 5$ , in each case).

#### Protein synthesis

Sandwich ELISAs determined protein production per million cells per 24 h in samples collected 1–3 days post thaw. Of the three quantified proteins, Alpha-fetoprotein (AFP) did not exhibit a significant difference at any time point.

In contrast, albumin production in the PS samples was significantly higher ( $p < 0.05$ ,  $n = 5$ ) 24 h post-thaw being measured at  $46.7 \pm 11.5$   $\mu\text{g}$  per million viable cells per 24 h, compared to  $30.9 \pm 4.4$   $\mu\text{g}$  per million viable cells per 24 h following NS.

Alpha-antitrypsin was also significantly improved ( $p < 0.05$ ,  $n = 5$ ) 24 h post thaw, at  $18.8 \pm 4.8$   $\mu\text{g}$  per million viable cells per 24 h, compared to  $12.2 \pm 2.0$   $\mu\text{g}$  per million viable cells per 24 h following NS.

All protein production capabilities in either NS or PS samples improved significantly from 24 h to 72 h post-thaw, mirroring the recoveries in viable cell numbers during progressive post-thaw culture (see Fig. 8).

#### Discussion

Ice solidification occurs in small and large volumes by two distinct processes. At small volumes network solidification (NS) manifests while at large volumes progressive solidification (PS) is the predominant process. These differences in bio-physical events presented as different ice crystal formats in this study. Similar differences in ice matrix ultrastructure have been presented for sperm processed either in straws or bags [22].

With ELS, the observed recovery following these two processes was very similar although the structure of ice and the freeze concentrated residual compartments within the two types of samples

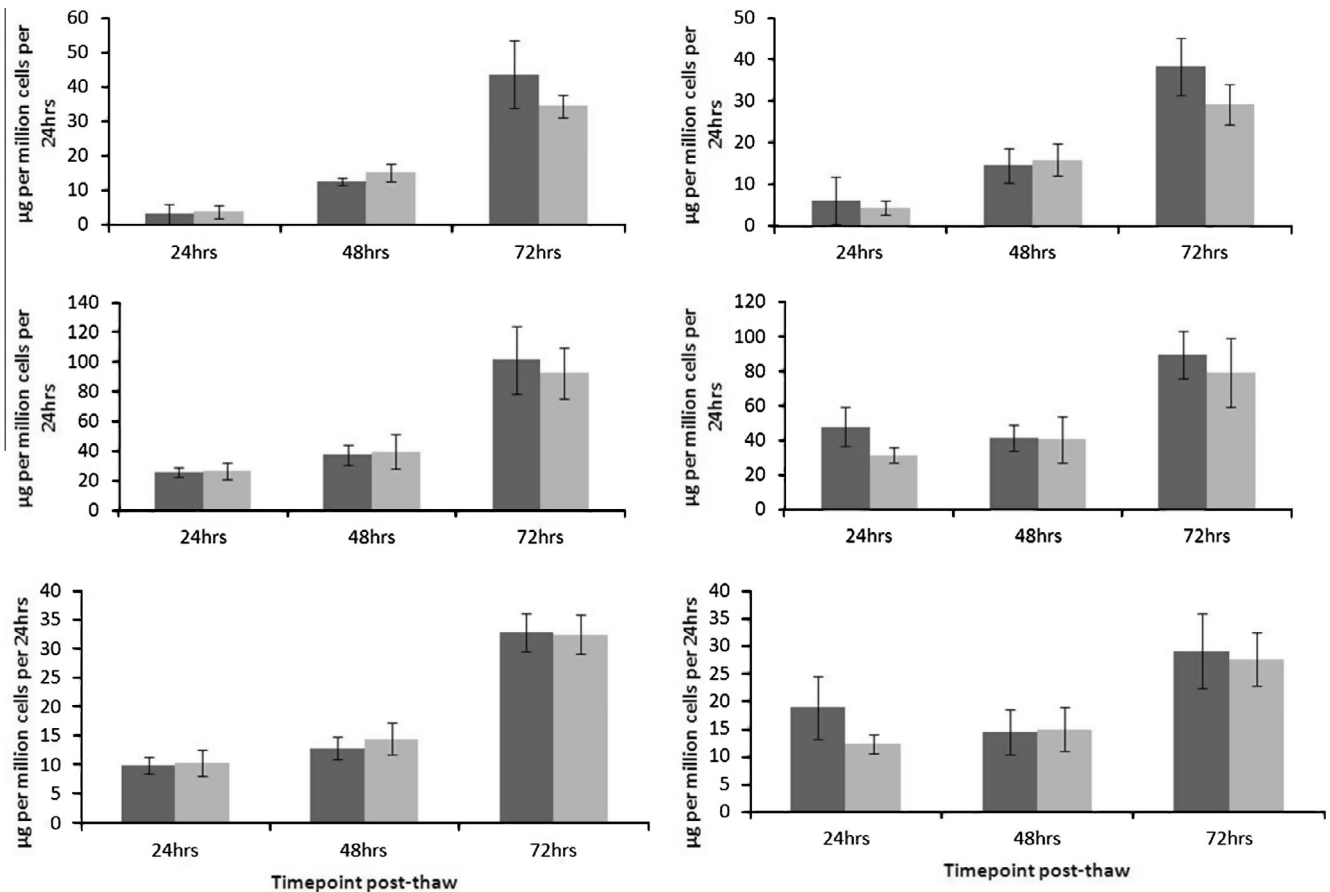


**Fig. 8.** The production of liver specific proteins by ELS, day 1 to day 3 post-thaw between samples experiencing either progressive solidification or network solidification during cryopreservation – alpha-fetoprotein (top), albumin (middle), and alpha-antitrypsin (bottom). Progressive solidification samples are shown dark in gray with network solidification samples lighter gray. Production was analyzed per million viable cells post-thaw per 24 h (right), and normalized per million viable cells pre-thaw that takes account of cells destroyed during the cryopreservation (left). Measurements on the left therefore present the overall outcome per sample cryopreserved – there are no statistically significant differences. Measurements on the right display production per million cells, but taking into account that there is now a different cell number between the two sets. Allowing for this different cell number, the progressive solidification samples have significantly improved production of albumin and alpha-antitrypsin in the first 24 h post thaw (at  $p < 0.05$ ). There are no significant differences at other time points or with alpha-fetoprotein  $N = 5 \pm SD$ . Intra either NS or PS sample sets, the measured protein production increased significantly from day 1 to day 3 for all measurements ( $p < 0.05$ ).

are very different. Post-thaw, samples experiencing NS had a higher post-thaw viability and viable cell numbers, significant after 24 h of recovery. When examining the functional outcomes, samples cryopreserved experiencing PS have an improved outcome per unit of viable cells, although overall differences were small. Our results suggest that NS allows more cells to survive cryopreservation, but those surviving cells have greater average damage than those experiencing PS. PS by contract showed a trend to fewer, healthier cells post thaw, especially at the 24 h time point following thawing.

During large scale cryopreservation the potential long exposure to cryoprotectants in the liquid state prior to phase transition, experienced for the central portion of the sample under condition of PS, may be a potential extra stress over and above those which result from cryopreservation in NS conditions. We had considered the possibility that PS would therefore result in greatly reduced post-thaw recoveries. This was in fact not the case, which is encouraging when planning further work on scaled-up cryopreservation in volumes  $> 1$  l. It could be hypothesised that under conditions of PS, the extra cryoprotectant stress experienced by part of the sample could act to remove an unhealthy, or poorly performing sub population of cells present before cryopreservation. NS, by reducing the time to which the ELS from the whole sample was exposed to the osmotic and chemical toxicities, where the central mixture was in the liquid state just at the point of nucleation,

may avoid injuring this already partially stressed population leading to significantly higher viable cell numbers (although metabolically less productive) by 24 h post-thaw. It is also possible that the temperature discontinuity present when an undercooled sample nucleates damages cells in subtle ways, so they survive cryopreservation though are no longer function effectively. Further studies will need to investigate these mechanisms.

It is important to differentiate the processes described above (NS and PS) from another way to control ice crystal progression – this being the so-called directional solidification (DS) where the sample is moved across a constantly low temperature gradient, sufficiently cold to induce ice nucleation in the portion of the sample in contact with the cold plate. DS allows the morphology of the ice interface to be varied under conditions where the local chemical conditions of the residual solution can be kept constant, which is different to what happens in PS where progressive exclusion of both solutes and cells occurs ahead of the ice front. The technique allowed investigation of whether different ice crystal morphologies (for example, with increasingly complex ice dendrite formation) impacted on cell survival, but this was not generally found to be the case [10]. Differential entrapment or exclusion of cells within the advancing ice front was also noted with DS [11], but the behavior of larger cell complexes (such as the ELS) has not been investigated as far as we are aware. PS would perhaps be expected to deliver ice fronts moving between and through the alginate

capsules containing the ELS, which were used in relatively high packing density in the current study, but further work will be needed to investigate this aspect. DS also allows better homogeneity of the cooling profile throughout the entire sample [2], whereas, as seen here, PS results in differential thermal profiles towards the sample centre as the excluded solutes, generating areas of local undercooling, result in variable release of latent heat of ice crystal formation. This heat has to be dissipated from the sample core before linear cooling can proceed. This results in a controllable progression of solidification through the specimen dependant on the rate at which the temperature gradient is passed through the sample [1,10,11]. DS allows the morphology of the ice interface to be varied under conditions where the local chemical conditions of the residual solution can be kept constant, which is different to what happens in PS where progressive exclusion of both solutes and, in some situations, cells occurs ahead of the ice front [11]. DS also allows better homogeneity of the cooling profile throughout the entire sample, whereas, as seen here, PS results in differential thermal profiles towards the sample centre as the excluded solutes, generating areas of local undercooling, result in variable release of latent heat of ice crystal formation which have to be dissipated from the sample core before controlled cooling can proceed. However, for large cell masses contained within an irregular geometry as investigated here, engineering a DS approach to cryo-cooling would prove to be challenging. In the current work, solidification proceeded only through static surface cooling conditions, with ice growth primarily determined by the thermal properties and 3-dimensional structure of the sample.

Another factor worthy of comment is that the experimental systems used here had little excess cryoprotectant additive and there would be little settling effect of ELS on the ice crystal progression – all the samples were in effect ‘settled’ by removing the extra CPA volume. The process of ice propagation in this system may differ compared with conventional cell and protein suspensions, where sedimentation of cells may occur before initiation of freezing and, secondly, cells and proteins may be pushed ahead of ice fronts during progressive solidification.

While success has been reported with large volumes in flat bag cryopreservation, these have generally been deliberately compressed into a thin wafer or ‘slab’ format with little internal temperature gradients and so often experience NS. It is possible to observe PS in bags however, if the bag temperature is not thermally equilibrated prior to the onset of solidification [15,25].

Such flat-bag approaches would be very difficult to adapt for BAL cryopreservation due to the geometries involved, where the end-product would ideally reside in a cylindrical fluidised bed format.

The varying temperature profiles throughout the sample when cooling a large cylinder have been recognized for some time [19]. Previous studies have shown that the level of freeze-concentration of solutes is dependent on the cooling rate and this has been studied in detail in cylindrical vessels [13]. In cylindrical configurations, the solutes increased in concentration radially from the edge of the cylinder to the centre, and this was accompanied by aggregation of some proteins within the core layers. Due to the alginate sphere composition of the test BAL, cell aggregation will not occur here as the cells are already immobilised. This increase in solutes centrally (as would be seen in a cylindrical BAL cassette) is a likely cause of lower cell number post thaw when progressive solidification is present in our current scale-down module.

Using inserts in the EF600-103 to emulate large volume cooling profiles within small samples gave similar thermal histories as were seen in a large volume. This allowed for the study of these thermal profiles as well as longer and variable cryoprotectant exposure and cryo-concentration of solutes in the system, in addition to accurately mimicking the variations in ice structure

between the two set-ups. Combining these three effects in a smaller volume format accurately provides more accessible and more economical methods of study of these sample configurations, without the additional variable of differing volume or thawing rate. This equipment modification may have application in studying other large volume freezing problems, such as those encountered with proteins.

Significantly this study informs us that PS may be applied to the BAL without major detrimental effects on the bulk ELS product, although there was a low level of early functional attrition seen after PS which requires further study.

## Conclusion

Previously our group reported good outcome when ELS (cryopreserved in typical small volume format in cryo-vials) experienced network solidification during cryopreservation [16,17]. Good outcomes can now be achieved in a more realistic large scale geometry that necessarily produces progressive solidification, and this can be modeled in an economical way using an adapted head plate for the EF600-103 freezer.

It has been demonstrated that both PS and NS exhibit very different biophysical conditions during ice crystal growth; this is reflected in the ultrastructural observations of the differing ice-matrices during solidification. However these different outcomes of cryo-solidification in reality made only small, mostly non-significant differences to viable cell recovery or function. ELS cryopreserved under both conditions each showed very good propensity to return to normal cell replication as post-thaw culture extended beyond the first 24 h. As progressive solidification is almost unavoidable in samples any larger than a few mls, an understanding of the differences between these two conditions may well be necessary for successful larger volume cryopreservation across a wide range of cell therapies.

## References

- [1] A. Arav, J. Saragusty, Directional freezing of spermatozoa and embryos, *Reprod. Fertil. Dev.* 26 (2014) 83–90.
- [2] A. Arav, Z. Gavish, A. Elami, Y. Natan, A. Revel, S. Silber, R.G. Gosden, P. Patrizio, Ovarian function 6 years after cryopreservation and transplantation of whole sheep ovaries, *Reprod. Biomed. Online* 20 (2010) 48–52.
- [3] V. Ayel, O. Lottin, M. Faucheux, D. Sallier, H. Peerhossaini, Crystallisation of undercooled aqueous solutions: experimental study of free dendritic growth in cylindrical geometry, *Int. J. Heat Mass Transfer* 49 (2006) 1876–1884.
- [4] E. Erro, J. Bundy, I. Massie, S.A. Chalmers, A. Gautier, S. Gerontas, M. Hoare, P. Sharratt, S. Choudhury, M. Lubowicki, I. Llewellyn, C. Legallais, B. Fuller, H. Hodgson, C. Selden, Bioengineering the liver: scale-up and cool chain delivery of the liver cell biomass for clinical targeting in a bioartificial liver support system, *Biores. Open Access* 2 (2013) 1–11.
- [5] H.R. Harmison, K.R. Diller, J.R. Walsh, C.M. Neils, J.J. Brand, Measurement of cell volume loss in the liquid region preceding an advancing phase change interface, *Biotransport: Heat Mass Transfer Living Syst.* 858 (1998) 276–283.
- [6] S. Hartmann, D. Niedermeier, J. Voigtlander, T. Clauss, R.A. Shaw, H. Wex, A. Kiselev, F. Stratmann, Homogeneous and heterogeneous ice nucleation at LACIS: operating principle and theoretical studies, *Atmos. Chem. Phys.* 11 (2011) 1753–1767.
- [7] R.B. Head, Steroids as ice nucleators, *Nature* 191 (1961) 1058–1059.
- [8] R. Heidemann, S. Lunse, D. Tran, C. Zhang, Characterization of cell-banking parameters for the cryopreservation of mammalian cell lines in 100-mL cryobags, *Biotechnol. Prog.* 26 (2010) 1154–1163.
- [9] R. Heidemann, M. Mered, D.Q. Wang, B. Gardner, C. Zhang, J. Michaels, H.J. Henzler, N. Abbas, K. Konstantinov, A new seed-train expansion method for recombinant mammalian cell lines, *Cytotechnology* 38 (2002) 99–108.
- [10] A. Hubel, E.G. Cravalho, B. Nunner, C. Korber, Survival of directionally solidified B-lymphoblasts under various crystal-growth conditions, *Cryobiology* 29 (1992) 183–198.
- [11] A. Hubel, T.B. Darr, A. Chang, J. Dantzig, Cell partitioning during the directional solidification of trehalose solutions, *Cryobiology* 55 (2007) 182–188.
- [12] M.I. Kleman, K. Oellers, E. Lullau, Optimal conditions for freezing CHO-S and HEK293-EBNA cell lines: influence of Me2SO, freeze density, and PEI-mediated transfection on revitalization and growth of cells, and expression of recombinant protein, *Biotechnol. Bioeng.* 100 (2008) 911–922.

- [13] P. Kolhe, A. Badkar, Protein and solute distribution in drug substance containers during frozen storage and post-thawing: a tool to understand and define freezing–thawing parameters in biotechnology process development, *Biotechnol. Prog.* 27 (2011) 494–504.
- [14] C. Korber, Phenomena at the advancing ice liquid interface – solutes, particles and biological cells, *Q. Rev. Biophys.* 21 (1988) 229–298.
- [15] I. Massie, C. Selden, H. Hodgson, B. Fuller, S. Gibbons, G.J. Morris, GMP cryopreservation of large volumes of cells for regenerative medicine: active control of the freezing process, *Tissue Eng. Part C: Methods* (2014) (ahead of print).
- [16] I. Massie, C. Selden, H. Hodgson, B. Fuller, Cryopreservation of encapsulated liver spheroids for a bioartificial liver: reducing latent cryoinjury using an ice nucleating agent, *Tissue Eng. Part C: Methods* 17 (2011) 765–774.
- [17] I. Massie, C. Selden, H. Hodgson, B. Fuller, Storage temperatures for cold-chain delivery in cell therapy: a study of alginate-encapsulated liver cell spheroids stored at –80 degrees C or –170 degrees C for up to 1 year, *Tissue Eng. Part C: Methods* 19 (2013) 189–195.
- [18] H.T. Meryman, Cryopreservation of living cells: principles and practice, *Transfusion (Paris)* 47 (2007) 935–945.
- [19] H.T. Meryman, *Cryobiology*, Academic Press, London, 1966.
- [20] G.J. Morris, E. Acton, Controlled ice nucleation in cryopreservation – a review, *Cryobiology* 66 (2013) 85–92.
- [21] R.G. Pereyra, I. Szleifer, M.A. Carignano, Temperature dependence of ice critical nucleus size, *J. Chem. Phys.* 135 (2011) 1–5. 0345081.
- [22] H. Rodriguez-Martinez, Cryopreservation of porcine gametes, embryos and genital tissues: state of the art, in: I. Katkov (Ed.), *Current Frontiers in Cryobiology*, InTech, 2012, pp. 231–260. Available at: <<http://www.intechopen.com/books/current-frontiers-in-cryobiology>>.
- [23] J. Saragusty, H. Gacitua, I. Rozenboim, A. Arav, Do physical forces contribute to cryodamage?, *Biotechnol Bioeng.* 104 (2009) 719–728.
- [24] J.A. Searles, J.F. Carpenter, T.W. Randolph, The ice nucleation temperature determines the primary drying rate of lyophilization for samples frozen on a temperature-controlled shelf, *J. Pharm. Sci.* 90 (2001) 860–871.
- [25] A. Sputtek, M. Lioznov, N. Kroger, A.W. Rowe, Bioequivalence comparison of a new freezing bag (CryoMACS (R)) with the Cryocyte (R) freezing bag for cryogenic storage of human hematopoietic progenitor cells, *Cytotherapy* 13 (2011) 481–489.
- [26] D.M. Stefanescu, *Science and Engineering of Casting Solidification*, second ed., Springer, New York, 2008.

# Modeling the effects of cyclodextrin on intracellular membrane vesicles from Cos-7 cells prepared by sonication and carbonate treatment

Peter Kilbride<sup>1</sup>, Holly J. Woodward<sup>1</sup>, Kuan Boone Tan<sup>2</sup>,  
Nguyễn T.K. Thanh<sup>2</sup>, K.M. Emily Chu<sup>1</sup>, Shane Minogue<sup>1</sup> and  
Mark G. Waugh<sup>1</sup>

<sup>1</sup> UCL Institute for Liver & Digestive Health, University College London, London, United Kingdom

<sup>2</sup> Biophysics Group, Department of Physics & Astronomy, University College London, London, United Kingdom

## ABSTRACT

Cholesterol has important functions in the organization of membrane structure and this may be mediated via the formation of cholesterol-rich, liquid-ordered membrane microdomains often referred to as lipid rafts. Methyl-beta-cyclodextrin (cyclodextrin) is commonly used in cell biology studies to extract cholesterol and therefore disrupt lipid rafts. However, in this study we reassessed this experimental strategy and investigated the effects of cyclodextrin on the physical properties of sonicated and carbonate-treated intracellular membrane vesicles isolated from Cos-7 fibroblasts. We treated these membranes, which mainly originate from the *trans*-Golgi network and endosomes, with cyclodextrin and measured the effects on their equilibrium buoyant density, protein content, represented by the palmitoylated protein phosphatidylinositol 4-kinase type II $\alpha$ , and cholesterol. Despite the reduction in mass stemming from cholesterol removal, the vesicles became denser, indicating a possible large volumetric decrease, and this was confirmed by measurements of hydrodynamic vesicle size. Subsequent mathematical analyses demonstrated that only half of this change in membrane size was attributable to cholesterol loss. Hence, the non-selective desorption properties of cyclodextrin are also involved in membrane size and density changes. These findings may have implications for preceding studies that interpreted cyclodextrin-induced changes to membrane biochemistry in the context of lipid raft disruption without taking into account our finding that cyclodextrin treatment also reduces membrane size.

**Subjects** Biophysics, Cell Biology, Mathematical Biology

**Keywords** TGN, Cholesterol, Cyclodextrin, Lipid raft, Membrane, PI 4-kinase

## INTRODUCTION

In this study we investigated the relationship between membrane composition, density, and size by using methyl- $\beta$ -cyclodextrin (cyclodextrin) to rapidly deplete membrane cholesterol from an isolated intracellular membrane preparation. Cyclodextrins are a family of cyclic oligosaccharides that adopt a cone-like structure in aqueous solution, with an internal hydrophobic core that can sequester lipids from membranes (*Heine et al., 2007*;

Submitted 16 July 2015  
Accepted 5 October 2015  
Published 27 October 2015

Corresponding author  
Mark G. Waugh,  
m.waugh@ucl.ac.uk

Academic editor  
Frances Separovic

Additional Information and  
Declarations can be found on  
page 14

DOI 10.7717/peerj.1351

© Copyright  
2015 Kilbride et al.

Distributed under  
Creative Commons CC-BY 4.0

**OPEN ACCESS**

*Pinjari, Joshi & Gejji, 2006*). Cyclodextrins have useful pharmaceutical applications as soluble carriers for hydrophobic molecules and are also commonly used in biochemical and cell biology studies to manipulate membrane lipid levels (*Loftsson & Brewster, 1996; Rodal et al., 1999; Welliver, 2006; Zidovetzki & Levitan, 2007*). Cyclodextrin efficaciously removes sterols such as cholesterol from biological membranes but can also remove other lipids such as sphingomyelin and phosphatidylcholine (*Ottico et al., 2003*). Recently cyclodextrin and the related molecule hydroxypropyl- $\beta$ -cyclodextrin have been shown to alleviate the pathological intracellular accumulation of free cholesterol in Niemann-Pick Type C disease models (*Camargo et al., 2001; Davidson et al., 2009; Holtta-Vuori et al., 2002; Lim et al., 2006; Liu et al., 2008; Liu et al., 2010; Liu et al., 2009; Mbua et al., 2013; Pontikis et al., 2013; Ramirez et al., 0000; Ramirez et al., 2010; Rosenbaum et al., 2010; Swaroop et al., 2012; Te Vruchte et al., 2014; Vance & Karten, 2014; Vite et al., 2015; Waugh, 2015*). These recent developments demonstrate a potential therapeutic use for cyclodextrins and also clearly establish their efficacy for reducing the cholesterol content of endosomal membranes (*Rosenbaum et al., 2010; Shogomori & Futerman, 2001*). In addition, we have previously reported that the addition of cyclodextrin to cultured cells leads to the vesicularization and contraction of the *trans*-Golgi network (TGN) and endosomal membranes (*Minogue et al., 2010*). These cyclodextrin-induced changes to intracellular biomembrane architecture are associated with alterations to intramembrane lateral diffusion and lipid kinase activity of phosphatidylinositol 4-kinase II $\alpha$  (PI4KII $\alpha$ ), a constitutively palmitoylated and membrane-associated enzyme (*Barylko et al., 2009; Lu et al., 2012*) that may be important in the etiology of some cancers and neurodegenerative disorders (*Chu et al., 2010; Clayton, Minogue & Waugh, 2013a; Li et al., 2010; Li et al., 2014; Simons et al., 2009; Waugh, 2012; Waugh, 2014; Waugh, 2015*).

Whilst cyclodextrin has been mainly used to remove cholesterol from the plasma membrane our focus here is on characterizing the effects of such treatment on intracellular membranes where cholesterol levels are known to be important for processes such as protein sorting and trafficking from the TGN (*Paladino et al., 2014*). Since the effects of cyclodextrin on intracellular membranes are important to understand both in a disease context (*Vite et al., 2015*) and for furthering our knowledge about the functions of cholesterol on intracellular membranes, we decided to investigate more comprehensively how cyclodextrin alters the biophysical properties of a lipid-raft-enriched membrane fraction isolated from intracellular TGN and endosomal membranes (*Minogue et al., 2010; Waugh et al., 2011a*). In particular, we sought to understand more fully the cyclodextrin-induced changes to the equilibrium buoyant densities of isolated cholesterol-rich membrane fractions that we and others have reported in a number of preceding publications (for examples, see *Hill, An & Johnson, 2002; Kabouridis et al., 2000; Matarazzo et al., 2012; Minogue et al., 2010; Navratil et al., 2003; Pike & Miller, 1998; Spisni et al., 2001; Xu et al., 2006; Zidovetzki & Levitan, 2007*). In these previous experiments, cholesterol depletion with cyclodextrin rendered the membrane fraction less buoyant, leading to the cyclodextrin-treated membranes banding to a denser region in an equilibrium density gradient. This cyclodextrin-induced change, sometimes referred to as a density shift, has allowed us to design, using sucrose density gradients, a membrane floatation assay in

which we have been able to separate cholesterol-replete and -depleted membranes before and after cyclodextrin treatment.

In many of these prior studies, a cyclodextrin-dependent redistribution of biomolecules to a denser membrane fraction was interpreted as a delocalization from cholesterol-rich lipid rafts or liquid-ordered domains to a less buoyant, liquid-disordered, non-raft fraction. This reasoning stems from the idea that raft-enriched membrane domains are intrinsically buoyant due to their high lipid-to-protein ratio. However, since density is defined as mass divided by volume we reassessed these inferences on the grounds that in the absence of a membrane volume change, a reduction in mass alone would result in a membrane becoming more buoyant, i.e., less dense.

To explore the relationship between cholesterol content and membrane density, we employed our membrane floatation assay to measure the change in the physical properties and biochemical composition of cholesterol-enriched membrane vesicles following cyclodextrin treatment. We then analyzed these changes to mathematically model, from first principles, the degree to which the mass and volume of the membrane domains would have to alter to account for the measured change in membrane density. Finally, we provide a mathematical solution to explain the relationship between membrane cholesterol mass and vesicle density.

## MATERIALS AND METHODS

### Materials

All cell culture materials, enhanced chemiluminescence (ECL) reagents and X-ray film were purchased from GE Healthcare Life Sciences, UK. Polyvinylidene difluoride (PVDF) membrane was bought from Merck Millipore UK. Horseradish peroxidase (HRP)-linked secondary antibodies were purchased from Cell Signalling Technology UK. The antibody to PI4KII $\alpha$  was previously described by us (*Minogue et al., 2010*). HRP-linked cholera toxin B subunit was purchased from Sigma-Aldrich UK. Sucrose was obtained from VWR International Ltd UK. Complete protease inhibitor tablets were purchased from Roche Ltd UK. All other reagents were from Sigma-Aldrich UK.

### Cell culture

Cos-7 cells obtained from the European Collection of Cell Cultures operated by Public Health England were maintained at 37 °C in a humidified incubator at 10% CO<sub>2</sub>. Cells were cultured in Dulbecco's Modified Eagle's Medium (DMEM) supplemented with Glutamax, 10% fetal calf serum, 50 i.u./mL penicillin, and 50  $\mu$ g/mL streptomycin. Cell monolayers were grown to confluency in 10 cm tissue culture dishes. Typically, four confluent plates of cells were used in each subcellular fractionation experiment.

### Subcellular fractionation by sucrose density gradient centrifugation

A buoyant subcellular fraction enriched for TGN and endosomal membranes was prepared according to our previously published method (*Minogue et al., 2010; Waugh et al., 2006*). Confluent cell monolayers were washed twice in ice-cold phosphate-buffered saline

(PBS) pH 7.4 and then scraped into 2 mL of homogenization buffer (Tris-HCl 10 mM, EGTA 1 mM, EDTA 1 mM, sucrose 250 mM, plus Complete™ protease inhibitors, pH 7.4). Post-nuclear supernatants were prepared by Dounce homogenization of the cells suspended in homogenization buffer followed by centrifugation at 1,000 g at 4 °C for 2 min to pellet nuclei and unbroken cells. Cellular organelles were separated by equilibrium density gradient centrifugation by overnight ultracentrifugation on a 12 mL, 10–40% w/v sucrose density gradient as previously described (Waugh *et al.*, 2003a; Waugh *et al.*, 2003b; Waugh *et al.*, 2006). Using this procedure, a buoyant TGN-endosomal enriched membrane fraction consistently banded in gradient fractions 9 and 10 and was harvested as described before (Waugh *et al.*, 2003b; Waugh *et al.*, 2006).

### **Refractometry to measure membrane density**

The refractive index of each membrane fraction was determined using a Leica AR200 digital refractometer. Refractive index values were then converted to sucrose densities using Blix tables (Dawson *et al.*, 1986) and linear regression carried out using GraphPad Prism software.

### **Membrane floatation assay to measure the equilibrium buoyant density of membrane vesicles**

This assay was previously described by us (Minogue *et al.*, 2010). Briefly, 400 µL of cyclodextrin (20 mM) dissolved in water was added to an equal volume of TGN/endosomal membranes on ice for 10 min to give a cyclodextrin concentration of 10 mM. Then, 200 µL of sodium carbonate (0.5 M, pH 11.0) was added to a final concentration of 50 mM in a 1 mL sample. The carbonate-treated membranes were probe-sonicated on ice using a VibraCell probe sonicator from Sonics & Materials Inc., USA at amplitude setting 40 in pulsed mode for 3 × 2 s bursts. To the 1 mL sonicated membrane samples, 3 mL of 53% w/v sucrose in Tris-HCl 10 mM, EDTA 1 mM and EGTA 1 mM, pH 7.4 was added to form 4 mL of sample in 40% w/v sucrose and a sodium carbonate concentration of 12.5 mM and, where applicable, a cyclodextrin concentration of 2 mM. A discontinuous sucrose gradient was formed in a 12 mL polycarbonate tube by overlaying the 40% sucrose layer with 4 mL 35% w/v and 4 mL 5% w/v sucrose in Tris-HCl 10 mM, EDTA 1 mM and EGTA 1 mM, pH 7.4. The gradient was centrifuged overnight at 185,000 g at 4 °C in a Beckman LE-80K ultracentrifuge and 12 × 1 mL fractions were harvested beginning at the top of the tube.

### **Immunoblotting of sucrose density gradient fractions**

The protein content of equal volume aliquots of each density gradient fraction was separated by sodium dodecyl sulfate-polyacrylamide gel electrophoresis (SDS-PAGE), transferred to PVDF membranes and probed with antibodies directed against proteins of interest. Western blots were visualized by chemiluminescence and bands were quantified from scanned X-ray films using image analysis software in Adobe Photoshop CS4.

### **Measurements of membrane lipid levels**

The cholesterol content of equal volume membrane fractions was assayed using the Amplex red cholesterol assay kit (Molecular Probes). The use of this assay to measure

membrane cholesterol mass has been previously validated (*Bate, Tayebi & Williams, 2008; Minogue et al., 2010; Nicholson & Ferreira, 2009*). Ganglioside glycosphingolipids were detected by dot blotting of membrane fractions (*Ilangumaran et al., 1996*) and probing with HRP-conjugated cholera toxin B subunit as described previously (*Ilangumaran et al., 1996; Mazzone et al., 2006; Waugh, 2013; Waugh et al., 2011a; Waugh et al., 2011b*). Membrane-bound cholera toxin was visualized by incubation with chemiluminescence detection reagents and spots were quantified as described for the analysis of immunoblotting data (*Waugh, 2013*).

### Dynamic light scattering measurement to measure hydrodynamic diameter of membrane vesicles

The hydrodynamic size of the membrane vesicles in the gradient fraction was studied with a Zetasizer Nano ZS90 (Malvern Instruments). All diluted samples were prepared in filtered (0.2  $\mu\text{m}$ ) Millipore ddH<sub>2</sub>O to avoid sample artifacts, and measurements were made at 25 °C in triplicate.

### Mathematical modelling of membrane compositional changes

Subscripts are used to specify a unit being examined, with *s* and *r* defining treatment sensitive (assuming that most of this fraction is composed of cholesterol with a density of around  $\rho = 1.067$  (*Haynes, 2013*)) and remaining components, respectively. The subscript—post is used to denote values for vesicles post cyclodextrin treatment.

The fractions are not considered discrete sections of the vesicles; rather they can be mixed and inter-connected.

The mass density of a particle is defined as the mass per unit volume. To determine the mass density of an object consisting of multiple discrete components in a steady state, a linear combination of its components can be used as in Eq. (1).

$$\rho = \frac{m_1 + m_2 + m_3 + \dots}{V_1 + V_2 + V_3 + \dots} \quad (1)$$

where the subscripts denote the mass and volume of the separate components. Through normalizing the total volume  $V = V_1 + V_2 + V_3 + \dots = 1$ , the density can simplify to

$$\rho = m_1 + m_2 + m_3 + \dots m_n$$

where  $m_n$  now refers to the mass of the volume fraction in question. Considering an object composed of *n* different materials the overall mass density is therefore

$$\begin{aligned} \rho_{\text{whole}} &= \rho_{\text{fraction1}} V_{\text{fraction1}} + \rho_{\text{fraction2}} V_{\text{fraction2}} + \rho_{\text{fraction3}} V_{\text{fraction3}} + \dots \\ &= \sum_{j=1}^{j=n} \rho_j V_j \end{aligned} \quad (2)$$

where  $\rho_j$  is the density of fraction *j*, and  $v_j$  is the volume fraction of material *j*.

To determine the % composition of the vesicles, boundary conditions were formulated and solved using simultaneous equations. Pre-treatment, the system was described

through Eq. (3):

$$V_r \times \rho_r + V_s \times \rho_s = \rho_{\text{pre}} \quad (3)$$

where the fractional volume of the residual component is given by  $V_r$ , the fractional volume of the treatment sensitive component =  $V_s$ , and  $\rho_{\text{pre}}$  was the measured density of the vesicle pre-treatment.

A second simultaneous equation arises through the physical definition of the system, which is the total volume has been normalised to one:

$$V_r + V_s = 1 \quad (4)$$

i.e., combining all the fractions in a vesicle together equaled fraction one of a vesicle.

The 3rd simultaneous equation was determined with respect to the post-treatment density. It can be derived that for the cyclodextrin sensitive fraction:

$$\rho_{\text{pre}} = \frac{m_{\text{pre}}}{V_{\text{pre}}} = \rho_{\text{post}} = \frac{m_{\text{post}}}{V_{\text{post}}} = 1.067. \quad (5)$$

While the mass and volume of the cholesterol fraction change, its intrinsic density does not. Hence:

$$\frac{m_{\text{pre}}}{V_{\text{pre}}} = \frac{m_{\text{post}}}{V_{\text{post}}} \Rightarrow V_{\text{post}} = \frac{m_{\text{post}}}{m_{\text{pre}}} \times V_{\text{pre}} \quad (6)$$

$\frac{m_{\text{post}}}{m_{\text{pre}}}$  = the mass post-treatment relative to the pre-treatment mass, which was defined as the dimensionless parameter  $M$ . The RHS of Eq. (6) then simplified to:  $V_{s\text{-pre}} \times M$ . A similar procedure was followed for  $V_r$ .

In order to define the mass density of the vesicles post-treatment, Eq. (3) was modified and normalized to take account of the change of mass. This yielded:

$$\rho_{\text{post}} = \frac{V_r \times \rho_r + V_s \times \rho_s \times M_{s\text{-post}}}{V_r + V_s \times M_{s\text{-post}}}. \quad (7)$$

## Statistical analysis

Data are presented as mean  $\pm$  SEM of at least three determinations. Statistical significance was assessed using the two-tailed student  $t$  test and  $P$  values  $< 0.05$  were deemed to be statistically significant.

## RESULTS

### Changes in membrane composition and density following cholesterol depletion

The starting material for this set of experiments was our previously characterized cholesterol-rich intracellular membrane fraction prepared from post-nuclear cell supernatants. These membranes were isolated on equilibrium sucrose density gradients and their identity as a TGN-endosomal fraction was confirmed by Western blotting for

PI4KII $\alpha$  and syntaxin-6 (Minogue *et al.*, 2010; Waugh *et al.*, 2006). To investigate in more detail the relationship between cholesterol levels, membrane composition and membrane biophysical properties, we employed our recently described floatation assay method to determine the equilibrium buoyant densities of TGN-endosomal membrane domains using sucrose gradients (see work flow chart in Fig. 1). This technique involved treating the membranes with cyclodextrin (10 mM) for 10 min to extract cholesterol followed by probe sonication to induce their vesicularization and fragmentation (Waugh, Lawson & Hsuan, 1999; Waugh *et al.*, 1998). The sonication step was carried out in alkaline carbonate buffer which is a well-established means for removing peripheral proteins including actin from membranes (Fujiki *et al.*, 1982; Nebl *et al.*, 2002). This procedure was necessary in light of the extensive literature demonstrating that peripherally associated membrane proteins can influence membrane architecture, geometry and density, and such additional heterogeneity in these membrane characteristics could potentially complicate subsequent biophysical analyses. This combination of probe sonication and carbonate addition was aimed at generating a population of membrane vesicles stripped of peripheral proteins including cyclodextrin-sensitive cytoskeletal proteins which have the potential to modify membrane microdomain stability. Furthermore, the inclusion of these treatments meant that the integral protein and lipid compositions of the vesicles would be the principal determinants of membrane density.

In this set of experiments we compared the effects of cyclodextrin treatment on the biochemical composition of the buoyant (fractions 5–8) and dense (fractions 9–12) regions of the sucrose gradient. Cyclodextrin addition resulted in a large ( $83.4 \pm 2.75\%$ ,  $n = 3$ ) decrease in the cholesterol mass of the buoyant fractions protein without any significant accumulation in the denser region of the sucrose gradient (Fig. 2). This large reduction in cholesterol also coincided with a relocalization of the membrane-associated PI4KII $\alpha$  protein to denser membrane fractions 9–12 (Fig. 2). We quantified this change in PI4KII $\alpha$  distribution, which was also noted in our previous publication (Minogue *et al.*, 2010), and found that unlike the situation with cholesterol, cyclodextrin did not result in an overall loss of PI4KII $\alpha$  from the membrane fractions.

We used refractometry to measure the sucrose density of the gradient fractions. Trial experiments revealed that the final, diluted cyclodextrin concentrations of 200 mM present in the dense gradient fractions did not impact on the refractive index readings for these samples. These measurements allowed us to determine that the inclusion of cyclodextrin caused the main protein fraction to shift in density from 1.096 to 1.126 g/mL (Fig. 3).

Finally, we measured cyclodextrin-effected changes to the hydrodynamic diameter of the vesicles by dynamic light scattering. Even though the isolated membrane vesicles were found to be heterogeneous we focused on a peak signal corresponding to a vesicle population in the biologically relevant size range of 10–1,000 nm. We ascertained that while there was no change in the total number of vesicles, the average vesicle diameter shrank from 780 to 42 nm in the buoyant fraction and from 453 to 271 nm in the dense fraction (Table 1). These results showed that the reduction in cholesterol levels

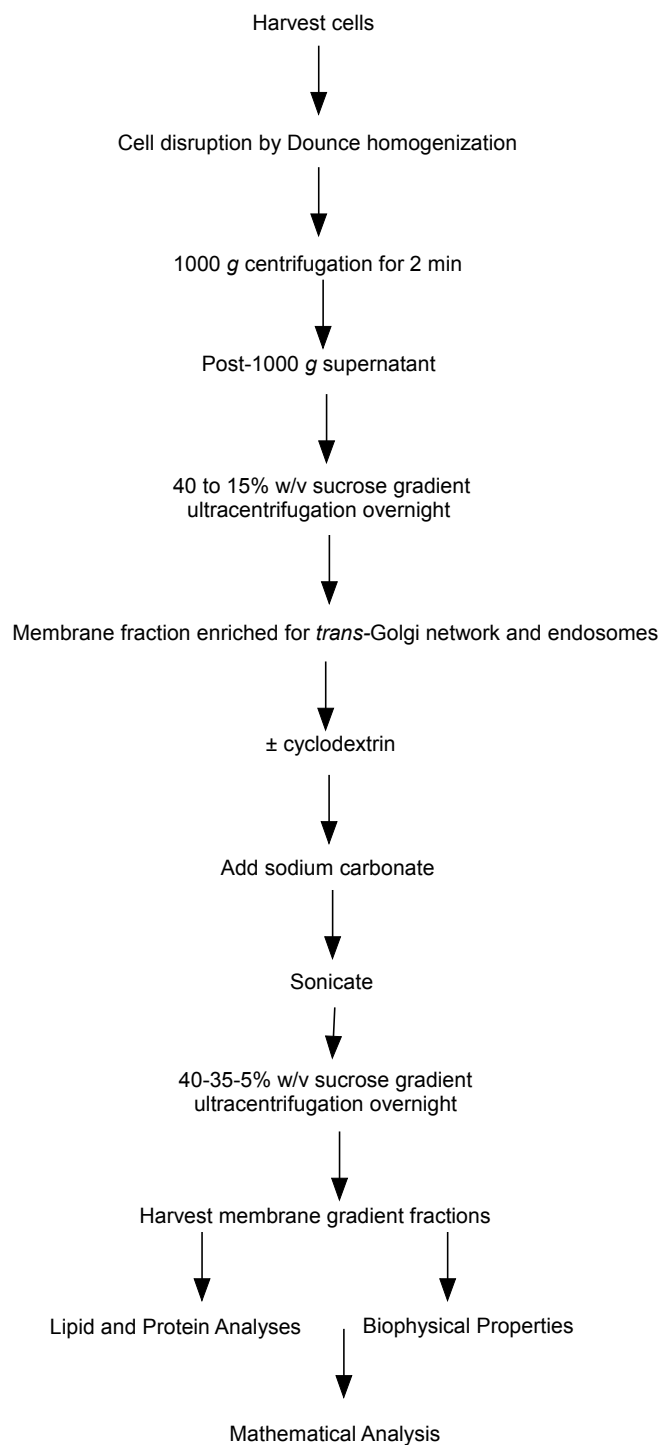


**Figure 1** Flow chart of steps involved in the subcellular fractionation procedures. Flow chart outlining the steps involved in the subcellular fractionation procedures, equilibrium density floatation assay and membrane analyses used in the experiments.

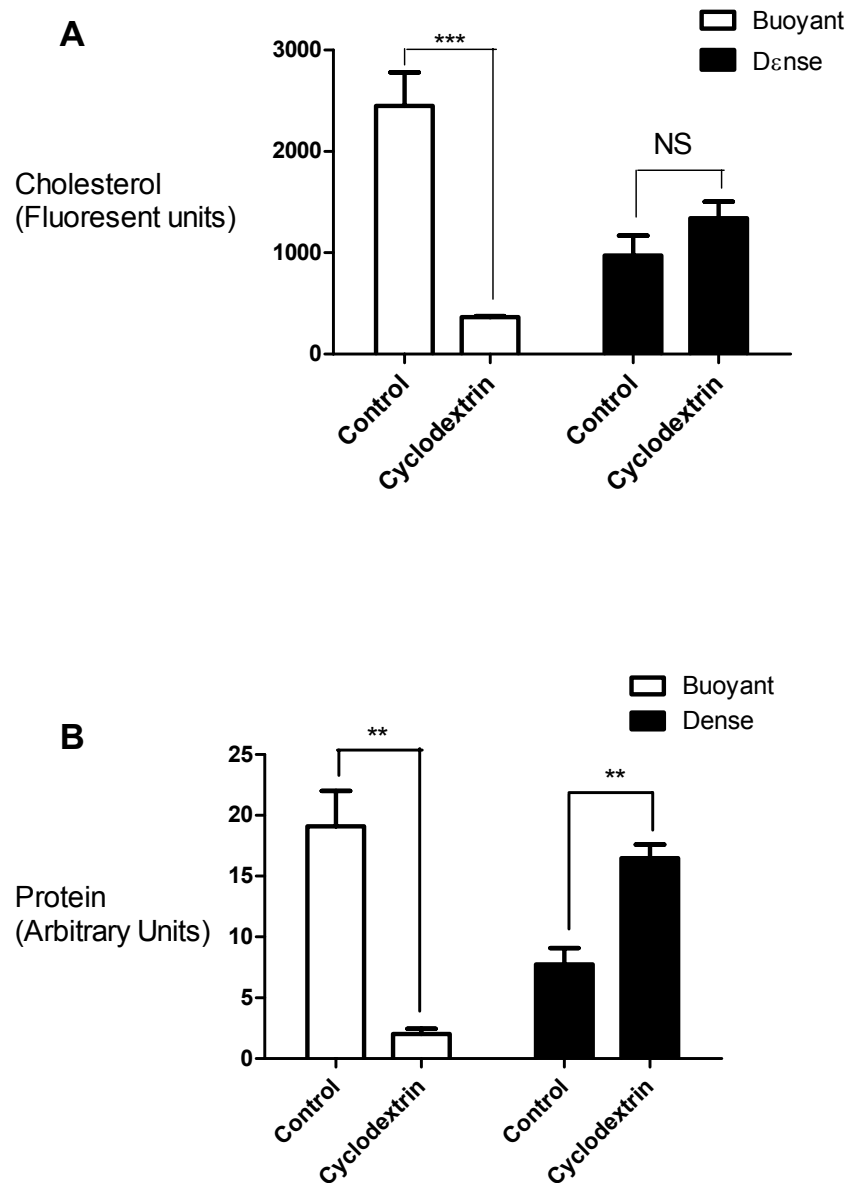


**Figure 2** Effects of cyclodextrin on vesicle composition. Comparing the effects of cyclodextrin treatment on the biochemical composition of buoyant and dense membrane fractions isolated on equilibrium sucrose density gradients. (A) Change in cholesterol levels as determined by Amplex Red cholesterol assays. Note that there was no significant change in the total amount of cholesterol present in the dense membranes. (B) Levels of the membrane-associated protein PI4KII $\alpha$  were determined by Western blotting and quantitated by image analysis software. Cyclodextrin addition causes a redistribution of PI4KII $\alpha$  from the buoyant to the dense fractions. Results are presented as mean  $\pm$  S.E.M from experiments repeated three times, \*\*\* $p$  < 0.001, \*\* $p$  < 0.01, NS not statistically significant using the two-tailed student  $t$ -test.

brought about by cyclodextrin treatment caused the membrane vesicle sizes to decrease considerably.

Together, these experiments revealed that cholesterol depletion with cyclodextrin resulted in a reduction in membrane buoyancy, as evidenced by the delocalization of

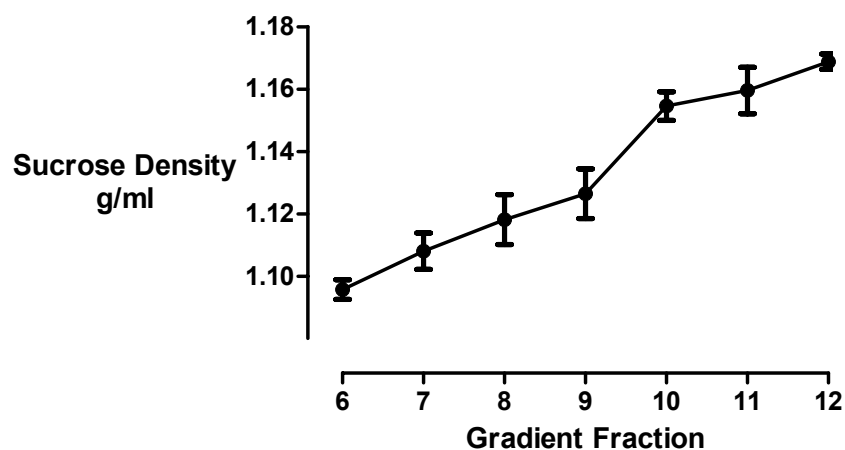


**Figure 3** Sucrose density gradient profile. The density of each gradient fraction was determined by refractometry and the conversion of refractive index values to sucrose concentrations was accomplished using Blix tables. Results are presented as mean  $\pm$  S.E.M. of an experiment repeated three times.

**Table 1** Size of membrane vesicles in different gradient fractions following cholesterol depletion with cyclodextrin. The size distributions, as measured by dynamic light scattering, of control and cyclodextrin-treated membrane vesicles from different gradient fractions. Results are presented as the mean  $\pm$  S.D. of triplicate determinations.

| Treatment             | Gradient fraction | Size (nm)         |
|-----------------------|-------------------|-------------------|
| Control               | Buoyant           | 779.5 $\pm$ 28.2  |
|                       | Dense             | 453.0 $\pm$ 177.1 |
| Cholesterol depletion | Buoyant           | 42.2 $\pm$ 11.5   |
|                       | Dense             | 270.2 $\pm$ 68.8  |

PI4KII $\alpha$ -containing membranes to a denser region of the sucrose gradient and also a reduction in membrane size. Therefore, we decided to mathematically model the relationship between these different parameters.

## MATHEMATICAL MODELING

In this model, we determined an expected value for vesicle size post cyclodextrin treatment in our system and compared it with experimental data. From our experimental measurements, there was an  $83.4 \pm 2.75\%$  reduction in the cyclodextrin sensitive cholesterol component with other components not directly affected by the treatment. The total increase in mass density of the vesicles through cyclodextrin treatment was known (from  $1.096 \pm 0.003$  mg/mL for fraction 5 to  $1.122 \pm 0.0005$  mg/mL for fraction 10). The % composition of these two components and the density of the non-cholesterol residual component were unknown and approximated in this work, based on the above assumptions.

To determine the volumetric fractional composition of the vesicles pre cyclodextrin treatment and the density of the residual component, the experimentally measured values

were inserted into Eqs. (4), (6) and (7), giving Eqs. (8)–(10):

$$V_r \times \rho_r + V_s \times 1.067 = 1.096 \pm 0.003 \quad (8)$$

$$V_r + V_s = 1 \quad (9)$$

$$\frac{V_r \times \rho_r + V_s \times 1.067 \times (0.166 \pm 0.00275)}{V_r + V_s \times (0.166 \pm 0.00275)} = 1.122 \pm 0.0005. \quad (10)$$

Calculating these Eqs. (8)–(10) allowed us to predict the volume fractions of the vesicle pretreatment as follows—cholesterol  $0.567 \pm 0.072$  ( $56.7 \pm 7.2\%$ ), residual component  $0.433 \pm 0.072$  ( $43.3 \pm 7.2\%$ ), and a density of the residual component of  $1.134 \pm 0.005$  mg/mL. As liquid-ordered domains typically comprises 20–30% cholesterol, the higher than expected value determined here is most likely the result of some membrane components being removed during the membrane isolation procedure and particularly by the alkaline carbonate addition step, leading to an apparent enrichment of cholesterol in the isolated fraction. Hence, the % value for cholesterol determined here is not the physiological proportion of cholesterol in TGN/endosomal membranes but rather, the amount present in the membrane vesicles after the extensive membrane disruption and isolation procedures used in this study. In concordance with this explanation, we have previously shown that membrane fractions prepared in the presence of carbonate are subject to substantial depletion of non-integral proteins (Waugh, 2013; Waugh et al., 2011a; Waugh et al., 2011b). As proteins have a density of 1.35 mg/mL (Chick & Martin, 1913; Fischer, Polikarpov & Craievich, 2004) and other membrane components such as lipids tend to have much lower densities, the value of  $1.134 \pm 0.005$  mg/mL calculated for the density of the residual component seems reasonable.

Cyclodextrin treatment resulted in the total amount of cholesterol in the system to be reduced by 83.4%; however, the absolute volumes of the other components remained constant. To calculate the volume concentrations post cyclodextrin, three more simultaneous equations were formulated and solved by the same method:

$$V_{r\text{-post}} \times \rho_r + V_{s\text{-post}} \times 1.067 = 1.122 \pm 0.0005 \quad (11)$$

$$V_{r\text{-post}} + V_{s\text{-post}} = 1 \quad (12)$$

$$\frac{V_{r\text{-post}} \times \rho_r + V_{s\text{-post}} \times 1.067 \times 6.02}{V_{r\text{-post}} + V_{s\text{-post}} \times 6.02} = 1.096 \pm 0.03. \quad (13)$$

The predicted vesicle composition post treatment obtained by solving any two of Eqs. (11)–(13) was: cholesterol  $0.179 \pm 0.047$  ( $17.9 \pm 4.7\%$ ) and residual component  $0.821 \pm 0.047$  ( $82.1 \pm 4.7\%$ ).

The relative volume of the treated vesicles was calculated through Eq. (14):

$$V_r + V_s \times 0.166 \pm 0.0275 = \text{New Volume} \quad (14)$$

giving a relative volume of  $0.527 \pm 0.073$ , i.e., post treatment, the vesicle was  $49.1 \pm 7.3\%$  of its original size. This corresponds to the diameter of the treated vesicles of  $0.81 \pm 0.04$ , i.e., the radius must have shrunk by  $19 \pm 4\%$ .

Experimental measurements showed the diameter of the vesicles falling from  $453 \pm 177.1$  nm to  $270.2 \pm 68.8$  nm post treatment, a 40.4% decline in diameter and thus an 88.8% fall in vesicle volume. This differs markedly from what has been calculated based on cyclodextrin affecting cholesterol alone and is consistent with previous work demonstrating that cyclodextrin can also sequester a range of hydrophobic molecules (reviewed in [Zidovetzki & Levitan, 2007](#)). These results imply that only about 50% of the change in membrane size is due to cholesterol desorption.

Since the mathematical analysis demonstrated that the decrease in membrane size could not be fully accounted for by cholesterol loss, we investigated the effect of cyclodextrin addition on the levels of membrane gangliosides which are glycosphingolipids that are structurally unrelated to sterols. Changes in ganglioside lipid distribution were determined using HRP-conjugated cholera toxin B subunit as a probe. Kuziemko and colleagues ([Kuziemko, Stroh & Stevens, 1996](#)) previously determined that Cholera-toxin binds to gangliosides in the order GM1 > GM2 > GD1A > GM3 > GT1B > GD1B > asialo-GM1, albeit with a >200 fold difference in binding affinity between GM1 and asialo-GM1. Therefore, unlike thin layer chromatography, dot-blotting immobilized sucrose density gradient fractions with cholera toxin B subunit does not permit the separation and quantitation of individual glycosphingolipid species. Furthermore there is a possibility that in addition to gangliosides, the toxin may also bind to the carbohydrate moieties of glycosylated proteins associated with the isolated vesicles ([Blank et al., 2007](#); [Uesaka et al., 1994](#)). Bearing in mind these limitations, we used this well established technique ([Clarke, Ohanian & Ohanian, 2007](#); [Correa et al., 2007](#); [Domon et al., 2011](#); [Ersek et al., 2015](#); [Ilangumaran et al., 1996](#); [Liu, Yao & Suzuki, 2013](#); [Liu et al., 2015](#); [Mazzone et al., 2006](#); [Nguyen et al., 2007](#); [Pang, Urquhart & Hooper, 2004](#); [Pristera, Baker & Okuse, 2012](#); [Russelakis-Carneiro et al., 2004](#); [Tauzin et al., 2008](#); [Waugh, 2013](#); [Waugh et al., 2011a](#); [Waugh et al., 2011b](#)) to generate a composite yet simple signal to assess if there was any redistribution of these structurally related non-sterol molecules in the density gradient following cyclodextrin addition ([Fig. 4](#)). We observed that the ganglioside content of the buoyant fractions was decreased by about 50% following cyclodextrin treatment and this is consistent with mathematical analysis that vesicle size reduction is due to the non-selective desorption of membrane lipids.

## DISCUSSION

Our combined biophysical, biochemical, and mathematical analyses demonstrate that cyclodextrin-induced cholesterol extraction can lead to an increase in equilibrium density by inducing membrane shrinkage. The cyclodextrin-induced shift of biomolecules to a denser membrane fraction can be accounted for by a large change in vesicle volume, without necessarily having to evoke the disruption of liquid-ordered membrane microdomains. These new findings have implications for the use of cyclodextrin-induced sterol depletion as a means of assessing whether a protein associates with cholesterol-rich lipid rafts. At high cholesterol levels, such as those reported here in the control buoyant membranes, one might expect significant levels of lipid rafts or even for the entire

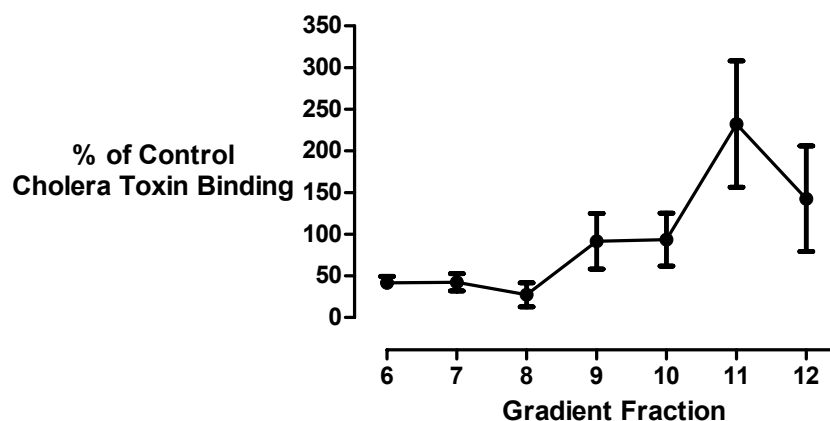


**Figure 4** Effect of cyclodextrin on ganglioside distribution profile. Dot blotting of equal volume membrane fractions and detection with HRP-conjugated cholera toxin B subunit was used to determine the levels of ganglioside lipids in control and cyclodextrin-treated membrane fractions. Cyclodextrin addition resulted in a decrease in HRP-conjugated cholera toxin B subunit binding to the buoyant membrane fractions. Results are presented as mean  $\pm$  S.E.M from experiments repeated three times.

membrane to exist solely in the liquid-ordered phase (Almeida, Pokorny & Hinderliter, 2005; Armstrong et al., 2013; Munro, 2003; Swamy et al., 2006) and hence, removal of cholesterol with cyclodextrin would be predicted to disrupt these rafts (Cabrera-Poch et al., 2004; Kabouridis et al., 2000; Larbi et al., 2004). However, in the context of the type of experiments described here, a cyclodextrin-dependent change in membrane density may only imply that a biomolecule is associated with a cholesterol-rich membrane and does not necessarily report the stable association of that component with lipid raft microdomains.

Our results suggest that at least under the experimental conditions employed here, cyclodextrin-induced reduction of membrane size can also be effected by the extraction of molecules other than sterols. The apparent lack of selectivity for cyclodextrin-induced biomolecule desorption demonstrated here leads us to speculate that these agents could potentially be repurposed to treat a range of conditions similar to Niemann-Pick type C, that feature enlarged endosomal membrane phenotypes due to defective lipid trafficking and/or metabolism but importantly, do not necessarily involve cholesterol accumulation. An example of a disease to consider in this regard could be oculocerebrorenal syndrome of Lowe (OCRL), a neurodevelopmental condition characterized by phosphatidylinositol 4,5-bisphosphate accumulation on endosomal membranes due to inactivating mutations in the OCRL phosphoinositide 5-phosphatase (reviewed in Billcliff & Lowe, 2014; Clayton, Minogue & Waugh, 2013b). Furthermore, whilst cyclodextrin has a high affinity for sterol lipids it is also known to bind phosphoinositides such as phosphatidylinositol 4-phosphate (Davis, Perera & Boss, 2004), and this further supports the idea that these macromolecules could have applications in the treatment of a number of inherited phospholipid storage disorders. This suggests a new type of drug action involving agents designed to alter membrane surface area through the reduction of membrane mass. The objective of such treatments would be to increase the membrane concentrations of more cyclodextrin-resistant biomolecules, in order to restore or amplify membrane-based

signaling or trafficking functions. This has already been shown for the epidermal growth factor receptor, which is subject to augmented levels of constitutive activation following cyclodextrin treatment (*Pike & Casey, 2002; Westover et al., 2003*). However, these possible uses for cyclodextrin remain speculative and further work is required to investigate if the biophysical changes documented here under specific *in vitro* conditions also occur on intracellular membranes in live cells.

In conclusion, this work throws new light on the mechanism of action of methyl- $\beta$ -cyclodextrin on biological membranes. This may lead to a reassessment of its use in cell-based laboratory experiments while at the same time widening its potential applications in the therapeutic arena. In particular, this study indicates that the cholesterol-independent effects of cyclodextrin on membrane area may have more general applications in the treatment of intracellular lipid storage diseases.

### Nomenclature

|        |                     |
|--------|---------------------|
| $\rho$ | mass density (kg/L) |
| $V$    | volume (L)          |

## ADDITIONAL INFORMATION AND DECLARATIONS

### Funding

Financial support was provided by the Royal Free Charity (Dr. Mark G. Waugh), and the Royal Society for University Research Fellowship (Prof Nguyễn T.K. Thanh). The funders had no role in study design, data collection and analysis, decision to publish, or preparation of the manuscript.

### Grant Disclosures

The following grant information was disclosed by the authors:

Royal Free Charity.

Royal Society for University Research Fellowship.

### Competing Interests

The authors declare there are no competing interests.

### Author Contributions

- Peter Kilbride performed the experiments, analyzed the data, wrote the paper, reviewed drafts of the paper.
- Holly J. Woodward performed the experiments.
- Kuan Boone Tan performed the experiments, analyzed the data, contributed reagents/materials/analysis tools, reviewed drafts of the paper.
- Nguyễn T.K. Thanh analyzed the data, contributed reagents/materials/analysis tools, wrote the paper, reviewed drafts of the paper.
- K.M. Emily Chu performed the experiments, wrote the paper, reviewed drafts of the paper.

- Shane Minogue contributed reagents/materials/analysis tools, reviewed drafts of the paper.
- Mark G. Waugh conceived and designed the experiments, performed the experiments, analyzed the data, contributed reagents/materials/analysis tools, wrote the paper, prepared figures and/or tables, reviewed drafts of the paper.

### Supplemental Information

Supplemental information for this article can be found online at <http://dx.doi.org/10.7717/peerj.1351#supplemental-information>.

### REFERENCES

- Almeida PF, Pokorny A, Hinderliter A. 2005.** Thermodynamics of membrane domains. *Biochimica et Biophysica ACTA/Biomembranes* **1720**:1–13 DOI [10.1016/j.bbamem.2005.12.004](https://doi.org/10.1016/j.bbamem.2005.12.004).
- Armstrong CL, Marquardt D, Dies H, Kucerka N, Yamani Z, Harroun TA, Katsaras J, Shi AC, Rheinstadter MC. 2013.** The observation of highly ordered domains in membranes with cholesterol. *PLoS ONE* **8**:e66162 DOI [10.1371/journal.pone.0066162](https://doi.org/10.1371/journal.pone.0066162).
- Barylko B, Mao YS, Wlodarski P, Jung G, Binns DD, Sun HQ, Yin HL, Albanesi JP. 2009.** Palmitoylation controls the catalytic activity and subcellular distribution of phosphatidylinositol 4-kinase II $\alpha$ . *Journal of Biological Chemistry* **284**:9994–10003 DOI [10.1074/jbc.M900724200](https://doi.org/10.1074/jbc.M900724200).
- Bate C, Tayebi M, Williams A. 2008.** Sequestration of free cholesterol in cell membranes by prions correlates with cytoplasmic phospholipase A2 activation. *BMC Biology* **6**:8 DOI [10.1186/1741-7007-6-8](https://doi.org/10.1186/1741-7007-6-8).
- Billcliff PG, Lowe M. 2014.** Inositol lipid phosphatases in membrane trafficking and human disease. *Biochemical Journal* **461**:159–175 DOI [10.1042/BJ20140361](https://doi.org/10.1042/BJ20140361).
- Blank N, Schiller M, Krienke S, Wabnitz G, Ho AD, Lorenz HM. 2007.** Cholera toxin binds to lipid rafts but has a limited specificity for ganglioside GM1. *Immunology and Cell Biology* **85**:378–382 DOI [10.1038/sj.icb.7100045](https://doi.org/10.1038/sj.icb.7100045).
- Cabrera-Poch N, Sanchez-Ruiloba L, Rodriguez-Martinez M, Iglesias T. 2004.** Lipid raft disruption triggers protein kinase C and Src-dependent protein kinase D activation and Kidins220 phosphorylation in neuronal cells. *Journal of Biological Chemistry* **279**:28592–28602 DOI [10.1074/jbc.M312242200](https://doi.org/10.1074/jbc.M312242200).
- Camargo F, Erickson RP, Garver WS, Hossain GS, Carbone PN, Heidenreich RA, Blanchard J. 2001.** Cyclodextrins in the treatment of a mouse model of Niemann-Pick C disease. *Life Sciences* **70**:131–142 DOI [10.1016/S0024-3205\(01\)01384-4](https://doi.org/10.1016/S0024-3205(01)01384-4).
- Chick H, Martin CJ. 1913.** The density and solution volume of some proteins. *Biochemical Journal* **7**:92–96 DOI [10.1042/bj0070092](https://doi.org/10.1042/bj0070092).
- Chu KM, Minogue S, Hsuan JJ, Waugh MG. 2010.** Differential effects of the phosphatidylinositol 4-kinases, PI4KII $\alpha$  and PI4KIII $\beta$ , on Akt activation and apoptosis. *Cell Death and Disease* **1**:e106 DOI [10.1038/cddis.2010.84](https://doi.org/10.1038/cddis.2010.84).
- Clarke CJ, Ohanian V, Ohanian J. 2007.** Norepinephrine and endothelin activate diacylglycerol kinases in caveolae/rafts of rat mesenteric arteries: agonist-specific role of PI3-kinase. *American Journal of Physiology Heart and Circulatory Physiology* **292**:H2248–H2256 DOI [10.1152/ajpheart.01170.2006](https://doi.org/10.1152/ajpheart.01170.2006).

- Clayton EL, Minogue S, Waugh MG. 2013a. Mammalian phosphatidylinositol 4-kinases as modulators of membrane trafficking and lipid signaling networks. *Progress in Lipid Research* 52:294–304 DOI 10.1016/j.plipres.2013.04.002.
- Clayton EL, Minogue S, Waugh MG. 2013b. Phosphatidylinositol 4-kinases and PI4P metabolism in the nervous system: roles in psychiatric and neurological diseases. *Molecular Neurobiology* 47:361–372 DOI 10.1007/s12035-012-8358-6.
- Correa JR, Atella GC, Vargas C, Soares MJ. 2007. Transferrin uptake may occur through detergent-resistant membrane domains at the cytopharynx of Trypanosoma cruzi epimastigote forms. *Memorias do Instituto Oswaldo Cruz* 102:871–876 DOI 10.1590/S0074-02762007005000117.
- Davidson CD, Ali NF, Micsenyi MC, Stephney G, Renault S, Dobrenis K, Ory DS, Vanier MT, Walkley SU. 2009. Chronic cyclodextrin treatment of murine Niemann-Pick C disease ameliorates neuronal cholesterol and glycosphingolipid storage and disease progression. *PLoS ONE* 4:e6951 DOI 10.1371/journal.pone.0006951.
- Davis AJ, Perera IY, Boss WF. 2004. Cyclodextrins enhance recombinant phosphatidylinositol phosphate kinase activity. *Journal of Lipid Research* 45:1783–1789 DOI 10.1194/jlr.D400005-JLR200.
- Dawson RMC, Elliot DC, Elliot WH, Jones KM. 1986. *Data for biochemical research*. 3rd edition. Oxford: Clarendon Press.
- Domon MM, Besson F, Bandorowicz-Pikula J, Pikula S. 2011. Annexin A6 is recruited into lipid rafts of Niemann-Pick type C disease fibroblasts in a Ca<sup>2+</sup>-dependent manner. *Biochemical and Biophysical Research Communications* 405:192–196 DOI 10.1016/j.bbrc.2010.12.138.
- Ersek A, Xu K, Antonopoulos A, Butters TD, Santo AE, Vattakuzhi Y, Williams LM, Goudevenou K, Danks L, Freidin A, Spanoudakis E, Parry S, Papaioannou M, Hatjiharissi E, Chaidos A, Alonzi DS, Twigg G, Hu M, Dwek RA, Haslam SM, Roberts I, Dell A, Rahemtulla A, Horwood NJ, Karadimitris A. 2015. Glycosphingolipid synthesis inhibition limits osteoclast activation and myeloma bone disease. *Journal of Clinical Investigation* 125:2279–2292 DOI 10.1172/JCI59987.
- Fischer H, Polikarpov I, Craievich AF. 2004. Average protein density is a molecular-weight-dependent function. *Protein Science* 13:2825–2828 DOI 10.1110/ps.04688204.
- Fujiki Y, Hubbard AL, Fowler S, Lazarow PB. 1982. Isolation of intracellular membranes by means of sodium carbonate treatment: application to endoplasmic reticulum. *Journal of Cell Biology* 93:97–102 DOI 10.1083/jcb.93.1.97.
- Haynes WM. 2013. *CRC handbook of chemistry and physics*. 94th edition. Boca Raton: CRC Press, Taylor & Francis Group.
- Heine T, Dos Santos HF, Patchkovskii S, Duarte HA. 2007. Structure and dynamics of beta-cyclodextrin in aqueous solution at the density-functional tight binding level. *The Journal of Physical Chemistry A* 111:5648–5654 DOI 10.1021/jp068988s.
- Hill WG, An B, Johnson JP. 2002. Endogenously expressed epithelial sodium channel is present in lipid rafts in A6 cells. *Journal of Biological Chemistry* 277:33541–33544 DOI 10.1074/jbc.C200309200.
- Holtta-Vuori M, Tanhuanpaa K, Mobius W, Somerharju P, Ikonen E. 2002. Modulation of cellular cholesterol transport and homeostasis by Rab11. *Molecular Biology of the Cell* 13:3107–3122 DOI 10.1091/mbc.E02-01-0025.
- Ilangumaran S, Arni S, Chicheportiche Y, Briol A, Hoessli DC. 1996. Evaluation by dot-immunoassay of the differential distribution of cell surface and intracellular proteins

- in glycosylphosphatidylinositol-rich plasma membrane domains. *Analytical Biochemistry* 235:49–56 DOI 10.1006/abio.1996.0090.
- Kabouridis PS, Janzen J, Magee AL, Ley SC. 2000.** Cholesterol depletion disrupts lipid rafts and modulates the activity of multiple signaling pathways in T lymphocytes. *European Journal of Immunology* 30:954–963 DOI 10.1002/1521-4141(200003)30:3<954::AID-IMMU954>3.0.CO;2-Y.
- Kuziemko GM, Stroh M, Stevens RC. 1996.** Cholera toxin binding affinity and specificity for gangliosides determined by surface plasmon resonance. *Biochemistry* 35:6375–6384 DOI 10.1021/bi952314i.
- Larbi A, Douziech N, Khalil A, Dupuis G, Gherairi S, Guerard KP, Fulop Jr T. 2004.** Effects of methyl-beta-cyclodextrin on T lymphocytes lipid rafts with aging. *Experimental Gerontology* 39:551–558 DOI 10.1016/j.exger.2003.10.031.
- Li J, Lu Y, Zhang J, Kang H, Qin Z, Chen C. 2010.** PI4KII $\alpha$  is a novel regulator of tumor growth by its action on angiogenesis and HIF-1 $\alpha$  regulation. *Oncogene* 29:2550–2559 DOI 10.1038/onc.2010.14.
- Li J, Zhang L, Gao Z, Kang H, Rong G, Zhang X, Chen C. 2014.** Dual inhibition of EGFR at protein and activity level via combinatorial blocking of PI4KII $\alpha$  as anti-tumor strategy. *Protein Cell* 5:457–468 DOI 10.1007/s13238-014-0055-y.
- Lim CH, Schoonderwoerd K, Kleijer WJ, De Jonge HR, Tilly BC. 2006.** Regulation of the cell swelling-activated chloride conductance by cholesterol-rich membrane domains. *Acta Physiologica* 187:295–303 DOI 10.1111/j.1748-1716.2006.01534.x.
- Liu B, Li H, Repa JJ, Turley SD, Dietschy JM. 2008.** Genetic variations and treatments that affect the lifespan of the NPC1 mouse. *Journal of Lipid Research* 49:663–669 DOI 10.1194/jlr.M700525-JLR200.
- Liu B, Ramirez CM, Miller AM, Repa JJ, Turley SD, Dietschy JM. 2010.** Cyclodextrin overcomes the transport defect in nearly every organ of NPC1 mice leading to excretion of sequestered cholesterol as bile acid. *Journal of Lipid Research* 51:933–944 DOI 10.1194/jlr.M000257.
- Liu B, Turley SD, Burns DK, Miller AM, Repa JJ, Dietschy JM. 2009.** Reversal of defective lysosomal transport in NPC disease ameliorates liver dysfunction and neurodegeneration in the npc1<sup>-/-</sup> mouse. *Proceedings of the National Academy of Sciences of the United States of America* 106:2377–2382 DOI 10.1073/pnas.0810895106.
- Liu Q, Yao WD, Suzuki T. 2013.** Specific interaction of postsynaptic densities with membrane rafts isolated from synaptic plasma membranes. *Journal of Neurogenetics* 27:43–58 DOI 10.3109/01677063.2013.772175.
- Liu T-M, Ling Y, Woyach JA, Beckwith K, Yeh Y-Y, Hertlein E, Zhang X, Lehman A, Awan F, Jones JA, Andritsos LA, Maddocks K, MacMurray J, Salunke SB, Chen C-S, Phelps MA, Byrd JC, Johnson AJ. 2015.** OSU-T315: a novel targeted therapeutic that antagonizes AKT membrane localization and activation of chronic lymphocytic leukemia cells. *Blood* 125:284–295 DOI 10.1182/blood-2014-06-583518.
- Loftsson T, Brewster ME. 1996.** Pharmaceutical applications of cyclodextrins. 1. Drug solubilization and stabilization. *Journal of Pharmaceutical Sciences* 85:1017–1025 DOI 10.1021/js950534b.
- Lu D, Sun HQ, Wang H, Barylko B, Fukata Y, Fukata M, Albanesi JP, Yin HL. 2012.** Phosphatidylinositol 4-kinase II $\alpha$  is palmitoylated by Golgi-localized palmitoyltransferases in cholesterol-dependent manner. *Journal of Biological Chemistry* 287:21856–21865 DOI 10.1074/jbc.M112.348094.

- Matarazzo S, Quitadamo MC, Mango R, Ciccone S, Novelli G, Biocca S. 2012.** Cholesterol-lowering drugs inhibit lectin-like oxidized low-density lipoprotein-1 receptor function by membrane raft disruption. *Molecular Pharmacology* **82**:246–254 DOI [10.1124/mol.112.078915](https://doi.org/10.1124/mol.112.078915).
- Mazzone A, Tietz P, Jefferson J, Pagano R, LaRusso NF. 2006.** Isolation and characterization of lipid microdomains from apical and basolateral plasma membranes of rat hepatocytes. *Hepatology* **43**:287–296 DOI [10.1002/hep.21039](https://doi.org/10.1002/hep.21039).
- Mbua NE, Flanagan-Steet H, Johnson S, Wolfert MA, Boons GJ, Steet R. 2013.** Abnormal accumulation and recycling of glycoproteins visualized in Niemann-Pick type C cells using the chemical reporter strategy. *Proceedings of the National Academy of Sciences of the United States of America* **110**:10207–10212 DOI [10.1073/pnas.1221105110](https://doi.org/10.1073/pnas.1221105110).
- Minogue S, Chu KM, Westover EJ, Covey DF, Hsuan JJ, Waugh MG. 2010.** Relationship between phosphatidylinositol 4-phosphate synthesis, membrane organization, and lateral diffusion of PI4KII $\alpha$  at the trans-Golgi network. *Journal of Lipid Research* **51**:2314–2324 DOI [10.1194/jlr.M005751](https://doi.org/10.1194/jlr.M005751).
- Munro S. 2003.** Lipid rafts: elusive or illusive? *Cell* **115**:377–388 DOI [10.1016/S0092-8674\(03\)00882-1](https://doi.org/10.1016/S0092-8674(03)00882-1).
- Navratil AM, Bliss SP, Berghorn KA, Haughian JM, Farmerie TA, Graham JK, Clay CM, Roberson MS. 2003.** Constitutive localization of the gonadotropin-releasing hormone (GnRH) receptor to low density membrane microdomains is necessary for GnRH signaling to ERK. *Journal of Biological Chemistry* **278**:31593–31602 DOI [10.1074/jbc.M304273200](https://doi.org/10.1074/jbc.M304273200).
- Nebi T, Pestonjamas KN, Leszyk JD, Crowley JL, Oh SW, Luna EJ. 2002.** Proteomic analysis of a detergent-resistant membrane skeleton from neutrophil plasma membranes. *Journal of Biological Chemistry* **277**:43399–43409 DOI [10.1074/jbc.M205386200](https://doi.org/10.1074/jbc.M205386200).
- Nguyen HT, Charrier-Hisamuddin L, Dalmasso G, Hiol A, Sitaraman S, Merlin D. 2007.** Association of PepT1 with lipid rafts differently modulates its transport activity in polarized and nonpolarized cells. *American Journal of Physiology Gastrointestinal and Liver Physiology* **293**:G1155–G1165 DOI [10.1152/ajpgi.00334.2007](https://doi.org/10.1152/ajpgi.00334.2007).
- Nicholson AM, Ferreira A. 2009.** Increased membrane cholesterol might render mature hippocampal neurons more susceptible to beta-amyloid-induced calpain activation and tau toxicity. *Journal of Neuroscience* **29**:4640–4651 DOI [10.1523/JNEUROSCI.0862-09.2009](https://doi.org/10.1523/JNEUROSCI.0862-09.2009).
- Ottico E, Prinetti A, Prioni S, Giannotta C, Basso L, Chigorno V, Sonnino S. 2003.** Dynamics of membrane lipid domains in neuronal cells differentiated in culture. *Journal of Lipid Research* **44**:2142–2151 DOI [10.1194/jlr.M300247-JLR200](https://doi.org/10.1194/jlr.M300247-JLR200).
- Paladino S, Lebreton S, Tivodar S, Formiggini F, Ossato G, Gratton E, Tramier M, Coppey-Moisan M, Zurzolo C. 2014.** Golgi sorting regulates organization and activity of GPI proteins at apical membranes. *Nature Chemical Biology* **10**:350–357 DOI [10.1038/nchembio.1495](https://doi.org/10.1038/nchembio.1495).
- Pang S, Urquhart P, Hooper NM. 2004.** N-glycans, not the GPI anchor, mediate the apical targeting of a naturally glycosylated, GPI-anchored protein in polarised epithelial cells. *Journal of Cell Science* **117**:5079–5086 DOI [10.1242/jcs.01386](https://doi.org/10.1242/jcs.01386).
- Pike LJ, Casey L. 2002.** Cholesterol levels modulate EGF receptor-mediated signaling by altering receptor function and trafficking. *Biochemistry* **41**:10315–10322 DOI [10.1021/bi025943i](https://doi.org/10.1021/bi025943i).
- Pike LJ, Miller JM. 1998.** Cholesterol depletion delocalizes phosphatidylinositol bisphosphate and inhibits hormone-stimulated phosphatidylinositol turnover. *Journal of Biological Chemistry* **273**:22298–22304 DOI [10.1074/jbc.273.35.22298](https://doi.org/10.1074/jbc.273.35.22298).

- Pinjari RV, Joshi KA, Gejji SP. 2006.** Molecular electrostatic potentials and hydrogen bonding in alpha-, beta-, and gamma-cyclodextrins. *The Journal of Physical Chemistry A* **110**:13073–13080 DOI [10.1021/jp065169z](https://doi.org/10.1021/jp065169z).
- Pontikis CC, Davidson CD, Walkley SU, Platt FM, Begley DJ. 2013.** Cyclodextrin alleviates neuronal storage of cholesterol in Niemann-Pick C disease without evidence of detectable blood–brain barrier permeability. *Journal of Inherited Metabolic Disease* **36**:491–498 DOI [10.1007/s10545-012-9583-x](https://doi.org/10.1007/s10545-012-9583-x).
- Priester A, Baker MD, Okuse K. 2012.** Association between tetrodotoxin resistant channels and lipid rafts regulates sensory neuron excitability. *PLoS ONE* **7**:e40079 DOI [10.1371/journal.pone.0040079](https://doi.org/10.1371/journal.pone.0040079).
- Ramirez CM, Liu B, Aqul A, Taylor AM, Repa JJ, Turley SD, Dietschy JM.** Quantitative role of LAL, NPC2, and NPC1 in lysosomal cholesterol processing defined by genetic and pharmacological manipulations. *Journal of Lipid Research* **52**:688–698 DOI [10.1194/jlr.M013789](https://doi.org/10.1194/jlr.M013789).
- Ramirez CM, Liu B, Taylor AM, Repa JJ, Burns DK, Weinberg AG, Turley SD, Dietschy JM. 2010.** Weekly cyclodextrin administration normalizes cholesterol metabolism in nearly every organ of the Niemann-Pick type C1 mouse and markedly prolongs life. *Pediatric Research* **68**:309–315 DOI [10.1203/PDR.0b013e3181ee4dd2](https://doi.org/10.1203/PDR.0b013e3181ee4dd2).
- Rodal SK, Skretting G, Garred O, Vilhardt F, Van Deurs B, Sandvig K. 1999.** Extraction of cholesterol with methyl-beta-cyclodextrin perturbs formation of clathrin-coated endocytic vesicles. *Molecular Biology of the Cell* **10**:961–974 DOI [10.1091/mbc.10.4.961](https://doi.org/10.1091/mbc.10.4.961).
- Rosenbaum AI, Zhang G, Warren JD, Maxfield FR. 2010.** Endocytosis of beta-cyclodextrins is responsible for cholesterol reduction in Niemann-Pick type C mutant cells. *Proceedings of the National Academy of Sciences of the United States of America* **107**:5477–5482 DOI [10.1073/pnas.0914309107](https://doi.org/10.1073/pnas.0914309107).
- Russelakis-Carneiro M, Hetz C, Maundrell K, Soto C. 2004.** Prion replication alters the distribution of synaptophysin and caveolin 1 in neuronal lipid rafts. *American Journal of Pathology* **165**:1839–1848 DOI [10.1016/S0002-9440\(10\)63439-6](https://doi.org/10.1016/S0002-9440(10)63439-6).
- Shogomori H, Futerman AH. 2001.** Cholesterol depletion by methyl-beta-cyclodextrin blocks cholera toxin transport from endosomes to the Golgi apparatus in hippocampal neurons. *Journal of Neurochemistry* **78**:991–999 DOI [10.1046/j.1471-4159.2001.00489.x](https://doi.org/10.1046/j.1471-4159.2001.00489.x).
- Simons JP, Al-Shawi R, Minogue S, Waugh MG, Wiedemann C, Evangelou S, Loesch A, Sihra TS, King R, Warner TT, Hsuan JJ. 2009.** Loss of phosphatidylinositol 4-kinase 2alpha activity causes late onset degeneration of spinal cord axons. *Proceedings of the National Academy of Sciences of the United States of America* **106**:11535–11539 DOI [10.1073/pnas.0903011106](https://doi.org/10.1073/pnas.0903011106).
- Spisni E, Griffoni C, Santi S, Riccio M, Marulli R, Bartolini G, Toni M, Ullrich V, Tomasi V. 2001.** Colocalization prostacyclin (PGI<sub>2</sub>) synthase–caveolin-1 in endothelial cells and new roles for PGI<sub>2</sub> in angiogenesis. *Experimental Cell Research* **266**:31–43 DOI [10.1006/excr.2001.5198](https://doi.org/10.1006/excr.2001.5198).
- Swamy MJ, Ciani L, Ge M, Smith AK, Holowka D, Baird B, Freed JH. 2006.** Coexisting domains in the plasma membranes of live cells characterized by spin-label ESR spectroscopy. *Biophysical Journal* **90**:4452–4465 DOI [10.1529/biophysj.105.070839](https://doi.org/10.1529/biophysj.105.070839).
- Swaroop M, Thorne N, Rao MS, Austin CP, McKew JC, Zheng W. 2012.** Evaluation of cholesterol reduction activity of methyl-beta-cyclodextrin using differentiated human neurons and astrocytes. *Journal of Biomolecular Screening* **17**:1243–1251 DOI [10.1177/1087057112456877](https://doi.org/10.1177/1087057112456877).
- Tauzin S, Ding H, Khatib K, Ahmad I, Burdevet D, Van Echten-Deckert G, Lindquist JA, Schraven B, Din NU, Borisch B, Hoessli DC. 2008.** Oncogenic association of the Cbp/PAG

- adaptor protein with the Lyn tyrosine kinase in human B-NHL rafts. *Blood* **111**:2310–2320 DOI [10.1182/blood-2007-05-090985](https://doi.org/10.1182/blood-2007-05-090985).
- Te Vruchte D, Speak AO, Wallom KL, Al Eisa N, Smith DA, Hendriksz CJ, Simmons L, Lachmann RH, Cousins A, Hartung R, Mengel E, Runz H, Beck M, Amraoui Y, Imrie J, Jacklin E, Riddick K, Yanjanin NM, Wassif CA, Rolfs A, Rimmele F, Wright N, Taylor C, Ramaswami U, Cox TM, Hastings C, Jiang X, Sidhu R, Ory DS, Arias B, Jeyakumar M, Sillence DJ, Wraith JE, Porter FD, Cortina-Borja M, Platt FM. 2014.** Relative acidic compartment volume as a lysosomal storage disorder-associated biomarker. *Journal of Clinical Investigation* **124**:1320–1328 DOI [10.1172/JCI72835](https://doi.org/10.1172/JCI72835).
- Uesaka Y, Otsuka Y, Lin Z, Yamasaki S, Yamaoka J, Kurazono H, Takeda Y. 1994.** Simple method of purification of *Escherichia coli* heat-labile enterotoxin and cholera toxin using immobilized galactose. *Microbial Pathogenesis* **16**:71–76 DOI [10.1006/mpat.1994.1007](https://doi.org/10.1006/mpat.1994.1007).
- Vance JE, Karten B. 2014.** Niemann–Pick C disease and mobilization of lysosomal cholesterol by cyclodextrin. *Journal of Lipid Research* **55**:1609–1621 DOI [10.1194/jlr.R047837](https://doi.org/10.1194/jlr.R047837).
- Vite CH, Bagel JH, Swain GP, Prociuk M, Sikora TU, Stein VM, O'Donnell P, Ruane T, Ward S, Crooks A, Li S, Mauldin E, Stellar S, Meulder M De, Kao ML, Ory DS, Davidson C, Vanier MT, Walkley SU. 2015.** Intracisternal cyclodextrin prevents cerebellar dysfunction and Purkinje cell death in feline Niemann-Pick type C1 disease. *Science Translational Medicine* **7**:276ra226 DOI [10.1126/scitranslmed.3010101](https://doi.org/10.1126/scitranslmed.3010101).
- Waugh MG. 2012.** Phosphatidylinositol 4-kinases, phosphatidylinositol 4-phosphate and cancer. *Cancer Letters* **325**:125–131 DOI [10.1016/j.canlet.2012.06.009](https://doi.org/10.1016/j.canlet.2012.06.009).
- Waugh MG. 2013.** Raft-like membranes from the trans-Golgi network and endosomal compartments. *Nature Protocols* **8**:2429–2439 DOI [10.1038/nprot.2013.148](https://doi.org/10.1038/nprot.2013.148).
- Waugh MG. 2014.** Chromosomal instability and phosphoinositide pathway gene signatures in glioblastoma multiforme. *Molecular Neurobiology* DOI [10.1007/s12035-014-9034-9](https://doi.org/10.1007/s12035-014-9034-9).
- Waugh MG. 2015.** PIPs in neurological diseases. *Biochimica et Biophysica ACTA/Molecular and Cell Biology of Lipids* **1851**:1066–1082 DOI [10.1016/j.bbalip.2015.02.002](https://doi.org/10.1016/j.bbalip.2015.02.002).
- Waugh MG, Chu KM, Clayton EL, Minogue S, Hsuan JJ. 2011a.** Detergent-free isolation and characterization of cholesterol-rich membrane domains from trans-Golgi network vesicles. *Journal of Lipid Research* **52**:582–589 DOI [10.1194/jlr.D012807](https://doi.org/10.1194/jlr.D012807).
- Waugh MG, Lawson D, Hsuan JJ. 1999.** Epidermal growth factor receptor activation is localized within low-buoyant density, non-caveolar membrane domains. *Biochemical Journal* **337**(Pt 3):591–597 DOI [10.1042/bj3370591](https://doi.org/10.1042/bj3370591).
- Waugh MG, Lawson D, Tan SK, Hsuan JJ. 1998.** Phosphatidylinositol 4-phosphate synthesis in immunisolated caveolae-like vesicles and low buoyant density non-caveolar membranes. *Journal of Biological Chemistry* **273**:17115–17121 DOI [10.1074/jbc.273.27.17115](https://doi.org/10.1074/jbc.273.27.17115).
- Waugh MG, Minogue S, Anderson JS, Balinger A, Blumenkrantz D, Calnan DP, Cramer R, Hsuan JJ. 2003a.** Localization of a highly active pool of type II phosphatidylinositol 4-kinase in a p97/valosin-containing-protein-rich fraction of the endoplasmic reticulum. *Biochemical Journal* **373**:57–63 DOI [10.1042/bj20030089](https://doi.org/10.1042/bj20030089).
- Waugh MG, Minogue S, Blumenkrantz D, Anderson JS, Hsuan JJ. 2003b.** Identification and characterization of differentially active pools of type IIalpha phosphatidylinositol 4-kinase activity in unstimulated A431 cells. *Biochemical Journal* **376**:497–503 DOI [10.1042/bj20031212](https://doi.org/10.1042/bj20031212).
- Waugh MG, Minogue S, Chotai D, Berditchevski F, Hsuan JJ. 2006.** Lipid and peptide control of phosphatidylinositol 4-kinase IIalpha activity on Golgi-endosomal rafts. *Journal of Biological Chemistry* **281**:3757–3763 DOI [10.1074/jbc.M506527200](https://doi.org/10.1074/jbc.M506527200).

- Waugh MG, Minogue S, Clayton EL, Hsuan JJ. 2011b.** CDP-diacylglycerol phospholipid synthesis in detergent-soluble, non-raft, membrane microdomains of the endoplasmic reticulum. *Journal of Lipid Research* 52:2148–2158 DOI [10.1194/jlr.M017814](https://doi.org/10.1194/jlr.M017814).
- Welliver M. 2006.** New drug sugammadex: a selective relaxant binding agent. *AANA Journal* 74:357–363.
- Westover EJ, Covey DF, Brockman HL, Brown RE, Pike LJ. 2003.** Cholesterol depletion results in site-specific increases in epidermal growth factor receptor phosphorylation due to membrane level effects. Studies with cholesterol enantiomers. *Journal of Biological Chemistry* 278:51125–51133 DOI [10.1074/jbc.M304332200](https://doi.org/10.1074/jbc.M304332200).
- Xu W, Yoon SI, Huang P, Wang Y, Chen C, Chong PL, Liu-Chen LY. 2006.** Localization of the kappa opioid receptor in lipid rafts. *Journal of Pharmacology and Experimental Therapeutics* 317:1295–1306 DOI [10.1124/jpet.105.099507](https://doi.org/10.1124/jpet.105.099507).
- Zidovetzki R, Levitan I. 2007.** Use of cyclodextrins to manipulate plasma membrane cholesterol content: evidence, misconceptions and control strategies. *Biochimica et Biophysica ACTA/General Subjects* 1768:1311–1324 DOI [10.1016/j.bbamem.2007.03.026](https://doi.org/10.1016/j.bbamem.2007.03.026).